

GROUNDWATER DEFLUORIDATION USING NOVEL METAL MODIFIED CLAY AND DIATOMACEOUS EARTH ADSORBENTS

Report to the
Water Research Commission

by

**WM Gitari¹, AA Izuagie¹, R Mudzielwana¹, GK Pindihama¹, ME Denga¹,
T Ngulube¹ and TAM Msagati²**

¹Environmental Remediation and Water Pollution Chemistry Group,
School of Environmental Sciences, University of Venda

²College of Science, Engineering and Technology, Nanotechnology Unit,
University of South Africa

WRC Report No. 2363/1/19

ISBN 978-0-6392-0096-5

November 2019



Obtainable from

Water Research Commission
Private Bag X03
Gezina, 0031

orders@wrc.org.za or download from www.wrc.org.za

DISCLAIMER

This report has been reviewed by the Water Research Commission (WRC) and approved for publication. Approval does not signify that the contents necessarily reflect the views and policies of the WRC, nor does mention of trade names or commercial products constitute endorsement or recommendation for use.

Printed in the Republic of South Africa

© Water Research Commission

EXECUTIVE SUMMARY

BACKGROUND

Groundwater is a source of drinking water for most rural communities in many developing countries due to lack of municipal water supply. However, the raw groundwater may contain chemical species above recommended limits for drinking water and could be detrimental to human health. One example of chemical species of concern in groundwater is fluoride, which is often present in high concentrations. Fluoride ion is essential for formation of teeth and bone if present in drinking water at the right concentrations. However, in concentrations above recommended limits (1.5 mg/l) it may have negative health impacts such as teeth mottling (dental fluorosis) and deformation of bones (skeletal fluorosis). Several studies have observed that the groundwater in North West, Limpopo and Northern Cape provinces contain fluoride in concentrations reaching 30 mg/l and may require partial defluoridation. A number of techniques have been developed for defluoridation of groundwater such as adsorption, ion exchange and precipitation processes, membrane process such as reverse osmosis, Donnan dialysis, electro dialysis and nanofiltration. Of these methods, adsorption has been identified as the only technology that is most suited for use in rural communities. However, the adsorption capacity of most of the developed adsorbents is low and they are costly, and in other instances requiring pH adjustment prior to application in the field. This project was designed to evaluate locally available smectite-rich clays soils and diatomaceous earth either in their raw form or modified with high charge density cations Al^{3+} , Fe^{3+} , Ce^{3+} , Mg^{2+} and Mn^{2+} , their oxides or mixed oxides/hydroxides for defluoridation of groundwater. The project was designed with a main objective and several specific objectives.

METHODS AND STUDY DESIGN

Initial groundwater sample collection and characterisation

Field groundwater samples were collected from selected community and private boreholes in various districts/villages in Limpopo province and their physicochemical parameters evaluated. This was done in an attempt to understand the groundwater chemistry with respect to major and minor metal species content and anions co-existing with F^- ions. This was crucial in designing anionic solutions for testing effect of co-existing anions on fluoride removal. Physical parameters were recorded in the field and in the laboratory.

Fluoride adsorption experiments

Two clay soil types (black smectite-rich and red-black silica-rich) were collected from Mukondeni Village in Limpopo province while Fluoride-rich groundwater was collected from a borehole in Ga-Matlala and Siloam village in Limpopo province. The diatomaceous earth (DE) for the study was obtained from an industrial supplier in South Africa and natural deposits in Gilgil, Nakuru County, Kenya. The clay soils were rinsed with deionized water, centrifuged, dried and milled to a fine powder to pass through a 250 μm sieve. Modification of the clay soils and diatomaceous earth by metal oxides was done through co-precipitation using Fe^{3+} , Al^{3+} , Ce^{3+} , Mn^{2+} and Mg^{2+} salt solutions at alkaline pH. Modification of bentonite clay with Mn^{2+} ions and coating with MnO_2 was done through cation exchange and in-situ reduction of $KMnO_4$ in presence of bentonite clay respectively. Iron(III) oxide modified bentonite clay-reddish/black Mukondeni clay soil composite ceramic pellets were synthesized by mixing the two components at various ratios.

The MnO_2 /clay soil composite adsorbent was prepared by mixing smectite-rich clay soil/ MnO_2 Na-bentonite at various ratios and then calcined at various temperatures to produce pellets. Factors optimized in the synthesis included, particle size, furnace temperature, firing time and clay ratios. Chemical and mineralogical analysis was carried out using XRD and XRF, morphological analysis by SEM, surface area by BET, surface functional groups by FTIR, pH_{pzc} by the solid addition method, Cation Exchange Capacity (CEC) by the ammonium acetate method. Optimization of the F^- adsorption conditions were done through

batch experiments. Operational conditions optimized included agitation time, adsorbent dosage, initial fluoride concentration, solution pH and effect of temperature. Adsorption modeling was done using Langmuir, Freundlich and Dubinin-Radushkevich adsorption isotherms while kinetic modeling was done using Lagergren's pseudo first and second order kinetic models. The Al/Fe modified diatomaceous earth was also tested for groundwater defluoridation and pathogen of faecal origin removal using a fixed bed.

RESULTS

The results are presented in five sections: (1) Field groundwater sampling and physicochemical characterization, (2) Synthesis, characterization and evaluation of iron(III) oxide coated bentonite clay red/black Mukondeni clay soil composites for the defluoridation of groundwater, (3) Synthesis, characterization and evaluation of groundwater defluoridation capacity of smectite-rich clay soils and Mn-modified bentonite clay composites, (4) Defluoridation of groundwater using raw, heat-treated and Al/Fe-oxide, Mn/Ce/Mg tri-metal oxide-modified diatomaceous earth, and (5) Defluoridation potential evaluation of Al/Fe oxide coated diatomaceous earth using fixed bed column.

Field groundwater sampling and physicochemical characterization

This first section presents a summary of groundwater sampling and physicochemical characterization in Limpopo province. Groundwater samples collected in various parts of Limpopo province and Sekhukhune district were observed to have neutral to circum-neutral pH and highly saline with high concentrations of Ca, Na, K, Mg, Cl⁻, NO₃⁻ and SO₄²⁻ [Na (65-1616 mg/l), K(1.33-20.38 mg/l), Mg(0.19-304.90 mg/l), Ca(1.14-142.40 mg/l), Cl⁻(38.6-478.5 mg/l), NO₃⁻ (8.52-507.82 mg/l), SO₄²⁻(17.60-183-53 mg/l), F⁻(0.3-3.2 mg/l)]. Metal species concentrations ranged as follows: Al (1.68-11.06 µg/l), V (0.19-36.93 µg/l), Mn (0.28-284.64 µg/l), Fe (1.80-7137 µg/l), Zn (1.15-3755 µg/l), Ba (3.38-288.71 µg/l). Some of the boreholes were observed to have fluoride levels above the admissible limits and require defluoridation.

Fluoride adsorption using raw and iron(III) oxide coated bentonite clay red/black Mukondeni clays

This second section presents a summary of the synthesis, characterization and evaluation of raw red/black Mukondeni clay soils, iron(III) oxide coated bentonite clay red/black Mukondeni clay soil and their composites for the defluoridation of groundwater. The CEC of the red/black mixed clay soils ranged from 70.6-137.7 meq/100 g at pH 5.4-7.4. The adsorption of fluoride was mainly by chemisorption. The mixed Mukondeni clay soils had low adsorption capacity (0.05-0.16) mg/g and might require surface modification to increase their adsorption capacity. Maximum adsorption of fluoride was observed at pH 2 which would not be applicable in rural communities since it will require pH adjustment of product water. Modification of the bentonite clay with Fe₂O₃ tripled the BET surface area (43.2 to 132.3 m²/g). However, CEC levels of the Fe³⁺/Fe-oxide modified bentonite was lower than of raw bentonite indicating cation exchange process was the main process for entry of Fe³⁺ ions during the modification process. Na⁺ and Mg²⁺ were observed to be the main exchangeable cations. The regeneration studies demonstrated a decrease in the adsorption of fluoride from 76.7% to 35.9% after four consecutive cycles indicating potential reusability of the adsorbent. A maximum fluoride removal was observed at a dosage of 3 g/100 ml. Overall, the residual concentration of chemical species in the treated water at initial pH of 6-9, were below the WHO drinking water guidelines. An experimental adsorption capacity of 1.52 mg/g was established by Langmuir model for the adsorbent. The results indicate that Fe₂O₃ coated bentonite clay is a potential adsorbent for defluoridation of groundwater with no secondary contamination of treated water. Its limitation would be interference by co-existing anions in field water. This would render the adsorbent unsuitable for defluoridation of field fluoride-rich groundwater.

To increase physical integrity and handleability of the adsorbent an attempt was made to fabricate Iron(III) oxide modified bentonite clay-red/black Mukondeni clay soils composite ceramic granules for use in household defluoridators. Optimum conditions for fabrication of the pellets were 250 µm particle size composite material, 600°C furnace temperature, 1 h firing time and 5:1 (iron(III) oxide coated bentonite:

clay-red/black Mukondeni clay soil) ratios. The results of F⁻ adsorption tests revealed a decrease in defluoridation capacity of the adsorbent with increasing firing temperature. The optimum adsorption capacity was 0.03 mg/g for a 10 mg/l initial F⁻ concentration and 2 g adsorbent at pH 6.8. The adsorption capacities of the ceramic pellets increased with increasing iron(III) oxide modified bentonite clay ratio. Their fluoride adsorption potential was observed to be low and further evaluation in a dynamic flow mode was not envisaged. However, the potential implications of the results are important in the development of future point-of-use water defluoridation devices for the removal of fluoride from water using clay composites.

Fluoride adsorption using smectite-rich clay soils and Mn-modified bentonite clay composites

This third section presents a summary on synthesis, characterization and evaluation of groundwater defluoridation capacity of smectite-rich clay soils, Mn²⁺-modified bentonite, MnO₂-coated bentonite clay and their composites. Batch experiments were carried out to evaluate the effects of contact time, effect of adsorbent dosage, adsorbate initial concentration and the effect of pH on fluoride adsorption by the adsorbent. The CEC for Mukondeni black clay soils varied from 74.2 (meq/100 g) at pH 5.4 to 79.9 (meq/100 g) at pH 7.4. It was further observed that 0.8 g/100 ml of black Mukondeni clay soils removed up to 91.89% from initial F⁻ concentration of 3 mg/l at pH of 2 and contact time of 30 min. Black Mukondeni clay soils showed high percentage F⁻ removal from field water at acidic pH 2 which would limit its application in household treatment devices since pH adjustment of product water would be required. However, the black clay soils showed significant F⁻ adsorption potential at pH range of 4-10 with an initial concentration of 3 mg/l. A removal of ≈ 85% was observed over this pH range indicating the potential of the soil for defluoridation of low fluoride containing groundwater. A maximum adsorption capacity of 0.34 mg/g was achieved at optimized conditions. A poor fluoride removal was observed with field water which was attributed to effect of co-existing anions. Modification of bentonite clay with Mn²⁺ ions and synthesis of Mn²⁺ intercalated bentonite clay at optimized conditions was carried out followed by physicochemical and mineralogical characterization and evaluation of F⁻ adsorption potential. Maximum F⁻ removal of 84.0% was achieved under optimal conditions. Co-existing ions decreased the percentage fluoride removal. Treatment of the field water at optimized conditions showed moderate F⁻ removal of 55.9% as compared to 84% in synthetic F⁻ water which was attributed to the presence of co-existing anions. Surface modification of NaOH activated bentonite with MnO₂ was carried out and the adsorbent evaluated for its fluoride adsorption capacity. Regeneration results indicated that the MnO₂ coated Na-bentonite could successfully be regenerated using 0.1 M NaOH and be reused for effective fluoride removal over five cycles. MnO₂ coated Na-bentonite was able to reduce F⁻ in field groundwater from 5.4 mg/l to 0.98 mg/l which is below the South African water limit of 1.5 mg/l. The maximum adsorption capacity of 0.64 mg/g was achieved at optimized conditions.

Fabrication of smectite-rich clay soil-MnO₂ coated bentonite clay composites was carried out in an attempt to form physically stable adsorbent and increase its handleability. Pellets were prepared by moulding the clay manually. Evaluation of the fluoride adsorption by the pellets was carried out as a function of the fabrication parameters such as the clay mixing ratios and calcination temperatures. Results showed that pellets prepared at 1:3 clay mixing ratio (MnO₂ coated Na-bentonite/Smectite-rich clay soils) exhibited highest fluoride removal capacity. The calcination temperature on the prepared pellets was observed to increase their fluoride adsorption capacity to a maximum at 550°C. Maximum fluoride removal was 63.3% for 10 mg/l initial fluoride solution indicating their potential for application in household defluoridation devices.

Defluoridation of groundwater using raw, heat-treated and Al/Fe-oxide, Mn/Ce/Mg tri-metal oxide-modified diatomaceous earth

This fourth section presents a summary of the evaluation of the groundwater defluoridation potential of raw, heat-treated Al/Fe-oxide, Mn/Ce/Mg tri-metal oxide-modified diatomaceous earth and the regeneration potential of the synthesized adsorbents. The highest percent fluoride removal at optimum adsorption

conditions was between 23.4 and 25.6% for the raw diatomaceous earth. Moreover, optimum fluoride removal was observed at acidic pH of 2, which would not be appropriate for household defluoridation. PO_4^{3-} in tested field water was observed to reduce the fluoride uptake capacity of raw DE. Results of batch fluoride adsorption experiments indicate that Al/Fe oxide-modified DE had a high fluoride removal potential. Optimum adsorption capacity was 7.6 mg/g for 100 mg/l F^- solution at 297 K. Co-existing ions were observed to have an effect on the adsorption of F^- . Fluoride adsorption > 45% was observed in the pH range 4-8 which is crucial for defluoridation of field groundwater since no pH adjustment is required. At 5 mg/l co-existing anion concentration, reduction in % F^- removal was at most 9.2% for PO_4^{3-} . The synthesized adsorbent was effective in defluoridation of field groundwater at optimized conditions registering 83.2% fluoride removal with an equilibrium $\text{pH} \approx 6.86$. Moreover, minimal leaching of Al, Fe and Si from the adsorbent was observed at pH range of 4-8 and there seemed to be no correlation between leaching quantities and the adsorbent dosage. Fluoride concentration in water could be reduced from initial 10 mg/l F^- solution by 81.8% at the 3rd cycle of defluoridation using 0.8 g/100 ml adsorbent dosage as compared to 27.8 and 8.6% recorded for NaOH and Na_2CO_3 respectively at the same cycle. The results indicate that Al/Fe oxide modified DE is a potential adsorbent for defluoridation of groundwater and can be easily regenerated for reuse making it suitable for point of use defluoridation devices in rural communities.

Successful modification of the diatomaceous earth with Mg/Ce/Mn oxides was confirmed through physicochemical and mineralogical analysis using TEM, SEM, SEM-EDX, FTIR and XRD. Adsorption capacity was established to be 1.16 mg/g for an initial adsorbate concentration of 10 mg/l. Several regenerants were tested for recovery and re-usability of the adsorbent. Regeneration of the adsorbent using dilute K_2SO_4 solution reduced the fluoride removal to 60.8% from 96.7% in the first cycle of reuse. The adsorbent was effective in defluoridation of field fluoride-rich groundwater, moreover other co-existing anions such as Br^- and NO_3^{2-} were removed to below detection limits. Sulphate and Cl^- ions were leached into the product water, which was attributed to SO_4^{2-} and Cl^- from the initial salts used in the modification of the DE. This property would be a limitation in the application of the adsorbent in defluoridation of field fluoride-rich groundwater.

Defluoridation potential of Al/Fe oxide coated diatomaceous earth using fixed bed

This fifth section presents a summary of the evaluation of the defluoridation potential of Al/Fe oxide coated diatomaceous earth using fixed bed. Optimization of treatment parameters: The effect of sorbent mass/bed height was evaluated at 0.5, 0.85 and 1 cm bed heights corresponding 0.1 g, 0.76 g and 1 g sorbent mass respectively. The breakthrough volume (V_b) was observed to increase with increasing bed height/adsorbent mass. The effect of influent flow rates on the adsorption of fluoride was evaluated at flow rates of 0.62, 1.18 and 1.32 ml/min respectively at adsorbent dosage of 1 g and $C_e = 10$ mg/l. The breakthrough volume decreased with increased flow rate. The effect of influent fluoride concentration was evaluated at flow rates of 0.62 ml/min and bed mass of 1 g. Initial F^- concentration used were 3.5, 10 and 18 mg/l. The variation of C_t/C_0 with increasing influent concentration indicated that the breakthrough time increased with decreasing influent concentration. Appearance of early breakthrough point and low breakthrough volume for high influent concentration indicates rapid exhaustion of the fluoride removal capacity of the

Field Water treatment: The efficiency of fixed-bed column to treat fluoride-rich groundwater was tested using field ground water collected from a community borehole in Lephalale with fluoride concentration of 9.14 mg/l. Treatment was carried out using 1 g of adsorbent at a flow rate of 0.62 ml/min. The adsorbent was observed to be efficient in groundwater treatment. The pH remained within the SANS-241 (2015) guidelines for drinking water. The adsorbent was also observed to remove other co-existing anions improving further the quality of the water. It was observed that 1 g adsorbent could treat 75 ml in 120 minutes at a flow rate of 0.62 ml/min. The column performance was not affected by the presence of the co-existing anions in the field water.

Removal of pathogens of faecal origin: The adsorbent was also tested for its potential to remove pathogens of faecal origin in addition to fluoride in groundwater. Field water (fluoride-rich) samples were spiked with 10 ml of wastewater effluent from a local wastewater treatment plant. Water samples, before and after passing through the prepared adsorbent bed (1 g material, 1 rpm flow rate) were analysed in triplicate for the presence of *E. coli* and other coliforms using the membrane filtration technique. The results of the experiments showed that the adsorbent bed was effective in removing both *E. coli* and other coliform bacteria in conjunction with fluoride. Both *E. coli* and total coliform were reduced from $\geq 30\,000$ cfu/100 ml to 0 cfu/100 l after passing through the column.

GENERAL DISCUSSION, CONCLUSION AND RECOMMENDATIONS

Several locally sourced clay soils, bentonite clay and diatomaceous earth (DE), either in their raw form, composite or modified with metal oxides, were evaluated for their potential to adsorb fluoride from groundwater in this project. The raw clay soils, bentonite and DE were observed to have low fluoride adsorption potential with most registering low adsorption capacity (0.05-0.16 mg/g F⁻). Moreover, their maximum fluoride removal was observed at acidic pH range which would be a challenge for application in field treatment due to pH adjustment requirement. The red/black clay soils were also observed to leach chemical species to levels beyond required limits. Modification of bentonite with Mn²⁺, Fe³⁺, Fe₂O₃ and MnO₂ was observed to increase their surface area and fluoride adsorption capacity. The Fe³⁺/Fe₂O₃ modified bentonite adsorbents showed a wide pH range of maximum F⁻ adsorption (2-12) but had low F⁻ adsorption potential for water samples, the adsorbed exhibited high affinity for Br⁻, SO₄²⁻, NO₃⁻, PO₄³⁻ than Cl⁻ and F⁻. The adsorbent was chemically stable and could be regenerated up to two cycles. The Fe₂O₃ modified bentonite-red/black clay soils composite pellets showed moderate fluoride adsorption capacity, the Fe₂O₃ content in the ceramic pellets was significant in the fluoride removal capacity.

The Mn²⁺ intercalated bentonite clay showed maximum fluoride adsorption (84%) at acidic pH 2 for a 3 mg/l F⁻ solution with a decreased removal observed for field water. Moreover, the adsorbent was chemically stable but had low adsorption capacity compared to similar materials reported in literature. MnO₂ modified bentonite clay had increased surface area compared to raw bentonite. It exhibited maximum F⁻ removal at pH 8 (5 mg/l F⁻ solution) and moreover reduced F⁻ in field water to below 1 mg/l (5.4 mg/l F⁻ solution). It was regenerated successfully using 0.01 M NaOH and reused up to 5 cycles and it was chemically stable except at extreme acidic and alkaline pH, Mn and K was observed to leach out at levels above prescribed guidelines. It decreased the pH of treated water and exhibited a moderate adsorption capacity (0.65 mg/l F⁻ (5 mg/l F⁻ solution). The black smectite-rich clay soil-MnO₂ coated bentonite clay composites ceramic pellets were observed to be stable at 500°C calcination temperature. They exhibited moderate fluoride removal potential of 63.3% (10 mg/l F⁻) and showed promising qualities for application in fixed bed defluoridation devices.

The raw DE exhibited Low F⁻ adsorption potential (23-25%) (8 mg/l F⁻ solution) and optimum F⁻ adsorption was observed at pH 2 which would limit application of the adsorbent in field water treatment. Although chemically stable at adsorption conditions it exhibited low F⁻ adsorption for field water. The Al/Fe oxide modified DE adsorbent exhibited high F⁻ removal potential at pH 6.7 (11 mg/l F⁻) at a wide pH range of 4-8. Moreover, its adsorption capacity was not significantly affected by co-existing anions. The adsorbent was effective in defluoridation of field groundwater at field pH (≈ 7.0) and minimal leaching of chemical species (Al, Fe, and Si at pH 4-8). The adsorbent is easily regenerable with K₂SO₄ solution and still retains high adsorption capacity after several cycles. It exhibited superior qualities for application in household water defluoridation devices and it is recommended for further technical testing and evaluation. The Mg/Ce/Mn-oxide modified DE remained amorphous and the metal oxides were deposited across pores but remained porous. The adsorbent exhibited high F⁻ adsorption capacity (1.16 mg/g) at 10 mg/l at 0.6 g/100 ml, moreover high defluoridation capacity for field groundwater was observed with no significant

change in pH. The adsorbent exhibited poor regeneration potential with low F⁻ adsorption capacity observed after regeneration and substantial leaching of Mn, Ce, Mg and Si in product water. Of all the adsorbents synthesized and evaluated for their fluoride adsorption potential, Al/Fe modified DE exhibited superior qualities for further testing and evaluation for application in household defluoridation devices and was subsequently tested using a fixed bed. Al/F oxide modified DE adsorbent bed exhibited potential for defluoridation of groundwater. It exhibited no leaching and therefore posed no risk for secondary contamination of the product water. Moreover, testing the bed with fluoride water spiked with wastewater confirmed the potential of the adsorbent to adsorb fluoride and remove microbial pathogens of faecal origin thus providing a dual process for delivery of fluoride and microbial contaminants free water at household level. Further evaluation and optimization of the Al/Fe, Mg/Ce/Mn-oxide modified DE/clay soils composites/mixtures is recommended for fabrication of ceramic candles and discs for application in household water treatment devices.

CAPACITY BUILDING

STUDENTS GRADUATED

- **Mudzielwana Rabelani (2016)**. Synthesis, characterization and performance evaluation of groundwater defluoridation capacity of smectite-rich clay soils and Mn-modified bentonite clay composites. *MSc Thesis*, University of Venda.
- **Tholiso Ngulube (2016)**. Synthesis, characterization and performance evaluation of iron(III) oxide coated bentonite clay-silica-rich reddish black Mukondeni clay soils composites for the defluoridation of groundwater. *MSc Thesis*, University of Venda.
- **Izuagie, Anthony Anabui (2016)**. Defluoridation of groundwater using raw, heat-treated and metal oxide-modified diatomaceous earth. *PhD Thesis*, University of Venda.
- **Masemula Komane Joseph (2016)**. Defluoridation of groundwater using Mn²⁺/Al³⁺ oxides modified Mukondeni black clay soil. *Honors mini Thesis*. University of Venda

SUBMITTED FOR EXAMINATION 2017

- **Denga Masindi Esther (2017)**. Fabrication of metal-oxide modified porous ceramic granules from aluminosilicate-rich clay soils for defluoridation of groundwater. *MSc Thesis*. University of Venda

PUBLICATIONS IN JOURNALS

- W.M. Gitari, A.A. Izuagie, J.R. Gumbo, Synthesis, characterization and batch assessment of groundwater fluoride removal capacity of trimetal Mg/Ce/Mn oxide-modified diatomaceous earth, Arabian Journal of Chemistry (2017), doi: <http://dx.doi.org/10.1016/j.arabjc.2017.01.002>
- T NGULUBE, MW GITARI AND H TUTU (2017). Defluoridation of groundwater using mixed Mukondeni clay soils. Water Science and Technology: 17(2): 480-492. DOI: **10.2166/ws.2016.157**
- IZUAGIE AA, WILSON M. GITARI AND JABULANI R. GUMBO. (2016). Effects of calcination temperature and solution pH on the defluoridation potential of Al/Fe oxide-modified diatomaceous earth: metal leaching and sorbent reuse. Water Science and Technology-Water Supply. 11 October 2016, ws2016142; DOI: **10.2166/ws.2016.142**
- Mudzielwana R, Gitari MW, Msagati TAM. (2017) Characterisation of smectite-rich clay soil: Implication for groundwater defluoridation. S Afr J Sci. 2016; 112(11/12), Art. #2015-0442, 8 pages. <http://dx.doi.org/10.17159/sajs.2016/20150442>
- IZUAGIE AA, WILSON M. GITARI AND JABULANI R. GUMBO (2016): Synthesis and performance evaluation of Al/Fe oxide coated diatomaceous earth in groundwater defluoridation: Towards fluorosis mitigation, Journal of Environmental Science and Health, Part A, DOI: 10.1080/10934529.2016.1181445
- IZUAGIE AA, WILSON M. GITARI AND JABULANI R. GUMBO (2015): Defluoridation of groundwater using diatomaceous earth: optimization of adsorption conditions, kinetics and leached metals risk assessment, Desalination and Water Treatment, DOI: 10.1080/19443994.2015.1083894

PATENTS

- 2016/08590 ~ Complete ~54: DEFLUORIDATION TREATMENT OF WATER WITH TRIMETAL MAGNESIUM/CERIUM/MANGANESE OXIDE MODIFIED DIATOMACEOUS EARTH ~71: UNIVERSITY OF VENDA, UNIVERSITY ROAD, THOHOYANDOU, 0950; P/BAG X5050, South Africa ~72: Anthony Anabui IZUAGIE; Jabulani Ray GUMBO; Wilson Mugeru GITARI~

CONFERENCE ABSTRACTS AND PROCEEDINGS

- MUDZIELWANA R, GITARI W. M AND MSAGATI T. A. M **(2016)**. Intercalation of Mn^{2+} ions onto bentonite clay: implication on groundwater defluoridation. 13th International conference on modelling, monitoring and management of water pollution. Water Pollution XIII. ISBN: 978-1-78466-139-7
- NGULUBE T, GITARI WM AND HLANGANANI T **(2016)**. Adsorptive removal of excess fluoride in drinking water using silica-rich reddish black clay soils: Adsorbent preparation, performance and study of adsorption mechanisms. International Conference on Industrial Chemistry. June 27-28, 2016 New Orleans, Louisiana, USA
- IZUAGIE AA, GITARI WM AND GUMBO JR **(2015)**. Defluoridation of groundwater using Al/Fe oxide-modified diatomaceous earth: synthesis, equilibria and kinetics of adsorption. 2015 FASC and Chemical Society of Nigeria (CSN) Conference. University of Lagos, Lagos, Nigeria
- NGULUBE T, GITARI WM AND HLANGANANI T. **(2015)**. Synthesis, characterization and performance of iron oxide coated bentonite clay in the removal of fluoride from drinking water. 1st UNIVEN-WSU International Research Conference. East London. 2nd to 4th Sept 2015. Research and innovation for sustainable development and the transformation of society.
- IZUAGIE AA, GITARI WM AND GUMBO JR **(2015)**. A novel Al/Fe oxide-modified silica-rich sedimentary powder for groundwater defluoridation: thermodynamics and kinetics of adsorption. 1st UNIVEN-WSU International Research Conference. 2nd to 4th Sept 2015, East London. Research and innovation for sustainable development and the transformation of society
- MUDZIELWANA R, GITARI WM AND MSAGATI TAM **(2015)**. Intercalation of Mn^{2+} ions onto bentonite clay: implication on groundwater defluoridation. 1st UNIVEN-WSU International Research Conference. 2nd to 4th Sept 2015, East London. Research and innovation for sustainable development and the transformation of society.

ACKNOWLEDGEMENTS

The project team wishes to thank the following people for their contributions to the project.

Reference Group	Affiliation
Dr N Kalebaila	Water Research Commission (Chairperson)
Prof PG Ndungu	University of Johannesburg
Prof C Ngila	University of Johannesburg
Prof T Godeto	University of Johannesburg
Prof H Tutu	University of Witwatersrand
Dr A Senzanje	University of KwaZulu-Natal
Prof V Somerset	Cape peninsula University of Technology
Prof LF Petrik	University of the Western Cape
Project Team	
Prof WM Gitari	University of Venda
Prof TAM Msagati	University of South Africa
Dr AA Izuagie	University of Venda
Mr Rabelani Mudzielwana	University of Venda
Miss Masindi Esther Denga	University of Venda
Miss Tholiso Ngulube	University of Venda
Mr Glynn Kuziva Pindihama	University of Venda

This page was intentionally left blank

CONTENTS

EXECUTIVE SUMMARY	iii
CAPACITY BUILDING	ix
ACKNOWLEDGEMENTS	xi
CONTENTS	xiii
LIST OF FIGURES	xxii
LIST OF TABLES	xxxii
ACRONYMS & ABBREVIATIONS	xxxv
1 BACKGROUND	1
1.1 INTRODUCTION.....	1
1.2 PROJECT AIM AND OBJECTIVES.....	2
1.3 SCOPE AND LIMITATIONS.....	2
2 LITERATURE REVIEW	3
2.1 OCCURRENCE AND SOURCES OF FLUORIDE IN GROUNDWATER.....	3
2.2 CHEMISTRY OF FLUORIDE IN GROUNDWATER.....	5
2.3 THE HEALTH IMPLICATIONS OF FLUORIDE CONSUMPTION.....	7
2.4 WATER DEFLUORIDATION TECHNOLOGIES.....	11
2.4.1 Precipitation processes.....	11
2.4.2 Coagulation-precipitation defluoridation.....	11
2.4.3 Membrane processes.....	13
2.4.4 Electrocoagulation/electroflotation technology.....	14
2.4.5 Adsorption processes.....	15
2.5 WATER DEFLUORIDATION BY ADSORPTION.....	16
2.5.1 Bone and bone charcoal.....	16
2.5.2 Activated alumina (AA).....	16
2.5.3 Clays and soils.....	18
2.5.3.1 Mechanisms of adsorption onto clay soils.....	18
2.5.3.2 Kaolin clay.....	19
2.5.3.3 Other clays.....	19
2.5.3.4 Application of clay materials in household defluoridators and filters.....	19
2.5.3.5 Shortcomings of raw clay filter media.....	21
2.5.4 Merits of the adsorption process.....	21
2.5.5 Summary of bench scale studies on various adsorbents for defluoridation of water.....	22
2.6 CURRENT PRACTICES IN WATER DEFLUORIDATION.....	25
2.6.1 The concept of appropriate technology.....	25
2.6.2 Water defluoridation in Tanzania using bone char.....	26
2.6.3 Nalgonda technique for domestic defluoridation.....	27
2.6.4 Defluoridators using Activated Alumina in India.....	28
2.7 SUMMARY.....	30

3	FIELD GROUNDWATER SAMPLING AND CHARACTERIZATION	37
3.1	SAMPLE COLLECTION AND CHARACTERIZATION	37
3.1.1	Sampling Sites	37
3.1.2	Sample collection and analysis	38
3.2	RESULTS AND DISCUSSION	38
3.2.1	Overview	38
3.2.2	Physicochemical and hydrochemical profiles	38
3.2.3	Graphical presentation of Hydrochemical properties of the groundwater.....	41
3.2.3.1	Schoeller and Stiff Diagrams	41
3.2.3.2	Trilinear Diagram (Piper Diagram)	42
3.2.3.3	Durov Diagram	44
3.2.4	Principal component analysis of water samples	45
3.3	SUMMARY.....	46
4	EVALUATION OF GROUNDWATER DEFLUORIDATION BY SILICA-RICH MIXED RED/BLACK MUKONDENI CLAY SOILS.....	47
4.1	INTRODUCTION	47
4.2	MATERIALS AND METHODS	47
4.3	PREPARATION OF THE SILICA-RICH RED/BLACK MUKONDENI CLAY SOILS	47
4.4	CHARACTERISATION OF SILICA-RICH RED/BLACK MUKONDENI CLAY SOILS.....	48
4.4.1	X-Ray Diffraction (XRD) analysis.....	48
4.4.2	Cation Exchange Capacity (CEC).....	48
4.4.3	Point of zero charge (PZC) of silica-rich reddish black Mukondeni clay soils	49
4.4.4	X-Ray Fluorescence (XRF) Analysis	50
4.4.5	Scanning Electron Microscopy (SEM) analysis	50
4.4.6	Brunauer-Emmett-Teller (BET) analysis	51
4.4.7	Fourier Transform Infrared (FTIR) analysis	52
4.5	BATCH ADSORPTION EXPERIMENTS	53
4.5.1	Effect of contact time on fluoride removal capacity	53
4.5.2	Effect of adsorbent dosage on fluoride removal capacity	54
4.5.3	Effect of fluoride ion concentration on fluoride removal capacity	56
4.5.4	Effect of temperature on fluoride removal capacity	56
4.5.5	Effect of competing ions on fluoride removal capacity	58
4.5.6	Effect of pH on fluoride removal capacity	58
4.6	GROUNDWATER DEFLUORIDATION AT OPTIMAL AND FIELD PH CONDITIONS.....	60
4.6.1	Adsorption of fluoride from field groundwater at optimised and field conditions	60
4.6.2	Chemical stability of the adsorbent at different pH	61
4.7	ADSORPTION MODELLING STUDIES	61
4.7.1	Adsorption isotherm parameters.....	61
4.7.2	Thermodynamic parameters	62
4.8	ADSORPTION KINETICS	63
4.8.1	Overview	63
4.8.2	The pseudo first-order and pseudo second-order models.....	63
4.8.3	Diffusion based models.....	63
4.9	ADSORPTION MECHANISM OF FLUORIDE ONTO SILICA-RICH RED/BLACK MUKONDENI CLAY SOILS	65
4.10	SUMMARY.....	65

5	EVALUATION OF GROUNDWATER DEFLUORIDATION BY IRON(III) OXIDE COATED BENTONITE CLAY	67
5.1	INTRODUCTION	67
5.2	MATERIALS AND METHODS	67
5.3	SYNTHESIS OF THE IRON(III) OXIDE COATED BENTONITE CLAY	68
5.3.1	Activating bentonite clay with NaOH	68
5.3.2	Coating NaOH-activated bentonite clay with Fe ₂ O ₃	68
5.4	CHARACTERIZATION STUDIES	68
5.4.1	Point of zero charge (PZC) of raw bentonite and Fe ₂ O ₃ coated bentonite clay	68
5.4.2	Cation Exchange Capacity (CEC)	69
5.4.3	X-Ray Fluorescence Analysis	70
5.4.4	X-Ray Diffraction Analysis	70
5.4.5	Scanning Electron Microscopy Analysis	71
5.4.6	Brunnet-Emmett-Teller (BET) analysis	72
5.5	BATCH F ⁻ ADSORPTION EXPERIMENTS	73
5.5.1	Overview	73
5.5.2	Effect of contact time on fluoride removal capacity	73
5.5.3	Effect of dosage on fluoride removal capacity	74
5.5.4	Effect of concentration on fluoride removal capacity	74
5.5.5	Effect of temperature on fluoride removal	76
5.5.6	Effect of pH on fluoride removal capacity	76
5.5.7	Effect of co-existing ions on fluoride removal capacity	77
5.6	TREATMENT OF FIELD GROUND WATER FROM SILOAM COMMUNITY BOREHOLE AT OPTIMIZED CONDITIONS	78
5.7	CHEMICAL STABILITY OF THE ADSORBENT	79
5.8	REUSE AND REGENERATION OF IRON(III) OXIDE COATED BENTONITE CLAY	80
5.9	ADSORPTION MODELLING	81
5.9.1	Isotherm models	81
5.9.1.1	Langmuir Isotherm	81
5.9.1.2	Freundlich Isotherm	82
5.9.1.3	Dubinin-Radushkevich isotherm model	82
5.9.2	Thermodynamics	84
5.9.3	Adsorption kinetics	84
5.9.3.1	Overview	84
5.9.3.2	Pseudo first- and second order kinetics	85
5.9.3.3	Intraparticle and external diffusion models	86
5.10	SUMMARY	88
6	EVALUATION OF GROUNDWATER DEFLUORIDATION BY RED/BLACK MUKONDENI CLAY SOILS – IRON(III) OXIDE MODIFIED BENTONITE CLAY COMPOSITE CERAMIC PELLETS	90
6.1	INTRODUCTION	90
6.2	MATERIALS	90
6.3	METHODS	90
6.3.1	Fabrication of ceramic composite pellets	90
6.3.2	Optimisation of fabrication conditions	90
6.3.2.1	Optimisation of particle size	91
6.3.2.2	(ii) Optimisation of furnace temperature	91
6.3.2.3	(iii) Optimisation of firing time	91
6.3.2.4	(iv) Optimisation of clay ratios	91
6.3.3	Characterisation studies	91
6.3.4	Defluoridation experiments	91

6.4	FLUORIDE ADSORPTION UNDER DIFFERENT ADSORBENT FABRICATION CONDITIONS	92
6.4.1	Effect of particle size	92
6.4.2	Effect of furnace temperature	92
6.4.2.1	X-ray Diffraction analysis	92
6.4.2.2	Morphological Analysis	94
6.4.2.3	Brunauer Emmett Teller (BET) analysis	95
6.4.2.4	Fluoride adsorption	95
6.4.3	Effect of firing time	96
6.4.3.1	Changing morphology with firing times	96
6.4.3.2	Mineralogical changes with firing times	97
6.4.3.3	Chemical composition changes with firing time	97
6.4.3.4	Changes in surface area, pore volume and pore size distribution with firing time	98
6.4.3.5	Changes in surface functional groups with firing time	98
6.4.3.6	Fluoride adsorption with increasing firing time	99
6.4.4	Effect of clay ratios	99
6.5	SUMMARY	99
7	EVALUATION OF GROUNDWATER DEFLUORIDATION BY Mn^{2+} MODIFIED BENTONITE CLAY ..	
	100	
7.1	INTRODUCTION	100
7.2	MATERIALS	100
7.3	METHODS	100
7.3.1	Preparation of Mn^{2+} modified bentonite clay	100
7.3.2	Characterisation techniques	101
7.3.3	Batch and field groundwater adsorption studies	101
7.3.4	Adsorption modelling studies	101
7.4	PHYSICO-CHEMICAL AND MINERALOGICAL CHARACTERIZATION STUDIES	101
7.4.1	X-ray diffraction analysis	101
7.4.2	X-ray fluorescence analysis	102
7.4.3	Scanning Electron microscopy (SEM) analysis	102
7.4.4	Cation Exchange Capacity	103
7.4.5	Determination of pH _{pzc}	104
7.4.6	Fourier Transform Infra-red Analysis	105
7.4.7	BET Surface Area Analysis	106
7.5	BATCH F- ADSORPTION EXPERIMENTS	107
7.5.1	Effect of contact time	107
7.5.2	Effect of adsorbent dosage	108
7.5.3	Effect of adsorbate concentration	108
7.5.4	Effect of pH	109
7.5.5	Effect of co-existing anions	111
7.6	CHEMICAL STABILITY OF Mn^{2+} MODIFIED BENTONITE CLAY FOR USE IN GROUNDWATER DEFLUORIDATION	111
7.7	REGENERATION AND REUSE OF ADSORBENT	113
7.8	DEFLUORIDATION OF FIELD GROUNDWATER	113
7.9	ADSORPTION MODELLING	114
7.9.1	Adsorption isotherms	114
7.9.2	Adsorption Kinetics	116
7.9.3	Mechanism of F- adsorption onto Mn^{2+} modified bentonite clay	118
7.10	SUMMARY	118

8	EVALUATION OF GROUNDWATER DEFLUORIDATION BY MnO_2 COATED BENTONITE CLAY ...	119
8.1	INTRODUCTION	119
8.2	MATERIALS.....	119
8.3	METHODS	120
8.3.1	Activation of bentonite clay with NaOH.....	120
8.3.2	Coating the Na-bentonite with MnO_2	120
8.3.3	Characterisation techniques	120
8.3.4	Batch and field groundwater adsorption studies.....	120
8.3.5	Adsorption modelling studies	121
8.4	SYNTHESIS OF MnO_2 COATED BENTONITE.....	121
8.4.1	Optimizing conditions for activating bentonite with NaOH.....	121
8.4.1.1	Effect of contact time	121
8.4.1.2	Effect of concentration.....	122
8.4.2	Optimisation of conditions for coating NaOH activated bentonite with MnO_2	123
8.4.2.1	Effect of $KMnO_4$ concentration	123
8.4.2.2	Effect of clay amount	123
8.4.2.3	Effect of reaction time	124
8.5	PHYSICOCHEMICAL AND MINERALOGICAL CHARACTERIZATION.....	125
8.5.1	X-ray diffraction analysis.....	125
8.5.2	X-ray fluorescence	127
8.5.3	Scanning electron microscopy.....	127
8.5.4	Surface area, pore distribution and pore volume.....	129
8.5.5	Fourier Transform Infra Red (FTIR) Analysis	130
8.5.6	pH point of zero charge (pH_{pzc}).....	131
8.6	BATCH F^- ADSORPTION EXPERIMENTS	133
8.6.1	Effect of contact time	133
8.6.2	Effect of adsorbent dosage	133
8.6.3	Effect of initial adsorbate concentration.....	134
8.6.4	Effects of pH.....	135
8.6.5	Effect of co-existing ions	136
8.7	REGENERATION AND REUSE OF ADSORBENT	137
8.8	CHEMICAL STABILITY OF THE ADSORBENT	138
8.9	DEFLUORIDATION OF FIELD GROUNDWATER.....	140
8.10	ADSORPTION MODELLING.....	141
8.10.1	Adsorption isotherms	141
8.10.2	Adsorption kinetics.....	143
8.11	MECHANISM OF FLUORIDE ADSORPTION.....	145
8.12	SUMMARY.....	146
9	EVALUATION OF GROUNDWATER DEFLUORIDATION BY SMECTITE-RICH CLAY SOILS	147
9.1	INTRODUCTION	147
9.2	MATERIALS.....	147
9.3	METHODS	148
9.3.1	Preparation and characterization of smectite-rich clay soils.....	148
9.3.2	Batch and field groundwater adsorption experiments	148
9.4	PHYSICOCHEMICAL AND MINERALOGICAL CHARACTERIZATION.....	148
9.4.1	X-ray diffraction analysis.....	148
9.4.2	X-ray fluorescence analysis	149
9.4.3	Scanning electron microscope analysis.....	150
9.4.4	Surface area and pore volume.....	150
9.4.5	Fourier Transform Infra-red analysis.....	151

9.4.6	Cation Exchange capacity	151
9.4.7	pH point of zero charge.....	152
9.5	BATCH DEFLUORIDATION EXPERIMENTS.....	153
9.5.1	Effect of contact time	153
9.5.2	Effect of adsorbent dosage.....	153
9.5.3	Effect of initial adsorbate concentration.....	154
9.5.4	Effect of initial pH	155
9.5.5	Effect of co-existing anion.....	157
9.6	REGENERATION OF SMECTITE-RICH CLAY SOILS.....	157
9.7	DEFLUORIDATION OF FIELD GROUNDWATER.....	158
9.8	ADSORPTION MODELLING.....	159
9.8.1	Isotherm modelling.....	159
9.8.1.1	Langmuir isotherm.....	159
9.8.1.2	Freundlich adsorption model.....	161
9.8.2	Adsorption Kinetics	161
9.8.2.1	Pseudo first- and second order kinetics	162
9.8.2.2	Intra-particle diffusion model	162
9.9	MECHANISM OF F ⁻ ADSORPTION ONTO SMECTITE-RICH CLAY SOILS	163
9.10	SUMMARY.....	164
10	EVALUATION OF GROUNDWATER DEFLUORIDATION BY SMECTITE-RICH CLAY SOIL-MNO₂ COATED BENTONITE CLAY COMPOSITES	165
10.1	INTRODUCTION	165
10.2	MATERIALS.....	165
10.3	METHODS.....	165
10.3.1	Synthesis and characterisation of smectite-rich clay soil-MNO ₂ coated bentonite clay composites.....	165
10.3.2	Batch and field groundwater adsorption experiments	166
10.4	RESULTS AND DISCUSSION	166
10.4.1	Effect of clay mixing ratio on F ⁻ adsorption	166
10.4.2	Effect of calcination temperature on F ⁻ adsorption	167
10.5	PHYSICOCHEMICAL AND MINERALOGICAL CHARACTERISATION.....	168
10.5.1	X-ray diffraction analysis.....	168
10.5.2	X-ray fluorescence.....	168
10.5.3	Scanning electron microscopy.....	169
10.6	SUMMARY.....	170
11	EVALUATION OF GROUNDWATER DEFLUORIDATION USING RAW DIATOMACEOUS EARTH	171
11.1	INTRODUCTION	171
11.2	MATERIALS.....	171
11.3	METHODS.....	172
11.3.1	Preparation and characterisation of the raw DE for adsorption.....	172
11.3.2	Batch and field groundwater adsorption experiments	172
11.4	PHYSICOCHEMICAL AND MINERALOGICAL CHARACTERIZATION.....	172
11.4.1	Morphology of natural diatomaceous earth	172
11.4.2	X-ray fluorescence analysis of diatomaceous earth	172
11.4.3	Surface area and pore volume of raw diatomaceous earth.....	174
11.4.4	X-ray diffraction of DE.....	175
11.4.5	Fourier transform infrared spectra of raw and fluoride-treated diatomaceous earth	175
11.4.6	Cation exchange capacity of diatomaceous earth	176
11.4.7	pH at point-of-zero charge (pH _{pzc})	176

11.5	BATCH FLUORIDE ADSORPTION EXPERIMENTS.....	177
11.5.1	Effect of shaking speed.....	177
11.5.2	Effect of contact time	178
11.5.3	Effect of adsorbent dosage.....	179
11.5.4	Effect of pH	180
11.5.5	Effect of adsorbate concentration	181
11.5.6	Effect of temperature	182
11.6	ADSORPTION MODELLING.....	184
11.6.1	Adsorption isotherms	184
11.6.2	Adsorption kinetics.....	186
11.6.2.1	Pseudo first and second order models.....	186
11.6.2.2	Intra-particle diffusion model	187
11.6.2.3	External diffusion model.....	187
11.7	EVALUATION OF METALS, NON-METALS AND ANIONS RELEASE FROM DIATOMACEOUS EARTH.....	190
11.8	DEFLUORIDATION OF FIELD GROUNDWATER.....	190
11.9	SUMMARY.....	193
12	EVALUATION OF GROUNDWATER DEFLUORIDATION USING TRIMETAL MG/CE/MN OXIDE-MODIFIED DIATOMACEOUS EARTH	194
12.1	INTRODUCTION	194
12.2	MATERIALS.....	194
12.3	METHODS	194
12.3.1	Preparation of solutions for DE modification.....	194
12.3.2	Synthesis and optimization of synthesis conditions for pure Mg/Ce/Mn oxide and Mg/Ce/Mn oxide-modified diatomaceous earth.....	195
12.3.3	Batch and field groundwater adsorption experiments	195
12.4	PHYSICOCHEMICAL AND MINERALOGICAL ANALYSIS OF THE TRIMETAL OXIDE MODIFIED DIATOMACEOUS EARTH	196
12.4.1	X-ray diffraction analysis (XRD).....	196
12.4.2	Scanning electron microscopic analysis.....	196
12.4.3	High resolution transmission electron microscopic (HR-TEM) analysis	199
12.4.4	Surface area analysis by Brunauer-Emmett-Teller method.....	200
12.4.5	Fourier Transform Infra-Red (FTIR) Spectroscopy.....	201
12.4.6	pH at Point-of-zero-charge (pH_{pzc}).....	201
12.4.7	Thermogravimetric analysis (TGA).....	202
12.5	BATCH ADSORPTION EXPERIMENTS	203
12.5.1	Effect of contact time	203
12.5.2	Effect of adsorbent dosage.....	204
12.5.3	Effect of adsorbate concentration	205
12.5.4	Effect of pH	207
12.5.5	Effect of temperature	208
12.5.6	Effect of co-existing anions.....	209
12.6	ASSESSMENT OF METAL LEACHING FROM SORBENT AT VARIOUS EQUILIBRIUM PH VALUES.....	210
12.7	DEFLUORIDATION OF FIELD WATER.....	210
12.8	REGENERATION AND REUSABILITY OF SPENT SORBENT	212
12.9	ADSORPTION MODELLING.....	213
12.9.1	Isotherms	213
12.9.2	Adsorption thermodynamics	215
12.9.3	Adsorption kinetics.....	216
12.9.3.1	Pseudo-first- and second-order models	216

12.9.3.2	Diffusion models	218
12.10	SUMMARY	221
13	EVALUATION OF GROUNDWATER DEFLUORIDATION USING AL/FE OXIDE-IMPREGNATED DIATOMACEOUS EARTH	222
13.1	INTRODUCTION	222
13.2	MATERIALS.....	222
13.3	METHODS	223
13.3.1	Optimising the modification of DE with Al ₂ O ₃ and Fe ₂ O ₃	223
13.3.2	Al/Fe oxide modification of diatomaceous earth at optimum conditions.....	223
13.3.3	Characterisation of the adsorbents	223
13.3.4	Batch and field groundwater adsorption experiments	223
13.4	SYNTHESIS OF AL ₂ O ₃ - AND FE ₂ O ₃ -MODIFIED DIATOMACEOUS EARTH	224
13.4.1	Effect of shaking speed on synthesis of Al ₂ O ₃ - and Fe ₂ O ₃ -modified DE.....	224
13.4.2	Effect of contact time	224
13.5	PHYSICOCHEMICAL AND MINERALOGICAL CHARACTERIZATION	225
13.5.1	Surface area and pore volume of Al/Fe oxide-modified DE	225
13.5.2	Morphological analysis of raw and Al/Fe oxide-modified diatomaceous earth by scanning electron microscope	226
13.5.3	Scanning Electron Microscope-Energy dispersive X-ray spectroscopy (EDX)	227
13.5.4	Morphological analysis of raw and Al/Fe oxide-modified diatomaceous earth by transmission electron microscope.....	228
13.5.5	Fourier Transform Infra-Red (FTIR) Spectroscopy.....	229
13.5.6	X-ray fluorescence (XRF) analysis	231
13.5.7	X-ray diffraction (XRD) analysis.....	231
13.5.8	pH at point-of-zero charge pH _{pzc}	232
13.5.9	Thermogravimetric analysis (TGA).....	233
13.6	OPTIMIZATION OF ADSORPTION CONDITIONS FOR FLUORIDE REMOVAL USING AL/FE OXIDE-MODIFIED DE	234
13.6.1	Effect of contact time on fluoride removal.....	234
13.6.2	Effect of Al/Fe oxide-modified DE dosage on fluoride removal	236
13.6.3	Effect of adsorbate concentration on fluoride removal by Al/Fe DE	236
13.6.4	Effect of pH on fluoride adsorption	237
13.6.5	Effect of temperature	239
13.6.6	Evaluation of defluoridation efficiency of different Al/Fe oxide-modified diatomaceous earth samples.....	240
13.7	EVALUATION OF THE DE MODIFICATION WITH AL ₂ O ₃ - AND FE ₂ O ₃ THROUGH ANALYSIS OF SUPERNATANTS.....	241
13.7.1	Relationship between leached metals and adsorbent dosage	241
13.7.2	Effect of co-existing anions on F ⁻ sorption	242
13.7.3	Metal speciation calculations	243
13.7.4	Effect of calcination.....	246
13.8	ADSORPTION MODELING.....	248
13.8.1	Isotherm models	248
13.8.2	Adsorption thermodynamics	250
13.8.3	Adsorption kinetics.....	251
13.8.4	Adsorption mechanisms.....	253
13.8.4.1	Intra-particle diffusion	253
13.8.4.2	External diffusion	253
13.9	DEFLUORIDATION OF FIELD WATER.....	254
13.10	REGENERATION AND REUSABILITY OF SPENT SORBENT	256
13.11	SUMMARY.....	257

14	EVALUATION OF GROUNDWATER DEFLUORIDATION By AL/FE OXIDE-MODIFIED DIATOMACEOUS EARTH IN A FIXED-BED COLUMN	258
14.1	INTRODUCTION	258
14.2	MATERIALS.....	258
14.3	METHODS	259
14.3.1	Adsorbent and adsorbate preparation	259
14.3.2	Reactor set up.....	259
14.3.3	Evaluation of adsorption parameters	260
14.3.4	Fixed bed column defluoridation studies	260
14.3.4.1	Chemical analysis of processed water	260
14.3.4.2	Microbial tests.....	260
14.4	EVALUATION OF ADSORPTION PARAMETERS	261
14.4.1	Effect of flow rate	261
14.4.2	Effect of sorbent mass/bed depth	261
14.4.3	Effect of initial fluoride concentration	262
14.4.4	Evaluation of adsorption capacity by batch method	263
14.5	DEFLUORIDATION OF FIELD WATER.....	264
14.6	SUMMARY.....	266
15	CONCLUSIONS & RECOMMENDATIONS	268
	REFERENCES	271
	APPENDIX A: ADSORBENT CHARACTERISATION METHODS.....	286
	APPENDIX B: BATCH AND FIELD ADSORPTION EXPERIMENTS	288
	APPENDIX C: ADSORPTION MODELS	290

LIST OF FIGURES

Figure 2.1. (a) South African groundwater with F ⁻ concentration greater than 1.5 mg/l. Figure (b) South African groundwater with F ⁻ concentration greater than 3.0 mg/l. (Source: McCaffery, 1998).....	4
Figure 2.2. Fluoride distribution in groundwater 1996-2000 (Ncube and Schuttle, 2005).....	5
Figure 2.3. The distribution of % morbidity of dental fluorosis (Ncube and Schutte, 2005).....	9
Figure 2.4. Dental fluorosis morbidity (North-West Province) (Ncube and Schutte, 2005).....	10
Figure 2.5. Activated alumina-based domestic defluoridation filter (Daw, 2004).....	17
Figure 2.6. Stratified column of brick chips used in household defluoridation (Padmasiri, 1998).....	20
Figure 2.7. Crushed brick fluoride filter combined with experimental sand filter.....	21
Figure 2.8. Bone char domestic defluoridator (Wondimagegn, 2008).....	27
Figure 2.9. The Nalgonda defluoridator as adopted for domestic use in Tanzania (Dahi, 2000).....	28
Figure 2.10. A schematic diagram of a domestic defluoridator using activated alumina.	28
Figure 2.11. A SIPP filter unit: A – the silver-impregnated clay pot that serves as the filtering unit; B – the clay pot fitted into a 10 l bucket and placed on top of a collection vessel; and C – skeletal view of a complete SIPP filter (Momba et al., 2013).....	29
Figure 2.12. A CCF unit: A – outside view of the filter with inset (dome-shaped filter covered with a cloth); B – dome-shaped filter; C – skeletal view of CCF showing the internal content of the complete filter unit (Momba et al., 2013).....	30
Figure 3.1. Field groundwater sampling sites in various sites in various districts of Limpopo Province.....	37
Figure 3.2. Schoeller diagram showing average composition of major cations anions in mg/l and meq/l of the water samples of study areas. Stiff diagram is shown at bottom side.....	42
Figure 3.3. Piper Trilinear diagram depicting hydrochemical facies of the study areas.....	43
Figure 4.1. XRD diffractogram of silica-rich red/black Mukondeni clay soils.....	48
Figure 4.2. Point of zero charge of silica-rich reddish black Mukondeni clay soils.....	49
Figure 4.3. SEM images of silica-rich reddish black Mukondeni clay soils before (a) and after (b) defluoridation.....	50
Figure 4.4. Plot of BJH Adsorption dV/dlog (w) and pore volume against pore diameter for silica-rich reddish black Mukondeni clay soils.....	52
Figure 4.5. FTIR spectra of silica-rich red/black Mukondeni clay soils before and after defluoridation.....	53
Figure 4.6. Percentage removal and adsorption capacity of silica-rich reddish black Mukondeni clay soils as a function of contact time (1, 2 and 3 g, 10 mg/l F ⁻ , 25°C room temperature, 100 ml, 250 rpm, pH _i = 6.423, n=3).....	54
Figure 4.7. Percentage removal and adsorption capacity of silica-rich reddish black Mukondeni clay soils as a function of dosage (60 min contact time, 10 mg/l F ⁻ , 25°C room temperature, 250 rpm, pH _i = 5.937, n=3).....	55
Figure 4.8. Percentage removal and adsorption capacity of silica-rich red/black Mukondeni clay soils as a function of initial fluoride concentration (60 min contact time, 1.5 g dosage, 25°C room temperature, 100 ml, 250 rpm, pH _i = 6.11, n=3).....	56
Figure 4.9. Percentage removal and adsorption capacity of silica-rich red/black Mukondeni clay soils as a function of temperature (60 min contact time, 1.5 g dosage, 100 ml, 250 rpm, pH _i = 6.11, n=3).....	57

Figure 4.10. Percentage removal of fluoride by silica-rich reddish black Mukondeni clay soils as a function of competing ions (60 min contact time, 9 mg/l, 1.5 g dosage, 25°C room temperature, 100 ml, 250 rpm, $pH_i = 6.59$, $n=3$).....	58
Figure 4.11. Percentage removal of fluoride by silica-rich reddish black Mukondeni clay soils as a function of pH (60 min contact time, 1.5 g dosage, 9 mg/l F^- , 25°C room temperature, 100 ml, 250 rpm, $n=3$).....	59
Figure 4.12. Data plots on the Weber Morris intraparticle diffusion model (1 g dosage, 10 mg/l adsorbate concentration, 25°C room temperature, and 250 rpm, $pH = 6.423$).....	64
Figure 5.1. pH_{pzc} of raw bentonite clay (a) and Fe_2O_3 coated bentonite clay (b).....	69
Figure 5.2. XRD diffractogram of raw bentonite and Fe_2O_3 coated bentonite clay.....	71
Figure 5.3. SEM micrographs of raw bentonite (a) and Fe_2O_3 coated bentonite clay (b) at different magnifications.....	72
Figure 5.4. Removal of fluoride by Fe_2O_3 coated bentonite clay as a function of contact time (0.5, 1 and 2 g adsorbent, 10 mg/l F^- , 25°C room temperature, 100 ml solution, 250 rpm, $n=3$).....	74
Figure 5.5. Percent fluoride removal by Fe_2O_3 coated bentonite clay as a function of dosage (60 minutes contact time, 5, 10, 20 mg/l F^- , 25°C room temperature, 250 rpm, $n=3$).....	75
Figure 5.6. Percent fluoride by Fe_2O_3 coated bentonite clay as a function of concentration (60 minutes contact time, 2 and 3 g, 25°C room temperature, 100 ml solution, 250 rpm, $n=3$).....	75
Figure 5.7. Percentage fluoride removal by Fe_2O_3 coated bentonite clay as a function of temperature. (60 minutes contact time, 25°C room temperature, 3 g/100 ml S/l ratio, 250 rpm, $n=3$).....	76
Figure 5.8. Percentage fluoride removal by Fe_2O_3 coated bentonite clay as a function of pH (60 minutes contact time, 5 mg/l F^- , 25°C room temperature, 3 g/100 ml, S/l ratio, 250 rpm, $n=3$).....	77
Figure 5.9. Percentage removal of fluoride by iron(III) oxide coated bentonite clay as a function of co-existing ions (30 min contact time, 10 mg/l F^- , 25°C room temperature, 3 g/100 ml S/l ratio, 250 rpm, $pH_i = 6.47$, $n=3$).....	77
Figure 5.10. Regeneration studies using 0.01 M NaOH (10 mg/l F^- , 100 ml solution, 2 g adsorbent dosage).....	80
Figure 5.11. Langmuir adsorption isotherm for adsorption of F^- by Fe_2O_3 modified bentonite clay (3 g adsorbent dosage, 60 minutes of equilibration time, 5-80 mg/l F^-).....	82
Figure 5.12. Freundlich adsorption isotherm (3 g adsorbent, 60 minutes of equilibration time, concentration was varied from 5-80 mg/l).....	83
Figure 5.13. The Dubinin-Radushkevich adsorption isotherm (3 g of adsorbent, 60 minutes of equilibration time, 5-80 mg/l F^-).....	83
Figure 5.14. Plot of equilibrium constants against $1/T$	84
Figure 5.15. Pseudo-first order kinetic plot for adsorption of fluoride by Fe_2O_3 coated bentonite clay (0.5, 1 and 2 g dosage, 10 mg/l F^- , 25°C room temperature, 100 ml solution, 250 rpm).....	85
Figure 5.16. Pseudo-second order kinetic plot for adsorption of fluoride by Fe_2O_3 coated bentonite clay (0.5, 1 and 2 g dosage, 10 mg/l F^- , 25°C room temperature, 100 ml solution, 250 rpm).....	85
Figure 5.17. Data fit into (a) Intraparticle diffusion model and (b) external diffusion model (0.5, 1 and 2 g, 10 mg/l F^- , 25°C room temperature, 100 ml fluoride solution, 250 rpm $pH_i = 6.653$).....	87
Figure 6.1. Iron(III) oxide modified bentonite-red/black clay soil composite ceramic pellets before (a) and after calcination (b, c and d).....	93

Figure 6.2. XRD diffractogram of iron(III) oxide coated bentonite-silica-rich reddish black Mukondeni clay soil composite pellets at 100, 600, 700, 800 and 900°C.....	93
Figure 6.3. SEM micrographs of iron(III) oxide modified bentonite-rich red/black clay soil composite ceramic pellets at different calcination temperatures ((a) 100, (b) 600 and (c) 800°C)	94
Figure 6.4. Morphology of iron(III) oxide coated bentonite-silica-rich reddish black clay soil composite pellets at two magnifications and different firing times (a) 1 h, (b) 2 h and (c) 3 h).....	96
Figure 6.5. The FTIR spectra of iron(III) oxide modified-red/black clay soil composite pellets at different firing times ((a) 1 h, (b) 2 h and (c) 3 h).....	98
Figure 7.1. SEM Micrographs [bentonite (a) and Mn ²⁺ modified bentonite (b) x 20 000.....	103
Figure 7.2. pH _{zpc} of raw and Mn ²⁺ modified bentonite clay.....	104
Figure 7.3. FTIR spectrum of raw bentonite, Mn ²⁺ bentonite and the F ⁻ loaded Mn ²⁺ bentonite clay.	105
Figure 7.4. a) N ₂ adsorption-desorption isotherm b) pore distribution of raw and Mn ²⁺ modified bentonite clay.	106
Figure 7.5. Variation of % F ⁻ removal as a function of contact time for various adsorbent dosages (3 mg/l F ⁻ , 100 ml vol, pH 5.54 ± 0.5 and 250 rpm shaking speed, Particle size <250 µm, N=3).....	107
Figure 7.6. Variation % F ⁻ removal and adsorption capacity by Mn ²⁺ bentonite clay as a function of adsorbent dosage (contact time of 30 min, adsorbent dosage, 3 mg/l F ⁻ , pH of 5.54±0.5 and shaking speed of 250 rpm, particle size <250 µm, N=3).....	108
Figure 7.7. Variation of % F ⁻ removal by Mn ²⁺ bentonite clay as a function of adsorbate concentration at various contact times (adsorbent dosage 1.0 g/100 ml, pH of 5.24 and shaking speed of 250 rpm, particle size <250 µm, N=3).	109
Figure 7.8. Variation of % F ⁻ removal by Mn ²⁺ bentonite clay as a function of pH (contact time 30 min, adsorbent dosage 1.0 g/100 ml, 3 mg/l F ⁻ and shaking speed of 250 rpm, particle size <250 µm, N=3)	110
Figure 7.9. ΔpH versus initial pH for the adsorption of F ⁻ onto Mn ²⁺ modified bentonite clay.	110
Figure 7.10. Effects of co-existing anions on F ⁻ removal and equilibrium pH by Mn ²⁺ modified bentonite clay (3 mg/l F ⁻ , 1.0 g/100 ml adsorbent dosage, 30 min contact time at 250 rpm and pH of 6.5, particle size <250 µm).....	111
Figure 7.11. Concentration of chemical species in treated water at various pH, a) in mg/l), and b) in µg/l) (1 g/100 ml) adsorbent dosage, 3 mg/l) initial F ⁻ concentration and 30 min contact time at 250 rpm, particle size <250 µm)	112
Figure 7.12. Percentage (%) fluoride removal onto Mn ²⁺ modified bentonite clay in successive regeneration cycles (3 mg/l, 30 min contact time at 250 rpm and pH 5.54, particle size <250 µm)	113
Figure 7.13. Langmuir isotherm plot for F ⁻ adsorption by Mn ²⁺ intercalated bentonite clay (at 30, 60 and 120 min contact time 250 rpm shaking speed, pH 5.54 ± 0.5 and adsorbent dosage of 1 g/100 ml).....	115
Figure 7.14. Calculated R _L values for adsorption of F ⁻ onto Mn ²⁺ intercalated bentonite clay at various contact times.	115
Figure 7.15. Freundlich isotherm plot for fluoride removal onto Mn ²⁺ intercalated bentonite clay at 30, 60 and 120 min contact time, 250 rpm shaking speed, pH 5.5.	116
Figure 7.16. Pseudo second order plot at various adsorbent doses (3 mg/l F ⁻ , pH 5.54 and shaking speed of 250 rpm).	117
Figure 7.17. Plot for intra-particle diffusion at various adsorbent dosages (3 mg/l F ⁻ , pH 5.54 and shaking speed of 250 rpm).....	117

Figure 8.1. Variation of chemical species concentration in mg/l and µg/l with contact time (0.1 M NaOH concentration, 0.1 g/100 ml adsorbent dosage, n=3, particle size=250 µm)	121
Figure 8.2. Variation of chemical species in mg/l and µg/l with contact time (0.1M NaOH concentration, 0.1 g/100 ml adsorbent dosage, n=3, particle size=250 µm)	122
Figure 8.3. Variation of % F ⁻ removal with initial fluoride concentration for MnO ₂ coated bentonite clay prepared at various KMnO ₄ concentration.	123
Figure 8.4. Variation of % F ⁻ removal with initial fluoride concentration (Na-bentonite doses: 2.5, 5, 7.5 and 10 g. Adsorption conditions: 0.5 g/100 ml adsorbent dosage, 30 min contact time at 250 rpm and initial pH 5.54±0.5, n=3, particle size <250 µm).	124
Figure 8.5. Variation of % F ⁻ removal as a function of initial fluoride concentration (contact times for coating bentonite clay: 30, 60 and 120 min, Adsorption conditions: 0.5 g/100 ml adsorbent dosage, 30 min contact time at 250 rpm and initial pH 5.54±0.5, particle size <250 µm, N=3)	125
Figure 8.6. XRD spectra for Na-bentonite and MnO ₂ -bentonite.....	126
Figure 8.7. Surface morphology for Na-bentonite and MnO ₂ coated bentonite.	128
Figure 8.8. N ₂ adsorption-desorption isotherms (a) and pore distribution (b).	130
Figure 8.9. FTIR spectra of Na-bentonite, MnO ₂ coated Na-bentonite, F ⁻ loaded MnO ₂ coated bentonite. .	131
Figure 8.10. a) pH _{pzc} of Na-bentonite and b)MnO ₂ coated Na-bentonite	132
Figure 8.11. Variation of % F ⁻ removal as a function of contact time for various adsorbent dosages (5 mg/l F ⁻ , pH 6.26 and 250 rpm shaking, particle size <250 µm, N=3, particle size <250 µm).....	133
Figure 8.12. Variation % F ⁻ removal and adsorption capacity by MnO ₂ bentonite clay as a function of adsorbent dosage (contact time of 30 min, adsorbent dosage, 5 mg/l F ⁻ , pH of 6.24 and shaking speed of 250 rpm, particle size <250 µm, N=3).	134
Figure 8.13. Variation of % F ⁻ removal with initial concentration at various contact time (adsorbent dosage 1.5 g/100 ml, pH 5.54 and shaking speed of 250 rpm, particle size <250 µm, N=3).....	135
Figure 8.14. Variation of % F ⁻ removal and ΔpH with initial pH (3 mg/l, 1.5 mg/l, and 30 min contact time at 250 rpm, particle size <250 µm, N=3).	136
Figure 8.15. Effects of co-existing anions on fluoride removal by MnO ₂ coated Na-bentonite (5 mg/l F ⁻ , 10 mg/l of co-existing ions, 1.5 g/100 ml adsorbent dosage, pH 8 and 30 min contact time at 250 rpm, N=3). 137	137
Figure 8.16. Percent fluoride removal onto MnO ₂ coated Na-bentonite clay in successive regeneration cycles (5 mg/l F ⁻ , S/l ratio 1.5 mg/100 ml, 30 min contact time at 250 rpm and pH 8, N=3, particle size<250 µm). 138	138
Figure 8.17. Concentration of chemical species in treated water at various pH. a) in mg/l, and b) in µg/l (1.5 g/100 ml adsorbent dosage, 3 mg/l initial F ⁻ concentration and 30 min contact time at 250 rpm, particle size <250 µm, n=3).....	139
Figure 8.18. Langmuir adsorption isotherm (30 min, 60 min, 120 min contact times at 250 rpm, 1.5 g/100 ml, pH 6.2)	141
Figure 8.19. R _L values for the adsorption of F ⁻ onto MnO ₂ coated Na-bentonite.	142
Figure 8.20. Freundlich adsorption isotherm (30 min, 60 min, 120 min contact times at 250 rpm, 1.5 g/100 ml, pH 6.2).....	143
Figure 8.21. Lagergren Pseudo-second-order plot at various adsorbent dosages (5 mg/l F ⁻ , pH 6.24 and 250 rpm shaking, particle size <250 µm).....	144
Figure 8.22. Intra-particle plot at various adsorbent dosages (5 mg/l F ⁻ , pH 6.24 and 250 rpm shaking)....	145
Figure 9.1. XRD spectra of the smectite clay soils.....	149

Figure 9.2. Scanning electron micrograph of smectite-rich clay soils.	150
Figure 9.3. Pore size distribution of smectite-rich clay soils.....	151
Figure 9.4. FTIR spectra for raw (a) and F ⁻ Loaded smectite-rich clay (b).....	152
Figure 9.5. Variation of initial pH with Δ pH (0.1, 0.01 and 0,001 M KCl, dosage of 0.5 g/50 ml and shaking time of 48 hrs).....	152
Figure 9.6. Variation of % F ⁻ removal by smectite-rich clay soils with contact time (adsorbent dosage 0.3 g/100 ml, 3 mg/l, 5 mg/l and 10 mg/l F ⁻ , pH 5.54 and shaking speed of 250 rpm, N=3, particle size <250 μ m).	153
Figure 9.7. Variation % F ⁻ removal and adsorption capacity with adsorbent dosage (contact time of 30 min, adsorbate concentration, 3 mg/l F ⁻ , pH 5.54 and shaking speed of 250 rpm, N=3, particle size=250 μ m)...	154
Figure 9.8. Variation of % F ⁻ removal with initial concentration at various contact time (adsorbent dosage 0.8 g/100 ml, pH 5.54 and shaking speed of 250 rpm, N=3).	155
Figure 9.9. Variation of % F ⁻ removal and equilibrium pH with initial pH (contact time 30 min, adsorbent dosage 0.8 g/100 ml, 3 mg/l F ⁻ and shaking speed of 250 rpm, N=3).....	156
Figure 9.10. Variation of Δ pH with initial pH during F ⁻ adsorption onto smectite-rich clay soils.....	156
Figure 9.11. Effects of co-existing anions on fluoride removal by smectite-rich clay soils (3 mg/l F ⁻ , 0.8 g/100 ml adsorbent dosage, 30 min contact time at 250 rpm, N=3, particle size <250 μ m)	157
Figure 9.12. Percentage (%) fluoride removal by smectite-rich clay soils in successive cycles (3 mg/l, 30 min contact time at 250 rpm and pH 5.54, N=3, particle size < μ m).	158
Figure 9.13. Langmuir isotherm (contact time 30 min, adsorbent dosage 0.8 g/100 ml and shaking speed of 250 rpm).	160
Figure 9.14. Values of R _L , for adsorption of fluoride onto smectite-rich clay soil.....	160
Figure 9.15. Freundlich isotherms (contact time 30 min, adsorbent dosage 0.8 g/100 ml and shaking speed of 250 rpm).	161
Figure 9.16. Pseudo second order plot at various adsorbate concentrations (0.8 g/100 ml adsorbent dosage, pH 5.54 at 250 rpm).....	162
Figure 9.17. Plot for intra-particle diffusion at various concentrations (0.8 g/100 ml, pH 5.54 and shaking speed of 250 rpm).....	163
Figure 10.1. Effect of clay mixing ratio on % F ⁻ removal (5 mg/l F ⁻ , 0.3 g/100 ml adsorbent dosage, 30 min contact time at 250 rpm shaking speed, and 6.03 \pm 0.5 pH, particle size <250 μ m).	166
Figure 10.2. Effect of calcination temperature on % F ⁻ removal (10 mg/l F ⁻ adsorbate concentration, 2 g/100 ml adsorbent dosage, 30 min contact time at 250 rpm shaking speed, and 6.03 \pm 0.5 pH, particle size <250 μ m)	167
Figure 10.3. Pellets calcined at different temperatures (a – 150°C, b – 250°C, c – 350°C, d – 450°C, e – 550°C, f – 650°C and g – 750°C).....	168
Figure 10.4. XRD Spectra for smectite-rich clay, MnO ₂ coated Na-bentonite and calcined composite clay soils.....	169
Figure 10.5. Surface morphology of smectite-rich clay soils, MnO ₂ -coated Na-bentonite and clay composite.	170
Figure 11.1. SEM micrograph of diatomaceous earth.....	173
Figure 11.2. X-ray diffractogram of natural diatomaceous earth.....	175

Figure 11.3. FTIR spectra of raw (RDE) and F-treated (FDE) diatomaceous earth.....	176
Figure 11.4. Plot of change in pH against initial pH (volume of 1 M KCl: 50 ml, adsorbent dosage: 1 g, temperature: 298 K, shaking speed: 250 rpm and contact time: 24 h).	177
Figure 11.5. Per cent fluoride removal as a function of shaking speed (initial F ⁻ concentration: 8 mg/l, volume of solution: 50 ml, adsorbent mass: 0.4 g, contact time: 30 min and temperature: 298 K).....	178
Figure 11.6. Variation of a. per cent fluoride removal and b. adsorption capacity with contact time (initial fluoride concentration: 8 mg/l, volume of solution: 50 ml, adsorbent dosage: 0.4 g, temperature: 298 K, initial pH: 2, and shaking speed: 200 rpm).	179
Figure 11.7. Variation of per cent fluoride removal and adsorption capacity with adsorbent dosage (initial fluoride concentration: 8 mg/l, volume of solution: 50 ml, contact time: 30 min, temperature: 298 K, initial pH: 2, and shaking speed: 200 rpm).	180
Figure 11.8. Variation of per cent fluoride removal with pH (initial F ⁻ concentration: 8 mg/l, volume of solution: 50 ml, contact time: 30 min, temperature: 298 K, and shaking speed: 200 rpm).	181
Figure 11.9. Variation of adsorption capacity and per cent fluoride removal with equilibrium fluoride concentration (volume of fluoride solution: 50 ml, contact time: 30 min, initial pH: 2, adsorbent dosage: 0.4 g and shaking speed: 200 rpm).	182
Figure 11.10. Langmuir's profiles at 298 K, 313 K and 323 K (volume of fluoride solution: 50 ml, contact time: 30 min, initial pH: 2, adsorbent dosage: 0.4 g and shaking speed: 200 rpm).	184
Figure 11.11. Freundlich profiles at 298 K, 313 K and 323 K (volume of fluoride solution: 50 ml, contact time: 30 min, initial pH: 2, adsorbent dosage: 0.4 g and shaking speed: 200 rpm).	185
Figure 11.12. Pseudo-second-order plots for equilibration at different contact times (initial fluoride concentration: 8 mg/l, volume of solution: 50 ml, adsorbent dosage: 0.4 g, initial pH: 2, temperature: 298 K and shaking speed: 200 rpm).	187
Figure 11.13. Verification of intra-particle diffusion using Weber-Morris model (initial fluoride concentration: 8 mg/l, volume of solution: 50 ml, adsorbent dosage: 0.4 g, initial pH: 2, temperature: 298 K and shaking speed: 200 rpm).....	188
Figure 11.14. External diffusion plots a. for contact time up to 30 min and b. for all contact time (initial fluoride concentration: 8 mg/l, volume of solution: 50 ml, adsorbent dosage: 0.4 g, initial pH: 2, temperature: 298 K and shaking speed: 200 rpm).	189
Figure 12.1. X-ray diffractogram of Mg/Ce/Mn oxide-modified diatomaceous earth.....	196
Figure 12.2. SEM images of raw diatomaceous earth (a and b), Mg/Ce/Mn oxide (c and d) and Mg/Ce/Mn oxide-modified diatomaceous earth (e and f).	197
Figure 12.3. SEM-EDX spectra of a. raw diatomaceous earth and b. Mg/Ce/Mn oxide-modified diatomaceous earth.....	198
Figure 12.4. HR-TEM images of Mg/Ce/Mn oxide (a and b), Mg/Ce/Mn oxide-modified diatomaceous earth (c to f) and b to f.....	199
Figure 12.5. Plot of BJH adsorption pore volumes and BJH dV/dlog(D) pore volumes against pore diameter (D) for a. raw and b. Mg/Ce/Mn oxide-modified diatomaceous earth.....	200
Figure 12.6. FTIR spectra of Mg/Ce/Mn oxide, Mg/Ce/Mn oxide-modified and F ⁻ loaded Al/Fe oxide-modified diatomaceous earth.	201
Figure 12.7. pH at point-of-zero charge of Mg/Ce/Mn oxide-modified DE evaluated in 1 M, 0.1 M and 0.01 M KCl (volume of solution: 25 ml, adsorbent dosage: 0.2 g, contact time: 24 h and shaking speed: 200 rpm).	202

Figure 12.8. The thermograms of Mg/Ce/Mn oxide and Mg/Ce/Mn oxide-modified diatomaceous earth. ...	203
Figure 12.9. Variation of a. Per cent fluoride removal and b. adsorption capacity with contact time at various adsorbent dosages (initial fluoride concentration: 10 mg/l, volume of solution: 100 ml, shaking speed: 200 rpm and temperature: 297 K).	204
Figure 12.10. Per cent fluoride removal and adsorption capacity as a function of adsorbent dosage (initial fluoride concentration: 10 mg/l, contact time: 60 min, shaking speed: 200 rpm and temperature: 297 K)...	205
Figure 12.11. Variation of a. per cent fluoride removal and b. adsorption capacity with equilibrium fluoride concentration at different temperatures (contact time: 60 min, volume of solution: 100 ml, and shaking speed: 200 rpm).....	206
Figure 12.12. Fluoride removal as a function of initial solution pH (initial fluoride concentration: 9 mg/l, volume of solution: 100 ml, contact time: 60 min, shaking speed: 200 rpm and temperature: 297 K).	207
Figure 12.13. Variation of a. per cent fluoride removal and b. adsorption capacity with temperatures (contact time: 60 min, volume of solution: 100 ml, and shaking speed: 200 rpm).....	208
Figure 12.14. Per cent fluoride removal in the presence of co-existing anions (initial F ⁻ concentration: 10 mg/l, initial anion concentration: 5 mg/l, volume of solution: 100 ml, contact time: 60 min, shaking speed: 200 rpm and temperature: 297 K).	209
Figure 12.15. Concentration of leached metals as a function of equilibrium pH (initial fluoride concentration: 9 mg/l, volume of solution: 100 ml, contact time: 60 min, temperature: 297 K and shaking speed: 200 rpm).	210
Figure 12.16. Concentrations of elements in treated field water in mg/l.....	211
Figure 12.17. Concentrations of elements in treated field water in µg/l (volume of water: 100 ml, adsorbent dosage: 0.6 g, contact time: 50 min, shaking speed: 200 rpm).....	212
Figure 12.18. Percent (%) fluoride removal as a function of defluoridation cycle using 0.01 M NaOH and 0.1 M K ₂ SO ₄ as regenerants (initial fluoride concentration: 10 mg/l, volume of solution: 100 ml, adsorbent dosage: 0.8 g contact time: 60 min, temperature: 297 K and shaking speed: 200 rpm).....	213
Figure 12.19. Langmuir isotherm plots at 297 K, 310 K and 326 K (contact time: 60 min, adsorbent dosage: 0.6 g, volume of solution: 100 ml, shaking speed: 200 rpm).....	214
Figure 12.20. Freundlich isotherm plots at 297 K, 310 K and 326 K (contact time: 60 min, adsorbent dosage: 0.6 g, volume of solution: 100 ml, shaking speed: 200 rpm).....	214
Figure 12.21. Values of dimensionless separation factor, R_L at different initial fluoride concentrations.....	215
Figure 12.22. $\ln K_L$ as a function of reciprocal of adsorption temperatures.	216
Figure 12.23. Pseudo-first-order plots for a. 0.1 g, b. 0.2 g and c. 0.3 g sorbent (initial fluoride concentration: 10 mg/l, volume of solution: 100 ml, shaking speed: 200 rpm and temperature: 297 K).	217
Figure 12.24. Pseudo-second-order plots for 0.1, 0.2 and 0.3 g sorbent (initial fluoride concentration: 10 mg/l, volume of solution: 100 ml, shaking speed: 200 rpm and temperature: 297 K).	217
Figure 12.25. Weber-Morris intra-particle diffusion plot for a) 0.1 g, b) 0.2 g and c) 0.3 g sorbent (initial fluoride concentration: 10 mg/l, volume of solution: 100 ml, shaking speed: 200 rpm and temperature: 297 K).	219
Figure 12.26. External diffusion plots for 0.1 g, 0.2 g and 0.3 g sorbent dosages (initial fluoride concentration: 10 mg/l, volume of solution: 100 ml, shaking speed: 200 rpm and temperature: 297 K).	220
Figure 13.1. Plot of BJH adsorption pore volume and BJH dV/dlog(D) pore volume against pore diameter (D) for a. raw and b. Al/Fe oxide-modified diatomaceous earth.	226
Figure 13.2. SEM images of a. raw diatomaceous earth, b. and c. Al/Fe oxide and d. to f. Al/Fe oxide-modified diatomaceous earth.	227

Figure 13.3. Energy dispersive spectrograph of (a). raw diatomaceous earth and (b). Al/Fe oxide-modified diatomaceous earth.	228
Figure 13.4. TEM images of (a) Al/Fe oxide and (b) to (f) Al/Fe oxide-modified diatomaceous earth.	229
Figure 13.5. FTIR spectra of Al/Fe oxide, Al/Fe oxide-modified and F-loaded Al/Fe oxide modified diatomaceous earth.	230
Figure 13.6. X-ray spectrum of Al/Fe oxide-modified diatomaceous earth.	232
Figure 13.7. Variation of initial solution pH with Δ pH of solutions at 0.01, 0.1 and 1 M KCl for Al/Fe modified DE (vol 50 ml, adsorbent dosage: 0.5 g, contact time: 24 h and shaking speed: 200 rpm).	233
Figure 13.8. The thermograms of Al/Fe oxide and Al/Fe oxide-modified diatomaceous earth.	234
Figure 13.9. Variation of a. per cent fluoride removal and b. adsorption capacity with contact time at adsorbent doses of 0.1, 0.2 and 0.3 g (initial fluoride concentration: 10 mg/l, volume of solution: 100 ml, and temperature: 297 K and shaking speed: 200 rpm).	235
Figure 13.10. Variation of per cent fluoride removal and adsorption capacity with adsorbent dosage (initial fluoride concentration: 10 mg/l, volume of solution: 100 ml, shaking speed: 200 rpm and temperature: 297 K).	236
Figure 13.11. a). Variation of per cent fluoride removal and, b). adsorption capacity with adsorbate concentration at 297, 317, and 329 K (contact time: 50 min, volume of solution: 100 ml and shaking speed: 200 rpm).	237
Figure 13.12. Variation of per cent fluoride removal and adsorption capacity with equilibrium pH (initial fluoride concentration: 11.25 mg/l, volume of solution: 100 ml, temperature: 297 K, shaking speed: 200 rpm).	238
Figure 13.13. Leached metals as a function pH (initial fluoride concentration: 11.25 mg/l, volume of solution: 100 ml, temperature: 297 K, shaking speed: 200 rpm).	239
Figure 13.14. a) Per cent fluoride removal and, b) adsorption capacity as a function of temperature (contact time: 50 min, temperature: 297, 317, and 329 K, volume of solution: 100 ml and shaking speed: 200 rpm).	240
Figure 13.15. Concentration of leached metals as a function of adsorbent dosage (initial fluoride concentration: 10 mg/l, volume of solution: 100 ml, contact time: 50 min, temperature: 297 K and shaking speed: 200 rpm).	242
Figure 13.16. Variation of concentrations of species of a. Al and b. Fe at different pH values.	244
Figure 13.17. Variation of concentrations of a. fluoride species, b. Al-F complexes and c. Fe-F complexes at different pH values.	245
Figure 13.18. Variation of per cent fluoride removal and adsorption capacity with calcination temperature (initial fluoride concentration: 10 mg/l, volume of solution: 100 ml, contact time: 50 min and shaking speed: 200 rpm).	246
Figure 13.19. Residual metal species concentration in Al/Fe oxide-modified DE at different calcination temperatures (Adsorbent dosage: 0.5 g/50 ml of acid solution).	247
Figure 13.20. Langmuir isotherm plots at 297, 317 and 329 K (contact time: 50 min, volume of solution: 100 ml, adsorbent dosage: 0.6 g and shaking speed: 200 rpm).	248
Figure 13.21. Freundlich isotherm plots at 297 K, 317 K and 329 K (contact time: 50 min, volume of solution: 100 ml, adsorbent dosage: 0.6 g, shaking speed: 200 rpm).	249
Figure 13.22. Values of dimensionless separation factor, R_L at different initial fluoride concentrations.	250
Figure 13.23. $\ln K_L$ as a function of reciprocal of adsorption temperatures.	251

Figure 13.24. Pseudo-first-order profiles at different adsorbent dosages of a. 0.1 g, b. 0.2 g and c. 0.3 g of Al/Fe oxide-modified DE (initial fluoride concentration: 10 mg/l, volume of solution: 100 ml, temperature: 297 K and shaking speed: 200 rpm).....	252
Figure 13.25. Pseudo-second-order profile at different adsorbent dosages (initial fluoride concentration: 10 mg/l, volume of solution: 100 ml, temperature: 297 K and shaking speed: 200 rpm).	252
Figure 13.26. Intra-particle diffusion profile at different adsorbent dosages of 0.1 g, 0.2 g and 0.3 g (initial fluoride concentration: 10 mg/l, volume of solution: 100 ml, temperature: 297 K and shaking speed: 200 rpm).....	253
Figure 13.27. External diffusion profiles at adsorbent dosages of 0.1 g, 0.2 g and 0.3 g (initial fluoride concentration: 10 mg/l, volume of solution: 100 ml, temperature: 297 K and shaking speed: 200 rpm).....	254
Figure 13.28. Loss of silica from diatomaceous earth as a function of solution pH (initial fluoride concentration: 10 mg/l, dosage of raw DE: 0.4 g/50 ml, shaking speed: 200 rpm, temperature: 297 K).....	257
Figure 14.1. Schematic diagram of a fixed-bed column continuous flow set up.	259
Figure 14.2. Breakthrough curves at different influent flow rates (influent concentration: 10 mg/l, sorbent dosage: 1 g, particle size <250 µm, N=3).....	261
Figure 14.3. Breakthrough curves at different sorbent masses/bed height (influent concentration: 8.17 mg/l, inflow rate 0.62 ml/min, particle size <250 µm, N=3).....	262
Figure 14.4. Breakthrough curves at different initial fluoride concentrations as function of time (sorbent dosage: 1 g and influent flow rate of 0.62 ml/min, particle size <250 µm, N=3).....	263
Figure 14.5. Field water defluoridation in a fixed bed-column packed with 1 g Al/Fe oxide modified DE and flow rate of 0.62 ml/min, particle size <250 µm, N=3.	264
Figure 14.6. Petri Dishes after incubation showing 'a' before & 'b' after treatment	265

LIST OF TABLES

Table 2.1. Solubility products of various fluoride-bearing minerals.....	6
Table 2.2. Health effects of long-term consumption of high or low fluoride in water.....	8
Table 2.3. Maximum allowable fluoride concentration for drinking water.....	8
Table 2.4. Different clay soils and their adsorption capacities in water defluoridation.....	18
Table 2.5. The performance of various adsorbents in water defluoridation	33
Table 3.1. Physicochemical properties of field groundwater samples	39
Table 3.2. Pearson's correlation matrix for physicochemical and hydrochemical parameters of studied waters	40
Table 3.3. Hydrogeochemical facies as worked out by Piper diagram and irrigation waters analysis.....	44
Table 3.4. Principal Component Analysis of site variation using water quality parameter.....	46
Table 4.1. CEC of silica-rich reddish black Mukondeni clay soils at pH 5.4 and 7.4	49
Table 4.2. Elemental composition of silica-rich reddish black Mukondeni clay soils	50
Table 4.3. Surface area, pore volume and pore size of silica-rich red/black Mukondeni clay soils	51
Table 4.4. Adsorption of F- onto silica-rich red/blackMukondeni clay soils.....	60
Table 4.5. Concentration of chemical species before and after defluoridation at field pH conditions.....	60
Table 4.6. Leaching of metals into solution after defluoridation at pH 2, 6 and 12	61
Table 4.7. Calculated adsorption isotherm parameters.....	62
Table 4.8. Activation energy values of removal of fluoride by silica-rich Mukondeni clay soils	63
Table 4.9. Pseudo-second-order kinetic parameters for different adsorbent dosages for fluoride removal by silica-rich reddish black Mukondeni clay soils.	63
Table 4.10. Kinetic parameters of the fluoride adsorption onto silica-rich red/black Mukondeni clay soils	65
Table 4.11. Comparison of different adsorption capacities of different clay adsorbents for fluoride	66
Table 5.1 Cation Exchange Capacity of raw bentonite and iron(III) oxide coated bentonite clay.....	69
Table 5.2. Chemical composition of raw and Fe ₂ O ₃ coated bentonite clay.....	70
Table 5.3. Surface area, pore volume and pore sizes of raw and Fe ₂ O ₃ coated bentonite clay.....	73
Table 5.4. Defluoridation of field groundwater by Fe ₂ O ₃ coated bentonite clay at field and optimized initial pH conditions. (60 minutes contact time, 25°C room temperature, 3 g/100 ml S/l ratio, 250 rpm).....	78
Table 5.5. Metal concentration before and after defluoridation	79
Table 5.6. Concentration of metals in solution after defluoridation at pH 2, 6 and 12	79
Table 5.7. Calculated Langmuir, Freundlich and Dubinin-Radushkevich isotherm parameters	81
Table 5.8. Calculated Thermodynamic parameters for the Van Hoff's plot.....	84
Table 5.9. Calculated pseudo-second-order kinetic parameters at various adsorbent dosages for fluoride removal by Fe ₂ O ₃ coated bentonite clay	86
Table 5.10. Kinetic parameters of the fluoride adsorption onto iron(III) oxide coated bentonite clay	88

Table 5.11. Adsorption capacities of various adsorbents compared to the present adsorbent	89
Table 6.1. Surface area, pore volume and pore sizes for iron(III) oxide modified bentonite-red/black clay soil composite ceramic pellets	95
Table 6.2. F ⁻ adsorption potential of the ceramic pellets fired at various furnace temperatures.....	95
Table 6.3. Mineralogical composition iron(III) oxide coated red/black clay soil composite pellets at different firing times	97
Table 6.4. Chemical composition of iron(III) oxide coated-red/black clay soil composite pellets at different firing times	97
Table 6.5. Surface area, pore volume and pore sizes of the composite pellets at different firing times	98
Table 6.6. Fluoride adsorption potential of the composite pellets prepared at different firing times.....	99
Table 6.7. Fluoride adsorption capacity of iron(III) oxide modified bentonite-red/black clay soil composite pellets fabricated at different clay ratios.	99
Table 7.1. Chemical composition of raw and Mn ²⁺ modified bentonite clay.....	102
Table 7.2. CEC of raw and Mn ²⁺ bentonite clay at pH 5.4 and 7.4	103
Table 7.3. Physicochemical parameters of field water before and after treatment	114
Table 7.4. Calculated parameters for the Langmuir and Freundlich adsorption isotherms	114
Table 7.5. Pseudo first and second order kinetic model calculated parameters.....	116
Table 8.1. Chemical composition of Na-bentonite and MnO ₂ coated Na-bentonite clay.	127
Table 8.2. Quantitative SEM-EDS of Na-bentonite and MnO ₂ coated Na-bentonite	128
Table 8.3. Surface area, pore diameter and pore volume of Na bentonite and MnO ₂ coated bentonite clay.....	129
Table 8.4. The South African National standards for drinking water for selected species.....	140
Table 8.5. Physicochemical parameters of groundwater before and after treatment.	140
Table 8.6. Constant values for Langmuir and Freundlich isotherms.....	142
Table 8.7. Calculated parameters for pseudo-first- and second-order reaction kinetics models	143
Table 8.8. Constant values of intra-particle diffusion model.....	144
Table 8.9. Comparison of different adsorption capacities of different adsorbents for fluoride.....	146
Table 9.1. Elemental composition of the clay soils.....	149
Table 9.2. BET surface area, pore volume and pore width of the smectite-rich clay soils.....	150
Table 9.3. Physicochemical parameters of field water before and after treatment	159
Table 9.4. Values of Langmuir and Freundlich isotherm models (contact time 30 min, adsorbent dosage 0.8 g/100 ml and shaking speed of 250 rpm).....	159
Table 9.5. Calculated adsorption kinetics model values.	163
Table 9.6. Comparison of adsorption capacities of different adsorbents for fluoride.	164
Table 10.1. Chemical composition of the composite clay soils.	169
Table 11.1. Physical and chemical parameters of diatomaceous earth.....	173
Table 11.2. Concentration of trace metals in diatomaceous earth.....	174
Table 11.3. Surface area and pore volume of diatomaceous earth by BET method	174
Table 11.4. Variation of per cent fluoride removal with temperature.....	183

Table 11.5. Variation of adsorption capacity with temperature	183
Table 11.6. Calculated Freundlich isotherm parameters.....	185
Table 11.7. Pseudo-first-order and pseudo-second-order parameters	186
Table 11.8. Concentrations of anions in raw and treated field groundwater	190
Table 11.9. Concentration of chemical species in treated water at different initial pH values (mg/l).....	191
Table 11.10. Concentration of chemical species in treated water at different initial pH values (µg/l)	191
Table 11.11. Concentration of elements in treated water at different contact times (mg/l)	192
Table 11.12. Concentration of elements in treated water at different contact times (µg/l)	192
Table 12.1. Mixtures of salt solutions at different proportions	195
Table 12.2. Surface area, pore area and pore volume of the raw and Mg/Ce/Mn oxide-modified diatomaceous earth	200
Table 12.3. Percent (%) fluoride removal and adsorption capacity at various adsorbent dosages	205
Table 12.4. Percent fluoride removal at different solution pH values	207
Table 12.5. Percent fluoride removal in the presence of co-existing anions (Initial 10 mg/l F ⁻).....	209
Table 12.6. Concentrations of competing anions in raw and treated field water	211
Table 12.7. Calculated Langmuir and Freundlich isotherm parameters	215
Table 12.8. Adsorption thermodynamic parameters	216
Table 12.9. Pseudo-second-order parameters at different adsorbent dosages.....	218
Table 13.1. Effect of shaking speed on modification of diatomaceous earth with Al ₂ O ₃ and Fe ₂ O ₃	224
Table 13.2. Effect of contact time on modification of diatomaceous earth with Al ₂ O ₃ and Fe ₂ O ₃	224
Table 13.3. Comparison of the surface area, and pore area and volume of the raw and Al/Fe oxide-modified diatomaceous earth	225
Table 13.4. Chemical composition of raw and Al/Fe oxide modified DE.....	231
Table 13.5. Effect of equilibrium pH on fluoride sorption.....	238
Table 13.6. Per cent fluoride removal by co-precipitated metal oxide-modified DE from different metal ratios	241
Table 13.7. Percent fluoride removal using different metal oxide-modified DE samples.....	241
Table 13.8. Effect of co-existing anions on fluoride adsorption (Initial adsorbate conc: 10 mg/l F ⁻).....	243
Table 13.9. Effect of phosphate ion concentration on fluoride removal (Initial adsorbate conc: 10 mg/l F ⁻)	243
Table 13.10. Per cent fluoride removal and adsorption capacity at various calcination temperatures (Initial conc: 10 mg/l).....	246
Table 13.11. Concentration of major elements in calcined adsorbent at different temperatures.....	247
Table 13.12. Calculated Langmuir and Freundlich isotherm parameters	249
Table 13.13. Adsorption thermodynamic parameters	250
Table 13.14. Pseudo-second-order parameters at different adsorbent dosages.....	251
Table 13.15. Concentrations of competing anions in raw and treated field water	254
Table 13.16. Concentrations of chemical species in raw and treated field water in mg/l	255

Table 13.17. Concentrations of elements in raw and treated field water in $\mu\text{g}/\ell$	255
Table 13.18. Comparison of the sorbent regeneration potentials for selected reagents	256
Table 14.1. Breakthrough curve parameters for F^- adsorption onto Al/Fe oxide modified DE at different operating conditions.....	262
Table 14.2. Percent F^- removal and adsorption capacity in batch and continuous flow fixed bed.....	264
Table 14.3. Physicochemical parameters of feet water and effluent water at breakthrough point.....	265
Table 14.4. Elemental analysis of processed Siloam water by ICP-MS/ICP-AES (conc in $\mu\text{g}/\ell$ except for Ca, K, Na, P and Si)	267

ACRONYMS & ABBREVIATIONS

BDH	Barret-Joyner-Halenda
BET	Brunauer Emmett and Teller
BF	Bucket filter
BSF	Biosand filter
BSF-Z	Biosand filter-Zeolite
CCF	Ceramic candle filter
CEC	Cation exchange capacity
DDU	Domestic defluoridation unit
DE	Diatomaceous Earth
DWA	Department of Water Affairs
DWAF	Department of Water Affairs and Forestry
EC	Electrical conductivity
EC	Electrocoagulation
ED	Electrodialysis
FTIR	Fourier transform infra-red
ICP-AES	Inductively coupled plasma-Atomic Emission spectroscopy
ICP-MS	Inductively coupled plasma-Mass spectroscopy
NEERI	National Environmental Engineering Research Institute-India
PCA	Principal Component Analysis
pHpzc	PH point of zero charge
POU	Point of use
RO	Reverse Osmosis
SANS	South African National Standard
SEM	Scanning electron microscopy
SEM-EDS	Scanning electron microscopy-Electron dispersive spectroscopy
SIPP	Silver impregnated porous pot
TDS	Total dissolved solids
TEM	Transmission electron microscopy
TEM-EDS	Transmission electron microscopy-Electron dispersive spectroscopy
TGA	Thermogravimetric analysis
TISAB	Total ionic strength adjustment buffer
UNICEF	United Nations Children Fund
WHO	World Health Organization
WRC	Water Research Commission
XRD	X-ray diffraction
XRF	X-ray fluorescence



This page was intentionally left blank

1 BACKGROUND

1.1 INTRODUCTION

Fluorosis is a chronic health hazard affecting a large population in South Africa. According to WRC (2001), North West, Limpopo, and Northern Cape have been identified as provinces having high levels of fluoride in groundwater, often as high as 30 mg/l. Taking into consideration the health effects that come with excessive fluoride in drinking water WHO has set the guidelines of 1.5 mg/l as the maximum permissible limit for fluoride in potable water (WHO, 2004). Ground waters may contain excess fluoride beyond WHO limits depending on the presence of fluoride-rich minerals as well as hydrogeological conditions. Atasoy et al. (2013) points out that, the presence of fluoride in water that is used for consumption within permissible limits is beneficial for human health. However, excessive consumption of fluoride leads to adverse health problems such as dental or skeletal fluorosis. Therefore, mitigation of fluorosis is a very significant area of research and reliable defluoridation technologies are required.

Technologies for removal of excess fluoride from groundwater can be divided into two main categories, namely precipitation and adsorption. Precipitation processes involve the addition of chemicals and formation of fluoride precipitates. Among these are precipitations with calcium and aluminium salts (Feenstra et al., 2007). In the adsorption method, raw water is passed through a bed containing the defluoridating material. The material retains fluoride either by physical, chemical or ion exchange mechanisms. The adsorbent gets saturated after a period of operation and requires regeneration. Precipitation methods however have many limitations which include, daily addition of chemicals, large volumes of sludge production; and are not effective with water sources with high total dissolved solids and hardness (Bulusu et al., 1993). The adsorption process is extensively used and gives satisfactory results (Cai et al., 2015; Wang et al., 2014). For this reason, adsorption seems to be a more attractive method for defluoridation in terms of cost, simplicity of design and operation. Moreover, the adsorbent can be easily recovered and reused (Ozean et al., 2005). Although a wide variety of adsorbents have been used for defluoridation, naturally available clays have been the adsorbents of choice in most developed countries. (Mlilo et al., 2010; Srinivasan, 2011; Atasoy and Ahin, 2013).

Several studies have indicated that chemical modification of clay and other aluminosilicate-based materials can alter their surface properties leading to increased surface area, in addition to new functional groups that increase their adsorption capacities for anionic species (Wanga et al., 2015; Yakub and Soboyejo, 2013; Dai and Huang, 1991). Zhu et al. (2007) and Tor et al. (2006) prepared granular red mud as low-cost adsorbent to remove cadmium ions and fluoride ion from water, respectively. The introduction of polysulfone increased the hydrophobicity of the prepared beads. Ma et al. (2011) also prepared granular acid treated bentonite with polyvinyl acetate to enhance its adsorption capacities. Gitari et al. (2013) modified bentonite clay with Fe³⁺ and observed increase in surface area and micropore area of the modified form. The modified bentonite exhibited high adsorption capacity for F⁻ as compared to raw bentonite. Introduction of functional groups such as OH, H-O-H and absorbed water are known to create physicochemical interactions with F⁻ in aqueous media. (Hauge et al., 1994). It is anticipated that modification of various clays materials such as bentonite clay and silica-rich natural materials such as diatomaceous earth will increase the functionality of their surfaces, modify their surface charge and ultimately increase their F⁻ adsorption capacity. This report presents results and discussions on chemical and mineralogical characterization of various locally obtained clay soils, bentonite clay and diatomaceous earth, their modification with metal oxides and evaluation of their fluoride adsorption potential.

1.2 PROJECT AIM AND OBJECTIVES

The main aim of the project was to evaluate locally available smectite-rich clays soils and diatomaceous earth either in their raw form or modified with high charge density cations Al^{3+} , Fe^{3+} , Ce^{3+} , Mg^{2+} and Mn^{2+} , their oxides or mixed oxides/hydroxides for defluoridation of groundwater. The following were the specific aims of the project:

1. Carry out detailed literature survey on various technologies of groundwater and surface water defluoridation. Emphasising on natural clay-based materials used in the adsorption systems and focusing on their application in rural areas in sub-Saharan Africa. Level of implementation and success of these systems at community and household levels. Status of fluoride problem and studies done in South Africa be highlighted
2. Evaluate the mineralogical and physicochemical properties of South African bentonite clay supplied by ECCA Holdings (Pty), clay soils corrected from Ga-Mashamba in Mukondeni, Vhembe district in Limpopo and commercial diatomaceous earth
3. Optimize the modification of the bentonite clay and diatomaceous earth with selected high charge density cations such as Fe^{3+} , Al^{3+} and Mn^{2+} . These metal species will be introduced as metal cations, metal hydroxides/oxy-hydroxides or metal oxides
4. Evaluate the mineralogical, surface properties, morphology and physicochemical properties of the metal modified bentonite and diatomaceous earth
5. Evaluate and optimize the F^- adsorption capacity of the raw, metal modified bentonite clay, diatomaceous earth and the clay soils from Ga-Mashamba using batch experiments
6. Evaluate and optimize the regeneration potential of the optimized F^- adsorbents using alkaline media such as NaOH and Na_2CO_3 and test their reusability
7. Test and evaluate optimized F^- adsorbents on a dynamic flow set-up, breakthrough and adsorption capacity determined
8. Test the optimized adsorbent for its potential to remove pathogen in a fixed bed

1.3 SCOPE AND LIMITATIONS

The study proposed to evaluate selected clay soils and minerals in South Africa for their capacity to adsorb fluoride from aqueous solutions. The clay soils were obtained from a selected area of Limpopo province in South Africa and was not extend to clay soils and minerals from other regions in South Africa. Minerals evaluated included bentonite clay mined in Western Cape and supplied by ECCA (Pty) in Western Cape. Diatomaceous earth was obtained from an industrial supplier in South Africa and also sourced from natural deposits in Gilgil, Nakuru County, Kenya. The clay soils, bentonite clay and diatomaceous earth were evaluated as obtained from sources or calcined at optimized temperatures. Metal modification of the soils, clay minerals and diatomaceous was done using Fe^{3+} , Al^{3+} and $\text{Mn}^{2+}/4+$, Ce^{3+} , Mg^{2+} salt solutions only. Detailed adsorption chemistry in the evaluation was limited to F^- anion but the effect of the adsorbents on other chemical constituents of the treated water were also be evaluated. The evaluation didn't look into the detailed removal mechanisms of pathogens, but rather tested the final optimized adsorbent for its potential to remove pathogens of faecal origin as a representation of the microbial community likely to be present in water resources.

2 LITERATURE REVIEW

2.1 OCCURRENCE AND SOURCES OF FLUORIDE IN GROUNDWATER

Fluorine is the lightest member of the halogen group and is one of the most reactive of all chemical elements. It is the most electronegative of all the elements (Hem, 1989). Being very reactive it is not found as fluorine in the environment but as fluoride, F⁻ in combination with other chemical elements. Fluoride ion has the same charge and almost the same ionic radius as hydroxide ion and may replace each other in mineral structures (Hem, 1985). Fluoride thus forms mineral complexes with a number of cations and some fairly common mineral species of low solubility contain fluoride (WHO, 2004). Fluoride occurs as minerals, fluorite, cryolite and fluorapatite and high concentrations in water are associated with underground sources (Nanyaro et al., 1984). Fluoride is a normal constituent of natural waters and its concentration varies depending on the water source. Seawater typically contains about 1 mg/l while rivers and lakes generally exhibit concentrations of less than 0.5 mg/l (WHO, 2004). The concentrations of fluoride in surface waters generally are hardly beyond 0.3 mg/l except in isolated cases. Concentrations of fluoride in water are limited by the solubility of fluorite such as CaF₂, the most common fluorine mineral (Rajkovic & Novakovic, 2007), so that in the presence of 40 mg/l calcium ions it should be limited to 3.1 mg/l (Hem, 1989). Therefore, concentration of fluoride is higher at lower concentration of calcium ions (that is, in water with low hardness), and it is the absence of calcium ions in solution which allows higher concentrations to be stable (Edmunds & Smedley, 1996).

Geological processes, weathering of fluoride containing minerals and hydro-geological conditions can lead to higher fluoride levels in groundwater in certain areas, which become endemic in certain areas (Daw, 2004). Elazhar et al. (2013) considered the natural concentration of fluoride in water to depend on the geological, chemical, and physical characteristics of the aquifer, the porosity and acidity of the soil and rocks, the temperature, the action of other chemical elements and the depth of wells. As a result of these factors, the fluoride concentrations in groundwater can range from less than 1 mg/l to more than 35 mg/l. Fluoride (F⁻) naturally occurs in rocks in many geological environments (Hem, 1989) but fluoride concentrations in groundwater are particularly high in groundwater associated with acid volcanic rocks, e.g. in Sudan, Ethiopia, Uganda, Kenya and Tanzania (Bailey et al., 2010). Gaciri and Davies (1993) attribute the abundance of F⁻ in groundwater in Rift valley to weathering of alkaline volcanic rocks rich in F⁻ and the interaction of groundwater with volcanic HF exhalations. Other countries with which have high F⁻ in groundwater include Sudan, Nigeria, Senegal, Algeria, Egypt, Zimbabwe, Morocco, Uganda and Somalia (Ibrahim et al., 1995; Smet, 1992). High concentrations of fluoride also occur in some metamorphic and sedimentary rocks that contain significant amounts of fluoride-bearing minerals such as fluorite and apatite. (Hem, 1989).

Ncube and Schutte (2002) observes that high F⁻ in South African groundwater is mainly found in areas underlain by sedimentary rocks, granites, metamorphic and volcanic rocks. Apart from the natural sources of fluoride in groundwater, the groundwater through some anthropogenic activities is getting polluted because of deep percolation from intensively cultivated fields, disposal of hazardous liquid and solid wastes. These wastes include effluents from aluminium smelters, electronic device and semiconductor industries (Arnesen et al., 1995; Haron and Yunus, 2001; Anwar, 2003; Oren et al., 2004; Amina et al., 2004; Kass et al., 2005). McCaffrey (1998) calculated groundwater distribution maps from the SA National Groundwater Database in the early 1990s and observed that large areas of the country are subject to F⁻ concentrations in groundwater in excess of 1.5 mg/l (Figure 2-1).

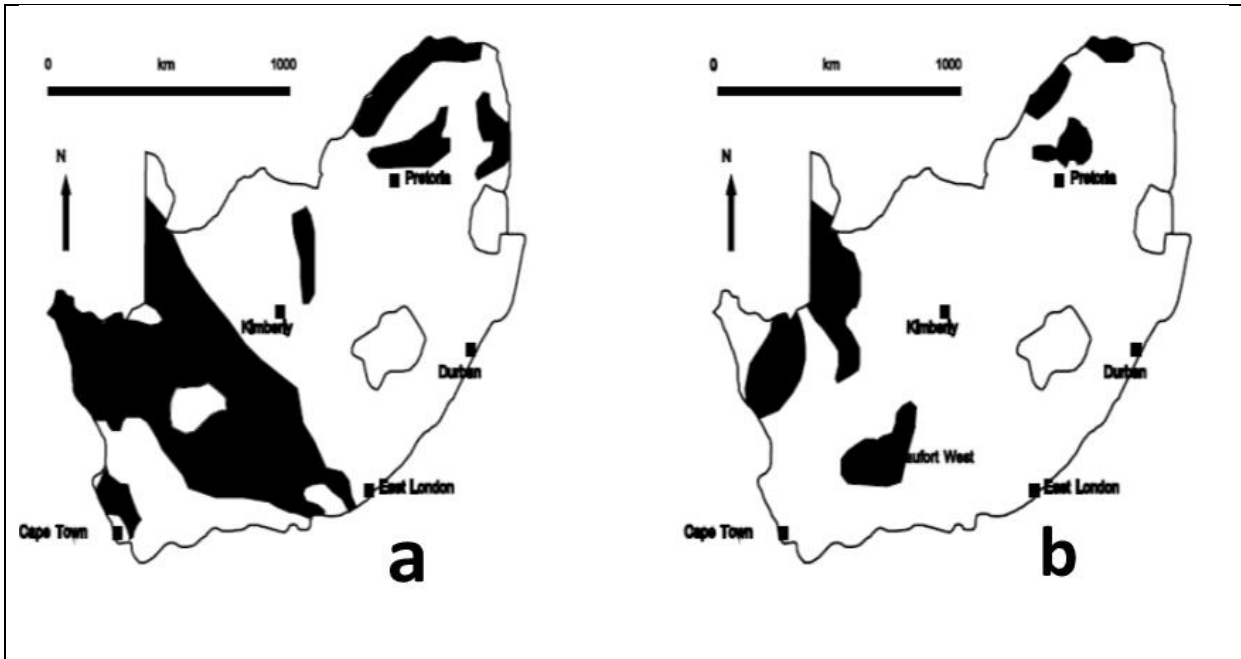


Figure 2.1. (a) South African groundwater with F⁻ concentration greater than 1.5 mg/l. Figure (b) South African groundwater with F⁻ concentration greater than 3.0 mg/l. (Source: McCaffery, 1998)

Marais (1998) also published groundwater maps showing high fluoride areas, detailing each province but excluding Gauteng and Western Cape. From his maps, sampling of 12 074 communities water points established that 10 295 were utilizing groundwater. Amongst these, with available information 625 were observed to be utilizing drinking water with high nitrates and/or fluorides. Figure 2.2 shows the current status of fluoride distribution in South Africa groundwater. The authors note that problems of high fluoride ion concentrations are concentrated in Limpopo, Northern Cape, North-West, and KwaZulu-Natal provinces. These populations have high populations still living in rural areas and dependent on groundwater for drinking purposes. Limpopo, Northern Cape, KwaZulu-Natal and Eastern Cape were noted to have fluoride ion concentration in groundwater of greater than 8 mg/l. Most of these areas were observed to be endemic in fluorosis. Underwood (1977) and WHO (1984) reports that South Africa has some of the highest recorded fluoride levels in ground water (20-40 mg/l). Ncube (2002) in a more recent survey of water quality data also confirms the fluoride levels varied from 2.75-42.05 mg/l on various sites across the country. This is further confirmed by Muller et al. (1997) who observed that dams and rivers in South Africa show fluoride levels below 0.5 mg/l while boreholes water has significantly higher levels of fluoride than other sources of drinking water. Other provinces had few cases or individual sources with high fluoride ion concentrations such as Mpumalanga and Free State. Although the authors conclude that groundwater in South Africa in general is of good quality, serious problems of high fluoride levels greater than, 1.5 mg/l occurs in the groundwater sources of the Limpopo, Northwest, Western Cape, KwaZulu-Natal and Northern Cape provinces and will require partial defluoridation. Moreover, a sizable population in communities in North-West and KwaZulu-Natal were observed to be dependent on groundwater for domestic purposes (Ncube and Schutte, 2005). The authors further noted that research must be initiated into investigating cheap and technologically simple processes for small-scale removal of fluoride from this fluoride-rich groundwater or alternative water supply in rural areas.

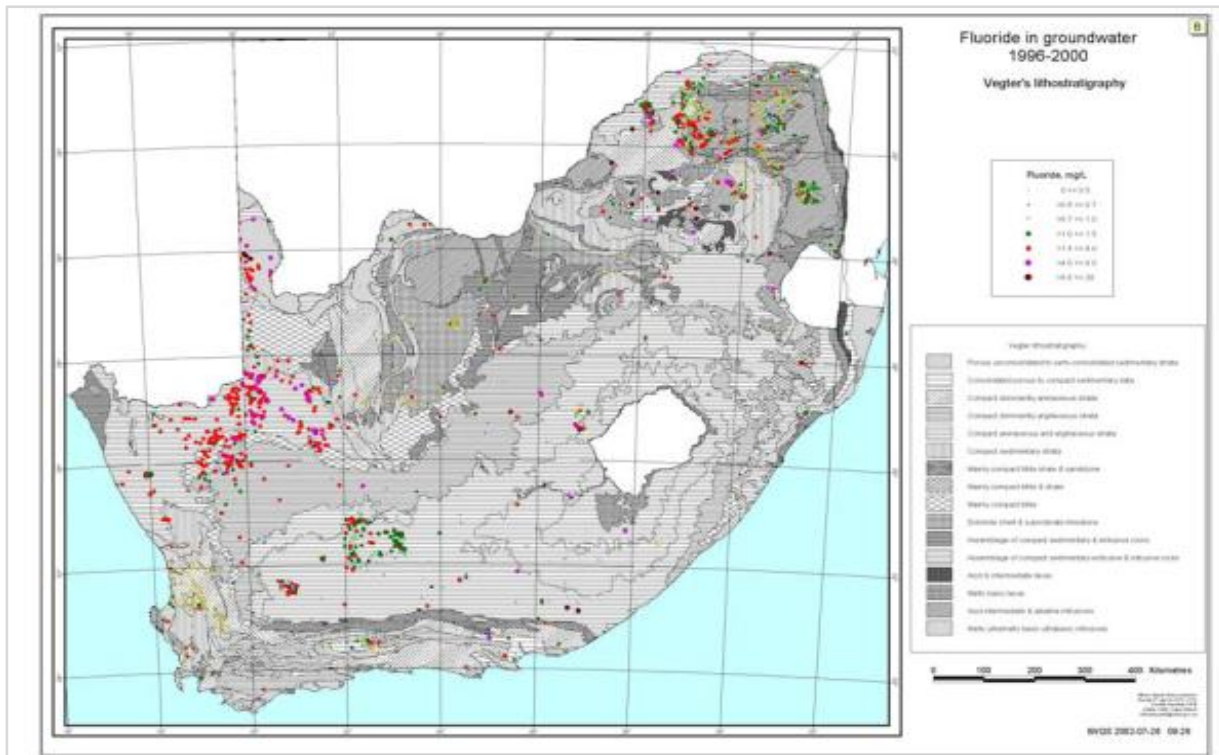


Figure 2.2. Fluoride distribution in groundwater 1996-2000 (Ncube and Schutte, 2005).

The authors further note another important aspect that, although they are aware of techniques developed in other countries, South Africa needs to develop techniques suitable for the local conditions and affordable by the lay person in the rural communities. This aspect is brought out more clearly by the site-specific study carried by Odiyo and Makungo (2012) on fluoride concentrations and impact on human health in Siloam Village in Limpopo Province. This study notes that in Siloam village, groundwater with high fluoride concentration is frequently used without treatment exposing the residents to excessive fluoride consumption. It is noted that the bulk water supply from the communal stand is inadequate leading the communities to use untreated groundwater. Makhado et al. (2006) also reports that most inhabitants of Dididi village, northwest of Thohoyandou in Limpopo suffered serious tooth damage. This was attributed to the high fluoride content (4.6 mg/l) of the Luwini springs that the community uses as source for drinking water. This could represent the scenario in most rural communities in South Africa where the groundwater has high fluoride concentrations and there is no sufficient supply of municipal treated water for drinking purposes. This provides a strong case for provision of point of use or community based defluoridation options. This project was about developing techniques/fluoride adsorbents suitable for local communities/point of use systems in South Africa utilizing locally available materials in the local communities.

2.2 CHEMISTRY OF FLUORIDE IN GROUNDWATER

Shrikant and Nitin (2012) observe that, the fluoride content of the surface and ground water is a function of many factors such as availability and solubility of the parent fluoride minerals with which this water comes in contact with, rock porosity, velocity of flowing water, temperature of the interactions between the rocks and the water, pH of the water and concentration of the calcium ions present in the water. When a fluoride compound is dissolved in water, the element fluorine will be present mainly as fluoride ions. However, depending on the ionic concentrations and pH of the solutions the fluoride is also present in solution as

HF₂ and undissociated HF (Killedar and Bhargava, 1998). Ncube (2002) summarises the factors controlling F⁻ concentrations in groundwater and other natural waters such as thermal springs, these include: temperature; presence or absence of complexing and precipitating ions; solubility of fluoride-bearing minerals; anion exchange capacity of aquifer materials (OH⁻ or F⁻); type of geological formations, and amount of time the water is in contact with a geological formation.

High temperatures increase the solubility of fluoride bearing mineral phases leading to increase in F⁻ concentrations in groundwater. A number of thermal springs in Waterberg area of Limpopo province of South Africa were observed to have high F⁻ concentrations (Olivier et al., 2008). Edmunds and Smedley (1996) observed that thermal springs of high pH are rich in fluoride. A thermal spring in Siloam Village in Limpopo province was observed to have F⁻ concentration > 5 mg/l. Makhado et al. (2006) reports a concentration of 4.6 mg F⁻/l for Luwini thermal spring, Northeast of Thohoyandou in Limpopo province. The authors attributed this to dissolution of F⁻ in fluoride bearing minerals in the nearby metamorphic granite and basalt rocks sedimentary sandstone and shale formations. Fluoride ion distribution in groundwater is largely dependent on the geology of the area amongst other factors. According to Ncube (2002), in Northern Cape: high F⁻ groundwater are found in areas underlain by compact sedimentary strata, unconsolidated to semi-consolidated sedimentary strata, Northwest: high F⁻ groundwater is found in areas underlain by porous unconsolidated to semi-unconsolidated sedimentary strata, dolomite chert, subordinate limestone and assemblage of compact sedimentary and extrusive rocks, KwaZulu-Natal in areas with arenaceous and argillaceous strata, Limpopo: in areas with mafic basic lavas. Fluorides occur abundantly in nature as fluorspar (CaF₂) and cryolite (Na₃AlF₆) (Rawhani, 1986) and various fluorosilicates.

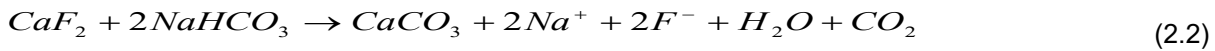
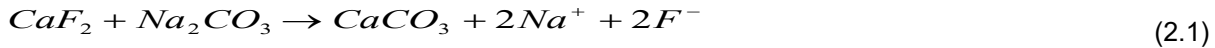
According to Oserse (1947) fluorspar contains 48.9% fluoride and cryolite 54.4%. Fluorspar is mainly found in phosphate bearing rocks and also widely associated with granite and dolomitic formations. South Africa's economically most significant deposits of fluorspar occur in dolomites of the malmani subgroup of the North West province and Felsic members of the Bushveld complex (Munzhelele, 1998). Fluorspar deposits are also found in some alkali and carbonatite complexes in the Northern Province. Mineralization of various fluoride bearing minerals plays a big role in the content of fluoride in groundwaters (Gachiri and Davies, 1993). Mineral solubility limits the concentration of fluoride in groundwater. Table 2-1 shows the solubility products of various fluoride bearing minerals that can potentially control fluoride concentration in groundwater

Table 2.1. Solubility products of various fluoride-bearing minerals

Mineral	Ksp	Temp °C/pH
Fluorite (CaF₂)	3.4 x 10 ⁻¹¹	18
Calcite (CaCO₃)	1 x 10 ⁻⁸	25
Aragonite (CaCO₃)	1 x 10 ⁻⁸	25
OH- (apatite)	2.6 x 10 ⁻⁴⁵	18/pH=7.0
OH- (apatite)	2.3 x 10 ⁻⁴¹	40/pH=74
Selaite (MgF₂)	6.4 x 10 ⁻⁹	27
Halite (NaCl)	1 x 10 ^{-1.58}	25
Siderite (FeCO₃)	1 x 10 ^{-10.5}	25
Magnesite (MgCO₃)	1x10 ⁻⁵	25
Dolomite	1x10 ^{-16.7}	25

Rivett et al. (2006) notes that in groundwater with pH>8 and dominated by Na⁺ ions and carbonate species, fluoride ions commonly exceed 1 mg/l and concentration in excess of 50 mg/l have been recorded in South Africa. This is attributed to low Ca²⁺ concentrations at alkaline pH which increases the solubility of fluoride-bearing formations. Ncube (2002) notes that the main source of F⁻ is the dissolution of various minerals of which the most important is fluorite High levels of Na⁺ are associated with high levels of (CaF₂) bicarbonate

ions which also leads to high alkaline levels. High bicarbonate levels lead to low levels of Ca^{2+} leaving high concentrations of F^- in solution (equation 2.1 and 2.2). Rao and Prasad (1997) observed that presence of sodium bicarbonate in weathered rock formations increases the dissolution of CaF_2 and hence increase of F^- in groundwater.



Odiyo and Makungo (2012) observed a high correlation between F^- and Na^+ in Siloam borehole water in Limpopo province. Moreover, he noted that high concentrations of Na^+ increases the solubility of fluorite in water. Raju et al. (2009) also noted that weathering and leaching of fluoride bearing minerals in rocks formation under alkaline environments lead to enrichment of fluoride in groundwater. Anion exchange (OH^- and F^-) involving various types of clay minerals can also lead to very high concentrations of fluorides. The process involves base exchange softening, i.e. Ca^{2+} and Mg^{2+} are exchanged for Na^+ as the pH is progressively increased to alkaline levels (9-10.5). Anion exchange can occur in sedimentary basins (Boyle and Chagnon, 1995).

2.3 THE HEALTH IMPLICATIONS OF FLUORIDE CONSUMPTION

Fluoride is beneficial to both bone and dental development in human beings when ingested at specific doses. Intake of fluoride in water at low-dose levels (<1 mg/l) is important in the formation of teeth and prevention of dental caries (Pontius, 1991; WHO, 2004). Too low fluoride intake levels during childhood may give rise to dental caries in later years. Dental caries is a disease caused by specific bacteria harboured in dental plaque, which ferments carbohydrates to produce acids that can demineralise tooth enamel (Hammer, 1986). If the demineralization of the enamel is allowed to continue, the invading bacteria would penetrate the enamel and lead to the eventual loss of tooth as a result of decay in the absence of restorative dental care (Hammer, 1986). The World Health Organization (WHO) has set a maximum allowable level of 1.5 mg/l for fluoride in drinking water (WHO, 2006). However, excess fluoride (above 4 mg/l) in drinking water is known to cause harmful effects such as teeth mottling, skeletal fluorosis (Jenkins, 1978; Teri, 1982; Abdulrahmani, 1996) and kidney damage (Odonnel, 1973). Absorbed fluoride is distributed throughout the body and retained in bones and teeth (WHO, 1984). The degree of dental fluorosis depends on the amount of fluoride exposure up to the age of 8-10 years, as fluoride stains only the developing teeth while they are being formed in the jawbones and are still under the gums (Choubisa and Sompura, 1996). Persons suffering from fluorosis manifest discoloured teeth and deformed bones (Ayoob and Gupta, 2006; Yoshimura et al., 2006; Tamer et al., 2007). Advanced skeletal fluorosis may result in crippling skeletal fluorosis, which is the most severe type whereby victims are faced with mobility difficulties (Mjengera and Mkongo, 2003). Table 2-2 summarizes the benefit and health effects of fluoride (WHO, 2004; NHMRC and ARMCANZ, 2005).

Table 2.2. Health effects of long-term consumption of high or low fluoride in water

Fluoride concentration (mg/l)	Effect on health
<0.5	Dental caries
0.5-1.5	Promotes dental health
1.5-4	Dental fluorosis
>4	Dental and Skeletal fluorosis

(Source: WHO, 2004)

Table 2-3 shows the maximum permissible levels of fluoride in drinking water on the basis of climatic conditions. The amount of water consumed and hence the amount of fluoride intake is related to temperature. There are more than 20 developed and developing nations that are reported to be endemic for dental and skeletal fluorosis. These are Argentina, United States of America, Algeria, Libya, Egypt, Jordan, Turkey, Iran, Kenya, Tanzania, South Africa, China, Australia, New Zealand, Japan, Thailand, Canada, Saudi Arabia, Persian Gulf, Sri Lanka, Syria, India, etc. (Mameri et al., 1998). A study by UNICEF shows that fluorosis is endemic in at least 27 countries across the globe (Qian et al., 1999). It is estimated that tens of millions of people in the world are affected. The fluoride problem in Tanzania, for example, was realized by the government as early as 1950 but owing to lack of technical knowhow defluoridation was considered complicated and expensive (Mjengera and Mkongo, 2003).

Table 2.3. Maximum allowable fluoride concentration for drinking water.

Annual average maximum daily air temperatures (°C)	Recommended fluoride concentration (mg/l)			Maximum allowable fluoride concentration (mg/l)
	Lower	Upper	Optimum	
10-12.0	0.9	1.2	1.7	2.4
12.1-14.6	0.8	1.1	1.5	2.2
14.7-17.7	0.8	1.0	1.3	2.0
17.8-21.4	0.7	0.9	1.2	1.8
21.5-26.3	0.7	0.8	1.0	1.6
26.4-31.5	0.6	0.7	0.8	1.4

Source: US Public Health Drinking Water Standards, 1962

There were no definite actions taken to solve the problem until some years after. Based on medical reports and other studies, the country set a temporary standard of 8 mg/l (Rural Water Supply Health Standard Committee, 1974). This value was quite high compared to the WHO guideline value of 1.5 mg/l in drinking water (WHO, 1984). Bardecki (1974) opined that if the WHO guideline were adopted by that time, about 30% of Tanzanian water sources in use would have been disqualified. The level of fluoride in drinking water in Arusha District, Tanzania ranged from 1.0 to 45.5 mg/l (Mjengera and Mkongo, 2003).

In Kenya, the levels of fluoride in drinking water were studied where 1,286 boreholes and wells from different parts of the country were analysed for their fluoride ion concentration. The highest level recorded was 57.0 mg/l (Nair and Gitonga, 1985). In India, as many as 25 million people in 15 of the 32 states were identified as endemic for fluorosis in 1993 (Ghandi, 1993). In Mexico, 5 million people, constituting about 6% of the population were reported to be affected by fluoride in groundwater (Amor et al., 2001). As a result of the large number of people affected by high level of fluoride in groundwater, India and China lowered

their permissible upper limit of fluoride in drinking water from 1.5 as given by World Health Organization (WHO, 1984) to 1.0 mg/l.

The issues of fluoridation, fluorides and fluorosis in South Africa have been recorded, debated and discussed since 1935. Several research studies (Maughan-Brown, 1935; Staz, 1938 and Abrahams, 1946) reported the presence of fluorosis amongst children in high fluoride areas. The most comprehensive work was undertaken by Ockerse (1941), he produced three reports on human fluorosis in various regions of the former Union of South Africa. During that time 805 areas where dental fluorosis occurred were known (Ockerse, 1947). Many of the dental fluorosis sufferers (primarily blacks) in South Africa lived in rural areas.

Ncube and Schutte (2005) using Water Management system Database at Resource Quality Services Directorate at DWAF for the period 1996-2000 established the occurrence of fluoride in groundwater sources (Figure 2-1 and 2-2) and its impact on dental health. The authors were able to delineate regions areas with higher fluoride concentrations or lower than that recommended for drinking water. They also delineated occurrence of dental fluorosis in selected provinces. However, the study was confined to a few provinces since the Oral health Care dental fluorosis data was available for a few provinces at that time. This includes Free State, Western Cape, KwaZulu-Natal and North-West (Figure 2-3). The authors were further able to link the high fluoride levels in groundwater, the consumption of this high fluoride groundwater and occurrence of dental fluorosis in the affected areas. A further scrutiny of the data showed that in provinces where communities depended largely on groundwater for drinking purposes such as North-West province the morbidity of dental fluorosis was very high. A percentage morbidity of dental fluorosis as high as 97% was recorded in North-West Province (Figure 2.4). A major and significant finding of this study was that high morbidity of fluorosis was observed in areas where fluoride concentrations were extremely high and in most of those areas exceeding the limits for drinking water. In another observation, in towns and villages where the fluoride concentrations were lower than the limits for drinking water, the morbidity of fluorosis was comparatively low.

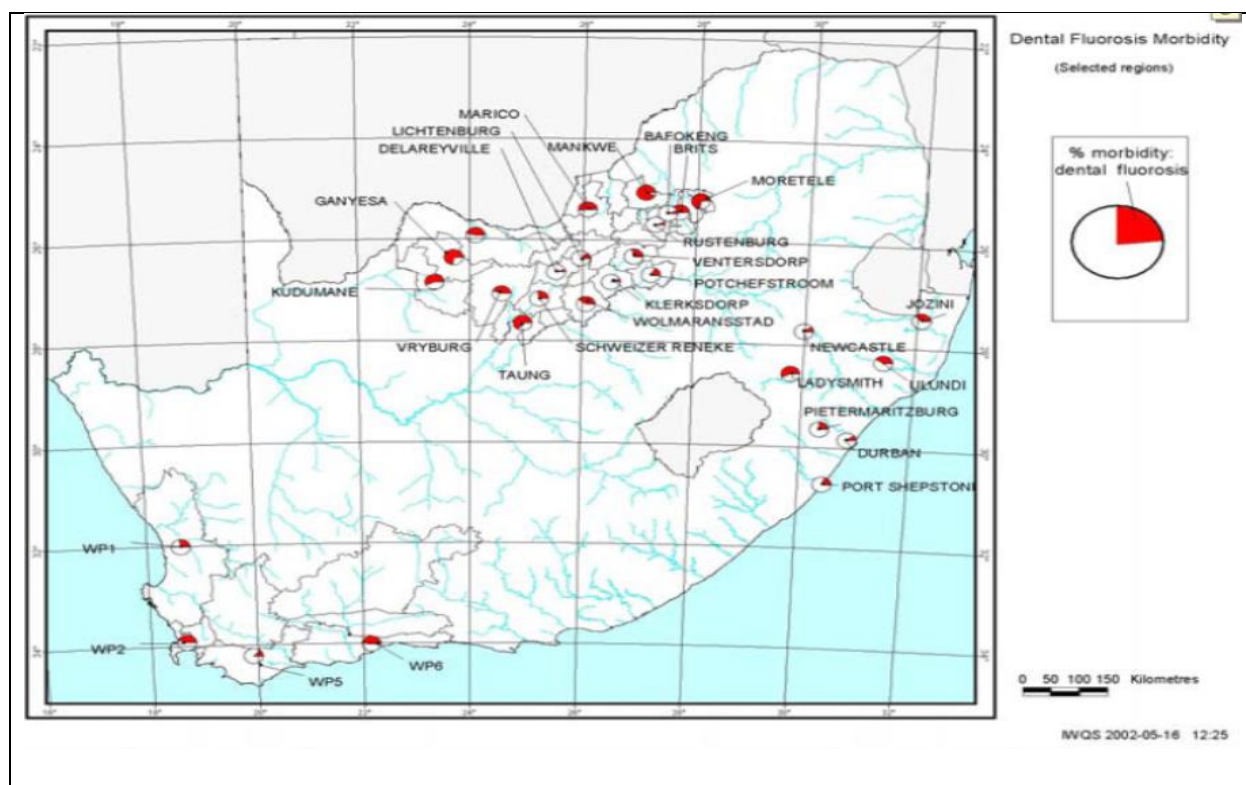


Figure 2.3. The distribution of % morbidity of dental fluorosis (Ncube and Schutte, 2005)

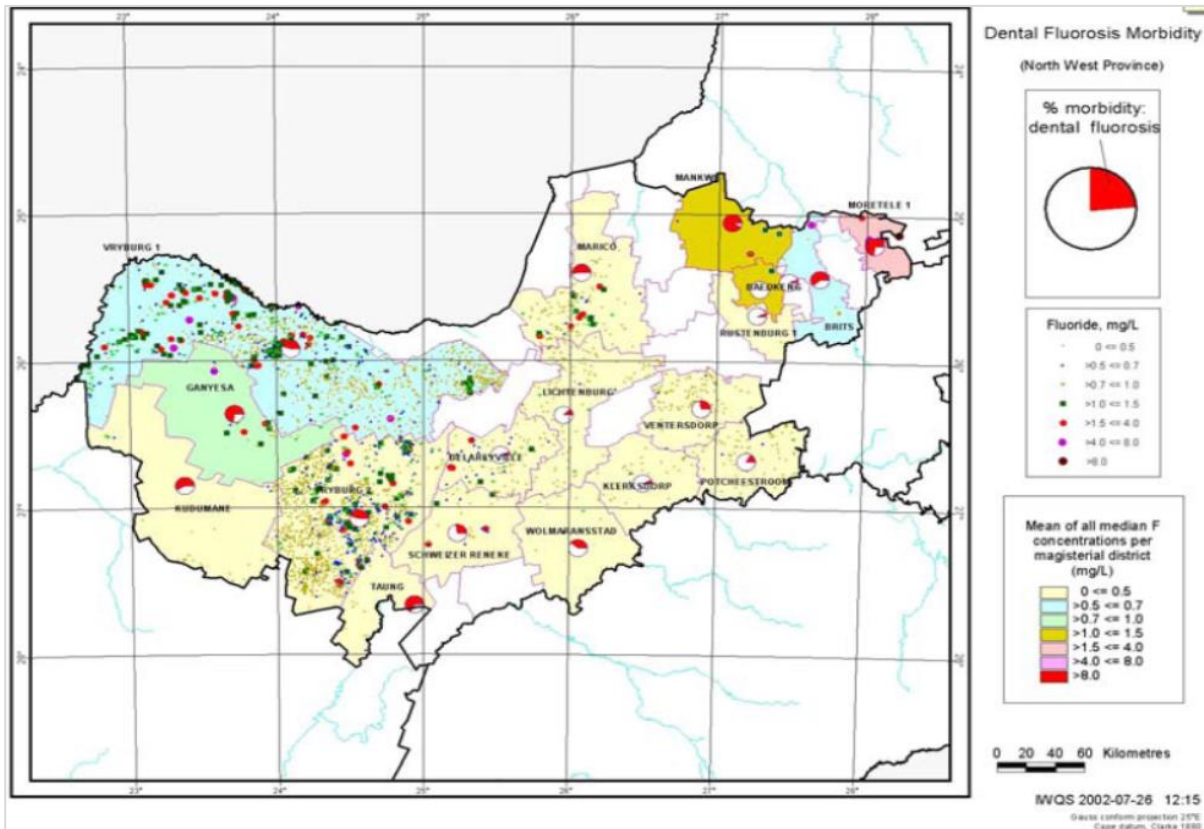


Figure 2.4. Dental fluorosis morbidity (North-West Province) (Ncube and Schutte, 2005)

Odiyo and Makungo (2012) carried out a case study on the link between fluoride concentrations and impact on human health of Siloam village, an example of a typical rural village in South Africa with high fluoride concentrations in groundwater. The study established a strong link between consumption of the high fluoride groundwater and incidences of mottled teeth in members of the rural community. The study showed that 87% of the households that use groundwater, 85% had members with mottled teeth and 50% of School learners between the ages of 11-14 also had mottled teeth.

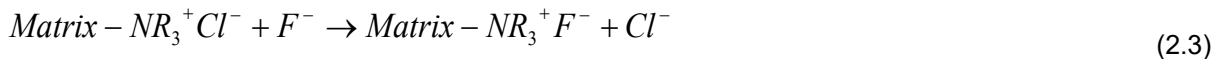
This section has presented studies done linking dental fluorosis morbidity to consumption of groundwater with high fluoride concentration. Moreover, the evidence from the data presented in the reviewed studies confirms that this is prevalent in rural communities that are dependent on groundwater for drinking purposes. There are several options proposed to address this challenge. This includes:

- Partial defluoridation of the groundwater sources if used for drinking purposes (for example the case of Siloam village in Limpopo Province)
- Development of alternative water supplies

For partial defluoridation of the groundwater, cheap and technologically simple processes that can be operated with minimal challenges by rural community members need to be developed.

2.4 WATER DEFLUORIDATION TECHNOLOGIES

Quite a number of techniques have been employed for the removal of excess fluoride from water over the years with each technique having its own merits and demerits. These technologies include adsorption, ion exchange, and precipitation processes (Karthikeyan et al., 2005). The recent technologies include membrane processes such as reverse osmosis (Joshi et al., 1992), Donnan dialysis (Dieye, 1995), electrodialysis (Adihikary et al., 1989), and nanofiltration (Simons, 1993). Ion-exchange defluoridation. Fluoride can be removed from water with a strongly basic anion-exchange resin containing quaternary ammonium functional groups. The removal takes place according to the reaction (equation 2.3):



The fluoride ions replace the chloride ions of the resin. This process continues until all the chloride ions on the resin are replaced. The resin is regenerated for reuse by backwashing with saturated sodium chloride solution in which case new chloride ions replace the fluoride ions (Meenakshi, 2006). The resin can therefore be used over and over again by simply washing with saturated sodium chloride solution. The defluoridation of the feed water is achieved on the basis that fluoride ions being more electronegative replace chloride ions on the resin. The defluoridation technology has the advantage of being able to remove (90-95%) fluoride. However, it is costly in-terms of capital and operating cost, releases fluoride-rich waste which requires specialized disposal, and treated water has a very low pH.

2.4.1 Precipitation processes

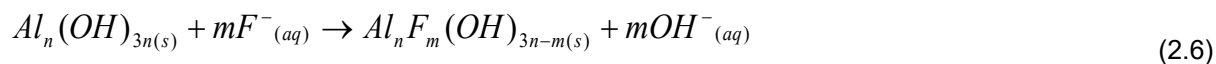
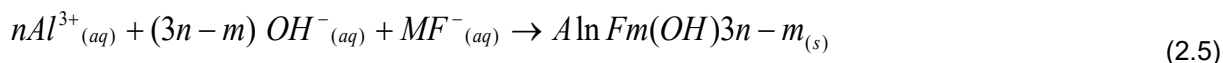
According to Feenstra et al. (2007), precipitation processes involve the addition of chemicals and formation of fluoride precipitates. Among these are precipitations with calcium and aluminium salts. Precipitation chemicals must be added daily in batches. Precipitation techniques produce a certain amount of sludge every day. Defluoridation by precipitation can be grouped into two types which are: precipitation of fluoride by a suitable reagent through a chemical reagent and co-precipitation of fluoride, which involves its simultaneous precipitation with a macro-component from the same solution through the formation of mixed crystals by adsorption or occlusion or mechanical entrapment. Addition of lime (Ca(OH)_2 or other calcium salts (CaSO_4 and CaCl_2) can be used to precipitate fluoride as insoluble CaF_2 and is the cheapest and most commonly used precipitation technique for defluoridation but principally used for high fluoride containing waste waters. (Huang and Liu, 1999 and Hu et al., 2003). The precipitation reaction using lime is as follows (equation 2.4):



2.4.2 Coagulation-precipitation defluoridation

This method is based on the addition of chemicals (coagulants and aids) to water and the subsequent formation of insoluble fluoride precipitates. Lime and alum are the most commonly used coagulants (Meenakshi, 2006). Ayoob et al. (2008) says that the chemistry of fluoride removal by alum is quite complex, though it has been widely applied in water treatment. In co-precipitation using Al salts, fluoride ions are considered to be removed from the solution by getting enmeshed onto Al(OH)_3 flocs. The most recent researches in this direction precisely concludes that the mechanism of fluoride removal in water due to the

addition of an aluminium salt may be due to co precipitation of fluoride and hydroxide ions with aluminium ions to yield a precipitate and/by adsorption/ligand exchange. (Equation 2.5 and 2.6)



An example of technology developed using this coagulation-precipitation process is Nalgonda technique developed in India makes use of both lime and alum for the removal fluoride from water (Eswar and Devaraj, 2011). The Nalgonda technique involves addition of lime, aluminium salts and bleaching powder as disinfectant to raw water by rapid mixing, flocculation, sedimentation and filtration (Gumbo and Mkongo, 1995; Eswar and Devaraj, 2011). The technique is a two-step process in which lime is first added and mixed rapidly with water to precipitate the fluoride as insoluble calcium fluoride. The addition of lime raises the pH value of water up to 11-12 (Meenakshi, 2006). The precipitation reaction occurs according to the following reaction (equation 2.7):



The second step involves the addition of alum either as aluminium sulphate or aluminium chloride for coagulation (Meenakshi, 2006). Aluminium salt is responsible for the removal of fluoride from water. Two reactions occur when alum is added to water. In the first reaction, alum reacts with OH⁻ to produce insoluble Al(OH)₃ (equation 2.8):



In the second reaction, alum reacts with fluoride ions present in the water (Meenakshi, 2006) (equation 2.9):



In the rural areas of India, where communities employ domestic defluoridation using the Nalgonda technique, stainless steel candle filters are used. The equipment consists of filters fitted with candle and an additional mixing device. People are advised to mix the raw water with lime and alum and leave it overnight so that the next morning, clear supernatant water is ready for consumption (Eswar and Devaraj, 2011). At domestic level, defluoridation is carried out in a container of 60 l capacity with a tap of 3.5 cm above the bottom of the container for withdrawal of water after precipitation and settling (Eswar and Devaraj, 2011). For small communities of up to 200 people, a fill and draw (FandD) defluoridation plant is put in place. The plant has a hoper bottom cylindrical tank with a depth of 2 m equipped with a hand operated or power-driven stirring mechanism (Eswar and Devaraj, 2011). In this setup, raw water is pumped or poured into the tank and the required quantities of lime, alum and bleaching powder are added with stirring. Stirring is done for about 10 minutes and content allowed to settle for 2 hours. The defluoridated water is withdrawn and supplied through stand posts while the settled sludge is discarded.

The coagulation-precipitation technique for defluoridation is cost effective, can be used at domestic and community levels, no regeneration of media, design and construction is simple, least disposal problems and no electricity is needed to power the unit. The technique however has its limitations. Only a small

portion of fluoride (18-33%) is removed. There is need for regular analysis of feed and treated water to calculate the correct dosage of chemicals to be added, addition of $\text{Ca}(\text{OH})_2$ increases the hardness of water. The use of aluminium sulphate as coagulant causes the sulphate ion to increase substantially and exceed the permissible limit of 400 mg/l. The residual aluminium in excess of 0.2 mg/l in treated water causes dangerous dementia disease as well as pathophysiological, neurobehavioral, structural and biochemical changes. It also affects musculoskeletal, respiratory, cardiovascular, endocrine and reproductive systems (Nayak, 2002).

2.4.3 Membrane processes

The membrane technology employs the use of semi-permeable membranes for removing ions from water. The three main types of membrane process are nanofiltration (NF), reverse osmosis (RO) and eletrodialysis (ED). Nanofiltration can be used to carry out selective desalination and is generally used to remove divalent ions such as calcium and sulphate ions from water (Nasr et al., 2013). The NF technology has the advantage of lower operating cost over RO and ED, partly because of the low cost of membrane materials. Since reverse osmosis cannot be used for partial and/or selective demineralization, nanofiltration or electro dialysis is more suitable for producing drinking water directly, without the need for remineralization (Nasr et al., 2013).

Electrodialysis (ED) is a type of technology which arranges ion-exchange membranes alternately in a direct current field (Strathmann, 2004; Xu, 2005; Pugazhenthii & Kumar, 2005; Huang et al., 2007). ED has been widely used to demineralize, concentrate and/or convert salt-containing solutions because of its distinguished functions (Audinos, 1997; Saracco, 2003; Huang and Xu, 2006; Huang et al., 2007).

Reverse osmosis (RO) is a physical process in which the contaminants are removed by applying pressure on the feed water to direct it through a semi-permeable membrane. The process is the reverse of natural osmosis because pressure is applied to the concentrated side of the membrane to overcome the natural osmotic pressure. The RO membrane rejects ions based on size and electrical charge (Meenakshi, 2006). In the recent years, RO membrane process for removing fluoride water has emerged as a preferred alternative for providing safe drinking water without posing the problems associated with other conventional methods.

In a study carried out by Babu et al. (2011) using RO membrane (a standard domestic spiral wound polyamide membrane) with 0.1 nm pore size, it was discovered that using the RO membrane alone for defluoridation of water could only achieve 18 to 65% fluoride rejection. But when the feed water containing about 10 to 30 mg/l fluoride was pre-treated by passing it through a calcium carbonate column before using RO membrane, fluoride rejection attained a maximum value of 93.5% at a concentration of 14 mg/l fluoride in feed water. At this concentration, the level of fluoride in permeate was 0.91 mg/l which is below the WHO permissible limit of fluoride in drinking water (WHO, 2004). Hence, with the calcium carbonate pre-treatment the RO membrane separation can reduce the final fluoride concentrations to 1 mg/l. In fact, a final concentration of 0.2 mg/l fluoride was obtained at pH 7.4 (Babu et al., 2011). The calcium carbonate aids in increasing the alkalinity of the feed water, which in turn helps in effective combination of fluoride ions with calcium. This increases the molecular size to levels higher than the molecular weight cut-off, of the membrane and hence higher rejection is obtained (Babu et al., 2011). Calcium carbonate increases the alkalinity of the feed water according to the following equation 2.10:



When hollow fibre ultrafiltration membranes were used with calcium carbonate pre-treatment, there was no significant fluoride rejection. Thus, establishing that RO membrane with pore size of 0.1 nm was essential for significant rejection of fluoride (Babu et al., 2011). The membrane process is effective for fluoride removal; it provides an effective barrier to suspended solids, inorganic pollutants, organic micropollutants, pesticides and microorganisms. No chemicals are required, life of membranes is long and it works under wide range of pH. The defluoridation technique has its limitations. The process is expensive. It removes all the ions present in water though some minerals are essential for growth. Therefore, addition of mineral is required after treatment. The treated water becomes acidic and needs pH correction. Lot of water is wasted as brine and the disposal of brine is a problem. All the methods using membrane technology require electricity supply and so they would not be applicable to households in rural areas due to high electricity bills or lack of connection to electricity grid.

2.4.4 Electrocoagulation/electroflotation technology

Electrocoagulation (EC) is a defluoridation technique involving in situ generation of coagulants by dissolving either aluminium or iron ion electrically at the anode. Electrolytic gases, usually H₂, are released at the cathode (Bennajah et al., 2009). For aluminium, the main reactions at the electrode during electrocoagulation (EC) are (equations 2.11 and 2.12):

Anode:



Cathode:



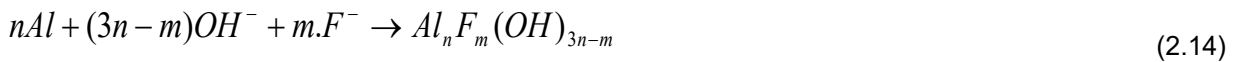
The dissolution of aluminium or iron at the anode produces hydroxides, oxyhydroxides or polymeric hydroxides as a function of pH (Holt et al., 2005). These can remove both soluble and colloidal polluting substances by adsorbing or precipitating the pollutants and promoting coagulation (Bennajah et al., 2009). "Flocs can be removed either by settling followed by filtration, floatation or a combination of these two techniques. In practice, settling is the most common option, while floatation can be achieved by hydrogen or air injection" (Bennajah et al., 2009).

Electrocoagulation is more effective for removing pollutants from water than added chemicals because microflocs are formed which are more likely to flocculate when an electric field is applied. The removal therefore does not require addition of chemicals for coagulation. Electrocoagulation also prevents the presence of co-anions from added chemicals such as sulphate ions in Al₂(SO₄).18H₂O (Hu et al., 2003). Since chemicals are not added then, there is no generation of large volumes of sludge which may release secondary pollutants as in the case of chemical coagulation. The main deficiency of electrocoagulation is the lack of dominant reactor design and modelling procedures (Mollah et al., 2001; Bennajah et al., 2009). Moreover, there is problem of complete understanding of the fluoride removal by EC because at least three mechanisms compete (Zhu et al., 2007):

Adsorption on Al(OH)₃ particles (equation 2.13):



Co-precipitation (equation 2.14):



Fluoride attachment to the electrodes.

The third mechanism is said to be closely linked to co-precipitation because it results simultaneously from the direct co-precipitation of fluoroaluminium compounds on the electrode surface and from the adsorption of colloidal particles of fluoroaluminium complexes formed in the vicinity of the electrode (Zhu et al., 2007). The defluoridation technology is expensive, requires technical skills and electricity supply. It therefore would not be applicable in households in rural areas.

2.4.5 Adsorption processes

Oremusova (2007) defines adsorption as a process that occurs when a gas or liquid solute accumulates on the surface of a solid or a liquid (adsorbent), forming a molecular or atomic film (the adsorbate). Usually, the sorbent has a fixed total uptake, where by one solute is exchanged for another (as in ion exchange processes). When a quantity of adsorbent is contacted with a given volume of a liquid containing an absorbable solute, adsorption occurs until equilibrium is achieved (Kalibantonga, 2005). In the adsorption method, raw water is passed through a bed containing the defluoridating material. The material retains fluoride either by physical, chemical or ion exchange mechanisms. The adsorbent gets saturated after a period of operation and requires regeneration. An ion exchange mechanism whereby F^- is exchanged with OH groups in the mineral structure is generally assumed to be the rate determining step in the adsorption process. This ion exchange process can be presented by the following equilibria (equations 2.15 and 2.16):



where MOH_2 and MOH_2^+ are metal oxides like Al/Fe oxides

Easily exchangeable OH^- groups are those found in metal hydroxides or hydrated metal oxides such as aluminium or iron oxides, although it is known that not all structural forms of metal oxides have exchangeable OH^- groups with F^- notably magnetite (Fe_4O_6) and corundum ($\alpha-Al_2O_3$). Lattice OH^- groups such as those found in aluminosilicates, for example kaolinite, have a low tendency to be replaced by F^- (Hauge et al., 1994).

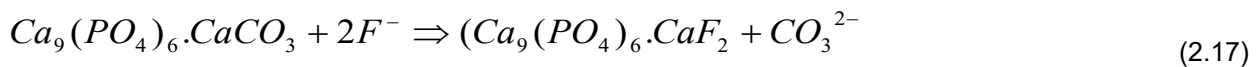
The extent of adsorption is proportional to specific area where the specific area is that portion of the total area that is available for adsorption. It is related to the grain size of the adsorbent. The choice of particle size is made by considering the following factors: the ease of mass transfer from the fluid to the surface, creation of as much interfacial surface area as possible and reduction of antiparticle diffusion path length, all of which favour smaller particles; and maintenance of a low pressure drop, which favours larger particles (Jimmy et al., 1997). Coetzee et al. (2006) points out that because hydrogen and hydroxide ions are adsorbed quite strongly, the adsorption of other ions is influenced by the pH of the solution. In general, adsorption of typical pollutants from water is increased with decreasing pH. The pH of the solution is a very important parameter and determines the degree of protonation of the OH^- exchange sites and the degree of protonation of F^- . The pH will therefore determine the specific charge of an exchange site and therefore ultimately also the adsorption tendency of the substrate.

2.5 WATER DEFLUORIDATION BY ADSORPTION

Normally, adsorption processes are exothermic, thus the extent of adsorption generally increases with decreasing temperature. A number of investigations have shown that temperature affects several factors which are important in the adsorption process. According to Robert (1988), for complete miscible systems, selective adsorption generally decreases with rise in temperature. It is the expected effect for an exothermic process. The physicochemical nature of the adsorbent can have profound effects on both rate and capacity for adsorption. Whereas solubility, molecular sizes, and charge (ionic species) are considered in the case of adsorbate (Benefield, 1982). The criteria for the selection of suitable adsorbents include adsorption capacity, cost of the medium, ease of operation, potential for reuse and possibility of regeneration. A wide range of materials have been assessed for fluoride uptake. Bhatnagar et al. (2011) points out that, bauxite, magnetite, kaolinite, serpentine, various types of clays and red muds are some of the naturally occurring materials studied. The mechanism of fluoride uptake and applications of some of the most frequently encountered adsorbents are reviewed in the preceding sections.

2.5.1 Bone and bone charcoal

Smith and Smith (1937) were the first to identify the potential of bone to remove fluoride from water. They reported that degreased, caustic and acid bone material could effectively reduce fluoride concentration from 3.5 to 0.2 mg/l. The suggested removal mechanism was of ion exchange in which the carbonate radical of the apatite ($Ca_9(PO_4)_6.CaCO_3$) comprising bone was replaced by fluoride to form an insoluble fluorapatite (equation 2.17).



According to Ayoob et al. (2008), the high cost factor of bone, became an inhibiting factor for its wider use. It was later recognized that bone char produced by carbonizing bone at temperatures of 1100-1600°C had superior fluoride scavenging potential compared to unprocessed bone. Thereafter bone char replaced bone as a defluoridating agent (Sorg, 1978). The adsorption mechanism of the fluoride ion onto bone char is suggested to be ion exchange. The phosphate ion in the bone char is exchanged for fluoride ion, Fan et al. (2003) explained the uptake of fluoride on hydroxyapatite (equation 2.18):



According to Ayoob et al. (2008), at the application level, the success of this technique hinges mainly on the quality of bone charcoal. The bone charring process is crucial as any failure may result in a product of low defluoridating capacity, affecting the quality of water treated. Poor bone charcoal may render water with bad taste and smell and would be unaesthetically unpleasant to consumers. The consumers may dislike the process once they are exposed to such smell or taste.

2.5.2 Activated alumina (AA)

The crystal structure of alumina contains cation lattice discontinuities giving rise to localized areas of positive charges (Clifford et al., 1978). This makes alumina to attract various anionic species. The maximum capacity of activated alumina was found to be 3.6 mg F⁻/g (Bulusu and Nawalakhe, 1988). Alumina has a

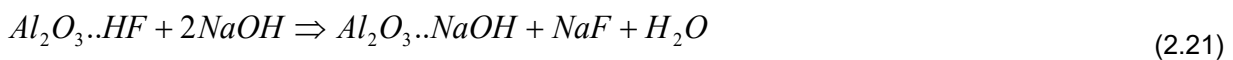
high preference for fluoride compared to other anionic species, and hence is an attractive adsorbent. In practice, alumina (Al_2O_3) is first treated with HCl to make it acidic (equation 2.19).



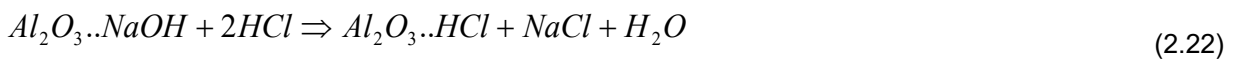
This acidic form of alumina when contacted with fluoride ions displaces the chloride ions and gets attached with the alumina (equation 2.20).



To regenerate the adsorbent a dilute solution of sodium hydroxide is mixed with the adsorbent to get a basic alumina (equation 2.21).



Further treatment with acid regenerates the acidic alumina (equation 2.22).



AA has been used for defluoridation of drinking water in industrialized countries. However, recently this technology is gaining a wide attention in developing countries like India where the AA is used as a filter media in household defluoridation units (Figure.2.5). Venkobachar et al. (1997) reported that around 500 to 1500 litres of safe water could be produced with 3 kg of activated alumina when the raw water fluoride is between 11 and 4 mg/l at natural water pH of 7.8-8.2. A disadvantage of this process is that the regeneration steps result in an aqueous solution containing high concentration of fluoride that requires safe disposal.

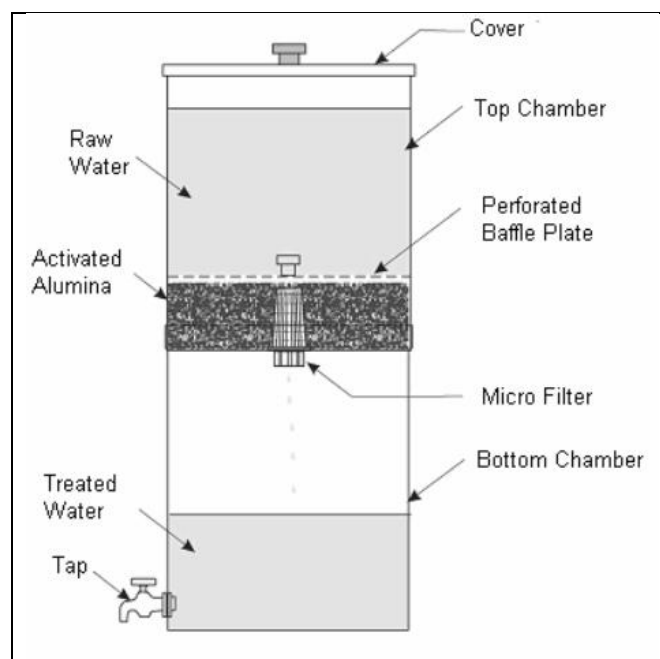


Figure 2.5. Activated alumina-based domestic defluoridation filter (Daw, 2004)

On the other hand, if the spent alumina is discarded, the cost of the defluoridation increases. Apart from that, spent alumina may leach out fluoride ions when it comes in contact with alkaline aqueous media. defluoridation of water in a rural area of Madibeng Municipality, North-West Province, South Africa. He observed that the plant reduced fluoride content from 6 mg/l in the feed water to 1.5 mg/l. An output of 940-1296 m³ of defluoridated water was achieved before a breakthrough at 2 mg/l F⁻. He demonstrated that a 1st world technology could be effectively operated and maintained in rural area with constant supervision and training of operators.

2.5.3 Clays and soils

The potential of clay and soil-based systems for defluoridation has been and is also under intense investigation in many fluoride endemic regions of the world, especially developing countries. The first comprehensive study of fluoride adsorption by minerals and soils was published by Bower and Hatcher (1967). They observed that excess fluoride in water could be removed to different degrees by adsorption onto a variety of mineral and soil types. Thereafter, fluoride adsorption onto soils and clays, both in natural and modified activated forms has been studied extensively. (Daifullah et al., 2003; Gitari et al., 2013; Jiang and Zeng, 2003). Research studies in this area includes Illinois soils in the US (Omueti and Jones, 1977); clay pottery (Chaturvedi, 1988); and soils in Kenya (Zevenbergen, 1996); activated clay, (Bjorvatn and Bårdsen, 1995); bentonite and kaolinite. (Kau et al., 1997 and Kau et al., 1998). Table 2-4 shows some of the clays that were applied in different countries for the removal of fluoride in water.

Table 2.4. Different clay soils and their adsorption capacities in water defluoridation

Type of clay	Adsorption capacity (mg/g)	Area of study	References
Fe³⁺ modified bentonite clay	2.91	South Africa	Gitari et al. (2013)
Bambawoha clay	0.168	Ethiopia	Hassen (2007)
Montmorillonite clay	1.485	India	Karthkeyan (2005)
Red mud	0.01	India	Rakshit (2004)
Fired clay	0.015	India	Rakshit (2004)

In general, it is observed that the adsorption capacity of the clays is low. Nevertheless, adsorption on clay-based systems is used in many parts of the world for defluoridation due to low cost and abundance within the communities having high fluoride in their groundwaters.

2.5.3.1 Mechanisms of adsorption onto clay soils

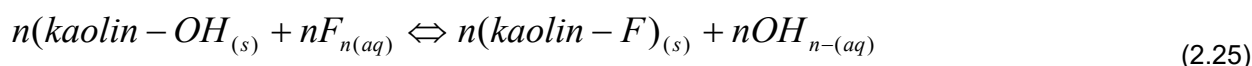
The fluoride adsorption process on clay mineral surfaces is based on the surface chemistry of the sorbent, the solution chemistry of fluoride, and a surface complex mechanism. An ion exchange mechanism where F⁻ is exchanged with OH⁻ groups in surface layer hydrated metal oxides such as aluminium or iron oxides, is generally assumed to be the determining step in the adsorption process. For a hydrated aluminium oxide surface these are (equations 2.23 and 2.24).



The surfaces of clays always contain ionizable functional groups which constitute the active sites on the surface, OH in this case, can undergo proton transfer depending on the pH. This process is one of the determinant surface charges. Since F⁻ is negatively charged, the more positive the surface of the adsorbent the more favourable it would be for fluoride adsorption.

2.5.3.2 Kaolin clay

The potential of kaolin clay for fluoride adsorption has been evaluated by several researchers. (Bower and Hatcher, 1967; Kau, 1997; Perrott, 1976; Semmens and Meggy, 1996). These studies established several factors that could influence fluoride sorption, which include solution pH, clay surface area, structure, aluminum content, and the presence of certain exchangeable cations capable of forming fluoride precipitates (Hiemstra and Van Riemsdijk, 2000). Although ion exchange reaction is regarded as the predominant form of fluoride sorption, fluoride may also be immobilized through the formation of complexes or precipitates with exchangeable cations such as magnesium, iron and calcium or be attracted to the clay electrostatically, in which case F⁻ may be retained in the electric double layer. (Kau, 1997). It was clearly demonstrated that disruption of the kaolin crystal structure occurred due to fluoride uptake and F/OH exchange occurred primarily with Al(OH)₃ rather than with OH⁻ from the crystal lattice of clay minerals. The reaction between kaolin and fluoride increases the pH of the solution through the release of hydroxide ions as represented in equation 2.25.



2.5.3.3 Other clays

Coetzee et al. (2006) carried out a comprehensive study on the fluoride adsorption characteristics of South African clay minerals and correlated this with mineral composition, structure and adsorption mechanisms. This study assessed the fluoride adsorption characteristics of clays (kaolinite, bauxite, goethite, bentonite, and palygorskite) collected from different regions in South Africa, where a high fluoride concentration in groundwater is a water quality issue. Bauxitic clays were found to have the best overall potential as fluoride adsorbents. Simple chemical activation using 1% Na₂CO₃ solutions, dilute hydrochloric acid and calcination could enhance adsorption capacity of certain clay types. (Coetzee et al., 2006). Chibi and Haarhoff (2000) evaluated samples of Sri Lankan Clay for defluoridation of groundwater in South Africa. They observed a reduction of fluoride in feed water from 5 mg/l to less than 2 mg/l. They observed that the geological analysis on these clay samples related to locally found F clay samples in South Africa. Several researchers have evaluated the removal of F⁻ using fired clays (Moges, 1996; Hauge et al., 1994) Hauge et al. (1994) studied the defluoridation of drinking water using pottery. The study investigated the effect of firing clay on F⁻ adsorption. The results show that clays fired at temperature up to 600°C gave higher F⁻ adsorption. (Hauge, 1994) Moges et al. (1996) studied the defluoridation of water using fired clay chips in Ethiopia. Their findings indicated that F⁻ adsorption is affected by factors such as initial concentration, mass of adsorbent and the pH of the solution (Moges, 1996).

2.5.3.4 Application of clay materials in household defluoridators and filters

Natural clays present a major advantage due to their abundance in nature (locally available). Since these clay minerals are widely available in many rural areas they can be used as alternative defluoridating materials. These clay soils can be packed in columns and used as adsorbents to remove fluoride from water. The use of clay powder in columns is possible but challenging mainly because of difficulties in packing the columns and controlling the flow. Domestic clay column filters are normally packed using clay chips found as waste from the manufacture of brick, pottery or tile (Figure 2-6). The filters are mostly based

on up-flow or plug-flow regimes. Figure 2.6 shows a household defluoridation unit using a column of brick chips.

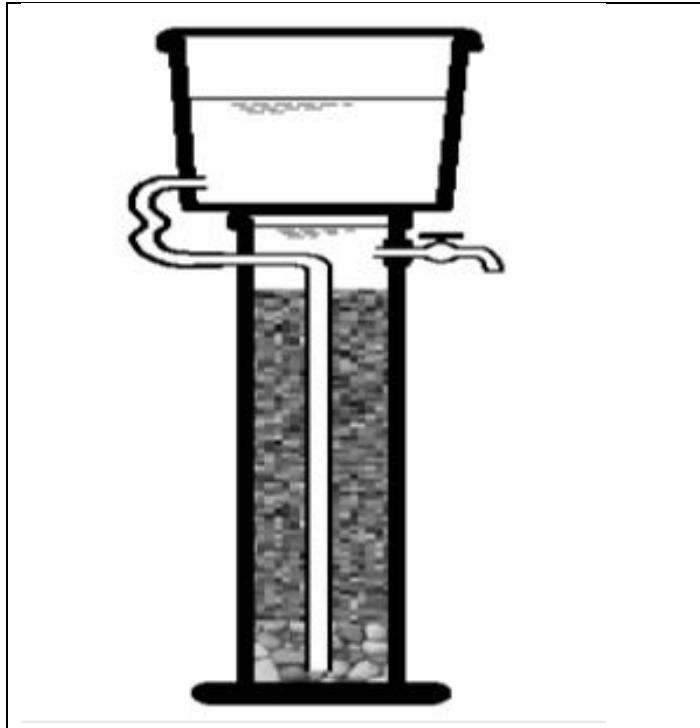


Figure 2.6. Stratified column of brick chips used in household defluoridation (Padmasiri, 1998).

Other column filters using clays also incorporate other materials to aid the filtration processes. Agonafir and Ambelu (2007) conducted a study to determine the treatment duration of a crushed brick fluoride filter media made with sand filter and the fluoride adsorption capacity of the crushed bricks material per unit weight. They reported that crushed bricks fluoride removal filter media with experimental sand filter containing charcoal (Figure 2-7) had a very good effect in the fluoride removal from water. During the filter run the residual fluoride concentration below the safe recommended limit ($<1.5 \text{ mg/l}$) was observed until about 300 litres of raw water that had fluoride concentration of 8 mg/l was treated. The crushed bricks material showed high fluoride adsorption capacity (91.76%) per unit weight (Agonafir and Ambelu, 2007). Figure 2.7 shows an experimental household sand filter for defluoridation of groundwater

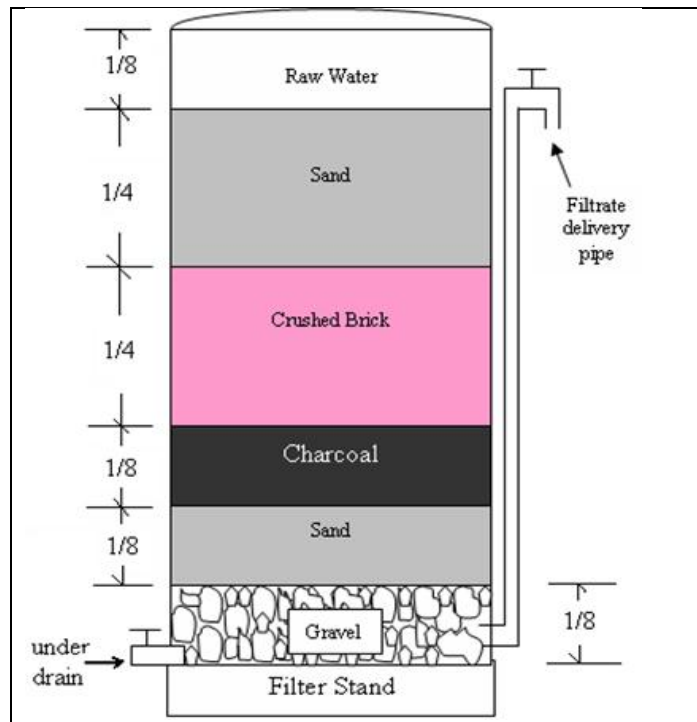


Figure 2.7. Crushed brick fluoride filter combined with experimental sand filter

2.5.3.5 Shortcomings of raw clay filter media

It has been observed that exhaustion time of the filter unit is one disadvantage that the clay filter media have. This might be due to complete saturation of anion-exchange sites indicating the complete exhaustion of the filter media. Agonafir and Ambelu (2007) reports that as the filtration process proceeded, about 300 litres of 8 mg/l fluoride water was defluoridated and the concentration observed to increase beyond the permissible upper limit (1.5 mg/l). This is a limitation because the media can only defluoridate and filter as much water during a certain period. Research reports recommend that only water to be used for drinking and cooking purposes (usually less than 5 litre per person per day) needs to be defluoridated. The entire water demand is often ten times higher and to defluoridate all these would be too expensive as well as producing a large amount of toxic sludge (SKAT, 2003). Another study done by Abaire (2009) in Ethiopia indicated that clay has low capacity as compared to bone char and therefore, the lifetime of the adsorption bed is very short. Nonetheless, clay mineral is widely available and adsorption by clay may be cost effective and easier to use in many situations.

2.5.4 Merits of the adsorption process

The adsorption process is extensively used and gives satisfactory results and adsorption modules easy to fabricate at household and community level. For this reason, adsorption seems to be a more attractive method for defluoridation in terms of cost, simplicity of design and operation. Moreover, the adsorbents can be easily recovered and reused (Ozean et al., 2005). The adsorption process may generate little or no toxic pollutants and has low initial capital and operating costs (Crini, 2006). Adsorption is safe from the environmental point of view as no sludge is produced. (Unuabonah et al., 2008). However, many studies point out that there exists considerable scope and need to develop new or modified adsorbents with improved fluoride uptake properties to meet the stringent legislative requirements of 1.5 mg/l of fluoride in

drinking water. Therefore, it is important to make efforts to understand various possible approaches to improve the fluoride uptake properties of potential materials including clay minerals and soils.

2.5.5 Summary of bench scale studies on various adsorbents for defluoridation of water

Adsorption has been considered to be the most efficient technology for fluoride removal from drinking water compared to other technologies (Mjengera and Mkongo, 2003; Amor et al., 2001; Hichour et al., 2000). In principle, any solid material with a microporous structure can be used as an adsorbent. Examples are bone and coal char, clays, iron oxides, synthetic natural zeolites, molecular sieves and activated carbon (Mohamedbaker, 2010).

Several research studies have been carried out using various materials as adsorbents for the defluoridation of water. Activated carbon is the most widely used adsorbent for water treatment but it has high operating costs owing to the high price of the activated carbon and high-water flow rate (Figureueiredo et al., 2005). These factors make activated carbon not suitable for use in developing countries (Panday et al., 1985). Activated charcoal has a very poor fluoride adsorption capacity (Janardhana et al., 2006).

Janardhana et al. (2006) studied the defluoridation of drinking water by impregnating activated coconut shell charcoal (CSC) with aluminium, zirconium, calcium and sodium metal ions using a continuous down flow adsorption mode at room temperature. The impregnation compounds were $ZrOCl_2$, alum, CaO, $CaCl_2$ and $Na_2B_4O_7$. Of the modified CSC, zirconium impregnated activated carbon (ZICSC) had the highest fluoride removal capacity. Starting with the initial fluoride concentration of 6.5 mg/l in test solution, the residual fluoride concentration in each of 1 l of solutions was 0.14, 0.12, 1.06, 1.87, 5.64 and 5.48 mg/l for $ZrOCl_2$, alum, CaO, $CaCl_2$ and $Na_2B_4O_7$ respectively. The unimpregnated charcoal had a very poor fluoride adsorption capacity (residual fluoride was 6.04 mg/l).

Sadiju et al. (2008) reported adsorption capacities of 94.8% and 95.3% respectively for raw and bauxite calcined at 200°C at a dose of 2.5 g/200 ml fluoride solution, equilibration shaking time of 30 min. Considering the effect of bauxite calcination temperature at 200, 300, 400 and 500°C on fluoride adsorption on bauxite, they observed that bauxite calcined at 500°C had the lowest defluoridation capacity of 87.1%. From the thermogram, at 400°C, gibbsite ($Al(OH)_3$) had started to transform to boehmite ($AlOOH$), and at 500°C, the kaolinite structure is completely destroyed resulting in highly amorphous phase that could be attributed to different activated aluminas (Sadiju et al., 2008).

Locally sourced gypsum calcined at 400°C was reported to show high defluoridation capacity of about 70% at a dose of 10 g/200 ml for 8 mg/l fluoride solution within equilibration time of 30 min (Masamba et al., 2005). The report by Zevenbergen et al. (2003) shows that Ando soil is an effective adsorbent for the defluoridation of drinking water at village level. The Ando soil was a local Kenyan soil derived from volcanic ash. The batch experiments involved suspension of 1 g of soil in 50 ml of NaF solution containing 4, 20 and 40 mg F/l respectively. The F^- solutions contained 0.3 M Ca + Mg concentration of 0.3 M therefore resembling typical Kenyan fluoride-rich groundwater. The soil suspensions were equilibrated by shaking at different time intervals from 0.16 to 24 hours at 18°C. The authors observed that the time required to reach equilibrium for F^- sorption increased with increasing initial concentration of F^- . A steady state was attained within a few hours with the initial concentration of 4 mg F^- /l whereas at an initial concentration of 20 and 40 mg F^- /l, the F^- concentration was still declining after 24-hour contact time. The observed high fluoride adsorption capacity is attributed to the high 'active' aluminium (e.g. allophone) content and acidic character which are typical characteristics of Ando soils and soils with 'andic' properties (Zevenbergen et al., 2003).

Bjorvatn et al. (1997) studied the defluoridation of water using five topsoil samples (mostly red, lateric clay) collected in Ethiopia. They reported that the soils reduced the fluoride content of water from about 15 to 1 mg/l, at dosage levels of about 100 g/l and optimum contact time of 24 hours. It was noted that the soil samples pre-heated at 50°C had similar fluoride efficiency as those pre-heated at 250°C.

Murugan and Subramanian (2006) carried out a study on defluoridation of water using Tamarind seed as an unconventional biosorbent. By batch experiment they varied experimental conditions which included agitation time, pH, initial fluoride concentration and sorbent dosage. For the batch experiment, 0.15 g of Tamarind seed powder was required for complete removal of fluoride from 1.0 l of field sample containing 2.7 mg/l of fluoride. This gave rise to sorption capacity of 18 mg/g which was the maximum defluoridation capacity of the seed at pH 7.0. Defluoridation decreased with increase in temperature and particle size (Murugan and Subramanian, 2006).

Activated alumina (AA) is the most widely used adsorbent for the removal of fluoride from drinking water because it is readily available and is not expensive (Wu et al., 2007). However, activated alumina has its limitation in that it has low adsorption capacity (4.04 mg F⁻/g) (Maliyekkal et al., 2008), slow adsorption rate and decrease of adsorption capacity after regeneration (Ghorai and Pant, 2004). The defluoridation with AA is pH specific. At pH<5, AA gets dissolved causing loss of adsorbent while at pH>7, silicate and hydroxide compete more strongly with fluoride ions for exchange sites on AA (Bishop and Sansoucy, 1978). A maximum fluoride uptake capacity of 1.450 mg/g at pH 7 was reported by Ghorai and Pant (2004) for batch studies involving water containing initially 13.4 mg F/l with pH range from 4 to 7 and AA dose of 4 g/l. The fluoride removal efficiency of AA at the initial fluoride concentration of 13.4 mg/l was therefore 43.28%. Regeneration studies of the AA carried out using different regenerants which included alum, HCl, H₂SO₄ and NaOH (Iyenger, 2005) have reported that efficient regeneration could be achieved with a combination of 1% NaOH and 0.4N H₂SO₄. However, residual aluminium in output water can range from 0.16 to 0.45 mg/l (Eswar and Devaraj, 2011).

Bone char has been demonstrated to be a good adsorbent for the defluoridation of drinking water. It is a blackish, porous, granular material, prepared by heating ground bone in a furnace with only limited admission of atmospheric oxygen at 550°C for about 4 h (Rao et al., 2009). Bone char consists of 57-80% calcium phosphate (mainly as hydroxyapatite, Ca₁₀(PO₄)₆(OH)₂), 6-10% calcium carbonate and 7-10% of activated carbon (Fawell et al., 2006). Bone char removes fluoride from contaminated water by replacement of its hydroxyl ions by the fluoride ions according to the equation (Fawell et al., 2006) (equation 2.26).



In Nalgonda District bone char-based community defluoridation systems, the defluoridation capacity of the bone char is monitored by measuring the fluoride concentration in the treated water samples. When the defluoridation capacity is exhausted, the spent char is removed from the defluoridation system and stored in sealed bags as bone char sludge (Durgaprasad and Sivaram, 2007).

A report of the laboratory evaluation on the performance of bone char-based bucket defluoridators by Jacobsen and Dahi (1997) reveals that bone char-based defluoridators are very efficient in removing fluoride from water at a capacity of 1.1 mg/g. A domestic defluoridator made of 20 l plastic bucket and 10 kg of bone char, on an average, was efficient in reducing the fluoride in raw water containing 8.5 mg F/l to 0.37 mg/l (achieving 95.6% fluoride removal), for a period of 2 months, with 32.5 l of water treated every day. In their field testing involving ten bone char plastic bucket defluoridators monitored in Tanzanian households, on average, fluoride concentration was reduced from 10.3 to 1 mg/l, that is 90% for a monitoring period of 408 days with the pH of treated water ranging between 9.0 and 8.3; on average 8.56.

They noted that if 1 mg/l F⁻ of treated water was taken as the breakthrough point, the defluoridator saturation point varied from 4 to more than 13 months depending on the loading and water consumption patterns in the different households.

Mjengera and Mkongo (2003) carried out a study on an appropriate defluoridation technology for use in fluorotic areas in Tanzania. Their report reveals that a bone char column containing 4 kg of the media could defluoridate as much as 7,000 l of water with an average concentration of 11.7 mg/l fluoride passed through it. The residual fluoride concentration was analysed to be around 2 mg/l. The technique was considered suitable for influent water containing a limit of 10 mg/l F⁻. According to the authors, bucket type defluoridators are cheaper.

Based on batch tests, the rate and capacity of F⁻ uptake by bone char were highest with black grade, followed by grey grade and lowest with white grade. Twenty-four-hour contact-time F⁻ sorption isotherms indicated saturation at capacities of 11.4 mg F⁻/g of black grade, 2.4 mg F⁻/g of grey grade, and less than 0.3 mg F⁻/g of white grade bone char (Mwaniki, 1992). As efficient as the bone char is for defluoridation, it is unacceptable to some communities such as Hindus and villages in North Thailand owing to socio-cultural reasons (Feenstra et al., 2007) and also because the final water quality after defluoridation process is low (Mwaniki, 1992). Sadiju et al. (2008) remarked that the treated water may be left with a rotten meat taste and smell if the bone charring process is not properly carried out. The low fluoride adsorption capacity of AA and the unacceptability of bone char in some communities due to social and cultural aspects has led to increased research on other potential adsorbents for defluoridation of groundwater especially for point-of-use (POU) systems. These include clays and metal modified clays

Karthikeyan et al. (2005) carried out a defluoridation study using montmorillonite clay at the pH range of 2-12. The percentage of fluoride removed at pH 2 was 97.0%. It was observed that defluoridation decreased with increase in pH. For example, at pH 7, the percentage of fluoride removed was 82, while at pH 10 it was about 60 and at pH 12, 56% of fluoride was removed. The amount of fluoride removed by montmorillonite at pH 7 is quite substantial for drinking water at a neutral pH. The pH is considered an important variable that controls the adsorption of the fluoride at the montmorillonite-solution interface. The high percentage of fluoride removed at low pH values is due to the protonation of the clay surface. Therefore, the lower the pH, the greater the adsorption of fluoride, as more of the surface sites are positively charged (Karthikeyan et al., 2005).

The adsorption of fluoride onto the surface of montmorillonite is due to the development of positively charged surface sites according to the following reactions (Appelo and Postma, 1994) (equation 2.27).



where 'M' is a metal ion in the mineral lattice. The positively charged sites are available for electrostatic attraction to fluoride ion as (equation 2.28).



Anion exchange may also occur by displacement of the hydroxyl species as (equation 2.29).



At a specific pH of defluoridation, a specific amount of adsorbent was required for optimum fluoride removal. Further addition of higher doses of the adsorbent did not result in considerable increase in defluoridation. This was due to the overlapping of the active sites at higher concentrations of the adsorbent, thus reducing the net surface area (Killedar and Bhatgava, 1990; Rai et al., 2004). High density of particles reduces migration and access of adsorption sites by adsorbate species.

The South African clay deposits can be broadly classified according to the dominant clay mineral present: 1. Kaolin Fields (dominant clay mineral being kaolinite) 2. Bentonite Fields (dominant clay mineral being montmorillonite, which is part of the smectite group) and 3. Palygorskite Fields (dominant clay mineral being palygorskite) (Coetzee et al., 2003). The results of the study by Coetzee et al. (2003) on the adsorption capacities of South African clays and bauxite show that bauxite samples had the best adsorption capacities, the adsorption capacities of bentonite and palygorskite samples were intermediate, while pure kaolin samples had poor adsorption capacities.

A study by Onyango et al. (2004) observed that surface-tailored zeolite using aluminium ion (Al-zeolite F9) had a greater fluoride adsorption capacity (28-41 mg/g) than most reported values for fluoride adsorbents: bone char by Mwaniki (1992) (0.3-11.4 mg F-/g), activated alumina (AA) (4.04 mg F-/g) and magnesia amended AA-10.1 mgF-/g (Maliyekkal et al., 2008). However, the zeolite used was a synthetic one so cost may be an inhibiting factor in its use.

Wu et al. (2007) developed a trimetal oxide as fluoride adsorbent by co-precipitating Fe(II), Al(III) and Ce(IV) salt solutions with a molar ratio 1:4:1 under alkaline condition. The trimetal (Fe-Al-Ce) oxide retained amorphous structure and maintained relatively stable fluoride adsorption performance at calcination temperatures lower than 600 °C. The adsorbent showed high defluoridation ability around pH 5.5-7.0, which is preferable for actual application. A high fluoride adsorption capacity of 178 mg/g was obtained under an equilibrium fluoride concentration of 84.5 mg/l, adsorbent dose of 150 mg/l and pH 7.0. A high desorption efficiency of 97% was achieved by treating fluoride loaded Fe-Al-Ce oxide with NaOH at pH 12.2. The limitation of the developed adsorbent would be the cost of production of a bulk quantity to meet household need in rural communities as no natural adsorbent support material is involved.

2.6 CURRENT PRACTICES IN WATER DEFLUORIDATION

2.6.1 The concept of appropriate technology

“Appropriate” means that besides being scientifically sound the technology is also acceptable to those who apply it and to those for whom it is used. This implies that technology should be compatible with the local culture. It must be easily adapted and further developed if necessary. In addition, it should be easily understood and applied by community health workers and in some instances even by individuals in the community. Although different forms of technologies are appropriate at different stages of development, their simplicity is always desirable. The most productive approach for ensuring that appropriate technology is available is to start by identifying the problem and then to seeking, or if necessary, developing a technology which is relevant to local conditions and resources. (WHO, 1978). According to Nemade et al. (2002), numerous commercial methods have been described employing various materials for the fluoride removal since 1930. For practical and financial reasons, however, high-technology water treatment is unavailable in many rural areas. Priority, therefore, should be given to the development of simple devices for defluoridation of drinking water at a (preferentially) home-based level. (Nemade et al., 2002). A number of methods have been proposed for the defluoridation of water. Defluoridation devices for household use in rural areas should meet a number of requirements: modest investment, low maintenance cost, simple

design, easy to operate by villagers, ability to reduce the fluoride content to permissible limits and improve the water quality in general. No single method seems to meet all the requirements, but some techniques are more widely used than others.

An in-depth analysis of defluoridation research reveals that very few proven sustainable solutions have been developed so far. The adsorption/ion exchange processes are still the most widely used for fluoride removal in endemic areas of the developing countries. The Nalgonda technique and adsorption by bone char or a combination of both have been used in many countries like India and Tanzania at both domestic and community levels (Dahi et al., 1996) Of late a major shift has occurred in the perception of people in India towards community-based water supply treatment systems, with many people preferring domestic defluoridation units (DDU), especially using activated alumina. However, these DDUs are not available to the people in the fluoride endemic rural areas. Other techniques like reverse osmosis, electro coagulation, electro dialysis and nanofiltration assure good quality water but are high technology and high cost options for most of the fluoride endemic areas. Appropriate technologies have been applied in many parts of the world where endemic fluorosis is a problem. These countries include India, Thailand, Kenya, Tanzania and Ethiopia. High fluoride levels occur in ground waters in some parts of Africa however the East African countries have higher levels compared to the Southern Countries. In Tanzania for example, fluoride concentrations in ground water of up to 40 mg/l have been reported hence in such countries the use of appropriate technologies is most popular. (Thole, 2013)

2.6.2 Water defluoridation in Tanzania using bone char

Removal of fluoride from water has been explored using a number of materials among which are bauxite, gypsum, magnesite and their composite filters (Thole et al., 2011a; Thole et al., 2011b; Thole et al., 2012), Calcium chloride (CaCl_2) and Sodium dihydrogen phosphate (NaH_2PO_4) as co-precipitation reagents in contact precipitation (Dahi, 1996; Dahi, 1997), cow bone char in batch and fixed bed (Mjengera and Mkongo, 2003; Bregnhøj et al., 1997), activated carbon and activated carbon loaded separately with alumina, magnesia and calcium (Bablia, 1996). The technology best demonstrated in Tanzania is the use of bone char at household level in fixed bed defluoridators (Figure 2-8). The bone char has high sorption capacity initially; however, the media gets saturated with fluoride with time. The general practice around Arusha (Tanzania) is to replace the media when the effluent has a fluoride concentration of 2 mg/l, the maximum permissible limit as per International Reference Centre (IRC) in Hague, Netherland. Results show that for water with an initial fluoride of 10 mg/l, the defluoridator can treat approximately 1300 litres of water to a final fluoride content of less than 2 mg/l. The mass of bone char used in such an investigation is 4 kg. Based on use of 20 litres per family per day of the treated water, the 4 kg of bone char can be employed to treat water for sixty-five days family use. This approximates to 20 to 25 kg of bone char in a year for a family. (Dahi, 1996).

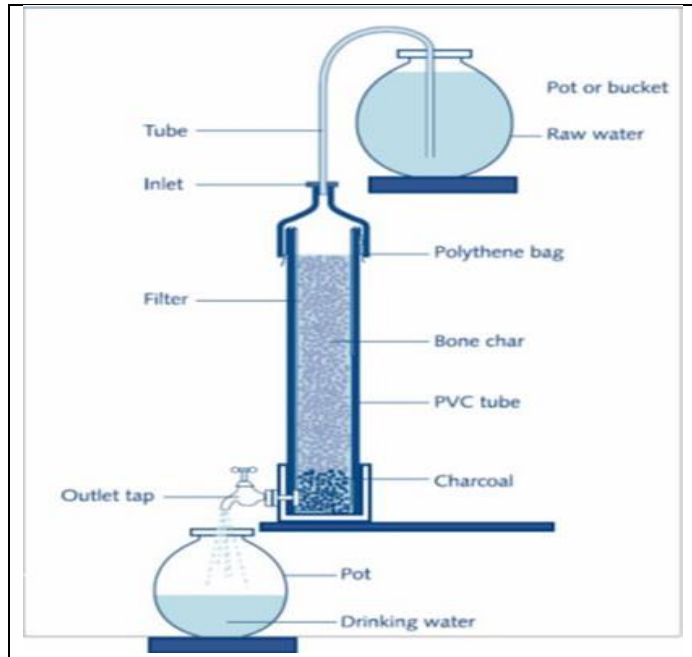


Figure 2.8. Bone char domestic defluoridator (Wondimagegn, 2008)

2.6.3 Nalgonda technique for domestic defluoridation

The Nalgonda technology was developed in India by National Environmental Engineering Research Institute (NEERI) to be used for the defluoridation of groundwater at both community and household levels. The defluoridation process is aluminium sulphate-based coagulation-flocculation sedimentation (Feenstra et al., 2007). The technique is reported to be limited in that it does not permit sufficient removal of fluoride, even when appropriate dosage is used, and residual fluoride concentration could be higher than 1 mg/l at high concentrations of fluoride in raw water (Feenstra et al., 2007). The treatment efficiency is limited to about 70 per cent, requiring a large dose of aluminium sulphate (700-1,200) mg/l. Thus, a dosage is reached where the users start complaining about residual sulphate salinity in the treated water (Feenstra et al., 2007). The Nalgonda Technique has been introduced in African villages and studied at pilot scale in Kenya, Senegal and Tanzania (Dahi, 1996). Any container of 20-50 litres capacity is suitable for this purpose (Figure 2.9). A tap, fitted 3-5 cm above the bottom of the container is useful to withdraw treated water. Adequate amount of lime water and bleaching powder are added to raw water and mixed well. Alum solution is added to it and stirred for 10 min. The contents are allowed to settle for 1 hour and the clear water is withdrawn either through the tap or decanted slowly, without disturbing the sediment and filtered (Eli et al., 1996). The settled sludge may be discarded away from the source of water or preferably collected and sent for recycling. With domestic treatment, there is no capital investment and the cost of the treatment is only that of the chemicals. Of late, stainless steel defluoridation filters, which function on Nalgonda technique, have been developed for use at domestic level (Hiremath, 2006; Mariappan and Vasudevan, 2011)

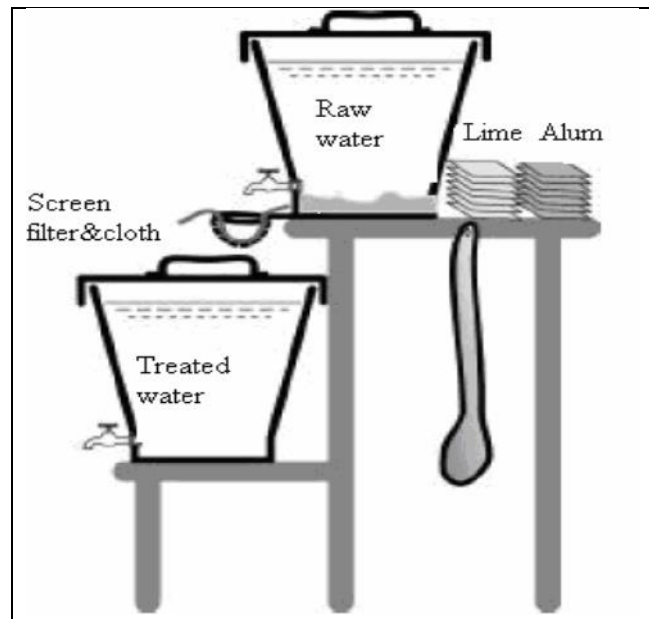


Figure 2.9. The Nalgonda defluoridator as adopted for domestic use in Tanzania (Dahi, 2000)

2.6.4 Defluoridators using Activated Alumina in India

In several rural areas of India having chronic fluoride problem, United Nations Children Educational fund (UNICEF) has funded voluntary organizations propagating activated alumina technique for defluoridation (Meenakshi, 2006). UNICEF assists the communities by providing a two-compartment bucket with upper chamber of approximately 20 litres capacity with a micro filter fitted to the bottom containing 5 kg of activated alumina (Figure 2.10).

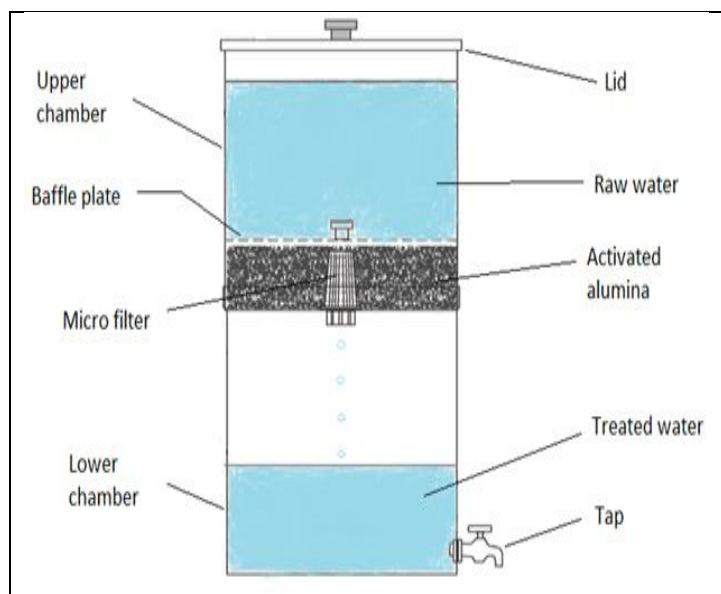


Figure 2.10. A schematic diagram of a domestic defluoridator using activated alumina.

However, AA has its limitations in that it has low adsorption capacity, slow adsorption rate and decrease of adsorption capacity after regeneration (Ghorai and Pant, 2004). A report by Chauhan et al. (2007) on the performance of AA in a DDU shows that AA has a fluoride uptake capacity (FUC) of 1.788 mg F/g at breakthrough point of 1.5 mg/l F- for 550 l of test water containing initial fluoride concentration of 10 mg/l if 3 kg of AA are used. The average influent water pH was 7.9 to 8.0 while 9-10 l of water flowed through the AA bed per hour. Household water treatment devices using biosand filter, zeolite sand composites, silver impregnated porous pots and ceramic candle filters.

Momba et al. (2013) have identified, selected and constructed household treatment devices using materials commonly or available in the market in South Africa. Five types of the treatment devices which seemed to be promising for South African conditions were identified. These include biosand filter (BSF) which comprises the conventional biosand filter (BSF-S) and a novel biosand filter with zeolite (BSF-Z), bucket filter (BF), a ceramic candle filter (CCF) and silver-impregnated porous pot (SIPP) filter (Figure 2.11 and 2.12.).

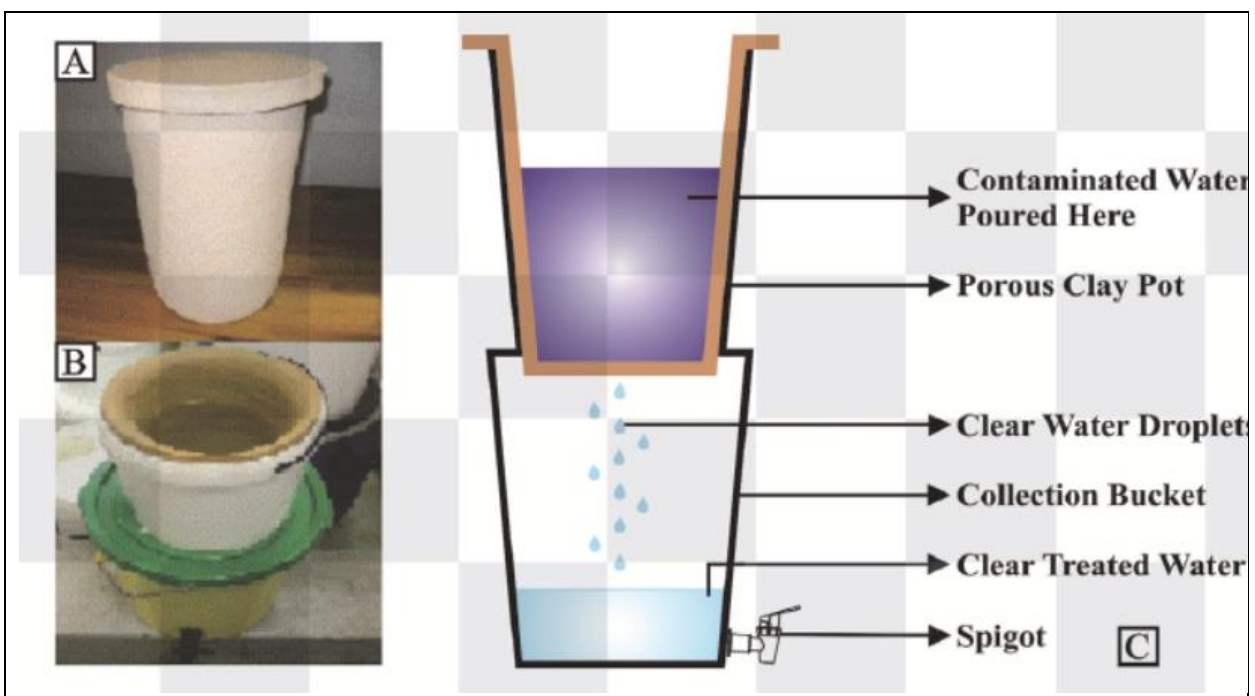


Figure 2.11. A SIPP filter unit: A – the silver-impregnated clay pot that serves as the filtering unit; B – the clay pot fitted into a 10 l bucket and placed on top of a collection vessel; and C – skeletal view of a complete SIPP filter (Momba et al., 2013)

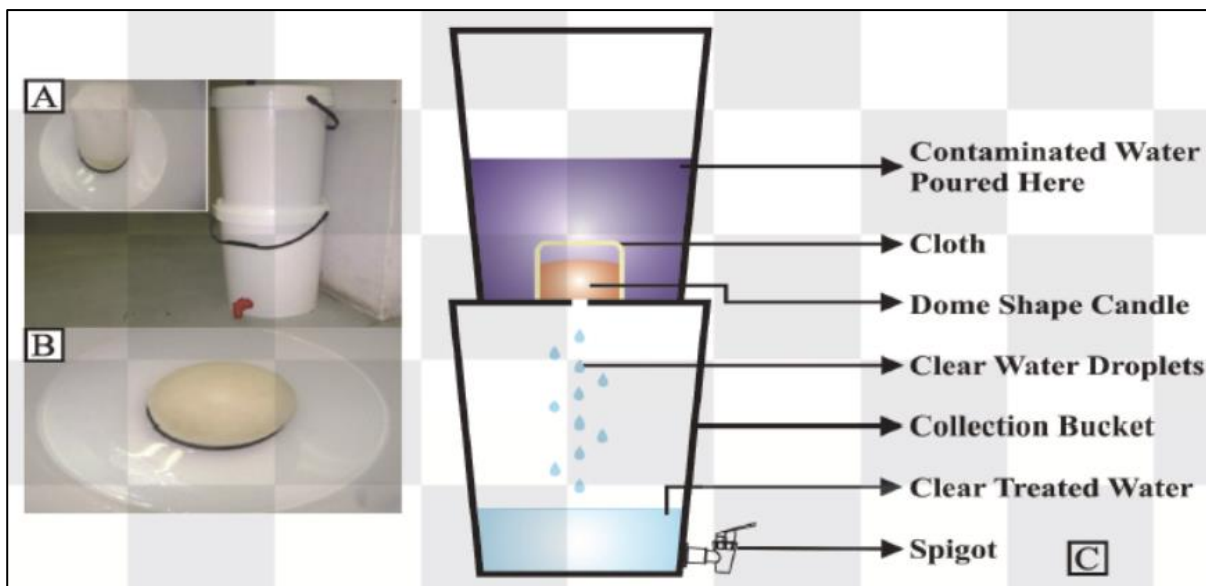


Figure 2.12. A CCF unit: A – outside view of the filter with inset (dome-shaped filter covered with a cloth); B – dome-shaped filter; C – skeletal view of CCF showing the internal content of the complete filter unit (Momba et al., 2013)

According to the authors all materials for construction of these devices were obtained locally except for CCF. The cost of the devices varied from R133-500 (USD 16-64). The filters were assessed for removal of pathogens, physical parameters and chemical constituents such as iron, arsenic, phosphates, calcium, nitrates and fluorides. All devices were able to remove selected chemical constituents to below South African national standard (SANS) 241 drinking water quality specifications (SANS 241: 2015). Of importance to this study is the efficiency of the BSF-S, SIPP, CCF and BF in the removal of F^- and other chemical constituents. This study points out the strong potential of clay materials locally sourced in South Africa to be successfully used in fabrication of household water treatment devices that are easy to operate and can treat water over an extended period of time.

2.7 SUMMARY

The literature review shows that high fluoride levels in groundwater is a worldwide problem and more so in developing countries whose largely rural population still lack continuous supply of clean piped drinking water. In South Africa, studies have revealed and delineated the regions with high fluoride concentrations in groundwater. The authors were able to delineate regions/areas with higher fluoride concentrations or lower than that recommended for drinking water. They also delineated occurrence of dental fluorosis in selected provinces. The authors pointed out that problems of high fluoride ion concentrations are concentrated in Limpopo, Northern Cape, North-West, and KwaZulu-Natal provinces. These provinces have high populations still living in rural areas and dependent on groundwater for drinking purposes. Limpopo, Northern Cape, KwaZulu-Natal and Eastern Cape were noted to have fluoride ion concentration in groundwater of greater than 8 mg/l. Most of these areas were observed to be endemic in fluorosis. A link was established between the high fluoride levels in groundwater, the consumption of this high fluoride groundwater and occurrence of dental fluorosis in the affected areas. A further scrutiny of the data showed that in provinces where communities depended largely on groundwater for drinking purposes such as North-West province, the morbidity of dental fluorosis was very high.

In the North-West Province a percentage morbidity of dental fluorosis as high as 97% has been recorded. Moreover, the evidence from the data presented in the reviewed studies in South Africa confirms that this is prevalent in rural communities that are dependent on groundwater for drinking purposes. Several options are suggested to address this challenge. This includes:

- Partial defluoridation of the groundwater sources if used for drinking purposes (for example the case of Siloam village in Limpopo Province)
- Development of alternative water supplies

For partial defluoridation of the groundwater, cheap and technologically simple processes, that can be operated with minimal challenges by rural community members needs to be developed.

Momba et al. (2013) brought out clearly the water supply situation in peri-urban and rural areas of South Africa. The authors point out that an estimated 5 million people in South Africa have no access to treated potable water within a reasonable distance from their dwellings. Lack of water supply is particularly acute in peri-urban and in scattered rural areas. It is this category of population that would rely on unsuitable water sources such as high fluoride groundwater. The authors further suggest that new approach to treat and deliver safe drinking water in the rural and peri-urban communities would be treatment at household level such as point of use (POP) systems which would be particularly suitable in geographically isolated regions. Numerous literature sources reveal numerous attempts at developing technologies for removal of fluoride from groundwater. The various technologies developed at commercial and bench scale includes: adsorption, ion exchange, precipitation and co-precipitation, electrolysis, donnan dialysis, electro dialysis and recently reverse osmosis and nanofiltration. Other techniques developed involve contact precipitation and co-precipitation using lime and alum.

Of the technologies developed so far adsorption has found extensive use and is observed to be the most suitable for household devices and community defluoridation plants. Moreover, research into the techniques available to defluoridate groundwater identified that those methods based on the principals of sorption as the methods most suited to rural and remote locations. The systems are relatively simple, requiring a reactor vessel to contain the media, which once it is exhausted can be regenerated or replaced. The adsorption process may generate little or no toxic pollutants and has low initial capital and operating costs. Adsorption is also safe from the environmental point of view as no sludge is produced. The challenge is to come up with a cheap and reliable adsorbent that has high F⁻ adsorption capacity and can be effectively regenerated.

Literature review further reveals that several locally sourced and fabricated adsorbents such as bone char and activated alumina have been successfully incorporated in domestic defluoridation units (DDU) for household use in communities in countries such as India, China, Tanzania, Ethiopia and Sri Lanka. Other adsorbents developed include layered clays like montmorillonite which have been observed to have low F⁻ adsorption capacity but are abundant and cheap to obtain. Some of the limitations observed for the developed adsorbents include, low adsorption capacity, high F⁻ removal at pH 2 for activated alumina with the process water requiring pH adjustment. Bone char has high adsorption capacity and it is cheap but the final process water quality depends on the method of preparing the bone char otherwise the process water is left with an odour and colour. In addition, bone char is not acceptable to some communities due to socio-cultural reasons. Although high adsorption capacity materials such as Fe-Al-Ce trimetal oxides have been developed, their application in household defluoridators would be prohibitive in terms of capital and running cost for rural communities. One of the important factors for construction and roll out of household water treatment devices in rural communities is cost. The devices use an adsorbent that needs to have an extended usage time, high fluoride adsorption capacity and of low cost.

Several natural clay materials and minerals have been tested internationally (Zevenbergen et al., 1996; Dongre et al., 2006; Sadiju et al., 2008) for defluoridation of groundwater with mixed success. Coetzee et al. (2006), Chibi and Haarhoff (2000) have evaluated the potential of South African clay soils and minerals for defluoridation of groundwater; they observed that some clay soils and minerals have the potential for fluoride adsorption. The authors point out the potential for beneficiation of these clay soils and minerals for improvement of their fluoride adsorption potential. Clay soils and minerals are abundantly available in the local communities which have high fluoride in their groundwater. It has been pointed out that utilization of local available materials in fabrication of fluoride adsorbents lowers the cost of the household defluoridators.

The literature reviewed points out that there are regions in South Africa that have high fluoride in groundwater in concentrations beyond the recommended limits and will require defluoridation. Moreover, a link to dental fluorosis on consumption of this water was established. Clay soils and minerals have been identified as the ideal candidates for fluoride adsorption due to their abundance in the rural communities having high fluoride in their ground water. This study evaluated several types of clay soils and clay minerals available locally in their natural or metal modified form. This includes lateritic soils from Ga-Mashaba village in Limpopo traditionally used for fabrication of ceramic pots and recently ceramic water filters. The study also evaluated the potential of South African bentonite clay, in its natural or metal modified form, diatomaceous earth obtained from suppliers in South Africa in its natural and metal modified form for defluoridation of groundwater.

Table 2-5 shows information on various adsorbents that have been developed and tested for defluoridation of groundwater either at batch scale or domestic defluoridation units (DDU). Table 2-5 shows that various materials have been designed and evaluated for fluoride adsorption in aqueous solutions with mixed success. Materials tested include surface tailored Zeolites, modified chitosans and natural clay materials such as montmorillonite, granular bentonite, humic acids and clays soils. Limitations established with these adsorbents include: low adsorption capacity, discoloration of processed water, low flow rate through the packed adsorbent bed, social-cultural issues, effective pH of adsorption too low, high S/L ratio and high cost of high adsorption capacity synthetic adsorbents such as zeolites.

Table 2.5. The performance of various adsorbents in water defluoridation

Defluoridation technique	Country	Author(s)	Material	F- concentration (mg/ℓ)	Volume of water treated at breakthrough (1.5 mg F/ℓ)	Optimum fluoride removal (%)	Adsorption capacity (mg/g)	Limitations
Adsorption: Batch studies	Malawi	Sadju et al. (2008)	Raw and calcined bauxite (12.5 g/ℓ)	8 reduced to 0.496		93.8 for raw bauxite. 95.3 bauxite calcined at 200°C. Equilibration time: 30 min	0.07504	Low adsorption capacity
Adsorption: Domestic defluoridation unit (DDU)		Sadju et al. (2012)	Raw bauxite (0.150 kg/ℓ)	6.17 reduced to < 1.5	ℓ/kg		≈ 0.1051	1. Very low adsorption capacity. 2. Very low volume of processed water at exhaustion of adsorbent bed. Discoloration of processed water.
Adsorption: Lab test of bucket defluoridator. Field test of bucket defluoridator.	Tanzania	Jacobsen & Dahi (1997)	Bone char (10 kg)	8.5 reduced to 0.37 (Lab test) 10.5 reduced to < 1 (Field test)	≈ 195 ℓ/kg	95.6 for a period of 2 months. 90% for 4 to 13 months.	1.1	1. Low adsorption capacity. 2. Treated water discoloration for the first few days. 3. Slow discharge from tap.
Adsorption: Household bone char filter		Mjengera & Mkongo (2003)	Bone char (4 kg)	11.7 reduced to ≈ 2	> 7,000 ℓ		17.0	Need to waste some batches of discoloured treated water from a fresh packed column.

column defluoridator.								
Adsorption: Lab test of DDU's on simulated water. Lab test of DDU's on natural waters.	India	Venkobachar et al. (1997)	Different grades of activated alumina, AA (3 kg).	10 reduced to 1.5 (3.3-17.0) reduced to < 1.5	500-800 ℓ 185-1300 ℓ		1.417-2.267	1. Low adsorption capacity. 2. Defluoridation cycle is affected by raw water alkalinity. Bone char is rejected by the Hindus for socio-cultural reasons.
Adsorption: Batch adsorption.		Tembhurkar & Dongre (2006)	Activated carbon (24 g/ℓ)	5 reduced to 0.38	-	92.5 at pH 2	0.1927	1. Low adsorption capacity. 2. pH for effective adsorption is too low.
Adsorption: Batch method		Karthikeyan et al. (2005)	Montmorillonite clay (70 g/ℓ)	3	-	97 at pH 2, 82 at pH 7	0.0416	Low adsorption capacity.
Adsorption: Batch studies Fixed-bed column		Ghorai & Pant (2004)	Activated alumina (4 g/ℓ)	13.5 5		92 at flow rate of 20 ml/min 86 at flow rate of 30 ml/min	1.450 mg/g	Low adsorption capacity.
Adsorption: Batch & column studies Adsorption: Batch studies	Kenya	Murugan & Subramanian (2006) Zevenbergen et al. (1996)	Tamarind seed (2 g/ℓ) for batch studies Ando soil (40 g/ℓ)			68.1 for batch studies at pH 7.	18 Adsorption increased with F-concentration	Leaching of polysaccharide into drinking water. Limited supply of the seed.
Adsorption: Batch studies		Wambu et al. (2011)	Acid-treated diatomaceous earth (500 g/ℓ)	1000		100 at 313 K		Large mass of adsorbent was used

								Need to examine defluoridation at normal groundwater F-concentration.
Adsorption: Fixed-bed column	South Africa	Onyango et al. (2009)	Surface-tailored zeolite (12.3 g/column) Adsorbent types: Al-F9 & Al-HUD	10	5.79 l for Al-F9 5.90 l for Al-HUD pH= 6.4, flow velocity= 4.87 x 10 ⁻² cm/s			The zeolite used was a synthetic adsorbent, so cost may be a hindrance.
Adsorption: Small-scale continuous flow column test for point-of-use systems		Murutu et al. (2012)	Phosphoric acid treated limestone (20 g)	10 reduced to 0.75 (break-through)	At 5 ml/min flow rate, V _b = 1,170 ml for 20 g bed; 1,740 ml for 30 g and 2,220 ml for 40 g. V _b increased with adsorbent mass/bed height; decreased with influent F-concentration and flow rate.			Low adsorption capacity.
Adsorption: Batch studies	Turkey	Tor (2006)	Montmorillonite (10 g/l)	20		≈ 49 at pH 6, 700 rpm, 298 K and 3 h of shaking		Low adsorption capacity.
Adsorption : Batch studies	Cameroon	Bjorvatn & Bardsen (1995)	Activated clay (100 g/l) Types: Humic and non-humic	5.47 to 0.09 for non-humus laterite 5.42 to 0.48 for		98.4 for non-humus laterite 91.1 for humus laterite. Contact time: 72 h	0.0538 0.0499	Low adsorption capacity

				humus laterite				
Adsorption: Batch studies Column studies	China	Ma et al. (2011)	Granular acid-bentonite (30 g/l)	5			Optimum value of 0.103 at initial pH of 6.28	Low adsorption capacity
Adsorption: Batch studies Column studies		Wu et al. (2007)	Fe-Al-Ce trimetal oxide (150 mg/l) 5 ml of pellets	84.5 5.5	 2,240 bed volumes at breakthrough of 1 mg/l	68.4	178 mg/g at pH 7 Accumulated adsorption capacity = 19 mg/g	Cost of producing bulk adsorbent for defluoridation at household levels.
Adsorption: Batch studies		Zhang et al. (2009)	Mn and Al salts modified attapulgite. Modification mass ratios of attapulgite: Mn ²⁺ :Al ³⁺ = 2:2:1, 2:1:2 & 4:3:3			Optimum F-removal for the modification mass ratio 2:1:2.	Optimum adsorption capacity for modified adsorbent of ratio 2:1:2 at 313 K.	
Defluoridation technique	Country	Author(s)	Material	F-concentration (mg/l)	Volume of water treated at breakthrough (1.5 mg F/l)	Optimum fluoride removal (%)	Adsorption capacity (mg/g)	Limitations
Adsorption: Batch studies	China	Yao et al. (2009)	Neodymium-modified chitosan (2 g/l)	20 reduced to 0.37		98.15 at pH 7, temperature 323 K and particle size 0.10 mm and contact time of 24 h.	9.815	Water quality after defluoridation was not accessed. There could be possibility of leaching of adsorbent groups into water.

3 FIELD GROUNDWATER SAMPLING AND CHARACTERIZATION

3.1 SAMPLE COLLECTION AND CHARACTERIZATION

3.1.1 Sampling Sites

Field groundwater samples were collected from various sites in various districts of Limpopo province to access their physicochemical properties with a special focus on fluoride levels. Samples were collected from the following sites Muraleni; Ga-Masemola (Ga-Sefoka, Molebeledi, Selolo and Nyala magnesium mine); Matlala (Phetole and Madietane) and Niani (Dambale, Tshikunda Malema and Zwigodini Malifa). Figure 3.1 below shows the location of the sampling sites

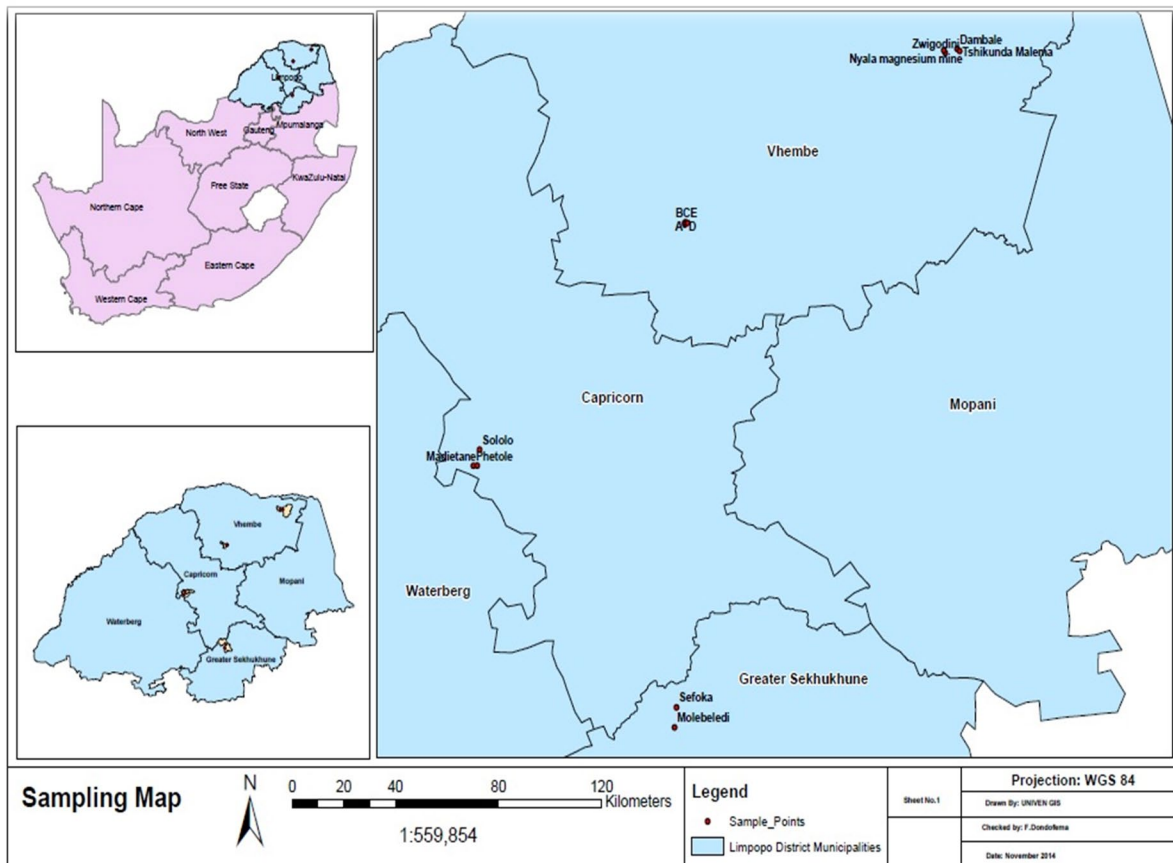


Figure 3.1. Field groundwater sampling sites in various sites in various districts of Limpopo Province

3.1.2 Sample collection and analysis

Samples were collected in selected boreholes in 1 l high density polyethylene bottles. pH, EC, TDS and temperature were immediately recorded in the field. Samples were stored in ice in cooler boxes and transported to the laboratory where they were stored in the fridge at 4°C until analysis for anions and cations. Samples for cation analysis were acidified to pH<2 by adding two drops of HNO₃ acid to minimize microbial activity. Metal species analysis was carried out at University of Stellenbosch Analytical Facility using ICP-MS for major metal species and ICP-AES for major metal species. Anionic species were analysed at both University of Venda laboratory using Metrohm 850 professional IC and University of Stellenbosch using a dionex Ion Chromatography on a Waters 432 Conductivity detector, coupled to a Waters 717plus Auto sampler and an Agilent 1100 series binary pump.

3.2 RESULTS AND DISCUSSION

3.2.1 Overview

The physicochemical properties of field groundwater samples from various boreholes in various districts of Limpopo province are presented in Table 3.1. Most of the groundwater was observed to be saline with high concentrations of alkaline (Na, K) and alkaline metal species (Ca, Mg), high anionic species concentrations (Cl⁻, SO₄²⁻, NO₃⁻). This was consistent with community members' comments and observation that the water tasted salty. Most of the borehole sampled registered less than 1 mg/l F⁻ but some of the boreholes had F⁻ concentrations greater than the SANS-241-1 (2015) recommended guideline for drinking water (1.5 mg/l) and will require partial defluoridation. pH of the sampled borehole ranges from 7-8 which is within the recommended guidelines for drinking water.

3.2.2 Physicochemical and hydrochemical profiles

The results of physicochemical properties and hydrochemical analysis are shown in the Table 3.1. The pH of the analysed water samples varied from 4.24 to 9.61 with mean value of 7.38 while temperature ranged between 19°C and 24.4°C with a mean of 22.45°C, which reflects the average air temperature during the sampling period. The pH values revealed the analysed water from the study area is acidic to slightly alkaline. Correlation matrix revealed strong correlation of pH with HCO₃⁻, SO₄²⁻ and TDS (Table 3.2). Temperature and pH influence dissolution and precipitation of minerals in surface and ground water. Accordingly, the average pH value (\cong 7.38) is indicative of the presence of dissolved anions that existed entirely as chloride and bicarbonate ions. The EC of the analysed water varied from 0.10 to 2.69 μ S/cm with a mean of 2.22 μ S/cm while TDS ranged between 7.57 mg/l and 1787 mg/l with a mean of 697.03 mg/l. Correlation matrix showed strong association of EC with Mg²⁺, Na⁺, K⁺, NO₃⁻, F⁻, SO₄²⁻ and Cl⁻, while TDS correlate with Ca²⁺, Mg²⁺, K⁺, NO₃⁻, HCO₃⁻ and SO₄²⁻. Forty percent of the samples analysed had the total dissolved solids value less than 1000 mg/l ranging from 7.57 to 586.7 mg/l. The low TDSs are indications of low mineralized water with limited migratory history and water-rock interactions (Talabi and Tijani, 2013).

Magnesium ion concentration ranged from 0.19 mg/l to 142.4 mg/l (\cong 86.47 mg/l). This was followed by calcium ion concentration which ranged between 1.4 mg/l and 142.4 mg/l (\cong 71.41 mg/l). With respect to the alkali metals, Na⁺ is the dominant ion with concentration ranging from 65.92 mg/l to 1616 mg/l with an average value of 304.89 mg/l, while K⁺ varied between 0.04 mg/l and 20.38 mg/l with an average value of 4.25 mg/l. Iron concentration varied between 1.84 mg/l and 7137 mg/l with an average of 657.1 mg/l while manganese ion ranged from 0.28 mg/l to 284.6 mg/l with an average value of 21.76 mg/l.

Table 3.1. Physicochemical properties of field groundwater samples

Major cationic species concentration (mg/ ℓ)																
species	Error (%)	Muraleni A	Muraleni B	Muraleni C	Muraleni D	Muraleni E	Dambale	Tshikiunda Malema	Zwigodini	Nyala	Pethole	Madietale	Selolo P	Selolo C	Sefoka	Molebeledi
Ba	4.33	0.03	0.02	0.08	0.05	0.07	0.0661	0.0034	0.0583	0.0241	0.1302	0.1643	0.2838	0.0484	0.0799	0.027
Ca	12.47	105.20	124.70	122.10	142.40	108.10	10.36	1.136	35.34	50.48	95.74	58.13	80.15	69.79	19.18	48.41
K	0.96	2.61	2.09	20.38	2.14	3.65	9.775	1.327	1.927	5.919	2.015	1.838	4.583	2.641	2.805	0.0435
Mg	1.68	106.40	83.96	118.30	141.10	134.30	304.9	0.189	19.3	147.2	68.09	48	52.65	40.63	11.91	17.16
Na	4.71	252.80	222.30	268.10	222.50	228.80	1616	65.92	87.09	148.1	334.6	271	324.6	283.9	175.2	72.51
Minor cationic species concentration (µg/ ℓ)																
Al	6.98	10.68	2.88	4.41	4.11	2.21	4.99	11.06	1.68	57.20	3.04	4.59	3.20	3.33	5.66	8.36
V	2.14	11.33	8.50	14.26	12.35	18.67	36.93	0.19	0.71	14.65	17.44	25.01	11.17	7.78	0.76	6.12
Cr	0.11	0.51	0.13	0.60	0.24	1.09	0.68	0.13	0.24	4.64	0.76	0.48	0.51	0.23	1.27	0.08
Mn	1.17	0.52	0.66	24.05	0.39	0.51	2.68	0.34	1.41	284.64	0.53	0.79	0.39	0.92	0.28	8.24
Fe	1.93	6.74	12.73	17.12	4.67	1.80	6.04	7.28	< 1.5	7137.00	1.51	10.36	24.23	< 1.5	< 1.5	< 1.5
Co	6.53	< 0.5	< 0.5	< 0.5	< 0.5	< 0.5	< 0.5	< 0.5	< 0.5	1.04	< 0.5	< 0.5	< 0.5	< 0.5	< 0.5	< 0.5
Ni	4.08	0.63	< 0.1	1.55	0.42	0.23	0.91	< 0.1	< 0.1	12.11	0.21	0.22	0.09	0.17	< 0.1	0.28
Cu	0.41	5.91	< 1	7.20	< 1	< 1	3.98	< 1	< 1	334.13	< 1	< 1	< 1	< 1	< 1	< 1
Zn	3.64	7.30	7.74	8.01	5.97	18.20	1.15	3.02	14.87	3755.00	14.65	751.18	14.92	122.10	12.31	384.89
As	3.16	0.18	0.10	0.24	0.18	0.24	3.89	3.14	0.82	1.70	0.56	0.63	0.72	0.34	0.31	0.51
Se	5.32	1.81	3.40	3.96	1.65	7.31	4.34	0.00	0.22	1.02	2.90	2.09	1.59	2.17	2.72	0.04
Mo	2.00	1.31	0.82	0.97	0.83	3.08	1.73	0.82	0.32	1.78	6.03	3.15	6.58	5.89	1.58	0.35
Cd	1.96	0.046	0.03	0.02	0.04	0.007	0.008	0.006	0.005	0.090	0.022	0.048	0.011	0.036	0.061	0.042
Sb	1.53	0.051	0.02	0.03	0.01	<0.000	0.067	0.097	0.005	0.190	0.003	0.008	0.010	0.052	0.020	0.020
Ba	1.90	29.634	22.86	84.46	47.57	78.59	70.73	3.38	58.65	24.11	132.37	163.01	288.71	50.25	81.46	27.03
Hg	1.75	0.018	0.01	0.02	0.02	0.02	0.036	0.011	0.013	0.014	0.065	0.020	0.018	0.018	0.011	0.009
Pb	1.80	0.988	0.56	0.37	0.52	1.19	0.362	0.961	0.097	16.901	0.458	5.216	0.488	0.204	0.169	0.321
Anionic species concentration (mg/ ℓ) and pH																
Cl ⁻		337.84	287.6	372.65	478.47	444.91	3140.6	38.57	104.2	190.86	255.21	257.15	348.4	343.42	138.32	62.5
NO ₃ ⁻		465.37	384.76	507.82	439.35	227.18	ND	ND	8.52	255.12	478.57	217.02	267.29	123.97	64.47	46.46
SO ₄ ²⁻		119.72	110.08	129.21	104.16	183.53	46.98	ND	17.60	28.35	92.48	32.98	ND	24.51	46.33	52.89
F ⁻		0.3	0.42	0.33	0.29	0.28	2.3	0.85	0.49	0.89	2.7	2.2	2.4	2.4	3.2	1.1
pH		7.09	7.27	7.85	7.09	7.28	7.24	9.55	7.26	6.92	7.48	7.1	7.35	7.35	8.54	7.06

Table 3.2. Pearson's correlation matrix for physicochemical and hydrochemical parameters of studied waters

	Ca ²⁺	Mg ²⁺	Na ⁺	K ⁺	HCO ₃ ⁻	SO ₄ ²⁻	Cl	TDS	EC	pH	Temp °C	Pb ²⁺	Ba ²⁺	Cd ²⁺	Hg ²⁺	As	Se	Cr ²⁺	Zn ²⁺	Mn ²⁺	Al ³⁺	V	
Ca ²⁺	1																						
Mg ²⁺	0.144	1																					
Na ⁺	-0.239	.806**	1																				
K ⁺	0.176	0.483	0.355	1																			
HCO ₃ ⁻	0.492	-0.204	-0.242	0.317	1																		
SO ₄ ²⁻	.762**	0.235	-0.096	0.237	.594*	1																	
Cl	-0.234	.844**	.988**	0.354	-0.232	-0.063	1																
TDS	.914**	0.148	-0.264	0.199	0.314	.726**	-0.276	1															
EC	-0.08	.900**	.964**	0.411	-0.163	0.067	.974**	-0.089	1														
pH	-0.046	-.800**	-.822**	-0.2	0.269	0.106	-.831**	0.057	-.832**	1													
Temp °C	-.780**	-0.076	0.269	-0.238	-.556*	-.823**	0.262	-.803**	0.131	-0.205	1												
Pb ²⁺	-0.132	0.183	-0.129	0.043	-.603*	-0.296	-0.12	0.058	-0.105	0.001	0.135	1											
Ba ²⁺	0.094	-0.079	0.12	0.098	-0.118	-0.03	0.024	0.147	0.012	-0.091	0.008	-0.118	1										
Cd ²⁺	0.055	-0.035	-0.285	-0.098	-0.305	-0.324	-0.288	0.143	-0.27	0.096	-0.175	.688**	-0.231	1									
Hg ²⁺	0.142	0.325	0.432	0.177	-0.102	0.114	0.341	0.215	0.414	-0.322	0.055	-0.125	0.302	-0.235	1								
As	-.701**	0.424	.620*	0.129	-0.467	-0.388	.640*	-.648**	.557*	-0.273	.636*	0.175	-0.157	-0.264	0.126	1							
Se	0.374	.527*	0.392	0.389	0.313	.692**	0.393	0.446	0.474	-0.336	-.547*	-0.174	0.128	-0.255	0.29	-0.121	1						
Cr ²⁺	-0.138	0.275	-0.044	0.162	-.524*	-0.18	-0.036	0.133	0.024	-0.011	0.026	.911**	-0.101	.630**	-0.024	0.156	0.021	1					
Zn ²⁺	-0.161	0.158	-0.141	0.039	-.583*	-0.356	-0.128	0.025	-0.107	-0.011	0.189	.986**	-0.16	.713**	-0.146	0.164	-0.232	.916**	1				
Mn ²⁺	-0.112	0.225	-0.117	0.162	-0.496	-0.265	-0.096	0.097	-0.041	0.005	0.125	.950**	-0.209	.661**	-0.12	0.183	-0.181	.946**	.974**	1			
Al ³⁺	-0.197	0.179	-0.134	0.061	-.542*	-0.278	-0.11	0.009	-0.071	0.06	0.146	.940**	-0.284	.686**	-0.171	0.256	-0.279	.916**	.939**	.975**	1		
V	0.085	.811**	.783**	0.36	-0.302	0.12	.759**	0.076	.756**	-.787**	0.023	0.172	0.265	-0.077	.525*	0.348	.542*	0.147	0.112	0.069	0.017	1	
Fe ²⁺	-0.222	0.157	-0.166	0.048	-0.556	-0.488	-0.142	0.023	-0.101	0.029	0.245	.960**	-0.246	.774**	-0.191	0.164	-0.286	.975**	.980**	.997**	.982**	-0.031	
NO ₃ ⁻	.865**	0.166	-0.164	0.195	0.216	0.574	-0.213	.905**	-0.049	-0.006	-.672**	0.081	0.22	0.222	0.464	-.559*	0.266	0.094	0.04	0.082	0.017	0.202	
F	-0.451	-0.122	0.325	-0.134	-0.333	-0.527	0.213	-0.312	0.153	-0.089	0.327	-0.087	.520*	0.071	0.398	0.154	-0.011	0.009	-0.072	-0.142	-0.145	0.18	

Barium ion concentration ranged from 3.38 mg/l to 288.71 mg/l with an average value of 77.52 mg/l, but Al³⁺ content varied from 1.68 mg/l to 57.20 mg/l with an average of 8.49 mg/l. Chloride is the dominant anion with concentration ranging from 62.5 to 3140.6 mg/l with an average value of 426.71 mg/l. Correlation analysis showed significant positive correlation of chloride ion with Mg²⁺, Na⁺ and K⁺ indicating their existence as MgCl, NaCl and KCl salts. This is followed by SO₄²⁻ concentration which varied between 0.00 mg/l and 183.53 mg/l with an average value of 65.92 mg/l. Sulphate ion showed a strong association with Ca²⁺, Mg²⁺, K⁺ and NO₃⁻, HCO₃⁻ suggesting their existence in form of CaCO₃, MgCO₃.

Hydrogen carbonate concentration varied between 0.0 mg/l and 605.96 mg/l (mean≅21.06 mg/l). Correlation matrix revealed significant positive correlation of HCO₃⁻ with Ca²⁺ and K⁺. In addition, the concentration of cations are in the order of Fe³⁺> Na⁺> Mg²⁺, Ca²⁺> Ba²⁺> K⁺, while anions concentration are in the order of Cl⁻> NO₃⁻> SO₄²⁻> F⁻. Nitrate concentration ranged from 12.28 mg/l to 773 mg/l with an average value of 346.4 mg/l. Nitrate shows strong correlation with such as HCO₃⁻ and SO₄²⁻. Fluoride contents varied between 0.28 mg/l and 3.2 mg/l (mean≅1.34 mg/l). Fluoride have strong association with Na²⁺, Cl⁻, EC, Temp, Ba²⁺, Cd, Hg²⁺, As, Cr and V.

Selenium is the dominant metal species with concentration ranging from 0.17 mg/l to 4.34 mg/l (mean≅ 2.35 mg/l). This is followed by Pb²⁺ concentration which ranged from 0.10 mg/l to 16.90 mg/l (mean≅1.92 mg/l). Arsenic concentration varied between 0.10 mg/l and 3.89 mg/l (mean≅0.90 mg/l), whereas chromium ion concentration ranged from 0.08 mg/l to 4.64 mg/l (mean≅0.77 mg/l). Cadmium concentration ranged between 0.01 mg/l and 0.09 mg/l (mean≅0.03 mg/l). Mercury ion concentration varied from 0.01 mg/l to 0.07 mg/l (mean≅ 0.02 mg/l). The metal species concentration are in the order of Se > Pb > As > Cr > Cd > Hg.

3.2.3 Graphical presentation of Hydrochemical properties of the groundwater

The chemical analysis results of water from the sampled boreholes was processed graphically using Schoeller, Stiff, Piper and Durov diagrams. The graphic representations are used to depict the water-rock interaction and hydrochemical facies which validates the groundwater chemistry.

3.2.3.1 Schoeller and Stiff Diagrams

Geochemistry of both surface and groundwater can be discussed in terms of its major ions. Stiff (1951) diagram is a graphical representation of the different water ions. The average ionic composition analysis by stiff diagram shown in Figure 3-2 and depicts dominance of Na-Cl, while Ca-HCO₃ and Mg-SO₄ are nearly equal in proportion. Schoeller (1977) diagram (Figure 3-2) presents average chemical composition of the groundwater. The relative tendency of ions in mg/l shows Na + K > Ca > Mg and Cl > HCO₃ + CO₃.

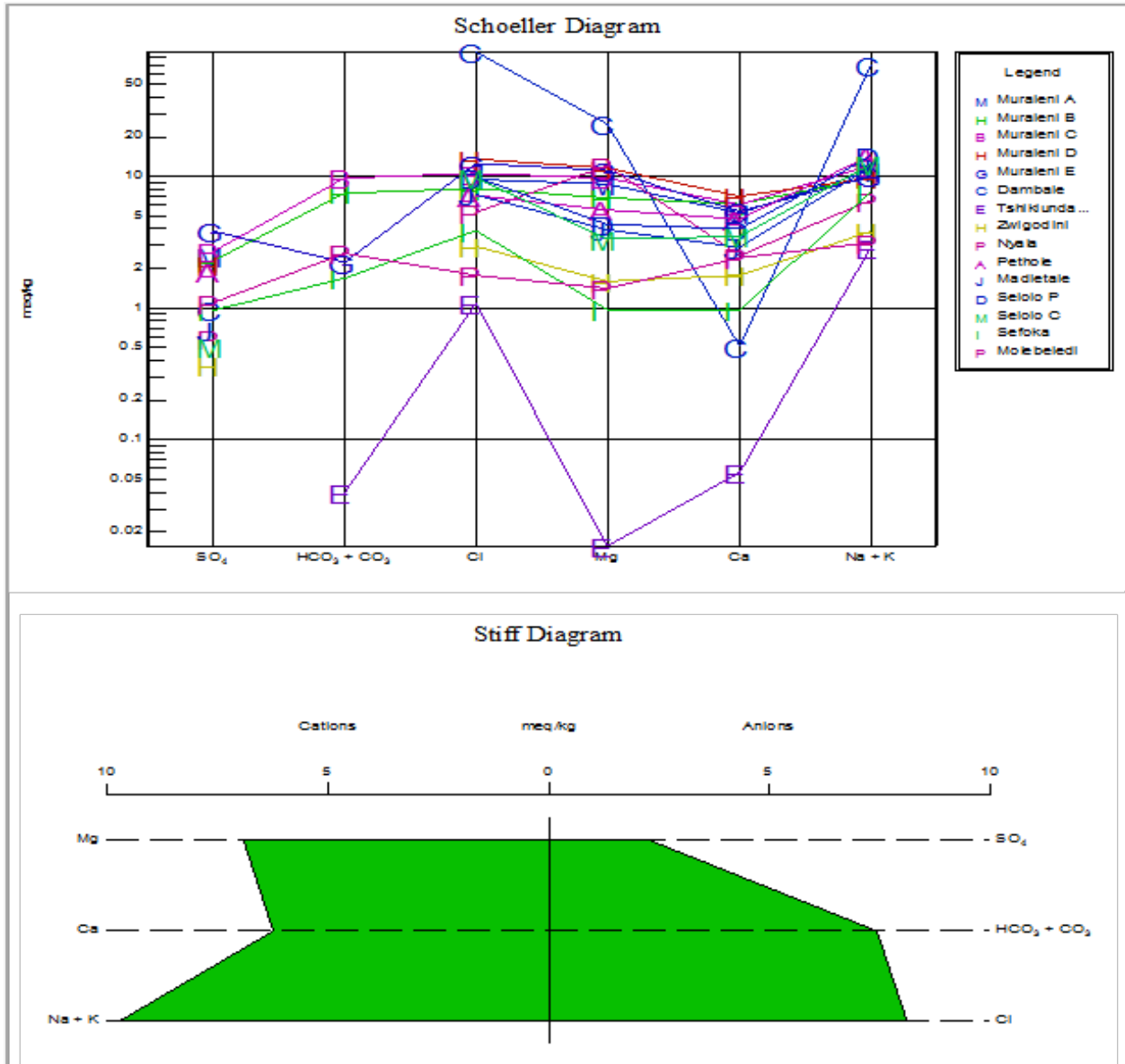


Figure 3.2. Schoeller diagram showing average composition of major cations anions in mg/l and meq/l of the water samples of study areas. Stiff diagram is shown at bottom side

3.2.3.2 Trilinear Diagram (Piper Diagram)

Piper Diagrams (Piper, 1944), are a combination anion and cation triangles that lie on a common baseline. Diamond shape between them can be used to make a tentative conclusion as to the origin of the water represented by the analysis and to characterize different water types. Piper diagram divides waters into four basic types according to their placement near the four corners of the diamond. Figure 3-3 shows representation of the chemistry of the groundwater in a piper diagram while Table 3-3 shows the various hydrochemical facies. The piper diagrams were generated using RockWare Aq.QA software (version 1.5.0). Water that plots at the

top of the diamond is high in $\text{Ca}^{2+} + \text{Mg}^{2+}$ and $\text{Cl}^- + \text{SO}_4^{2-}$, which results in region of permanent hardness. The water that plots near the left corner is rich in $\text{Ca}^{2+} + \text{Mg}^{2+}$ and HCO_3^- and is the region of water of temporary hardness.

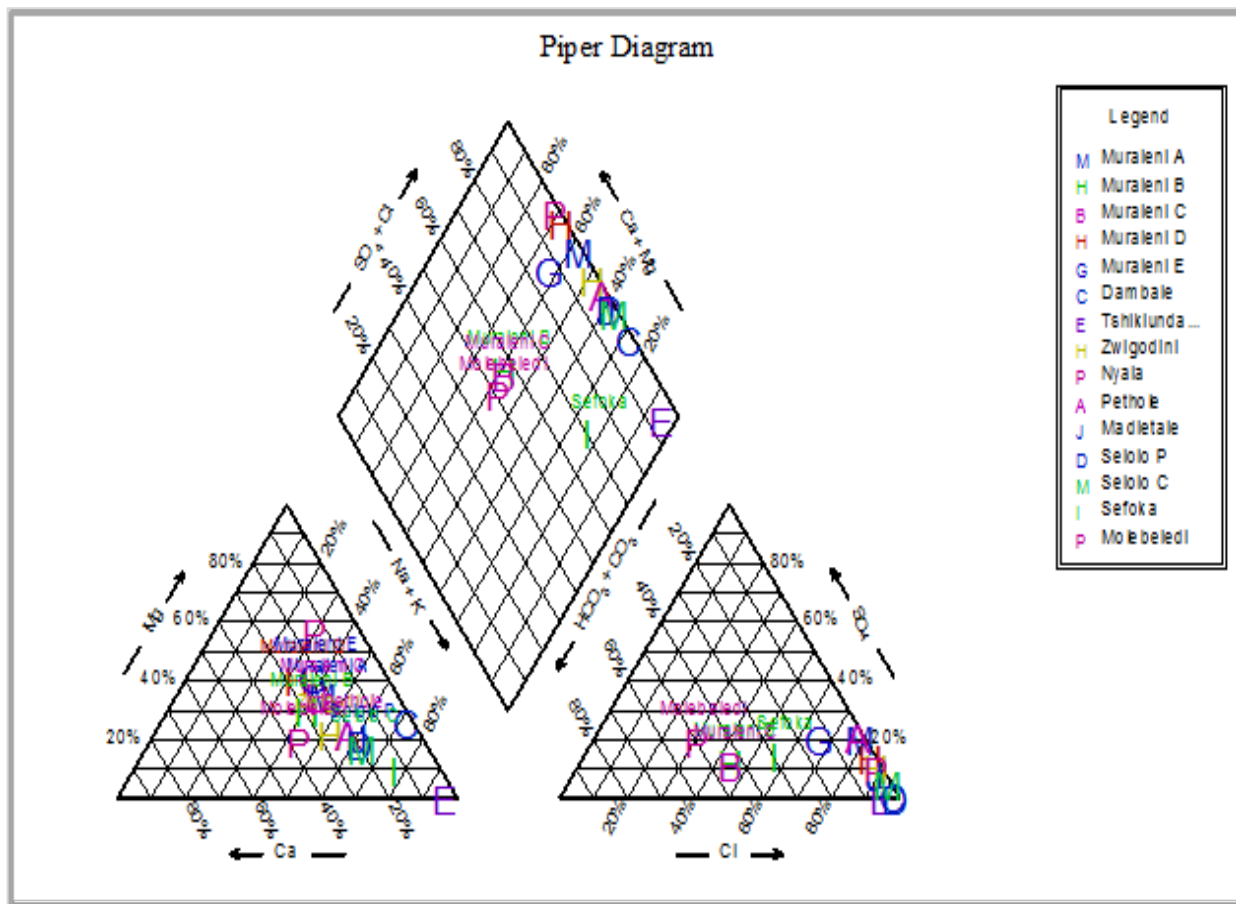


Figure 3.3. Piper Trilinear diagram depicting hydrochemical facies of the study areas.

Water plotted at the lower corner of the diamond is primarily composed of alkali carbonates ($\text{Na}^+ + \text{K}^+$ and $\text{HCO}_3^- + \text{CO}_3^{2-}$). Water lying near the right-hand side of the diamond may be considered saline ($\text{Na}^+ + \text{K}^+$ and $\text{Cl}^- + \text{SO}_4^{2-}$) (Ghoraba and Khan, 2013). Figure 3-3 depicts five different groups of samples that have been summarized in Table 3-3. About 13.33% occupy middle upper side of the diamond shape. This group indicates mixed water (chloride-zinc, chloride-iron water type). Over seventy nine percent of samples occupy the upper corner of the diamond shape, these samples belong to chloride-sodium and chloride-magnesium water type). Nonetheless, 6.67% of samples has a slight individualization of different facies (Table 3-3 and Figure 3-3).

Table 3.3. Hydrogeochemical facies as worked out by Piper diagram and irrigation waters analysis

Locations	Facies type	SH	SAR	ESR	MH
Muraleni A	Na - Cl	Low	4.15	0.17	62.5
Muraleni B	Na - Cl	"	3.77	0.74	52.6
Muraleni C	Na - Cl	"	4.14	0.74	61.5
Muraleni D	Mg - Cl	"	3.16	0.52	62
Muraleni E	Mg - Cl	"	3.47	0.61	67.2
Dambale	Na - Cl	"	19.6	2.75	98
Tshikiunda	Na - Cl	"	15.1	39.69	21.5
Malema					
Zwigodini	Na - Cl	"	2.92	1.13	47.4
Nyala	Fe -Cl	"	2.38	0.44	82.8
Pethole	Na - Cl	"	6.39	1.4	54
Madietale	Zn - Cl	"	6.36	1.72	57.7
Selolo P	Na - Cl	"	6.91	1.7	52
Selolo C	Na - Cl	"	6.68	1.81	49
Sefoka	Na - Cl	"	7.74	3.93	50.6
Molebeledi	Zn - HCO ₃	"	2.28	0.82	36.9

SH = Salinity hazard; SAR = Sodium absorption ratio; ESR = Exchangeable sodium ratio; MH = Magnesium hazard.

3.2.3.3 Durov Diagram

Durov (1948) diagram provides more information on the hydrochemical facies, identifies the water types and can also illustrate some possible geochemical processes that could explain groundwater quality and its evolution. The diagram is a composite plot consisting of 2 ternary diagrams where the cations of interest are plotted against the anions of interest; the sides form a binary plot of total cation versus total anion concentrations, expanded version includes electrical conductivity ($\mu\text{S}/\text{cm}$) and pH data added to the sides of the binary plot to allow further comparisons. The Durov Diagram for the major cations and anions was plotted using RockWare Aq.QA software (version 1.5.0) as represented in Figure 3-4. The Durov plot indicates that most of the samples are in the phase of ion exchange and reverse ion exchange with few in mixing dissolution phase. The pH part of the plot reveals that the groundwater is alkaline. The electrical conductivity of most of the surface water samples lies within the drinking water range (SANS 241-1, 2015).

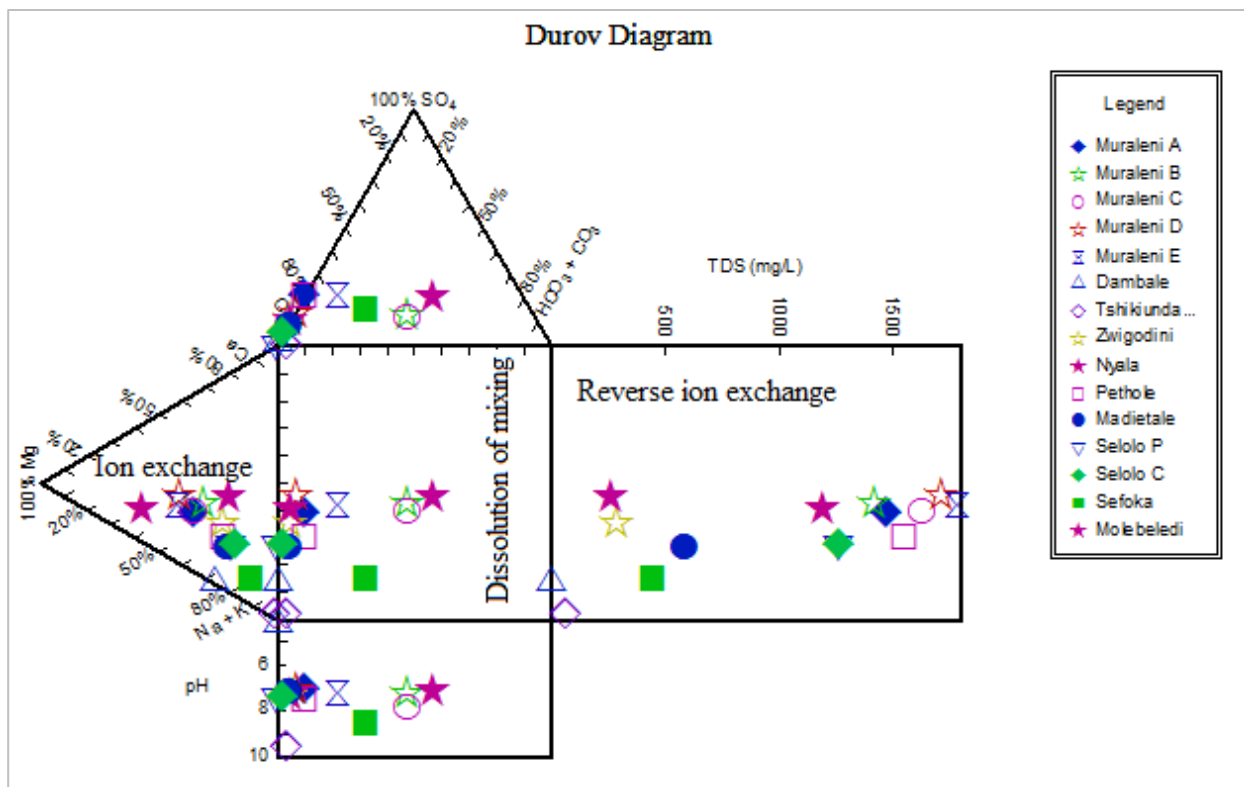


Figure 3.1. Durov diagram depicting geochemical processes in the groundwater

3.2.4 Principal component analysis of water samples

The increase in the degree of physical mixing of the water body with the pollutants (i.e. heavy metals had introduced changes in parameters' patterns. Despite this, five clusters of parameters that are controlling the distribution of anions and cations in the water body was identified from the principal component analysis (PCA). (Table 3.4). First component (i.e. PC1) contributes 39.96% to the total data variation in the water body from these sample locations. PC1 reveals higher loadings of the variables such as Mg^{2+} , Na^+ , Cl^- , EC, As and V which suggest that the sodium chloride salt is controlling distribution of the cations in the water (Table 3-2). Second component (i.e. PC2) accounts for 32.8% of the total variance and comprises higher loadings of Mn^{2+} , Pb^{2+} , Cd^{2+} , Cr^{2+} , Zn^{2+} , Al^{3+} and Fe^{2+} . This observed trend corroborates the correlation matrix (Table 3.2A). Third component (i.e. PC3) contains 12.12% of total variation. Third component reveals higher loadings of F^- , V, Hg^{2+} , Ba^{2+} and lower loadings of temperature. Fourth component (i.e. PC4) contributes 5.54% of the total variance and comprises higher loadings of K^+ and Se with lower loadings of SO_4^{2-} and HCO_3^- indicating the pH of the sampled water are principally controlled by these anions. Fifth component (i.e. PC5) accounts for 1.13% of the total data variation and comprises of lower loadings of Hg^{2+} and NO_3^- indicating they have similar sources.

Table 3.4. Principal Component Analysis of site variation using water quality parameter

Variables	PC1	PC2	PC3	PC4	PC5	Communalities
Ca ²⁺	-0.753	-0.413	-0.412			0.964
Mg ²⁺	0.909					0.959
Na ⁺	0.960					0.999
K ⁺				0.742		0.599
HCO ₃ ⁻		-0.607		0.445		0.812
SO ₄ ²⁻	-0.431	-0.545		0.498		0.9
Cl ⁻	0.974					0.999
TDS	-0.824					0.922
EC	0.941					0.991
pH	-0.982					0.993
Temp ^{°C}	0.694		0.528			0.964
Pb ²⁺		0.979				0.999
Ba ²⁺			0.892			0.944
Cd ²⁺		0.807		-0.447		0.969
Hg ²⁺			0.769		0.476	0.925
As	0.943					0.999
Se		-0.441		0.631	-0.540	0.903
Cr ²⁺		0.974				0.968
Zn ²⁺		0.991				0.997
Mn ²⁺		0.990				0.996
Al ³⁺		0.983				0.991
V	0.806		0.488			0.973
Fe ²⁺		0.989				0.989
NO ₃ ⁻	-0.800				0.573	0.987
F ⁻			0.882			0.98
EV	9.989	8.192	3.029	1.384	1.128	
VAR (%)	39.956	32.768	12.116	5.536	4.513	
CVAR (%)	39.956	72.725	84.841	90.376	94.889	

3.3 SUMMARY

The physical parameters pH, EC and TDS were within recommended limits by SANS 241-1 (SANS 241-1, 2015) while most chemical parameters of sampled groundwater were above the limits by SANS 241-1 (SANS 241-1, 2015) for drinking water. Na⁺ was observed to be the main cation and while Cl⁻ was the dominant anion. Low TDS indicates low mineralized water with limited migratory history and water-rock interactions. The assessment of the hydrochemical results showed that the surface water systems were fresh, low mineralised and with limited water-rock interactions. The principal hydrochemical facies in the study area were chloride-sodium and chloride-magnesium water type waters. Principal component analysis identified sodium chloride, temperature, sulphate and hydrogen bicarbonate as the main ions controlling the chemistry of the sampled waters.

4 EVALUATION OF GROUNDWATER DEFLUORIDATION BY SILICA-RICH MIXED RED/BLACK MUKONDENI CLAY SOILS

4.1 INTRODUCTION

Clay materials have been identified as appropriate adsorbent mediums for removal of fluoride from groundwater. Mukondeni clay soils are used for pottery making and ceramic water filters and are recently getting more attention in water treatment applications (Abebe et al., 2014; Denga, 2013; Hackett et al., 2013; Tyeryar, 2012). However, there seems to be very few scientific studies done to investigate their physicochemical characteristics and the link to water treatment. Many studies have shown that clay soils are good adsorbents for fluoride removal (Thakre et al., 2010; Karthkeyan et al., 2005; Srimurali et al., 2005). Thus, it becomes significant that the basic characteristics of Mukondeni clay soils are evaluated and their scientific application in the treatment of water be assessed. Moreover, these clay soils are locally and readily available, hence a breakthrough in their ability to remove contaminants from drinking water will come as an advantage to the local communities as this can lead to fabrication of cheap and readily available household defluoridation units. This chapter reports on the preparation of the adsorbent (silica-rich mixed red/black Mukondeni clay soils); physicochemical and mineralogical characterisation of the adsorbent; optimisation of the fluoride adsorption conditions; adsorption capacity, kinetic modelling and mechanisms of fluoride adsorption on red/black Mukondeni clay soils.

4.2 MATERIALS AND METHODS

All chemicals used in the present study were of analytical reagent grade. Silica-rich red/black Mukondeni clay soils were collected from Mukondeni Village in Limpopo province. Fluoride-rich water was collected from a borehole in Siloam village in Limpopo province. Sodium fluoride and (TISAB-III) were obtained from Rochelle Chemicals and Lab Equipment CC, South Africa Ltd. Several techniques were used to characterize the adsorbents (detailed in Appendix A). These included Cation Exchange Capacity (CEC), Point of Zero Charge (PZC), X-ray diffraction (XRD), X-ray fluorescence (XRF), Scanning Electron Microscopy (SEM), Scanning Electron Microscopy coupled with Energy Dispersive Spectroscopy (SEM-EDS), Transmission Electron Microscopy (TEM), Brunauer-Emmett-Teller (BET) and Fourier Transform Infrared (FTIR). Detailed methods for batch and field adsorption studies, as well as data modelling studies are presented in Appendix B and C, respectively.

4.3 PREPARATION OF THE SILICA-RICH RED/BLACK MUKONDENI CLAY SOILS

The silica-rich reddish black Mukondeni clay soils were washed by rinsing with MilliQ water. 200 g of clay soil was washed by 1 l of MilliQ water. The rinsing was done by stirring the mixture for 5 min and then rinsing again with MilliQ water. After that, the mixture was agitated in a reciprocating shaker for 30 min. The samples were then centrifuged for 15 min at 3000 rpm. The supernatant which carried colloidal clay particles was filtered through a 0.45 µm pore cellulose nitrate membranes and the residual clay particles collected. The residual clay

was left to dry in the oven for 12 h at 105°C. After drying the samples were milled into fine powder and passed through a 250 µm sieve.

4.4 CHARACTERISATION OF SILICA-RICH RED/BLACK MUKONDENI CLAY SOILS

4.4.1 X-Ray Diffraction (XRD) analysis

Figure 4.1 shows the XRD spectrum of silica-rich red/black Mukondeni clay soils. Figure 4.2 shows presence of quartz (SiO_2), vermiculite and albite which are $\text{Mg}_3\text{Si}_4\text{O}_{10}(\text{OH})_2$ and $\text{Na,Ca,Al}(\text{Si,Al})_3\text{O}_8$ respectively. Quantitative XRD further confirmed presence of pargasite – $\text{NaCa}_2\text{Mg}_4\text{Al}_3\text{Si}_6\text{O}_{22}(\text{OH})_2$ (3.12%) as the other minor mineral phases in addition to anthophyllite ($\text{Mg}_5\text{Fe}_2\text{Si}_8\text{O}_{22}(\text{OH})_2$) (1.82%).

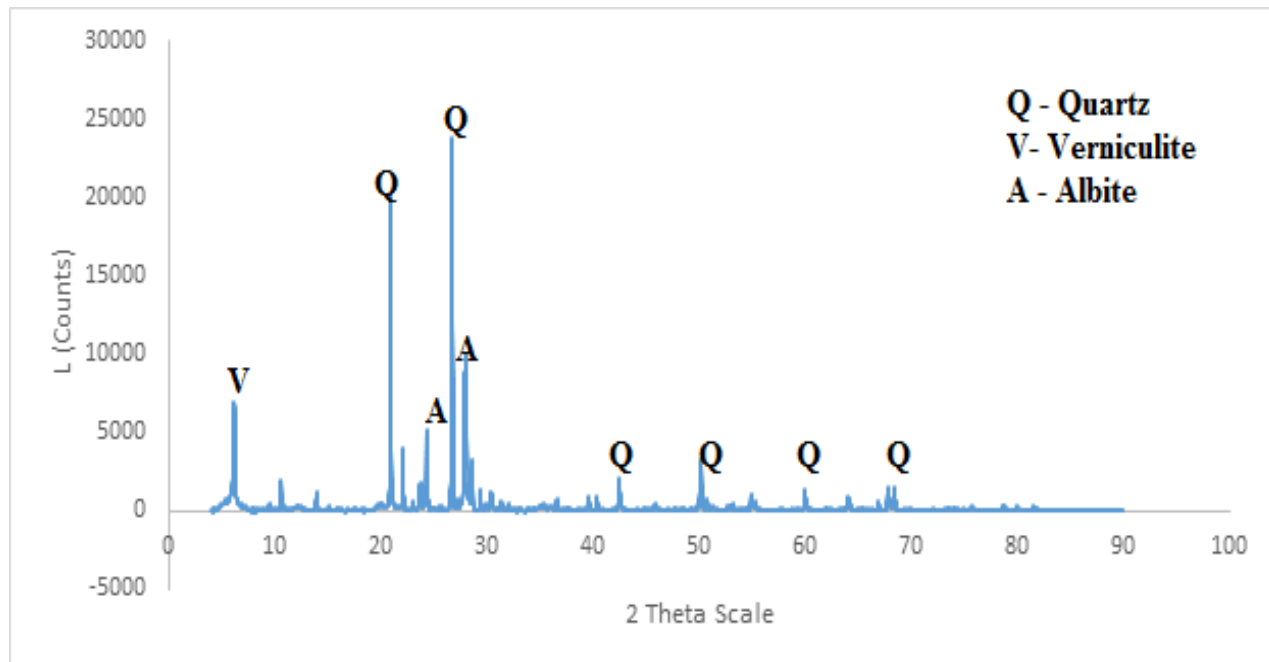


Figure 4.1. XRD diffractogram of silica-rich red/black Mukondeni clay soils.

4.4.2 Cation Exchange Capacity (CEC)

Table 4.1 shows the concentration of exchangeable cations in silica-rich red/black Mukondeni clay soils. Table 4.1 shows the concentration of exchangeable cations in silica-rich reddish black Mukondeni clay soils. The exchangeable cations identified were Na^+ , Ca^{2+} , Mg^{2+} and K^+ . The concentrations of the exchangeable cations were measured in mg/l and then converted to milliequivalent per 100 g ($\text{meq}/100 \text{ g}$) as shown in Table 4.1. The CEC results showed a high concentration of exchangeable Na^+ at both pHs and Ca^{2+} had the least concentration. Since CEC is an intrinsic property of soil defining the concentration of negatively charged sites on soil colloids that can adsorb exchangeable cations, the identified exchangeable cations in silica-rich

Mukondeni clay soils shows that it can be a good material for use in the adsorption process. This clay typically contains SiO₂, Al₂O₃ and oxides of Mg, Ca and K which might contribute towards the fluoride adsorption (Thakre et al., 2011). It is well documented that fluoride has a strong affinity for electropositive species and therefore these cations can enhance the fluoride adsorption.

Table 4.1. CEC of silica-rich reddish black Mukondeni clay soils at pH 5.4 and 7.4

pH	Exchangeable cations				CEC (meq/100 g)
	Na ⁺	K ⁺	Ca ²⁺	Mg ²⁺	Total
5.4	44.79	1.4	0.40	24.00	70.59
7.4	111.30	2.00	0.40	24.00	137.70

4.4.3 Point of zero charge (PZC) of silica-rich reddish black Mukondeni clay soils

Figure 4.2 shows the point of zero charge of silica-rich red/black Mukondeni clay soils. The point of zero charge (PZC) is one of the most important parameters used to describe variable-charge surfaces (Morais et al., 1976). If the pH of a soil is above its PZC the soil surface will have a net negative charge and predominantly exhibit an ability to exchange cations (CEC – exchange of one positive ion by another), while the soil will mainly retain anions (electrostatically) if its pH is below its PZC (AEC – exchange of one negative ion for another) (Appela et al., 2003). Figure 4.1 shows that mixed Mukondeni clay soils have a PZC at pH 6.5 which is slightly acidic. This means that adsorption of anions by mixed Mukondeni clay soils is effective only in acidic conditions below pH 6 since the surfaces will be positively charged.

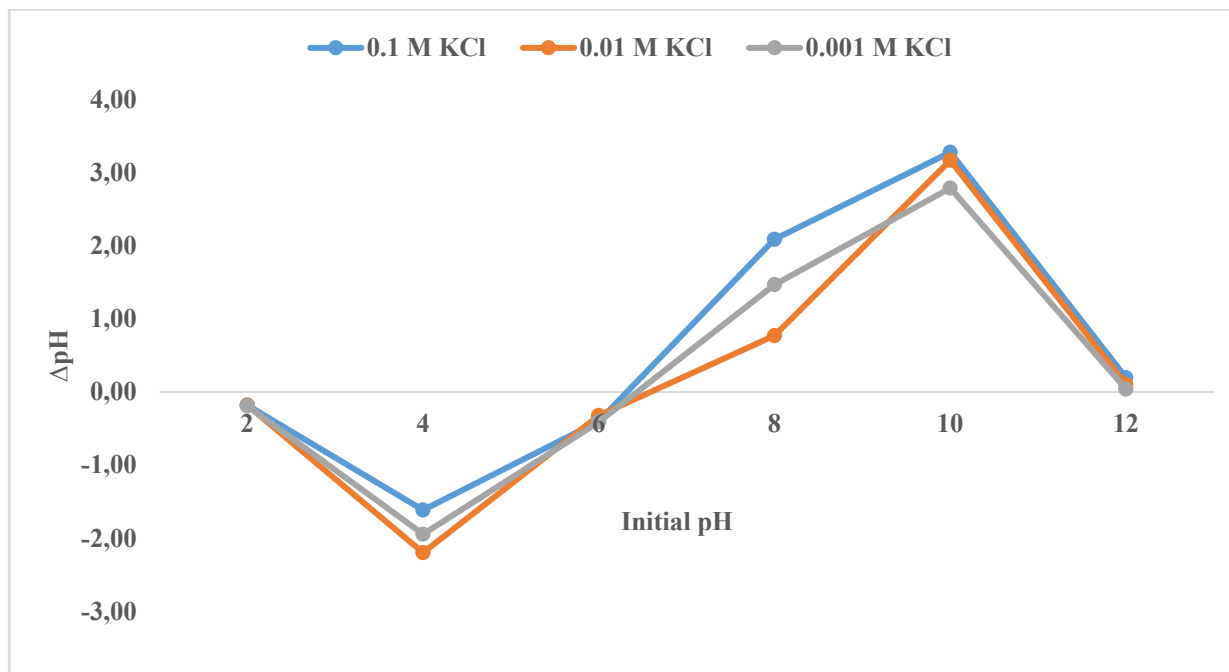


Figure 4.2. Point of zero charge of silica-rich reddish black Mukondeni clay soils

4.4.4 X-Ray Fluorescence (XRF) Analysis

Table 4.2 presents the chemical composition of Mukondeni clay soils. Results show that the clay soils are mainly composed of SiO₂ and Al₂O₃ confirming their alumino-silicate nature.

Table 4.2. Elemental composition of silica-rich reddish black Mukondeni clay soils

Elements as oxides	% w/w
Al ₂ O ₃	14.36
CaO	1.75
Cr ₂ O ₃	0.04
Fe ₂ O ₃	5.52
K ₂ O	0.9
MgO	2.68
MnO	0.08
Na ₂ O	2.53
P ₂ O ₅	0.04
SiO ₂	61.76
TiO ₂	0.57
L.O.I.	9.3
Total	99.53

4.4.5 Scanning Electron Microscopy (SEM) analysis

Figure 4.3 shows the morphology of mixed Mukondeni clay soils at different magnifications before (a) and after defluoridation (b). Examination of the SEM images shows clay particles of varying sizes that do not conform to any pattern of arrangement. Some individual well crystalline pseudo-hexagonal edges of clay particles as well as some roll, rough- and sharp-edged particles are also observed. Figure 4.3a reveals a rough texture with an irregular structure and shapes in the surface morphology.

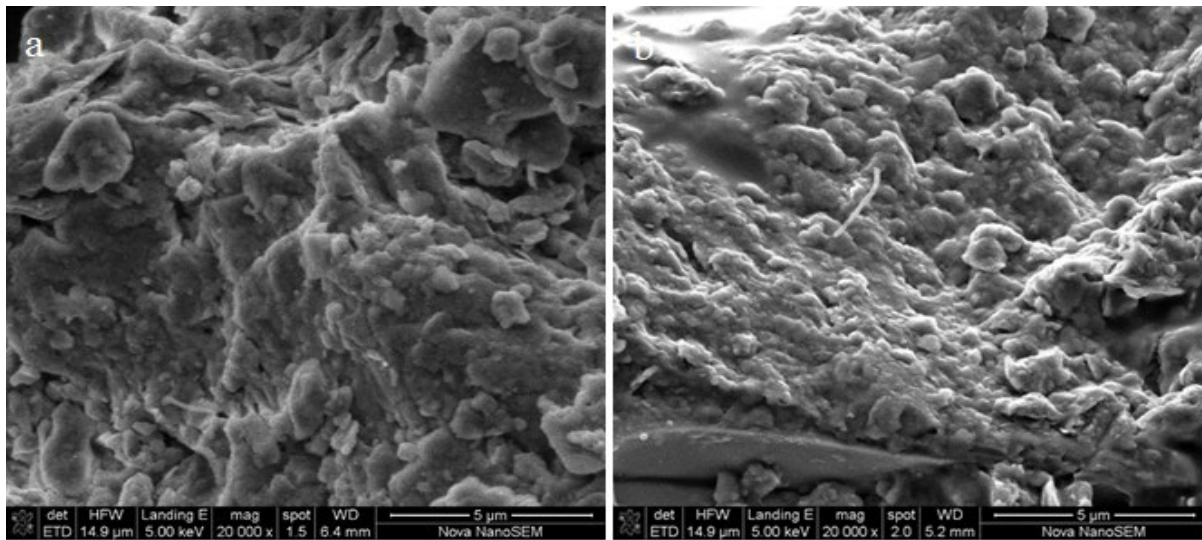


Figure 4.3. SEM images of silica-rich reddish black Mukondeni clay soils before (a) and after (b) defluoridation

However, after defluoridation the clay soils appear to have small particle sizes with undefined shapes (Fig 4.3b). The adsorption of fluoride seemed to have made the clay soils to agglomerate in form of very fine particles clustered together with some appearing threadlike and some having very flat surfaces.

4.4.6 Brunauer-Emmett-Teller (BET) analysis

Surface area is a surface phenomenon and it is dependent upon soil particle size, the smaller the soil particle size the higher the surface area and the bigger the soil particle size the smaller the surface area. In contrast to sand, clay minerals have the smallest particle size which ultimately leads to large surface area. The large specific surface area of clay soils provides sites in which molecules from soil solution can bind through weak van der Waal forces. Clay soils are charged colloid fractions which contain electrostatic surface charge, a property which accounts for adsorption, binding, and exchange of ions and molecules on particle surface (WHO, 2005). Table 4.3 gives the surface area, pore volume and pore size of silica-rich red/black Mukondeni clay soils.

Table 4.3. Surface area, pore volume and pore size of silica-rich red/black Mukondeni clay soils

Parameter	Silica-rich reddish black Mukondeni clay soils
Surface area (m²/g)	
Single point surface area	35.4612
BET Surface Area	43.2077
BJH Adsorption cumulative surface area of pores	30.9090
BJH Desorption cumulative surface area of pores	28.7297
Pore Volume (cm³/g)	
Single point adsorption total pore volume of pores	0.037698
BJH Adsorption cumulative volume of pores	0.035524
BJH Desorption cumulative volume of pores	0.034952
Pore Size (Å)	
Adsorption average pore width (4V/A by BET)	41.8647
BJH Adsorption average pore diameter (4V/A)	45.9720
BJH Desorption average pore diameter (4V/A)	48.6640

The BET-N₂ surface area represents the total surface area (external surface area + micro pore area). Results in Table 4.3 show that silica-rich red/black Mukondeni clay soils has a BET surface area of 35.46 m²/g. The surface area is high compared to typical soils but lower than pure phase goethite and illite, which range from 45 to 169 and 65 to 100 m²/g, respectively (Langmuir, 1997). Compared to other adsorbents used in defluoridation, it has a moderate surface area. A study by Gitari et al. (2013) showed that raw bentonite clay has a surface area of 16,015 m²/g while Goswami and Purkait (2013) used schwertmannite with a surface area of 314.55 m²/g.

Figure 4.4 shows the pore diameters of silica-rich red/black Mukondeni clay soils which helps us to differentiate between the materials in terms of their pores. Most of the particles have pore sizes which fall between 2 and 500 Å (Fig 4.4) meaning that silica-rich red/black Mukondeni clay soils are mesoporous.

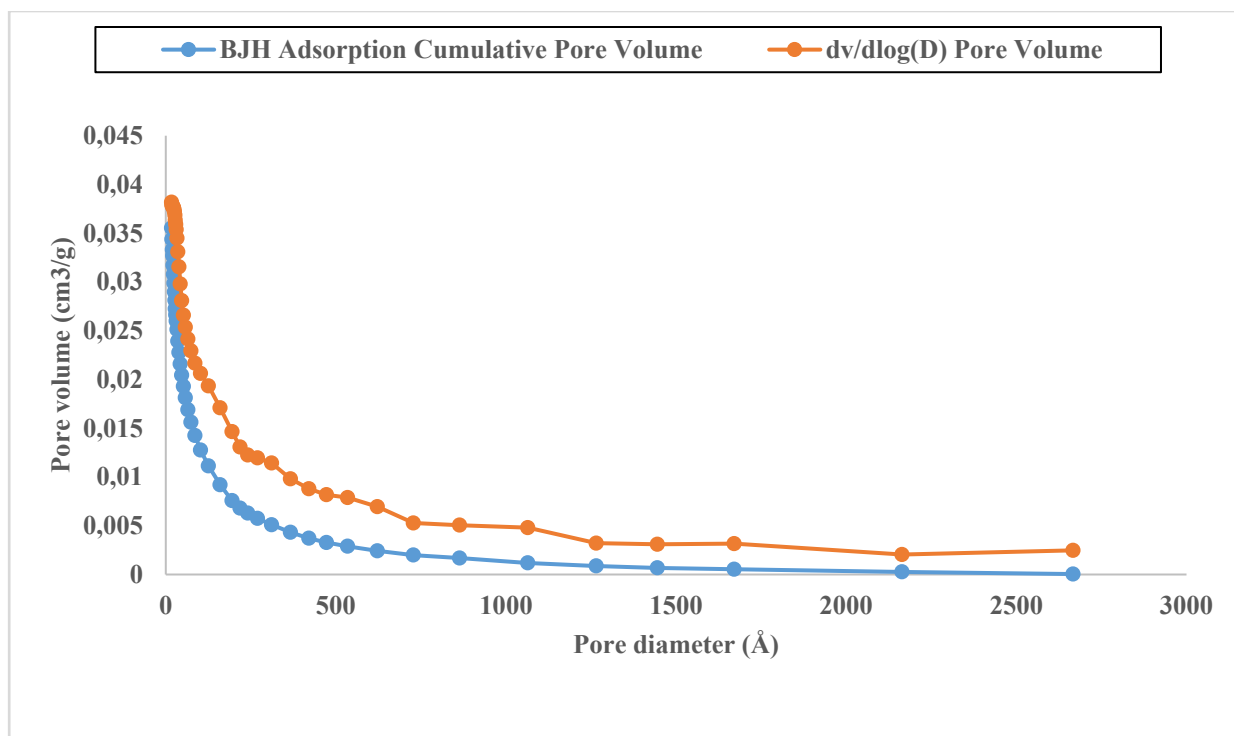


Figure 4.4. Plot of BJH Adsorption $dV/d\log(w)$ and pore volume against pore diameter for silica-rich reddish black Mukondeni clay soils

4.4.7 Fourier Transform Infrared (FTIR) analysis

The FTIR spectra of silica-rich red/black Mukondeni clay soils is shown in Figure 4.5. FTIR spectroscopy was utilized to indicate the functional groups present on the surface of the adsorbent. The pattern of vibration obtained indicates that there are a number of functional groups in the clay material. The FTIR spectra of the samples show a number of sharp and small bands. The presence of absorption bands at 457, 529 and 670 cm^{-1} on the spectrum corresponds to the Si-O-Si bending hence showing that that the material under study is a silicate (Madejova and Komadel, 2001). Silica-rich red/black Mukondeni clay soils showed a very high absorbance at wavelength number 910 and 995 cm^{-1} which corresponds to OH deformations linked to Al^{3+} (Madejova and Komadel, 2001). Peaks at 1635 cm^{-1} indicates presence of H-O-H bonding for water molecules (Yuan-hu et al., 2006). A wide but small absorption band is observed between 3690 and 3370 cm^{-1} which corresponds to a variety of OH bonds like OH stretching and crystalline hydroxyl, H-O-H stretching and absorbed water. The results corroborates the XRD and XRF results confirming that the material under study is an alumino silicate. There is no major difference between the raw clay soils and the fluoride adsorbed clay soils. However, on the fluoride adsorbed clay soils, the transmittance is quite high at $\approx 1000 \text{ cm}^{-1}$. This wavenumber corresponds to various forms of OH groups and that high transmittance is probably due to the OH ions which were exchanged for the fluoride ions during the adsorption process hence the reduction in the amount of OH ions leading to a higher transmittance.

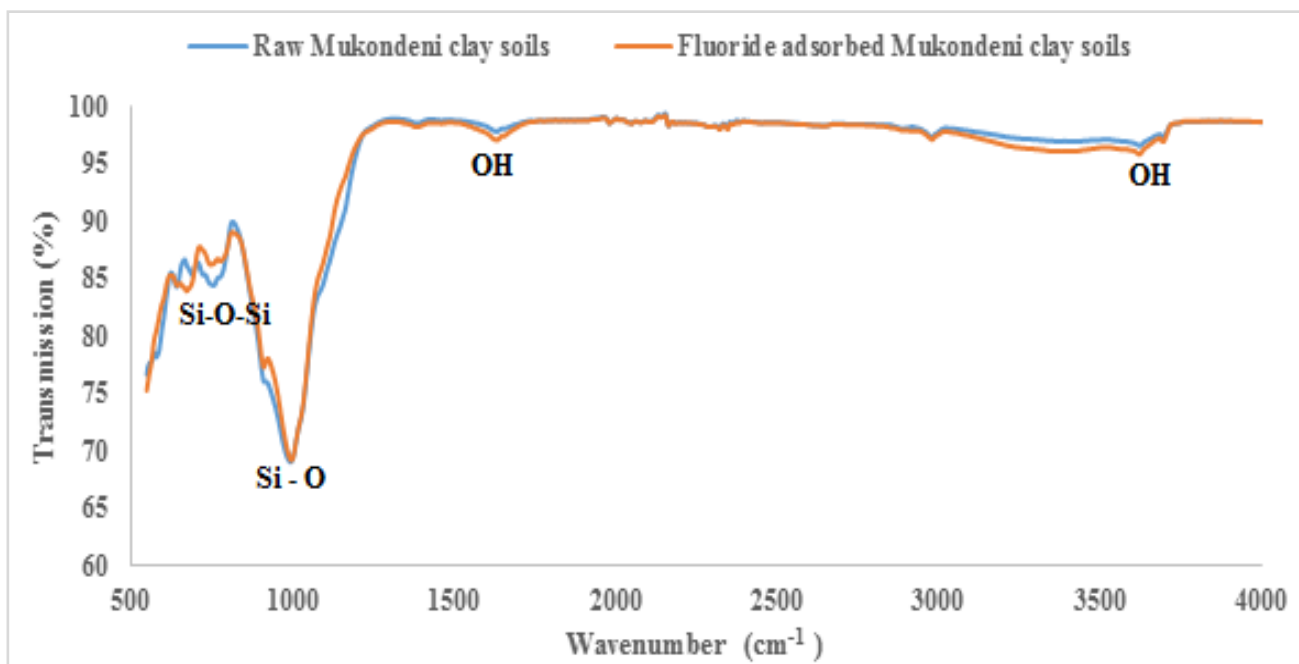


Figure 4.5. FTIR spectra of silica-rich red/black Mukondeni clay soils before and after defluoridation

4.5 BATCH ADSORPTION EXPERIMENTS

4.5.1 Effect of contact time on fluoride removal capacity

Fluoride removal by silica-rich red/black Mukondeni clay soils as a function of contact time is presented in Figure 4.6. In order to establish the equilibrium time of adsorption of fluoride onto silica-rich red/black Mukondeni clay soils, the effect of contact time was evaluated (1 min to 180 min) at an initial fluoride concentration of 10 mg/l (Fig 4.6). There was a rapid rise in fluoride removal from the first minute of contact up to 30 min followed by a gradual decrease at all adsorbent dosages. The same trend is also observed with adsorption capacity. Further increase in contact time did not increase the fluoride uptake due to saturation of adsorption sites. It can be observed that after 60 min the system seems to have reached equilibrium. Therefore, 60 min was taken as the optimum contact time and was used for subsequent experiments.

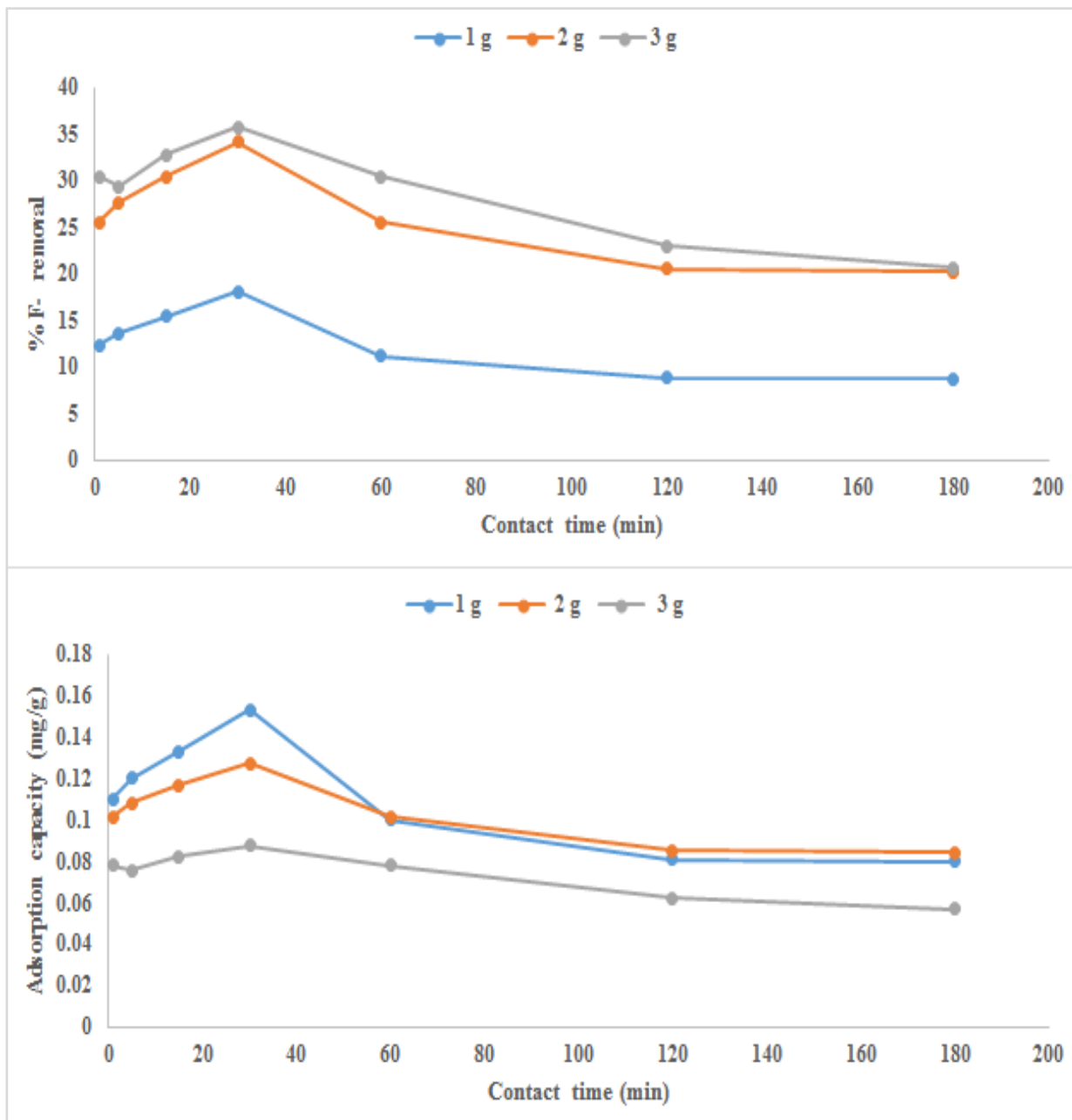


Figure 4.6. Percentage removal and adsorption capacity of silica-rich reddish black Mukondeni clay soils as a function of contact time (1, 2 and 3 g, 10 mg/l F⁻, 25°C room temperature, 100 ml, 250 rpm, pH_i = 6.423, n=3)

4.5.2 Effect of adsorbent dosage on fluoride removal capacity

Fluoride removal by silica-rich red/black Mukondeni clay soils as a function of clay soil dosage is presented in Figure 4.7. WHO stipulates that fluoride concentrations in drinking water should be 1.5 mg/l. Therefore, to determine the minimum amount of adsorbent required to bring the fluoride concentration to the prescribed levels, the effect of adsorbent dose on fluoride removal was evaluated. The % removal of fluoride was observed

to increase with an increase in dosage. As dosage increases, more adsorption sites suitable for the uptake of fluoride become available. At low adsorbent dosage the fluoride adsorption rate is rapid since the active sites are easily available and at high adsorbent dosage, the adsorbate species find it increasingly difficult to access the adsorption sites and equilibrium is established. Similar results have been reported in literature by various researchers (Tomar et al., 2014; Gitari et al., 2013; Tomar et al., 2013; Paudyal et al., 2011). It is observed that at dosages ≥ 1.5 g, the % removal remained fairly constant indicating that the reaction had reached equilibrium. Thus 1.5 g adsorbent mass was adopted as the optimum dosage for further experiments.

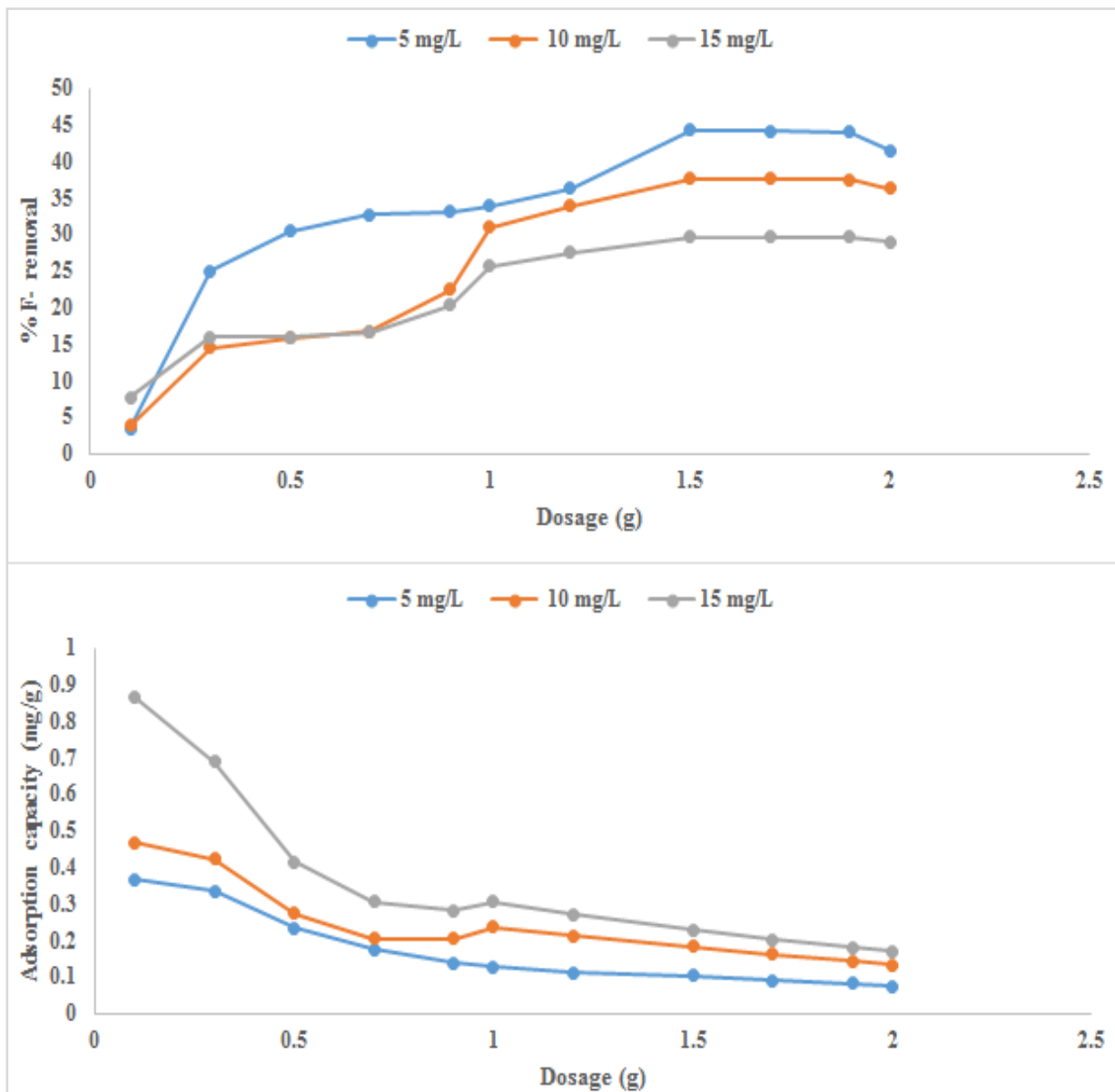


Figure 4.7. Percentage removal and adsorption capacity of silica-rich reddish black Mukondeni clay soils as a function of dosage (60 min contact time, 10 mg/l F⁻, 25°C room temperature, 250 rpm, pH = 5.937, n=3)

4.5.3 Effect of fluoride ion concentration on fluoride removal capacity

Fluoride removal by silica-rich red/black Mukondeni clay soils as function of initial F^- concentration is presented in Figure 4.8. The concentrations were varied from 1 to 15 mg/l. The effect of initial concentration on the adsorption and uptake of fluoride from solution by the silica-rich red/black Mukondeni clay soils was evaluated by varying the fluoride concentration from 1 to 15 mg/l. The adsorption capacity of the adsorbent rose with increasing initial fluoride concentration until 9 mg/l then dropped gradually at higher F^- concentration. Percentage fluoride removal decreased with increase in initial fluoride concentration. This may be attributed to the presence of more fluoride ions than the adsorption capacity of the adsorbent. Similar results have been reported by Ghandi et al. (2012) and Chen et al. (2010). The maximum adsorption capacity was observed at 9 mg/l and therefore it was taken as the optimum initial fluoride concentration for subsequent experiments.

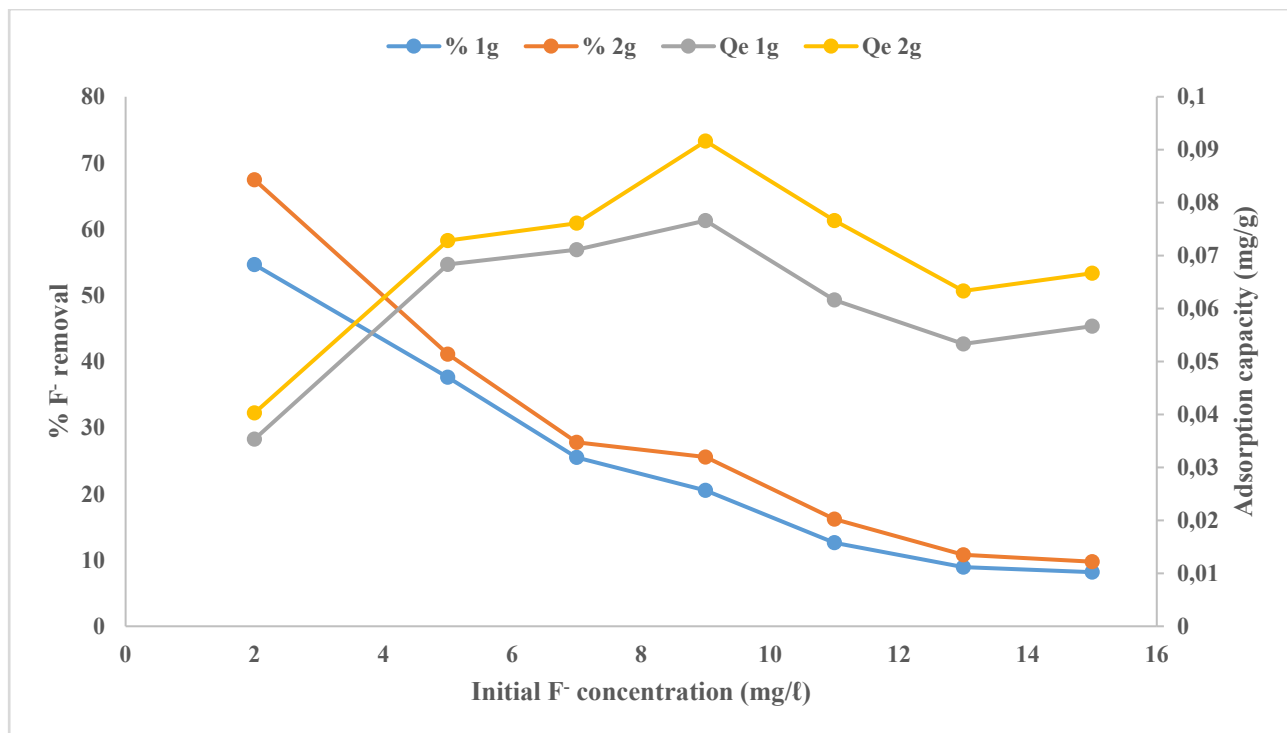


Figure 4.8. Percentage removal and adsorption capacity of silica-rich red/black Mukondeni clay soils as a function of initial fluoride concentration (60 min contact time, 1.5 g dosage, 25°C room temperature, 100 mL, 250 rpm, pH/= 6.11, n=3).

4.5.4 Effect of temperature on fluoride removal capacity

Percentage fluoride removal by silica-rich red/black Mukondeni clay soils as a function of temperature is presented in Figure 4.9. Temperature usually has a notable effect on reaction rate. If temperature increases, the rate of chemical reaction also increases. As the temperature was increased, adsorption capacity was also observed to increase at lower fluoride concentrations ($C_e < 7$ mg/l) but at higher initial fluoride concentrations ($C_e > 9$ mg/l) the temperature had little or no effect at all on adsorption capacity. It is observed that at ($C_e = 13$

and 15 mg/l), the adsorption capacity was the same. The highest adsorption capacity was observed at 9 mg/l across the 3 different temperatures and the difference in adsorption capacities between 318 K and 298 K is only 0.02 mg/g. On the basis of this observation, variation of temperature at the optimum initial fluoride concentration had little effect on fluoride removal hence all subsequent defluoridation experiments were carried out at room temperature.

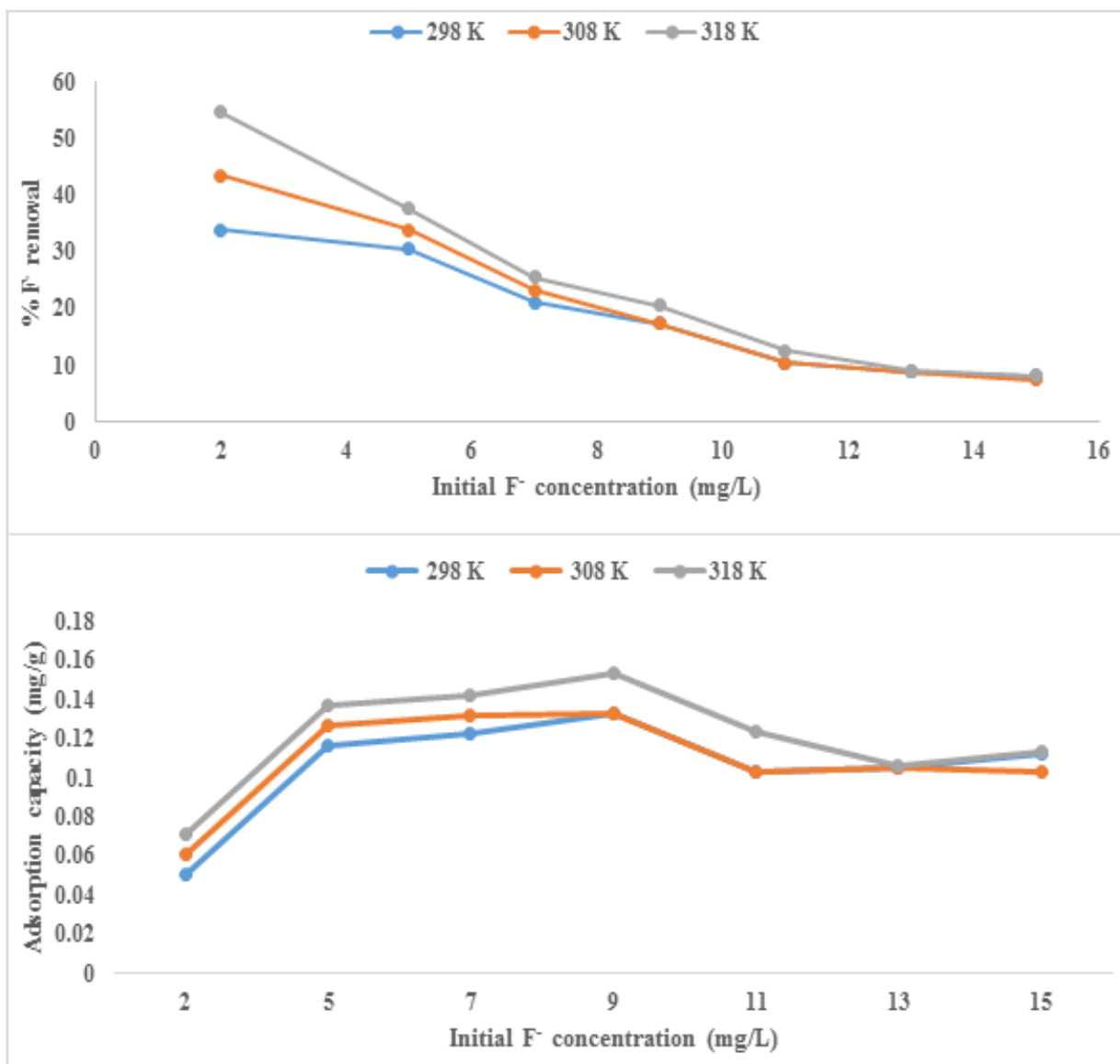


Figure 4.9. Percentage removal and adsorption capacity of silica-rich red/black Mukondeni clay soils as a function of temperature (60 min contact time, 1.5 g dosage, 100 mL, 250 rpm, pH = 6.11, n=3).

4.5.5 Effect of competing ions on fluoride removal capacity

Percentage fluoride removal by silica-rich red/black Mukondeni clay soils is presented in Figure 4.10. Groundwater may contain other anions such as sulphate, phosphate, carbonate and nitrate. Co-existing with fluoride and these may compete with fluoride for adsorption sites, thus affecting the adsorption efficiency. Thus, the effect of various co-existing anions on adsorption of fluoride was evaluated. The carbonate, phosphate and nitrate had a slight negative effect on fluoride adsorption while sulphate enhanced fluoride removal.

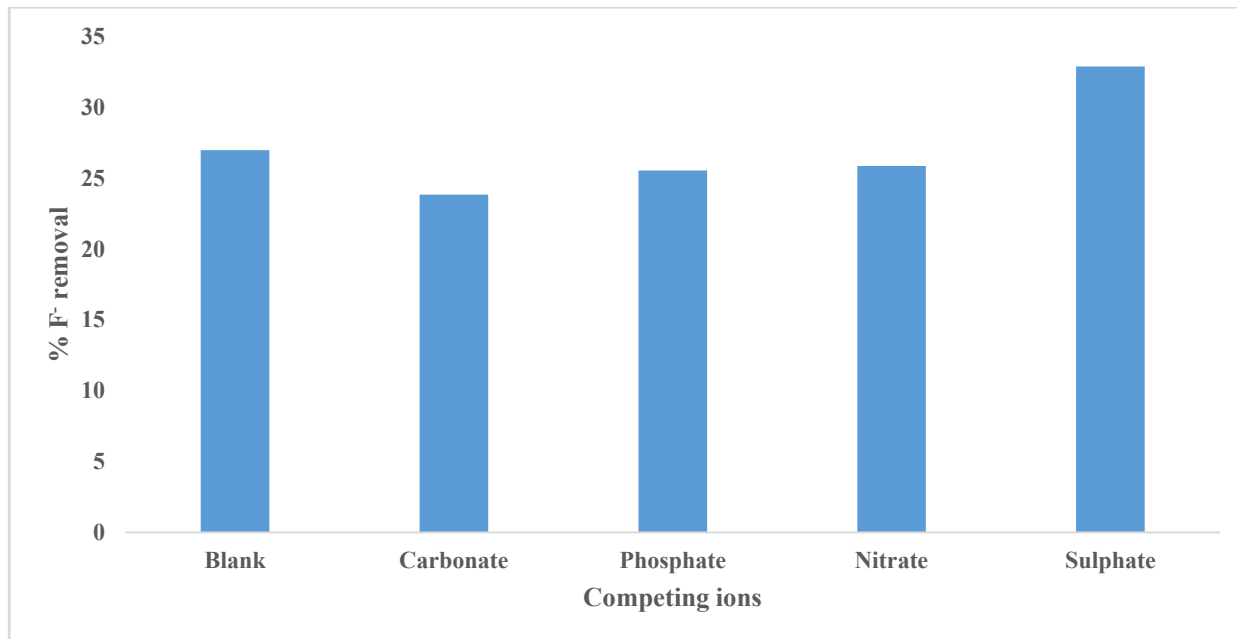


Figure 4.10. Percentage removal of fluoride by silica-rich reddish black Mukondeni clay soils as a function of competing ions (60 min contact time, 9 mg/l, 1.5 g dosage, 25°C room temperature, 100 mL, 250 rpm, pH = 6.59, n=3).

4.5.6 Effect of pH on fluoride removal capacity

Fluoride removal by silica-rich red/black Mukondeni clay soils as a function of pH is presented in Figure 4.11. The pH of a media is one of the most important parameters that can influence fluoride removal. It also helps in understanding the fluoride uptake mechanism of the adsorbent. It is observed that adsorption decreases with increase in pH. At low pH the surface of the adsorbent will be positively charged enhancing F⁻ adsorption. An interaction between the metal hydroxides (Si-OH, Al-OH and Fe-OH) at the surface of the clay adsorbent and fluoride ions is depicted in equation (4.1) and (4.2).

At acidic pH.



Whereas at higher pH (basic condition), there is dissolution of metal hydroxides from the adsorbents and this leads to increase in OH ions in the water

At alkaline pH



The progressive decrease of fluoride uptake with increase in pH is mainly due to the electrostatic repulsion of fluoride ions by the negatively charged surface of the adsorbent and competition of adsorption sites with OH⁻, since both OH⁻ and F⁻ are isoelectronic and have the same charge and similar ionic radii. Thus, the adsorption of fluoride ion followed ligand exchange mechanism. Maximum fluoride removal was observed at pH 2, hence was used in subsequent experiments

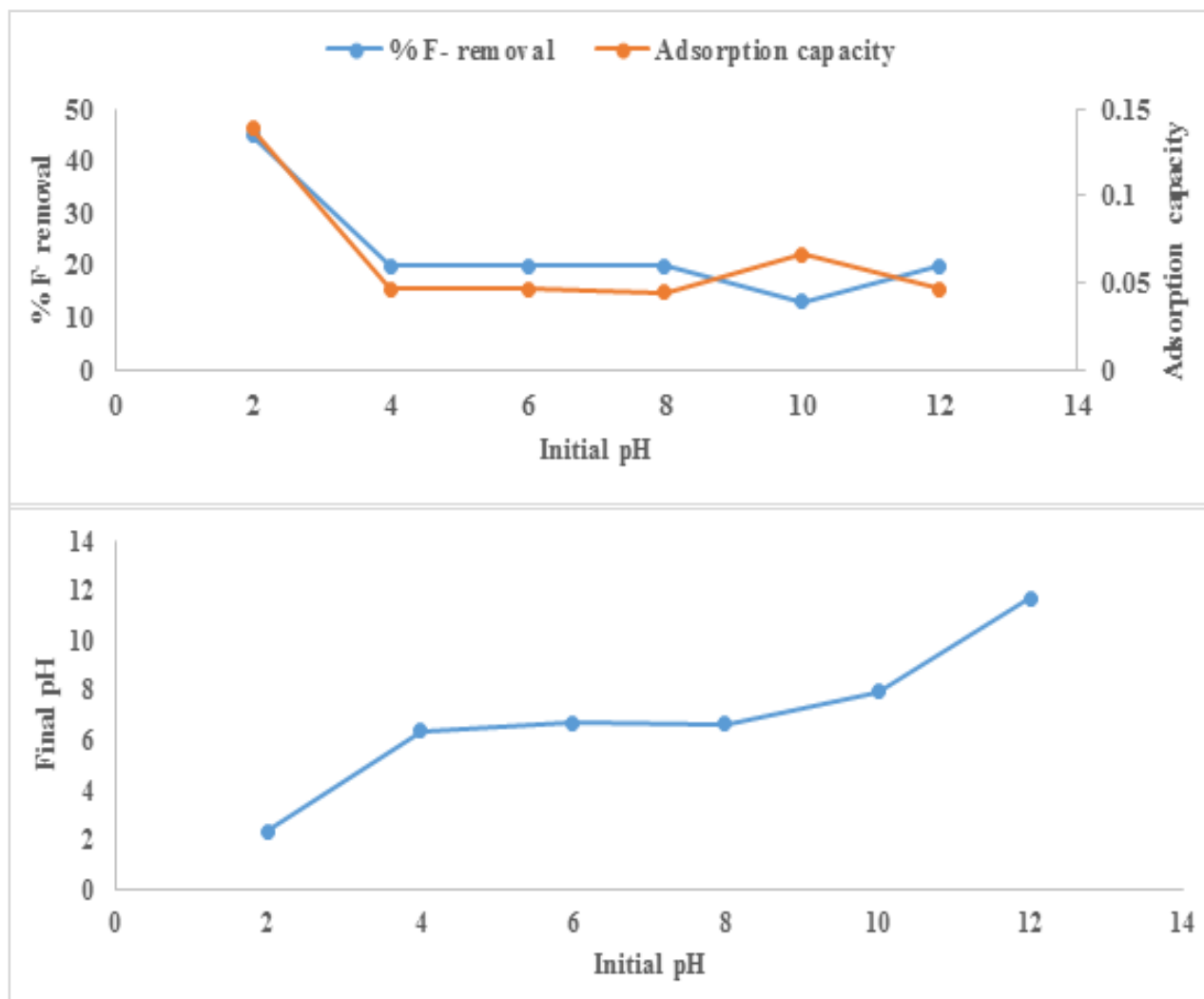


Figure 4.11. Percentage removal of fluoride by silica-rich reddish black Mukondeni clay soils as a function of pH (60 min contact time, 1.5 g dosage, 9 mg/l F⁻, 25°C room temperature, 100 ml, 250 rpm, n=3)

4.6 GROUNDWATER DEFLUORIDATION AT OPTIMAL AND FIELD PH CONDITIONS

4.6.1 Adsorption of fluoride from field groundwater at optimised and field conditions

Table 4.4 shows the adsorption of fluoride from field groundwater by silica-rich red/black Mukondeni clay soils at optimized pH and field pH conditions. Tables 4.4 and 4.5 display the physicochemical characteristics of the groundwater sample, demonstrating the complexity of its chemistry and the high fluoride concentration. The established optimum conditions for removal of fluoride were 60 min of contact time, 1.5 g of adsorbent dosage, pH of 2.12 and room temperature. Fluoride removal efficiency at field pH was observed to be slightly lower than at optimized pH. A possible explanation to this could be that, the pH of field water being at circum-neutral meant the surface of adsorbent was slightly negatively charged hence would repel negatively charged fluoride ions. However, fluoride levels remained above recommended limits. The other parameters are however within the permitted ranges of the DWA water quality guidelines. However, Al and Fe seemed to leach out of the adsorbent. However, at these concentrations both elements are not known to have any adverse health effects.

Table 4.4. Adsorption of F⁻ onto silica-rich red/black Mukondeni clay soils

Parameter	Borehole water	Field pH (pH= 7.81)	Optimized pH (pH = 2.12)	SANS 241-1(2015)
pH	7.81	7.09	6.42	5.0-9.5
EC (µS/cm)	25.74	25.22	25.20	150-370 (mS/m)
F ⁻ (mg/l)	5.53	4.233	3.95	1-1.5
Cl ⁻ (mg/l)	31.6	38.1	67.1	<200
SO ₄ ⁻ (mg/l)	11.9	10.5	9.6	<400
Br ⁻ (mg/l)	2.08	N.D	N.D	-
NO ₃ ⁻ (mg/l)	1.13	N.D	N.D	<50
PO ₄ ³⁻ (mg/l)	ND	N.D	N.D	-

Table 4.5. Concentration of chemical species before and after defluoridation at field pH conditions

Metals (µg/l)	Field water (pH = 7.81)	Treated water (pH = 7.82)	Metals (mg/l)	Field water (pH = 7.81)	Treated water (pH = 7.82)
Li	8.82	5.85	Al	0.04392	1.985
Be	<0.005	0.095	Ca	3.163	3.783
B	22.61	20.01	Fe	0.163251	2.175
V	0.085	11.36	K	2.544	3.746
Cr	0.227	26.73	Mg	0.0396	3.195
Mn	17.46	134.61	Na	67.58	69.69
Co	0.028	3.56	P	< 0.01	0.0126
Ni	0.741	23.38	Si	45.51	43.98
Cu	10.74	9.60	Sr	0.0234	0.016
Zn	11.47	24.46			
As	<0.03	0.227			
Se	< 0.54	0.897			
Mo	1.35	1.57			
Cd	< 0.04	0.0101			
Sb	< 0.01	0.063			
Ba	40.68	28.57			
Hg	< 0.01	<0.004			
Pb	0.592	1.11			

4.6.2 Chemical stability of the adsorbent at different pH

The changes in water quality of synthetic fluoride water after treatment with the red/black clay soils were evaluated and results are presented in Table 4.6. It is observed that highest leaching of metals occurred at pH 12. This could be attributed to dissolution of the aluminosilicate materials leading to release of the chemical species within the matrix. However, with Al, Mn and Fe leaching occurred at all the tested pHs, this is attributed to these chemical species being the main building blocks of the clay soils. Al exceeds the recommended limits as recommended by DWA all evaluated pH. pH 6 exhibited limited leaching of chemical species and would be the optimum pH for defluoridation since no pH adjustment is required. Contrary to other metals, Na shows a quite different trend. According to DWA water quality guidelines, Na should range between 0-100 mg/l (Table 4.4 & 4.6), the Na concentration at pH 12 is 272.7 mg/l which is above the recommended water quality guidelines. The high Na concentration is attributed to the NaOH which was used to adjust the pH to 12.

Table 4.6. Leaching of metals into solution after defluoridation at pH 2, 6 and 12

Metals ($\mu\text{g/l}$)	2	6	12	Metals (mg/l)	2	6	12
Li	3.54	4.33	6.31	Ca	22.95	1.43	6.23
Be	2.93	0.27	1.60	K	2.465	0.973	2.23
B	4.46	2.61	<0.000	Mg	20.33	1.314	9.39
Al	5681.6	3851.3	17337.4	Na	12.99	9.35	272.7
V	15.83	4.70	66.38	P	0.039	0.017	0.068
Cr	14.05	23.94	171.75	Si	5.49	8.22	40.62
Mn	1405.1	44.11	396.36				
Fe	112.866	2486.13	16615.10				
Co	43.15	1.70	18.45				
Ni	220.08	19.59	166.86				
Cu	24.88	2.86	54.54				
Zn	25.55	5.41	40.26				
As	0.11	0.08	0.39				
Se	0.73	0.45	2.76				
Sr	169.07	6.99	35.88				
Mo	0.07	0.25	0.14				
Cd	0.23	0.01	0.05				
Sb	0.01	0.01	0.02				
Ba	424.07	7.26	124.48				
Hg	< 0.01	0.01	0.01				
Pb	1.62	0.42	5.94				

4.7 ADSORPTION MODELLING STUDIES

4.7.1 Adsorption isotherm parameters

The adsorption data was modelled using Langmuir, Freundlich and Dubinin-Radushkevich isotherm models (Appendix C). Table 4.7 presents the various parameters calculated from these models. It is observed that the

Langmuir isotherm couldn't describe the adsorption data and had weak fit as described the by R^2 . The constant b is related to the affinity between the adsorbent and adsorbate (Vijayaraghavan et al., 2005). A low value of b indicates favourable adsorption. R_L values between 0 and 1 indicate favourable adsorption, 0 indicates irreversible adsorption, 1 means linear adsorption while a value greater than 1 indicates an unfavourable adsorption. The values of R_L obtained at different temperatures are shown in Table 4.7. The values lie between 0 and 1 which shows that the adsorption of F^- on silica-rich red/black Mukondeni clay soils is a favourable adsorption process. The calculated adsorption capacities (Q_m) are high compared to the experimental adsorption capacity (0.08 mg/g) indicating unconformity of the adsorption data to Langmuir isotherm.

Table 4.7. Calculated adsorption isotherm parameters

Adsorption isotherms and parameters				
Langmuir Isotherm				
Temp (K)	Q_m (mg/g)	b (L/mg)	R_L	R^2
298	0.18	1.74	0.06	0.5203
308	0.11	3.25	0.03	0.3107
328	0.11	1.9	0.06	0.2893
Freundlich Isotherm				
Temp (K)	K_F	$1/n$	n	R^2
298	0.06	3.33	0.2997	0.9529
308	0.07	5.23	0.191	0.9687
328	0.09	6.03	0.1658	0.9558
Dubinin-Radushkevich Isotherm				
Temp (K)	Q_D	B_D	E (J/mol)	R^2
298	0.9	0.518	1.03	0.7793
308	0.78	0.6553	1.40	0.6093
328	0.51	0.7246	1.64	0.5793

The Freundlich isotherm was applied to deduce the adsorption intensity of the adsorbent towards the adsorbate. Unlike the Langmuir isotherm the Freundlich isotherm assumes that the removal of ions occurs on a heterogeneous surface, involving a multilayer adsorption of ions. The high R^2 values suggest the applicability of the Freundlich adsorption isotherm in describing the adsorption data and that the adsorption process is on a heterogeneous surface. Furthermore, the calculated adsorption capacities (0.06, 0.07 and 0.09 mg/g) were comparable to the experimental adsorption capacity (0.08 mg/g) further confirming that Freundlich adsorption isotherm best describes the adsorption data.

The Dubinin-Radushkevich is generally applied to express the adsorption mechanism with a Gaussian energy distribution onto a heterogeneous surface (Dabrowski, 2001 and Dubinin, 1960). This isotherm is more general than Langmuir isotherm because it does not assume a homogenous surface or a constant adsorption potential (Vermeulen et al., 1996). The value of the regression ($R^2=0.78$) indicates adsorption data can be equally described by this model. The free energy E for the transfer of 1 mol of solute from infinity to the surface of the adsorbent was computed and established to be 1.03 kJ/mol.

4.7.2 Thermodynamic parameters

In order to evaluate the feasibility of the adsorption process, thermodynamic parameters were evaluated by conducting the adsorption experiments at different temperatures. Table 4.8 shows the activation energy for the

removal of fluoride from solution by red/black Mukondeni clay soils. The magnitude of the activation energy is commonly used as the basis for differentiating between physical and chemical adsorption (see Appendix C). Physical adsorption reactions are readily reversible, equilibrium attained rapidly and thus energy requirements are small, ranging from 5 to 40 kJ/mol. Chemical adsorption is specific, involves stronger forces and thus requires larger activation energies, e.g. 40-800 kJ/mol (Unuabonah, 2007; Ozcan, 2007). The activation energy for F⁻ adsorption onto red/black Mukondeni clay soils was 58.86 kJ/mol suggesting that the F⁻ ions were chemically adsorbed.

Table 4.8. Activation energy values of removal of fluoride by silica-rich Mukondeni clay soils

Chemical element	K ₁	K ₂	Ea (kJ/mol)
Fluoride	0.79	0.8	58.8554

4.8 ADSORPTION KINETICS

4.8.1 Overview

The kinetics of adsorption controls the efficiency of the process and the equilibrium time. It also describes the rate of adsorbate uptake on a given adsorbent. To identify the potential rate controlling steps involved in the process of adsorption, two kinetic models were evaluated and utilized to fit the experimental data. These models are the pseudo-first-order and the pseudo-second-order models (see Appendix C).

4.8.2 The pseudo first-order and pseudo second-order models

To evaluate the kinetics of the adsorption process, the pseudo first-order and pseudo second order models were tested to interpret the experimental data. Fitting of the data to the pseudo first-order model revealed low R² values (0.012-0.261) indicating poor fit of the data to this model. A fit of the kinetic data to pseudo second-order model revealed high R² values (Table 4.9) indicating a strong fit of the data to the model. The fluoride adsorption kinetics followed pseudo second-order kinetics model and suggests that fluoride adsorption was by chemical interaction.

Table 4.9. Pseudo-second-order kinetic parameters for different adsorbent dosages for fluoride removal by silica-rich reddish black Mukondeni clay soils.

Dosage (g)	q _e exp (mg/g)	K ₂ (gmh)	q _e cal (mg/g)	R ²
1	0.15	2.02.	0.078	0.9933
2	0.12	2.52	0.083	0.9959
3	0.08	32.91	0.057	0.9915

4.8.3 Diffusion based models

The kinetic data of fluoride adsorption was also analysed using the Weber-Morris intraparticle diffusion model. Adsorption mechanism involves three steps. Mass transfer of adsorbate from the bulk phase to particle surface

takes place. The second step involves the boundary layer diffusion, sorption on the sites and the final step is given by intra particle diffusion (Alshameri, 2014). The sorption on the sites is considered to be a very rapid step, hence requirement of longer contact time for equilibrium is said to be governed by intraparticle diffusion. To analyse the adsorption process controlled by intraparticle diffusion, the amount adsorbed Q_t versus \sqrt{t} was plotted as shown in Figure 4.12 and the kinetic parameters obtained are shown in Table 4.10. The plots show two stages of adsorption indicating the occurrence of surface diffusion and internal diffusion, i.e. initial and final phase respectively. The slowest of the steps controls the overall rate of the process. Generally, pore diffusion and intra-particle diffusion are often rate-limiting in a batch reactor, which for continuous flow system film diffusion is more likely the rate limiting step (Kalavathy et al., 2005). As shown in the diagram, the surface diffusion was rapid in the first 30 min and thereafter intraparticle diffusion became slow. The intraparticle diffusion constant, K_{id} values are obtained from the slope of the linear portion of the curve as shown in Table 4.10. From the results obtained, it is clear that the intraparticle diffusion was slow and the rate limiting step because the K_{id2} values are smaller than the K_{id1} values for all adsorbent dosages. The deviation of straight lines from the origin, was observed which may be because of the difference between the rate of mass transfer in the initial and final steps of adsorption. Further, such deviation of the straight line from the origin indicates that the intraparticle diffusion is not the sole rate controlling step (Thilagavathy and Santhi, 2014).

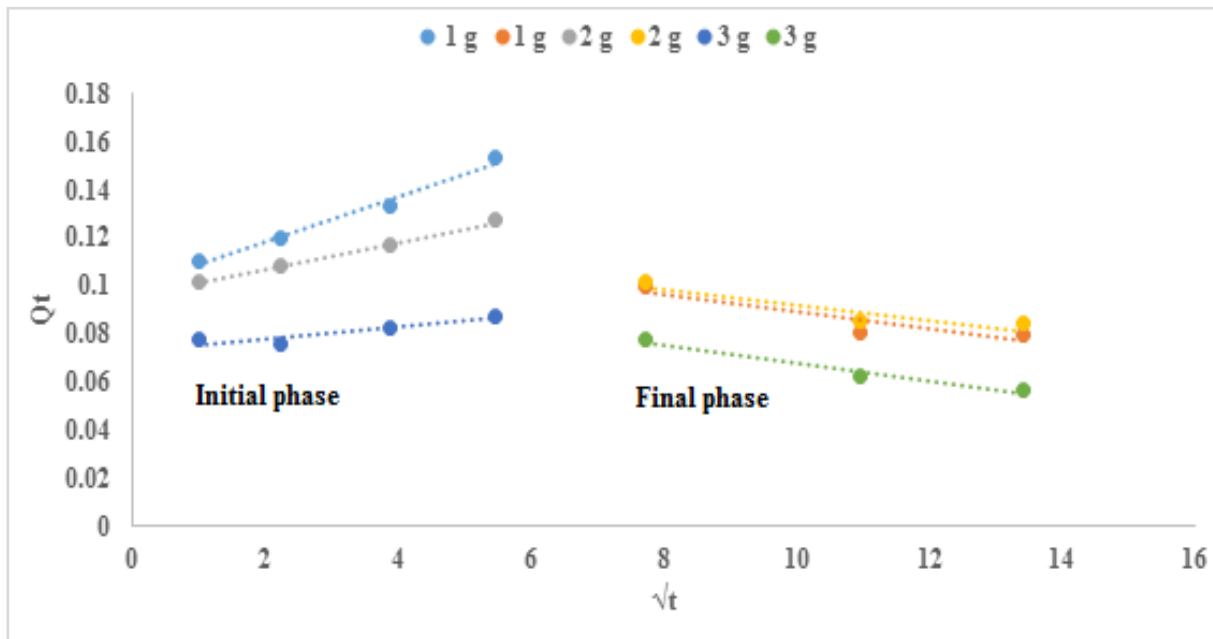


Figure 4.12. Data plots on the Weber Morris intraparticle diffusion model (1 g dosage, 10 mg/l adsorbate concentration, 25°C room temperature, and 250 rpm, pH= 6.423).

Table 4.10. Kinetic parameters of the fluoride adsorption onto silica-rich red/black Mukondeni clay soils

Dosage (g)	K _{id1}	K _{id2}	C1	C2
1	0.0090	-0.0036	0.9991	0.1260
2	0.0056	-0.0320	0.0957	0.1247
3	0.0025	0.00370	0.0730	0.1057

4.9 ADSORPTION MECHANISM OF FLUORIDE ONTO SILICA-RICH RED/BLACK MUKONDENI CLAY SOILS

The two most suggested mechanisms of fluoride sorption onto various adsorbents including clays are ion exchange and electrostatic attraction (Guo and Guo, 2013). However, no substantial fluoride removal was achieved by using silica-rich Mukondeni clay soils which is attributed to the low anion exchange capacity of these claysoils. The ion exchange between fluoride and hydroxyl ions was not the predominant mechanism of fluoride adsorption in this case. This can be observed from the FTIR results shown in Figure 4.5 where the transmission bands of the OH ions are not that different before and after defluoridation. Having observed that, it can be concluded that much of the fluoride adsorption occurred through electrostatic attraction. The metal oxides which are usually present in interlayer spaces of a layered clay can form aqua complex with water and develop charged surface through amphoteric dissociation (Kim et al., 2013). At acidic pH, more positively charged surface sites are developed which attract the negatively charged fluoride ions by electrostatic attraction, resulting in enhanced fluoride removal at acidic pH as expressed in equations. (4.4-4.6).



Overall reaction can be written as follows:



where M represents metal ion in this case which can be Mg, Ca, Na and K

4.10 SUMMARY

The potential of silica-rich red/black Mukondeni clay soils as an adsorbent for fluoride from aqueous solution was evaluated in an attempt to develop cheap readily available adsorbent. Characterisation was done by XRF, XRD, SEM, BET and FTIR. CEC and PZC. Fluoride adsorption parameters optimized included: contact time, adsorbent dosage, initial concentration, competing ions, pH and temperature. Optimisation experiments were done following batch procedures. The results showed that the optimum conditions for the defluoridation of water using these clay soils were 60 min, 1.5 g, 9 mg/l, 1.5/100 S/l ratios a pH of 2 at room temperature. A substantial amount of literature is available on fluoride sorption by a wide variety of low-cost adsorbents as shown in Table 4.11. It is observed that silica-rich red/black Mukondeni clay soils has the lowest adsorption capacity compared to other low-cost adsorbents and that highest adsorption capacities are observed with modified clays.

Table 4.11. Comparison of different adsorption capacities of different clay adsorbents for fluoride

Adsorbent	Adsorption capacity	Experimental conditions	References
Silica-rich red/black Mukondeni clay soils	0.08 mg/g	pH 2, 9 mg/l	Present study
Kaolinite	0.7 mg/g	pH 6-7, 5 mg/l	Srimurali et al. (1998)
Mg²⁺ bentonite	2.3 mg/g	pH 3-10, 5 mg/l	Thakre et al. (2010)
Montmorillonite clay	1.5 mg/g	Neutral	Karthkeyan et al. (2005)
Bentonite	1.2 mg/g	pH 2.8, 5 mg/l	Srimurali et al. (1998)

Equilibrium modelling showed that the Freundlich isotherm ($R^2=0.95$) gave a better fit than the Langmuir isotherm ($R^2=0.52$), and the Dubinin-Radushkevich isotherm ($R^2=0.78$) which indicates multilayer adsorption. The value of the activation energy of (58.9 kJ/mol) obtained from the Arrhenius Equation indicates chemisorption as the main mechanism for F^- adsorption. Kinetic modelling revealed the adsorption followed pseudo second order kinetics. This study indicated that silica-rich red/black Mukondeni clay soils are poor F^- adsorbents. Modification of their surface properties by introducing metal oxides could enhance their adsorption capacity.

5 EVALUATION OF GROUNDWATER DEFLUORIDATION BY IRON(III) OXIDE COATED BENTONITE CLAY

5.1 INTRODUCTION

Bentonite clay is known to adsorb many pollutants, but its use as an adsorbent in a filtration mode is limited in practice because on contact with water, bentonite clay swells and forms a highly stable colloidal suspension, making its separation from water following adsorption very difficult (Kapoor, 1998). Modification of bentonite is vital to increase its applicability potential for the adsorption of fluoride in a continuous or dynamic flow regime. The existence of various functional groups like OH, H-O-H and absorbed water were confirmed on the surfaces of bentonite clay by FTIR in section 4.2 of this chapter 4 and these functional groups are believed to have physicochemical interactions, e.g. inner-sphere complex formation or ion exchange with ion charge balancing alkaline/alkaline earth metal ions such as Na^+ , Mg^{2+} and Ca^{2+} in the clay interlayers. Easily exchangeable OH groups are those found in metal hydroxides or hydrated metal oxides such as aluminium or iron oxides. An ion exchange mechanism whereby F^- is exchanged with OH groups in the mineral structure is generally assumed to be the rate determining step in the adsorption process (Hauge et al., 1994). Modifying bentonite clay with iron oxides introduces OH groups that increases the capacity of the modified material to adsorb fluoride from solution. This is because the modification process increases the surface area of the bentonite clay and provides centres of positive charge which enhances the uptake of the negatively charged fluoride ions. This chapter presents findings on:

- a. Preparation and activation of bentonite clay with NaOH
- b. Modification of bentonite clay with Fe^{3+} -oxides/oxyhydroxides, physicochemical and mineralogical characterization of the products
- c. Evaluation of fluoride adsorption and regeneration potential.

5.2 MATERIALS AND METHODS

All chemicals used in the present study were of analytical reagent grade and were obtained from Rochelle Chemicals and Lab Equipment CC, South Africa Ltd. The bentonite clay was collected from Cape Bentonite, a mining company in Cape Town, South Africa. Fluoride-rich water was collected from a borehole in Siloam village in Limpopo province. Several techniques were used to characterize the adsorbents (detailed in Appendix A). These included Cation Exchange Capacity (CEC), Point of Zero Charge (PZC), X-ray diffraction (XRD), X-ray fluorescence (XRF), Scanning Electron Microscopy (SEM), Scanning Electron Microscopy coupled with Energy Dispersive Spectroscopy (SEM-EDS), Transmission Electron Microscopy (TEM), Brunauer-Emmett-Teller (BET) and Fourier Transform Infrared (FTIR). Detailed methods for batch and field adsorption studies, as well as data modelling studies are presented in Appendix B and C, respectively.

5.3 SYNTHESIS OF THE IRON(III) OXIDE COATED BENTONITE CLAY

5.3.1 Activating bentonite clay with NaOH

NaOH solutions of 0.01, 0.05 and 0.1 M concentrations were prepared by dissolving a known mass of the NaOH pellets in MilliQ water. A known weight of the bentonite clay was added to 100 ml of the desired NaOH solution in a 250 ml plastic bottle and then stirred on a reciprocating shaker at 250 revolutions per minute (rpm) at room temperature at different contact times. After continuous stirring for a fixed time interval, the samples were centrifuged for 15 min at 3000 rpm and the residual solution was analysed for fluoride by a fluoride ion selective electrode (Thermo Scientific Orion Star A215 pH/Conductivity Benchtop Meter, USA). This experiment was repeated with different bentonite clay masses and agitation times.

5.3.2 Coating NaOH-activated bentonite clay with Fe₂O₃

Anhydrous FeCl₃ was dissolved in MilliQ water to form solutions at molar concentrations of 0.1 M, 0.3 M and 0.5 M. 10 g of the Activated bentonite (AB) was added to 100 ml of the solutions of different concentrations. The pH of the mixture was adjusted with 10 M NaOH solution until the final pH reached 6.5 and the solution was then shaken at 250 rpm on a reciprocating shaker. The mixture formed precipitates which were reddish brown in colour. The precipitates were then centrifuged and washed with distilled water until the pH of the filtrate was between 6 and 7. The residue was collected and dried in an oven at 105°C for 12 h. Afterwards, the sample was milled into fine powder by a Retsch RS 200 miller. It was then later on analysed for surface area using the Brunauer Emmett Teller method of analysis using a Micromeritics TriStar II 3020 Version 2.00. The same procedure was repeated with varying shaking times of 1 h, 3 h and 6 h for each different concentration of FeCl₃. Parameters optimised were FeCl₃ concentration and agitation time.

5.4 CHARACTERIZATION STUDIES

5.4.1 Point of zero charge (PZC) of raw bentonite and Fe₂O₃ coated bentonite clay

The point (pH) where the electrical charge density is zero, is called the point of zero charge (PZC) and is a fundamental phenomenon in the process of adsorption. If the pH of a soil is above its PZC the soil surface will have a net negative charge and predominantly exhibits an ability to exchange cations, while the soil will mainly retain anions if its pH is below its PZC (Appela et al., 2003). Figure 5.1 shows the point of zero charge of raw bentonite clay and Fe₂O₃ modified bentonite clay respectively. Raw bentonite has a pHPZC at pH 8.8 (Fig 5.1). Spark (1997) reported that aluminium and iron oxides have high PZC values that can go up to 8. Hence, the high PZC of bentonite clay could be due to the presence of aluminium and iron oxide or hydroxides in the clay. On the contrary, the iron(III) oxide coated bentonite has a PZC at pH 7.5 which is slightly lower than that of the raw bentonite. Similar observations were made by Schwertmann and Fechter (1982) on natural and synthetic ferrihydrated clays. They pointed out that, the point of zero charge (pzc) of synthetic Fe-oxides is well documented and usually ranged between pH 7 and 9 (Parks, 1965; Schwertmann and Taylor, 1977). A PZC at 7.5 means that adsorption of fluoride using iron(III) oxide coated bentonite clay will be effective in acidic and circum-neutral pH conditions since the surfaces of the clay will be positively charged at that pH range.

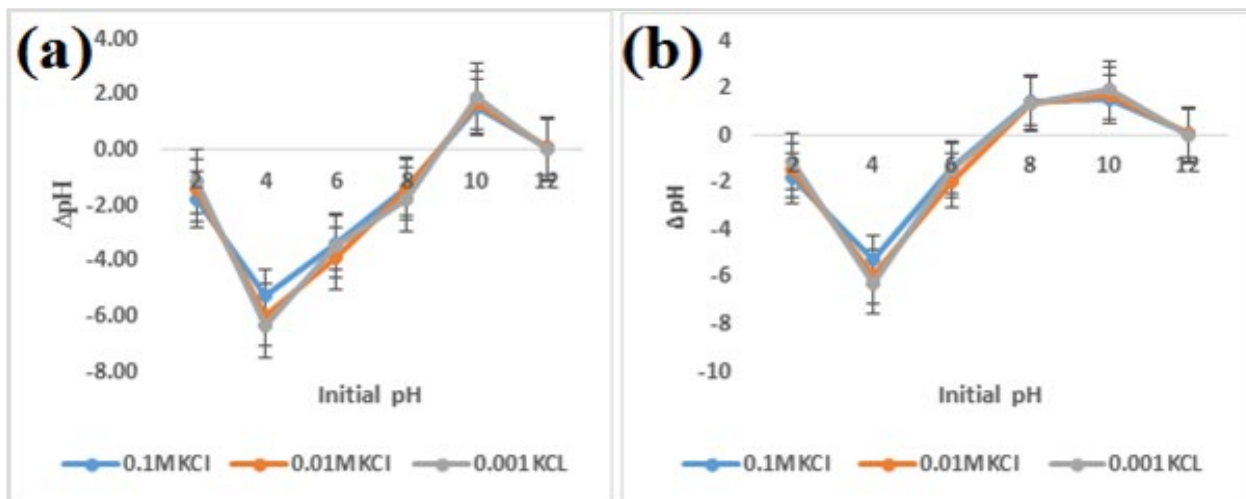


Figure 5.1. pH_{pzc} of raw bentonite clay (a) and Fe_2O_3 coated bentonite clay (b)

5.4.2 Cation Exchange Capacity (CEC)

The cation exchange capacity (CEC) of a soil is a measure of the quantity of negatively charged sites on soil surfaces that can retain positively charged ions (cations) such as Ca^{2+} , Mg^{2+} and K^+ by electrostatic forces. Cations retained electrostatically are easily exchangeable with cations in the soil solution. So, a soil with a higher CEC has a greater capacity to maintain adequate quantities of Ca^{2+} , Mg^{2+} and K^+ than a soil with a low CEC. (Ross and Ketterings, 2011) Table 5.1 shows the concentration of exchangeable cations identified in raw and iron(III) oxide coated bentonite clay.

Table 5.1 Cation Exchange Capacity of raw bentonite and iron(III) oxide coated bentonite clay

Raw bentonite clay	Concentration of Exchangeable cations (mg/l)				CEC (meq/100 g)
	Na^+	K^+	Ca^{2+}	Mg^{2+}	
pH 5.4	75.54	7.00	1.08	127.54	127.54
pH 7.4	111.34	6.9	1.90	142.04	142.04
Fe_2O_3 coated bentonite					
pH 5.4	49.2	6.8	1.0	45.7	97.5
pH 7.4	47.6	6.6	1.8	22.9	88.9

The main exchangeable cations in bentonite clay are Na^+ , K^+ , Ca^{2+} and Mg^{2+} . Mg^{2+} had the highest concentration with Ca^{2+} having the lowest concentration. Comparing the CEC of the iron(III) oxide coated and raw bentonite clay it can be seen that after modification the CEC was greatly reduced at all pHs. A significant reduction was noted on the concentration of Na^+ and Mg^{2+} . This may mean that these cations were exchanged for the trivalent Fe^{3+} during the modification with $FeCl_3$.

5.4.3 X-Ray Fluorescence Analysis

The percentage composition of major elements in raw and Fe₂O₃ coated bentonite clay are presented in Table 5.2. XRF analysis shows an appreciable amount of SiO₂ and Al₂O₃ for both the raw and Fe₂O₃ coated bentonite clay suggesting that this is an aluminosilicate material. There is reduction in Al₂O₃ and SiO₂, this could be attributed to dilution effect on addition of Fe₂O₃. An increase in Fe₂O₃ is observed. This confirms that Fe₂O₃ was successively coated on the bentonite clay surface and interlayers. An increase in Na₂O is observed for the modified bentonite, this is attributed to residue Na from the NaOH activation process.

Table 5.2. Chemical composition of raw and Fe₂O₃ coated bentonite clay

Element	% w/w (Raw)	% w/w (Fe₂O₃-bentonite)
Al₂O₃	14.04	8.80
CaO	0.93	0.37
Cr₂O₃	0.00	0.02
Fe₂O₃	3.31	28.35
K₂O	1.01	0.70
MgO	2.68	1.64
MnO	0.05	0.09
Na₂O	2.69	8.99
P₂O₅	0.06	0.05
SiO₂	58.84	37.33
TiO₂	0.47	0.18
L.O.I	14.79	14.44
TOTAL	98.87	100.96

5.4.4 X-Ray Diffraction Analysis

Hydrolysis of Fe³⁺ with NaOH may lead to formation of crystalline iron oxides-oxyhydroxides on the surfaces of the bentonite clay. Furthermore, adsorption reactions may lead to changes in molecular and crystalline structure of the adsorbent and hence an understanding of the molecular and crystalline structures of the adsorbent and the resulting changes thereof would provide valuable information regarding adsorption reactions. (Namasivayam and Yamuna, 1995). The X-ray diffraction (XRD) patterns of the raw and Fe₂O₃ coated bentonite clay were recorded and are shown in Figure 5.2. The XRD pattern of both the raw bentonite and Fe₂O₃ coated bentonite clay suggests that the clays are highly crystalline and have quartz and montmorillonite as the major mineral components. Intense peaks for montmorillonite on the raw bentonite clay at 27degrees (2-theta) and the wide distribution of quartz from 20-85 degrees (2-theta) are evidence of this fact. The XRD spectra presented in Figure 5.2 shows formation of new mineral phases. The new mineral phases clinoptilolite, heulandite and cristobalite are zeolitic and silica-like phases formed due to the high alkaline conditions created during the NaOH activation of the bentonite. The halite formation could be attributed to the high residue Na⁺ and Cl⁻ ions from the FeCl₃ used for the modification process. The observations indicate that a very dilute NaOH solution should be used for the activation to reduce changes in the structural integrity of the bentonite clay.

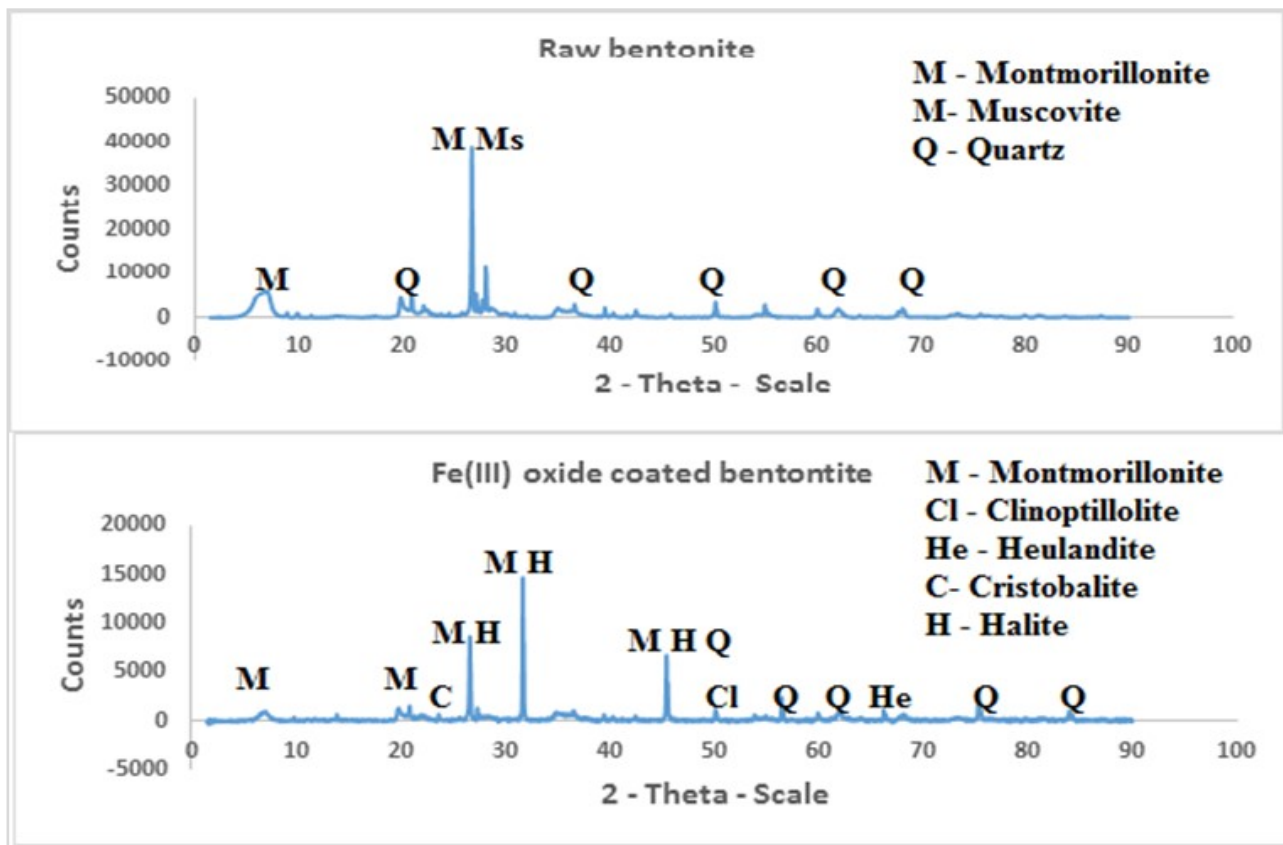


Figure 5.2. XRD diffractogram of raw bentonite and Fe₂O₃ coated bentonite clay

5.4.5 Scanning Electron Microscopy Analysis

The morphologies of raw bentonite and Fe₂O₃ coated bentonite clay are shown in Figure 5.3. The micrographs show that the morphology of bentonite clay changed after modification (Fig. 5.3 A1-B2). The micrographs reveal the clay platelets characteristic of layered clays (Fig 5.3 A2). At higher magnification the micrographs reveal deposition of layers and granules which are attributed to Fe-oxides and oxyhydroxides that precipitated on the platelet's surfaces (Fig 5.3 B2). The modified bentonite shows increased smoothing and loss of the opening between the platelets (Fig 5.3 B1-B2).

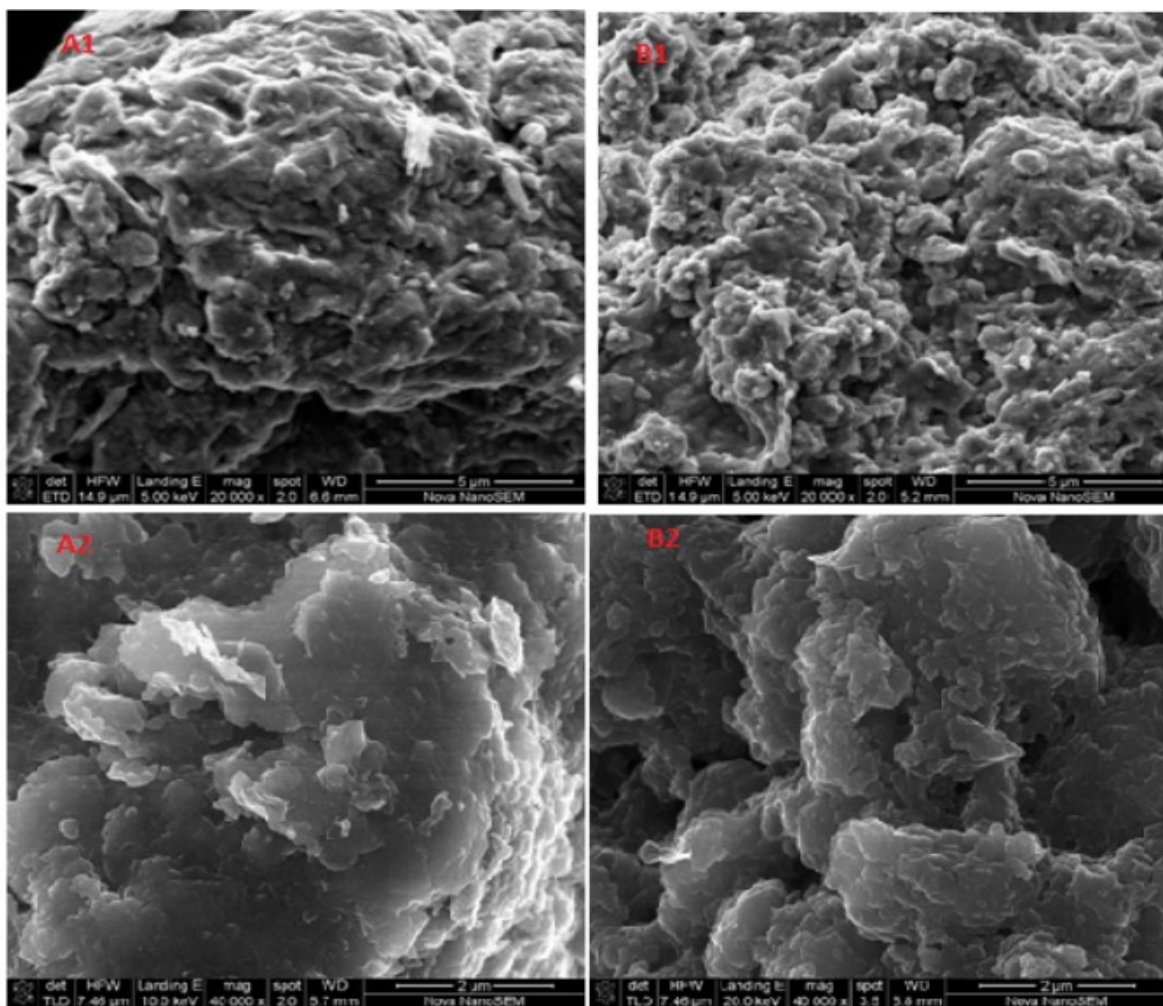


Figure 5.3. SEM micrographs of raw bentonite (a) and Fe_2O_3 coated bentonite clay (b) at different magnifications

5.4.6 Brunnet-Emmett-Teller (BET) analysis

Table 5.3 presents the surface area, pore volume and pore size of the raw and Fe_2O_3 coated bentonite clay. The BET surface area of the Fe_2O_3 coated bentonite tripled that of raw bentonite ($43.2077\text{-}132.3018\text{ m}^2/\text{g}$). The coatings of Fe_2O_3 substantially changed the surface area. The pore volume was also observed by one order of magnitude. A reduction in pore width and pore diameter was observed indication filling of the bentonite pores with Fe-oxides/oxyhydroxides. This is collaborated by XRF data that showed increased concentration of Fe_2O_3 in the modified bentonite.

Table 5.3. Surface area, pore volume and pore sizes of raw and Fe₂O₃ coated bentonite clay

	Raw bentonite clay	Fe ₂ O ₃ coated bentonite clay
Surface area (m ² /g)		
Single point surface area	42.9136	128,4410
BET Surface Area	43.2077	132,3018
BJH Adsorption cumulative surface area of pores	27.816	129.660
BJH Desorption cumulative surface area of pores	33.8529	125.3499
Pore Volume (cm ³ /g)		
Single point adsorption total pore volume of pores	0.066285	0.147116
BJH Adsorption cumulative volume of pores	0.059269	0.150779
BJH Desorption cumulative volume of pores	0.064930	0.155407
Pore Size (Å)		
Adsorption average pore width (4V/A by BET)	61.3637	14.4863
BJH Adsorption average pore diameter (4V/A)	85.231	17.106
BJH Desorption average pore diameter (4V/A)	76.720	18.596

5.5 BATCH F⁻ ADSORPTION EXPERIMENTS

5.5.1 Overview

Fluoride stock solution (100 mg/l) was prepared by dissolving 0.221 g anhydrous sodium fluoride in 1 l of MilliQ water. This was further diluted to the desired concentrations for practical use. A known weight of the adsorbent was added to 100 ml of the desired fluoride solution in a 250 ml plastic bottle and then stirred on a reciprocating shaker at 250 revolutions per minute (rpm) at room temperature. After continuous stirring for a fixed time interval, the samples were filtered using a 0.45 µm pore cellulose nitrate membranes and the fluoride concentration in the residual solution was measured by a fluoride ion selective electrode (Thermo Scientific Orion Star A215 pH/Conductivity Benchtop Meter (USA) coupled to a 8157BNUMD Orion ROSS Ultra Triode pH/ATC electrode). A similar ion meter coupled with a pH electrode was used for measuring pH of the treated samples. Before fluoride determination, a total ionic strength adjusting buffer (TISAB 111) was added to the solutions in a ratio of 10:1 in order to maintain ionic strength and pH, and eliminate the interference effect of F⁻ ion complexing metal cations. The procedures were repeated to investigate the effect of adsorbent dose, initial concentration, pH and temperature (refer to Appendix B for detailed experimental procedures).

5.5.2 Effect of contact time on fluoride removal capacity

Fluoride removal by Fe₂O₃ bentonite clay as a function of contact time is presented in Figure 5.4. The contact times were varied from 1 to 360 minutes. The % fluoride removal as a function of contact time is presented in Fig 5.4. It was observed that for all adsorbent dosages tested % F⁻ removal increased rapidly to a maximum at 30 mins followed by a dip at 60 mins. Thereafter the system seemed to have attained equilibrium with no significant change in % removal over 60-360 minutes of agitation. The initial rapid adsorption is likely due to the availability of a large number of active sites on the adsorbent surface. Similar phenomena were also observed on Fe (III) modified zeolite and other metal-loaded adsorbents for fluoride adsorption (Sun et al., 2011 and Liu et al., 2014). Based on these observations, 60 min was adopted as optimum contact time and was used in subsequent experiments.

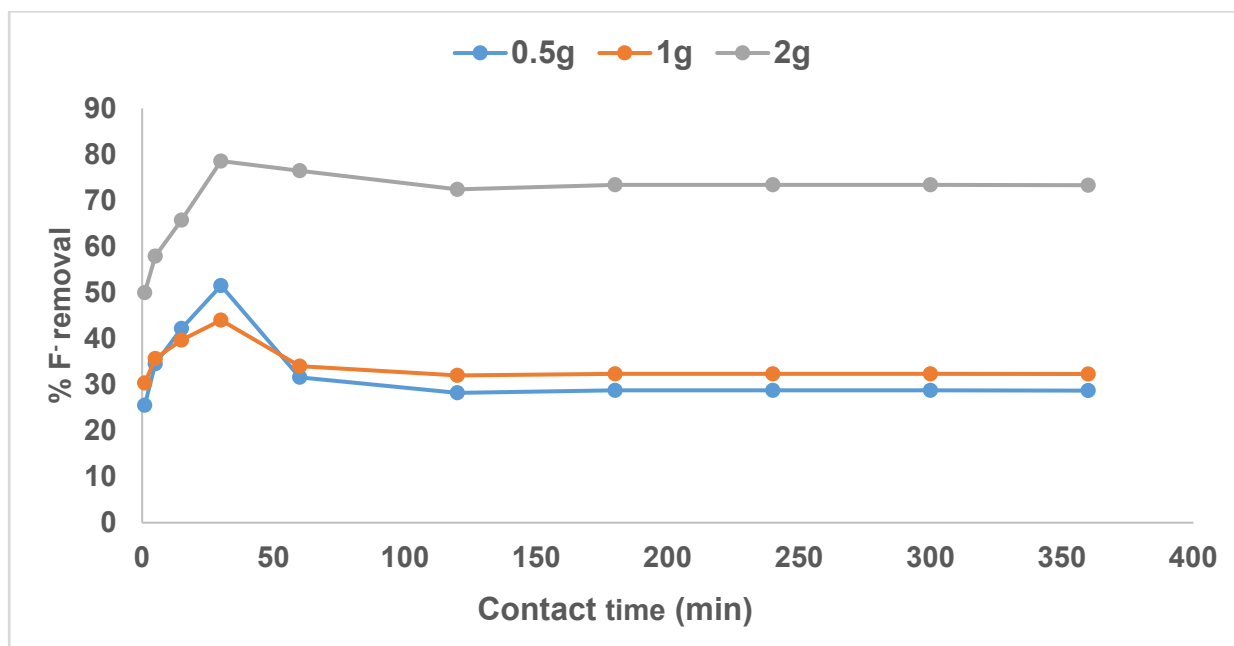


Figure 5.4. Removal of fluoride by Fe₂O₃ coated bentonite clay as a function of contact time (0.5, 1 and 2 g adsorbent, 10 mg/l F⁻, 25°C room temperature, 100 ml solution, 250 rpm, n=3)

5.5.3 Effect of dosage on fluoride removal capacity

Percent fluoride removal by Fe₂O₃ coated bentonite clay as a function of dosage is presented in Figure 5.5. The dosages were varied from 0.1 to 5 g. Figure 5.5 shows that % F⁻ removal increased with increase in adsorbent dosage. The maximum adsorption capacity was established to be 5.92 mg/g at a dosage of 0.1 g/100 ml (20 mg/l F⁻). The increase in the fluoride removal with dosage of the adsorbent is likely driven by the enhanced availability of active sites (Sundaram et al., 2009). The maximum F⁻ removal was observed with 3 g adsorbent dose at all initial fluoride concentrations. It was noted that a further increase in the adsorbent dosage did not significantly change the equilibrium concentration. Moreover, higher adsorbent dosage would be unsustainable in a field application. A dosage of 3 g was adopted as optimum dosage for subsequent experiments.

5.5.4 Effect of concentration on fluoride removal capacity

Percent fluoride removal by Fe₂O₃ coated bentonite clay as a function of initial fluoride concentration is presented in Figure 5.6. The concentrations were varied from 5 to 80 mg/l. The effect of initial concentration on fluoride removal is presented in Figure 5.6. It is observed that the percent fluoride removal decreases with increase in the fluoride concentration. This indicates that the adsorption depends upon the availability of binding sites.

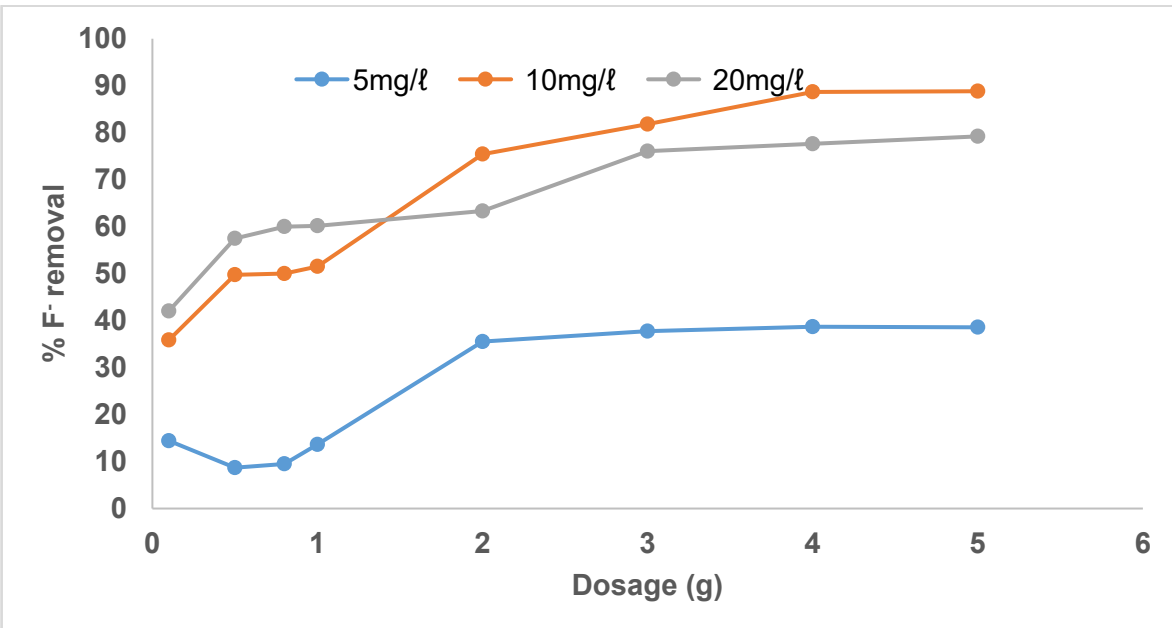


Figure 5.5. Percent fluoride removal by Fe₂O₃ coated bentonite clay as a function of dosage (60 minutes contact time, 5, 10, 20 mg/l F⁻, 25°C room temperature, 250 rpm, n=3)

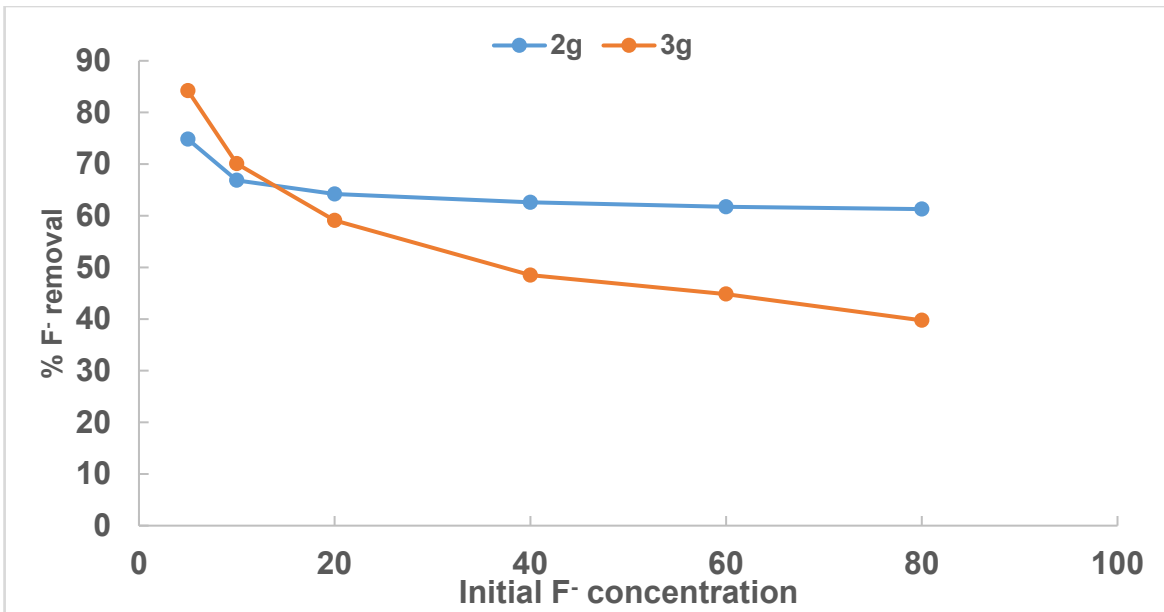


Figure 5.6. Percent fluoride by Fe₂O₃ coated bentonite clay as a function of concentration (60 minutes contact time, 2 and 3 g, 25°C room temperature, 100 mL solution, 250 rpm, n=3)

At low adsorbate concentration, the ratio of surface-active sites to total fluoride is high, hence the fluoride ions could interact with the sorbent to occupy the active sites on the adsorbent surface and be removed from solution. But with the increase in adsorbate concentration, the ratio of active sites to fluoride content decreases hence the decrease in percentage removal. When the initial fluoride concentration is 5 mg/l, a 3 g adsorbent dose reduces the equilibrium concentration of fluoride to below 1.5 mg/l.

5.5.5 Effect of temperature on fluoride removal

Percentage fluoride removal by Fe_2O_3 coated bentonite clay as a function of temperature is presented in Figure 5.7. The temperature was varied from 298-328°K. Figure 5.7 shows that temperature had a negligible influence on the % fluoride removal. Subsequent experiments were conducted at 298°K (room temperature).

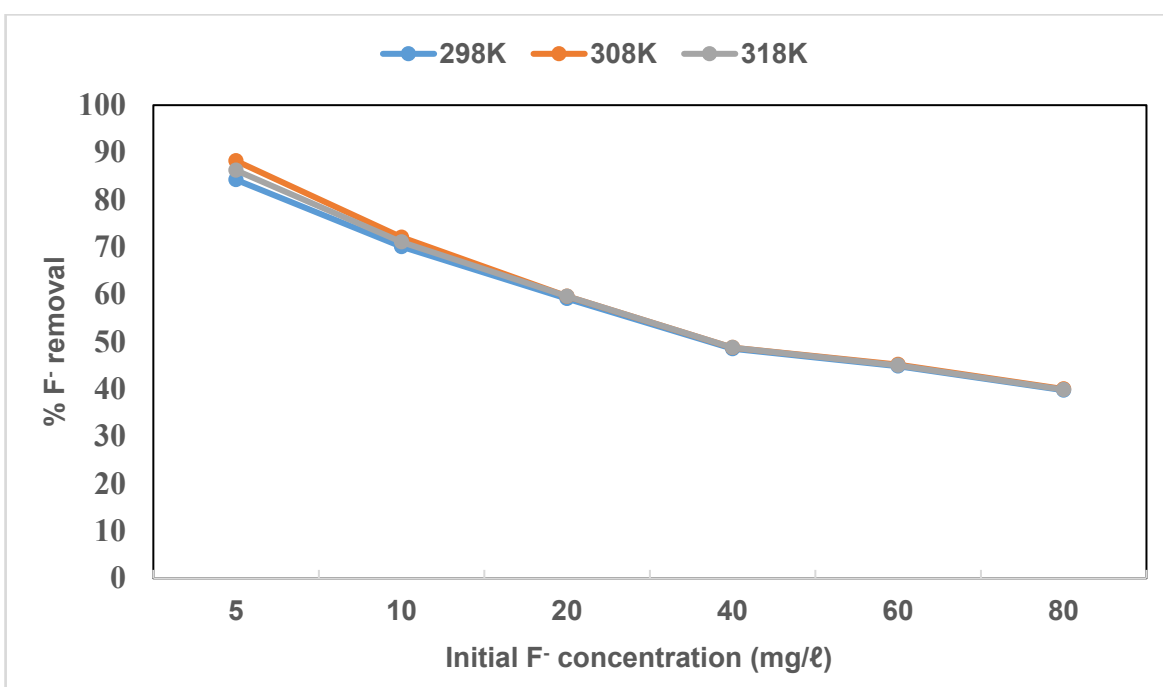


Figure 5.7. Percentage fluoride removal by Fe_2O_3 coated bentonite clay as a function of temperature. (60 minutes contact time, 25°C room temperature, 3 g/100 mL S/l ratio, 250 rpm, n=3).

5.5.6 Effect of pH on fluoride removal capacity

Percentage fluoride removal by Fe_2O_3 coated bentonite clay as a function of pH is presented in Figure 5.8. The pH was varied from 2 to 12. The pH of medium is one of the crucial parameters that can influence the fluoride removal capacity of an adsorbent. The effect of pH on the fluoride removal efficiency of Fe_2O_3 coated bentonite clay was evaluated over the pH range 2-12. The Fe_2O_3 coated bentonite clay exhibited high fluoride removal over a wide range of pH 2-12. Decline of about 19% in the fluoride removal at pH > 10 was observed which may be due to the abundance of OH^- on the adsorbent surface which may affect the fluoride uptake due to extreme competition for adsorption sites.

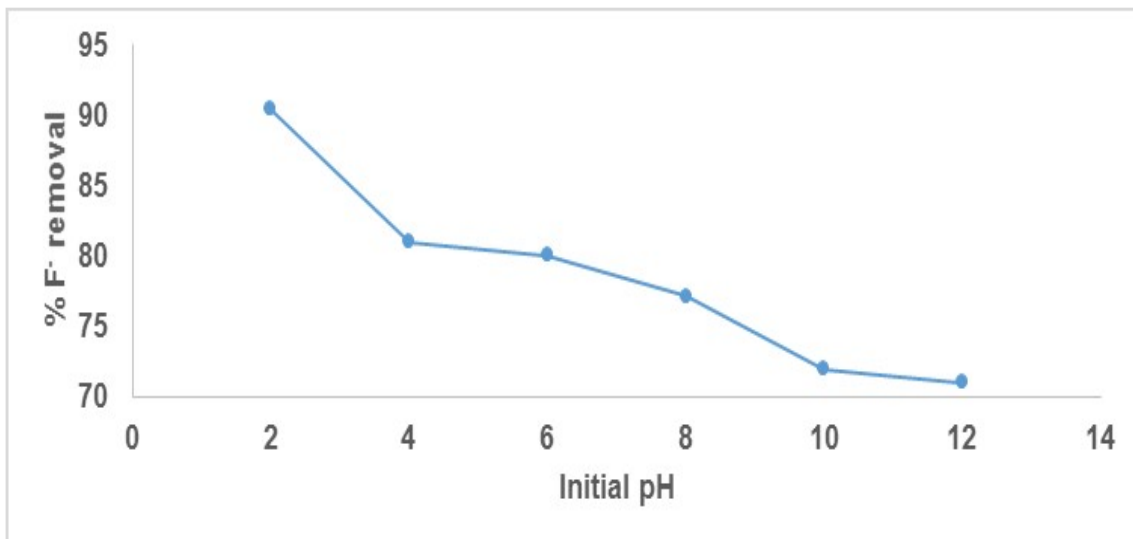


Figure 5.8. Percentage fluoride removal by Fe₂O₃ coated bentonite clay as a function of pH (60 minutes contact time, 5 mg/l F⁻, 25°C room temperature, 3 g/100 ml, S/l ratio, 250 rpm, n=3)

5.5.7 Effect of co-existing ions on fluoride removal capacity

Percentage fluoride removal by iron(III) oxide coated bentonite clay as a function of co-existing ions is presented in Figure 5.9. The influence of coexisting ions, carbonate, phosphate, nitrate and sulphate on fluoride adsorption was evaluated. Tests were conducted in the presence of 10 mg/l of fluoride and 10 mg/l each of co-existing ion.

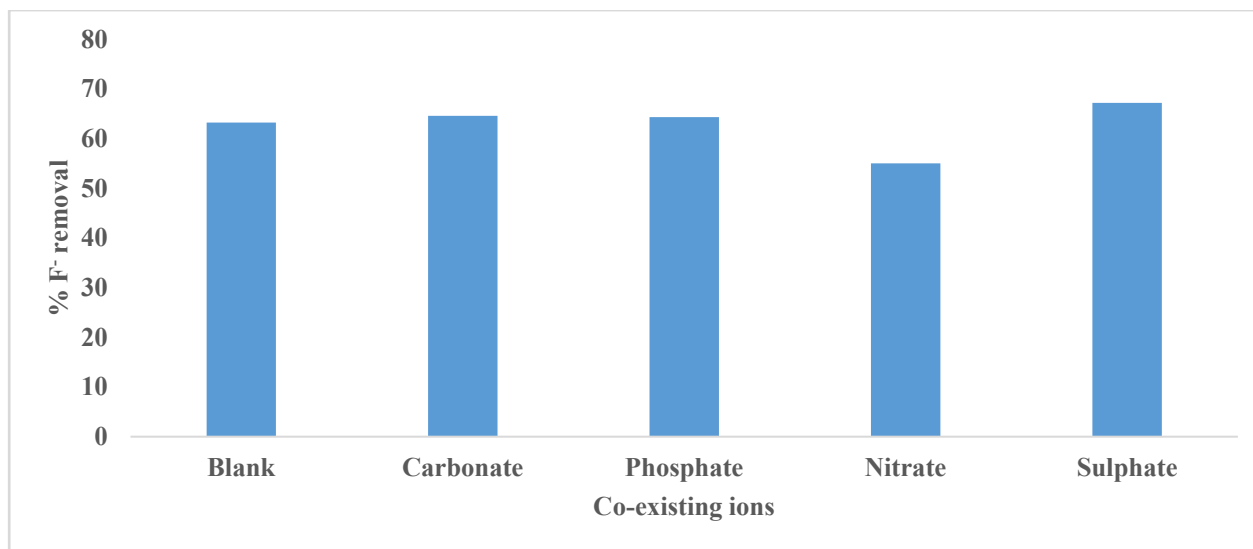


Figure 5.9. Percentage removal of fluoride by iron(III) oxide coated bentonite clay as a function of co-existing ions (30 min contact time, 10 mg/l F⁻, 25°C room temperature, 3 g/100 ml S/l ratio, 250 rpm, pH_i = 6.47, n=3)

It was observed that the adsorption capacity for fluoride decreased from 63 to 55% in the presence of nitrate. It is expected that the presence of anions in solution would enhance coulombic repulsion forces between the anions and fluoride or would compete with fluoride for the active sites. However, the other ions did not negatively affect fluoride removal. In the presence of sulphate, the fluoride removal efficiency was even higher compared to the blank sample.

5.6 TREATMENT OF FIELD GROUND WATER FROM SILOAM COMMUNITY BOREHOLE AT OPTIMIZED CONDITIONS

Table 5.4 shows the physicochemical properties of field groundwater from a community borehole before and after defluoridation at field and at optimised initial pH. The optimised conditions of 30 min of contact time, 3 g of adsorbent dosage, 298 K temperature and a pH of 2 established in the optimization stage were applied to defluoridation of Siloam borehole water. Measured parameters were within the SANS241 (2015) water quality guidelines except for F⁻ and Cl⁻ at both initial field and optimised pH conditions.

Table 5.4. Defluoridation of field groundwater by Fe₂O₃ coated bentonite clay at field and optimized initial pH conditions. (60 minutes contact time, 25°C room temperature, 3 g/100 ml S/l ratio, 250 rpm)

Parameter	Siloam borehole water	Field pH = 7.81	Initial adjusted = pH 2	SANS241-1 (2015)
		Equilibrium parameters after Treatment		
pH	7.81	7.624	7.11	6-9
EC (µS/cm)	25.74	25.12	25.10	0-150
F ⁻ (mg/l)	5.53	4.23	3.23	1-1.5
Cl ⁻ (mg/l)	31.60	180.10	189.10	0-250
SO ₄ ⁻ (mg/l)	11.9	N.D	N.D	0-250
Br ⁻ (mg/l)	2.08	N.D	N.D	0-6
NO ₃ ⁻ (mg/l)	1.13	N.D	N.D	0-6
PO ₄ ³⁻ (mg/l)	ND	N.D	N.D	0-5

ND= not detected

However, the removal efficiency for F⁻ efficiency was higher at optimised pH conditions. The lower % F⁻ removal at initial field pH conditions could be due to the effect of co-existing ions which competed for adsorption sites with F⁻. It is expected that the presence of anions in solution would enhance coulombic repulsion forces between the anions and fluoride or would compete with fluoride for the active sites (Onyango et al., 2004). Daifulla et al. (2007) observed that the adsorption capacity for fluoride decreased from 100 to 91% in the presence of sulphate and to 94% in the presence of bromide but chloride does not affect fluoride adsorption. Another study by Thakre et al. (2010) showed a significant drop in the fluoride removal efficiency in the presence of bicarbonate ion. Chloride seemed to be released into solution, this could be attributed to the residue Cl⁻ during the modification of bentonite with FeCl₃ solution as the Fe³⁺ source. Metal species before and after defluoridation were also evaluated to inform on the final water quality and impact of the adsorbent (Table 5.5). Metal species leaching from the adsorbent at neutral pH were within permissible limits except for Al, Na and Fe. However, at these levels Al and Fe have no known health effects but rather aesthetic effects. At 1423 mg/l Na will cause a highly salty taste and there is a likelihood of nausea and vomiting. At those levels the Na may be highly undesirable for infants or persons on a sodium restricted diet (DWAF, 1996). This would be one of the limitations of this adsorbent in defluoridation, however the high Na content is attributed to the NaOH used for pH adjustment and during co-precipitation of the Fe³⁺ solutions with bentonite clay. This could be reduced through repeated rinsing of the adsorbents with MilliQ water after preparation.

Table 5.5. Metal concentration before and after defluoridation

Metals ($\mu\text{g}/\ell$)	Field water (pH = 7.81)	Treated water (pH = 7.11)	Metals (mg/ℓ)	Field water (pH = 7.81)	Treated water (pH = 7.11)
Li	8.824888	9.071993	Al	0.04392	0.8336
Be	< 0.005	0.039969	Ca	3.163	10.56
B	22.61723	12.401841	Fe	0.163251	10.25
V	0.084905	0.373527	K	2.544	4.916
Cr	0.227367	4.165272	Mg	0.0396	8.992
Mn	17.46683	39.14397	Na	67.58	1423
Co	0.028445	0.549693	P	< 0.01	0.0043
Ni	0.741724	2.789933	Si	45.51	13.38
Cu	10.74428	7.319199	Sr	0.0234	0.1277
Zn	11.47378	8.552546			
As	< 0.03	0.124786			
Se	< 0.54	0.721939			
Mo	1.352091	0.508769			
Cd	< 0.04	0.007985			
Sb	< 0.01	0.053063			
Ba	40.61815	104.776			
Hg	< 0.01	<0.004			
Pb	0.592015	0.789663			

5.7 CHEMICAL STABILITY OF THE ADSORBENT

The chemical stability of the adsorbent under various pH conditions was evaluated by measuring the concentration of dissolved metals in the solution after adsorption (refer to Appendix B for detailed methods). Data on concentration of metals leached at various initial pH is presented in Table 5.6. pH had a major influence on the chemical stability of iron(III) oxide modified bentonite clay. It is observed that high leaching of chemical species occurred at pH 2 and 12. However at pH 6 which is near neutral, the leaching of chemical species was minimal. When compared to the SANS 241-1 (2015) guidelines, the concentration of metals Al, Mn and Fe exceeds the recommended limits at pH 2 and 12. This indicates that defluoridation at pH 2 using the iron oxide coated bentonite would be undesirable.

Table 5.6. Concentration of metals in solution after defluoridation at pH 2, 6 and 12

Metals($\mu\text{g}/\ell$)	pH 2	pH 6	pH 12	Metals(mg/ℓ)	pH 2	pH 6	pH 12
Li	20.20	15.87	7.08	Ca	37.15	18.67	1.42
Be	2.82	<0.000	0.74	K	6.06	7.40	5.18
B	32.37	15.06	30.21	Mg	27.61	14.54	1.10
Al	3202.86	17.10	6397.2	Na	2200.0	2142.0	2236.0
V	<0.000	<0.000	1.88	P	0.01	0.01	0.06
Cr	<0.000	0.56	8.21	Si	8.47	0.94	13.84
Mn	1180.86	6.79	27.48				
Fe	30.549	15.774	5668.28				
Co	25.96	0.08	0.51				
Ni	91.02	0.67	2.58				
Cu	14.20	0.20	4.48				
Zn	30.95	2.00	7.38				
As	<0.1	<0.1	0.54				
Se	2.12	2.56	3.99				
Sr	895.00	267.53	4.96				
Mo	0.27	0.31	10.97				
Cd	0.41	0.05	0.05				

Metals($\mu\text{g}/\ell$)	pH 2	pH 6	pH 12	Metals(mg/ℓ)	pH 2	pH 6	pH 12
Sb	0.08	0.11	0.16				
Ba	1059.14	110.00	11.66				
Hg	0.01	<0.05	0.04				
Pb	<0.05	<0.05	1.08				

However, it can be seen that it is only Na that considerably leached into solution at all the tested pHs. This is attributed to the Na introduced during pH adjustment and residual Na during the modification and activation process. According to SANS 241-1 (2015) guidelines, Na should be <200 mg/l and the Na concentration was \approx 2000 mg/l which is above the recommended water quality guidelines and is highly undesirable for infants or persons on a sodium restricted diet.

5.8 REUSE AND REGENERATION OF IRON(III) OXIDE COATED BENTONITE CLAY

Regeneration of the spent adsorbent is a key factor which targets the real economy of an adsorption system. Therefore, in the present work the spent adsorbent was regenerated to assess its reusability. For detailed procedures refer to Appendix B. A fluoride adsorption experiment was performed with fresh and regenerated iron(III) oxide coated bentonite clay to determine the effectiveness of the regeneration process and adsorption capacity of regenerated adsorbent. The results are presented in Figure 5.10. The regenerated adsorbent has less adsorption capacity as compared to fresh iron(III) oxide coated bentonite clay. The adsorption capacity decreases as the regeneration cycles increase. However, for the first 2 regeneration cycles the adsorbent has a fairly good fluoride removal capacity indicating potential for reuse of the adsorbent. This further substantiates the mechanism of fluoride uptake through the replacement of hydroxyl group/anions from the metal oxide sites of bentonite clay.

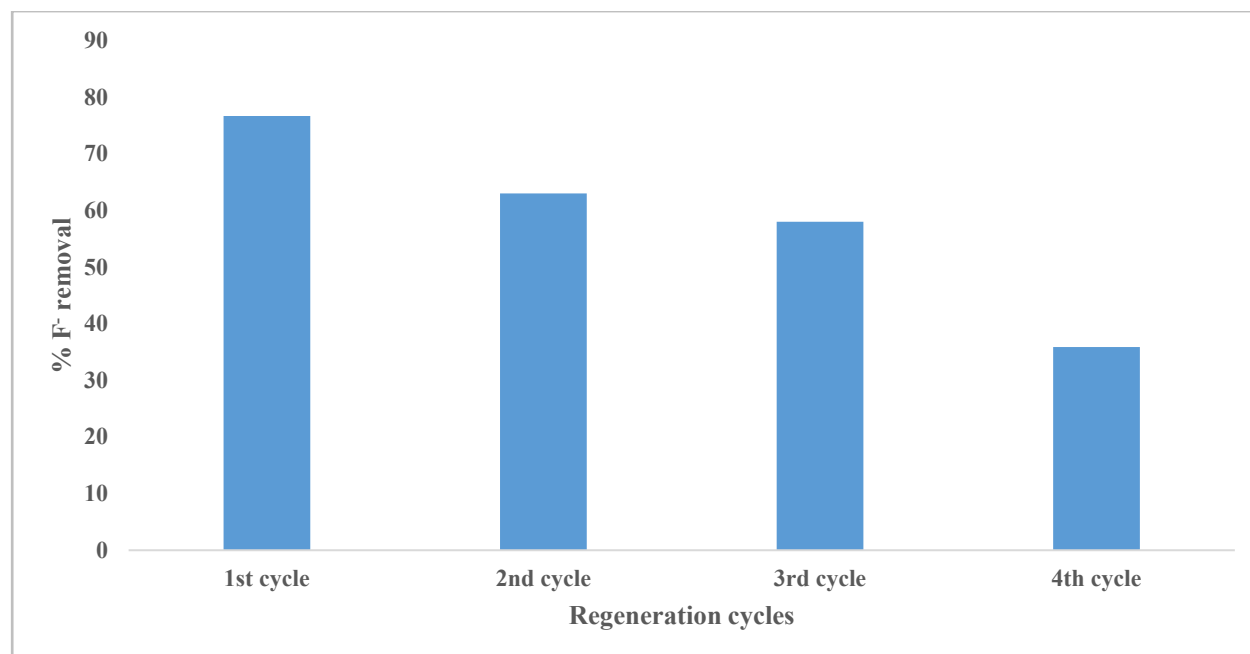


Figure 5.10. Regeneration studies using 0.01 M NaOH (10 mg/l F⁻, 100 ml solution, 2 g adsorbent dosage)

5.9 ADSORPTION MODELLING

5.9.1 Isotherm models

The concentration of an adsorbate (F^-) in a bulk solution is in dynamic balance with that of the adsorbent interface. The analysis of equilibrium data helps to develop mathematical models that could be used for the quantitative description of the results. The equation parameters and the underlying assumptions of these equilibrium models are capable of predicting ion adsorption and generating vital information on the mechanism of sorption. The Langmuir, Freundlich and Dubinin-Radushkevich isotherms were tested in this study (refer to Appendix C for details). Table 5.7 presents calculated parameters for the Langmuir, Freundlich and Dubinin-Radushkevich adsorption Isotherm models for the Fe_2O_3 coated bentonite adsorption data. The Dubinin-Radushkevich also describes a multilayer surface and with the high values of R^2 is an indication that adsorption onto the Fe_2O_3 coated bentonite clay is a heterogeneous surface. Adsorption phenomena. This is also corroborated by the good fit shown by the Freundlich isotherm. The magnitude of the mean free energy of adsorption (E) calculated from DR equation is useful for estimating the type of adsorption. If (E) is less than 16 kJ/mol, the adsorption type can be explained by ion exchange (Qadeer et al., 1995). From Table 5.7 it can be seen that all the (E) values are less than 16 kJ/mol, implying that fluoride ions in the solution were exchanged with the OH groups on the Fe_2O_3 coated bentonite clay.

Table 5.7. Calculated Langmuir, Freundlich and Dubinin-Radushkevich isotherm parameters

Langmuir Isotherm				
Temp (K)	Q_m (mg/g)	b (l/mg)	R_L	R^2
298	1.93	0.072	0.148	0.9303
308	1.88	0.0816	0.133	0.9207
328	1.9	0.077	0.139	0.9293
Freundlich Isotherm				
Temp (K)	K_F (mg/g)	$1/n$	n	R^2
298	1.2186	0.5031	1.9877	0.9929
308	1.2385	0.4783	2.0907	0.9887
328	1.2467	0.4666	2.1432	0.9858
Dubinin-Radushkevich Isotherm				
Temp (K)	Q_D (mg/g)	B_D	E (J/mol)	R^2
298	1.1489	0.6145	0.5543	0.9993
308	1.1611	0.5936	0.3852	0.9993
328	1.1628	0.5899	0.3840	0.9993

5.9.1.1 Langmuir Isotherm

Figure 5.11 shows the Langmuir adsorption isotherm for fluoride adsorption onto Fe_2O_3 coated bentonite clay at various temperatures. Figure 5.11 shows that the R^2 values at different temperatures, which ranged from 0.92-0.94 confirming that the sorption data fitted well to Langmuir Isotherm. Calculated R_L (separation factors) value indicates the adsorption nature to be either unfavourable if $R_L > 1$, linear if $R_L = 1$, favourable if $0 < R_L < 1$ and irreversible if $R_L = 0$. The calculated R_L values were 0.148, 0.133 and 0.139 respectively. They were all greater than 0 but less than 1 indicating F^- adsorption is a favourable process. The maximum Langmuir monolayer coverage capacity (Q_m) at all temperatures was determined to be 1.93, 1.88 and 1.9 mg/g. This is

comparable to the experimental adsorption capacity 1.52 mg/g further confirming that this adsorption process can be described by Langmuir model.

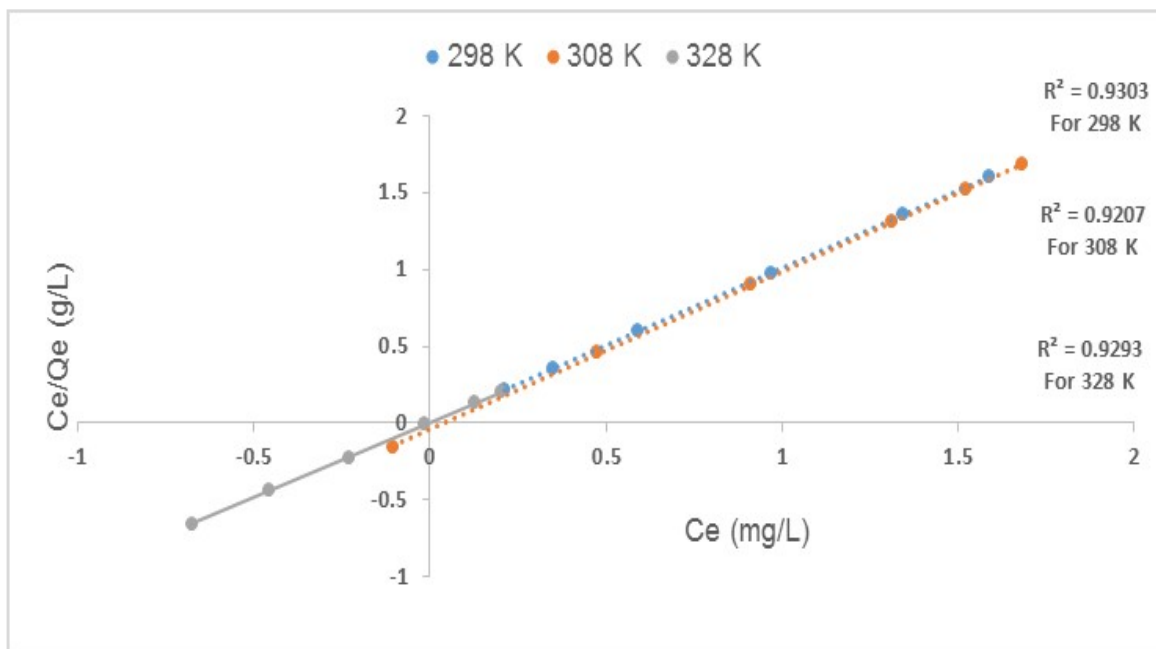


Figure 5.11. Langmuir adsorption isotherm for adsorption of F⁻ by Fe₂O₃ modified bentonite clay (3 g adsorbent dosage, 60 minutes of equilibration time, 5-80 mg/l F⁻)

5.9.1.2 Freundlich Isotherm

The plot of log Q_e against log C_e is shown in Figure 5.12. The constants n and K_f were determined from the slope and the intercept respectively. The constant K_f is an approximate indicator of adsorption capacity, while 1/n is a function of the strength of adsorption in the adsorption process (Voudrias et al., 2002). If n lies between 1-10, this indicates a favourable sorption process (Goldberg, 2005). The values of n were between 1 and 3, which indicates that the sorption of fluoride onto Fe₂O₃ coated bentonite clay is favourable and the R² values are above 0.98 showing a good fit to the Freundlich adsorption isotherm compared to the Langmuir isotherm. The experimental adsorption capacity (1.52 mg/g) was also close to the calculated adsorption capacity (K_f)(1.21 mg/g).

5.9.1.3 Dubinin-Radushkevich isotherm model

lnQ_e was plotted against ln (1+1/C_e) (Figure 5.13), and the constants B_D and Q_D were deduced from the slope and intercept are shown in Table 5.7.

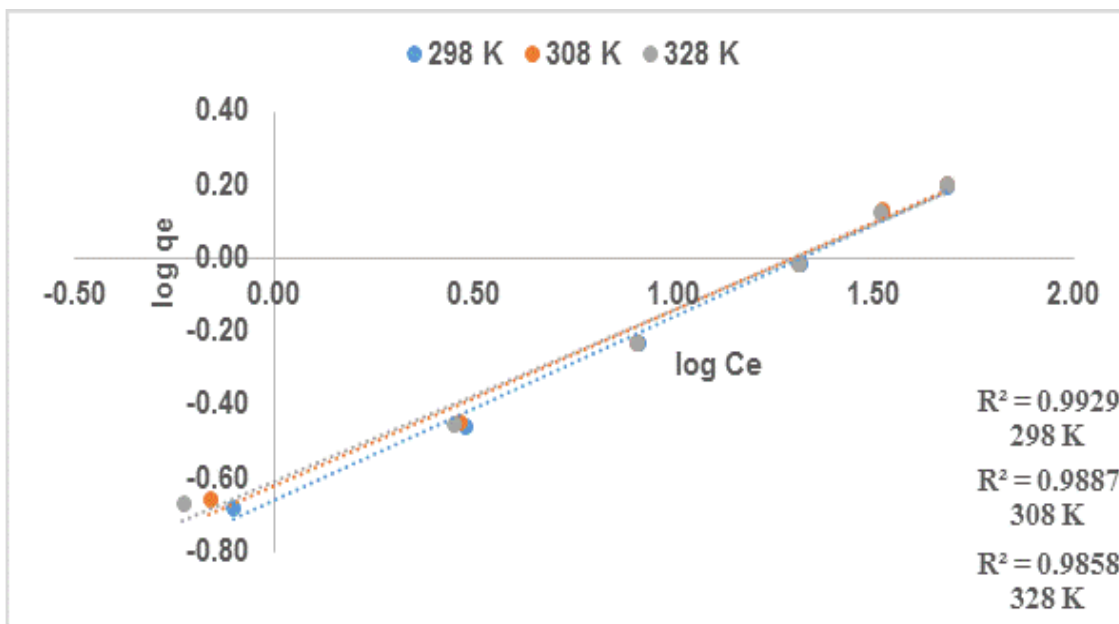


Figure 5.12. Freundlich adsorption isotherm (3 g adsorbent, 60 minutes of equilibration time, concentration was varied from 5-80 mg/ℓ)

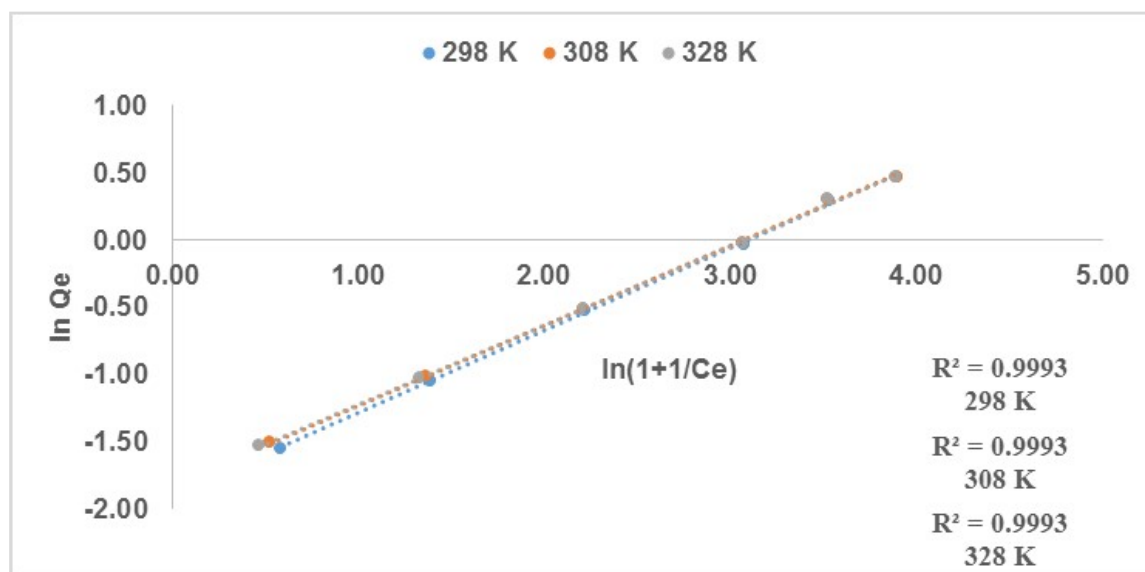


Figure 5.13. The Dubinin-Radushkevich adsorption isotherm (3 g of adsorbent, 60 minutes of equilibration time, 5-80 mg/ℓ F⁻)

5.9.2 Thermodynamics

In order to evaluate the feasibility of the adsorption process, thermodynamic parameters were evaluated (refer to Appendix C for details). Table 5.8 presents calculated thermodynamic parameters from the Van Hoff's plot of $\ln(K_a)$ vs $1/T$ (Figure 5.14). The values of ΔH and ΔS can be obtained from the slope and intercept of the Van Hoff's plot of $\ln(K_a)$ vs $1/T$. The positive value of enthalpy change suggests that the fluoride adsorption process is endothermic in nature and corroborates with the findings reported in literature (Sundaram et al., 2009). The negative value of free energy change at all temperatures evaluated and positive value of entropy change suggests that fluoride adsorption process is favourable and spontaneous.

Table 5.8. Calculated Thermodynamic parameters for the Van Hoff's plot

Parameter	ΔG (kJ/mol)	ΔH (kJ/mol)	ΔS (kJ/mol/K)	K_a (l/g)
	-10604.0082	58.74	5.891	72

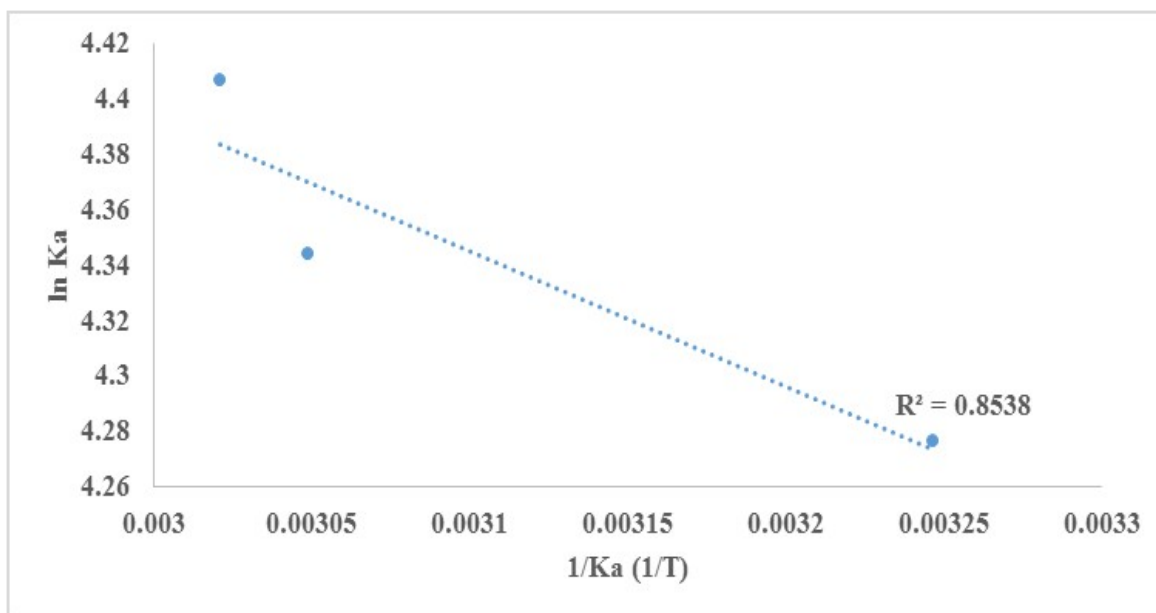


Figure 5.14. Plot of equilibrium constants against 1/T

5.9.3 Adsorption kinetics

5.9.3.1 Overview

Adsorption is a time-dependent process and it is very important to know the rate of the adsorption process for design purposes. The kinetics data of the fluoride adsorption onto the Fe_2O_3 coated bentonite clay were tested by fitting the data onto two adsorption kinetic models (detailed in Appendix C). This was done to determine the reaction order, rate limiting steps and the mechanism of the adsorption process.

5.9.3.2 Pseudo first- and second order kinetics

The fit of the pseudo first-order model to the fluoride adsorption kinetic data is shown in Figure 5.15, while Figure 5.16 shows the fit of the pseudo second-order model. The corresponding pseudo-second order calculated parameters are listed in Table 5.9.

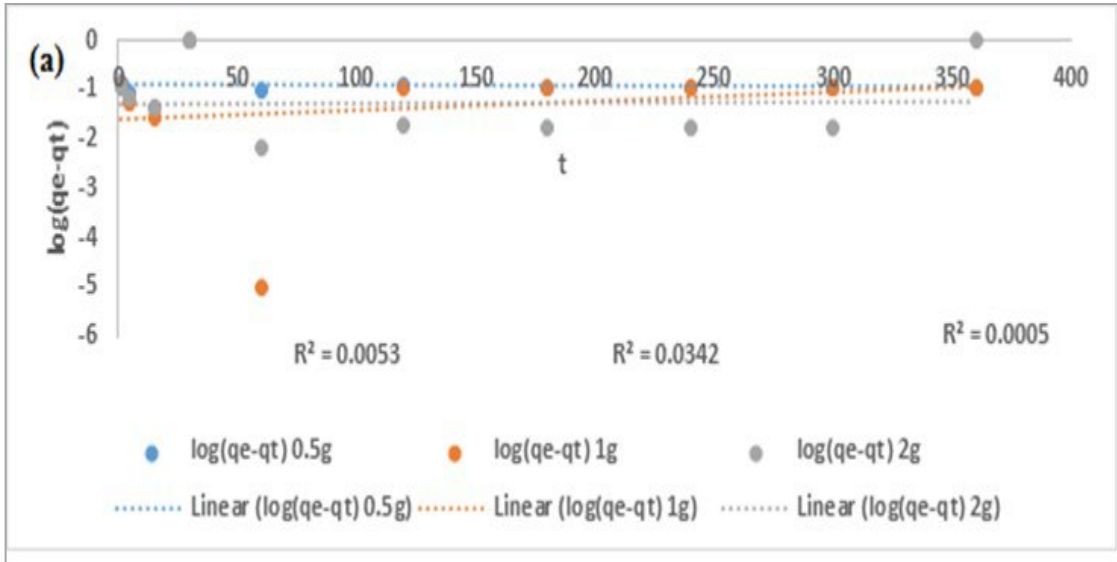


Figure 5.15. Pseudo-first order kinetic plot for adsorption of fluoride by Fe_2O_3 coated bentonite clay (0.5, 1 and 2 g dosage, 10 mg/l F^- , 25°C room temperature, 100 ml solution, 250 rpm).

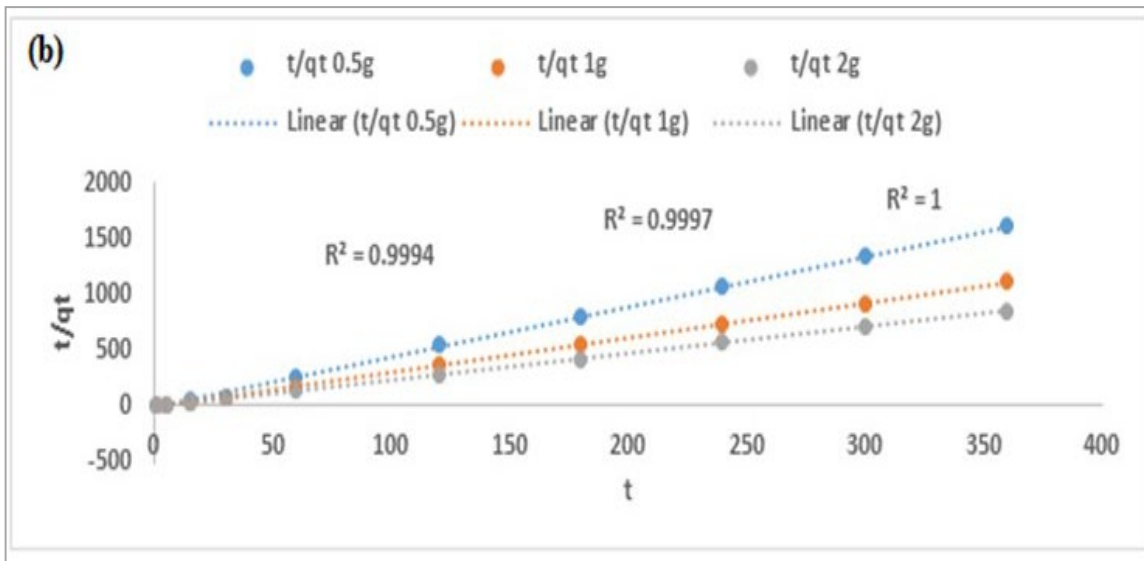


Figure 5.16. Pseudo-second order kinetic plot for adsorption of fluoride by Fe_2O_3 coated bentonite clay (0.5, 1 and 2 g dosage, 10 mg/l F^- , 25°C room temperature, 100 ml solution, 250 rpm).

Table 5.9. Calculated pseudo-second-order kinetic parameters at various adsorbent dosages for fluoride removal by Fe₂O₃ coated bentonite clay

Dosage (g)	q _e exp (mg/g)	K ₂ (gmh)	q _e cal (mg/g)	R ²
0.5	0.34	1.4082	0.2205	0.9994
1	0.44	1.2554	0.3203	0.9997
2	0.44	3.9003	0.4232	1

The pseudo-second-order kinetic model proved to be more suitable in describing the adsorption kinetics of fluoride based on the correlation coefficient ($R^2 > 0.99$) as shown in Table 5.9, suggesting a chemisorption process (Ho et al., 1995). Moreover, it is observed that the theoretical adsorption capacity, q_e , (0.44 mg/g) (Table 5.9) were all very close to the experimental capacity (0.34 mg/g). Similar results were observed for the adsorption of fluoride by various adsorbents (Caia, 2015; Tchomgui-Kamga et al., 2010).

5.9.3.3 Intraparticle and external diffusion models

There are three steps involved in adsorption of the fluoride ions: (i) the fluoride ions diffuse from liquid phase to liquid-solid interface; (ii) the fluoride ions move from liquid-solid interface to solid surfaces; and (iii) the fluoride ions diffuse into the particle pores (Liao, 2012). To evaluate the relative contribution of intraparticle and external diffusion to the kinetic processes, the kinetic adsorption data were further fitted to the intraparticle and external diffusion models (refer to Appendix C for details). The intraparticle and external diffusion parameters were obtained from the slope of the linear portion of the curves shown in Figure 5.17 (a) and (b). Intraparticle diffusion is assumed to be the sole rate-controlling step if the regression of Q_t versus $t^{1/2}$ is linear and the plot passes through the origin (Arami, 2008). The fitting results (Figure 5.17a) show that the regression was linear, but the plot did not pass through the origin ($C \neq 0$). Therefore, the adsorption kinetics of fluoride ions onto iron(III) oxide coated bentonite clay was regulated by both external and intraparticle diffusion processes. It is observed from both figures that fluoride exchange by iron(III) oxide coated bentonite clay involves two stages. These two stages suggest that the ion exchange process proceeds by surface sorption and intraparticle diffusion. The first sharp linear region is a diffusion adsorption stage, attributing to the diffusion of fluoride molecules through the solution to the external surface of adsorbent (film diffusion). The second linear region is a gradual adsorption stage, where the intraparticle diffusion is rate-controlled (intraparticle diffusion) (Yao et al., 2010).

The intra-particle rate constants K_{id1} and K_{id2} obtained at both adsorbent dosages (Fig. 5.17a), the K_{id1} value is greater than the K_{id2} value, indicating that the initial step is faster than the final step, i.e. during the first 30 min, external diffusion took place and it was faster than intraparticle diffusion which occurred from 30 min onwards. The values of intercept C provide information about the thickness of the boundary layer and the resistance to the external mass transfer. The constant C was found to increase from initial phase (C_1) to final phase (C_2) for all adsorbent dosages as shown in Table 5.10, which indicates the increase of the thickness of the boundary layer and decrease of the chance of the external mass transfer and hence increase of the chance of internal mass transfer at the final phase (Alshameri, 2014). The linear plot at each concentration does not pass through the origin, indicating that the intraparticle diffusion is not the only rate controlling step (Das et al., 2012).

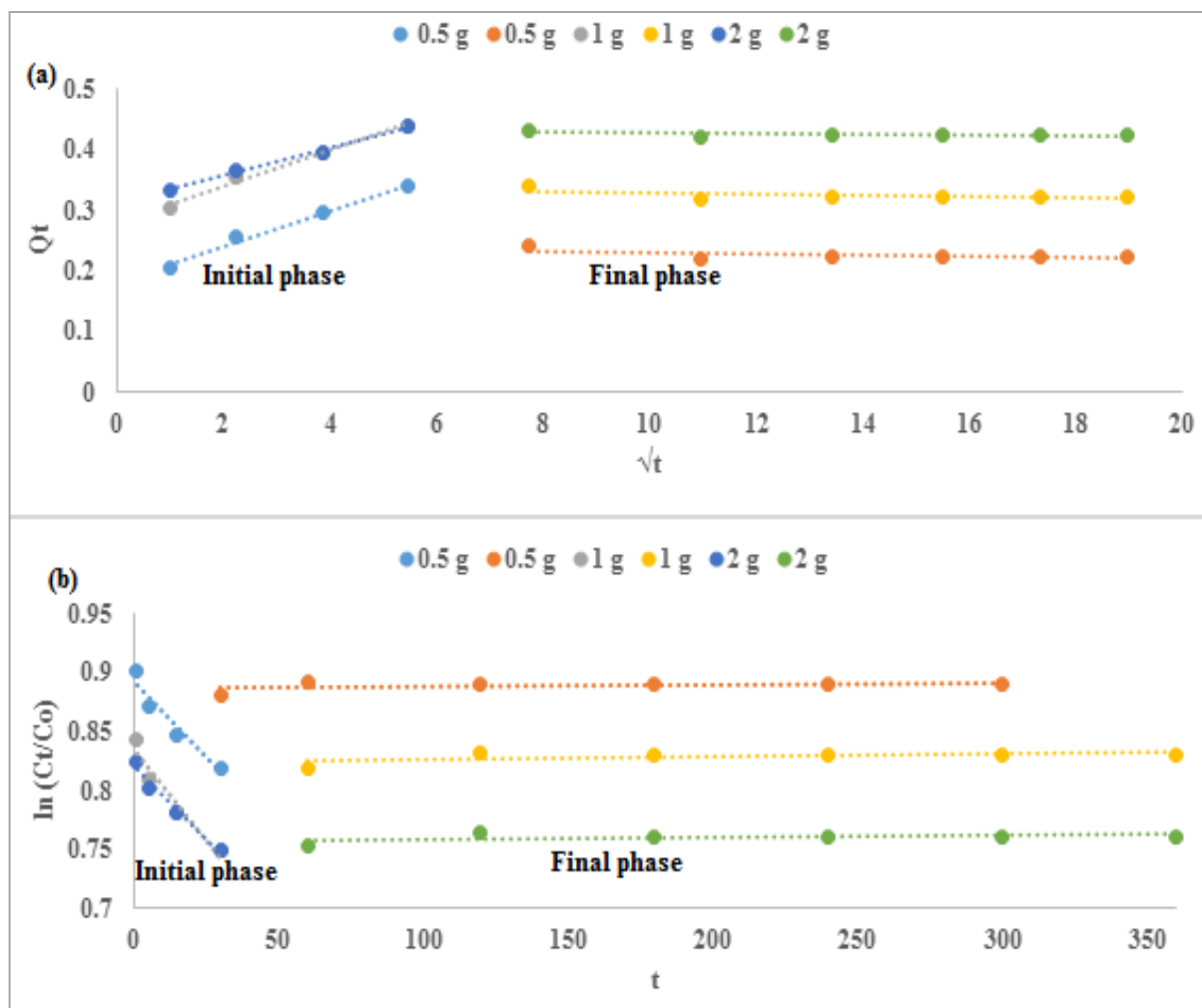


Figure 5.17. Data fit into (a) Intraparticle diffusion model and (b) external diffusion model (0.5, 1 and 2 g , 10 mg/l F^- , 25°C room temperature, 100 ml fluoride solution, 250 rpm $pH_i = 6.653$)

Table 5.10. Kinetic parameters of the fluoride adsorption onto iron(III) oxide coated bentonite clay

Model	Parameter	Dosage		
		0.5 g	1 g	2 g
Intraparticle diffusion	K_{id1}	0.0296	0.0296	0.0232
	K_{id2}	-0.011	-0.011	0.006
	$C1$	0.1809	0.2809	0.3112
	$C2$	0.2409	0.3409	0.4331
	R^21	0.9849	0.9849	0.9941
	R^22	0.4042	0.4042	0.3221
External diffusion	$kf1$	-0.0026	-0.03	-0.0025
	$kf2$	-0.5	-0.5	-0.5
	R^21	0.9294	0.9298	0.9718
	R^22	0.2336	0.3104	0.2402

5.10 SUMMARY

Iron(III) oxide/oxyhydroxides coated bentonite was synthesized through co-precipitation of Fe^{3+} solutions and bentonite clay. Bentonite clay was initially activated with NaOH to remove geological fluoride. Physicochemical and mineralogical characterisation was done by XRF, XRD, SEM-EDS, FTIR and BET. CEC and pH_{pzc} were evaluated using standard methods.

Modification of the bentonite clay with Fe-oxides increased the surface area compared to the raw bentonite. Batch adsorption variables evaluated included, adsorbate concentration, contact time, adsorbent dose, co-existing ions, pH and temperature. The Fe-oxides modified bentonite showed high F^- adsorption, >70% F^- removal was observed over the pH range 2-12 which is significant for field defluoridation of groundwater since no pH adjustment will be required. An adsorption capacity of 1.596 mg/g was recorded at an initial fluoride concentration of 80 mg/l, which was higher compared to the unmodified bentonite. Moreover, the residual concentration of chemical species in the treated water at initial pH of 6-9, were below the WHO drinking water guidelines. Solution pH played a major role in fluoride removal by Fe-oxides modified bentonite clay with maximum adsorption being observed at pH 2.

To assess how the fluoride adsorption capacity of iron(III) oxide coated bentonite clay compares with other adsorbents, a comparison is done with adsorbents reported in literature (Table 5.11)

Table 5.11. Adsorption capacities of various adsorbents compared to the present adsorbent

Adsorbent	Adsorption capacity	Experimental conditions	References
Fe(III) oxide bentonite	1.59 mg/g	pH 2, 80 mg/l	Present study
Al³⁺ bentonite	5.7 mg/g	pH 2-12, 60 mg/l	Vhahangwele et al. (2014)
Fe³⁺ bentonite	2.91 mg/g	pH 2, 60 mg/l	Gitari et al. (2013)
Mg²⁺ bentonite	2.3 mg/g	pH 3-10, 5 mg/l	Thakre et al. (2010)
La modified bentonite	1.5 mg/g	Neutral	Maiti et al. (2011)
Bentonite	1.2 mg/g	pH 2.8, 5 mg/l	Srimurali et al. (1998)

It is observed that modified bentonite clays have better fluoride removal capacities than raw bentonite clay. But compared with other non-clay adsorbents they are poor adsorbents but have advantage of being abundant and cheap for application in rural set-ups. Examples of high capacity adsorbents reported in literature include modified double layered hydroxides of Mg-Al-CO₃ with adsorption capacity of 303.54 mg/g (Batistella et al., 2011) and aluminium hydroxide impregnated with lime stone with adsorption capacity of 84.03 mg/g (Jain and Jayaram, 2009), however they will be costly to fabricate driving the cost of treatment out of reach of rural population.

The adsorption kinetics could be described by pseudo second order model suggesting chemisorption process. The developed adsorbent shows potential for further development and application in defluoridation devices at household level.

6 EVALUATION OF GROUNDWATER DEFLUORIDATION BY RED/BLACK MUKONDENI CLAY SOILS – IRON(III) OXIDE MODIFIED BENTONITE CLAY COMPOSITE CERAMIC PELLETS

6.1 INTRODUCTION

The ceramic pellets were an attempt to develop a material that is conducive for use in fixed bed devices. Adsorbent composites usually have combined advantages of their components when used for water treatment (Tran et al., 2013). Findings presented in this Chapter include;

- a. Optimization of fabrication conditions for the ceramic composite pellets
- b. Fabrication of the ceramic composite pellets at the optimized conditions
- c. Evaluation of the defluoridation potential of the ceramic pellets

6.2 MATERIALS

All chemicals used in the present study were of analytical reagent grade and were obtained from Rochelle Chemicals and Lab Equipment CC, South Africa Ltd. Both red/black clay soils and iron(III) oxide modified bentonite clay were collected and prepared as described in Chapters 4 and 5, respectively. Fluoride-rich water was collected from a borehole in Siloam village in Limpopo province.

6.3 METHODS

6.3.1 Fabrication of ceramic composite pellets

The two clays were mixed with MilliQ water (18.2M Ω cm) at room temperature manually to prepare the ceramic composite pellets. First, the clay samples were milled into a fine powder using a Retsch RS 200 miller. For the clay to be moulded, 10 ml of MilliQ water was added to 40 g of clay. The resulting mixtures were then moulded into pellets, using a cylindrical plastic mould (a plastic lid in this case was used in the lab because of the absence of an extruder) with internal dimensions of approximately 10- and 5-mm diameter and depth, respectively. The pellets were then allowed to cool at room temperature for 12 h before sintering in a furnace.

6.3.2 Optimisation of fabrication conditions

To determine which parameters are effective for the fabrication of ceramic pellets and the effect of these parameters on fluoride adsorption, four parameters were evaluated, namely; particle size; furnace temperature for drying; firing time and clay ratios. These are discussed below.

6.3.2.1 *Optimisation of particle size*

Clay particle size was the first parameter to be optimised since it would determine the appropriate size of clay particles which will not crack upon heating. Three particle sizes were used and these were obtained by using different sized sieves to obtain 125, 250 and 500 µm grains of clay. Pellets were fabricated as described above and thereafter dried in the oven at 105°C for 12 h. The pellets were then allowed to cool at room temperature for 12 h thereafter heated in the furnace at 600°C for an hour.

6.3.2.2 *(ii) Optimisation of furnace temperature*

Pellets were fabricated using the procedure described above and thereafter dried in the oven at 105°C for 12 h. The pellets were then allowed to cool at room temperature for 12 h after which they were heated in the furnace for an hour. The sintering temperatures were 600, 700, 800 and 900°C. These pellets were then crushed into fine powder and used for defluoridation experiments.

6.3.2.3 *(iii) Optimisation of firing time*

Fabricated pellets were dried in the oven at 105°C for 12 h. The pellets were then allowed to cool at room temperature for 12 h after which they were heated in the furnace at 600°C. The firing times were 1 h, 2 h and 3h. These pellets were then crushed into fine powder and used for defluoridation experiments.

6.3.2.4 *(iv) Optimisation of clay ratios*

The clay ratios were varied as follows iron(III) oxide coated bentonite (FeB): silica-rich reddish black Mukondeni clay soil (SRRBM) (1:1, 1:2, 2:1, 3:1, 4:1, 5:1 and 6:1), i.e. ([10 g (FeB): 10 g (SRRBM)], [10 g (FeB): 20 g (SRRBM)], [20 g (FeB): 10 g (SRRBM)], [30 g (FeB): 10 g (SRRBM)], [40 g (FeB): 10 g (SRRBM)] [50 g (FeB): 10 g (SRRBM)] [60 g (FeB): 10 g (SRRBM)]). After drying in the oven at 105°C for 12 h, the pellets were then allowed to cool at room temperature for 12 h after which they were heated in the furnace at 600°C for 1 h. These pellets were then crushed into fine powder and used for defluoridation experiments.

6.3.3 **Characterisation studies**

Several techniques were used to characterize the ceramic pellets fabricated according to each of the conditions described above. Procedures for adsorbent characterisation are detailed in Appendix A.

6.3.4 **Defluoridation experiments**

To determine the optimum conditions for fabricating the ceramic pellets that would effectively remove fluoride from water, a defluoridation experiment was carried out at each stage of optimisation to determine which conditions gave the highest fluoride removal. The defluoridation experiments were carried out as follows:

A known weight (2 g) of the adsorbent was added to 100 ml of 10 mg/l fluoride solution in a 250 ml plastic bottle and then agitated on a reciprocating shaker at 250 rpm at room temperature. After continuous stirring for 60 min, the samples were filtered using a 0.45 µm pore cellulose nitrate membranes and the samples were analysed for F-, pH, Temp and EC using a Thermo Scientific Orion Versa Star Advanced Electrochemistry

meter. Thereafter the final ceramic pellets were fabricated using the procedure described in 6.3.1 using the following optimised conditions: (i) particle size = 250 μm , (ii) furnace temperature = (600°C), (iii) firing time = 1 h and (iv) clay ratio = 5:1.

6.4 FLUORIDE ADSORPTION UNDER DIFFERENT ADSORBENT FABRICATION CONDITIONS

6.4.1 Effect of particle size

The effect of particle size on the fabrication efficiency of the ceramic pellets was evaluated by synthesis using particles of various sizes. A range of sizes 125, 250 and 500 μm particles for both red/black clay soils-iron(III) oxide modified bentonite clay, the 250 μm particle size produced ceramic pellets with minimum cracks and therefore this particle size was selected as the optimum for subsequent experiments.

6.4.2 Effect of furnace temperature

Different types of clay minerals exhibit characteristic behaviour on heating. Earlier work consisted for the most part, of correlating the amounts of water lost on ignition with the temperature, of determining the thermal energy associated with the dehydration, and of identifying the products formed at high temperatures (Warsha, 1960). Firing clays causes the aggregates to have a rough and microscopic porous surface with an increased surface area. High temperatures can also change the lattice structure of various minerals in the clays. Since firing clays alters the clay materials physicochemically and mineralogically, it becomes imperative that these properties be evaluated to determine which ones improve the adsorption capacity of the clay materials.

6.4.2.1 X-ray Diffraction analysis

Figure 6.1 shows images of iron(III) oxide modified bentonite-red/black clay soil composite ceramic pellets before and after calcination at 100, 600, 700 and 800°C. The prepared iron(III) oxide modified bentonite clay-red/black clay soil composite ceramic pellets are greyish in colour (a) before calcination but after calcination were reddish brown in colour (Figure 6.1 (b, c and d)). The reddish brown-colour is an indication of the presence of iron oxides. Figure 6.2 shows XRD diffractograms of iron(III) oxide modified bentonite-red/black clay soil composite pellets at 100, 600, 700, 800 and 900°C. Main mineral phase identified in the fired ceramic pellets are quartz and halite. Other minor phases identified include hematite, and muscovite which are iron bearing mineral phases. Microcline (KAlSi_3O_8) typically contains minor amounts of sodium.



Figure 6.1. Iron(III) oxide modified bentonite-red/black clay soil composite ceramic pellets before (a) and after calcination (b, c and d)

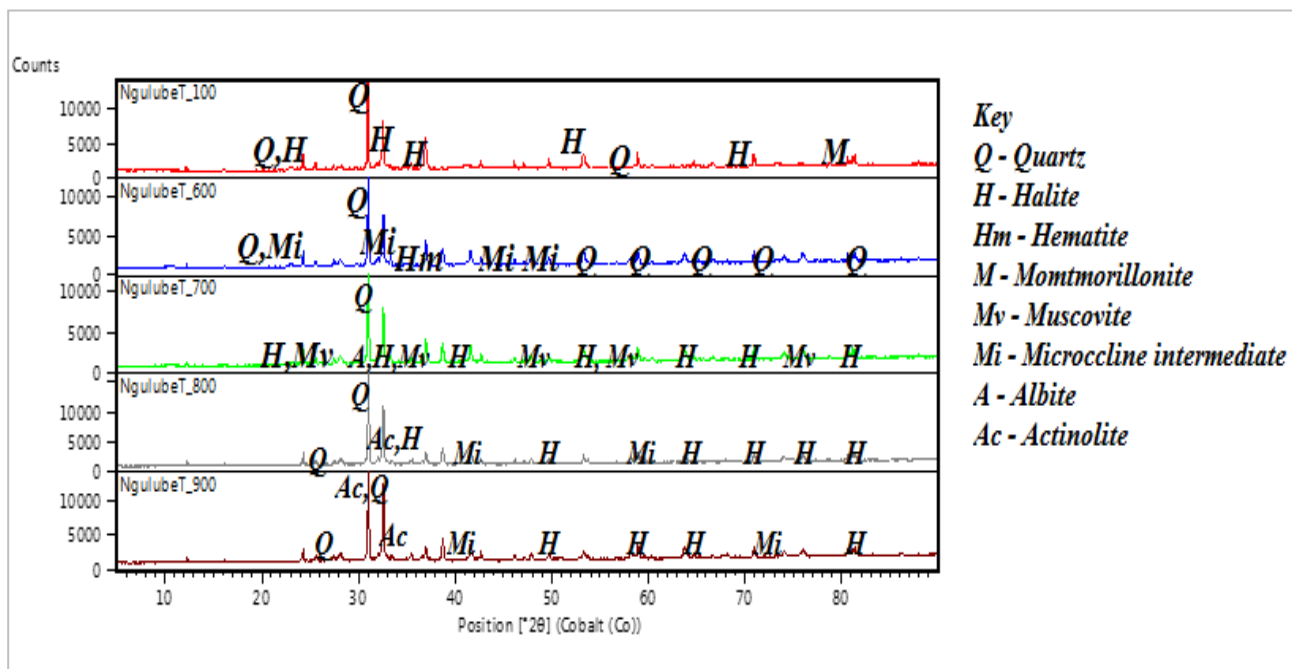


Figure 6.2. XRD diffractogram of iron(III) oxide coated bentonite-silica-rich reddish black Mukondeni clay soil composite pellets at 100, 600, 700, 800 and 900°C

6.4.2.2 Morphological Analysis

Morphological aspects of the iron(III) oxide modified bentonite clay-red/black clay soil composite ceramic pellets are presented in Figure 6.3. The scanning electron micrographs (SEM) show typical irregular plate like structures characteristics of bentonite clay. 100 and 600°C. This morphology seems to be lost as the firing temperature is increased to 800°C and replaced by angular small particles (Fig 6.35c). The porous nature of the material seems to be lost.

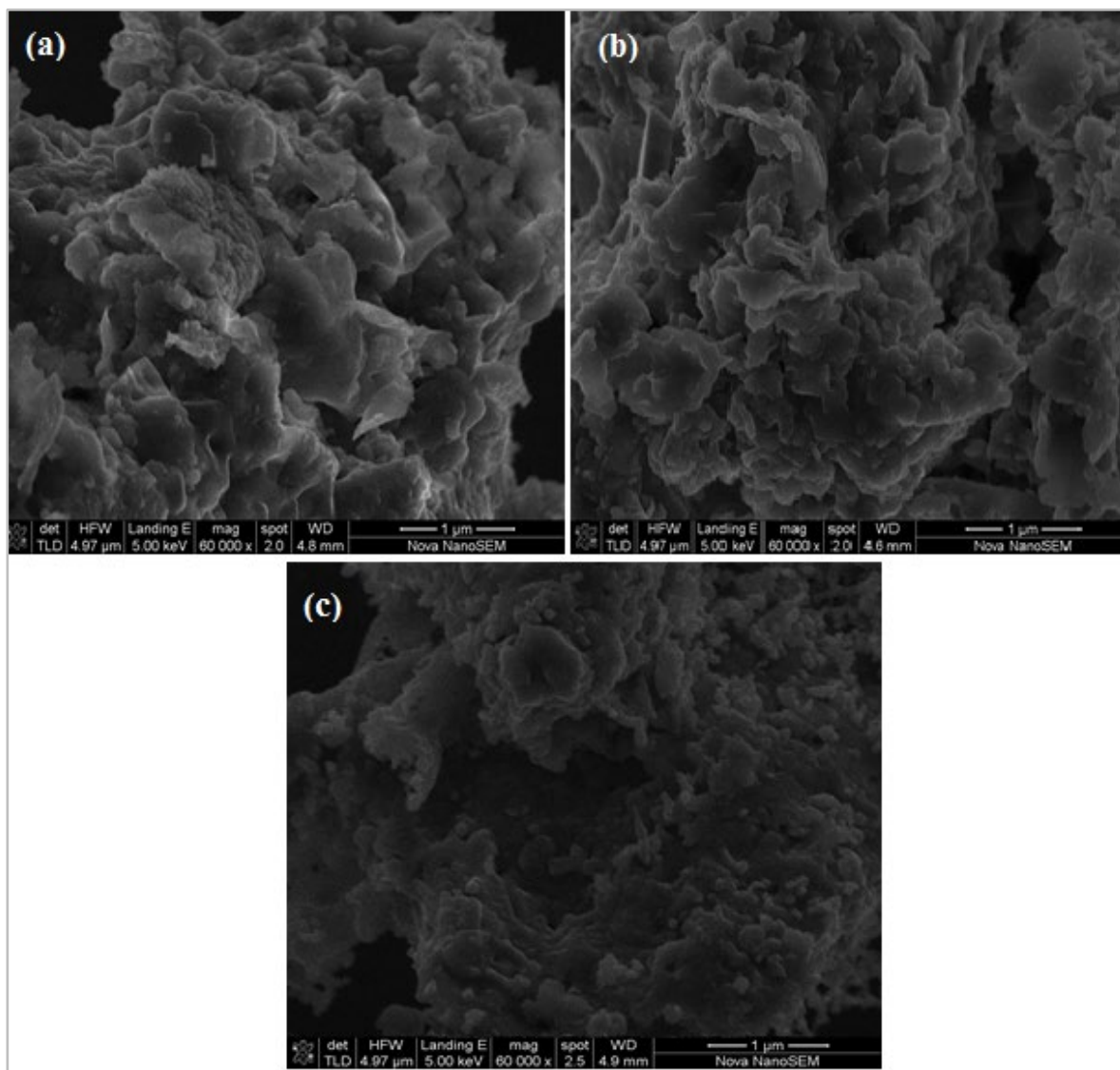


Figure 6.3. SEM micrographs of iron(III) oxide modified bentonite-rich red/black clay soil composite ceramic pellets at different calcination temperatures ((a) 100, (b) 600 and (c) 800°C)

6.4.2.3 Brunauer Emmett Teller (BET) analysis

Table 6.1 presents values of the surface area, pore volume and pore size of iron(III) oxide modified bentonite-red/black clay soil composite ceramic pellets. The BET surface area of the iron(III) oxide modified bentonite-red/black clay soil composite ceramic pellets were observed to be 174.89 m²/g on drying in the oven at 100°C. It is observed that increasing firing temperatures substantially changed the surface area. Surface area increased with increased firing temperatures. The pore volume was also observed to decrease with temperature. However, pore sizes seemed to increase with increasing firing temperatures. A compromise temperature of 600° was adopted as the optimum firing temperature and was adopted for fabrication of the ceramic pellets.

Table 6.1. Surface area, pore volume and pore sizes for iron(III) oxide modified bentonite-red/black clay soil composite ceramic pellets

	100°C	600°C	700°C	800°C
Surface area (m²/g)				
Single point surface area	174.89	67.40	20.95	10.70
BET Surface Area	181.42	70.00	21.69	11.18
BJH Adsorption cumulative surface area of pores	0.2508	79.96	24.32	11.49
BJH Desorption cumulative surface area of pores	0.2554	95.74	28.61	10.64
Pore Volume (cm³/g)				
Single point adsorption total pore volume of pores	0.2471	0.2546	0.1023	0.0378
BJH Adsorption cumulative volume of pores	0.2508	0.2631	0.1049	0.0367
BJH Desorption cumulative volume of pores	0.2554	0.2944	0.1206	0.0399
Pore Size (Å)				
Adsorption average pore width (4V/A by BET)	54.49	145.51	188.63	135.26
BJH Adsorption average pore diameter (4V/A)	57.11	131.59	172.48	127.57
BJH Desorption average pore diameter (4V/A)	58.60	123.02	168.54	150.31

6.4.2.4 Fluoride adsorption

Table 6.2 shows the fluoride adsorption potential of the ceramic pellets prepared at various firing temperatures. It is observed that as the firing temperature increased from 600 to 900°C, the percentage fluoride removal decreased by a factor of 2.03. This decrease in fluoride adsorption capacity is attributed to the decrease in surface area reported earlier. Reduction in fluoride adsorption capacity could also be due to the dehydration hydrous Fe(III) oxide phases leading to loss of hydroxyl groups.

Table 6.2. F⁻ adsorption potential of the ceramic pellets fired at various furnace temperatures

Parameter	Initial	(600°C)	(700°C)	(800°C)	(900°C)	SANS 241-1 (2015)
pH	6.02	6.44	6.79	6.68	6.64	5.0-9.5
TDS (mg/ℓ)	18.6	121.5	114.2	113.7	112.3	<1000
EC (µS/cm)	12.42	111.3	111.3	110.4	111.9	<150(mS/m)
F ⁻ (mg/ℓ)	10	7.12	7.34	8.26	8.34	1-1.5
% F removal	-	40.5	36.2	21.1	19.9	-

6.4.3 Effect of firing time

The duration in which the clays stay in the furnace is also critical in fabricating ceramic pellets. The effective time period in the furnace varies between types of clay. Tests were conducted to establish the optimum firing time at the optimized firing temperature. The optimized firing time was established through morphological changes, mineralogical and chemical composition, pore size distribution and specific surface area changes of the final product, as well as fluoride adsorption capacity at the different firing times. The results obtained are discussed individually in the sub-sections below.

6.4.3.1 Changing morphology with firing times

The morphology of the iron(III) oxide coated bentonite-red/black clay soil composite pellets at different firing times is shown in Figure 6.4. Morphology of the ceramic pellets do not change considerably at different firing times. The micrographs reveal clay particles with different shapes and sizes depicting a rough surface.

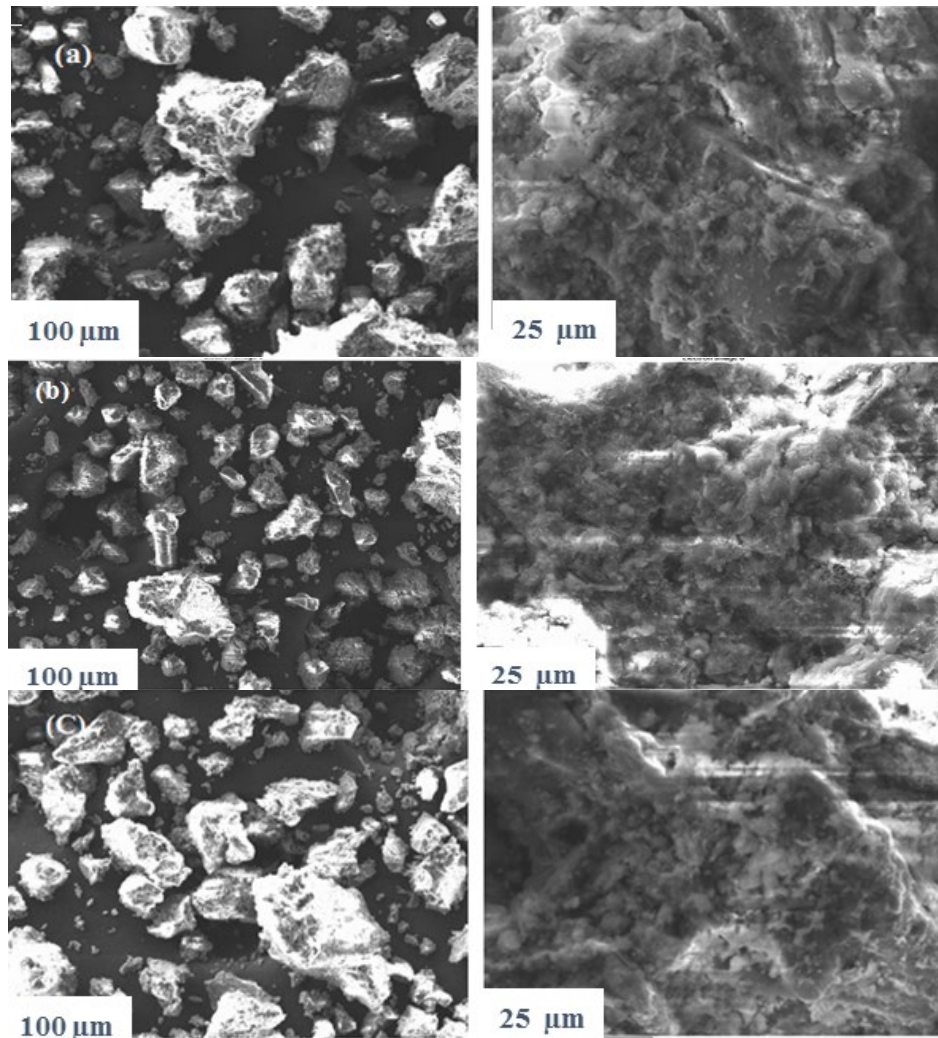


Figure 6.4. Morphology of iron(III) oxide coated bentonite-silica-rich reddish black clay soil composite pellets at two magnifications and different firing times (a) 1 h, (b) 2 h and (c) 3 h)

6.4.3.2 Mineralogical changes with firing times

The percentage composition of minerals in the iron(III) oxide coated bentonite-red/black clay soil composite pellets is presented in Table 6.3. The major minerals in the two clay soils forming the ceramic composite were quartz, plagioclase and hematite/goethite. Statistical analysis by One-way Analysis of Variance (ANOVA) showed that there was no significant variation at the various firing times.

Table 6.3. Mineralogical composition iron(III) oxide coated red/black clay soil composite pellets at different firing times

SAMPLE (W %)	1 h	2 h	3 h
Hematite/Goethite (FeO(OH))	18	20	18
K-feldspar (KAlSi ₃ O ₈ - NaAlSi ₃ O ₈ - CaAl ₂ Si ₂ O ₈)	1	6	1
Plagioclase (NaAlSi ₃ O ₈ - CaAl ₂ Si ₂ O ₈)	23	20	24
Quartz (SiO ₂)	29	29	34
Mica AB – 2-3 (X, Si) ₄ O ₁₀ (O, F, OH) ₂	6	6	6
Amphibole (SiO ₄)	9	3	4
Clinoptilolite (Na,K,Ca) ₂₋₃ Al ₃ (Al,Si) ₂ Si ₁₃ O. ₁₂ H ₂ O	3	7	5
Halite (NaCl)	7	6	6
I/S Interstratification	4	5	4

6.4.3.3 Chemical composition changes with firing time

The percentage composition of major elements given as metal oxides in iron(III) oxide coated bentonite-red/black clay soil composite pellets is presented in Table 6.4. It can be observed that there was no change in the chemical composition of the ceramic pellets at different firing times indicating no loss of modified iron(III) oxide.

Table 6.4. Chemical composition of iron(III) oxide coated-red/black clay soil composite pellets at different firing times

Sample	1 h	2 h	3 h
SiO ₂	54.72	54.78	54.76
TiO ₂	0.49	0.49	0.49
Al ₂ O ₃	12.87	12.96	12.91
Fe ₂ O ₃	16.45	16.66	16.67
MnO	0.081	0.082	0.082
MgO	2.64	2.59	2.65
CaO	1.64	1.64	1.64
Na ₂ O	5.65	5.67	5.66
K ₂ O	1.07	1.12	1.14
P ₂ O ₅	0.030	0.028	0.029
Cr ₂ O ₃	0.058	0.058	0.060
LOI	3.36	2.99	3.03
Total	99.05	99.07	99.10

6.4.3.4 Changes in surface area, pore volume and pore size distribution with firing time

Table 6.5 gives the surface area, pore volume and pore size for iron(III) oxide modified bentonite-red/black clay soil composite pellets. It can be observed that the firing times didn't affect the surface area and pore volume properties of the ceramic pellets.

Table 6.5. Surface area, pore volume and pore sizes of the composite pellets at different firing times

	1 h	2 h	3 h
Surface area (m²/g)			
Single point surface area	16.4828	15.1817	16.2468
BET Surface Area	16.8741	15.5784	16.6521
BJH Adsorption cumulative surface area of pores	15.655	15.257	16.245
BJH Desorption cumulative surface area of pores	23.7305	21.9098	24.0498
Pore Volume (cm³/g)			
Single point adsorption total pore volume of pores	0.063804	0.061239	0.072138
BJH Adsorption cumulative volume of pores	0.073067	0.070720	0.081151
BJH Desorption cumulative volume of pores	0.079739	0.076082	0.086606
Pore Size (nm)			
Adsorption average pore width (4V/A by BET)	15.12479	15.72402	17.32834
BJH Adsorption average pore diameter (4V/A)	16.6691	18.5411	19.9822
BJH Desorption average pore diameter (4V/A)	13.4407	13.8901	14.4044

6.4.3.5 Changes in surface functional groups with firing time

The FTIR spectra of iron(III) oxide modified bentonite-red/black clay soil composite pellets is shown in Figure 6.5. The FTIR spectrum shows prominent absorption bands at 3500, 1550, 1000 and 700 cm⁻¹. The absorption band at 1000 cm⁻¹ increased in intensity with firing times. This indicates loss of Si-O bonds as firing time increased meaning firing time of more than 1 hour is not desirable.

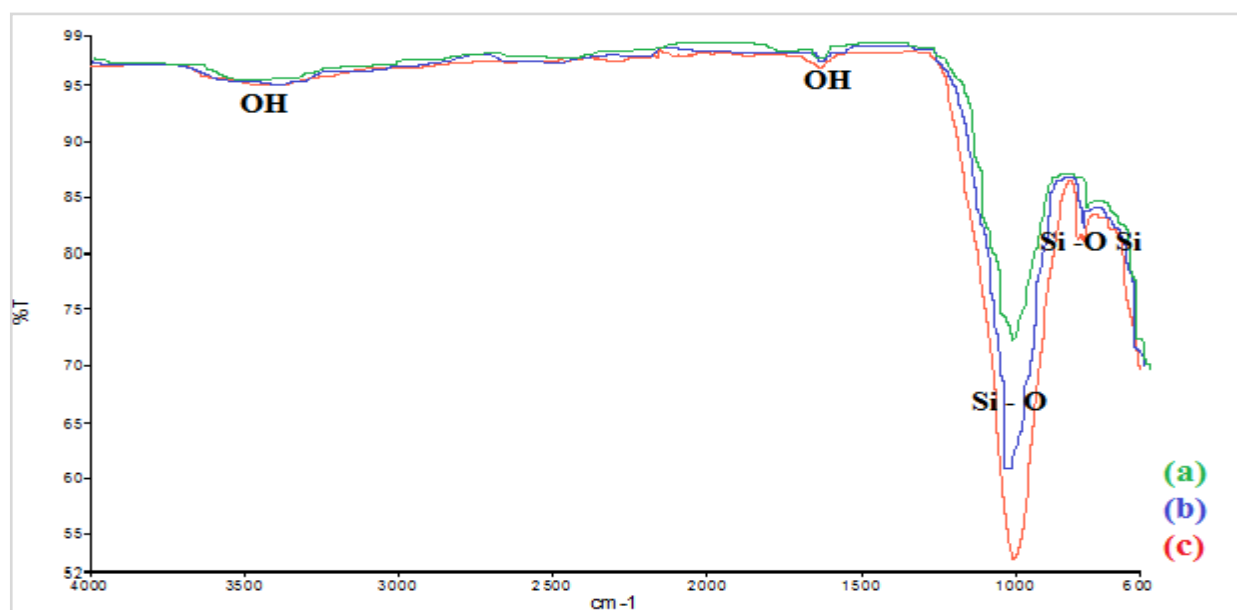


Figure 6.5. The FTIR spectra of iron(III) oxide modified-red/black clay soil composite pellets at different firing times ((a) 1 h, (b) 2 h and (c) 3 h)

6.4.3.6 Fluoride adsorption with increasing firing time

Table 6.6 shows the fluoride adsorption potential of the ceramic pellets. Percentage fluoride removal was observed to increase marginally as the firing time increased with maximum adsorption at 3 h. Ceramic pellets fired for 3 h showed the largest pore width and this could explain the increased fluoride adsorption.

Table 6.6. Fluoride adsorption potential of the composite pellets prepared at different firing times

Parameter	Initial parameters	1 h	2 h	3 h	SANS 241-1 (2015)
pH	6.02	6.34	6.66	6.86	5.0-9.5
TDS (mg/ℓ)	16.4	138.53	273	294.34	<1000
EC (μS/cm)	13.46	109.27	216.33	225.87	<150
F ⁻ (mg/ℓ)	10	7.20	7.18	7.14	1-1.5
% F removal	-	38.89	39.28	40.06	-

6.4.4 Effect of clay ratios

The potential defluoridation capacity of the iron(III) oxide modified bentonite-red/black clay soil composite pellets fabricated at different modified bentonite/clay soil ratios was evaluated and results are presented in Table 6.7. The clay soils had low fluoride adsorption potential and increasing their ratio in the pellets decreased the adsorption capacity of the composite pellets. The iron(III) oxide coated bentonite clay increased the fluoride adsorption capacity of the composite pellets. Analysis of the variation between one clay ratio and the next by Tukey-Kramer Multiple Comparisons Test showed that there was a significant variation between ratios. A 5:1 iron(III) oxide modified bentonite/clay: soil ratio was adopted for fabrication of the ceramic composite pellets.

Table 6.7. Fluoride adsorption capacity of iron(III) oxide modified bentonite-red/black clay soil composite pellets fabricated at different clay ratios.

Parameter	Initial	1:1	1:2	2:1	3:1	4:1	5:1	6:1	SANS 241-1
pH	6.02	6.34	6.66	6.86	6.47	6.49	6.61	6.78	5.0-9.5
TDS (mg/ℓ)	16.4	138.5	273.0	294.3	301.2	332.6	345.3	348	<1000
EC (μS/cm)	13.4	109.27	216.33	225.87	264.5	278	294.5	306	<150
F ⁻ (mg/ℓ)	10	7.15	7.23	7.03	6.87	6.45	6.41	6.38	1-1.5
% F-removal	-	39.86	38.31	42.23	45.56	55.04	56.01	56.74	-

6.5 SUMMARY

Iron(iii) oxide modified bentonite clay-red/black Mukondeni clay soils composite ceramic pellets were fabricated at established optimum conditions and its fluoride adsorption evaluated. The optimized conditions included particle size, furnace temperature, firing time and clay ratios. XRD and TEM analysis indicated the ceramic pellets to be crystalline. Optimum conditions for fabrication of the pellets based on fluoride adsorption capacity were: 250 μm particle size, 600°C furnace temperature, 1 h firing time and 5:1 (iron(iii) oxide coated bentonite: red/black clay soil) ratios. The optimum adsorption capacity was found to be 0.03 mg/g for a 10 mg/ℓ F⁻ initial concentration and 2 g adsorbent dosage at pH 6.8. The adsorption capacity of the ceramic pellets was observed to increase with increasing iron(iii) oxide modified bentonite clay content. The potential implications of the results are important in the development of future point-of-use water filtration devices for the removal of fluoride from water using locally available clays.

7 EVALUATION OF GROUNDWATER DEFLUORIDATION BY Mn²⁺ MODIFIED BENTONITE CLAY

7.1 INTRODUCTION

Fluoride in drinking water may have beneficial or harmful effects on human health depending on its concentration. Optimal concentration of fluoride in drinking water set by World Health Organization is at 1.5 mg/l (WHO, 2011). A concentration higher than this can lead to fluorosis. The disease is manifested by mottled teeth in dental fluorosis and deformation of bones in skeletal fluorosis (Coetzee et al., 2003). Groundwater in many regions contains fluoride concentration greater than 1.5 mg/l and will therefore require defluoridation. Various techniques such as precipitation, co-precipitation, ion exchange and adsorption for defluoridation of groundwater have been reviewed by Meenakshi and Maheshwari (2006). Among these techniques, adsorption is popular due to its viability and sustainability and its potential for utilising locally available and cost-effective materials. The challenge is to come up with high fluoride adsorption capacity adsorbents that are cheap and easily fabricated using locally sourced materials. This Chapter 5 presents findings on:

- a. Optimization of synthesis conditions for intercalation of Mn²⁺ onto bentonite clay interlayers
- b. Physicochemical and mineralogical characterization of the Mn²⁺ intercalated bentonite clay
- c. Evaluation of the effect of various operating parameters (contact time, adsorbent dosage, adsorbate concentration and pH) on the adsorption capacity of F⁻ by the Mn²⁺ intercalated bentonite clay
- d. Evaluation of the chemical stability and reusability of the Mn²⁺ intercalated bentonite clay adsorbent.

7.2 MATERIALS

All reagents and TISAB-III were obtained from Rochelle Chemicals & Lab Equipment CC, South Africa Ltd and they were of analytical grade. Bentonite clay was collected from ECCA pty (Ltd) in Cape Town. A stock solution containing 1000 mg/l fluoride was prepared by dissolving 2.21 g analytical grade sodium fluoride in 1 l of ultra-pure water (18.2 MΩ/cm). Fluoride solutions for batch experiments were prepared from fresh stock fluoride solution by appropriate dilution. A stock solution containing 1000 mg/l fluoride was prepared by dissolving 2.21 g NaF in 1 l of MilliQ water (18.2 MΩ/cm) and fluoride solutions for batch experiments were prepared from fresh stock fluoride solution by appropriate dilution. Field water was collected from a community borehole in Siloam, Vhembe district in South Africa.

7.3 METHODS

7.3.1 Preparation of Mn²⁺ modified bentonite clay

Raw bentonite clay was washed by mixing with ultra-pure water at a ratio of 1:5 in a 1000 ml beaker, the mixture was stirred for 5 min, and the procedure was repeated twice. After stirring, mixtures were agitated for 15 min using Stuart reciprocating shaker and then centrifuged for 10 min at 5 000 rpm. Samples were then

dried in an oven for 12 hrs at 110°C. Clay samples were then milled to pass through <250 µm sieve. Intercalation of Mn²⁺ ions onto bentonite clay was done according to the procedure developed in preliminary work conducted in 2014 (Mudzielwana, 2014). Optimum conditions (i.e. contact time, adsorbate concentration, adsorbent dosage, and pH) for modifying bentonite clay with Mn²⁺ ions were evaluated using batch experiments. The obtained conditions were: 60 min contact time, 4 g/100 ml adsorbent dosage, 50 mg/l Mn²⁺ adsorbate concentration and initial pH of 8.

To synthesize Mn²⁺ modified bentonite, 200 ml of 50 mg/l Mn²⁺ solution was mixed with 8 g of raw bentonite to make up S/L ratio of 4 g/100 ml, the pH of the mixture was then adjusted to 8 using 0.1 M NaOH and 0.1 M HCl. The mixture was put on a 1 l Erlenmeyer flask in order to avoid spillage during agitation. The mixture was agitated for 60 min at 250 rpm on a table shaker and filtered. The solid residue left on the filter paper was dried for 12 hrs at a temperature of 105°C in the oven. The modified clay was then milled to pass through <250 µm sieve. The experiments were repeated five times to generate enough Mn²⁺ modified bentonite for subsequent experiments.

7.3.2 Characterisation techniques

Several techniques were used to characterize the smectite-rich clay soils for adsorption (detailed in Appendix A). These included Cation Exchange Capacity (CEC), Point of Zero Charge (PZC), X-ray diffraction (XRD), X-ray fluorescence (XRF), Scanning Electron Microscopy (SEM), Scanning Electron Microscopy coupled with Energy Dispersive Spectroscopy (SEM-EDS), Transmission Electron Microscopy (TEM), Brunauer-Emmett-Teller (BET) and Fourier Transform Infrared (FTIR).

7.3.3 Batch and field groundwater adsorption studies

Methods followed for batch and field groundwater fluoride adsorption studies are detailed in Appendix B.

7.3.4 Adsorption modelling studies

Adsorption models used for describing the adsorption process using Mn modified bentonite are detailed in Appendix C. Equation 1 (Appendix C) was used to calculate the percentage of removal and adsorption capacity.

7.4 PHYSICOCHEMICAL AND MINERALOGICAL CHARACTERIZATION STUDIES

7.4.1 X-ray diffraction analysis

X-ray diffraction analysis indicated presence of montmorillonite and quartz as the major minerals and muscovite as one of the trace minerals in bentonite and Mn²⁺ modified bentonite clay (data not shown).

7.4.2 X-ray fluorescence analysis

The chemical composition of raw and Mn²⁺ bentonite clay was evaluated using X-ray fluorescence (XRF). The results for major chemical elements are presented in Table 7.1. The analysis reveals that silica (SiO₂) and Al₂O₃ are the major components. High concentration of SiO₂ and Al₂O₃ reveal that bentonite clay is an aluminosilicate material. MnO₂ is higher in Mn²⁺-modified bentonite (0.29%) than in raw bentonite (0.09%) confirming introduction of Mn²⁺ ions in the interlayers. The relatively high concentrations of MgO, Na₂O, CaO, and K₂O in the raw bentonite indicates that Mg²⁺, Na⁺, Ca²⁺, and K⁺ are the main exchangeable cations. This is confirmed by the subsequent decrease of the content of these chemical species in the Mn²⁺ modified bentonite clay. This is a further confirmation of entry of Mn²⁺ ions in the interlayers through ion exchange.

Table 7.1. Chemical composition of raw and Mn²⁺ modified bentonite clay

Oxide	Raw bentonite (w/w %)	Mn ²⁺ bentonite (w/w %)
Al ₂ O ₃	15.30	15.84
CaO	0.88	1.50
Cr ₂ O ₃	0.01	0.00
Fe ₂ O ₃	3.41	3.18
K ₂ O	0.98	0.39
MgO	3.20	3.06
MnO	0.06	0.29
Na ₂ O	2.12	0.94
P ₂ O ₅	0.09	0.04
SiO ₂	66.88	62.48
TiO ₂	0.46	0.12
L.O.I.	6.45	11.65
Total	99.89	99.49

7.4.3 Scanning Electron microscopy (SEM) analysis

SEM analysis was conducted to assess the effect of modification on the surface morphology of the bentonite clay. Figure 7.1 shows the surface morphology of raw and Mn²⁺ bentonite clay. The analysis reveals that raw bentonite has rough and spongy like material. After the modification of bentonite, formation of larger agglomerates is observed. This could be due to swelling due to ingress of water molecules in the interlayers and entry of hydrated Mn²⁺ ions in the interlayers.

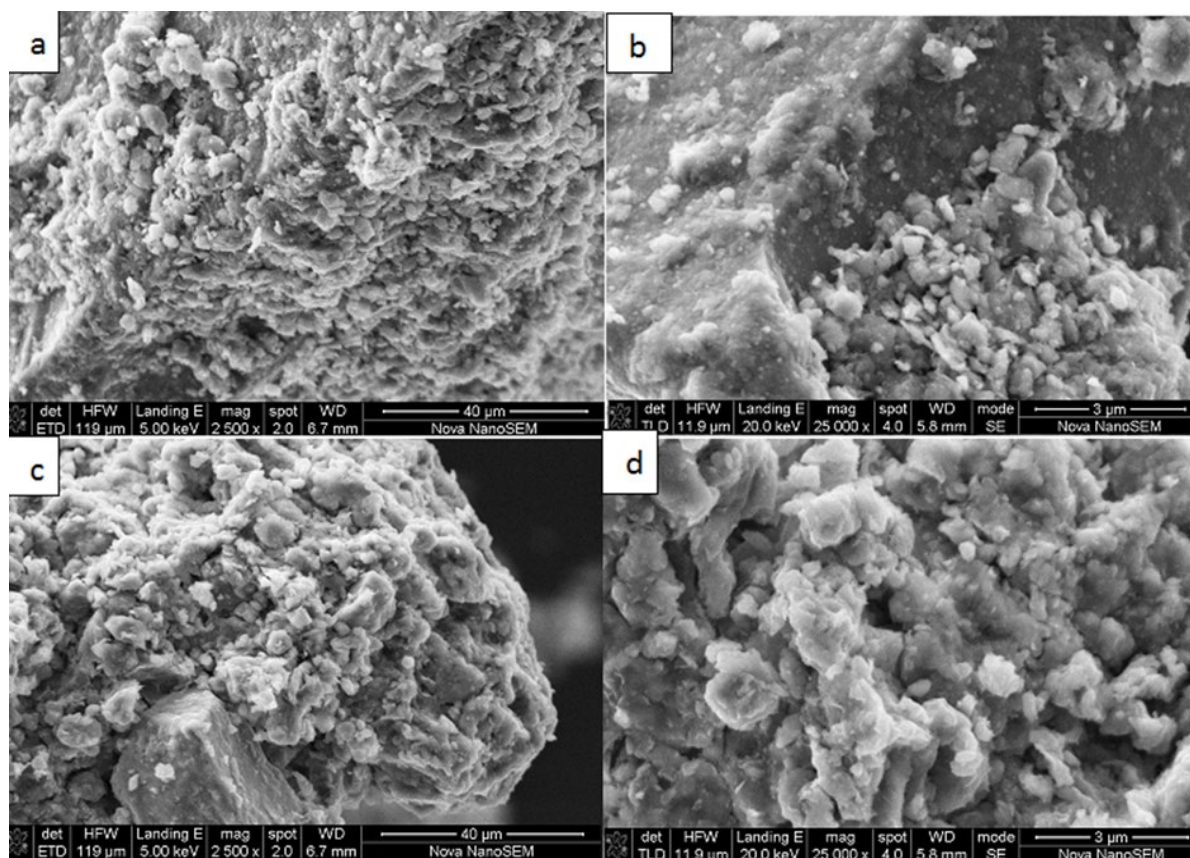


Figure 7.1. SEM Micrographs [bentonite (a) and Mn²⁺ modified bentonite (b) x 20 000

7.4.4 Cation Exchange Capacity

Table 7.2 shows the concentration of the exchangeable cations and the calculated CEC of raw and Mn²⁺ bentonite clay extracted at pH 5.4 and 7.4. CEC for raw bentonite was found to be higher than the CEC of Mn²⁺ modified bentonite. This confirms that the dominant mechanism during the reaction of Mn²⁺ solution with raw bentonite is ion exchange. The CEC results show that Na⁺ is the main exchangeable cation. pH of the buffering media does not seem to have significant influence on the exchangeable cation's concentration and subsequently the CEC.

Table 7.2. CEC of raw and Mn²⁺ bentonite clay at pH 5.4 and 7.4

	Exchangeable cation (mg/ℓ)				CEC (meq/100 g)
	Na ⁺	Ca ²⁺	K ⁺	Mg ²⁺	
Raw bentonite					
pH 5.4	153.0	8.36	51.4	75.56	288.32
pH 7.4	156.4	8.43	52.03	77.46	293.92
Mn²⁺ bentonite					
pH 5.4	51.9	3.1	23.7	32.04	110.74
pH 7.4	52.2	3.9	25.0	33.56	114.66

7.4.5 Determination of pH_{pzc}

pH_{pzc} of the clay was determined using the batch equilibration methods. Figure 7.2 shows the variation of initial pH versus ΔpH and the pH_{pzc} at the x-axis intercept. It is observed that there is an increase in pH_{pzc} of bentonite clay after the introduction of Mn²⁺ cation (Raw bentonite: 8.4 and Mn²⁺-modified bentonite: 8.8). Both raw and Mn²⁺-modified bentonite clay have high pH_{pzc} characteristic of clay materials dominated by aluminosilicate materials and manganese oxides. Modification of the raw bentonite clay with Mn²⁺ increases the pH_{pzc} and which extends the pH range for adsorption of anions meaning that the Mn²⁺-modified bentonite clay will have high adsorption capacity for anions than the raw bentonite clay.

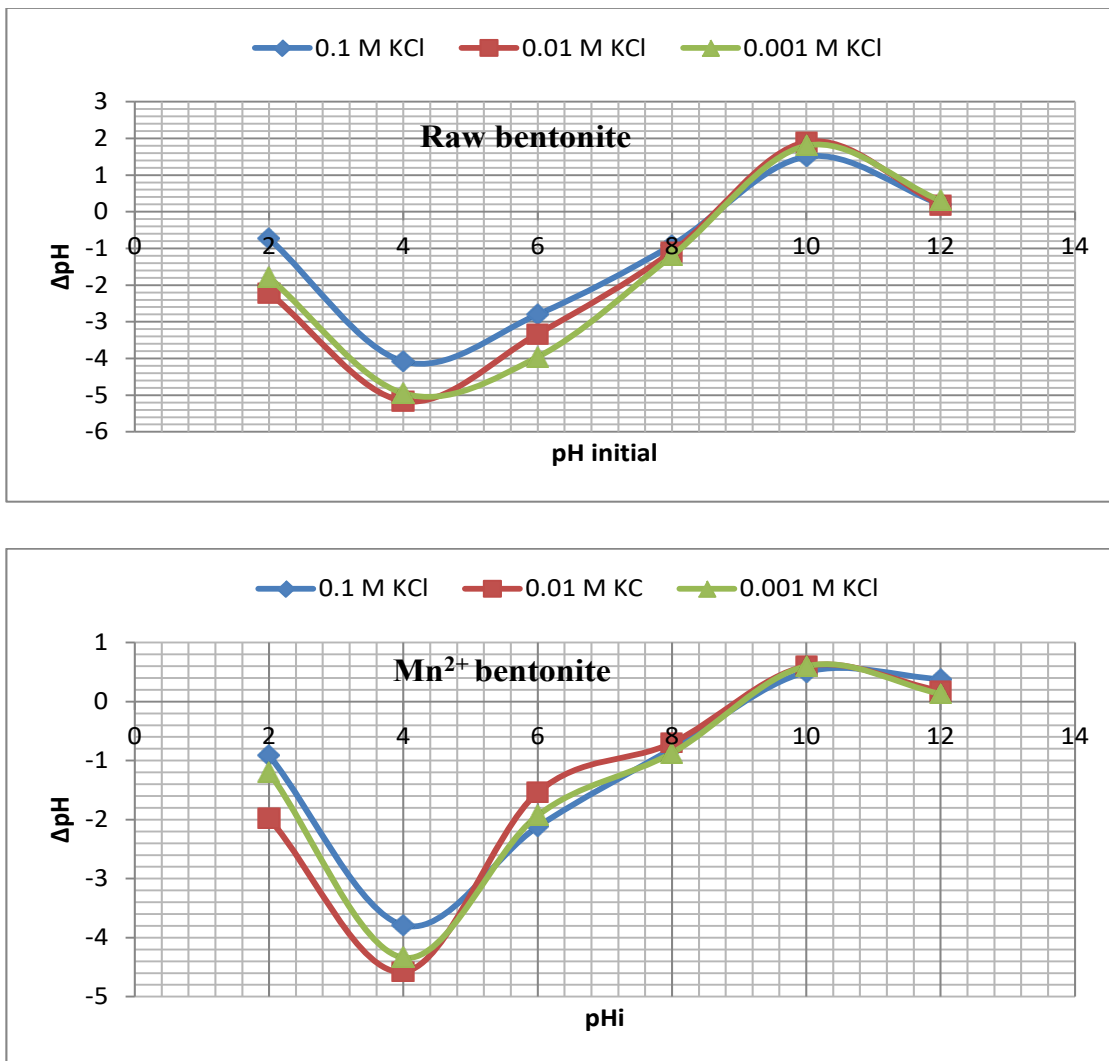


Figure 7.2. pH_{pzc} of raw and Mn²⁺ modified bentonite clay

7.4.6 Fourier Transform Infra-red Analysis

FTIR analysis were carried out in order to evaluate the effect of Mn^{2+} ion on the surface chemistry of bentonite clay and also deducing the mechanisms of F^- uptake by the modified bentonite clay. Figure 7.3 present the FTIR spectra of raw bentonite, Mn^{2+} modified bentonite and F^- loaded Mn^{2+} bentonite. According to Toor et al. (2014), three main absorption regions of bentonite clay are $3000-3800\text{ cm}^{-1}$, $1300-1800\text{ cm}^{-1}$ and $500-1200\text{ cm}^{-1}$ and notable difference can be observed in each region of raw, Mn^{2+} and F^- loaded bentonite.

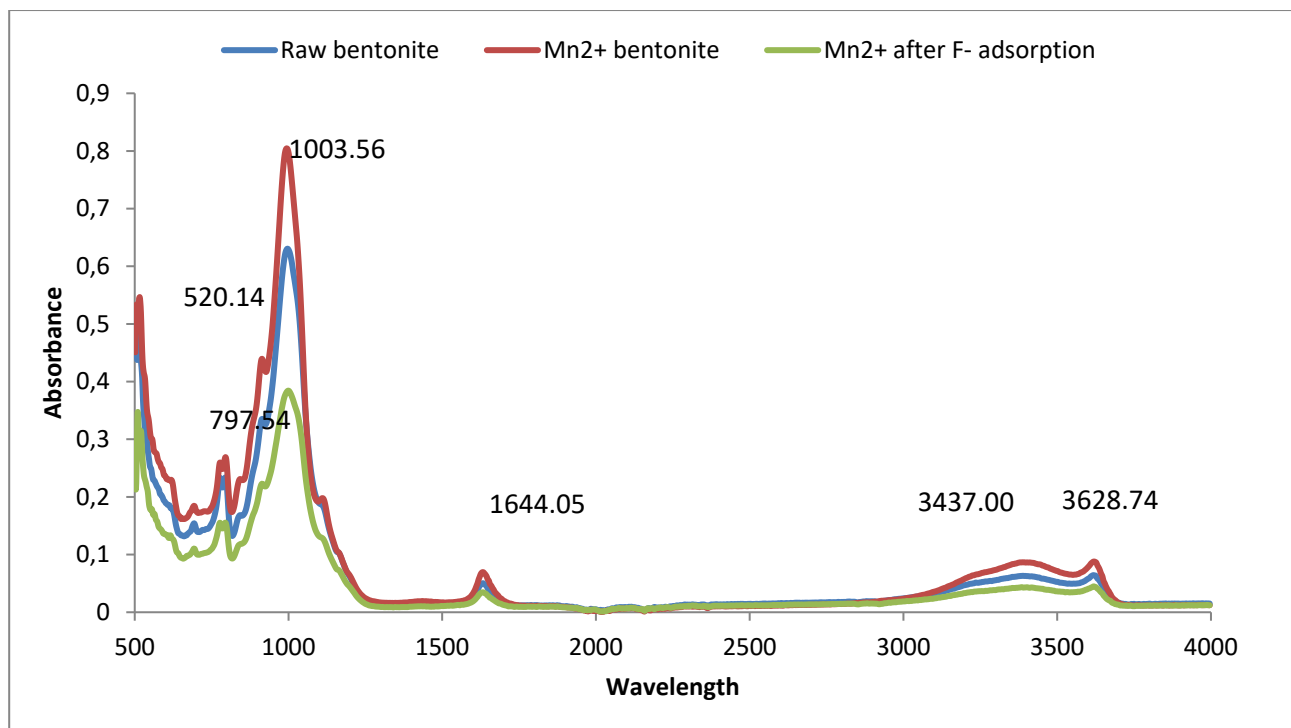


Figure 7.3. FTIR spectrum of raw bentonite, Mn^{2+} bentonite and the F^- loaded Mn^{2+} bentonite clay.

The absorption band between 3619.12 and 3623.81 cm^{-1} is due to stretching vibrations of structural OH^- groups of montmorillonite and water. At lower frequency bentonite showed a strong broad band at 999.10 cm^{-1} due to the stretching and vibration of Si-OH. The band at 914.93 cm^{-1} is attributed to Al-O-Al. The 795 cm^{-1} band corresponds to coupled Al-O and Si-O vibrations. Quartz was present as indicated by the bands at 791 cm^{-1} . Mn^{2+} bentonite showed an increased intensity of transmittance of all peaks observed for raw bentonite indicating the formation of new bonds such as Mn-O, Mn-OH and Mn- H_2O at those frequencies. The spectra for F^- loaded Mn^{2+} bentonite indicated reduction in intensities. This could be attributed to interaction of these groups with F^- . These observations indicate that structural hydroxides groups and water molecules had important role in F^- adsorption process. Moreover, it is an indication that F^- was removed through the exchange of OH^- or formation of bonds with Mn, Al, Si oxyhydroxyl groups on the surface of the modified clay.

7.4.7 BET Surface Area Analysis

Brunauer Emmet Teller (BET) and Barrett-Joyner-Halenda (BJH) analysis were carried out in order to assess the surface area, pore volume and the pore size and distribution of the Mn^{2+} modified bentonite clay. Figure 7.4a shows N_2 adsorption-desorption isotherm while Figure 7.4b shows pore size distribution of raw and Mn^{2+} modified bentonite.

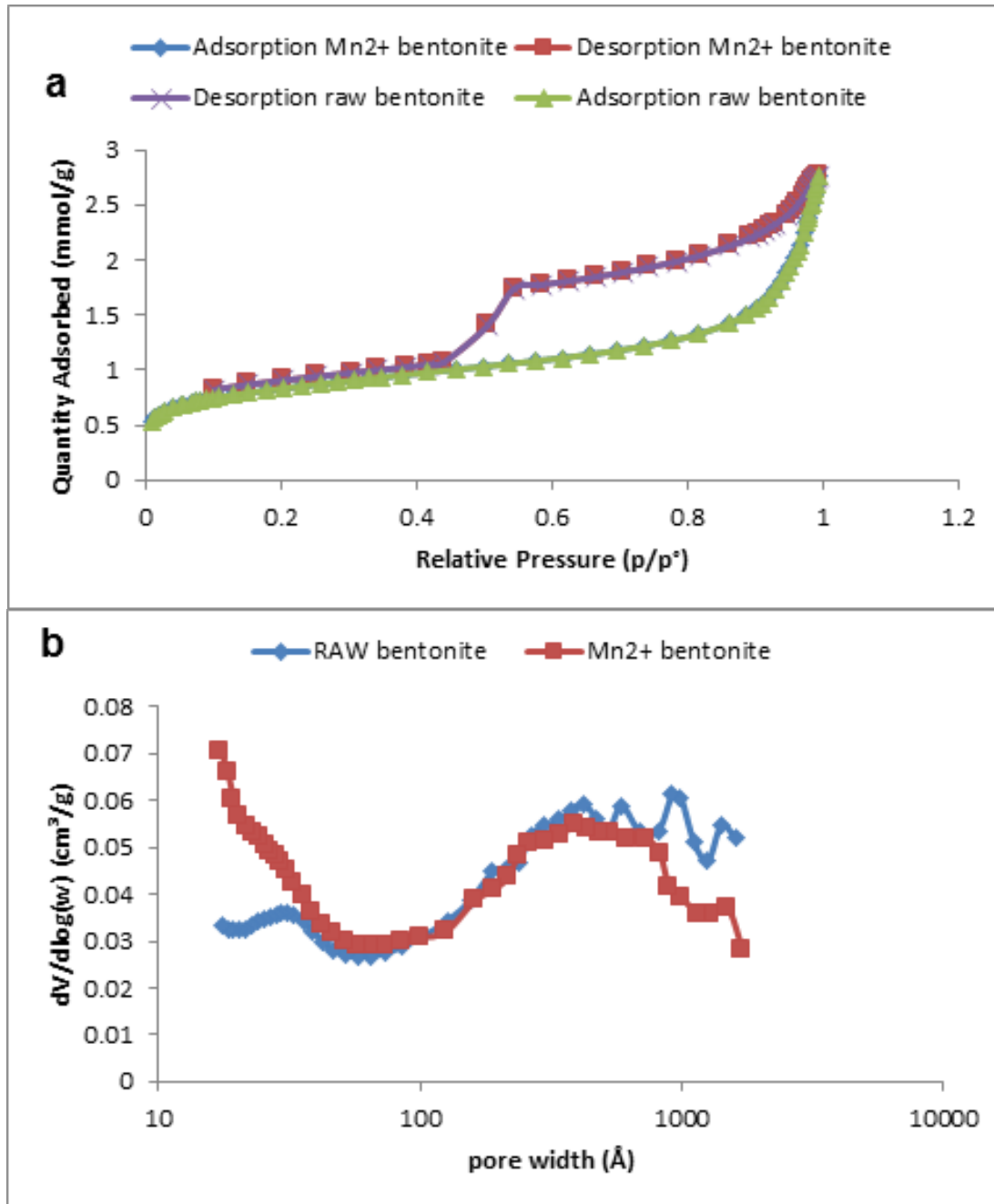


Figure 7.4. a) N_2 adsorption-desorption isotherm b) pore distribution of raw and Mn^{2+} modified bentonite clay.

BET results indicated that there was increase in total surface area (43.48 to 66.41 m²/g) and pore volume (0.088 to 0.092 cm³/g) after the intercalation of Mn²⁺ ions. This may be attributed to swelling of the bentonite clay during intercalation of Mn²⁺ ions or due to hydration of the intercalated Mn²⁺ ions. Pore diameter of raw bentonite was found to be higher compared to that of Mn²⁺ modified bentonite clay. This indicates that Mn²⁺ ions were incorporated onto the surface of the clay, including adsorption on the edges. Nitrogen adsorption-desorption Isotherms exhibited type IV isotherm with hysteresis loop indicating the mesoporous nature of the bentonite clay and Mn²⁺ modified bentonite clay (Zhang et al., 2012; Xu et al., 2013). Figure 8.4b shows pore distribution of raw and Mn²⁺ modified bentonite, it is observed that a significant number of the pore sizes for both raw and Mn²⁺ bentonite are in the range of 2 to 50 nm which indicate that bentonite clay is a mesoporous material.

7.5 BATCH F⁻ ADSORPTION EXPERIMENTS

7.5.1 Effect of contact time

The effect of contact time on the adsorption of F⁻ onto Mn²⁺ bentonite clay was evaluated by varying contact time from 5 to 270 min at various adsorbent dosages (0.1, 0.3, 0.5 g/100 ml), 3 mg/l initial F⁻ concentration, pH 5.54 ± 0.5 and 250 rpm shaking speed. Figure 7.5 presents % fluoride removal with contact time. Percent fluoride removal was rapid at initial contact reaching a maximum at 30 minutes. A slight decrease was observed thereafter with the system attaining equilibrium with no significant change after 60 minutes. The increase in fluoride removal may be attributed to the availability of sorption sites in the adsorbent and the decrease may be due to the saturation of the adsorbent surface with time. The same trend was observed at other adsorbent dosages. The percentage F⁻ removal was also observed to be increase with increase in adsorbent dosage. Contact time of 30 min was taken as the optimum time and was applied in subsequent experiments.

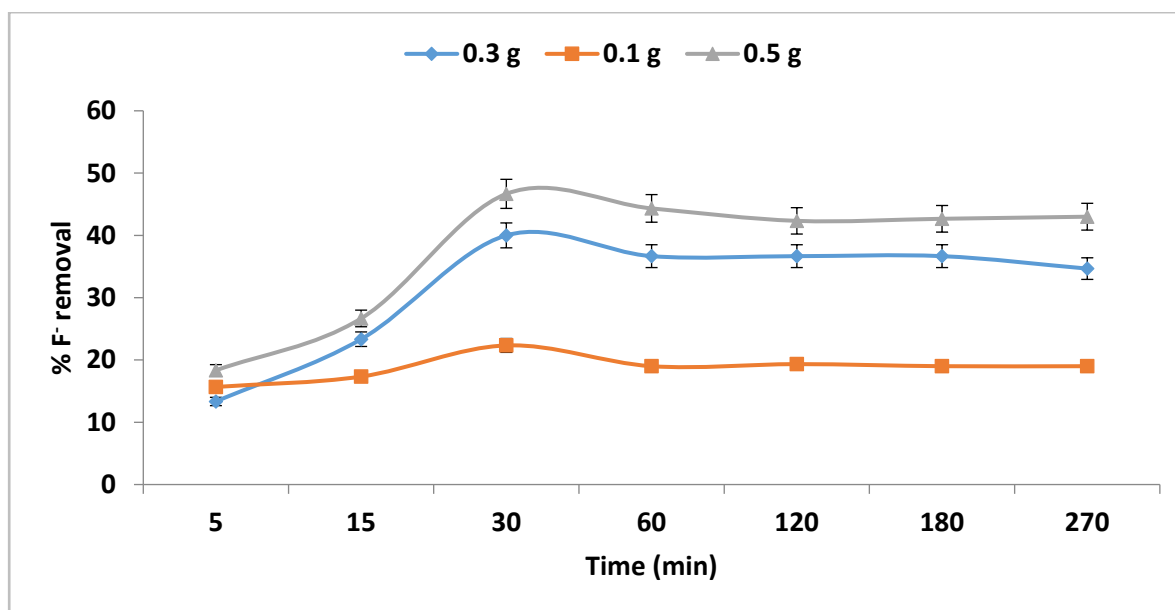


Figure 7.5. Variation of % F⁻ removal as a function of contact time for various adsorbent dosages (3 mg/l F⁻, 100 ml vol, pH 5.54 ± 0.5 and 250 rpm shaking speed, Particle size <250 μm, N=3).

7.5.2 Effect of adsorbent dosage

The effect of adsorbent dosage on the adsorption of F^- onto Mn^{2+} bentonite clay was evaluated at 30 minutes contact time, shaking speed of 250 rpm, 3 mg/l initial concentration of F^- and pH of 5.54 ± 0.5 . The adsorbent dosage was varied from 0.1 g/100 ml to 2 g/100 ml. The plot of percentage fluoride removal and adsorption capacity against adsorbent dosage is presented in Figure 7.6. It is observed that percentage fluoride removal by Mn^{2+} modified bentonite clay increased with an increase in the adsorbent dosage from 0.1 up to 1 g/100 ml were optimum uptake occurred and the system seemed to stabilize thereafter. This may be attributed to the increase in the sorption sites for fluoride ions as the adsorbent dosage increases. No significant change was observed for dosages greater than 1 g/100 ml adsorbent dosage, this may be attributed to high density of the adsorbent particles limiting mobility of the F^- hence limiting access to adsorption sites. The adsorption capacity on the other hand decreased with increase in adsorbent dosage. At dosage of 1 g/100 ml, $\approx 50\%$ of fluoride was removed. This dosage was adopted as the optimum and was used in subsequent experiments.

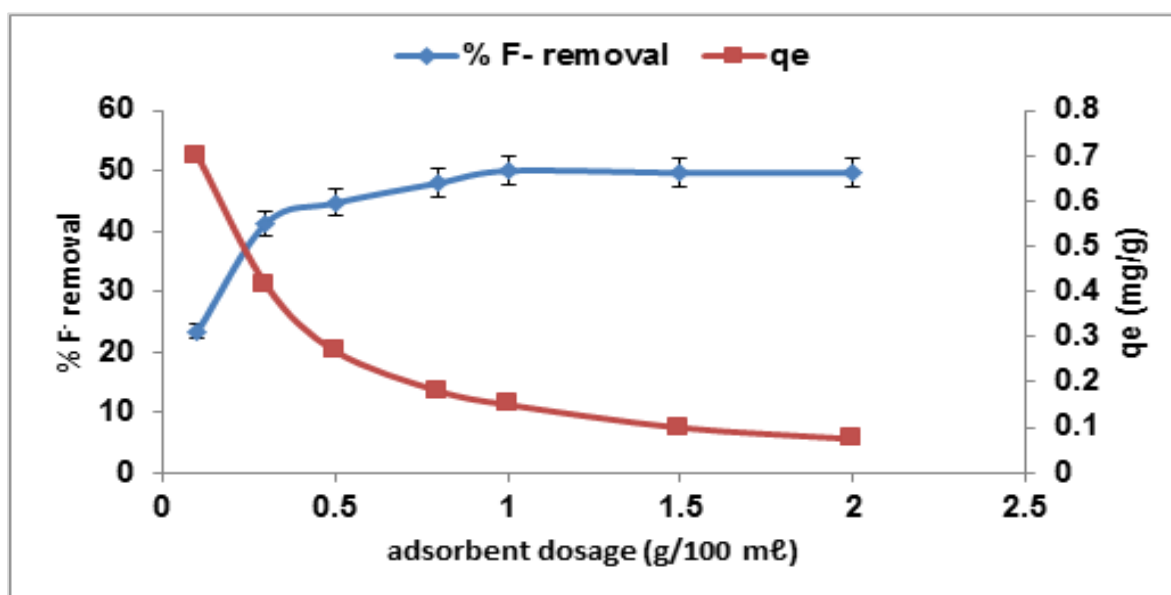


Figure 7.6. Variation % F^- removal and adsorption capacity by Mn^{2+} bentonite clay as a function of adsorbent dosage (contact time of 30 min, adsorbent dosage, 3 mg/l F^- , pH of 5.54 ± 0.5 and shaking speed of 250 rpm, particle size $<250 \mu m$, $N=3$).

7.5.3 Effect of adsorbate concentration

The effect of initial concentration in the adsorption of F^- onto Mn^{2+} bentonite clay was evaluated at various contact times (30, 60 and 120 min), at 250 rpm shaking speed, 1.0 g/100 ml adsorbent dosage and pH of 5.54 ± 0.5 . The initial concentration was varied from 3 mg/l to 25 mg/l. Plot of % F^- removal with adsorbate concentration is presented in Figure 7.7. Percentage F^- removal decreased with an increase in the initial concentration, the same trend was observed at other contact times. This is due to availability of more fluoride ions in solution at higher concentration and the adsorption sites become the limiting factor in the adsorption process. At contact times > 30 minutes the adsorption capacity was lower, this was earlier observed in the

contact time experiments where maximum absorption was at 30 minutes. An adsorbate concentration of 3 mg/l was adopted for subsequent experiments since the adsorbent exhibited optimum removal at this concentration.

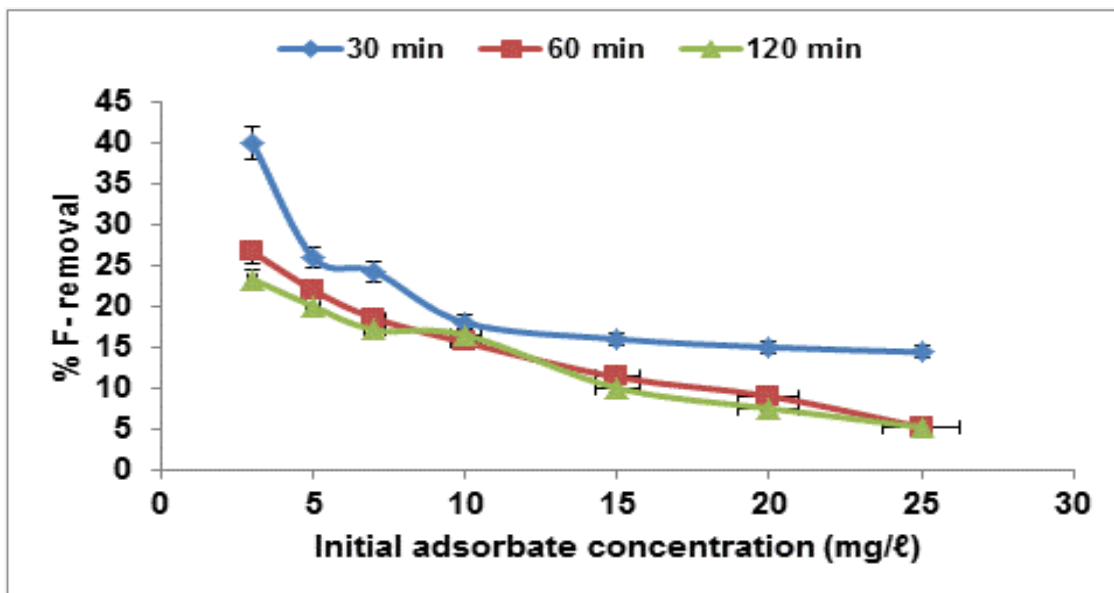


Figure 7.7. Variation of % F⁻ removal by Mn²⁺ bentonite clay as a function of adsorbate concentration at various contact times (adsorbent dosage 1.0 g/100 ml, pH of 5.24 and shaking speed of 250 rpm, particle size <250 μm, N=3).

7.5.4 Effect of pH

To study the effects of pH in the adsorption of F⁻ onto Mn²⁺ bentonite clay, the initial pH was adjusted from 2 to 12 using 0.1 M NaOH and 0.1 M HCl. The effect of pH was evaluated under the condition of 30 min contact time at 250 rpm, 1 g/100 ml adsorbent dosage, 3 mg/l initial concentration. The plot of pH with percentage F⁻ removal is shown in Figure 7.8 while Figure 7.9 shows the change (pH_{initial}-pH_{final}) in pH as a function of the initial pH. The pH of the medium is the most important parameter that influences the fluoride removal and helps in elucidating fluoride uptake mechanisms. From the results in Figure 7.8, it is observed that % fluoride removal decreases with an increase in initial pH, from 84% removal at pH 2 to 24.33% at pH 6, thereafter a slight increase was observed up to 30% at pH 10. The drastic decrease in F⁻ removal was observed at pH>10. This may be due to the abundance of OH⁻ ions in alkaline media that competes with F⁻ for adsorption sites. Maximum F adsorption was observed at pH 2, this could be attributed to the protonation of the exposed hydroxyl and O groups on the clay surface leading to electrostatic attraction of the F⁻ ions. Subsequent experiments were therefore conducted at pH 2. At pH below 8.8, the final pH increased resulting in positive ΔpH. At pH above 8.8, final pH decreased during adsorption of pH leading to negative value for ΔpH. Nur et al. (2014) observed the same trend of ΔpH for F⁻ adsorption onto hydrous ferric oxide. The increase in final pH at low initial pH values was attributed to the release of OH⁻ from the adsorbent during adsorption by ligand exchange process. At pH above 8.8 the final pH decreased from the initial pH probably due to the release of H⁺ from the surface of the adsorbent and removal of OH⁻ from solution as they compete for adsorption sites with F⁻ on the clay surface.

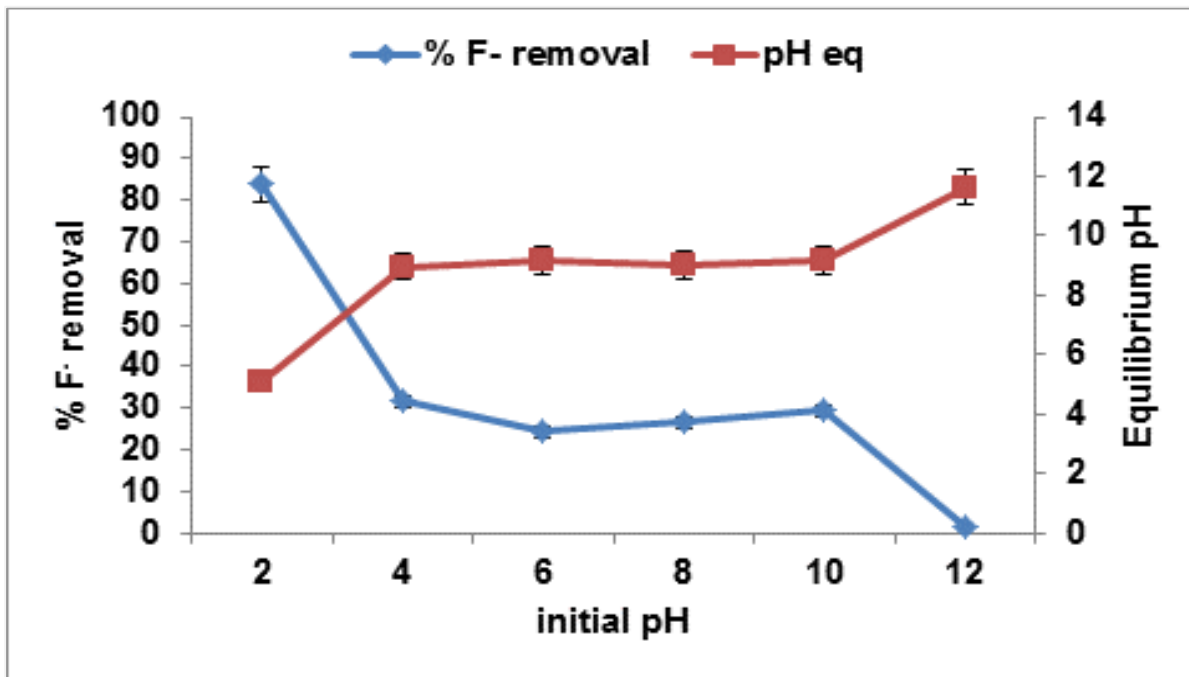


Figure 7.8. Variation of % F⁻ removal by Mn²⁺ bentonite clay as a function of pH (contact time 30 min, adsorbent dosage 1.0 g/100 mL, 3 mg/L F⁻ and shaking speed of 250 rpm, particle size <250 μm, N=3)

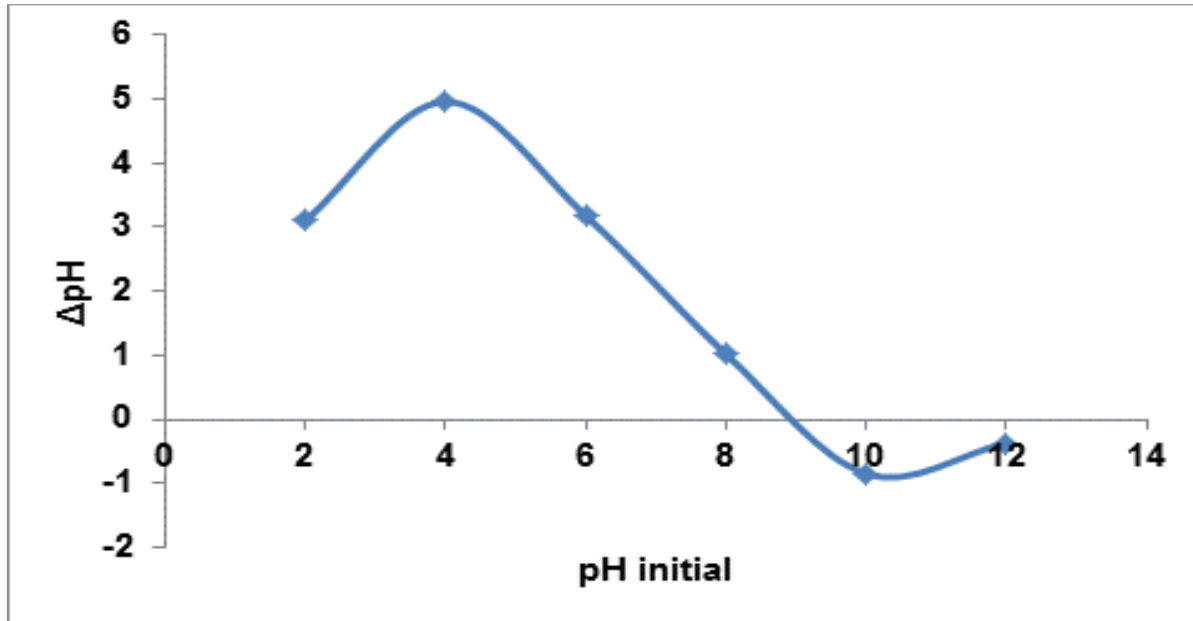


Figure 7.9. ΔpH versus initial pH for the adsorption of F⁻ onto Mn²⁺ modified bentonite clay.

7.5.5 Effect of co-existing anions

Co-existing ions such as Cl^- , NO_3^- , SO_4^{2-} and CO_3^{2-} are generally present in groundwater and can interfere with F^- adsorption. In order to evaluate the effects of co-existing anions on adsorption of fluoride by Mn^{2+} modified bentonite clay, defluoridation was conducted in the presence of 5 mg/l of SO_4^{2-} , Cl^- , CO_3^{2-} and NO_3^- separately at initial fluoride of 3 mg/l, a control experiment with initial F^- concentration of 3 mg/l was also included in the set up. The results are presented in Figure 7.10. Percentage F^- removal is slightly affected by the presence of Cl^- , NO_3^- and SO_4^{2-} . The presence of CO_3^{2-} decreased fluoride removal by up to 18%. This may be due to increased equilibrium pH which promoted competition for adsorption sites. The same observation was reported by Chen et al. (2011) and Yi et al. (2014). Effect of the co-existing ion in adsorption of F^- increases in the following order: $\text{NO}_3^- < \text{Cl}^- < \text{SO}_4^{2-} < \text{CO}_3^{2-}$.

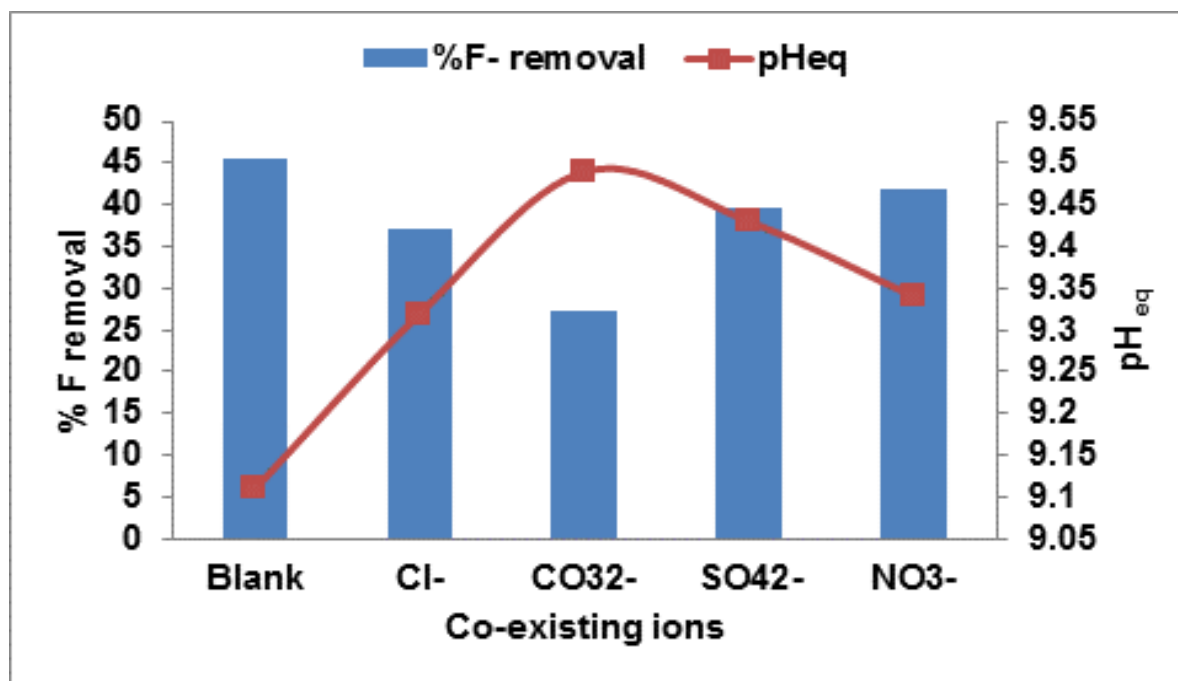


Figure 7.10. Effects of co-existing anions on F^- removal and equilibrium pH by Mn^{2+} modified bentonite clay (3 mg/l F^- , 1.0 g/100 ml adsorbent dosage, 30 min contact time at 250 rpm and pH of 6.5, particle size <250 μm)

7.6 CHEMICAL STABILITY OF Mn^{2+} MODIFIED BENTONITE CLAY FOR USE IN GROUNDWATER DEFLUORIDATION

Stability of Mn^{2+} modified bentonite clay for use in groundwater defluoridation was assessed by determining the extent of chemical species release from Mn^{2+} modified bentonite at different initial pH. Detailed methodologies are presented in Appendix C. The results on leaching of chemical species during defluoridation of groundwater at various initial pH are presented in Figure 7.11a (mg/l) and Figure 7.11b ($\mu\text{g}/\text{l}$). It was observed that the concentration of Na was very high at pH 4 and 12. This may be attributed to the use of NaOH

for pH adjustment. High Si and Al concentrations were observed at higher pH levels and this may be due to dissolution of Si and Al at high alkaline conditions. Mn, Fe, and Cu were released at minor concentration. Mn²⁺ modified bentonite is likely to be stable at field defluoridation conditions and over wide pH range and will not lead to secondary contamination of treated water.

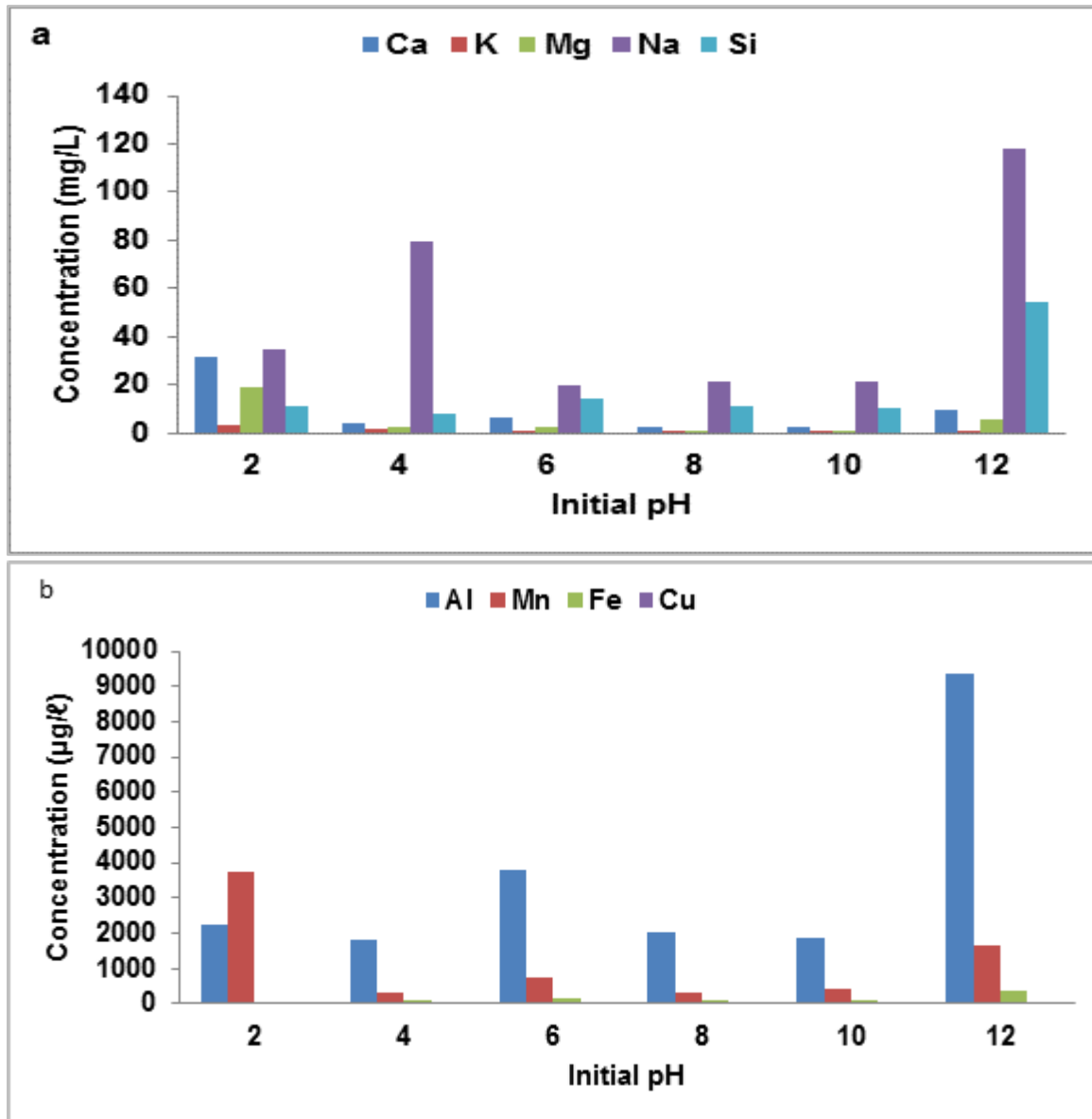


Figure 7.11. Concentration of chemical species in treated water at various pH, a) in mg/ℓ, and b) in µg/ℓ (1 g/100 ml) adsorbent dosage, 3 mg/ℓ initial F- concentration and 30 min contact time at 250 rpm, particle size <250 µm)

7.7 REGENERATION AND REUSE OF ADSORBENT

An adsorbent is economically viable if it can be regenerated and reused in many cycles of operation. To evaluate the regeneration and recyclability of the Mn^{2+} modified bentonite clay, experiments. Five successive adsorption and desorption cycles were performed at initial $3\text{ mg/l } F^-$ concentration, at pH 5.54 and contact time of 30 min using dilute NaOH. An adsorbent is economically viable if it can be regenerated and reused in many cycles of operation. To evaluate the regeneration and recyclability of the Mn^{2+} modified bentonite clay, experiments, five successive adsorption and desorption cycles were performed at initial $3\text{ mg/l } F^-$ concentration, at pH 5.54 and contact time of 30 min using dilute NaOH. The results are presented in Figure 7.12. From the results in Figure 7.12, it can be observed that percentage fluoride removal decreases with increasing cycles of reuse. However, a very slight decrease was observed up to the second cycle and a drastic decrease by 20% was observed at fifth cycle. Jia et al. (2015) reported the same trend and attributed it to inadequate regeneration of the adsorbent.

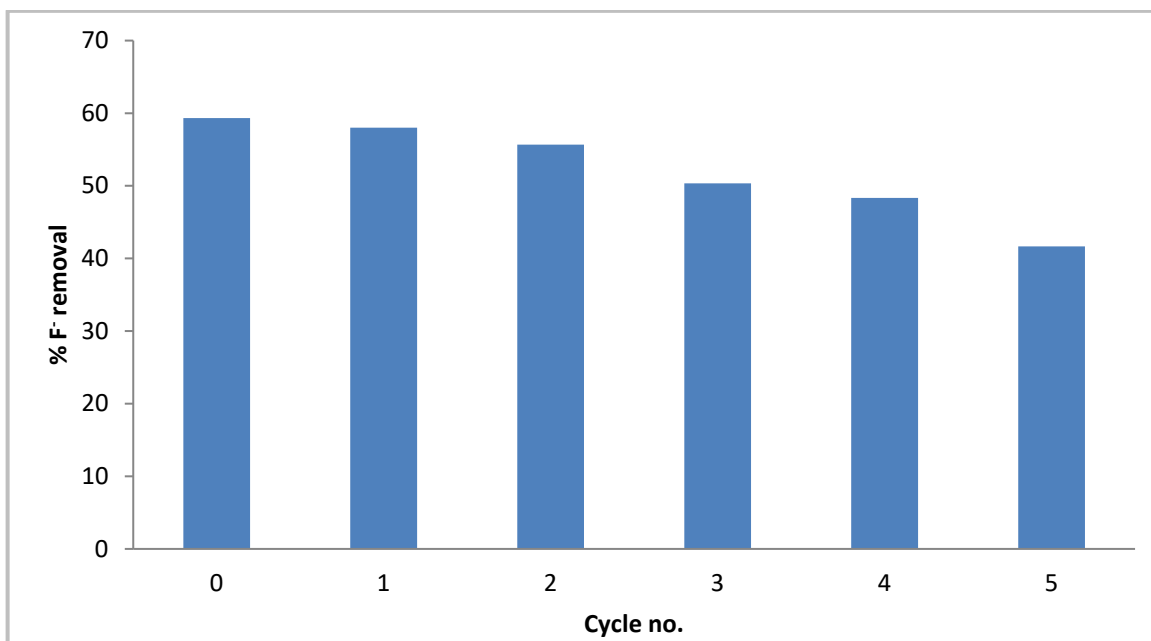


Figure 7.12. Percentage (%) fluoride removal onto Mn^{2+} modified bentonite clay in successive regeneration cycles (3 mg/l , 30 min contact time at 250 rpm and pH 5.54, particle size $<250\text{ }\mu\text{m}$)

7.8 DEFLUORIDATION OF FIELD GROUNDWATER

The effectiveness of Mn^{2+} bentonite clay in fluoride removal was tested on field water from Siloam community borehole containing 5.6 mg/l fluoride ion concentration. Field water was treated at optimized pH of 2, adsorbent dosage $1/100\text{ ml}$ and the mixture was agitated for 30 min at 250 rpm shaking speed. Results are presented in Table 7.3. Percentage F^- removal of 55.9% was achieved from field water at optimized conditions this is lower than the percentage F^- removal achieved at the same conditions from the synthetic F^- solution (84.0%) (Fig. 8.8). This may be attributed to the competition for adsorption sites between co-existing anion and F^- ion. Results

show there was reduction in Br⁻ and PO₄³⁻ ions indicating that they were also adsorbed alongside F⁻ ions. The results indicate that the adsorbent can potentially be used for defluoridation of groundwater but the efficiency of removal will depend on the chemistry of the water.

Table 7.3. Physicochemical parameters of field water before and after treatment

Parameters	Before treatment	After treatment
	Initial pH adjusted to 2	
pH	8.62	3.2
Conductivity (μS/cm)	338	402
Total dissolved solids (mg/ℓ)	203	84.1
F ⁻ (mg/ℓ)	5.4	2.7
Cl ⁻ (mg/ℓ)	31.59	37.15
SO ₄ ²⁻ (mg/ℓ)	11.89	11.89
NO ₃ ⁻ (mg/ℓ)	1.13	2.07
Br ⁻ (mg/ℓ)	2.08	ND
PO ₄ ³⁻ (mg/ℓ)	2.67	ND

7.9 ADSORPTION MODELLING

7.9.1 Adsorption isotherms

The F⁻ adsorption as a function of adsorbate concentration was modelled using both Langmuir and Freundlich and values derived from the equations calculated and are presented in Table 7.4. This was necessary to elucidate the surface adsorption properties of the adsorbent. The Langmuir plots are shown in Figure 7.13. For further analysis on the feasibility of the adsorption process, the dimensionless parameter or adsorption intensity (R_L) was calculated and used for further analysis of Langmuir model. R_L values <1 indicate favourable adsorption and >1 indicate unfavourable adsorption. Calculated R_L were within the range 0-1 indicating the adsorption process was favourable at room temperature (Fig 7.14). Figure 7.15 shows Freundlich isotherm plots for fluoride adsorption onto Mn²⁺ intercalated bentonite clay. Based on the correlation coefficient values (R^2), the experimental data fitted well to Langmuir suggesting a monolayer surface coverage phenomenon. The value of R_L , dimensionless equilibrium parameter and the value of $1/n$ Freundlich adsorption intensity were both between 0 and 1, which indicates that the adsorption of F⁻ onto Mn²⁺ bentonite was favourable.

Table 7.4. Calculated parameters for the Langmuir and Freundlich adsorption isotherms

	Langmuir isotherm			Freundlich isotherm		
	q_m (mg/g)	b (L/mg)	R^2	K_f (mg/g)	$1/n$	R^2
30 min	0.14	0.88	0.99	0.08	0.45	0.93
60 min	0.17	0.55	0.96	0.07	0.26	0.64
120 min		0.10	0.87	0.06	0.27	0.63

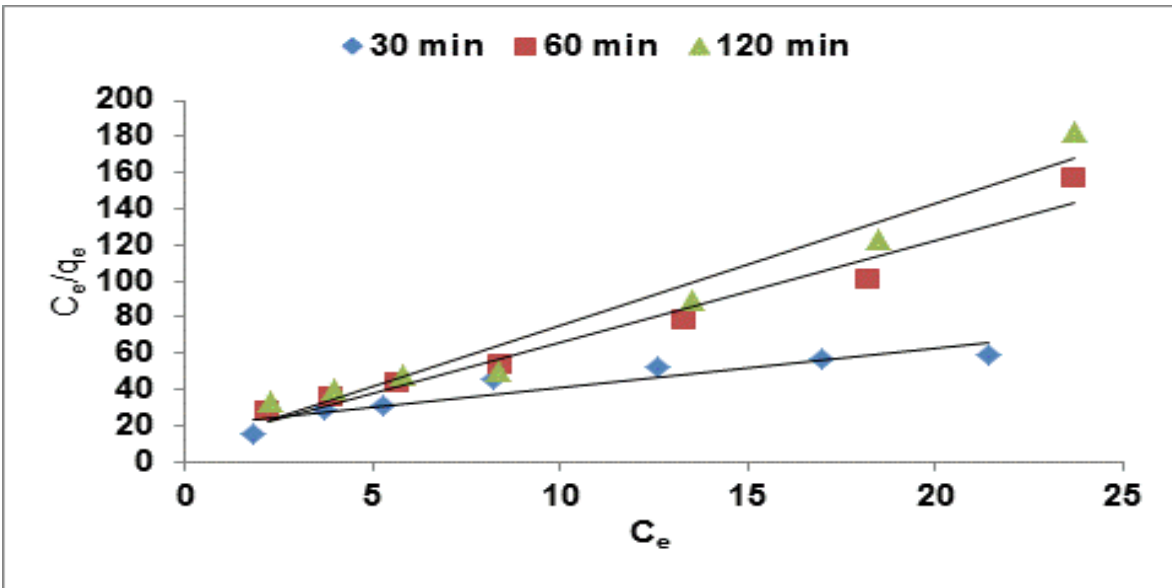


Figure 7.13. Langmuir isotherm plot for F^- adsorption by Mn^{2+} intercalated bentonite clay (at 30, 60 and 120 min contact time 250 rpm shaking speed, pH 5.54 ± 0.5 and adsorbent dosage of 1 g/100 mL).

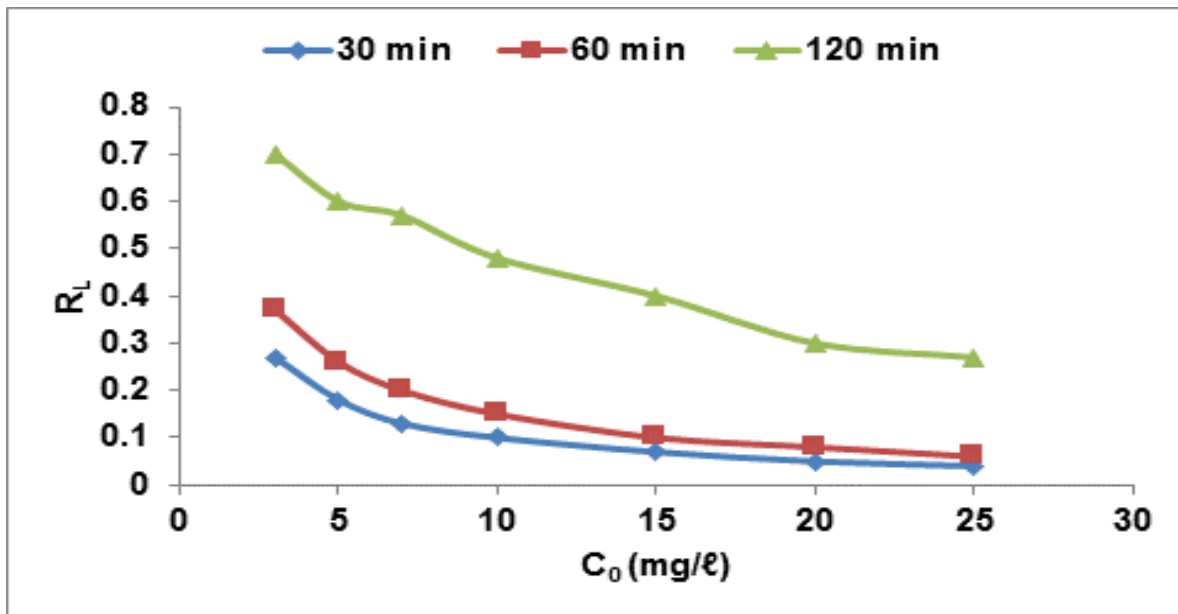


Figure 7.14. Calculated R_L values for adsorption of F^- onto Mn^{2+} intercalated bentonite clay at various contact times.

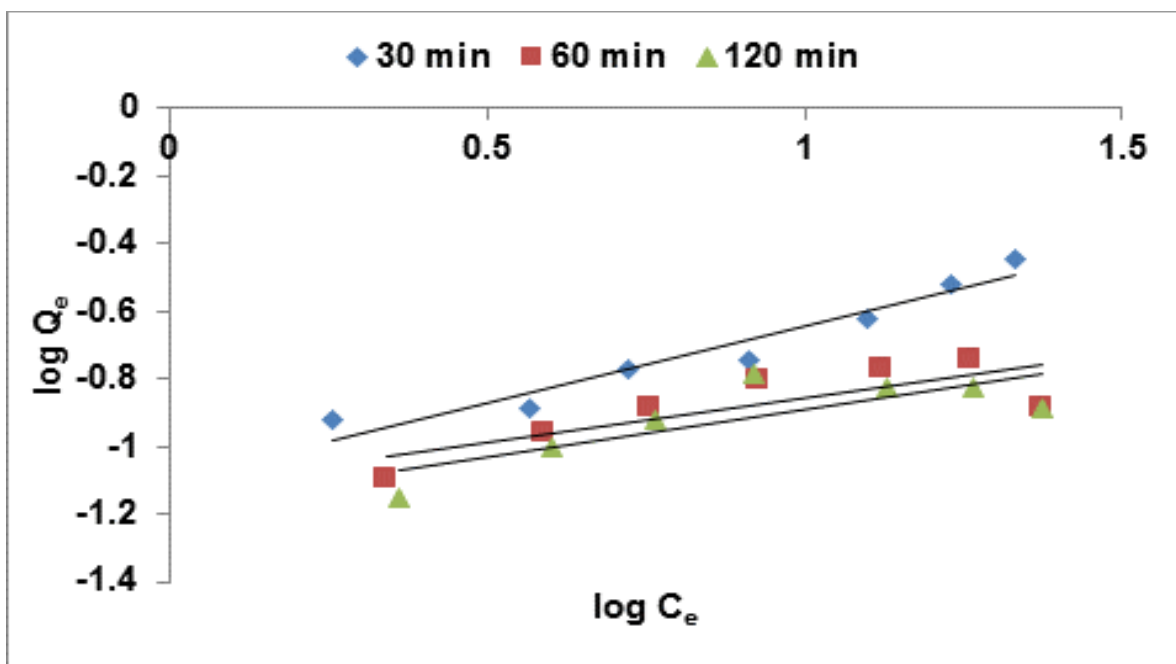


Figure 7.15. Freundlich isotherm plot for fluoride removal onto Mn^{2+} intercalated bentonite clay at 30, 60 and 120 min contact time, 250 rpm shaking speed, pH 5.5.

7.9.2 Adsorption Kinetics

The adsorption kinetics were evaluated to determine the mechanisms of fluoride adsorption onto Mn^{2+} bentonite clay as well as the potential rate controlling steps. Pseudo first and second order kinetics reaction based and the Webber Morris intra-particle diffusion models were used to explain the kinetics. The pseudo first order is used to describe liquid-solid phase adsorption systems, and it is the earliest known kinetic model describing the adsorption rate based on the adsorption capacity (Oladoja et al., 2014). Pseudo second order is used to describe chemisorption, as well as cation exchange reactions. Parameters in Table 7.5 shows that the adsorption of fluoride onto Mn^{2+} bentonite clay couldn't be described by the pseudo first order kinetics.

Table 7.5. Pseudo first and second order kinetic model calculated parameters

	Pseudo first order		Pseudo second order			Intra-particle diffusion	
	$K_{ad}(min^{-1})$	R^2	$q_e(mg/g)$	$K_{2a}(g/mg/min)$	R^2	K_{i1}	K_{i2}
0.1 g/100 mL	2.1×10^{-2}	0.47	0.56	2.73	0.99	0.016	-3×10^{-5}
0.3 g/100 mL	5.06×10^{-3}	0.35	0.33	1.36	0.99	0.022	-0.2×10^{-5}
0.5 g/100 mL	4.6×10^{-3}	0.05	2.4	0.52	0.99	0.13	-8×10^{-8}

A pseudo second order plot of the F^- adsorption data shows indicates a good fit of the data to this kinetic model (Fig 7.16). This suggests chemisorption as the mechanism for interaction of the F^- with the adsorbent. Figure 7.17 shows the plot of amount of fluoride adsorbed and $t^{0.5}$.

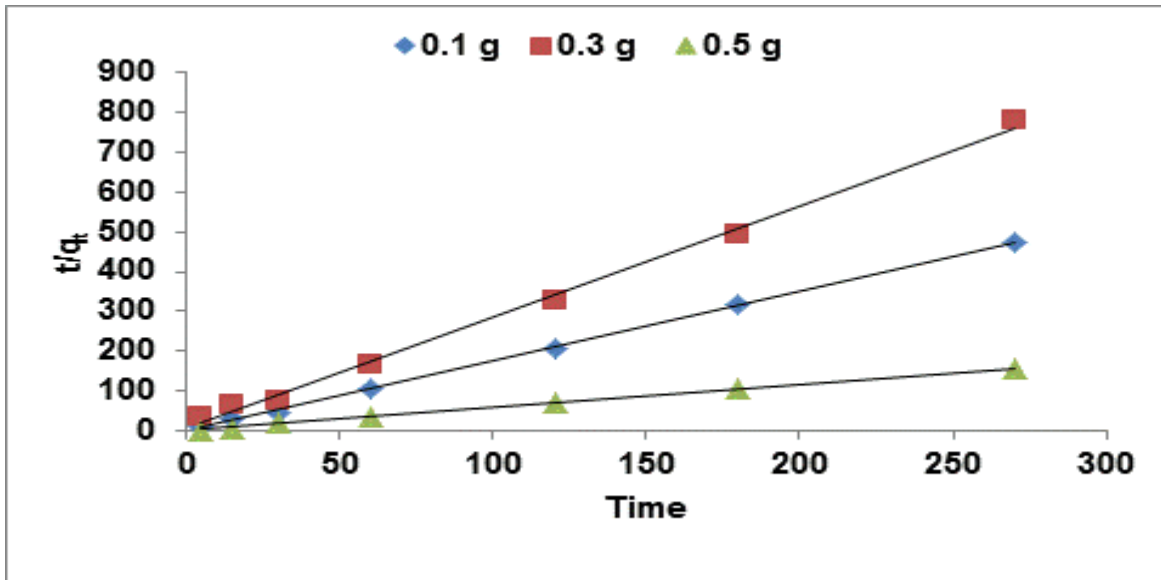


Figure 7.16. Pseudo second order plot at various adsorbent doses (3 mg/ℓ F⁻, pH 5.54 and shaking speed of 250 rpm).

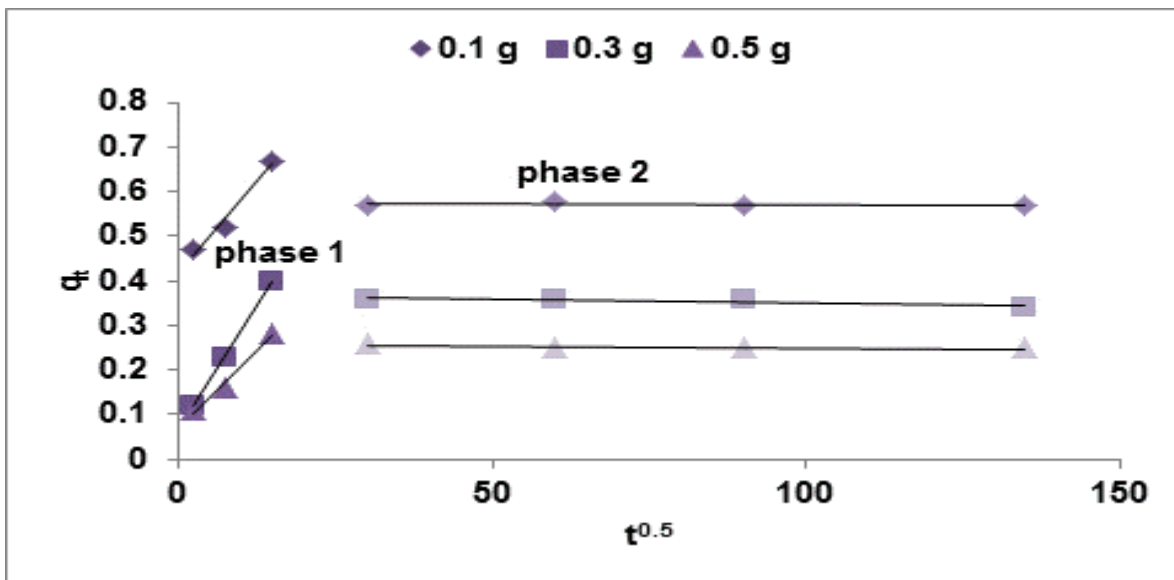


Figure 7.17. Plot for intra-particle diffusion at various adsorbent dosages (3 mg/ℓ F⁻, pH 5.54 and shaking speed of 250 rpm).

Intra particle diffusion model indicates that if the plot of q_t against $t^{0.5}$ gives straight line passing through the origin, then the adsorption is solely controlled by intra particle diffusion, while a bilinear plot indicates that adsorption occurred via film and intra particle diffusion mechanism (Ghosh et al., 2015). Adsorption of fluoride onto Mn²⁺ bentonite showed bilinear plot with the initial plot (phase 1) indicating external diffusion and the second plot (phase 2) indicating intra-particle diffusion. The intra-particle rate constants K_{i1} and K_{i2} obtained

from the plot are presented in Table 8.5. At both adsorbent dosages, K_{i1} value is greater than the K_{i2} value, indicating that the initial step is faster than the final step where equilibrium was established. This may be attributed to difference in the rate of mass transfer in the initial and second phase of adsorption (Jia et al., 2015). From these observations it is concluded that the process of adsorption of F^- involves an external mass transfer followed by diffusion into micro- and mesoporous surfaces. Moreover, it is concluded that F^- adsorption onto Mn^{2+} modified bentonite is a complex process involving external and internal diffusion of F^- ions.

7.9.3 Mechanism of F- adsorption onto Mn^{2+} modified bentonite clay

Ma et al. (2012) indicated that fluoride adsorption depends on the number of hydroxyl sites on an adsorbent surface. FTIR results showed that Mn^{2+} modified bentonite clay has highly accessible hydroxyl groups positioned on the layers which favours F^- adsorption. After F^- adsorption a decrease in intensity of transmittance was observed in transmittance bands associated with OH groups indicating an exchange of OH^- from the adsorbent surface for F^- ion. The adsorption of F^- was also dependent on pH (Fig 7.8) being optimum at acidic pH with a decrease at alkaline levels. Its pH dependence may be explained through the pH_{pzc} of the adsorbent. The pH_{pzc} of Mn^{2+} bentonite was observed to be 8.8. At pH below 8.8, the surface of the clay is positively charged (equation 7.1) and therefore F^- ions will be electrostatically adsorbed to the surface of the clay (equations 7.2-7.3). Loganathan et al. (2013) suggested that at low pH adsorption of F^- follows the ligand exchange mechanism because of stronger attractive force between F^- and the adsorbent surface and the presence of more hydroxylated sites for exchange of F^- than at high pH. At moderate pH, F^- adsorption occurs via ion exchange (equation 7.4). At pH above the pH_{pzc} where the surface of the clay is negatively charged fluoride adsorption also occurs via ion exchange (equation 7.5).



Where $\equiv M$ represent Metal in the adsorbent surface (Mn, Si, and Al).

7.10 SUMMARY

Bentonite clay was successfully modified by intercalation of Mn^{2+} in the interlayers through ion exchange. At 3 mg/l F^- concentration and 1 g/100 l volume and 30 min contact time, a maximum F^- removal of 84.0% was achieved at the optimized pH 2. Regeneration study revealed that Mn^{2+} bentonite can be successfully regenerated with 0.1 M NaOH. Stability assessment showed that there is minimal release of chemical species from the adsorbent at various pH levels. Fluoride adsorption onto Mn^{2+} bentonite occurred via ligand exchange at lower pH and ion exchange at higher pH. Mn^{2+} bentonite clay showed low F^- adsorption capacity compared to other adsorbent reported in the literature. The optimal adsorption capacity was at low pH which would limit application in rural areas due to requirement for pH adjustment. The Mn^{2+} intercalated bentonite clay removed $\approx 55.89\%$ of fluoride from field groundwater. However significant fluoride adsorption was observed over the pH range 4-10 indicating that Mn^{2+} intercalated bentonite clay has a potential for application in defluoridation of groundwater containing moderate levels of fluoride.

8 EVALUATION OF GROUNDWATER DEFLUORIDATION BY MnO₂ COATED BENTONITE CLAY

8.1 INTRODUCTION

The presence of chemical species such as fluoride in high concentration in drinking water is a serious concern from the health point of view. Fluoride is classified as one of the major contaminants of groundwater for human consumption by the World Health Organization (WHO, 2011). The consumption of water containing fluoride concentration above 1.5 mg/l for extended period of time may lead to dental fluorosis and higher concentrations may lead to major health hazards such as deformation of bones (skeletal fluorosis) (Ncube and Schutte, 2005). In South Africa dental fluorosis has been observed in provinces such as, Limpopo, North West, Mpumalanga, KwaZulu-Natal and Northern Cape (Ncube and Schutte, 2005; Odiyo and Makungo, 2012). Fluorosis is an incurable disease and as such efforts should be directed towards prevention. In trying to reduce the effect of fluoride, WHO has set a standard for fluoride concentration in water at 1.5 mg/l (WHO, 2011) while South African National Standard (SANS 241-1, 2015) has set a guideline of 1.0 mg/l. Ncube and Schutte (2005) suggested that areas with fluoride concentration above the permissible limit will require defluoridation. They further recommended that proper research must be initiated into investigating cheap and technologically simple processes for small-scale removal of fluoride from fluoride-rich groundwater or developing alternative methods of fluoride free water supply in such areas. Chapters 7 and 8 presented findings on the application of black smectite-rich clay soils and Mn²⁺ modified bentonite in defluoridation of groundwater. The two adsorbents showed higher percentage fluoride removal at acidic pH of 2 and they showed low adsorption capacity which limits their application in rural areas. There is therefore need to develop a high adsorption capacity fluoride adsorbent based on locally available clay materials which can show high fluoride binding capacity at wide pH range and which also offer the advantage of large surface area. Coating various materials with MnO₂ was observed to increase their surface area and moreover MnO₂ coated materials showed higher fluoride binding efficiency at wider pH range (Teng et al., 2009; Li et al., 2013). The current Chapter presents findings on:

- a. Optimization of activation parameters for bentonite clay with dilute NaOH.
- b. Optimization of conditions for coating activated bentonite clay with MnO₂.
- c. Evaluation of the physicochemical and mineralogical properties of the MnO₂ modified bentonite clay
- d. Evaluation of the optimum conditions for fluoride removal using MnO₂ coated bentonite clay, adsorption modelling, adsorption kinetics, its regeneration and reuse potential.

8.2 MATERIALS

All reagents and TISAB-III were obtained from Rochelle Chemicals & Lab Equipment CC, South Africa Ltd and they were of analytical grade. Bentonite clay was collected from ECCA pty (Ltd) in Cape Town. A stock solution containing 1000 mg/l fluoride was prepared by dissolving 2.21 g analytical grade sodium fluoride in 1 l of ultra-pure water (18.2 MΩ/cm). Fluoride solutions for batch experiments were prepared from fresh stock fluoride solution by appropriate dilution. A stock solution containing 1000 mg/l fluoride was prepared by dissolving 2.21 g NaF in 1 l of MilliQ water (18.2 MΩ/cm) and fluoride solutions for batch experiments were prepared from fresh stock fluoride solution by appropriate dilution. Field water was collected from a community borehole in Siloam, Vhembe district in South Africa.

8.3 METHODS

8.3.1 Activation of bentonite clay with NaOH

Prior to activation, optimal conditions for were determined by varying contact time and NaOH concentration. The Na-bentonite was prepared using optimised conditions as follows: 12 g of bentonite clay was suspended in 300 ml of 0.1 M NaOH solution. The mixture was agitated for 15 min, after agitation the suspension was centrifuged for 10 min at 2 500 rpm, the obtained residues were then rinsed with MilliQ water (18.2 MΩ/cm) and then dried at 110°C for 12 hrs in the oven.

8.3.2 Coating the Na-bentonite with MnO₂

Na-bentonite was then coated with MnO₂ through *in-situ* reduction of KMnO₄ with 2 M HCl. Optimum coating conditions were determined by varying KMnO₄ concentration, clay dosages and reaction time. Na-bentonite was coated at optimum conditions as follows:

Concentration of 1.5 M KMnO₄ was prepared by dissolving 5.0 g of KMnO₄ in 20 ml of distilled water in 500 ml beaker and kept in a water bath at 90°C for 15 min. To this 2.5 g of Na-bentonite was added and the suspension was mixed gently and kept in a water bath for 5 min. To this 300 ml of 2 M HCl was then added and the mixture was then vigorously stirred at 300 rpm using a magnetic stirrer followed by continuous heating in a water bath at 90°C for 60 min under continuous stirring. After the completion of reaction, mixtures were left for 15 min to cool. pH of the mixture was measured and found to be 3.2. The mixture was then filtered through 0.45 µm pore cellulose filter membrane, obtained residues were further rinsed with 0.05 perchloric acid and distilled water until the runoff was clear and then dried in an oven at 110°C for 12 h in the oven. Obtained MnO₂ coated Na-bentonite was then milled to pass through <250 µm sieve and stored in lockable sample bags.

8.3.3 Characterisation techniques

Several techniques were used to characterize the smectite-rich clay soils for adsorption (detailed in Appendix A). These included Cation Exchange Capacity (CEC), Point of Zero Charge (PZC), X-ray diffraction (XRD), X-ray fluorescence (XRF), Scanning Electron Microscopy (SEM), Scanning Electron Microscopy coupled with Energy Dispersive Spectroscopy (SEM-EDS), Transmission Electron Microscopy (TEM), Brunauer-Emmett-Teller (BET) and Fourier Transform Infrared (FTIR).

8.3.4 Batch and field groundwater adsorption studies

Methods followed for batch and field groundwater fluoride adsorption studies are detailed in Appendix B.

8.3.5 Adsorption modelling studies

Adsorption models used for describing the adsorption process using smectite-rich clay soils are detailed in Appendix C. Equation 1 (Appendix C) was used to calculate the percentage of removal and adsorption capacity.

8.4 SYNTHESIS OF MNO_2 COATED BENTONITE

8.4.1 Optimizing conditions for activating bentonite with NaOH

8.4.1.1 Effect of contact time

The activation was meant to extract competing anions/cations from the exchangeable sites of the bentonite clay. Figure 8.1 shows the concentration of anionic and cationic species leached from bentonite clay during the activation process. Results showed that the leaching of both anionic and cationic species was high at 15 min contact time and decreased at contact time > 15 min.

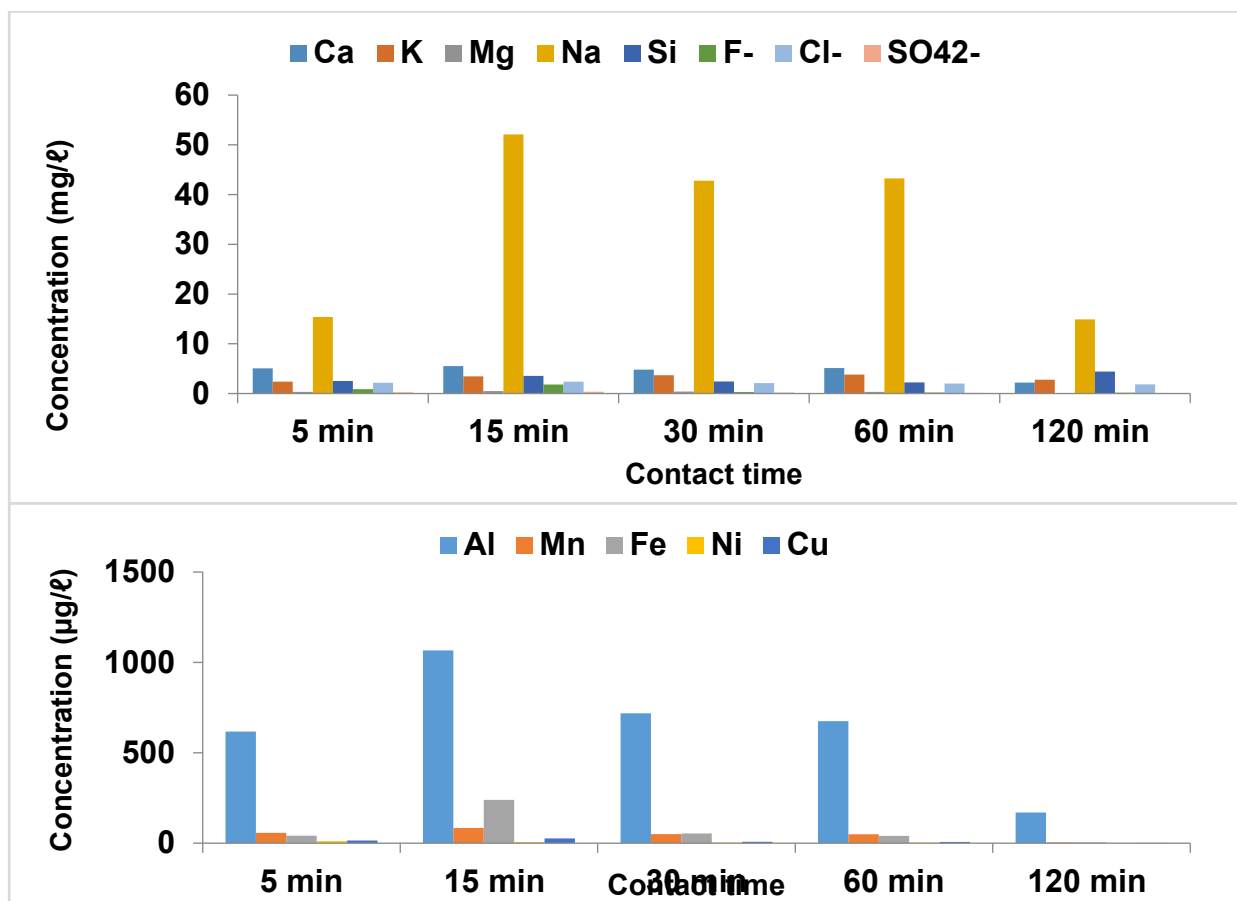


Figure 8.1. Variation of chemical species concentration in mg/l and µg/l with contact time (0.1 M NaOH concentration, 0.1 g/100 ml adsorbent dosage, n=3, particle size=250 µm)

8.4.1.2 Effect of concentration

Figure 8.2 shows the effect of NaOH concentration on the leaching of chemical species from bentonite clay. It was observed that as the concentration increases from 0.1 to 0.5 M, the concentration of both anionic and cationic species decreases except for Na which increased with increased concentration which may be due to the increase in Na added in the form of NaOH. Therefore 0.1 M NaOH concentration was adopted as the optimum concentration for activating bentonite clay. Based on the above results the optimum conditions for activating bentonite with NaOH were established to be 15 min contact time and 0.1 M NaOH.

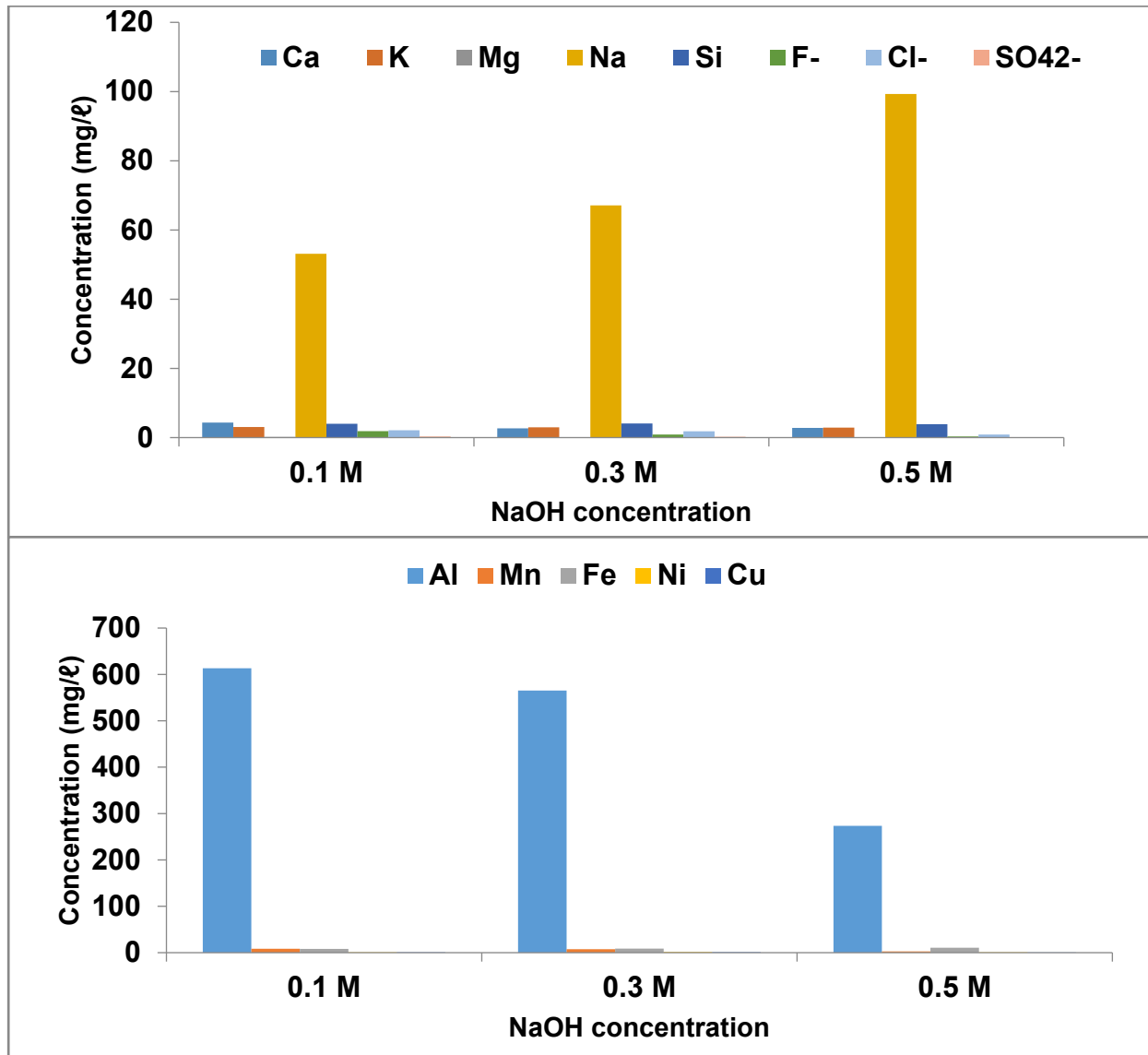


Figure 8.2. Variation of chemical species in mg/l and µg/l with contact time (0.1M NaOH concentration, 0.1 g/100 ml adsorbent dosage, n=3, particle size=250 µm)

8.4.2 Optimisation of conditions for coating NaOH activated bentonite with MnO_2

8.4.2.1 Effect of $KMnO_4$ concentration

Results of % fluoride removal of MnO_2 coated bentonite clay prepared at various $KMnO_4$ concentrations are presented in Figure 8.3. Fluoride removal was used as an indicator of the efficiency of the coating process. Results in Figure 8.3 show that % F^- removal was optimum for MnO_2 coated bentonite clay prepared with 1.5 M $KMnO_4$ concentration and these conditions were applied for synthesis of the bulky MnO_2 coated bentonite clay used in subsequent experiments.

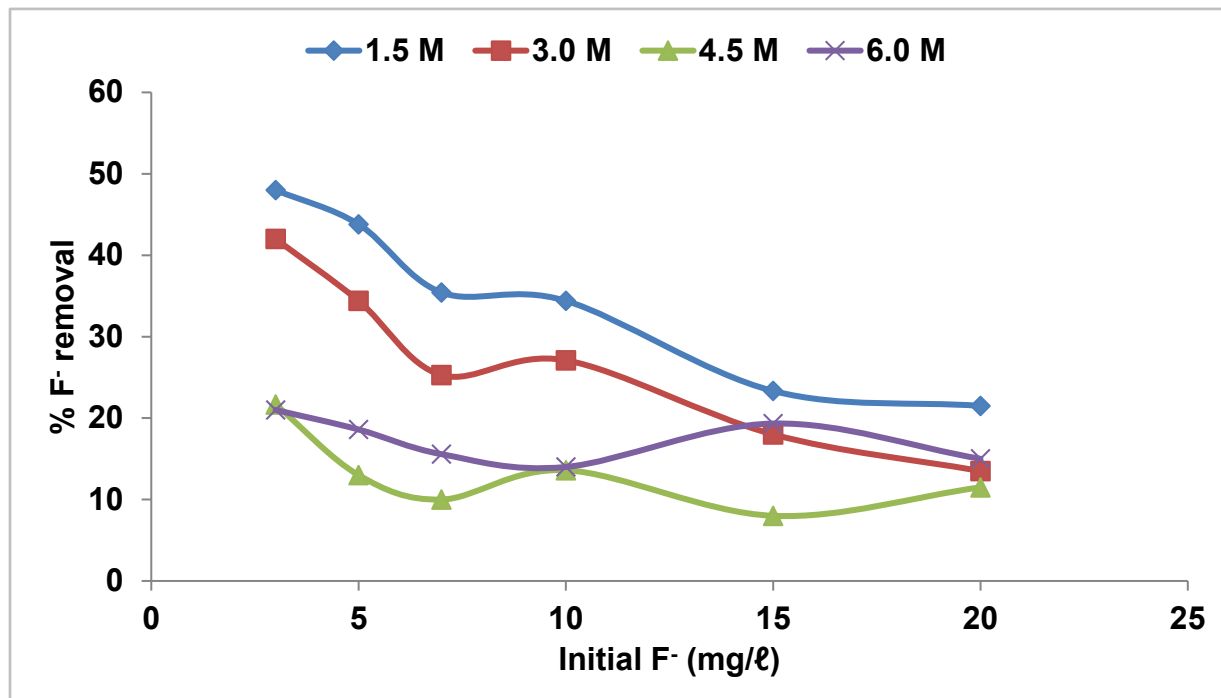


Figure 8.3. Variation of % F^- removal with initial fluoride concentration for MnO_2 coated bentonite clay prepared at various $KMnO_4$ concentration.

8.4.2.2 Effect of clay amount

Results of % fluoride removal by MnO_2 coated bentonite clay prepared at various clay dosages at optimized $KMnO_4$ solution are presented in Figure 8.4. Fluoride removal was used as the indicator of the efficiency of the coating process. Results in Figure 8.4 show that MnO_2 modified bentonite clay prepared with 2.5 g Na bentonite dosage had higher % F^- removal at all initial F^- concentrations compared to higher dosages and was adopted as the optimum dosage for subsequent experiments.

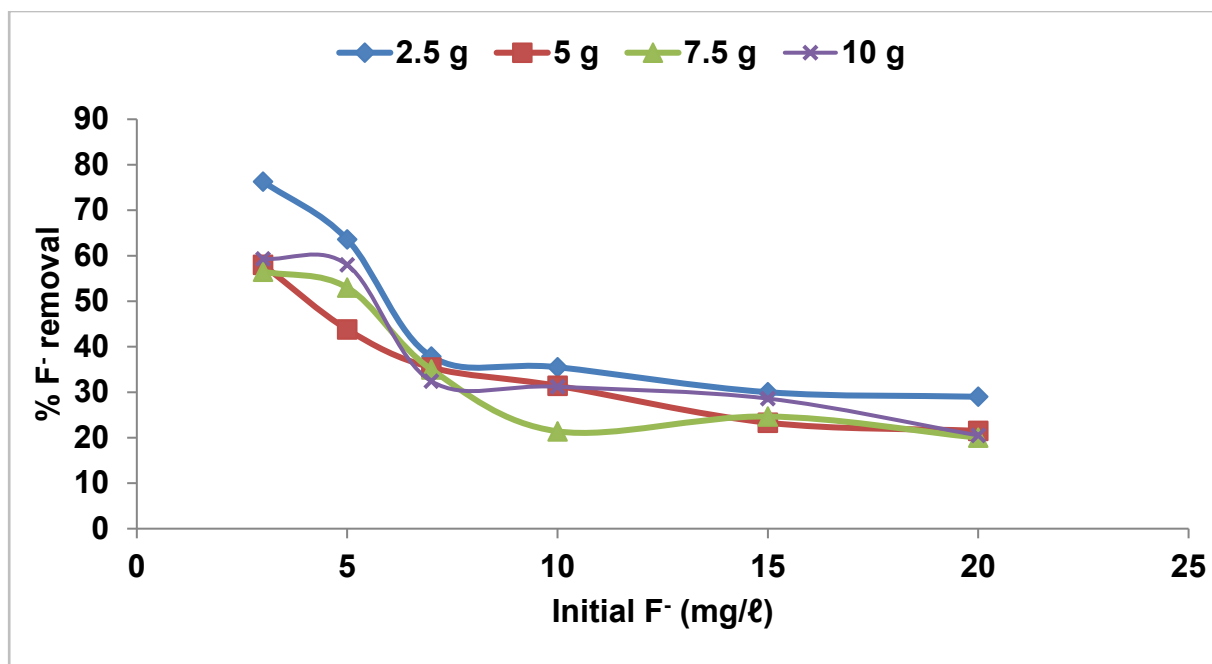


Figure 8.4. Variation of % F⁻ removal with initial fluoride concentration (Na-bentonite doses: 2.5, 5, 7.5 and 10 g. Adsorption conditions: 0.5 g/100 mL adsorbent dosage, 30 min contact time at 250 rpm and initial pH 5.54±0.5, n=3, particle size <250 μm).

8.4.2.3 Effect of reaction time

Results of % F⁻ removal with contact time for optimized KMnO₄ concentration and Na-bentonite clay dosage are presented in Figure 8.5. It is observed that MnO₂ modified clay prepared at 60 minutes of in situ oxidation showed highest percentage F⁻ removal at all initial concentrations tested and was adopted as the optimum reaction time for preparation of the final adsorbent. Based on the above findings, the optimum conditions for coating Na-bentonite with MnO₂ were established as: 1.5 M KMnO₄ concentration, 2.5 g clay amount and 60 min reaction time.

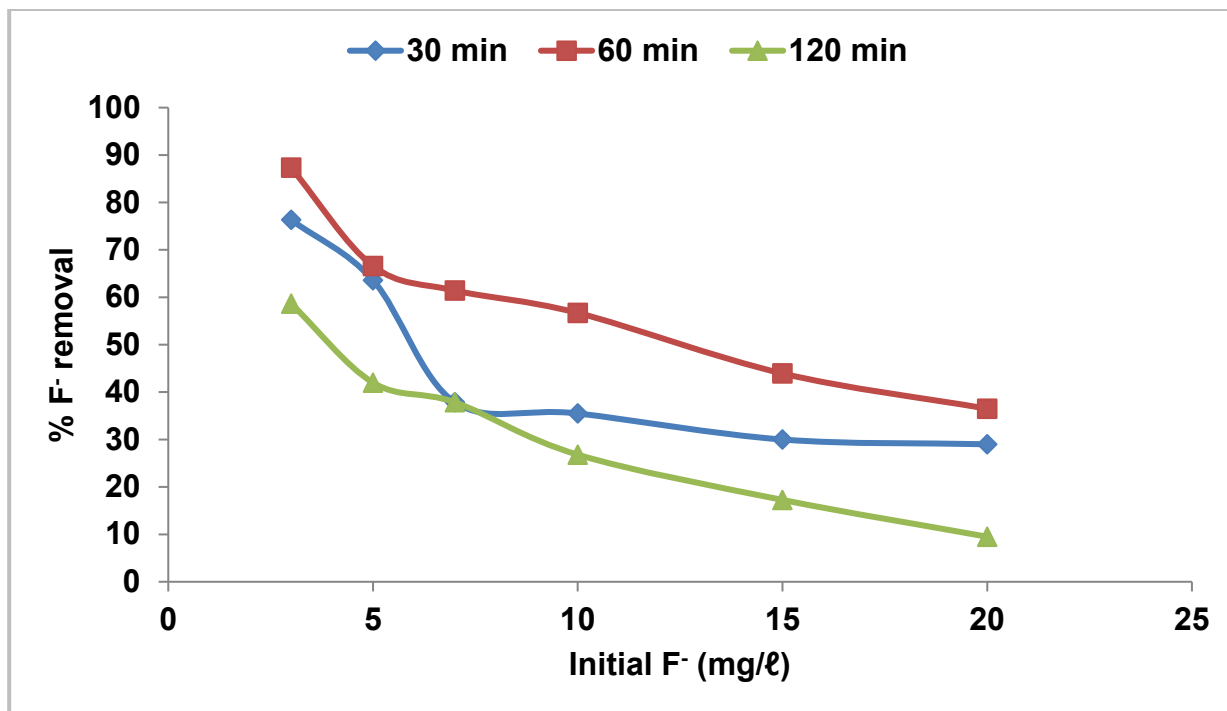


Figure 8.5. Variation of % F⁻ removal as a function of initial fluoride concentration (contact times for coating bentonite clay: 30, 60 and 120 min, Adsorption conditions: 0.5 g/100 mL adsorbent dosage, 30 min contact time at 250 rpm and initial pH 5.54±0.5, particle size <250 μm, N=3)

8.5 PHYSICOCHEMICAL AND MINERALOGICAL CHARACTERIZATION

8.5.1 X-ray diffraction analysis

X-ray diffraction analysis was carried out to evaluate the change in mineralogical content of Na-bentonite after modification with MnO₂. Figure 8.6 presents the XRD spectra of Na-bentonite and MnO₂ modified bentonite clay. Main minerals in Na-bentonite clay were quartz, montmorillonite. After modification with MnO₂, formation of new minerals, cryptomelane (KMn₈O₁₆), jacobsonite (Mn₆Fe₄)O₄ and pyrolusite (MnO₂) were observed in the Na-bentonite which are both oxides of manganese.

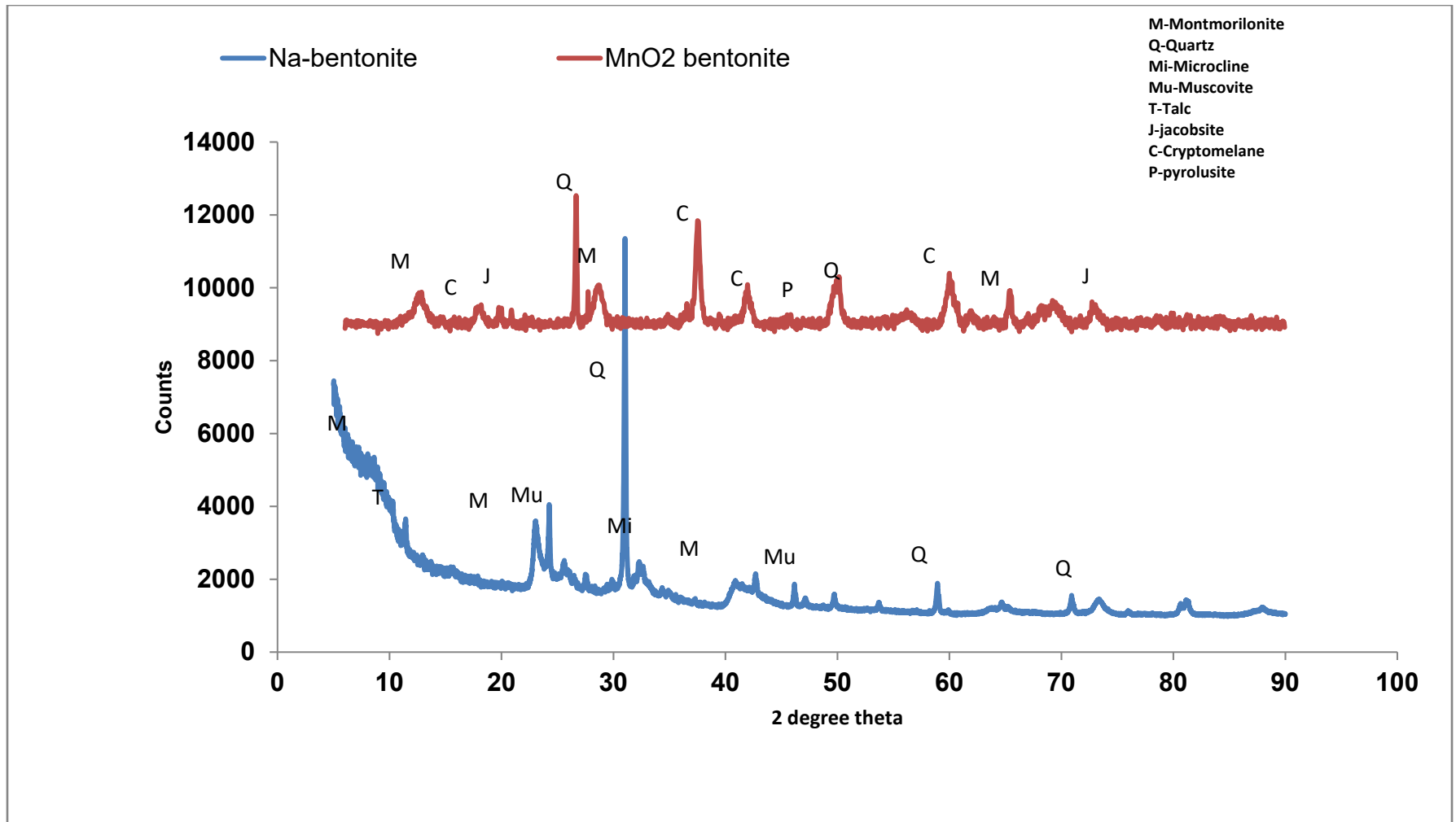


Figure 8.6. XRD spectra for Na-bentonite and MnO₂-bentonite

8.5.2 X-ray fluorescence

Table 8.1 shows the elemental composition of Na-bentonite and MnO₂ coated Na-bentonite clay. The results shows that SiO₂ and Al₂O₃ are the main oxides of Na-bentonite followed by Na₂O, MgO and Fe₂O₃. After coating Na-bentonite with MnO₂ there was a decrease in major oxides which may be attributed to dilution effect after introduction of MnO₂. A significant increase in K₂O was observed which is attributed to the residue K from the KMnO₄ solution.

Table 8.1. Chemical composition of Na-bentonite and MnO₂ coated Na-bentonite clay.

Composition	Na-bentonite	MnO ₂ coated
SiO ₂	64.11	34.30
TiO ₂	0.44	0.16
Al ₂ O ₃	15.90	7.80
Fe ₂ O ₃	3.34	1.41
MnO	0.05	39.20
MgO	3.35	1.17
CaO	0.81	0.10
Na ₂ O	4.22	0.23
K ₂ O	0.90	4.47
P ₂ O ₅	0.09	<0.01
Cr ₂ O ₃	0.01	<0.01
NiO	0.01	0.22
V ₂ O ₅	0.01	<0.01
ZrO ₂	0.02	<0.01
CuO	0.00	<0.01
LOI	6.90	10.90
Total	100.0	99.9

8.5.3 Scanning electron microscopy

Figure 8.7 presents the morphology of Na-bentonite clay and MnO₂ coated Na-bentonite clay. The morphology of Na-bentonite is largely granular with irregular structures. After modification with MnO₂ the morphology appears largely fibrous coatings on the granules which indicate precipitates of manganese oxides on the surface of the clay. The semi-quantitative SEM-EDS analysis confirmed the presence of Mn (44.2%) on the surface of the MnO₂ coated bentonite clay (Table 8.2). The analysis also revealed that coating Na-bentonite with MnO₂ decreased the concentration of the main elements of Na-bentonite this includes Si, Al, Na and Mg due to the dilution effect. However increase in K and Cl was observed which may be due to KMnO₄ and HCl used for coating.

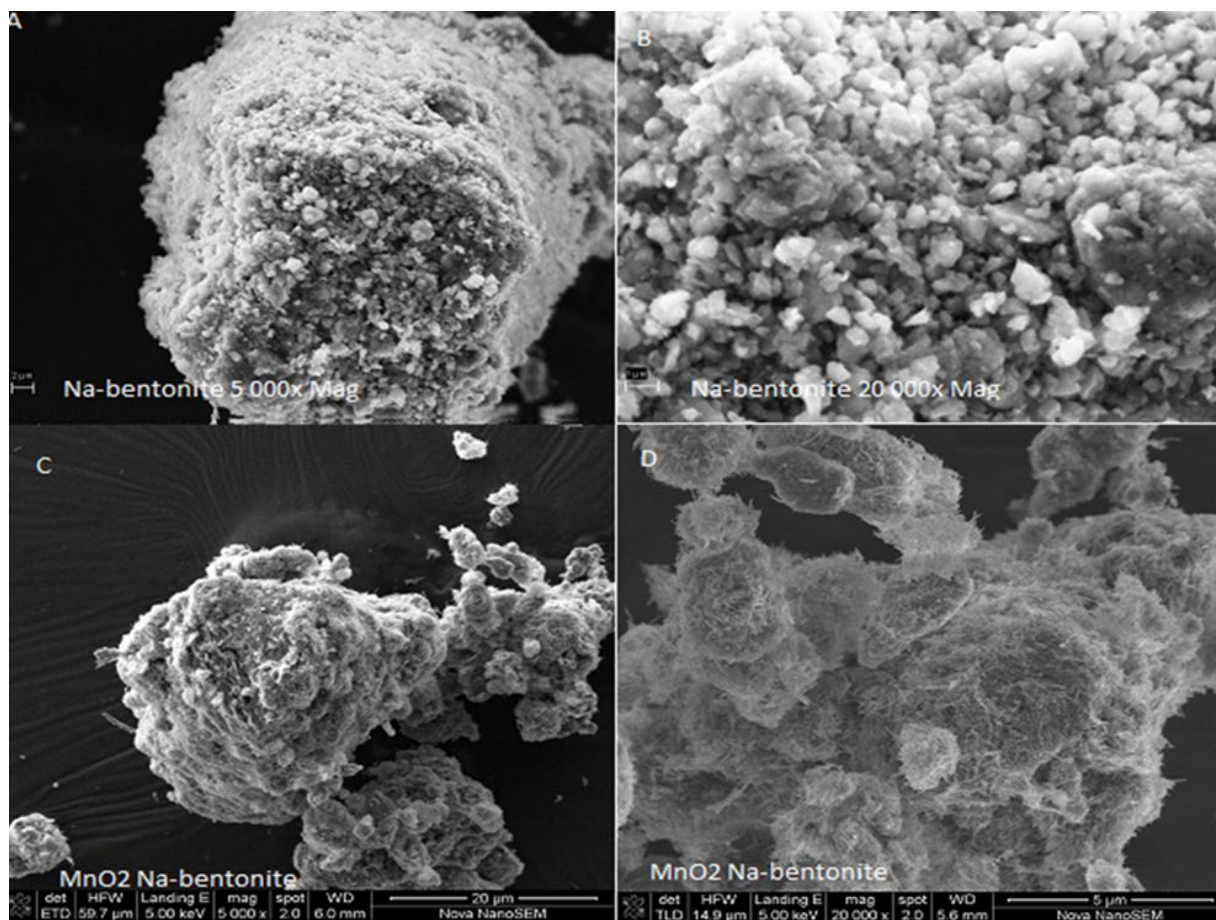


Figure 8.7. Surface morphology for Na-bentonite and MnO₂ coated bentonite.

Table 8.2. Quantitative SEM-EDS of Na-bentonite and MnO₂ coated Na-bentonite

Elements	Na-bentonite	MnO ₂ coated
O	59.33	36.29
Si	26.57	10.51
Al	8.32	3.99
Na	4.07	-
Mg	2.65	-
C	13.20	-
Fe	1.73	-
K	0.95	3.23
Mn	-	44.17

8.5.4 Surface area, pore distribution and pore volume

The surface area and pore distribution are important physical properties of an adsorbent. In order to determine the surface area and pore distribution of the adsorbent, BET and BJH techniques were used and the results are reported in Table 8.3. After coating with MnO₂ the surface area of Na-bentonite increased two fold from 29.03 m²/g to 58.25 m²/g. An increase in the external surface area could be due to surface adsorption and surface precipitation of the fibrous manganese oxides. An increase in surface area makes the MnO₂ coated Na-bentonite clay a better adsorbent.

Table 8.3. Surface area, pore diameter and pore volume of Na bentonite and MnO₂ coated bentonite clay

	Surface area (m ² /g)	Pore diameter (nm)	Pore volume (cm ³ /g)
Na-bentonite clay	29.03	12.45	0.092
MnO ₂ coated	52.5142	5.91	0.11

Figure 8.8a and b shows the nitrogen adsorption-desorption curves and the pore distribution for Na-bentonite and MnO₂ coated Na-bentonite respectively. The N₂ adsorption-desorption curves for both Na-bentonite and the MnO₂ coated Na-bentonite displayed type IV isotherm with wider hysteresis loop at high relative pressures suggesting that both Na-bentonite and MnO₂ coated bentonite are mesoporous in nature. Similar isotherms were reported by Xu et al. (2013) for the hydrous manganese oxide. Figure 8.8b shows the pore distribution of Na-bentonite and MnO₂ coated Na-bentonite. A sharp peak was observed for the Na-bentonite which shows the pore size distribution is monomodal meaning pores are largely of the same size with an average pore size of 12.83 nm. The pore distribution curve for MnO₂ coated Na-bentonite showed that greater amount of pores lies between 17.35-100 Å (1.75-10 nm) indicating that the pore size ranges from micro-mesoporous with the average 5.39 nm. Pore size of the Na-bentonite decreased after coating with MnO₂. Wang et al. (2012) also reported decrease in pore size for the MnO₂ coated bamboo charcoal.

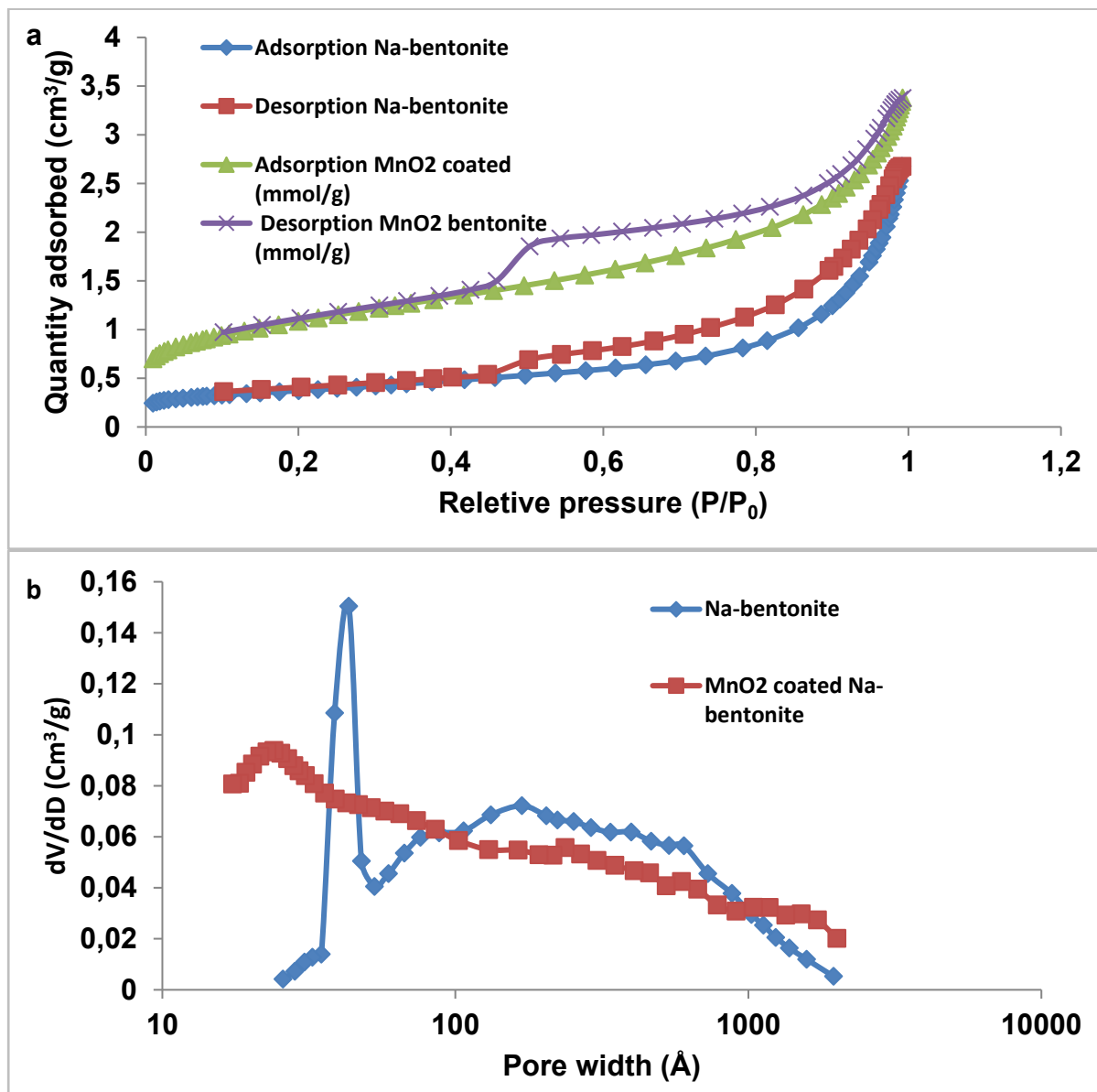


Figure 8.8. N₂ adsorption-desorption isotherms (a) and pore distribution (b).

8.5.5 Fourier Transform Infra-Red (FTIR) Analysis

FTIR was used for identification of functional groups of the adsorbent as well as for establishing the chemical interaction responsible for F⁻ adsorption. Figure 8.9 shows the FTIR spectra of Na-bentonite, MnO₂ coated Na-bentonite and F⁻ loaded MnO₂ coated Na-bentonite. From the Na-bentonite in Figure 5.43 the main absorption peaks observed were 3628.3 cm⁻¹, 1649.4 cm⁻¹, 1037 cm⁻¹ and 797.7 cm⁻¹ which were attributed to the vibration and stretching of H-O-H, Si-OH, Al-OH and Si-O-Al groups. The peaks observed at lower wavelength range could be attributed to the metal-oxygen-metal bonds vibrations. After coating Na-bentonite with MnO₂ there was a shift in these peaks to 3343.4 cm⁻¹, 1626.7 cm⁻¹, 1040.6 cm⁻¹ and 713.4 cm⁻¹.

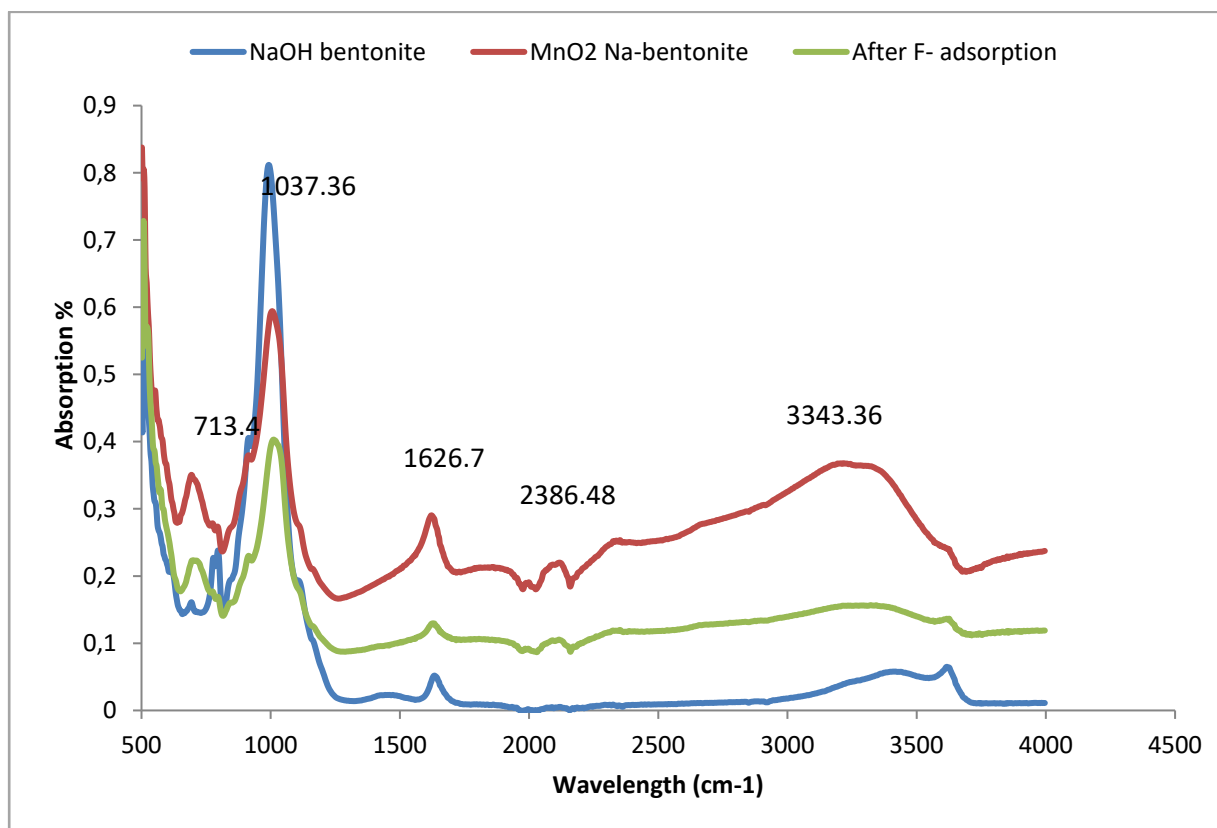


Figure 8.9. FTIR spectra of Na-bentonite, MnO₂ coated Na-bentonite, F⁻ loaded MnO₂ coated bentonite.

Their transmission intensity also increased and this may be ascribed to the interaction between the Mn oxides and the silanol and aluminol groups in the adsorbent surface leading to the formation of Mn-O bonds. A new band was observed at 2386.5 cm⁻¹ which may be attributed to the formation of Mn-O-Mn bonds indicating successful coating of Na-bentonite with MnO₂. Similar findings were reported for Mn oxide coated bentonite (Eren et al., 2009) and modified vermiculite (Sari and Tuzen, 2013). After F⁻ adsorption there was a decrease in transmission of all the bands and also the formation of a new band at 3629.1 cm⁻¹ which may be ascribed to the vibration of physisorbed water (Wang et al., 2013). The absorption band at 2386.5 cm⁻¹ in MnO₂ coated Na-bentonite also disappeared after F⁻ adsorption. These changes indicate that structural oxides/oxyhydroxides groups and water molecules had an important role in F⁻ adsorption process. From these observations it can be concluded that the adsorption of F⁻ occurred through the exchange of OH⁻ in Mn, Al, Si oxides for F⁻ and through interaction with oxyhydroxide groups.

8.5.6 pH point of zero charge (pH_{pzc})

Point of zero charge is the pH where the material has net zero surface charge. pH below the pH_{pzc} the clay surface is positively charged and above is negatively charged. Figure 8.10a and b shows the variation of initial pH of solutions at various ionic strength versus the ΔpH. The pH at X-axis gives the pH_{pzc} of the material. Coating Na-bentonite with MnO₂ lowered the pH_{pzc} of the clay from 8.4 to 3.0±0.2. Ma et al. (2012)

and Teng et al. (2009) also reported low pH_{pzc} for MnO_2 coated adsorbents and the property was attributed to acidic nature of the adsorbent. The pH_{pzc} helps to establish the pH region where the adsorption of F^- will be optimum. Adsorption of F^- onto MnO_2 coated Na-bentonite is likely to be optimum at pH below 3.0 ± 0.2 .

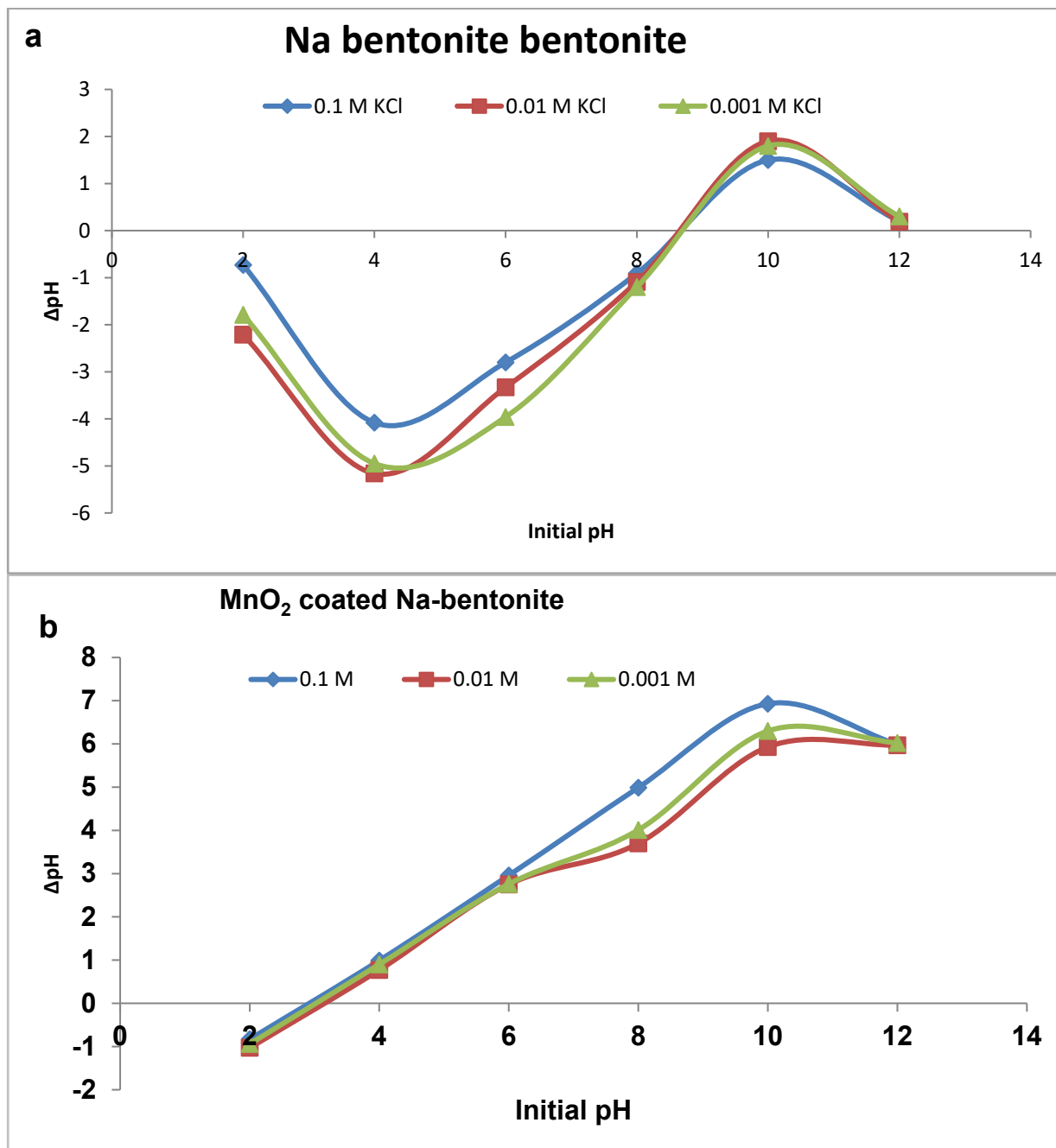


Figure 8.10. a) pH_{pzc} of Na-bentonite and b) MnO_2 coated Na-bentonite

8.6 BATCH F⁻ ADSORPTION EXPERIMENTS

8.6.1 Effect of contact time

Figure 8.11 presents the variation of % F⁻ removal with contact time. It is observed that at allevaluated dosages, significant adsorption of F⁻ occurred within the first 5 min of contact and increased to a maximum at 30 min. Initially high number of adsorption sites are available for fluoride adsorption and this number decreases with increased contact time. Eventually the adsorption sites become the limiting factor in the adsorption process and the system approaches equilibrium. A slight decrease in F⁻ removal is thereafter observed as the system approaches equilibrium. In this case 30 min contact time was adopted as the optimum contact time for subsequent experiments.

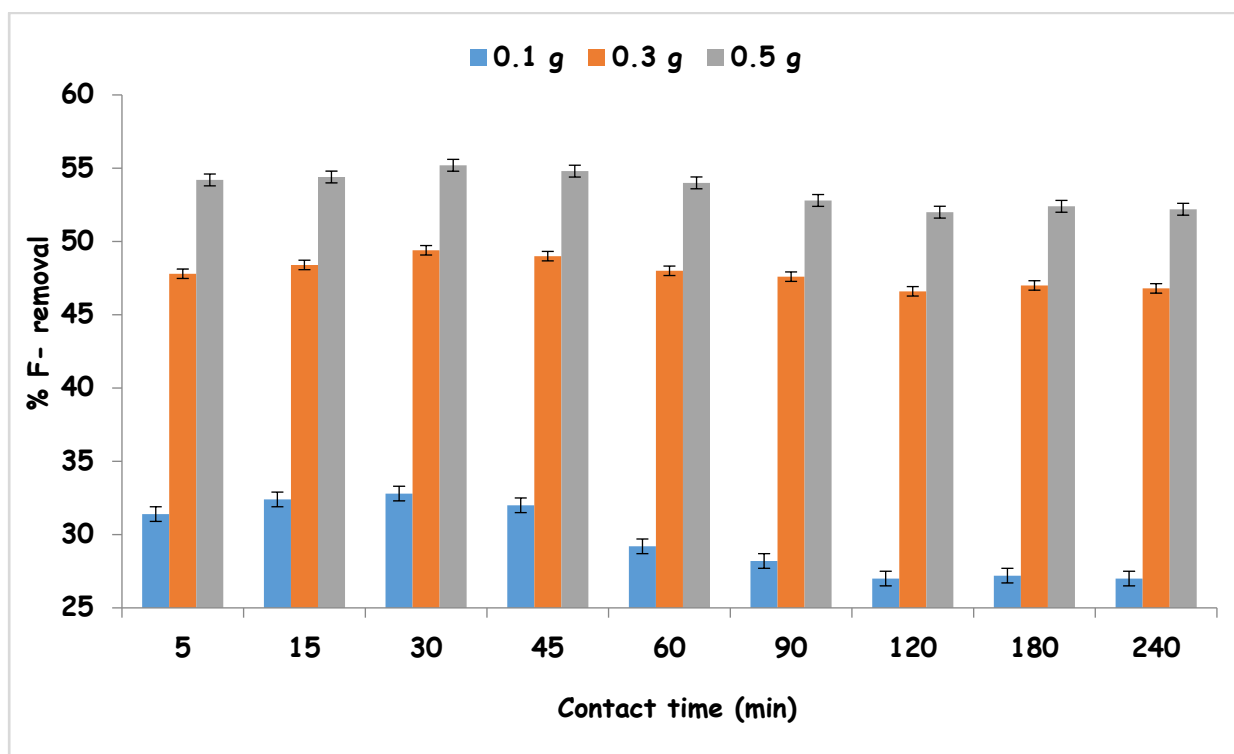


Figure 8.11. Variation of % F⁻ removal as a function of contact time for various adsorbent dosages (5 mg/l F⁻, pH 6.26 and 250 rpm shaking, particle size <250 μm, N=3, particle size <250 μm)

8.6.2 Effect of adsorbent dosage

The plot of percentage fluoride removal and adsorption capacity against adsorbent dosage is presented in Figure 8.12. It is observed that percentage F⁻ removal increased with increase in adsorbent dosage. The % F⁻ removal increased to a maximum of 86% at 2 g/100 ml dosage. However further increase in sorbent dose did not show any remarkable increase in % F⁻ removal. This may be attributed to high density of the adsorbent

particles limiting mobility of the F^- hence limiting access to adsorption sites. Adsorption capacity on the other hand decreased with increasing dosage. A balance is therefore struck between obtaining a high % removal and retaining a significant adsorption capacity. A dosage of 1.5 g/100 ml was adopted as the optimum adsorbent dosage for subsequent experiments.

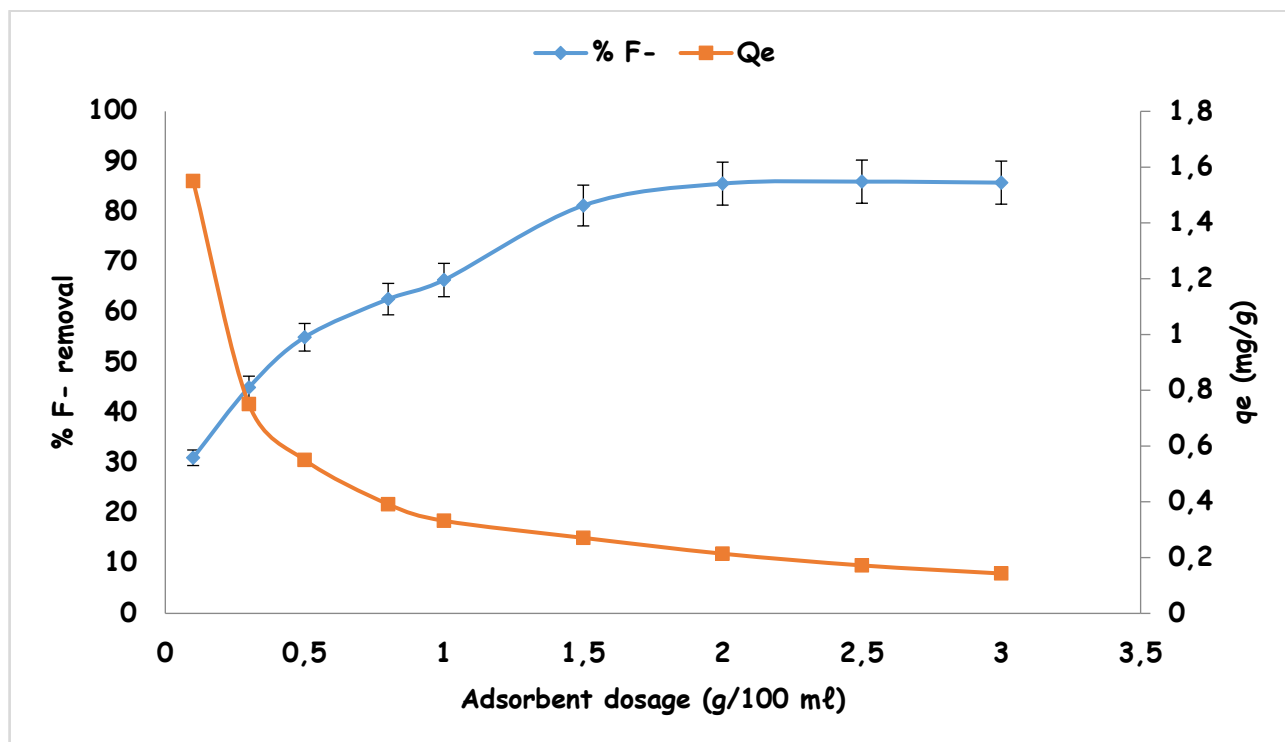


Figure 8.12. Variation % F^- removal and adsorption capacity by MnO_2 bentonite clay as a function of adsorbent dosage (contact time of 30 min, adsorbent dosage, 5 mg/l F^- , pH of 6.24 and shaking speed of 250 rpm, particle size <250 μm , N=3).

8.6.3 Effect of initial adsorbate concentration

The percentage F^- removal trends against initial adsorbate concentration at three different contact times are presented in Figure 8.13. It is observed that the % F^- removal decreased with increase in initial concentration and reached a plateau at initial concentration above 20 mg/l indicating that the adsorbent was saturated. This was observed at all contact times. The decrease may be attributed to decrease in the binding capacity of the adsorbent as the concentration increases (Thakre et al., 2010). There was no significant difference in the adsorption trends at 30 and 60 mins contact times. This confirms earlier observations in contact time experiments where maximum adsorption was at contact times of between 30-60 min. The percentage adsorption was > 80% for initial adsorbate concentration of <7 mg/l. However, 5 mg/l was chosen as the working initial adsorbate concentration for subsequent experiments. This was based on the fact that in Limpopo groundwater in most of the areas has F^- concentration at or below 5 mg/l.

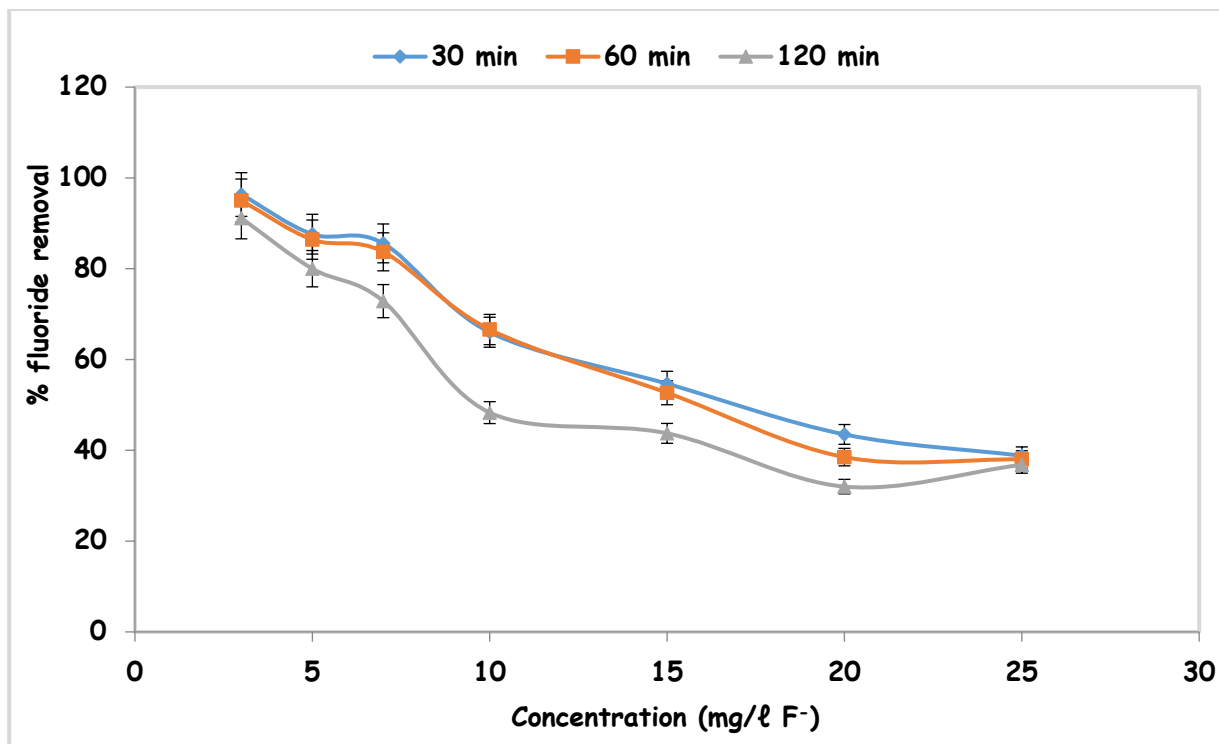


Figure 8.13. Variation of % F⁻ removal with initial concentration at various contact time (adsorbent dosage 1.5 g/100 mL, pH 5.54 and shaking speed of 250 rpm, particle size <250 μm, N=3).

8.6.4 Effects of pH

The percentage F⁻ removal and change in pH (Δ pH) results as a function of initial solution pH are presented in Figure 8.14. The pH of the media is one of the important parameters, which significantly affects the fluoride adsorption. It is observed that % F⁻ removal by MnO₂ coated Na-bentonite is above 90% at all evaluated pH levels (2-12). Initially % F⁻ removal decreased from 93.7% at pH 2 to 92.7% at pH 4 and increased again to 94.7% at pH 8 thereafter decreased to 93.3% at pH 12. The decrease in % removal at pH >8 may be due to the presence of OH⁻ ions which compete with F⁻ for adsorption. Δ pH trend showed that at initial pH 2, the equilibrium pH of the mixture increased leading to positive value of Δ pH. This may be due to the release of OH⁻ from the surface of the adsorbent during F⁻ adsorption. At pH 4 and above, the final pH decreased leading to negative value of Δ pH. This may be due to the release of H⁺ ions and adsorption of OH⁻ ions by the adsorbent. Highest % F⁻ removal was observed pH 8 and was adopted as the optimum pH for subsequent experiments.

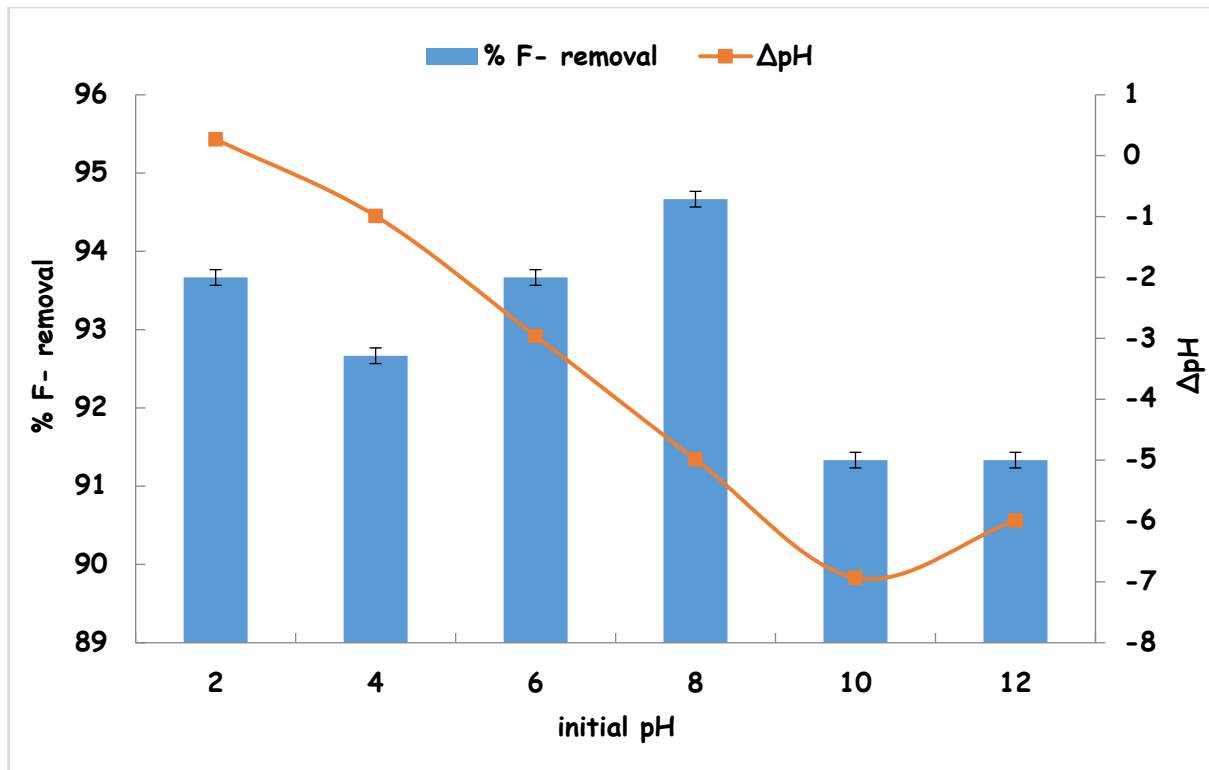


Figure 8.14. Variation of % F⁻ removal and ΔpH with initial pH (3 mg/ℓ, 1.5 mg/ℓ, and 30 min contact time at 250 rpm, particle size <250 μm, N=3).

8.6.5 Effect of co-existing ions

Various anionic species such as Cl⁻, NO₃⁻, SO₄²⁻, and CO₃²⁻ are generally present in groundwater and may compete with F⁻ for adsorption. Their effects on F⁻ adsorption was evaluated by preparing solutions of these anions in presence of F⁻ ions. The % fluoride removal in presence of 10 mg/ℓ of each of these anions are presented in Figure 8.15. It is observed that the presence of Cl⁻, NO₃⁻ and SO₄²⁻ decreased the % F⁻ removal by ≈24% while the presence of CO₃²⁻ decreased the % F⁻ removal significantly by ≈50%. Zhang et al. (2011) also reported significant decrease in % F⁻ removal in the presence of CO₃²⁻ and attributed it to the competition between F⁻ and CO₃²⁻ for active sites on adsorbent surface.

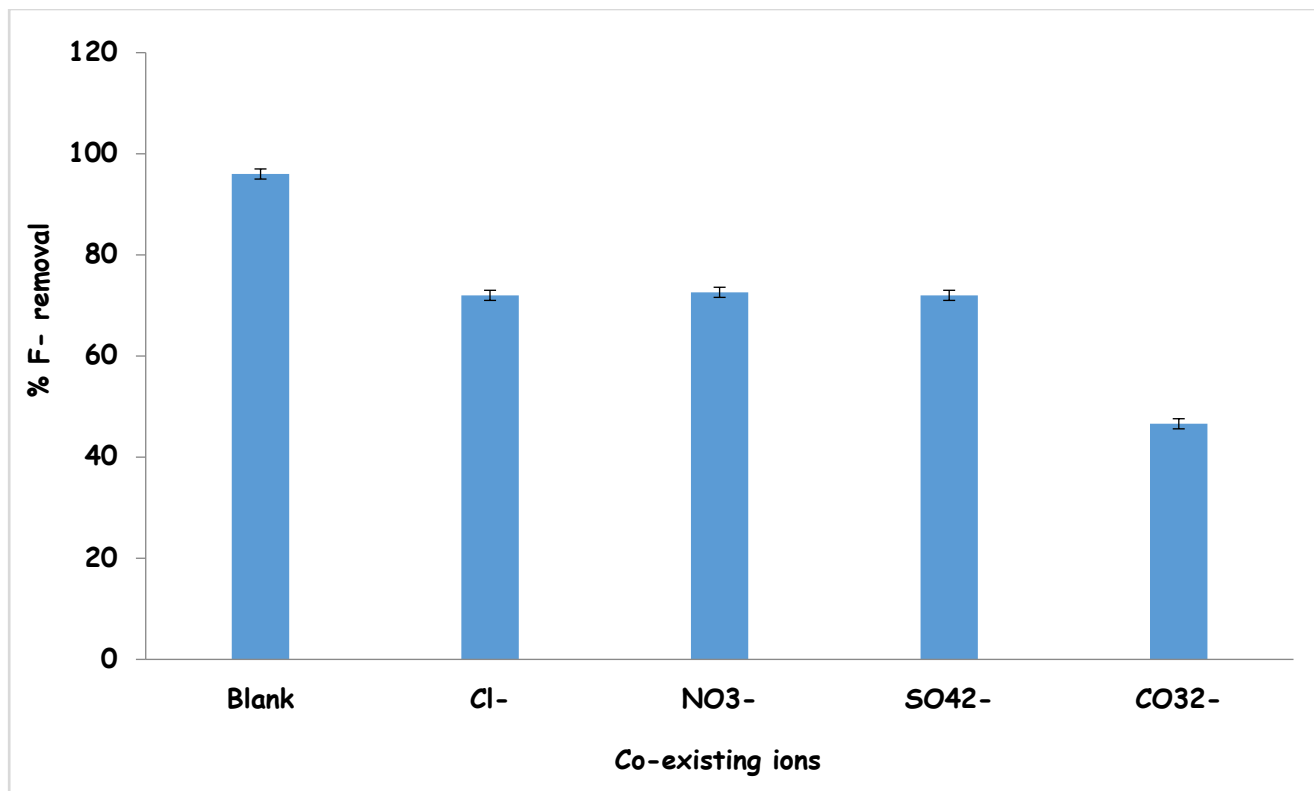


Figure 8.15. Effects of co-existing anions on fluoride removal by MnO₂ coated Na-bentonite (5 mg/l F⁻, 10 mg/l of co-existing ions, 1.5 g/100 ml adsorbent dosage, pH 8 and 30 min contact time at 250 rpm, N=3).

8.7 REGENERATION AND REUSE OF ADSORBENT

For the adsorbent to be cost effective, it must be regenerable and reused for fluoride adsorption. Regeneration of the adsorbent was carried out using dilute NaOH as the regenerant. After regeneration the adsorbent was collected on filter membrane and washed with MilliQ water and dried at 110°C for 3 hrs and re-used for defluoridation for up to five times. The filtrates were also diluted appropriately with MilliQ water and analysed for desorbed fluoride. Detailed methodologies are presented in appendix C. The percentage F⁻ removal as a function of regeneration cycle is presented in Figure 8.16. Results show that MnO₂ coated Na-bentonite can be successfully regenerated upto five cycles and still retain significant F⁻ adsorption potential. After the first regeneration cycle, MnO₂ coated Na-bentonite showed significantly high percentage fluoride removal of 97.8% which is almost equal to the percentage removal achieved by the fresh adsorbent. This could be attributed to the activating nature of the NaOH. Thereafter the percentage removal decreased with increasing cycle of reuse up to fifth cycle where up to 71.6% F⁻ removal was achieved. The decrease of fluoride adsorption is probably due to the gradual dissolution of MnO₂ at alkaline conditions from the surface of the adsorbent during the regeneration process (Xiang et al., 2014).

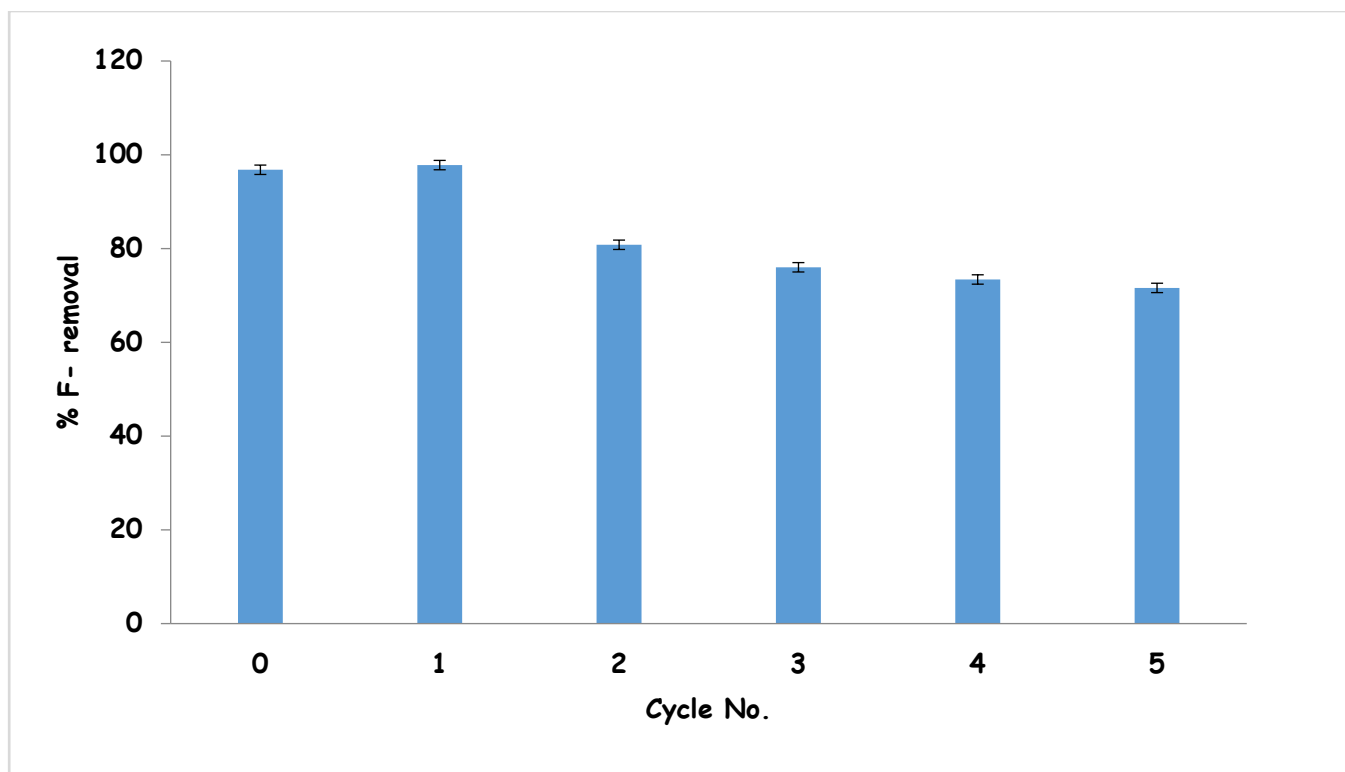


Figure 8.16. Percent fluoride removal onto MnO₂ coated Na-bentonite clay in successive regeneration cycles (5 mg/l F⁻, S/l ratio 1.5 mg/100 ml, 30 min contact time at 250 rpm and pH 8, N=3, particle size < 250 μm).

8.8 CHEMICAL STABILITY OF THE ADSORBENT

The chemical stability of MnO₂ coated Na-bentonite was assessed by measuring the release of metal and non-metal species at various pH levels (2-12) during the defluoridation process. The trends of metal and non-metal chemical species release as a function of initial pH are presented in Figure 8.17a and b in mg/l and μg/l respectively. Results show that pH has a significant impact on the chemical stability of the adsorbent. At pH below 8, the leaching of Al and Ni was observed to be higher which may be attributed to the dissolution at extreme acidic pH conditions. The increasing Na is mainly attributed to the contribution from the NaOH used for pH adjustment. However concentration of these species was found to be within the South African National Standards (SANS 241-1, 2015). The leaching of K was also observed to be higher at both pH levels which may be an indication that K was not stable in the adsorbent. The K levels in the product water was observed to be above the SANS 241-1 (2015) limits. Concentration above these guidelines may lead to aesthetic effects. The release of Mn was found to be above 10 mg/l at pH < 6 and > 11 which is above SANS 241-1 (2015) limits. Similar findings were observed by Teng et al. (2009) for MnO₂ coated alumina and it was attributed to dissolution of Mn at those extreme pH conditions. The release of Mn from the adsorbent would be the limitation for the application of MnO₂ coated Na-bentonite in drinking water due to secondary contamination of the treated water. Table 9.4 shows the SANS 241-1 (2015) guideline for selected species of metals and non-metals.

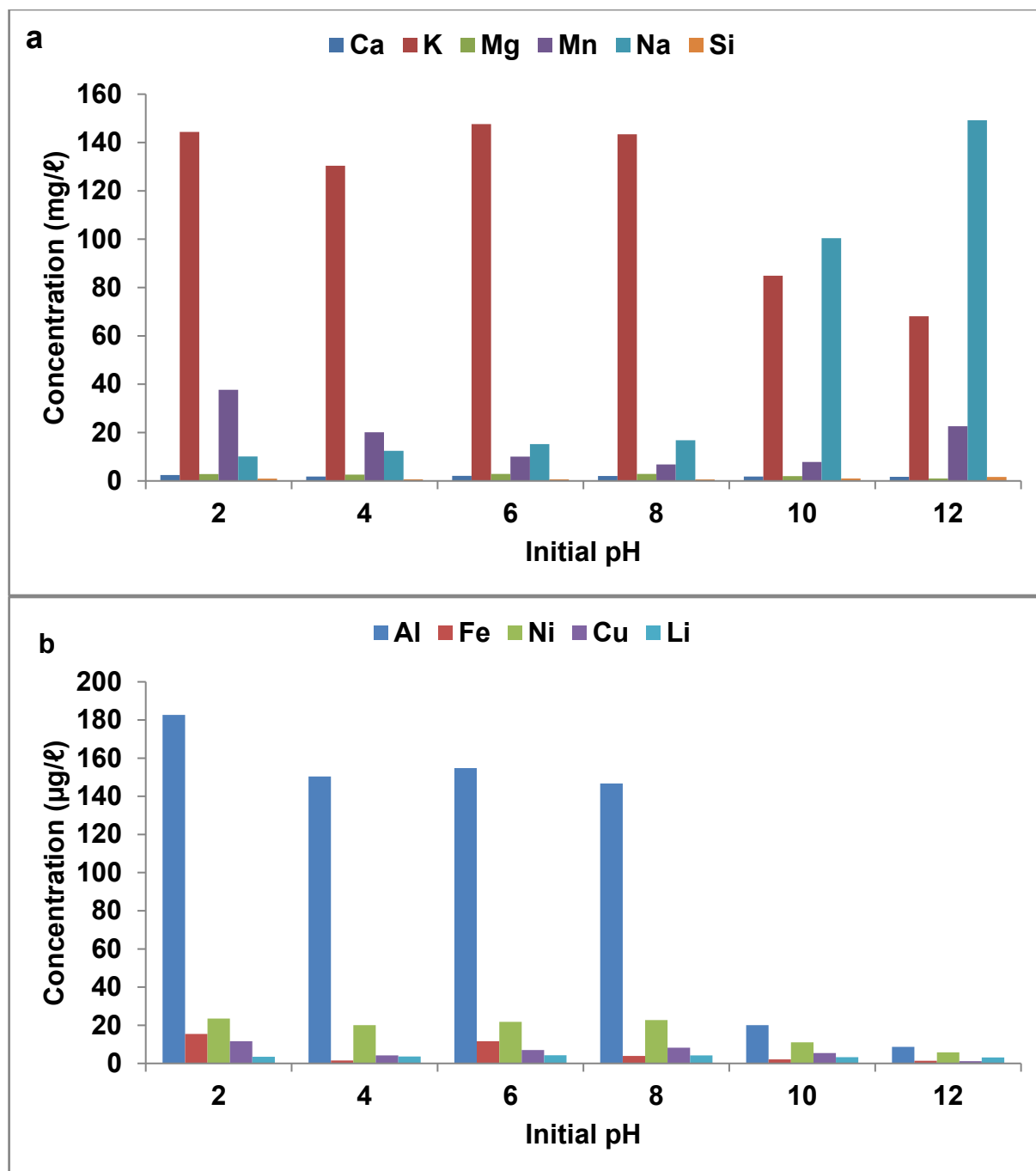


Figure 8.17. Concentration of chemical species in treated water at various pH. a) in mg/ℓ, and b) in µg/ℓ (1.5 g/100 mL adsorbent dosage, 3 mg/ℓ initial F⁻ concentration and 30 min contact time at 250 rpm, particle size <250 µm, n=3).

Table 8.4. The South African National standards for drinking water for selected species.

Elements	SANS 241-1 (2015)
Ca	<150 mg/l
K	<50 mg/l
Mg	<70 mg/l
Na	<200 mg/l
Si	-
Al	<300 µg/l
Mn	<100 µg/l
Fe	<200 µg/l
Cu	<1000 µg/l

8.9 DEFLUORIDATION OF FIELD GROUNDWATER

The defluoridation efficiency of MnO₂ coated Na-bentonite clay was tested on field groundwater collected from Siloam borehole with initial F⁻ concentration of 5.4 mg/l and natural pH (8.07). Optimized adsorbent dosage of 1.5 g/100 ml was used and the mixture was agitated for 30 min at 250 rpm. Water was treated at its natural pH (8.07). The physicochemical parameters of groundwater before and after treatment are presented in Table 5.16. MnO₂ coated Na-bentonite was able to reduce F⁻ in groundwater from 5.4 mg/l to 0.98 mg/l which is below the South African water quality standard value of 1.5 mg/l. The concentration of other co-existing ions such as SO₄²⁻, NO₃⁻, Br⁻ and PO₄³⁻ were not detected after treatment indicating that they were also adsorbed alongside F⁻. However the concentration of Cl⁻ increased after treatment which may be due to the release of residue Cl⁻ resulting from treatment with HCl during modification. pH of the mixture decreased from 8.07 to 5.7 after treatment and this may be due to the release of H⁺ ions into the solution. K and residue Mn was observed to be above prescribed SANS 241-1 (2015) limits (Table 8.5).

Table 8.5. Physicochemical parameters of groundwater before and after treatment.

Parameter	Before treatment	After treatment	SANS 241-1 (2015)
pH	8.07	5.72	5.0-9.5
EC (µS/cm)	194	451	<150 mS/m
TDS (mg/l)	116.7	270	<1000
F ⁻ (mg/l)	5.4	0.98	<1
Cl ⁻ (mg/l)	31.59	72.9	<200
SO ₄ ²⁻ (mg/l)	11.89	N.D	<400
NO ₃ ⁻ (mg/l)	1.13	N.D	<50
Br ⁻ (mg/l)	2.08	N.D	-
PO ₄ ³⁻ (mg/l)	2.67	N.D	-
Ca (mg/l)	2.09	3.3	<150
K (mg/l)	2.74	112.90	<50
Na (mg/l)	71.91	79.85	<200
Mg (mg/l)	0.04	2.84	<70
Mn (mg/l)	0.02	1.66	<100 µg/l
Al (µg/l)	11.11	102.69	<300
Si (mg/l)	46.31	42.26	-
Fe (µg/l)	16.55	1.06	<200

N.D= Not detected.

8.10 ADSORPTION MODELLING

8.10.1 Adsorption isotherms

In order to explain the relationship between the equilibrium amount of solute on the adsorbent and the solute concentration in solutions two commonly used isotherms, i.e. Langmuir and Freundlich adsorption isotherms were employed (Tang and Zhang, 2016; Mariapan et al., 2015). The adsorption data was fitted into these adsorption models. Figure 8.18 shows the plots of Langmuir adsorption isotherm for adsorption data at different contact times. It is observed that the data yielded straight line with higher correlation coefficient at all contact times. This indicates that the data is well described by the Langmuir adsorption model. Calculated values of R_L for different initial concentrations are presented in Figure 8.19. Calculated values lie between 0 and 1 indicating that the adsorption of F^- onto MnO_2 coated Na-bentonite was favourable, which means the adsorption is a spontaneous process which can take place at room temperature.

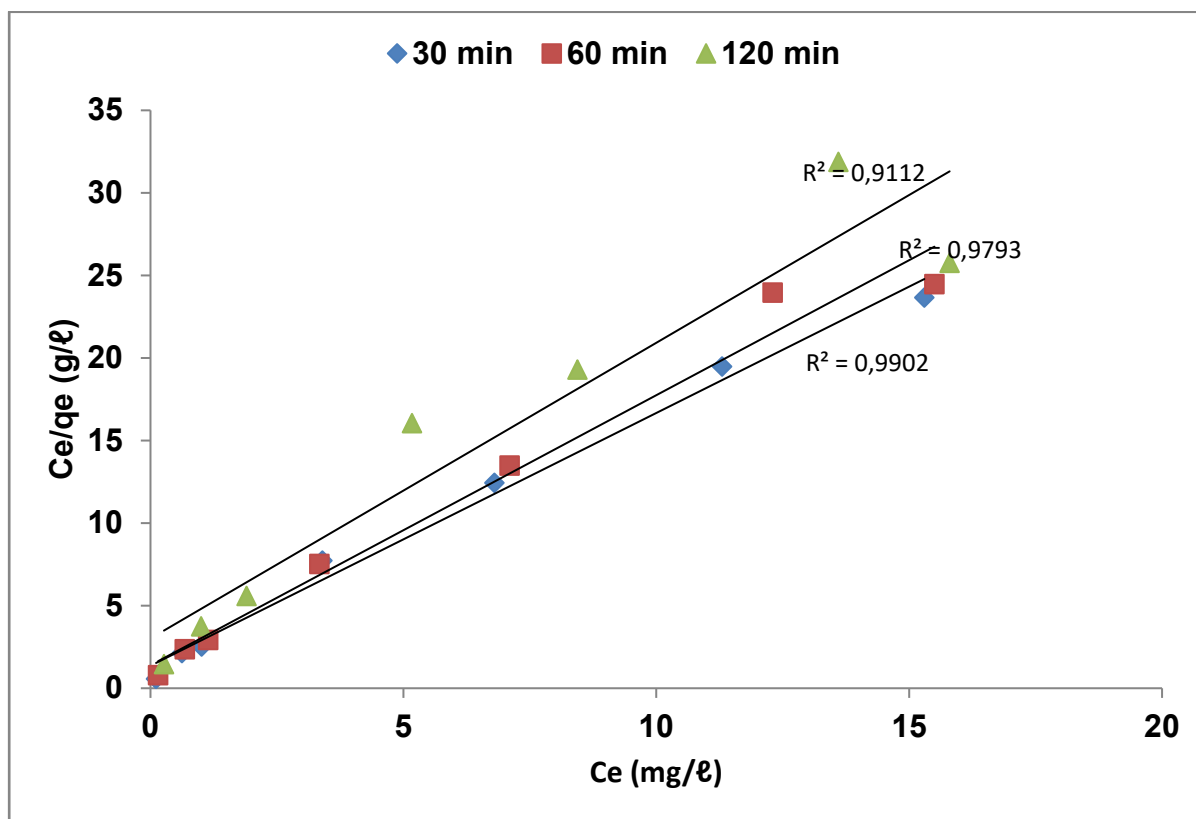


Figure 8.18. Langmuir adsorption isotherm (30 min, 60 min, 120 min contact times at 250 rpm, 1.5 g/100 mL, pH 6.2)

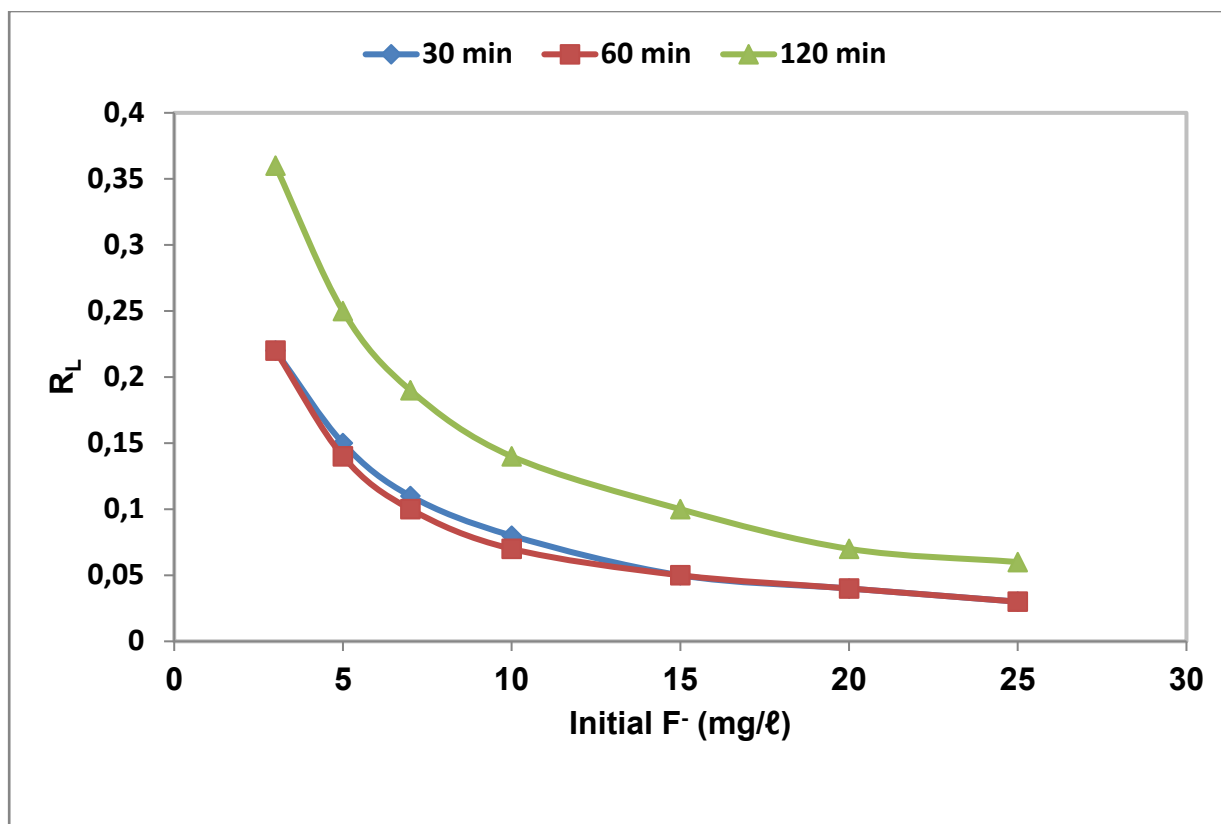


Figure 8.19. R_L values for the adsorption of F^- onto MnO_2 coated Na-bentonite.

Freundlich adsorption model is empirical model which is an indicative of the surface heterogeneity of adsorbent and considers multilayer adsorption. Figure 8.20 shows a plot of Freundlich isotherm. Calculated values of K_f and $1/n$ are reported in Table 8.6. Based on the correlation coefficient values for both contact times, adsorption data fits better to Langmuir than Freundlich adsorption isotherm. Moreover the theoretical adsorption capacity for Langmuir isotherm is almost equal to the experimental adsorption capacity which further confirms the fact that the data is best described by Langmuir model. Better fit of data to Langmuir isotherm model suggests monolayer adsorption coverage. Calculated model constants for Langmuir and Freundlich isotherms are shown in Table 8.6. The value of R_L , dimensionless equilibrium parameter and the value of $1/n$ Freundlich adsorption intensity were both between 0 and 1, which indicate that the adsorption of F^- onto MnO_2 coated Na-bentonite was favourable.

Table 8.6. Constant values for Langmuir and Freundlich isotherms

Contact time (min)	q_{exp} (mg/g)	Langmuir isotherm			Freundlich isotherm		
		Q_m (mg/g)	b (L/mg)	R^2	K_f (mg/g)	$1/n$	R^2
30	0.64	0.65	1.12	0.99	0.34	0.23	0.97
60	0.63	0.61	1.17	0.97	0.32	0.23	0.94
120	0.61	0.55	0.59	0.91	0.25	0.23	0.88

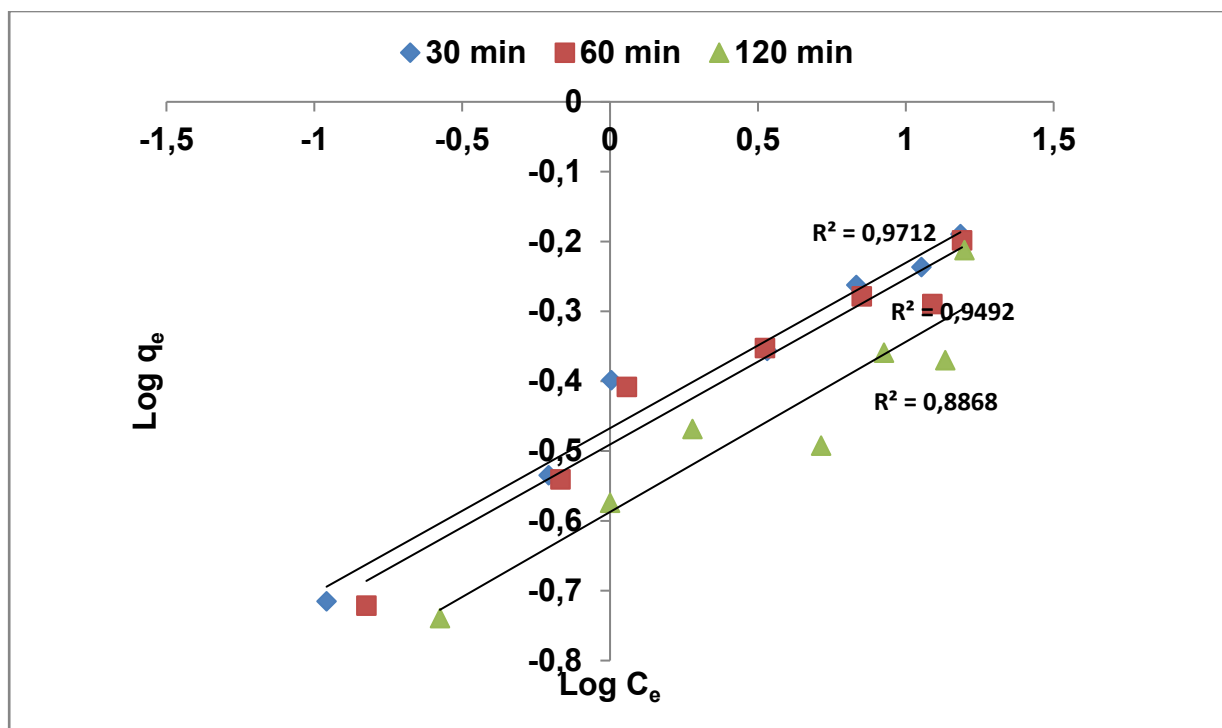


Figure 8.20. Freundlich adsorption isotherm (30 min, 60 min, 120 min contact times at 250 rpm, 1.5 g/100 mL, pH 6.2)

8.10.2 Adsorption kinetics

To understand the kinetics of the adsorption process, the data was fitted to pseudo first and second order Lagergren rate equations. These kinetics rates models are used to describe the relationship between the adsorption capacity and contact time. They also aid in identifying the potential rate-limiting step (Wang et al., 2015). Figure 8.21 shows plots of Lagergren pseudo second order of the kinetic data respectively. The pseudo second order plots fitted adequately to the kinetic data and higher correlation coefficient at both concentrations were evident. The pseudo first order plots did not fit adequately to the kinetic data. This indicates adsorption of fluoride onto MnO₂ coated Na-bentonite follows pseudo second order and occurs through chemisorption. Calculated model constants for pseudo first and second order are presented in Table 8.7.

Table 8.7. Calculated parameters for pseudo-first- and second-order reaction kinetics models

C ₀ (mg/L)	Pseudo-first-order			Pseudo-second-order		
	q _{e(exp)} (mg/g)	K _{1ad} (min ⁻¹)	R ²	K _{2ad} (g.mg ⁻¹ min ⁻¹)	q _{e(cal)} (mg/g)	R ²
3	0.19	9.67 x10 ⁻³	0.57	0.18	1.32	0.99
5	0.13	4.83 x10 ⁻⁴	0.39	1.09	0.77	0.99
10	0.21	6.90 x10 ⁻⁴	0.57	1.5	0.51	0.99

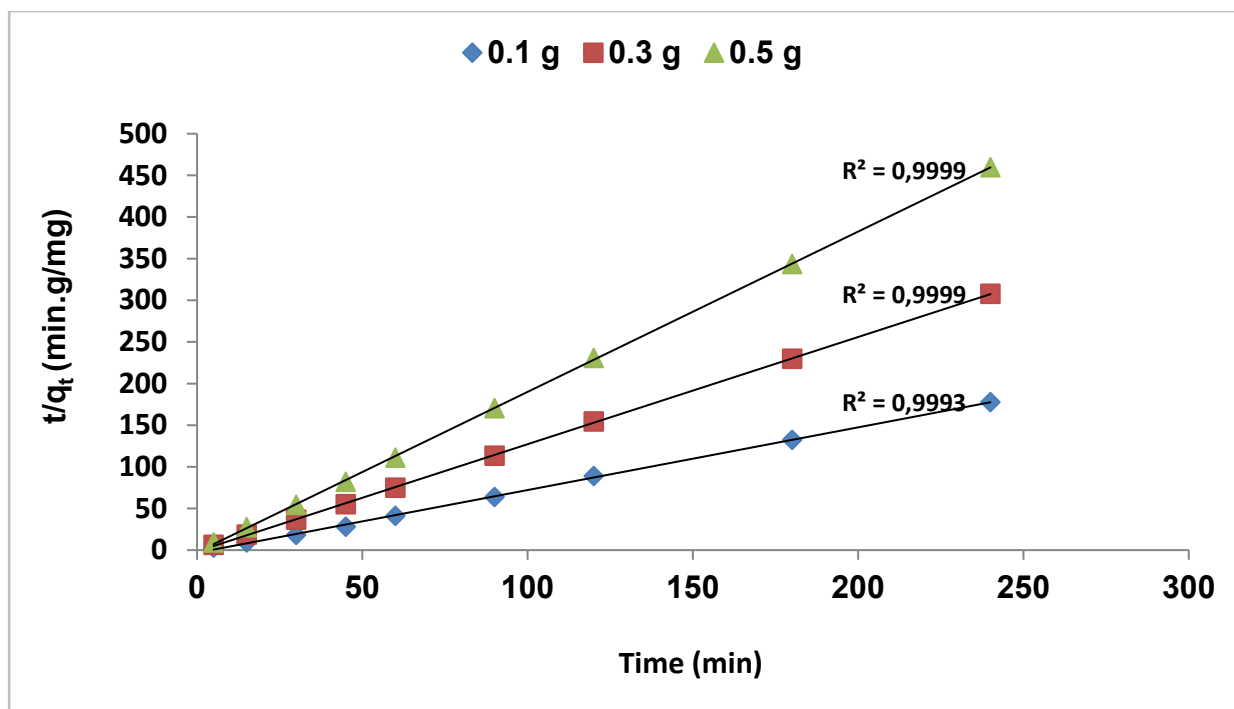


Figure 8.21. Lagergren Pseudo-second-order plot at various adsorbent dosages (5 mg/ℓ F⁻, pH 6.24 and 250 rpm shaking, particle size <250 μm).

Besides adsorption at the outer surface of the adsorbent, the adsorbate molecules may also diffuse into the interior of the porous adsorbent. The possibility of intra-particle diffusion was evaluated using Weber-Morris intra-particle diffusion model. Weber-Morris plots of F⁻ adsorption onto MnO₂ coated Na-bentonite clay at different adsorbent dosages are presented in Figure 8.22. If adsorption of a solute is controlled by the intra-particle diffusion process, a plot of qt versus t^{0.5} gives a straight line and pass through the origin (Daifullah et al., 2007, Chen et al., 2010). It is observed that at both evaluated adsorbent dosages, the plot did not pass through the origin however it gave three phases of the adsorption process are evident. First phase between 5 and 30 min shows external diffusion followed by second phase between 45 to 90 min representing the intra-particle diffusion and lastly phase 3 after 90 min showing the equilibrium stage. The values of K_{i1}, K_{i2} and K_{i3} (intra-particle diffusion co-efficient rate constant for phase 1, phase 2 and phase 3 respectively) obtained from the plots are shown in Table 8.8.

Table 8.8. Constant values of intra-particle diffusion model

Adsorbent dosage(g/100 mℓ)	K _{i1}	K _{i2}	K _{i3}
0.1	0.0210	-0.0640	0.0001
0.3	0.0920	-0.0070	0.0020
0.5	0.0025	-0.0072	0.0005

. For both adsorbent dosages the values of K_{i1} is higher than the value of K_{i2} and K_{i3} indicating that the first phase was faster compared to phase 2 and 3 (Shang and Gou, 2013; Tang and Zhang, 2016). This may be due to difference in the rate of mass transfer in the initial and final phase of adsorption. The Correlation coefficient values for the phase 2 was higher compared to phase 1 and 3. This may be an indication that intra-particle diffusion dominated the adsorption process. Pore distribution analysis showed that the pores of the

MnO₂ coated Na-bentonite ranged from micro to macro with average pores being mesoporous. External diffusion occurred in the micro pores, followed by intra-particle diffusion in the mesoporous and lastly equilibrium adsorption in the macro-porous of the adsorbent. These results show that adsorption of F⁻ onto MnO₂ coated Na-bentonite is not only controlled by intra-particle diffusion and but a complex process.

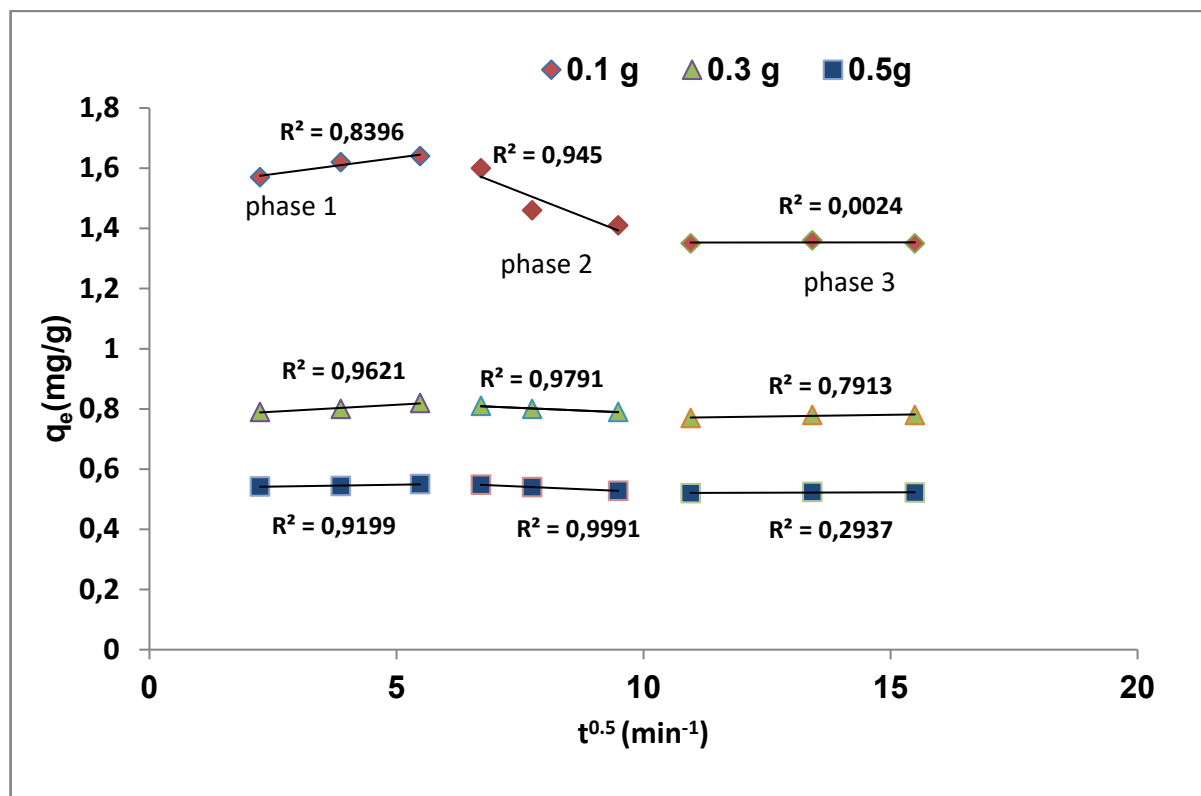


Figure 8.22. Intra-particle plot at various adsorbent dosages (5 mg/l F⁻, pH 6.24 and 250 rpm shaking)

8.11 MECHANISM OF FLUORIDE ADSORPTION

Possible mechanism for fluoride adsorption onto MnO₂ coated bentonite can be elucidated by looking at the effect of pH on F⁻ adsorption and the change in pH during F⁻ adsorption Figure. 8.14. At pH below 3, where final pH was higher than the initial pH and the surface of the adsorbent is positive, fluoride adsorption would be via ligands exchange mechanism because of stronger attractive force between fluoride and the adsorbent surface and the presence of more hydroxylated sites for exchange of F⁻. At solution pH above 3, the surface of the adsorbent becomes negatively charged and stronger electrostatic repulsion between active sites and F⁻ ions exists. Thus, fluoride removal would be mainly due to the ion exchange mechanism.

8.12 SUMMARY

MnO₂ coated bentonite clay was synthesised and evaluated for fluoride removal in groundwater. Bentonite clay was activated using NaOH and then coated with MnO₂ through *in-situ* reduction of KMnO₄. Physicochemical and mineralogical properties of the adsorbent were evaluated using XRD, XRF, BET, SEM, FTIR and pH_{pzc}. XRD showed that coating Na-bentonite leads to formation of new minerals such as, Jacobsite, cryptomelane and pyrolusite. Optimum conditions for fluoride removal were established using batch experiments. Optimum conditions were found to be, 30 min contact time, 250 rpm, 1.5 g/100 ml adsorbent dosage, 5 mg/l adsorbate concentration and pH 8. Maximum F⁻ removal of ≈94.7% was achieved under optimum conditions. The adsorption data was adequately described by Langmuir model, while kinetics data fitted well to pseudo second order kinetics model. Intra-particle diffusion model of Weber-Morris indicated that the removal of fluoride by MnO₂ coated Na-bentonite is a highly complex process, involving boundary layer diffusion and intra-particle diffusion as well as equilibrium adsorption. Sorption of fluoride occurred via ligands exchange mechanism at pH<3 and at pH> 3 via ion exchange mechanism. MnO₂ coated Na-bentonite can be successfully regenerated up to 5th cycle with 0.1 M NaOH. MnO₂ coated bentonite was able to remove fluoride from 5.4 mg/l to 0.98 mg/l. Toxicity assessment showed that MnO₂ coated Na-bentonite leaches out Mn ions which can result in secondary contamination. Its recommended that MnO₂ coated Na-bentonite has potential for application in defluoridation of groundwater in areas where no alternative sources of safe clean water are available and further modification should be carried out to make MnO₂ coated Na-bentonite more chemically stable

Comparison between MnO₂-coated Na-bentonite and previously reported MnO₂based adsorbents was carried out based on the pH, Initial F⁻ concentration and maximum adsorption capacity. The comparison is presented in Table 8.9. It seemed as MnO₂ coated Na-bentonite has lower adsorption capacity compared to other MnO₂ coated adsorbents except for activated alumina (Tripathy et al., 2008). Although MnO₂ coated Na-bentonite showed lower maximum adsorption capacity compared to other adsorbents, the adsorption capacity was sufficient for F⁻removal from groundwater. Moreover the percentage F⁻ removal was above 90% at evaluated pH values (2-12).

Table 8.9. Comparison of different adsorption capacities of different adsorbents for fluoride.

Adsorbent	pH	Initial F ⁻ (mg/l)	Adsorption capacity (mg/g)	Reference
MnO ₂ activated alumina	7	10	0.15	Tripathy et al. (2008)
MnO ₂ granular activated carbon	7.5-8	10	0.82	Ma et al. (2009)
Hydrous MnO ₂ coated activated alumina	3.5-7	6	7.1	Teng et al. (2009)
MnO ₂ coated earthenware	7.5	2	1.55	Sivasankar et al. (2011)
MnO ₂ graphene oxide	5.5-6.7	10	4.35	Li et al. (2013)
MnO ₂ coated Na-bentonite	8	5	0.65	Present study

9 EVALUATION OF GROUNDWATER DEFLUORIDATION BY SMECTITE-RICH CLAY SOILS

9.1 INTRODUCTION

Groundwater is the most affordable and widely used natural resource for many of the rural communities in South Africa. However, the presence of chemical species such as fluoride in high concentration is a serious concern from the health point of view. Meenakshi and Maheshwari (2006), reported various treatment methods for defluoridation, this includes adsorption, ion exchange, membrane techniques and precipitation method. Among these methods, adsorption is considered the most effective and appropriate for defluoridation of groundwater in rural communities. Different materials such as clay soils (Coetzee et al., 2003), activated alumina (Ghorai and Pant, 2004), activated carbon (Ma et al., 2009) and other low cost material have been tested for defluoridation of groundwater. Recent studies have focused on the use of clay soils due to their good adsorptive properties such as large specific surface area, chemical and mechanical stability, layered structure and high cation exchange capacity. Examples of such studies include; a study on illite-geothite soils in China (Wang and Reardon, 2001), adsorption studies using selected South African clays (Coetzee et al., 2003), use of chemically modified bentonite clay (Kamble et al., 2009) and magnesium incorporated bentonite clay (Thakre et al., 2010), Fe³⁺ modified bentonite clay (Gitari et al., 2013) and Al³⁺ modified bentonite (Vhahangwele et al., 2014). Smectite-rich clay soils and minerals have been identified as appropriate adsorbent for hosting high charge metal cations/oxides that inturn modify their surface properties. One of the most important impacted properties is positive charge that makes them suitable for adsorption of anions. Smectite-rich clay soils from Mukondeni in Limpopo has been used for a very long time in making ceramic water filters which are effective in improving water quality (Tyeryar et al., 2012). Its application in adsorption of inorganic pollutants has never been investigated although it is known to be rich in smectite (Dacosta et al., 2013).

This chapter presents results on the evaluation of the physicochemical, mineralogical properties of the smectite-rich black Mukondeni clay soil and its potential application in defluoridation of groundwater. Optimum operating conditions, contact time, adsorbent dosage, initial adsorbate concentration and initial pH were evaluated and optimized. The regeneration and re-usability of the smectite-rich clay soils as well as the effects of co-existing ions on defluoridation efficiency was also evaluated. Lastly the mechanism of fluoride adsorption on the clay soils are proposed.

9.2 MATERIALS

All reagents and TISAB-III were obtained from Rochelle Chemicals & Lab Equipment CC, South Africa Ltd and they were of analytical grade. Smectite-rich clay soil was collected from Mukondeni Village, Vhembe district in South Africa. A stock solution containing 1000 mg/l fluoride was prepared by dissolving 2.21 g NaF in 1 l of MilliQ water (18.2 MΩ/cm) and fluoride solutions for batch experiments were prepared from fresh stock fluoride solution by appropriate dilution. Field water was collected from a community borehole in Siloam, Vhembe district in South Africa.

9.3 METHODS

9.3.1 Preparation and characterization of smectite-rich clay soils

Clay soils were washed by mixing the soil with MilliQ water (18.2 M Ω /cm at a ratio of 1:5 in a 1 l beaker, the mixture was stirred for 5 min, and the procedure was repeated twice. After stirring, mixtures were agitated for 15 min using Stuart Reciprocating shaker and then centrifuged for 10 min at 5000 rpm. Samples were then dried in an oven for 12 hrs at 105°C and milled to pass < 250 μ m sieve. Several techniques were used to characterize the smectite-rich clay soils for adsorption (detailed in Appendix A). These included Cation Exchange Capacity (CEC), Point of Zero Charge (PZC), X-ray diffraction (XRD), X-ray fluorescence (XRF), Scanning Electron Microscopy (SEM), Scanning Electron Microscopy coupled with Energy Dispersive Spectroscopy (SEM-EDS), Transmission Electron Microscopy (TEM), Brunauer-Emmett-Teller (BET) and Fourier Transform Infrared (FTIR).

9.3.2 Batch and field groundwater adsorption experiments

Methods followed for batch and field groundwater fluoride adsorption studies are detailed in Appendix B. Adsorption models used for describing the adsorption process using smectite-rich clay soils are detailed in Appendix C. Equation 1 (Appendix C) was used to calculate the percentage of removal and adsorption capacity.

9.4 PHYSICOCHEMICAL AND MINERALOGICAL CHARACTERIZATION

9.4.1 X-ray diffraction analysis

XRD analysis was carried out to identify the mineral phases of the adsorbent. Its observed in Figure 9.1, that the smectite-rich clay soil is mainly composed of montmorillonite, quartz, albite and anthophyllite. Quantitative results further confirmed the presence of smectite (60.34%) as the major mineral and quartz (20.21%) and plagioclase (20.39%) as minor minerals.

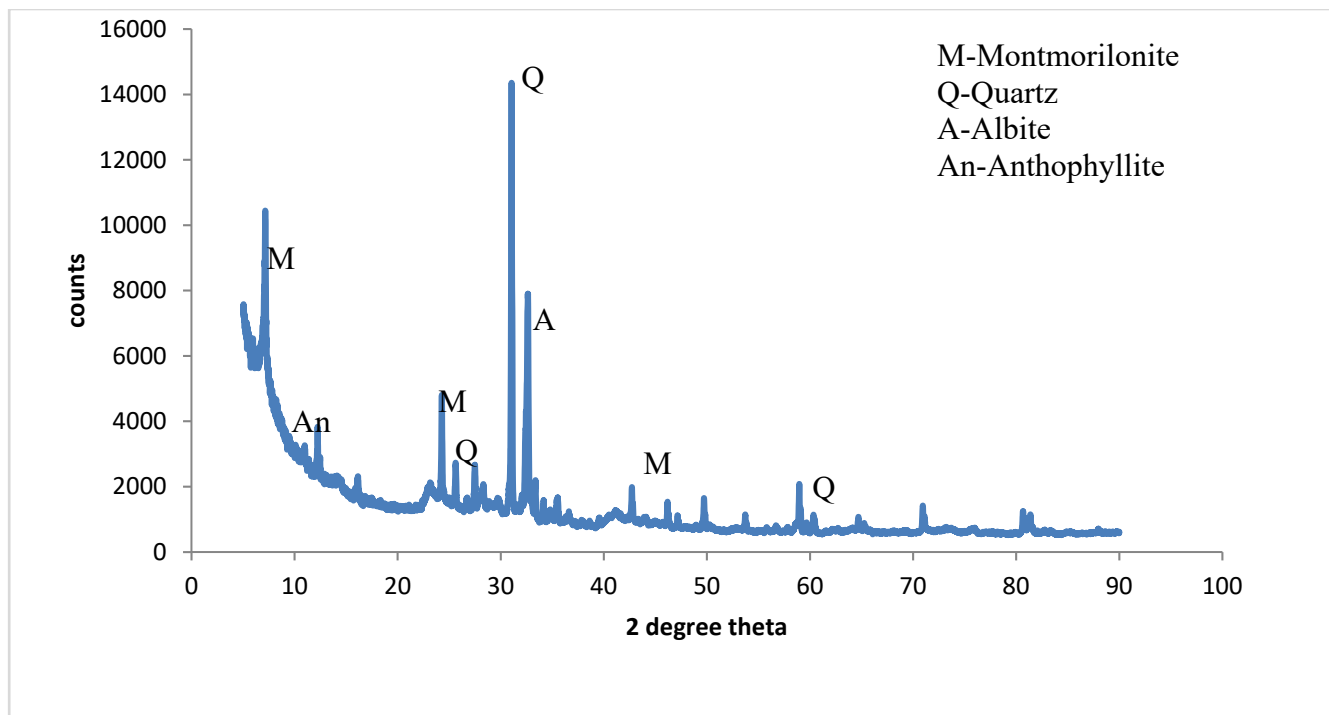


Figure 9.1. XRD spectra of the smectite clay soils.

9.4.2 X-ray fluorescence analysis

Table 9.1 presents the major chemical components of the smectite-rich clay soils. Results indicate that silica (SiO_2) is the main component followed by Al_2O_3 . High concentration of SiO_2 and Al_2O_3 reveal that the clay soil is an aluminosilicate material.

Table 9.1. Elemental composition of the clay soils

Major elements	% w/w
Al_2O_3	14.35
CaO	1.79
Cr_2O_3	0.02
Fe_2O_3	5.45
K_2O	0.93
MgO	2.79
MnO	0.08
Na_2O	2.52
P_2O_5	0.04
SiO_2	62.90
TiO_2	0.75
L.O.I	7.71
Total	99.15

9.4.3 Scanning electron microscope analysis

Surface morphology of smectite-rich clay is presented in Figure 9.2. At lower magnifications, smectite-rich clay soils showed irregular porous structure and micrographs at higher magnifications reveals that smectite-rich clay soil has a smooth surface layered structures.

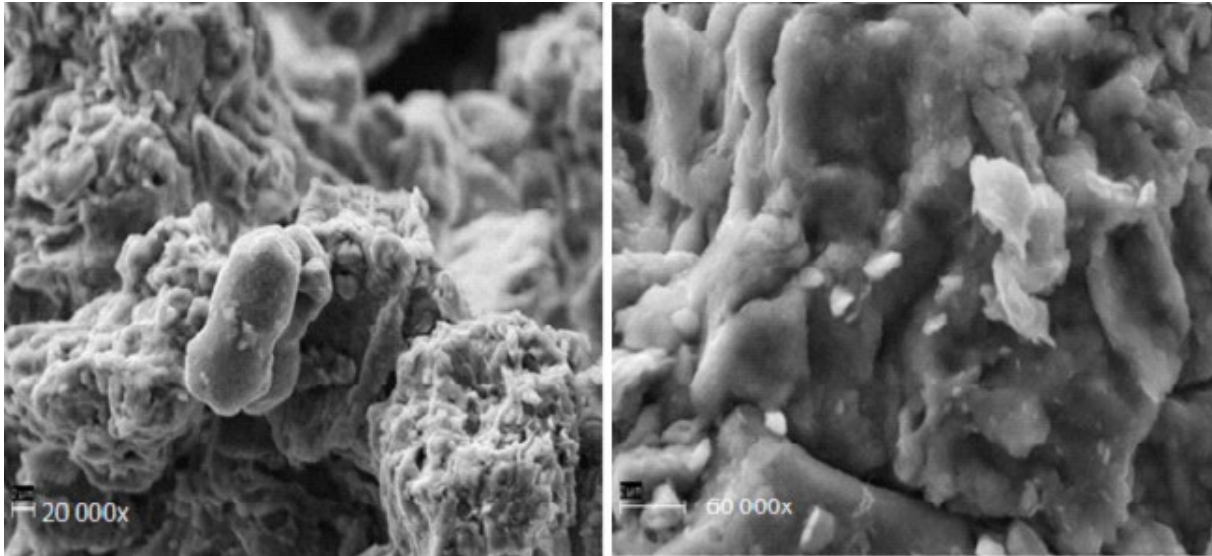


Figure 9.2. Scanning electron micrograph of smectite-rich clay soils.

9.4.4 Surface area and pore volume

The surface area and pore size of the clay soils are significant properties that influence the sorption of ions by the clay. Surface area, pore volume and pore size of smectite-rich clay soil was determined using BET method and the results are summarized in Table 9.2. Figure 9.3 shows the distribution of pores sizes. It was observed that highest amount of pores lies between 17.34 and 157.22 Å (1.73 nm and 15.72 nm) with an average pore diameter of 70.46 Å (7.04 nm). This suggests that smectite-rich clay contains significant range of poresizes ranging from microporous to mesoporous.

Table 9.2. BET surface area, pore volume and pore width of the smectite-rich clay soils

Surface area (m ² /g)	Pore volume (cm ³ /g)	Pore width (nm)
20.3437	0.03027	7.04

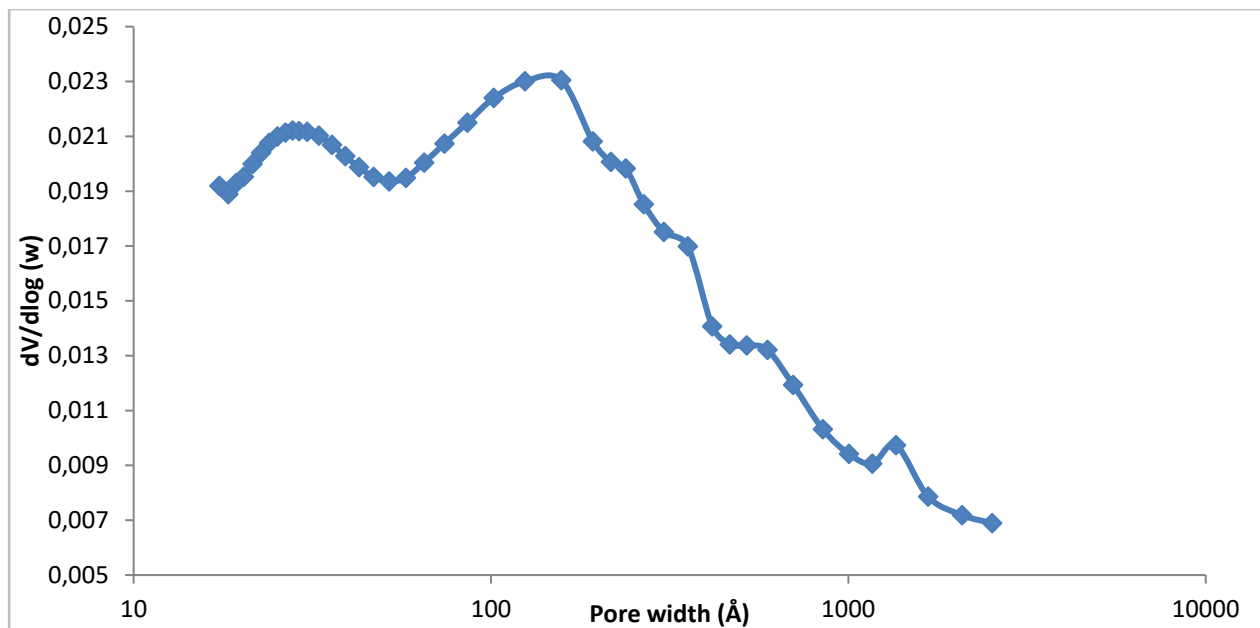


Figure 9.3. Pore size distribution of smectite-rich clay soils.

9.4.5 Fourier Transform Infra-red analysis

FTIR spectra analysis were carried out in order to understand the surface chemistry and functional groups of smectite-rich clay soils and elucidating adsorption mechanisms. Figure 9.4 shows the FTIR spectrum of raw and fluoride loaded smectite clay soil. Three main absorption regions ($3000-3800\text{ cm}^{-1}$, $1300-1800\text{ cm}^{-1}$ and $500-1200\text{ cm}^{-1}$) are observed. Toor et al. (2014) observed similar absorption bands for a montmorillonite clay. A notable difference was observed in those regions in raw smectite clay soils and F^- loaded smectite clay soils. The absorption band at 3694.4 cm^{-1} may be due to stretching and vibration of structural OH^- group and the broad band at 3620.5 cm^{-1} may be attributed to the stretching and vibration of structural hydroxyl groups and water. A strong band at 996.1 cm^{-1} may be attributed to the stretching and vibration of Si-O groups in the clay mineral. A peak at 910 cm^{-1} may be attributed to stretching and vibration of Al-OH-Al. After F^- sorption there was a decrease in the intensity of transmittance in all the peaks. This confirms that the fluoride adsorption in smectite-rich clay soils was mainly through interaction with OH groups and also direct interaction with the metal surface.

9.4.6 Cation Exchange capacity

Cation exchange capacity (CEC) refers to the total quantity of exchangeable cations that the soil can retain on their surfaces at given pH by electrostatic force. The cation exchange capacity for smectite-rich clay was identified by measuring the concentrations of Na^+ , K^+ , Mg^{2+} and Ca^{2+} in mg/l released in solution and the concentrations were then converted to milli-equivalent per 100 g ($\text{meq}/100\text{ g}$). The CEC for smectite-rich clay soils varied from 74.2 ($\text{meq}/100\text{ g}$) at pH 5.4 to 79.9 ($\text{meq}/100\text{ g}$) at pH 7.4 (Figure 9.4). It is observed that CEC is not dependent on pH since there is no significant difference in the concentration of cations at different pH. It can also be concluded that the clay soils have moderate CEC.

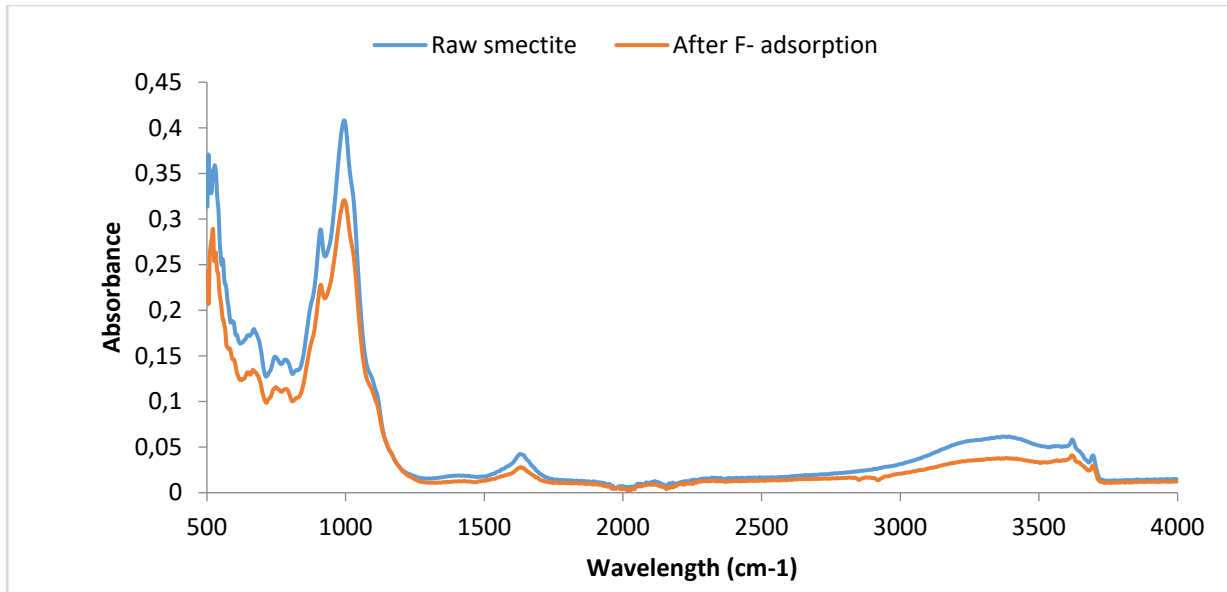


Figure 9.4. FTIR spectra for raw (a) and F⁻ Loaded smectite-rich clay (b).

9.4.7 pH point of zero charge

Figure 9.5 shows the variation of pH against Δ pH for the smectite-rich clay soil at various ionic strengths. pH_{pzc} refers to the suspension pH where the clay soil has zero net charges on the surface (Sparks, 1997). The pH_{pzc} of the smectite-rich clay soils is 5.8 which is lower than that of bentonite clay reported by Gitari et al. (2013) at 8.2. Above the pH_{pzc} the clay is negatively charged and below the pH_{pzc} the clay is positively charged (Bohn et al., 1975) therefore, adsorption of anions is likely to be high at pH below 5.8.

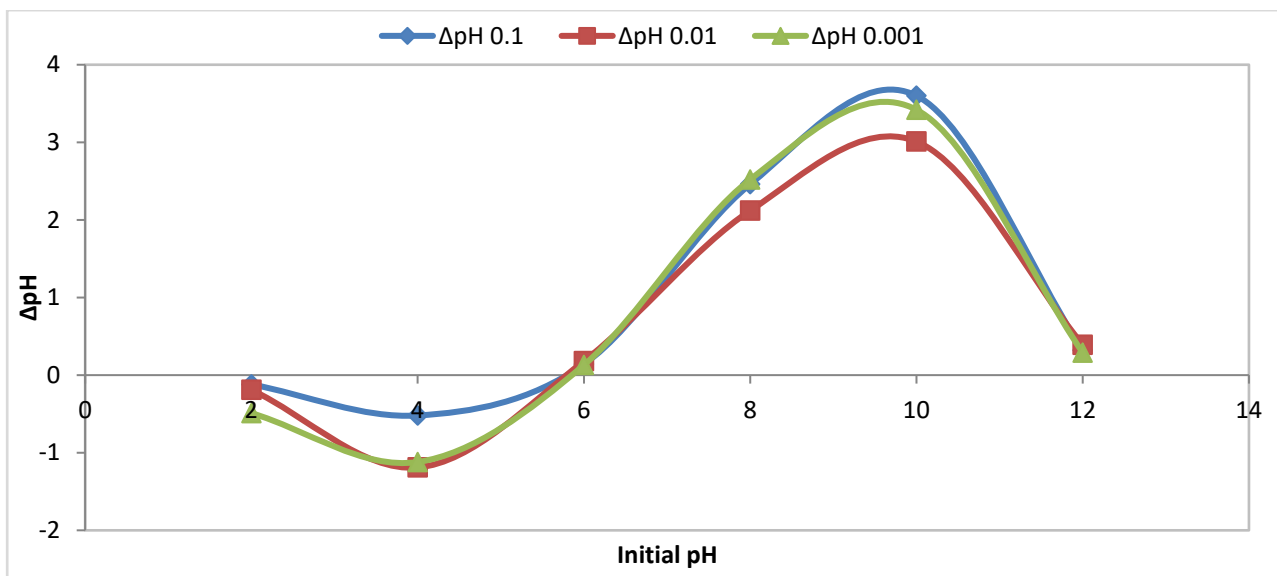


Figure 9.5. Variation of initial pH with Δ pH (0.1, 0.01 and 0,001 M KCl, dosage of 0.5 g/50 ml and shaking time of 48 hrs)

9.5 BATCH DEFLUORIDATION EXPERIMENTS

9.5.1 Effect of contact time

The effect of contact time on adsorption of fluoride was evaluated at various initial concentrations ranging from 3 mg/l to 10 mg/l and adsorbent dosage of 0.3 g/100 ml. Contact time was varied from 5 to 270 min at 250 rpm shaking speed. Figure 9.6 shows the plot of percentage fluoride removal with time. The percentage fluoride removal increased gradually to a maximum 30 min for all adsorbate concentrations. Gradual decrease in % removal was thereafter observed and the system seemed to approach equilibrium at all initial concentrations. The increase might be attributed to the availability of active sites for fluoride sorption which result in more exchange of ions and the decrease might be an indication that the active sites were getting saturated as the interaction continued with the system reaching equilibrium. The % fluoride removal was observed to decrease with increase in initial fluoride concentration. Optimum fluoride uptake was observed at 30 min and this contact time was applied in subsequent experiments.

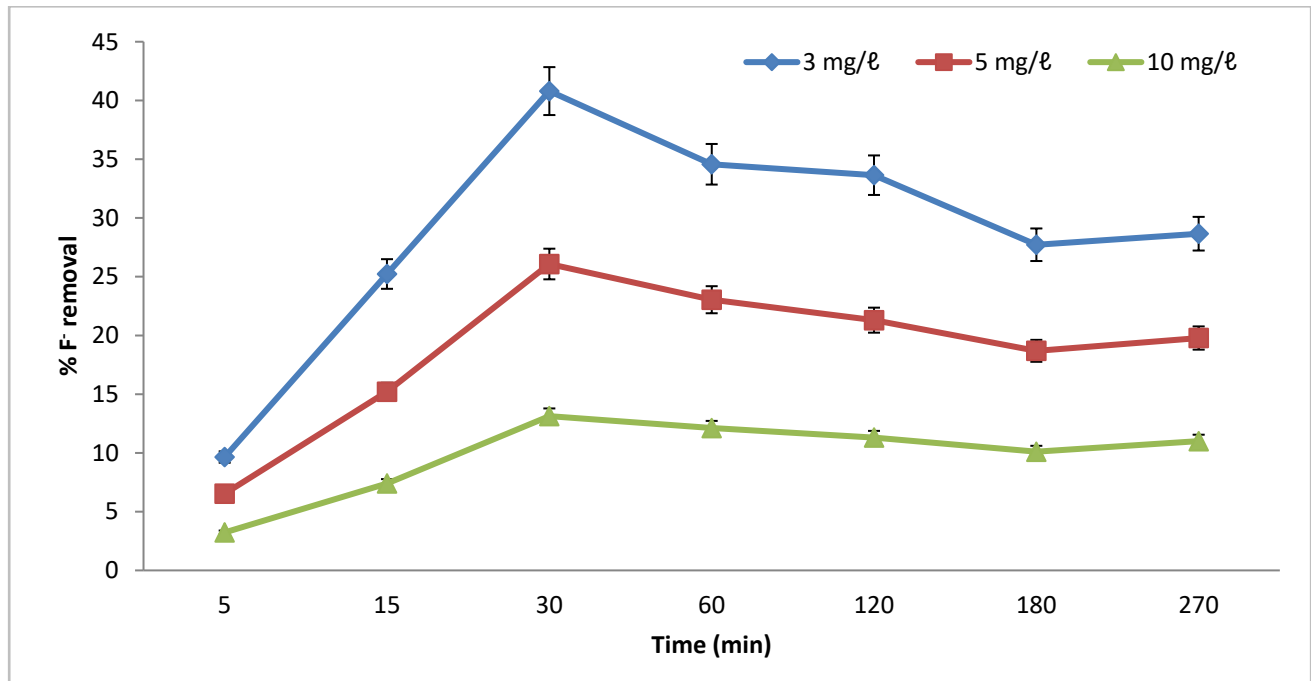


Figure 9.6. Variation of % F⁻ removal by smectite-rich clay soils with contact time (adsorbent dosage 0.3 g/100 ml, 3 mg/l, 5 mg/l and 10 mg/l F⁻, pH 5.54 and shaking speed of 250 rpm, N=3, particle size <250 μm).

9.5.2 Effect of adsorbent dosage

The effect of adsorbent dosage was evaluated by varying the amount of clay from 0.1 to 2.0 g/100 ml. An initial fluoride concentration of 3 mg/l was used. The mixtures were agitated for 30 min at 250 rpm shaking speed. The results were reported as % fluoride removal in Figure 9.7. Percentage fluoride removal increased gradually

from 46.5% at 0.1 g adsorbent dosage to 62.2% at 0.8 g/100 ml and the removal pattern seemed to flatten out suggesting the system had reached equilibrium and that increased adsorbent dosage did not have any further effect on adsorption of fluoride. The increase is due to an enhancement in the number of active sites available for adsorption of F^- as the adsorbent mass increased (Thakre et al., 2010). Adsorption capacity on the other hand decreased with increase in adsorbent dosage. Similar results have been reported by Kamble et al. (2009) with chemically modified bentonite for which they have cited two reasons: (i) better utilization of the available active sites at low adsorbent dose in comparison to high adsorbent dose where too many sites are available for limited quantity of adsorbate, (ii) reduced driving force for adsorption as high adsorbent dose causes lower equilibrium fluoride concentration. 0.8 g/100 ml was then chosen as the optimum adsorbent dosage and was applied in subsequent experiments.

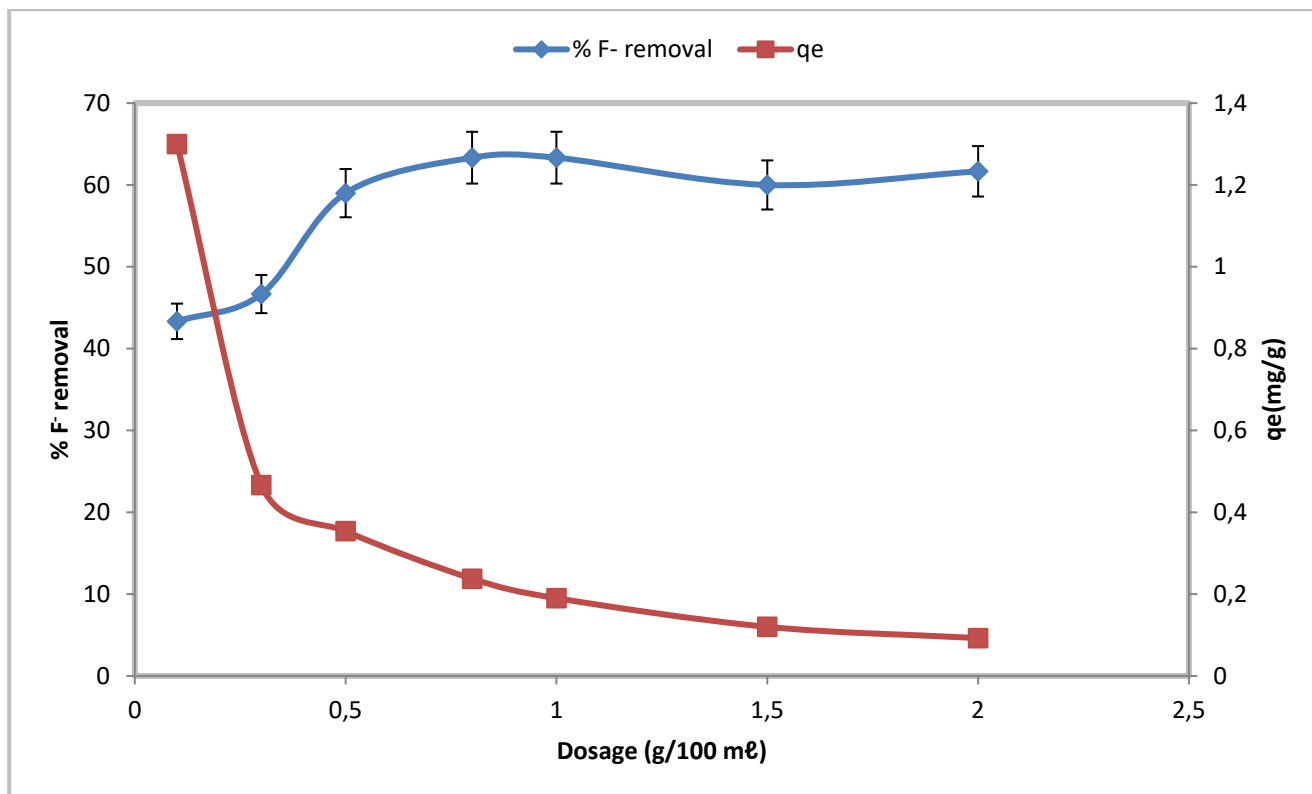


Figure 9.7. Variation % F⁻ removal and adsorption capacity with adsorbent dosage (contact time of 30 min, adsorbate concentration, 3 mg/l F⁻, pH 5.54 and shaking speed of 250 rpm, N=3, particle size=250µm).

9.5.3 Effect of initial adsorbate concentration

Effect of adsorbate concentration was evaluated by varying initial concentration from 3 mg/l to 15 mg/l at 30, 60 and 120 min contact time at 250 rpm shaking speed and 0.8 g/100 ml. Results were reported in terms of percentage removal in Figure 9.8. Percentage F⁻ removal decreased with an increase in initial concentration, same trend was observed for the three contact times. According to Thakre et al. (2010), the decrease in fluoride adsorption is due to the availability of more fluoride ions in solution at higher fluoride concentration, which also

indicates that the fluoride binding capacity of smectite-rich clay soil was getting exhausted. Initial adsorbate concentration of 3 mg/l was chosen to be the optimum concentration for subsequent experiments.

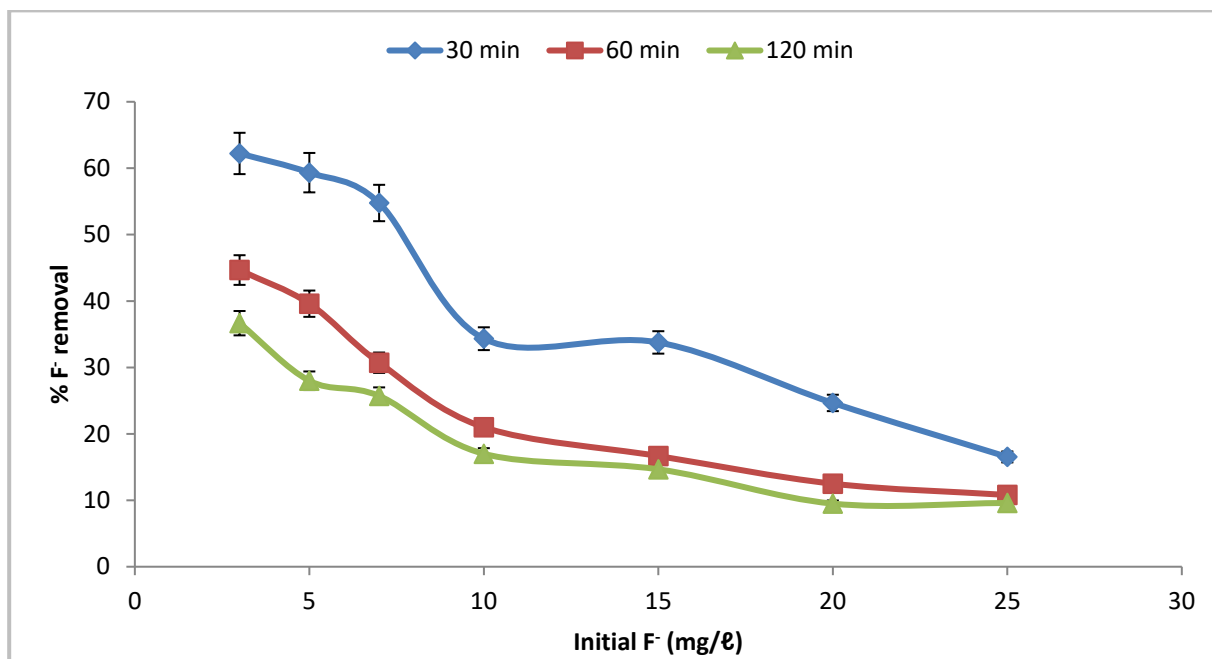


Figure 9.8. Variation of % F⁻ removal with initial concentration at various contact time (adsorbent dosage 0.8 g/100 mL, pH 5.54 and shaking speed of 250 rpm, N=3).

9.5.4 Effect of initial pH

Effect of initial pH was evaluated by varying the initial pH of the solution from 2 to 12 using 0.1 M NaOH and 0.1 M HCl. The results are presented in Figure 9.9 in terms of percentage fluoride removal and Figure 9.10 shows the change in pH during adsorption. The pH of the medium is one of the important parameters that influence fluoride removal efficiency significantly and helps in the understanding of fluoride uptake mechanism of the adsorbent (Loganathan et al., 2013). It is evident that smectite-rich clay showed significantly high fluoride removal over a wide pH range. The optimal pH was at acidic pH of 2 with fluoride removal of about 91.9%. Decline by 31.3% was observed at pH > 10. At pH 2 the surface of the clay is positively charged and F⁻ would be electrostatically attracted to the clay surface which explains the high F⁻ adsorption at pH 2. At pH below 5.8, the final pH was higher than the initial pH while at pH above 5.8 the solution pH decreases. The increase may be attributed to the release of OH⁻ ions from the adsorbent surface during ion exchange and the decrease in final pH at initial pH above the p_H_{pzc} may be attributed to the release of H⁺ ions from the adsorbent surface.

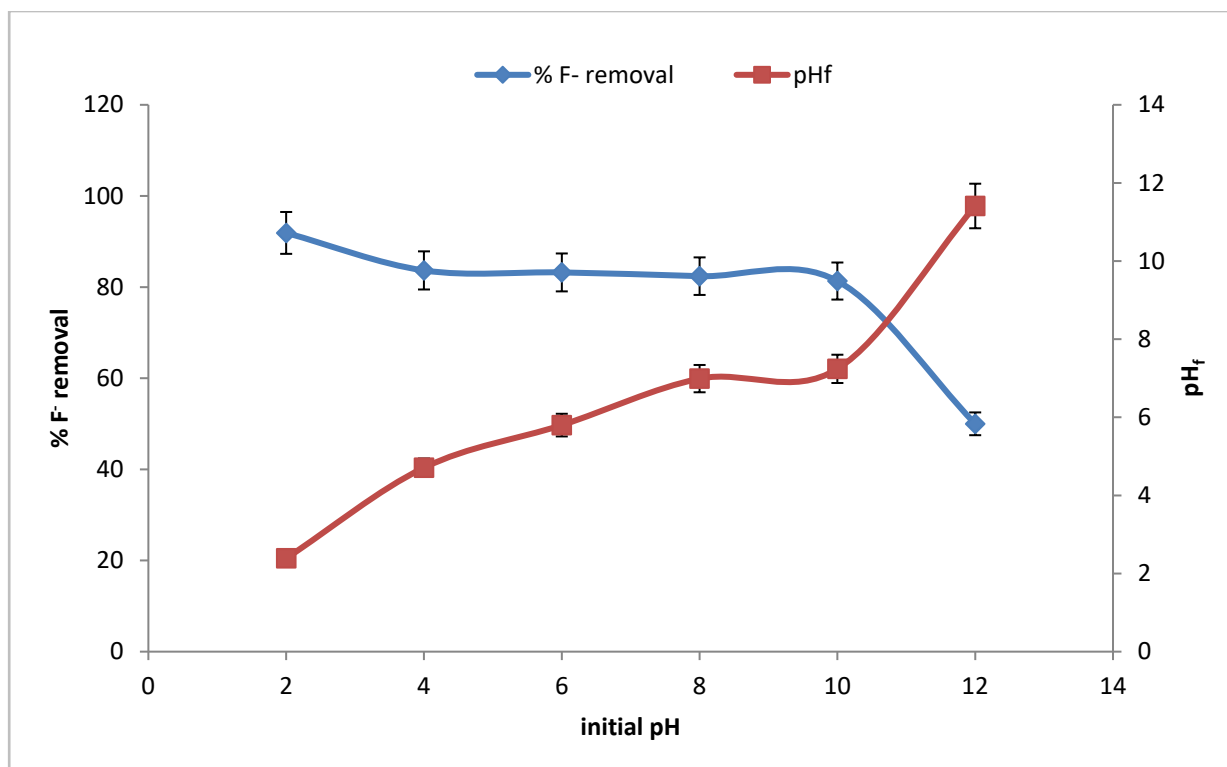


Figure 9.9. Variation of % F⁻ removal and equilibrium pH with initial pH (contact time 30 min, adsorbent dosage 0.8 g/100 mL, 3 mg/L F⁻ and shaking speed of 250 rpm, N=3).

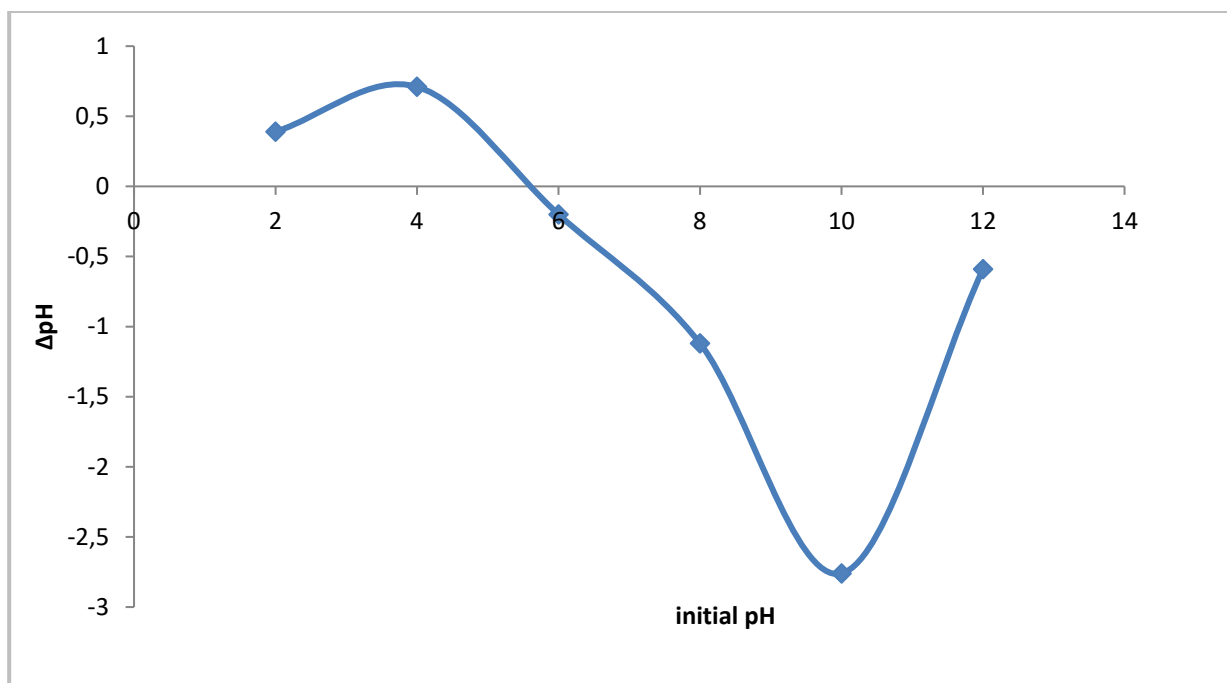


Figure 9.10. Variation of ΔpH with initial pH during F⁻ adsorption onto smectite-rich clay soils.

9.5.5 Effect of co-existing anion

Natural water sources have complex chemistry and may contain anions such as sulphates, chlorides, bicarbonates and nitrates in addition to fluoride and might affect the efficiency of fluoride removal by an adsorbent. In order to evaluate the effects of co-existing anions on adsorption of fluoride by smectite-rich clay soils, defluoridation was conducted in the presence of 5 mg/l of SO_4^{2-} , Cl^- , CO_3^{2-} and NO_3^- separately at initial fluoride concentration of 3 mg/l, blank experiment was done for control with initial F^- concentration of 3 mg/l. The results are presented in Figure 9.11. It is observed that presence of NO_3^- increased the percentage of fluoride removal to 57%. This may be due to an increase in the ionic strength of the solution or a weakening of lateral repulsion between adsorbed fluoride ions. However, the presence of Cl^- , SO_4^{2-} and CO_3^{2-} decreased the fluoride adsorption to 44%, 33.3% and 31.7% respectively; this may be due to the fact that these ions compete with fluoride ions for the surface functional groups on adsorbent surface and thereby decreasing the fluoride removal. Fluoride removal in the presence of anions increased in the order of $\text{CO}_3^{2-} < \text{SO}_4^{2-} < \text{Cl}^- < \text{NO}_3^-$.

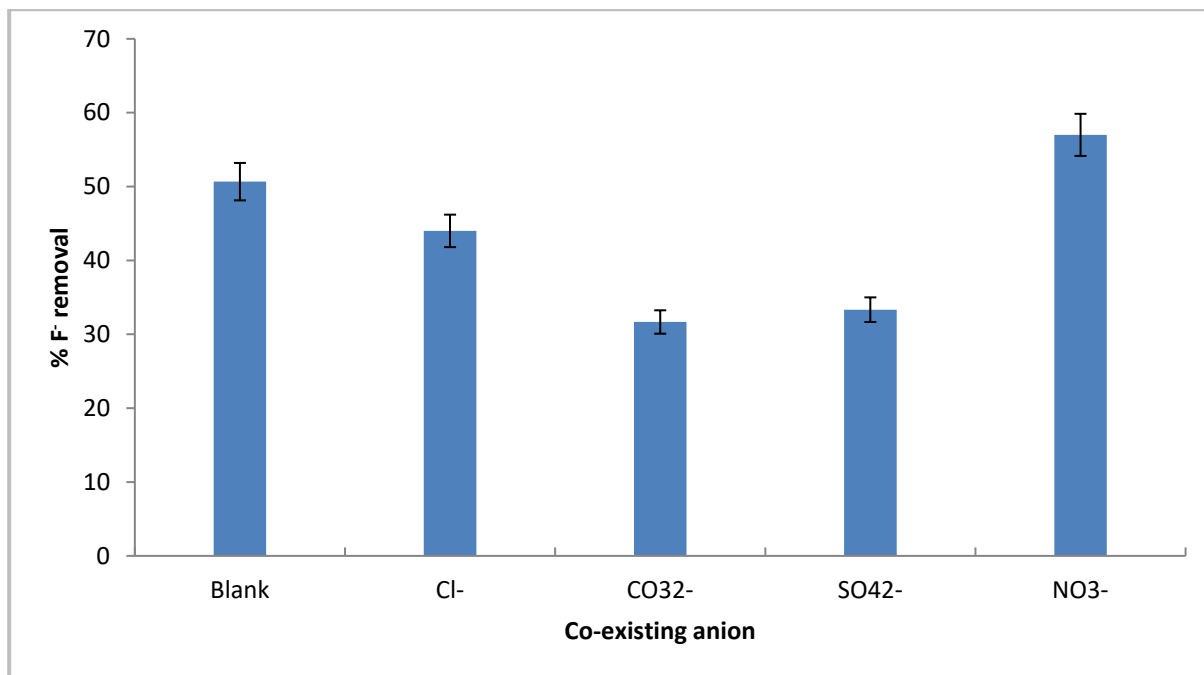


Figure 9.11. Effects of co-existing anions on fluoride removal by smectite-rich clay soils (3 mg/l F^- , 0.8 g/100 ml adsorbent dosage, 30 min contact time at 250 rpm, N=3, particle size <250 μm)

9.6 REGENERATION OF SMECTITE-RICH CLAY SOILS

Regeneration of the adsorbent was carried out as follows; 0.8 g of fluoride loaded clay was agitated with 100 ml of 0.1 M NaOH for 30 min on a table shaker. After agitation, the adsorbent was filtered through 0.45 μm pore membrane filter and the filtrate was diluted to 100 ml and then analysed for desorbed fluoride. The collected adsorbent on filter paper was washed with MilliQ water and then dried at 110°C for 3 hrs. To evaluate the regeneration and reusability of smectite-rich clay soils, five successive adsorption and desorption cycles.

Fluoride removal decreased from 55.6% to 54.7% after the first cycle and continued to decrease after each cycle (Figure 9.12). The same trend was reported in Zhang et al. (2011) and Jia et al. (2015) and it was attributed to inadequate regeneration of the adsorbent.

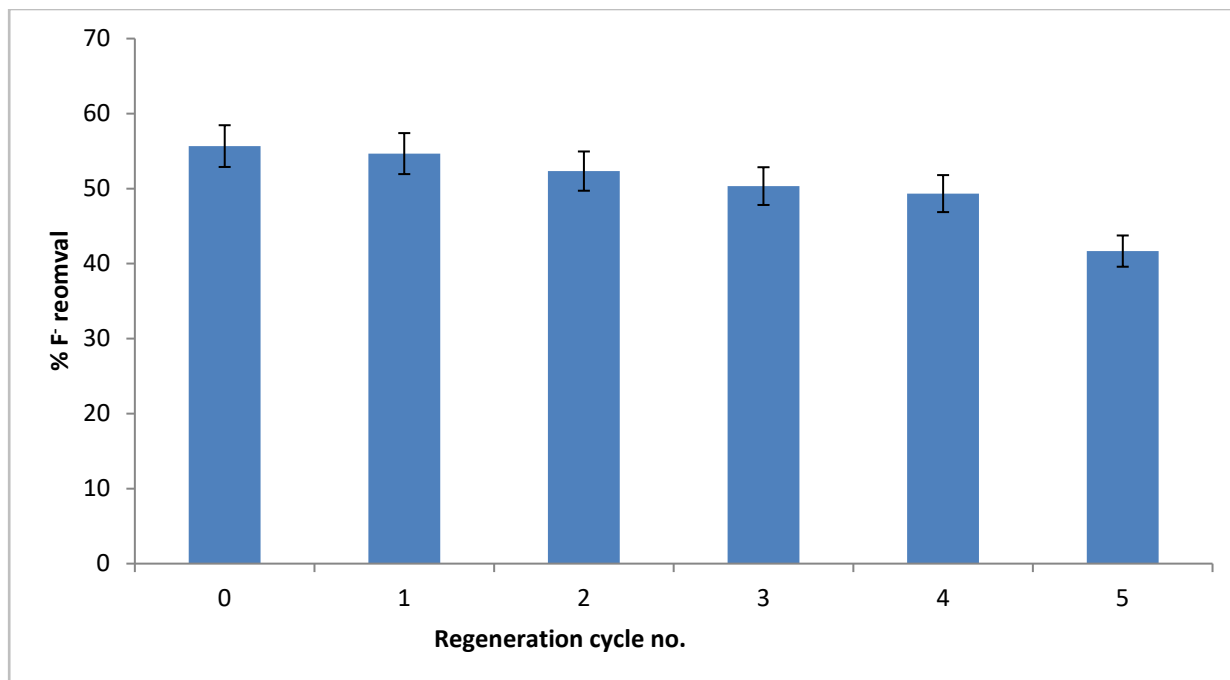


Figure 9.12. Percentage (%) fluoride removal by smectite-rich clay soils in successive cycles (3 mg/l, 30 min contact time at 250 rpm and pH 5.54, N=3, particle size <math>< \mu\text{m}</math>).

9.7 DEFLUORIDATION OF FIELD GROUNDWATER

The efficiency of smectite-rich clay soils on fluoride removal was tested by using field groundwater collected from Siloam borehole at the established optimum conditions of pH, contact time, and adsorbent dosage. The experiment was conducted at optimized pH (pH 2). Table 9.3 shows physicochemical parameters of the field water before and after treatment. Percentage F⁻ removal of 51.7% from field water was achieved at optimized conditions. This is lower than the percentage F⁻ removal achieved with synthetic fluoride solution (91.9%) at the same conditions. This is attributed to the presence of competing anions such as Br⁻, PO₄³⁻ and SO₄²⁻ present in the field water. The concentration of these co-existing ions decreased indicating that they were removed during the adsorption process. The results shows that smectite-rich clay soils from Mukondeni can be used for defluoridation of groundwater containing F⁻ concentration below 3 mg/l to below recommended limits. The fact that optimum fluoride adsorption by the smectite clay soils occurs at pH would be the limitation since the treated water will require pH adjustment.

Table 9.3. Physicochemical parameters of field water before and after treatment

Parameters	Before treatment	After treatment (initial pH adjusted to 2)
pH	7.8	2.68
Conductivity ($\mu\text{S/cm}$)	192.0	140.0
Total dissolved solids (mg/ℓ)	203	135.2
F ⁻ (mg/ℓ)	5.4	2.8
Cl ⁻ (mg/ℓ)	31.59	37.15
SO ₄ ²⁻ (mg/ℓ)	11.89	8.11
NO ₃ ⁻ (mg/ℓ)	1.13	2.07
Br ⁻ (mg/ℓ)	2.08	N.D
PO ₄ ³⁻ (mg/ℓ)	2.67	1.59

N.D= Not Detected

9.8 ADSORPTION MODELLING

9.8.1 Isotherm modelling

Langmuir and Freundlich equations are generally used to describe the equilibrium relationship between adsorbate concentration and amount of adsorbate adsorbed on the surface of the adsorbent. Refer to Appendix C for details on these models.

9.8.1.1 Langmuir isotherm

Figure 9.13 shows the plot of Langmuir isotherm for the adsorption data. The Langmuir plots show a strong fit. The calculated Langmuir parameters Q_m and b are reported in Table 9.4. An R_L value less than 1 generally indicates favourable adsorption, whereas greater than 1 indicates unfavourable adsorption. Calculated R_L values at various contact times lie within the range 0-1 (Figure 9.14) indicating adsorption process was favourable at room temperature for all the adsorbate concentrations tested.

Table 9.4. Values of Langmuir and Freundlich isotherm models (contact time 30 min, adsorbent dosage 0.8 g/100 mL and shaking speed of 250 rpm).

	Langmuir isotherm			Freundlich isotherm		
	Q_m (mg/g)	b (L/mg)	R^2	K_f (mg/g)	$1/n$	R^2
30 min	0.58	1.36	0.97	0.28	0.27	0.73
60 min	0.35	0.53	0.99	0.17	0.22	0.85
120 min	0.31	0.36	0.99	0.12	0.27	0.63

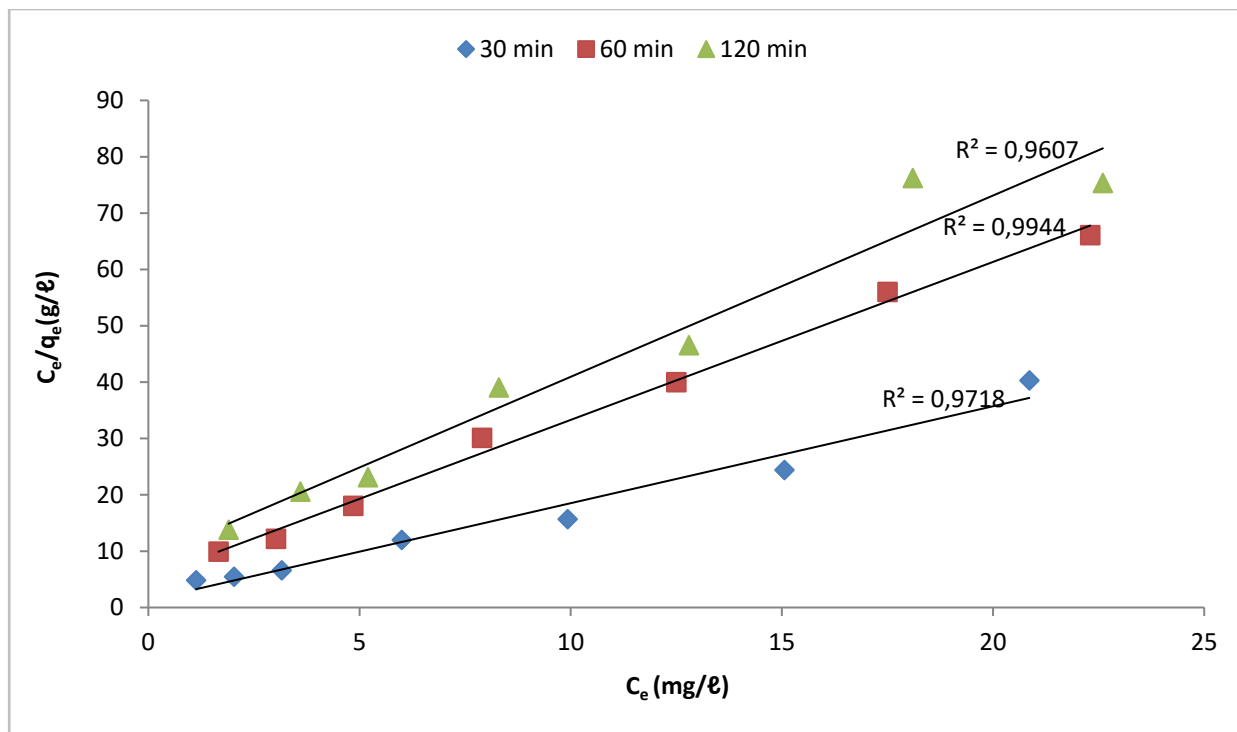


Figure 9.13. Langmuir isotherm (contact time 30 min, adsorbent dosage 0.8 g/100 ml and shaking speed of 250 rpm).

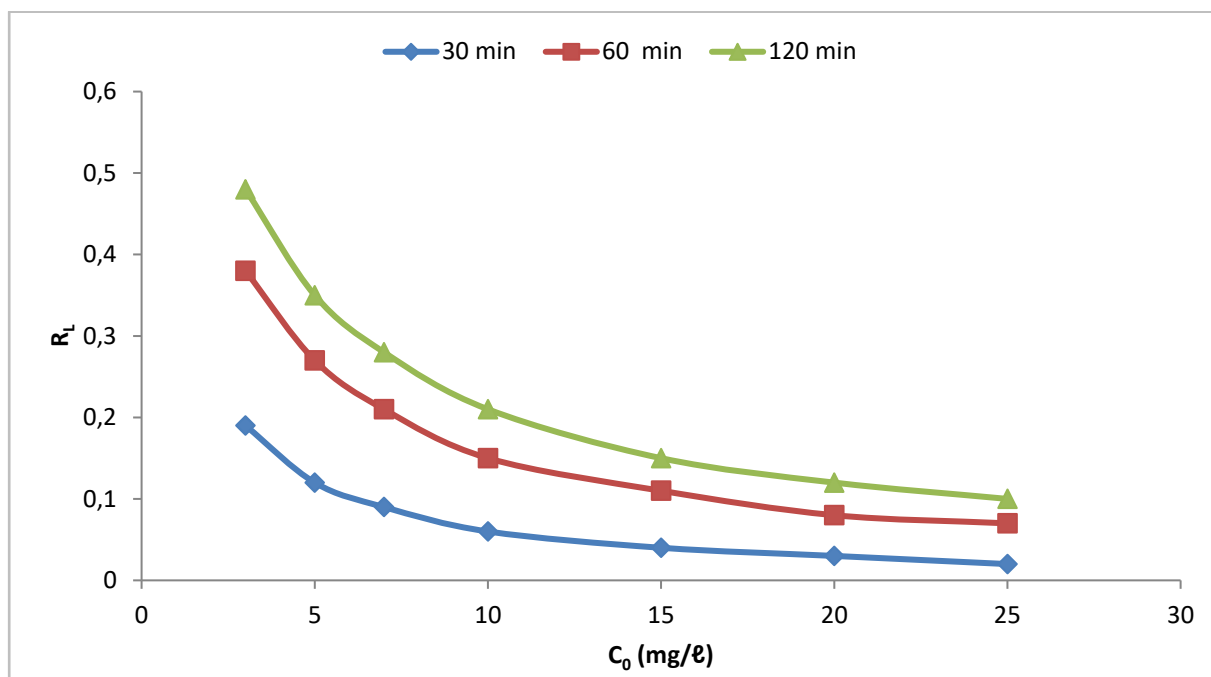


Figure 9.14. Values of R_L , for adsorption of fluoride onto smectite-rich clay soil.

9.8.1.2 Freundlich adsorption model

Freundlich adsorption model is empirical model which is an indicative of the surface heterogeneity of adsorbent and considers multilayer adsorption (Kamble et al., 2009). Figure 9.15 shows Freundlich isotherm. Values of K and $1/n$ are reported in Table 9.4.

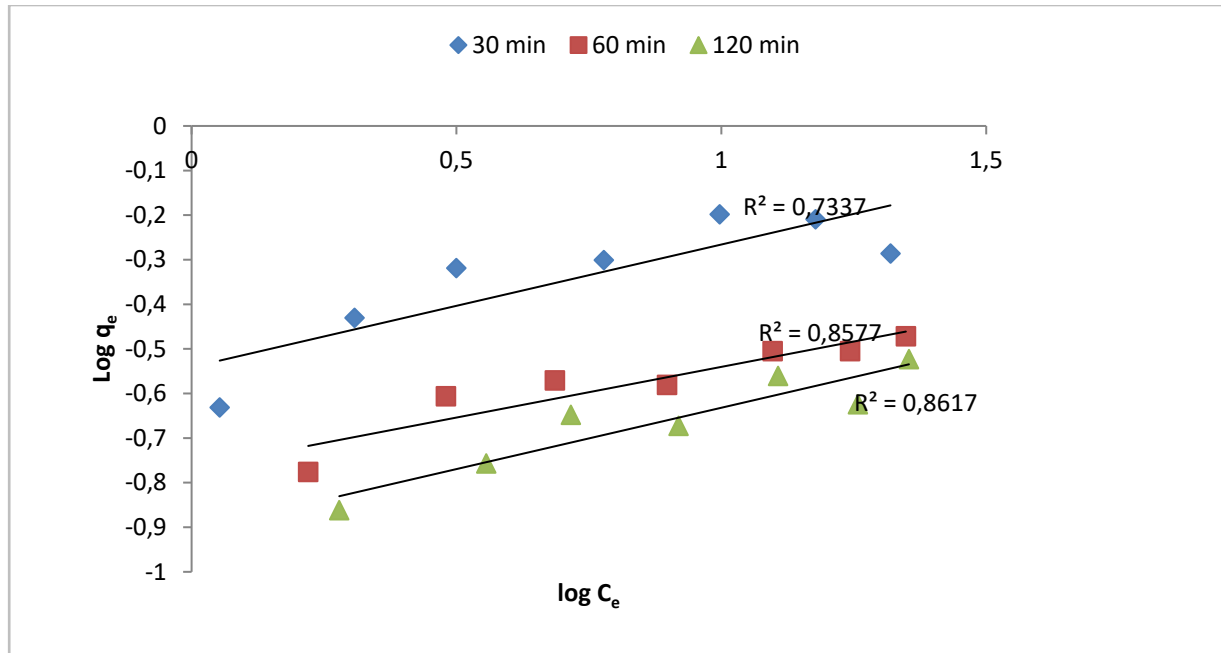


Figure 9.15. Freundlich isotherms (contact time 30 min, adsorbent dosage 0.8 g/100 mL and shaking speed of 250 rpm).

Based on the correlation coefficient values for both contact times, adsorption data fits well to Langmuir adsorption isotherm than Freundlich adsorption isotherm. Better fit of Langmuir isotherm model suggests monolayer uniform adsorption on the surface of adsorbent. Calculated model constants for Langmuir and Freundlich isotherms are shown in Table 9.4. The value of R_L , dimensionless equilibrium parameter and the value of $1/n$ Freundlich adsorption intensity were both between 0 and 1, which indicate that the adsorption of F^- onto smectite-rich clay soil was favourable.

9.8.2 Adsorption Kinetics

Theoretically, the adsorption of fluoride onto a solid particle is controlled by different mechanisms, these mechanisms involves diffusion or transport of fluoride from bulk solution to the exterior surface of adsorbent particle, adsorption of F^- onto particle surface, movement of solute within the pores of particle, attachment of solute at site on the interior surface of the adsorbent via sorption, complexation or intra-particle diffusion phenomenon (Maliyekaal et al., 2006; Chen et al., 2011). Pseudo first and second order rate reaction and the intra-particle diffusion models are widely used to elucidate the adsorption mechanisms and the rate limiting factors.

9.8.2.1 Pseudo first- and second order kinetics

The pseudo first-order model is widely used to describe liquid-solid phase adsorption systems, and it is the earliest known kinetic model describing the adsorption rate based on the adsorption capacity. The plots of pseudo first order had a poor fit (data not shown). This indicates that adsorption of fluoride onto smectite-rich clay soils followed pseudo second order and it occurred through chemisorption. Pseudo second order is used to describe chemisorption, as well as cation exchange reactions. The plots of pseudo second order yielded straight lines and higher correlation coefficient at all concentrations (Figure 9.16).

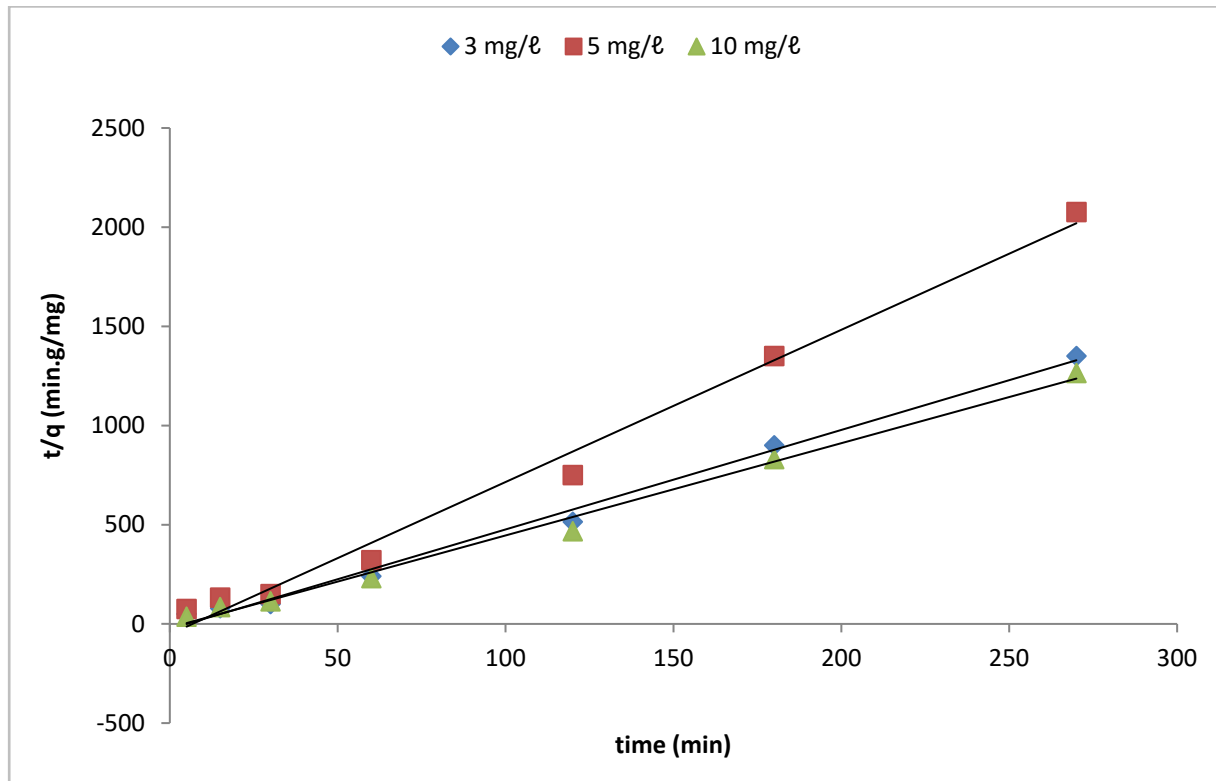


Figure 9.16. Pseudo second order plot at various adsorbate concentrations (0.8 g/100 ml adsorbent dosage, pH 5.54 at 250 rpm)

9.8.2.2 Intra-particle diffusion model

In order to predict the rate limiting step in the adsorption of F^- onto smectite-rich clay soils, the possibility of intra-particle diffusion was evaluated using Weber-Morris model of intra-particle diffusion expressed by equation 7.8 (Chen et al., 2011). Figure 9.17 shows the plot of the amount of fluoride adsorbed and $t^{0.5}$. As can be seen from Figure 7.17, the intercept did not pass through the origin at each of the evaluated concentrations and the data showed a bilinear plot, with the initial portion (phase 1) indicating the boundary layer diffusion and the other represents the intra-particle diffusion (phase 2) and the values of K_{i1} and K_{i2} (intra-particle diffusion co-efficient rate constant for phase 1 and phase 2 respectively) obtained from the plot are shown in Table 7.5. At both initial concentrations, the K_{i1} value is higher than the K_{i2} value, suggesting that the initial sorption step is rapid than the final step (phase 2), which may be due to difference in the rate of mass transfer in the initial

and final stages of adsorption (Jia et al., 2015). This observation is connected to a mechanism consisting of an external mass transfer followed by diffusion into micro- and mesoporous surfaces. This means adsorption of F^- onto smectite-rich clay soils is a complex process involving both boundary and intra-particle diffusion adsorption processes.

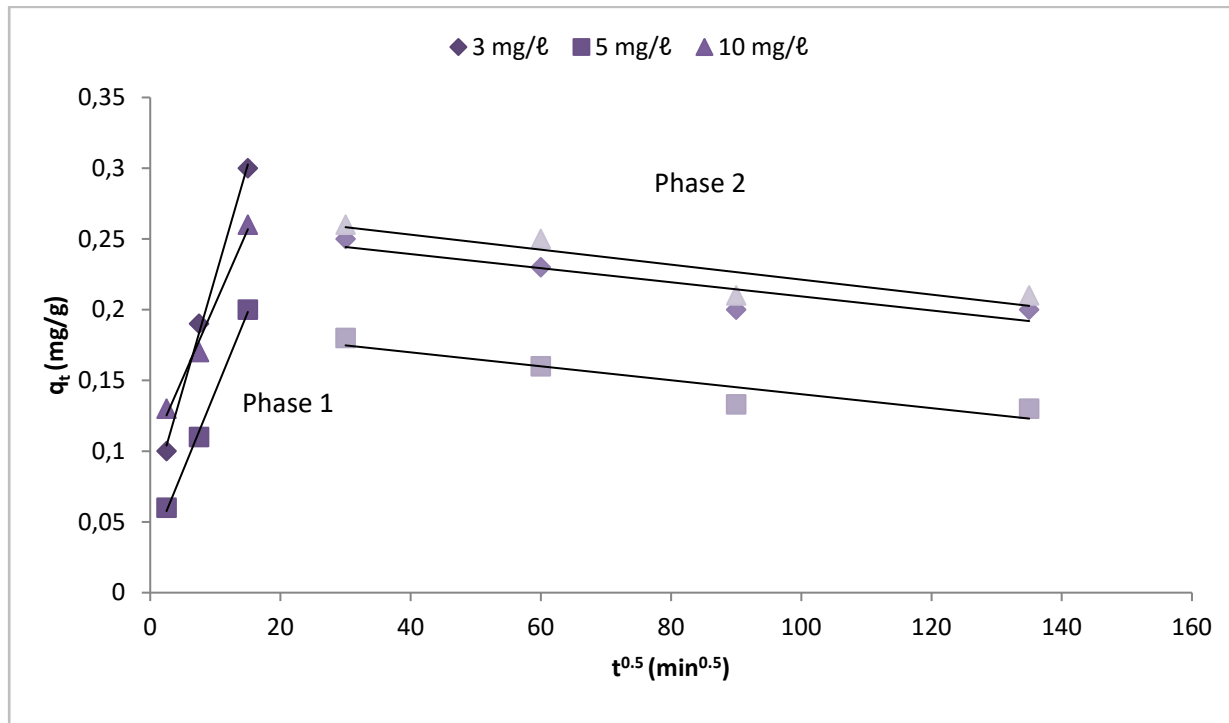


Figure 9.17. Plot for intra-particle diffusion at various concentrations (0.8 g/100 mL, pH 5.54 and shaking speed of 250 rpm).

Table 9.5. Calculated adsorption kinetics model values.

	Pseudo first order			Pseudo second order			Intra-particle diffusion	
	$q_{e(exp)}(mg/g)$	$K_{ad} (min^{-1})$	R^2	$K_{2ad} (g \cdot mg^{-1} \cdot min^{-1})$	$q_{e(cal)}(mg/g)$	R^2	K_{i1}	K_{i2}
3 mg/l	0.19	1.15×10^{-3}	0.05	0.986	0.23	0.99	0.015	-0.005
5 mg/l	0.13	2.3×10^{-4}	0.001	1.13	0.2	0.98	0.01	-0.005
10 mg/l	0.21	6.9×10^{-4}	0.003	1.12	0.21	0.99	0.011	-0.005

9.9 MECHANISM OF F^- ADSORPTION ONTO SMECTITE-RICH CLAY SOILS

The mechanism of fluoride adsorption onto smectite-rich clay was evaluated by comparing the FTIR spectra of smectite-rich clay soils before and after adsorption (Fig 9.4). FTIR spectra showed that the clay soils surface is mainly characterised by Si-OH and Al-OH groups which may be easily modified by changing the pH of the medium. pH_{pzc} determination showed that at pH 5.8 the surface has neutral charge, below 5.8 the surface is positively charged and above that it is negatively charged. Figure 9.9 showed that the adsorption of F^- onto

smectite-rich clay soil was optimum at low pH and decreases as the pH increases which may have been due to the increase in OH⁻ which compete with F⁻ for adsorption sites. After F⁻ adsorption the FTIR spectra showed a decreased peak intensity of transmittance indicating that during adsorption there was ion exchange between OH⁻ in the surface and F⁻ in bulk solution leading to the formation of new bonds such as SiF and AlF. The following mechanisms can be suggested at various pH levels; at pH below 5.8, the surface of the clay is positively charged (Eq. 9.1) and therefore F⁻ ions will be electrostatically adsorbed to the surface of the clay (Eq. 9.2). Ma et al. (2012) suggested that low pH causes protonation of surface –OH groups to –OH₂⁺ which facilitates the ligand exchange mechanism because of stronger attractive force between fluoride and the adsorbent surface and the presence of more hydroxylated sites for exchange of F⁻ than at high pH. At moderate pH, fluoride adsorption occurs via ion exchange (Eq. 9.3). At higher pH above the p*H*_{pzc} where the surface of the clay is negatively charged fluoride adsorption also occurs via ion exchange (Eq. 9.4).



Where $\equiv M$ represent Si and Al in the adsorbent surface.

9.10 SUMMARY

From the results obtained it was observed that 0.8 g/100 ml of black Mukondeni clay soils removed up to 91.89% of F⁻ from an initial F⁻ concentration of 3 mg/l at pH of 2 and contact time of 30 min. The experimental data fitted well to Langmuir adsorption isotherm than Freundlich isotherm and follows pseudo second order of reaction kinetics. The clay soils showed high percentage of F⁻ removal from field water at acidic pH 2 which would limit its application in household treatment devices since pH adjustment of product water would be required. However, significant F⁻ adsorption potential (of \approx 85%) at pH range of 4-10 was observed (F⁻ concentration of 3 mg/l) indicating the potential of the soil for defluoridation of low fluoride containing groundwater. A poor fluoride removal was observed with field water which was attributed to effect of co-existing anions. Comparison of adsorption capacity of smectite-rich clay soils with other developed adsorbents is presented in Table 9.6. From Table 9.6 it is observed that smectite-rich clay soil has lower adsorption capacity compared to other fluoride reported adsorbents. Therefore its surface modification will be essential to improve its adsorption capacity.

Table 9.6. Comparison of adsorption capacities of different adsorbents for fluoride.

Adsorbent	Adsorption capacity (mg/g)	Experimental conditions	Reference
Al/Fe granular ceramic adsorbent	1.79	pH 6, 10 mg/l F ⁻	Chen et al. (2011)
Fe ³⁺ zeolite	2.31	pH 6.94, 10 mg/l F ⁻	Sun et al. (2011)
Red mud	0.6	pH 3-4, 20 mg/l F ⁻	Lv et al. (2012)
La ³⁺ Bentonite/chitosan beads	2.31	pH 5, 10 mg/l F ⁻	Yi et al. (2014)
Smectite-rich clay soils	0.34	pH 2, 3 mg/l F ⁻	Present study

10 EVALUATION OF GROUNDWATER DEFLUORIDATION BY SMECTITE-RICH CLAY SOIL-MNO₂ COATED BENTONITE CLAY COMPOSITES

10.1 INTRODUCTION

Findings from previous studies have shown that smectite-rich clay soils as well Mn²⁺ modified bentonite clay have high fluoride removal efficiency at acidic pH, however, this limits their application in groundwater defluoridation. This section reports on attempts to fabricate stable MnO₂- modified bentonite clay-smectite-rich clay soil composite pellets that can be used in household defluoridation devices. The fabrication of the ceramic pellets involved optimization of the smectite-rich clay soils/MnO₂ coated bentonite clay mixing ratios, calcination temperatures and evaluating their fluoride adsorption potential. This was done in an attempt to fabricate a physically handlable and chemically stable material that can be used in household defluoridation devices.

10.2 MATERIALS

All reagents and TISAB-III were obtained from Rochelle Chemicals & Lab Equipment CC, South Africa Ltd and they were of analytical grade. Smectite-rich clay soil was collected from Mukondenani Village, Vhembe district in South Africa. Bentonite clay was collected from ECCA pty (Ltd) in Cape Town. A stock solution containing 1000 mg/l fluoride was prepared by dissolving 2.21 g analytical grade sodium fluoride in 1 l of ultra-pure water (18.2 MΩ/cm). Fluoride solutions for batch experiments were prepared from fresh stock fluoride solution by appropriate dilution. A stock solution containing 1000 mg/l fluoride was prepared by dissolving 2.21 g NaF in 1 l of MilliQ water (18.2 MΩ/cm) and fluoride solutions for batch experiments were prepared from fresh stock fluoride solution by appropriate dilution. Field water was collected from a community borehole in Siloam, Vhembe district in South Africa.

10.3 METHODS

10.3.1 Synthesis and characterisation of smectite-rich clay soil-MNO₂ coated bentonite clay composites

Smectite-rich clay soils were prepared as described in Section 9.3.1 and MnO₂ coated Na-bentonite was prepared using the method described in Section 8.3. Two factors were considered for the preparation of the smectite-rich clay soil/MnO₂ Na-bentonite clay composite; clay mixing ratio and the calcination temperature. The composite adsorbent prepared using optimised conditions was then characterised using several techniques (detailed in Appendix A). These included Cation Exchange Capacity (CEC), Point of Zero Charge (PZC), X-ray diffraction (XRD), X-ray fluorescence (XRF), Scanning Electron Microscopy (SEM), Scanning Electron Microscopy coupled with Energy Dispersive Spectroscopy (SEM-EDS), Transmission Electron Microscopy (TEM), Brunauer-Emmett-Teller (BET) and Fourier Transform Infrared (FTIR).

10.3.2 Batch and field groundwater adsorption experiments

Optimum fabrication conditions were established through evaluation of fluoride adsorption potential of materials prepared at different synthesis conditions. Methods followed for batch fluoride adsorption studies are detailed in Appendix B. Equation 1 (Appendix C) was used to calculate the percentage of removal and adsorption capacity.

10.4 RESULTS AND DISCUSSION

10.4.1 Effect of clay mixing ratio on F⁻ adsorption

In order to find the optimum clay mixing ratio, MnO₂ coated bentonite clay and smectite-rich clay soils were mixed at mass ratios of 1:1, 1:2, 1:3, 2:1 and 3:1 and put into 50 ml glass beaker. To this 20 ml of MilliQ water was added and the mixture was stirred to homogenise for 15 min. After stirring, mixtures were then centrifuged at 2500 rpm and the solid residues were then dried at 110°C for 12 hours in an oven. Thereafter samples were then milled to pass through <250 µm pore sieve. In order to find the optimum clay mixing ratio, defluoridation experiments were conducted as follows: 100 ml of 5 mg/l F⁻ solution was prepared and pipetted into five (5) 250 ml plastic bottles, to this 0.3 g of composite adsorbent prepared at various ratios was added to make up S/L ratio of 0.3 g/100 ml. Mixtures were then agitated for 30 min at 250 rpm on a Table shaker. After agitation samples were then filtered using 0.45 µm pore filter membrane. Filtrates were analysed for residual fluoride using ion selective electrode calibrated with four standards containing 1 ml of total ionic strength buffer (TISAB-III) per 10 ml of solution. Same ratio was maintained for the sample. Figure 10.1 shows the % F⁻ removal as a function of clay mixing ratio employed during fabrication of the composite pellets. Results shows that clay mixed at ratio of 1:3 (MnO₂ coated Na-bentonite/smectite-rich clay soils) achieved the highest % F⁻ removal, it was subsequently adopted as the optimum clay mixing ratio for subsequent experiments.

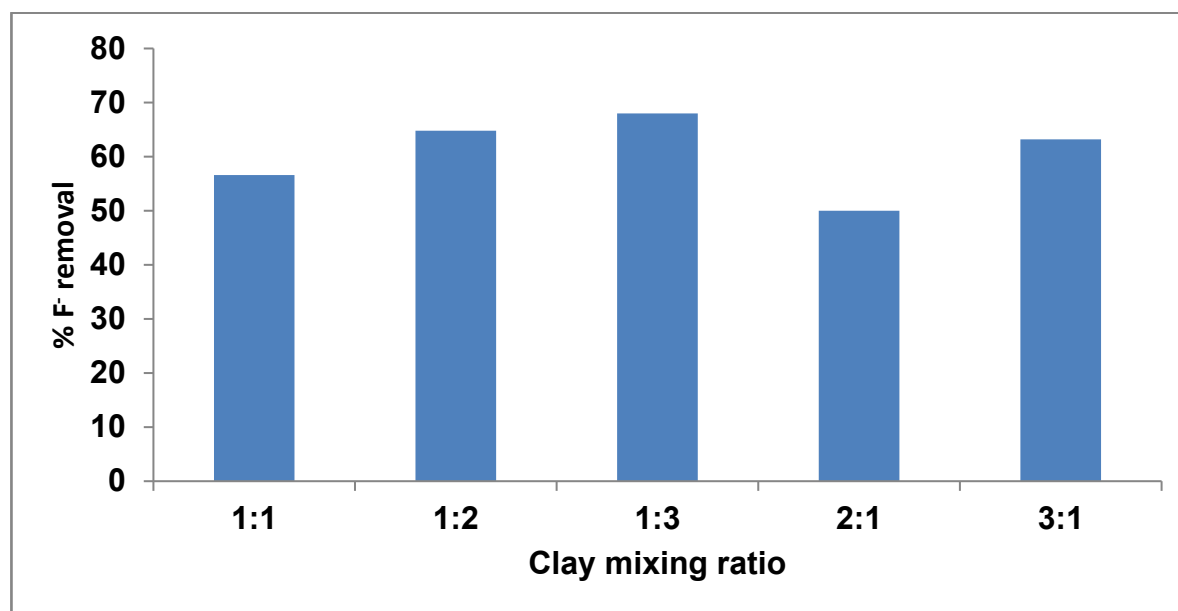


Figure 10.1. Effect of clay mixing ratio on % F⁻ removal (5 mg/l F⁻, 0.3 g/100 ml adsorbent dosage, 30 min contact time at 250 rpm shaking speed, and 6.03±0.5 pH, particle size <250 µm).

10.4.2 Effect of calcination temperature on F⁻ adsorption

In order to evaluate the effect of calcination temperature, the clay was mixed at various ratios and moulded manually into pellets. The pellets were then air dried for 3 hours followed by oven drying at 110°C for 12 hours. After drying pellets were calcined at various temperatures ranging from 150 to 750°C for 1 hour in a marble furnace. The obtained pellets were then used for defluoridation of synthetic fluoride solutions. In order to evaluate the effect of calcination temperature on defluoridation, pellets prepared were used for fluoride removal and the experiments were conducted as follows: 100 ml of 10 mg/l F⁻ solution was prepared and pipetted into five (5) 250 ml plastic bottles, to this 2 g of pellets composite adsorbent prepared at various calcination was added to make up S/L ratio of 2 g/100 ml. Mixtures were then agitated for 30 min at 250 rpm on a table shaker. After agitation samples were then filtered using 0.45 µm pore filter membrane. Filtrates were analysed for residual fluoride using ion selective electrode calibrated with four standards containing 1 ml of total ionic strength buffer (TISAB-III) per 10 ml of solution. Same ratio was maintained for the sample. Figure 10.2 shows the % F⁻ removal as a function of calcination temperature employed during fabrication of the composite pellets. Results show that the % F⁻ removal decreased from 44% to 38.7% as the calcination temperature increased from 150 to 250°C. Pellets calcined at 150°C did not stabilise in solution during agitation and this may have resulted in higher fluoride removal at 150°C as a result of adsorbent particle dispersion in the media. A gradual increase in fluoride removal was thereafter observed as the calcination temperatures increased with a maximum being observed at 550°C. A gradual decrease was thereafter observed as the calcination temperature was increased. A maximum % fluoride removal of 63.3% was attained at 550°C.

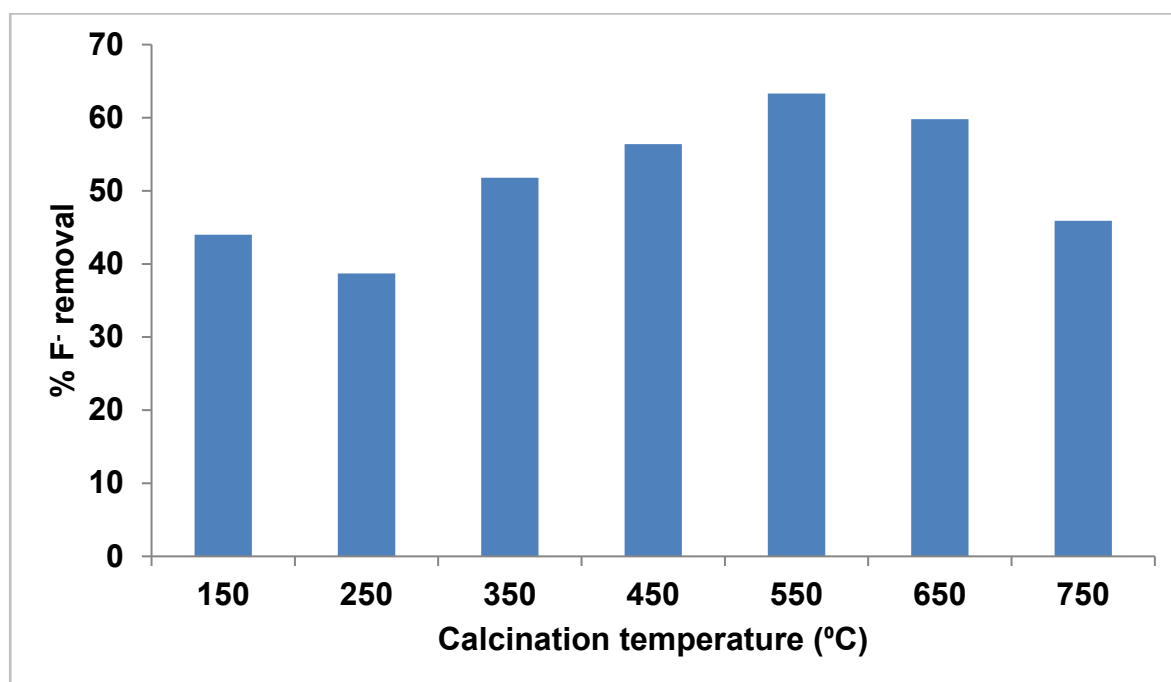


Figure 10.2. Effect of calcination temperature on % F⁻ removal (10 mg/l F⁻ adsorbate concentration, 2 g/100 ml adsorbent dosage, 30 min contact time at 250 rpm shaking speed, and 6.03±0.5 pH, particle size <250 µm)

Clay contains aluminium hydroxides and subjecting it to calcination at high temperatures results in dehydration and subsequent formation of new mineral phases. Figure 10.3 shows a photo of pellets calcined at different temperatures. It can be observed that pellets calcined at higher temperatures appear brown in colour. This can be attributed to surface property modification and the increased F^- removal with temperature increases. It has been reported that clay calcined at approximately 600°C are most effective for fluoride removal, temperatures above 650°C causes a decline in fluoride adsorption (Hauge et al., 1994; Piddennavar, 2013). Decrease in removal of F^- at temperature above 550°C may be attributed to loss of surface hydroxyl groups from the adsorbent.

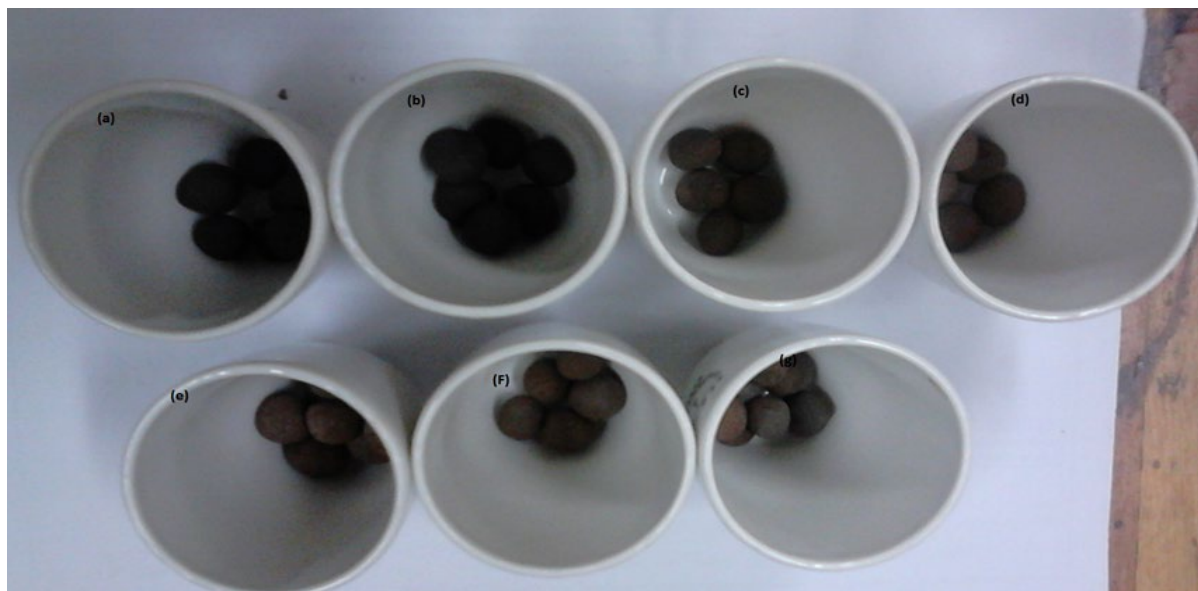


Figure 10.3. Pellets calcined at different temperatures (a – 150°C , b – 250°C , c – 350°C , d – 450°C , e – 550°C , f – 650°C and g – 750°C).

10.5 PHYSICOCHEMICAL AND MINERALOGICAL CHARACTERISATION

10.5.1 X-ray diffraction analysis

The XRD spectra of smectite-rich clay, MnO_2 coated Na-bentonite and ceramic composite is presented in Figure 10.4. The spectra shows that the ceramic clay composite is composed of quartz, albite, cryptomelane and microcline. Montmorillonite mineral is missing in the clay composite confirming the mineral transformation on calcination.

10.5.2 X-ray fluorescence

Table 10.1 shows the chemical composition of smectite-rich clay, MnO_2 coated Na-bentonite and the ceramic clay composite. The results show that the ceramic clay composite consisted of SiO_2 , Al_2O_3 , MnO and Fe_2O_3 as the major oxides with traces of MgO , Na_2O , K_2O and CaO . All these oxides are also the major constituents of MnO_2 coated Na-bentonite and smectite-rich clay soils. MnO content was found to be low in ceramic composite as compared to MnO_2 coated bentonite. This was expected due to the dilution effect on mixing with smectite-rich clay soil.

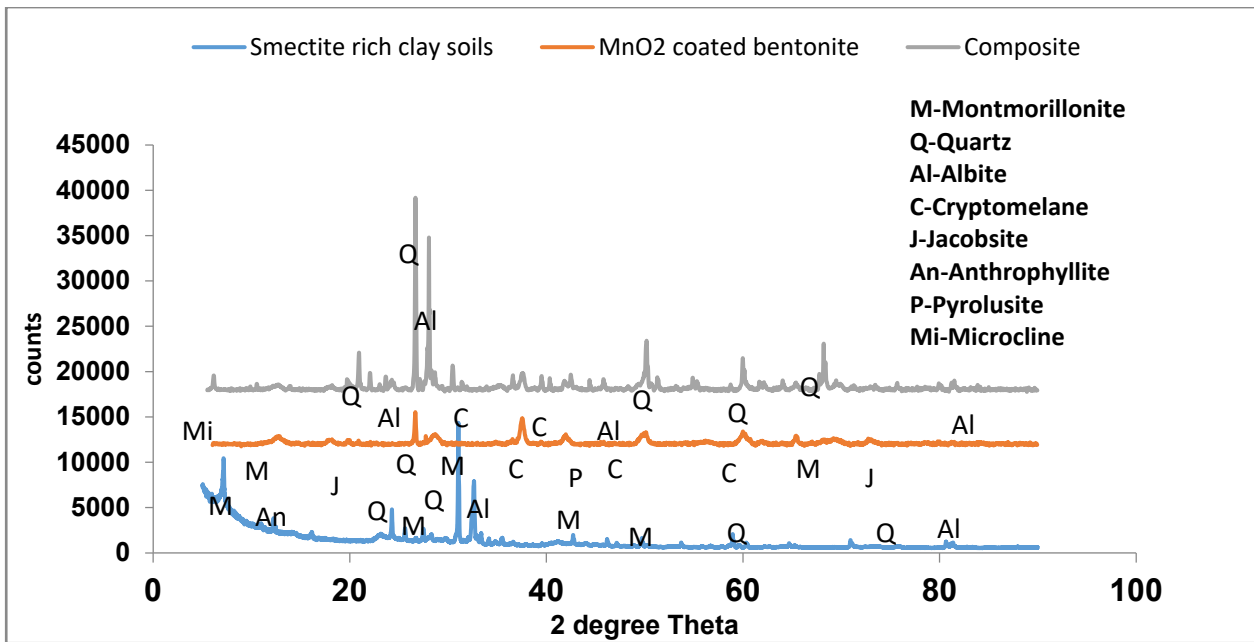


Figure 10.4. XRD Spectra for smectite-rich clay, MnO₂ coated Na-bentonite and calcined composite clay soils.

Table 10.1. Chemical composition of the composite clay soils.

Oxides	MnO ₂ coated Na-bentonite	Smectite-rich clay soil	Ceramic composite
SiO ₂	34.30	62.9	58.40
TiO ₂	0.16	<0.01	0.40
Al ₂ O ₃	7.80	14.35	12.10
Fe ₂ O ₃	1.41	5.45	4.55
MnO	39.20	0.08	9.75
MgO	1.17	2.79	2.06
CaO	0.10	1.79	1.49
Na ₂ O	0.23	2.52	2.07
K ₂ O	4.47	0.93	1.89
P ₂ O ₅	<0.01	0.04	<0.01
Cr ₂ O ₃	<0.01	0.02	0.06
SO ₃	0.22	<0.01	0.13
LOI	10.90	7.71	6.83
Total	99.96	99.15	99.88

10.5.3 Scanning electron microscopy

Figure 10.5 shows the morphology of smectite-rich clay soils, MnO₂ coated Na-bentonite and ceramic clay composite. The analysis reveals platy-like, angular structures and smooth surface features characteristics of smectite clay. The surface of MnO₂ coated Na-bentonite reveals angular and fibrous structures. The ceramic clay composite largely retains the morphology of the smectite-rich clay soils except the rough surface.

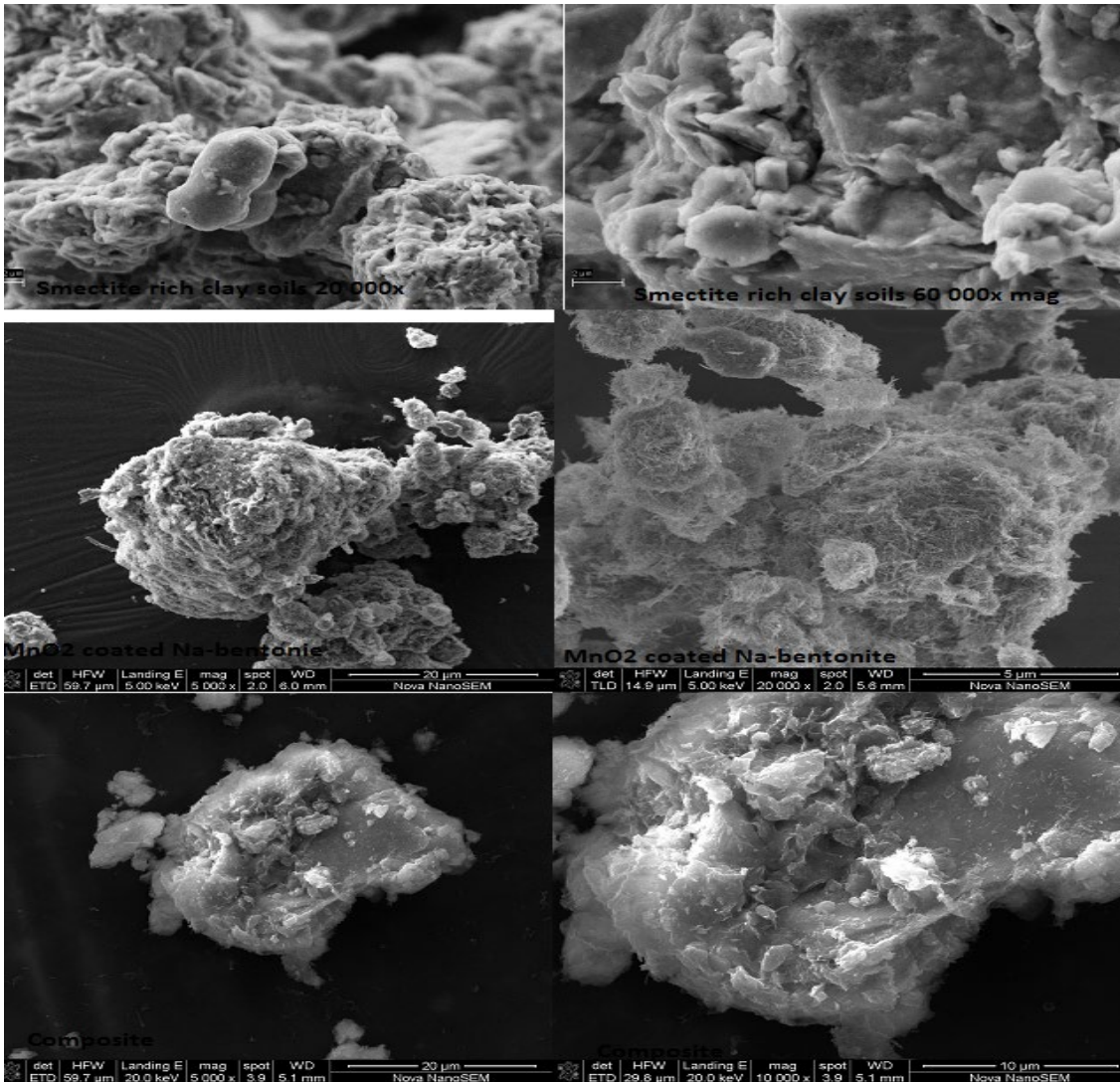


Figure 10.5. Surface morphology of smectite-rich clay soils, MnO₂-coated Na-bentonite and clay composite.

10.6 SUMMARY

In previous Chapters, bentonite clay was activated and converted into Na-bentonite which was then coated with MnO₂ via in-situ oxidation process which was then evaluated for fluoride adsorption. Further, the MnO₂ coated bentonite was blended with locally available black clay soil and fabricated into ceramic pellets in an attempt to fabricate physically handlable and chemically stable material for application in household defluoridation devices. In fabrication of the ceramic pellets two factors were optimized: MnO₂ coated bentonite clay/smectite-rich clay soils ratios and calcination temperatures. Optimum ratio for mixing MnO₂ coated Na-bentonite/smectite-rich clay soils for fabrication of the composite pellets was established to be 1:3 and calcination temperature was 550°C. XRF analysis showed that SiO₂, Al₂O₃, MnO and Fe₂O₃ are the major oxides of the clay composite. Mineralogical characterisation of the clay composite showed the presence of quartz, albite, cryptomelane and microcline as the main minerals of the calcined pellets. Pellets prepared under the established optimum conditions removed ≈63.3% F⁻ from an initial F⁻ concentration of 10 mg/l under batch experimental conditions.

11 EVALUATION OF GROUNDWATER DEFLUORIDATION USING RAW DIATOMACEOUS EARTH

11.1 INTRODUCTION

Groundwater is considered to be the most preferred drinking water for most rural communities in countries such as India, Tanzania, Kenya and South Africa. Groundwater is relatively free from pathogens associated with surface water if the borehole is well constructed and protected from entry of pathogens from surface. However due to geological formations some of the boreholes may have high fluoride concentrations beyond recommended limits by World Health Organization for drinking water and this limits utilization of this resource and also poses a health hazard to many rural communities. Fluoride is important for healthy teeth at concentration of 0.5-1.0 mg/l in drinking water. A guideline of 1.5 mg/l for fluoride in drinking water has been set by WHO (1984). In South Africa, South African National Standards (SANS 241-1, 2015) sets a value of 1.0 mg/l fluoride in drinking water. Several technologies have been developed for defluoridation of groundwater and the most versatile technology has been identified to be adsorption. The major component in adsorption as defluoridation technique is the adsorbent. Many natural and synthetic materials have been evaluated for their defluoridation potentials. These include activated alumina, natural and metal oxide-modified bentonite clay, activated coconut charcoal, surface-tailored zeolite, magnesia-amended activated alumina granules, lanthanum hydroxide and synthetic hydroxyapatite (Ghorai et al., 2005; Gitari et al., 2015; Janardhana et al., 2006; Maliyekkal et al., 2008; Sundaram et al., 2008). The limitation of the adsorption as defluoridation technology is cheap, easily available and high capacity adsorbents. Key aspects of a good candidate adsorbent is that it is locally available, cheap, abundant and has high fluoride adsorption capacity or can be easily modified to increase its adsorption capacity. These factors made diatomaceous earth (DE) a good candidate for investigation. DE is non-toxic and naturally abundant. A study by Yuan et al. (2004) reveals that the structure of DE contains bonded hydroxyl groups which could be exchangeable with electronegative fluoride ions in solution. In addition, the DE offers abundant surface area in form of a network of porous structure which can be easily modified through doping or coating high charge metal oxides. The porous structure allows easy flow of water during the treatment process. This chapter reports on the evaluation of the fluoride adsorption potential of raw diatomaceous earth and metal oxide modified diatomaceous earth and their regeneration potential.

11.2 MATERIALS

All reagents and TISAB-III were obtained from Rochelle Chemicals & Lab Equipment CC, South Africa Ltd and they were of analytical grade. The DE for the study was obtained from natural deposits at Kariandusi in Gilgil District, Nakuru County, Kenya and a second supply sourced in South Africa. A stock solution containing 1000 mg/l fluoride was prepared by dissolving 2.21 g analytical grade sodium fluoride in 1 l of ultra-pure water (18.2 MΩ/cm). Fluoride solutions for batch experiments were prepared from fresh stock fluoride solution by appropriate dilution. A stock solution containing 1000 mg/l fluoride was prepared by dissolving 2.21 g NaF in 1 l of MilliQ water (18.2 MΩ/cm) and fluoride solutions for batch experiments were prepared from fresh stock fluoride solution by appropriate dilution. Field water was collected from a community borehole in Siloam, Vhembe district in South Africa.

11.3 METHODS

11.3.1 Preparation and characterisation of the raw DE for adsorption

The obtained diatomaceous earth (DE) was washed in deionized water to remove dirt and silt. The colloidal particles were recovered from suspension through centrifugation. The cleaned DE was dried in the oven at 110°C for 8 hours, cooled in the desiccator, crushed in a mortar until the particles could pass through 250 µm pore sieve and then stored in tightly stoppered plastic bottles to prevent moisture absorption. The clean DE was then characterised using several techniques (detailed in Appendix A). These included Cation Exchange Capacity (CEC), Point of Zero Charge (PZC), X-ray diffraction (XRD), X-ray fluorescence (XRF), Scanning Electron Microscopy (SEM), Scanning Electron Microscopy coupled with Energy Dispersive Spectroscopy (SEM-EDS), Transmission Electron Microscopy (TEM), Brunauer-Emmett-Teller (BET) and Fourier Transform Infrared (FTIR).

11.3.2 Batch and field groundwater adsorption experiments

Methods followed for batch and field fluoride adsorption studies are detailed in Appendix B. Equation 1 (Appendix C) was used to calculate the percentage of removal and adsorption capacity.

11.4 PHYSICOCHEMICAL AND MINERALOGICAL CHARACTERIZATION

11.4.1 Morphology of natural diatomaceous earth

The micrograph in Figure 11.1 shows that each elongated or pinnate diatom contains a set of regular arrays of rectangular pores arranged along the void tube.

11.4.2 X-ray fluorescence analysis of diatomaceous earth

The result of the XRF analysis of DE (Table 11.1) shows that silica (SiO₂) is the major composition of the natural DE, while the main minor components are Al₂O₃ and Fe₂O₃. Full suite of trace elements in the DE sample was analysed by laser ablation ICP-MS on fusion disk. The results are presented in Table 11.2. Of the trace elements, zirconium had the largest concentration (453.2 mg/kg) followed by cerium (109.6 mg/kg).

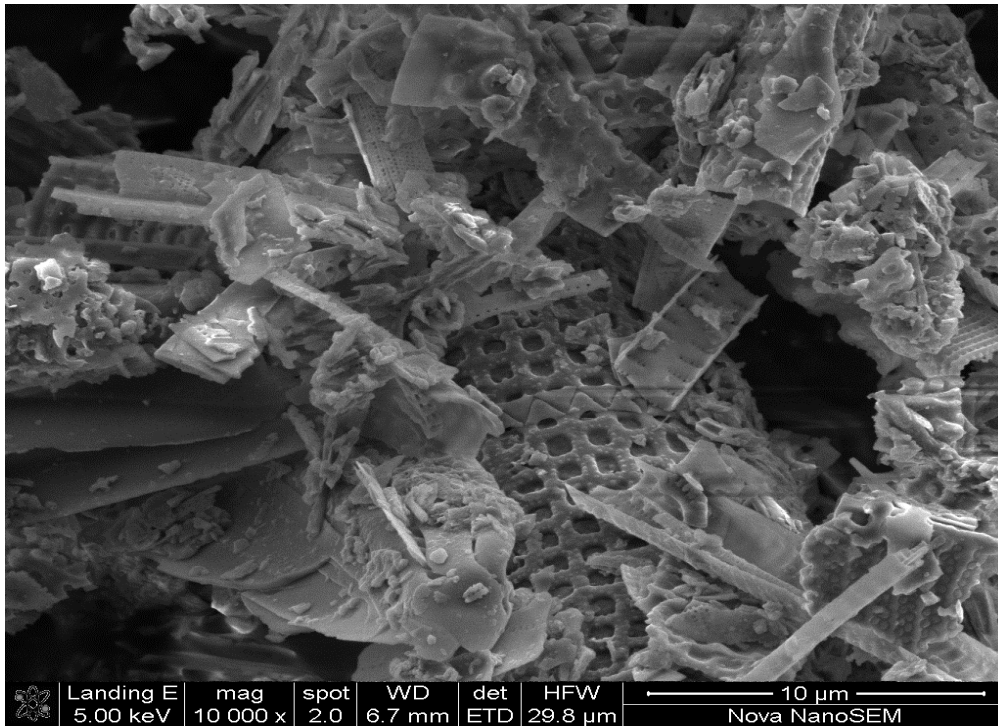


Figure 11.1. SEM micrograph of diatomaceous earth.

Table 11.1. Physical and chemical parameters of diatomaceous earth

Oxide	Composition (%)
SiO ₂	84.17
Al ₂ O ₃	4.01
Fe ₂ O ₃	2.96
Na ₂ O	0.61
K ₂ O	0.75
MgO	0.11
CaO	0.24
ZrO ₂	0.06
TiO ₂	0.17
MnO	0.04
P ₂ O ₅	0.04
LOI ^a	7.52
pHpzc ^b	8.68
WRC ^c	2.25

^aLoss on ignition.

^bpH at point-of-zero charge.

^cWater retention capacity (ml/g).

Table 11.2. Concentration of trace metals in diatomaceous earth

Trace element	Concentration (mg/kg)	Trace element	Concentration (mg/kg)
Sc	3.85	Pr	13.00
V	25.20	Nd	49.75
Cr	11.84	Sm	9.65
Co	1.43	Eu	0.90
Ni	7.38	Gd	8.42
Cu	17.55	Tb	1.48
Zn	86.93	Dy	9.41
Rb	44.67	Ho	2.05
Sr	26.74	Er	6.13
Y	51.45	Tm	0.91
Zr	453.15	Yb	6.24
Nb	85.41	Lu	0.89
Mo	2.36	Hf	11.32
Cs	1.20	Ta	5.04
Ba	30.97	Pb	11.08
La	58.50	Th	13.70
Ce	109.58	U	2.95

11.4.3 Surface area and pore volume of raw diatomaceous earth

The results of the BET analysis of the surface area, pore volume and pore of raw diatomaceous earth are shown in Table 11.3.

Table 11.3. Surface area and pore volume of diatomaceous earth by BET method

Surface area type	Area (m ² /g)	Pore volume type	Volume (cm ³ /g)	Pore size type	Size (nm)
Single point surface area	31.17	Single point adsorption total pore volume of pores	0.083	Adsorption average pore width (4V/A by BET)	10.37
BET surface area	31.89	BJH Adsorption cumulative volume of pores	0.089	BJH Adsorption average pore diameter (4V/A)	16.64
BJH Adsorption cumulative surface area of pores	21.41	BJH Desorption cumulative volume of pores	0.090	BJH Desorption average pore diameter (4V/A)	15.92
BJH Desorption cumulative surface area of pores	22.70				

11.4.4 X-ray diffraction of DE

The X-ray diffractogram of the DE (Figure 11.2) shows that the material is completely amorphous, containing no crystalline mineral phase.

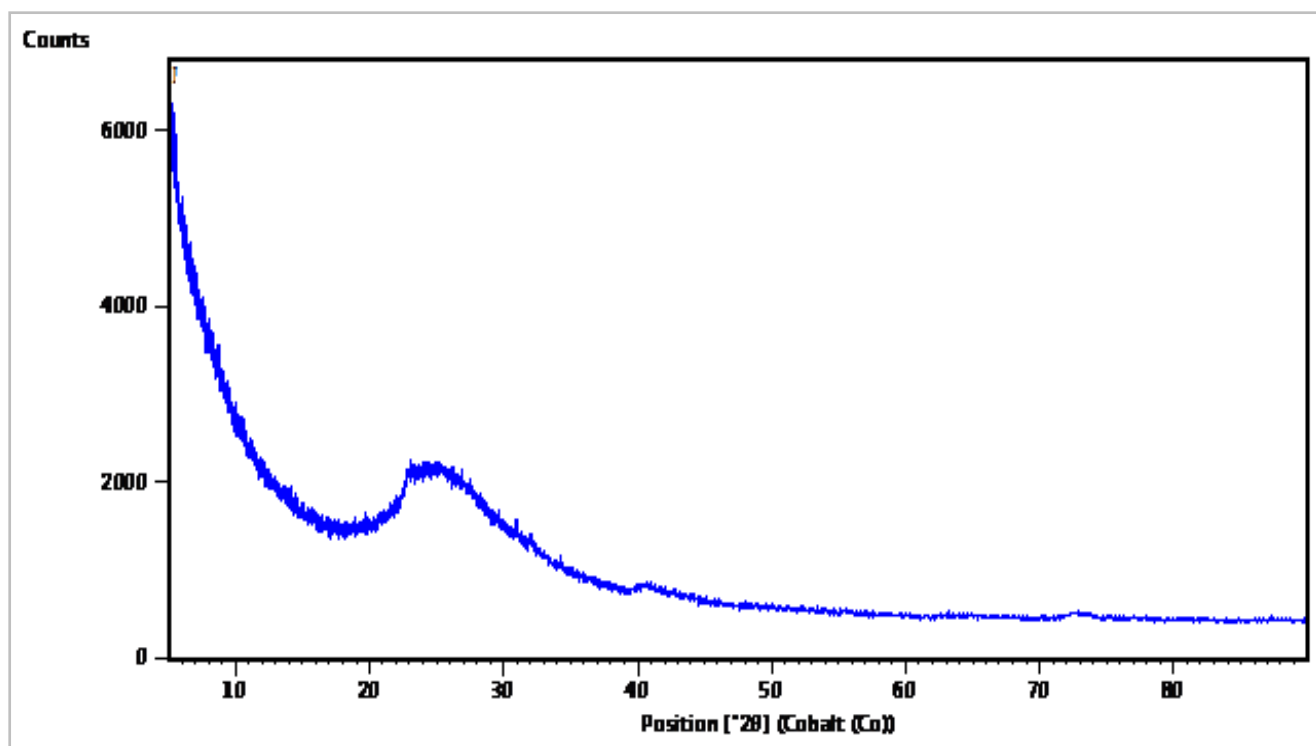


Figure 11.2. X-ray diffractogram of natural diatomaceous earth.

11.4.5 Fourier transform infrared spectra of raw and fluoride-treated diatomaceous earth

Figure 11.3 shows the FTIR spectra of DE and fluoride loaded DE. The transmittance at 453 cm^{-1} represents the Si-O-H stretching vibration, while the one at $1,055\text{ cm}^{-1}$ represents Si-O-Si stretching vibration. The overlap of the bands at 453 cm^{-1} and $1,055\text{ cm}^{-1}$ for the raw DE and fluoride-loaded DE is an evidence of low sorption of fluoride onto the DE surface. There was no significant change in the functional groups of the original material with fluoride sorption.

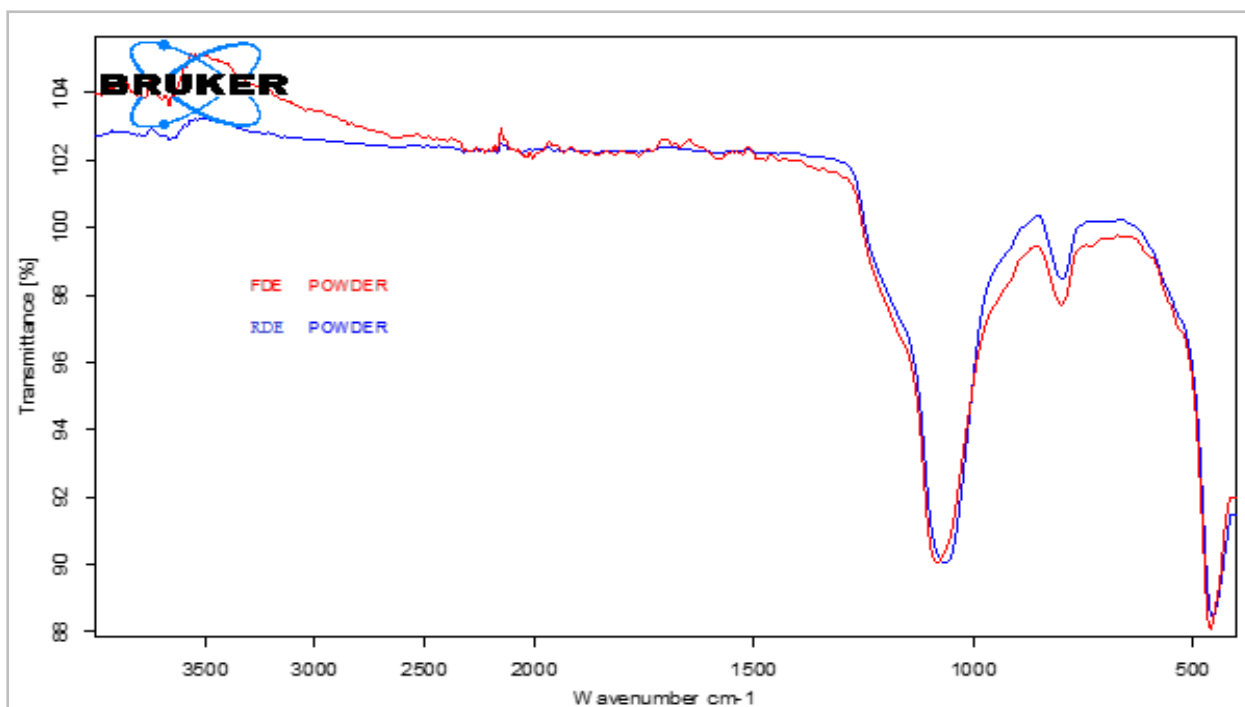


Figure 11.3. FTIR spectra of raw (RDE) and F-treated (FDE) diatomaceous earth.

11.4.6 Cation exchange capacity of diatomaceous earth

The concentration of exchangeable cations in DE were very low. The highest value was recorded for sodium (3.46 mg/g) while magnesium gave the least value (0.17 mg/g). K had a concentration of 2.49 mg/g and Ca 2.30 mg/g.

11.4.7 pH at point-of-zero charge (pH_{pzc})

In the ΔpH -initial pH profile, the point of intersection of the curve with the abscissa gives pH_{pzc} , the value abscissa is 8.7. The implication of this value to defluoridation is that fluoride removal from solution at $\text{pH} \geq 8.68$ will be by exchange of OH^- ion on sorbent for F^- in solution since the surface will be negatively charged while at $\text{pH} < 8.68$ fluoride would be removed from solution by attraction to the positively charged sorbent surface (Figure 11.4).

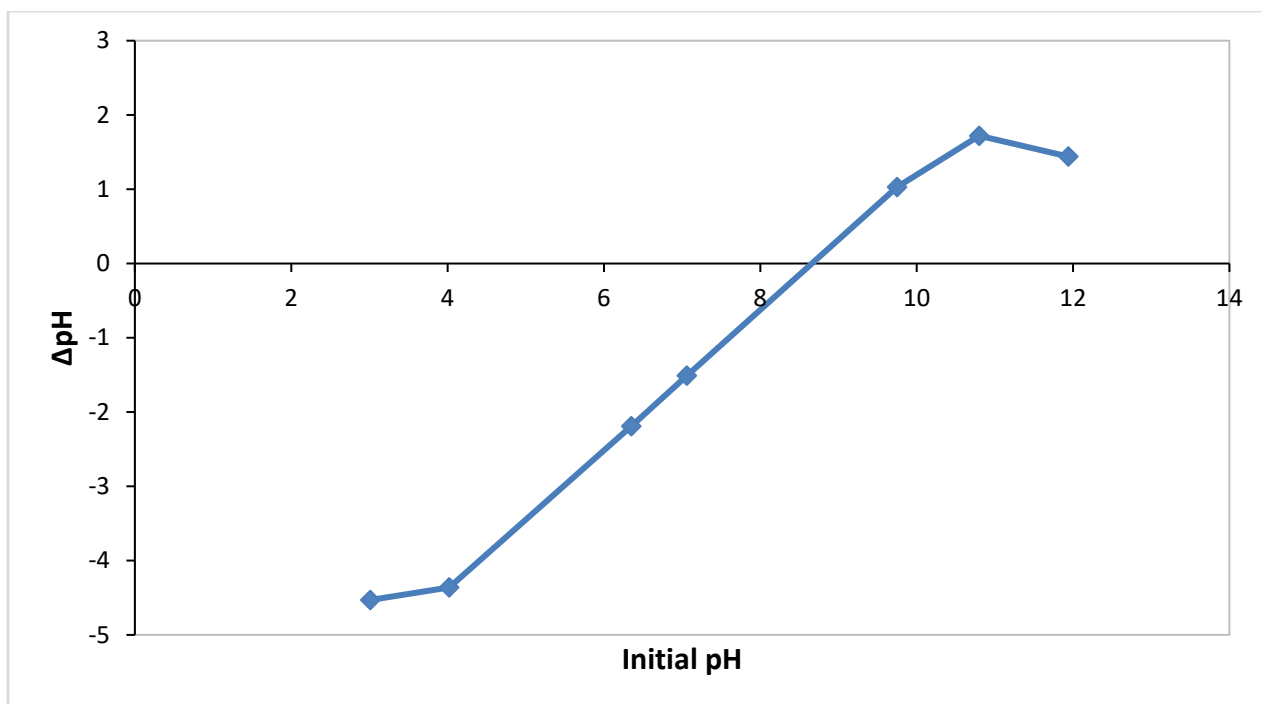


Figure 11.4. Plot of change in pH against initial pH (volume of 1 M KCl: 50 mL, adsorbent dosage: 1 g, temperature: 298 K, shaking speed: 250 rpm and contact time: 24 h).

11.5 BATCH FLUORIDE ADSORPTION EXPERIMENTS

11.5.1 Effect of shaking speed

The effect of shaking speed on fluoride sorption onto DE was evaluated at shaking speeds of 180, 200, 230 and 250 rpm. The equilibration of the mixtures consisting of 8 mg/l fluoride and adsorbent dosage of 0.4 g/50 mL were carried out at pH 2 and temperature of 298 K. After equilibration, the mixtures were centrifuged. The supernatants obtained were analysed for fluoride. Figure 11.5 shows the trend in the per cent fluoride removal and the equilibrium pH as the shaking speed increased. It is observed that % fluoride removal remained constant (25.6%) for all the evaluated shaking speeds. This implies that the fluoride removal was independent of increase in shaking speed above the minimum shaking speed evaluated. The equilibrium pH was observed to increase slightly from 2.09 at 180 rpm to a constant value of 2.13 at 230 rpm. As the shaking speed increased, the rate of collision between the fluoride and adsorbent would increase. Non-increase in the rate of fluoride sorption was probably due to increase in the equilibrium pH which would make the adsorbent surface less electropositive for fluoride attraction and removal from solution.

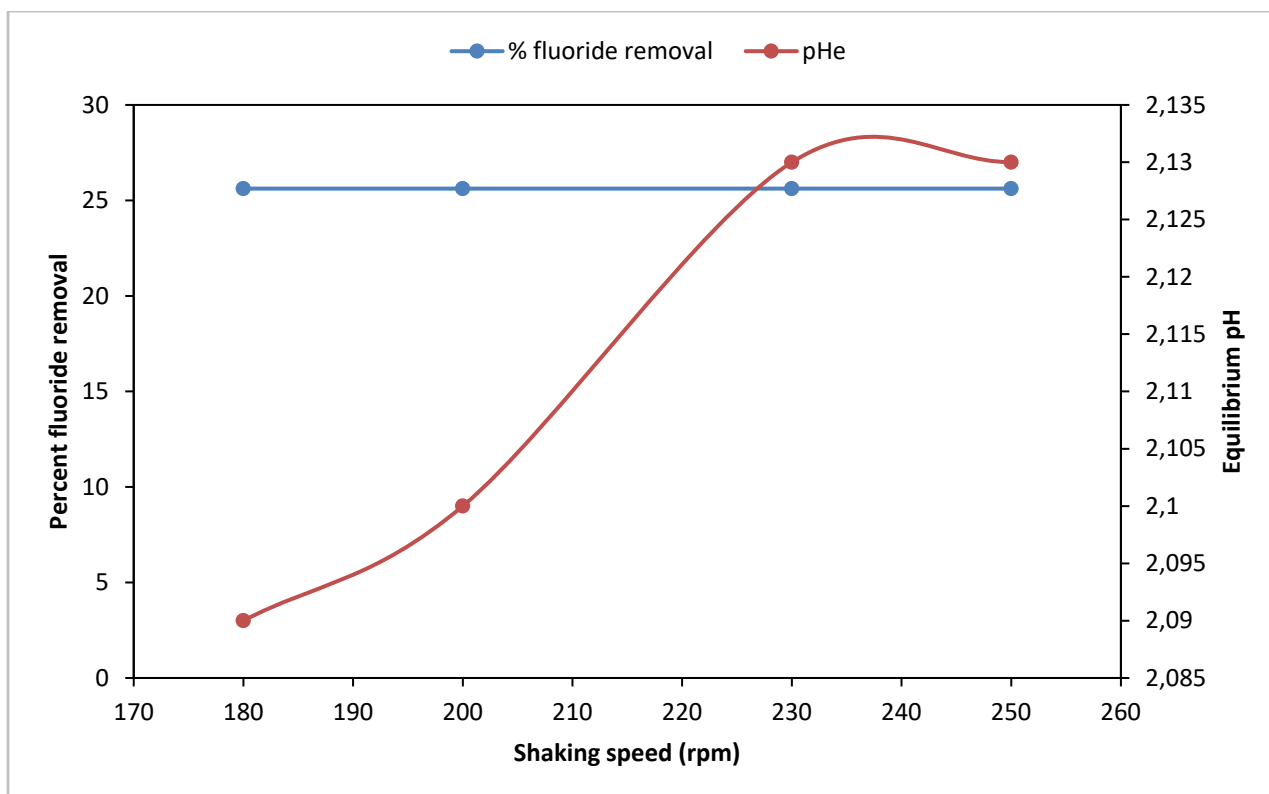


Figure 11.5. Per cent fluoride removal as a function of shaking speed (initial F⁻ concentration: 8 mg/l, volume of solution: 50 ml, adsorbent mass: 0.4 g, contact time: 30 min and temperature: 298 K).

11.5.2 Effect of contact time

The effect of contact time on fluoride sorption was evaluated at an initial fluoride concentration of 8 mg/l F⁻ and 0.4 g/50 ml sorbent dosage, initial pH 2 and contact times of 5, 10, 20, 30, 40 and 50 min at 298 K and shaking speed of 200 rpm (Fig 11.6). After equilibration, the mixtures were centrifuged and the supernatants analysed for fluoride. The results of the equilibrium fluoride concentration, adsorption capacity (q_e) and per cent fluoride removal at each contact time were calculated and the trends in these parameters are displayed in 6.6 at different equilibration times. Defluoridation is an equilibrium process involving sorption and desorption of adsorbate. At the start of defluoridation process, fluoride ions migrate to the adsorbent surface where the concentration of fluoride is lower. As the reaction proceeds, some of the adsorbed ions are desorbed from the surface. The optimum contact time is the time at which the highest fluoride removal is recorded. Maximum fluoride removal from solution was observed at 30 min contact time. The lowest and highest % fluoride removal was 21.9% and 25.6%, occurring at 20 min and 30 min contact times respectively. However, the difference in the two values was marginal (3.75%).

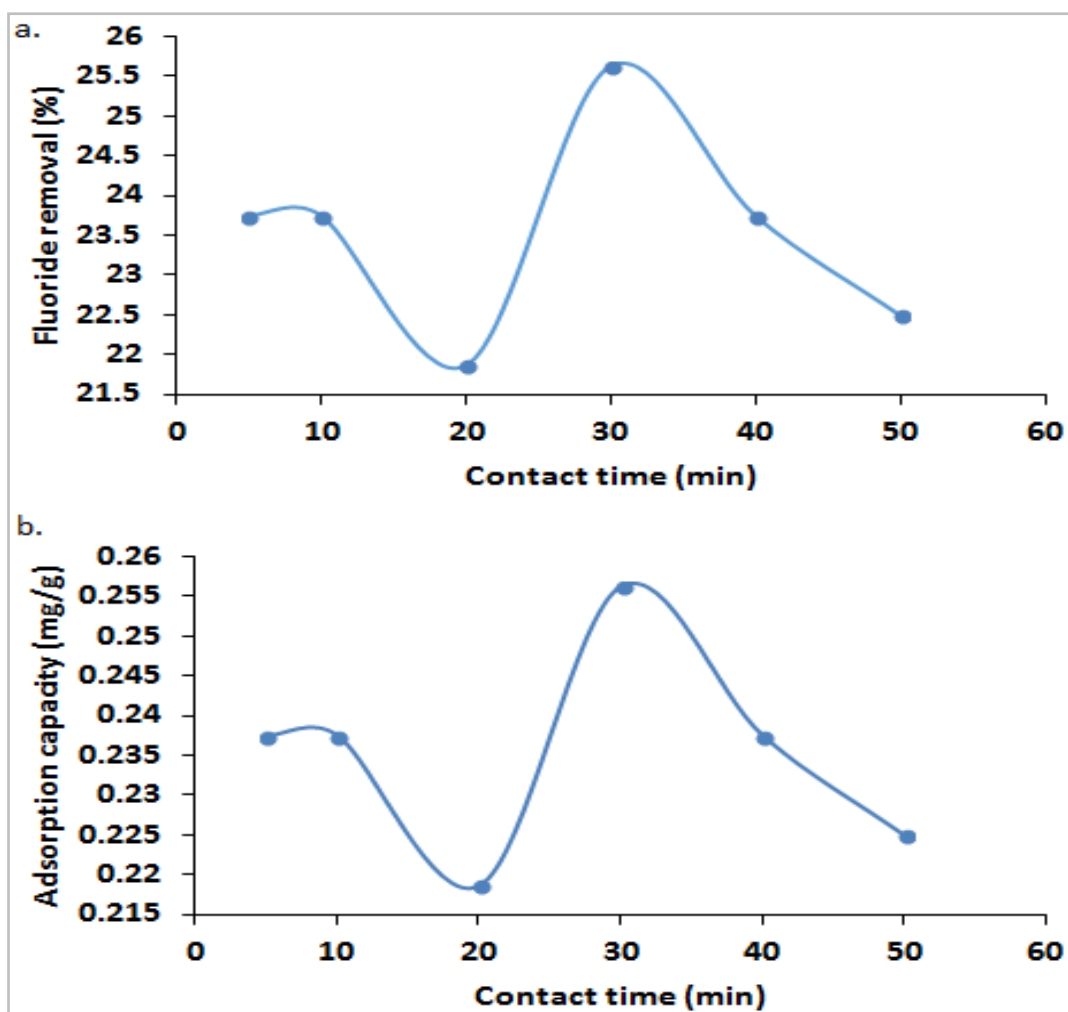


Figure 11.6. Variation of a. per cent fluoride removal and b. adsorption capacity with contact time (initial fluoride concentration: 8 mg/l, volume of solution: 50 ml, adsorbent dosage: 0.4 g, temperature: 298 K, initial pH: 2, and shaking speed: 200 rpm).

11.5.3 Effect of adsorbent dosage

The effect of adsorbent dosage on fluoride sorption was evaluated with the view of obtaining the optimum sorbent dosage. Sorbent dosage was varied from 0.1 to 1.2 g/50 ml. The initial concentration of fluoride solution was 8 mg/l while the initial pH of the sorbent-fluoride mixture was 2. The mixtures were equilibrated for 30 min at 200 rpm. After equilibration, the mixtures were centrifuged to remove the solid residues. The supernatants obtained were analysed for residual fluoride as explained previously. The values of the equilibrium fluoride concentration, adsorption capacity and the per cent fluoride removal at different adsorbent dosages are presented in Figure 11.7. It was observed that % fluoride removal increased from adsorbent dosage of 0.1 to 0.4 g/50 ml where the optimum per cent fluoride removal of 23.4% occurred. The increase in per cent fluoride removal was due to increase in the number of adsorption sites as the dosage increased. The % fluoride removal at adsorbent dosage of 0.6 g/50 ml was similar to that of 0.4 g/ 50 ml.

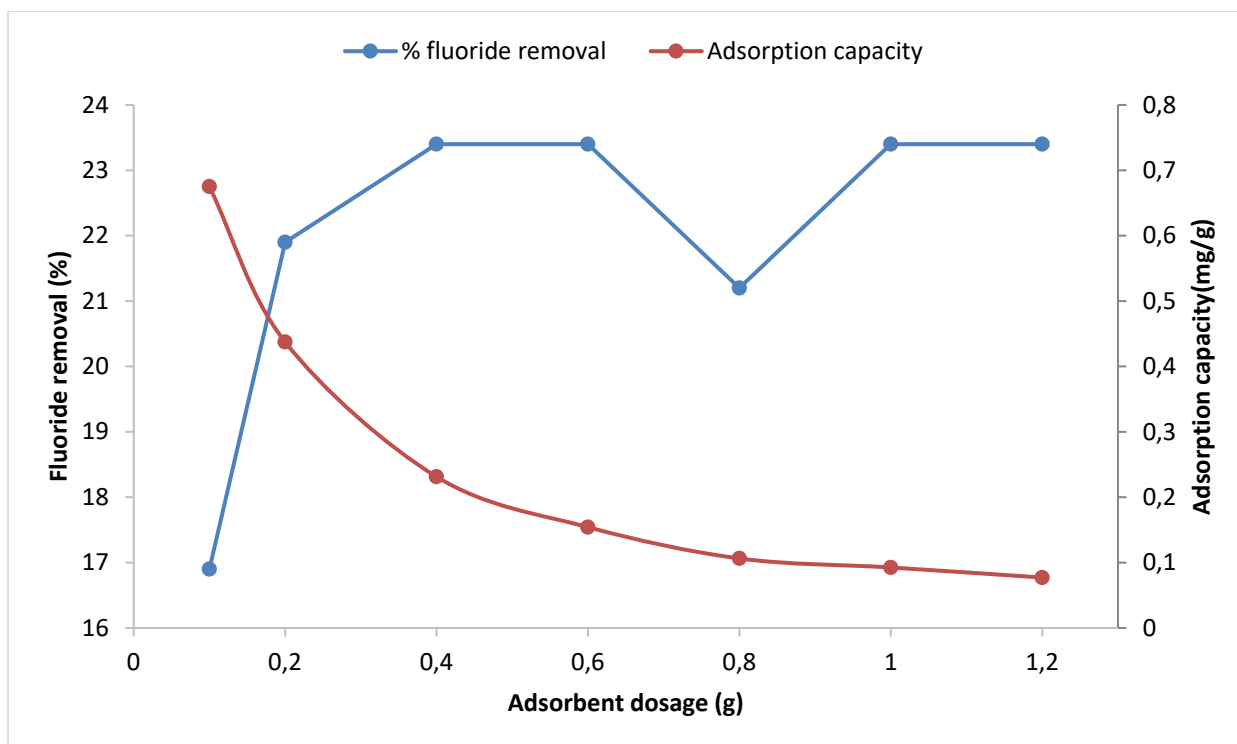


Figure 11.7. Variation of per cent fluoride removal and adsorption capacity with adsorbent dosage (initial fluoride concentration: 8 mg/l, volume of solution: 50 ml, contact time: 30 min, temperature: 298 K, initial pH: 2, and shaking speed: 200 rpm).

The increase in dosage must have resulted in overlapping of some active adsorption sites such that the net number of active adsorption sites equalled that obtained at 0.4 g dosage. At 0.8 g/50 ml dosage, more active sites overlapped, thereby reducing the number of net adsorption sites and the net surface area. Hence, a reduction of per cent fluoride removal. Similar observations have been reported in previous studies (Killedar and Bhatgava, 1990; Rai et al., 2004). The per cent fluoride removal increased to an optimum value of 23.4% at dosages of 1.0 g/50 ml and 1.2 g/50 ml. There was no observable increase in the per cent fluoride removal at these dosages because the number of overlapping sites was probably equal to the number of active sites. A 0.4 g/50 ml was therefore adopted as the optimum dosage and was used in subsequent experiments. The adsorption capacity decreased all through with increasing adsorbent dosage. This was notably because there was no appreciable increase in fluoride removal with increasing adsorbent dosage.

11.5.4 Effect of pH

To evaluate the effect of pH on fluoride sorption onto DE, mixtures consisting of 0.4 g/50 ml of adsorbent and 8 mg/l fluoride at initial pH 2-12 were equilibrated for 30 min at 200 rpm and 298 K. After equilibration, the sorbent was separated from solution by centrifuging, followed by analysis of the supernatants for residual fluoride. The equilibrium fluoride and per cent fluoride removal at different equilibrium pH are presented in Figure 11.8. The positive values of per cent fluoride removal at equilibrium pH of 2.05 and 4.27 are indicative of fluoride removal from solution at those pH values.

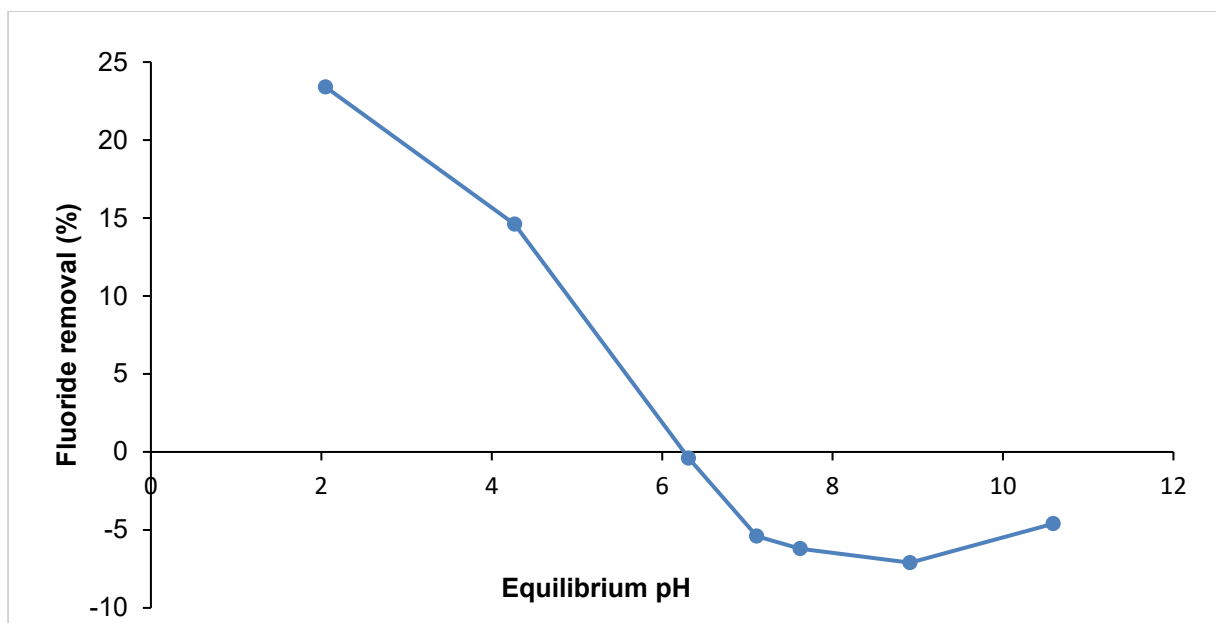


Figure 11.8. Variation of per cent fluoride removal with pH (initial F⁻ concentration: 8 mg/l, volume of solution: 50 ml, contact time: 30 min, temperature: 298 K, and shaking speed: 200 rpm).

The lower the pH, the higher the amount of fluoride removed. This is attributed to the increase in the electropositivity of the adsorbent surface which enhanced attraction for the negatively charged fluoride. Above pH 6, negative values were obtained for per cent fluoride removal. Thus, fluoride was being leached from the sorbent rather than being removed from solution. The fluoride release is evidence that the DE contained geological fluoride as later confirmed in stability experiments. Generally, fluoride removal decreased with increasing pH. The optimum pH for fluoride removal from solution was at pH of 2.05. The chemistry of the fluoride removal at different pH may be explained in relation to the pH at point-of-zero-charge (pHpzc) of the material. At pH_{pzc} = 8.68, the surface charge of DE in solution is neutral. The surface of particles at pH less than the pH_{pzc} is positively charged (Gavriloaiei and Gavriloaiei, 2008). Fluoride removal at the adsorbent surface therefore at pH < pH_{pzc} is expected to be by electrostatic attraction of the fluoride ions by the positively charged surface. The more electropositive the surface is, the more the attraction for fluoride ions. This explains why the maximum fluoride removal (23.4%) occurred at pH 2.05 (Figure 11.8). Protonation of the silanols at the adsorbent surface provides sites for electrostatic attraction for fluoride.

11.5.5 Effect of adsorbate concentration

A number of studies have shown that within a certain range of adsorbate concentration, the amount of adsorbate removed from solution increases with adsorbate concentration (Yao et al., 2009; Sadiju et al., 2012; Khraisheh et al., 2014; Oladoja and Helmreich, 2014). Defluoridation was therefore carried out at various initial fluoride concentrations to evaluate the effect of adsorbate concentration on fluoride sorption onto DE. Figure 11.9 shows how the adsorption capacity and the per cent fluoride removal varied with the equilibrium fluoride concentration. The adsorption capacity was observed to increase with the equilibrium concentration. A sharp increase in adsorption capacity observed at adsorbate concentration range 6-32 mg/l F⁻ decreased as the system approached equilibrium concentration > 38 mg/l F⁻. This is attributed to the adsorbent surface being completely saturated with fluoride ions. This is

evident from the drop in per cent fluoride removal at the equilibrium fluoride concentration of 53.67 mg/l. The optimum fluoride removal was observed at an initial 80 mg/l F⁻ concentration, while the optimum adsorption capacity was 5.79 mg/g for an initial 100 mg/l F⁻ (data not shown). However, for this study, defluoridation of solution containing 8 mg/l F⁻ was emphasized because the average fluoride concentration of the groundwater in the area of study ranged from 5-8 mg/l.

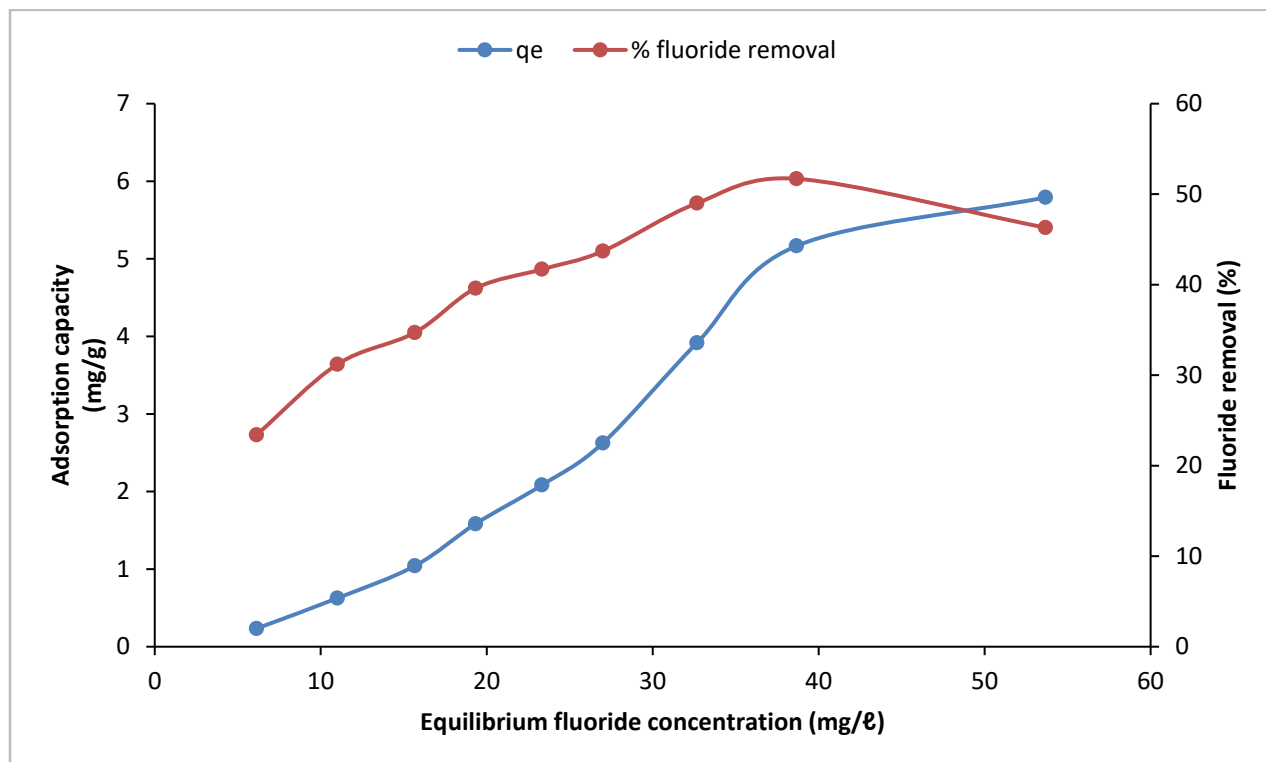


Figure 11.9. Variation of adsorption capacity and per cent fluoride removal with equilibrium fluoride concentration (volume of fluoride solution: 50 mL, contact time: 30 min, initial pH: 2, adsorbent dosage: 0.4 g and shaking speed: 200 rpm).

11.5.6 Effect of temperature

The effect of temperature on fluoride sorption was evaluated by repeating the experiment presented in Figure 11.9 at temperatures of 313 and 323 K, respectively. The values of the per cent fluoride removal and the adsorption capacity for single determinations at the evaluated temperatures are given in Tables 11.4 and 11.5, respectively.

Table 11.4. Variation of per cent fluoride removal with temperature

Temperature (K)	% F- removal for $C_0 = 8$ mg/l	% F- removal for $C_0 = 16$ mg/l	% F- removal for $C_0 = 24$ mg/l	% F- removal for $C_0 = 32$ mg/l	% F- removal for $C_0 = 40$ mg/l	% F- removal for $C_0 = 48$ mg/l	% F- removal for $C_0 = 64$ mg/l	% F- removal for $C_0 = 80$ mg/l	% F- removal for $C_0 = 100$ mg/l
298	23.4	31.2	34.7	39.6	41.7	43.7	49.0	51.7	46.3
313	22.5	31.2	37.5	40.6	43.3	47.2	52.1	54.6	56.0
323	19.1	31.2	34.7	37.5	41.7	45.1	47.8	53.7	57.0
Mean	-	21.7	31.2	35.6	39.2	42.2	45.3	49.6	53.1
Confidence	-	2.566	-	1.829	1.790	1.046	1.994	2.511	1.679
$t_{0.95}$	-	2.920	2.920	2.920	2.920	2.920	2.920	2.920	2.920

Table 11.5. Variation of adsorption capacity with temperature

Temperature (K)	q_e (mg/g) for $C_0 = 8$ mg/l	q_e (mg/g) for $C_0 = 16$ mg/l	q_e (mg/g) for $C_0 = 24$ mg/l	q_e (mg/g) for $C_0 = 32$ mg/l	q_e (mg/g) for $C_0 = 40$ mg/l	q_e (mg/g) for $C_0 = 48$ mg/l	q_e (mg/g) for $C_0 = 64$ mg/l	q_e (mg/g) for $C_0 = 80$ mg/l	q_e (mg/g) for $C_0 = 100$ mg/l
298	0.235	0.625	1.041	1.584	2.084	2.625	3.916	5.166	5.791
313	0.225	0.625	1.125	1.625	2.166	2.834	4.166	5.459	7.000
323	0.191	0.625	1.041	1.500	2.084	2.709	3.584	5.375	7.125

From the statistical analysis of the sorption data, there was no significant difference between the per cent fluoride removal for initial fluoride concentrations of 8, 16, 24, 32, 40, 48, 64 and 80 mg/l evaluated at 298 K, 313 K and 323 K. For those evaluations, the confidence at alpha 0.05 for one-tail data was lower than the corresponding $t_{0.95}$ obtained from the t Table. However, there was a significant difference in the per cent fluoride removal involving solution with initial fluoride concentration of 100 mg/l. This was attributed to the low value of amount fluoride removed at 298 K. Hence, a moderate increase in temperature at this fluoride concentration would enhance fluoride removal.

11.6 ADSORPTION MODELLING

11.6.1 Adsorption isotherms

The sorption data were modelled using Langmuir and Freundlich isotherms. Langmuir isotherm is used to test whether there was a monolayer adsorption of an adsorbate onto a smooth surface or not. The isotherm if applicable assumes that the surface containing the adsorbing sites is a perfectly flat (smooth) plane. Detailed description of the Langmuir and Freundlich isotherms is presented in Appendix C. The data at the various temperatures resulted in a poor fit and could thus not be described by Langmuir model (data not shown). The various values of the quantities and for Langmuir plots at evaluated temperatures 298, 313 and 323 K are shown in Figure 11.10 which confirm that the adsorption data did not conform to Langmuir isotherm.

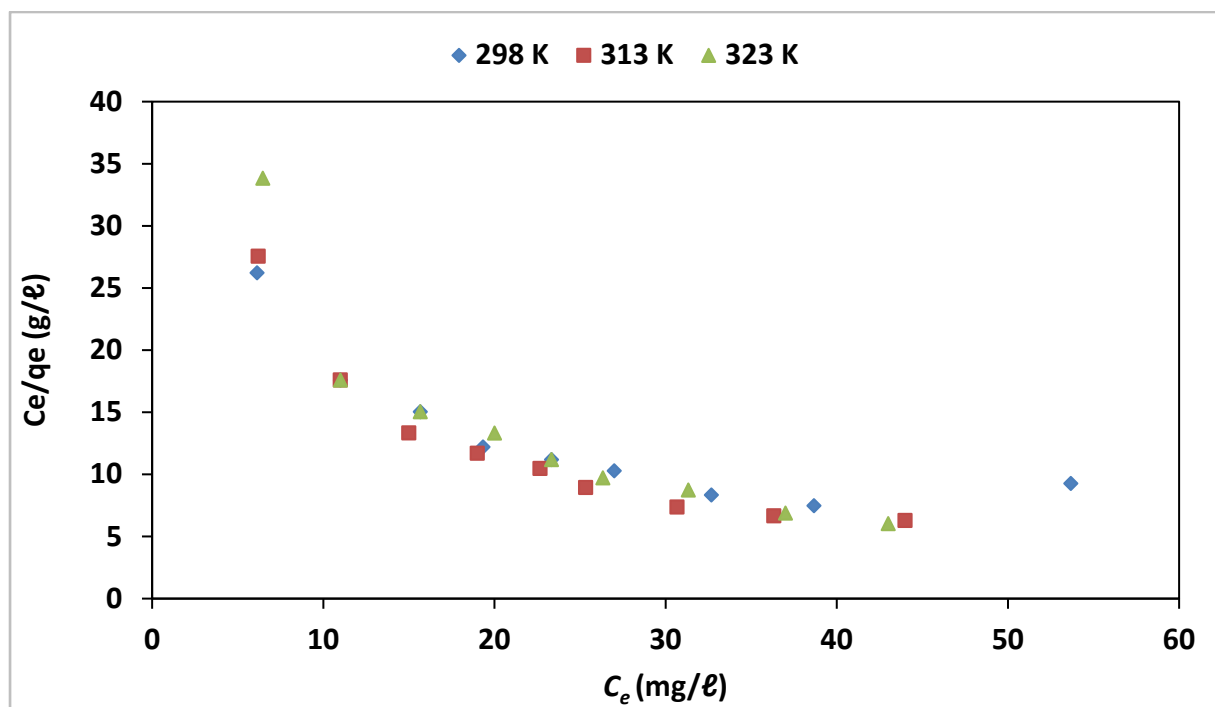


Figure 11.10. Langmuir's profiles at 298 K, 313 K and 323 K (volume of fluoride solution: 50 mL, contact time: 30 min, initial pH: 2, adsorbent dosage: 0.4 g and shaking speed: 200 rpm).

The sorption data were also modelled using Freundlich isotherm (Freundlich, 1906) (eq 4.8). Freundlich isotherm describes a multi-site adsorption isotherm for rough surfaces K_F and n are Freundlich constants whose values depend on experimental conditions. K_F represents the adsorption capacity while $1/n$ is the heterogeneity factor. $1/n$ values much less than 1 show that the adsorbents are heterogeneous. K_F and $1/n$ can be obtained from the plots of $\log q_e$ against $\log C_e$. A linear plot means that the adsorption process conforms to the Freundlich isotherm. Values of $1/n$ close to 1 indicate a material with relatively homogeneous binding sites (Papageorgiou et al., 2006). The plots of $\log q_e$ and C_e at the evaluated temperatures gave plots with high linearity as shown in Figure 11.11. It is therefore evident from the result that the fluoride adsorption onto raw DE is a multi-site adsorption. The calculated K_F , $1/n$ and correlation coefficients R^2 are reported in Table 11.6.

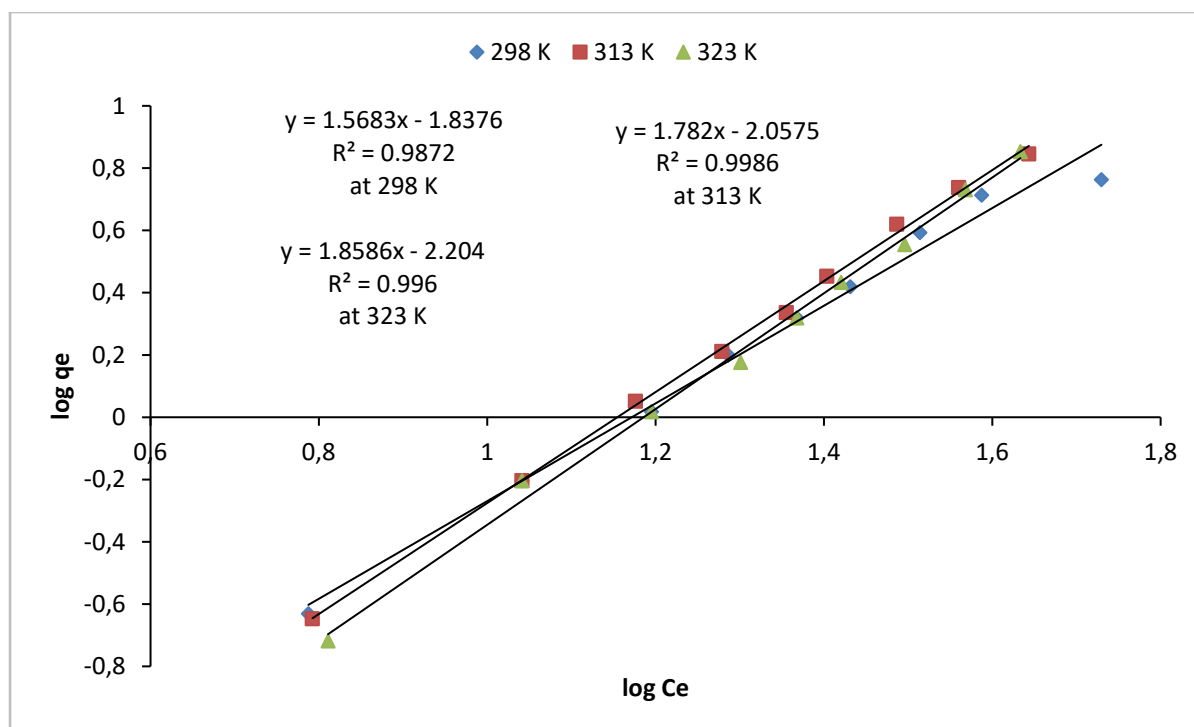


Figure 11.11. Freundlich profiles at 298 K, 313 K and 323 K (volume of fluoride solution: 50 mL, contact time: 30 min, initial pH: 2, adsorbent dosage: 0.4 g and shaking speed: 200 rpm).

Table 11.6. Calculated Freundlich isotherm parameters

Temperature (K)	K_F (mg/g)	$1/n$	R^2
298	0.0145	0.6376	0.9872
313	0.0088	0.5612	0.9986
323	0.0063	0.5380	0.9960

11.6.2 Adsorption kinetics

The aims of studying chemical kinetics include (1) to determine experimentally the rate of chemical reaction and its dependence on parameters such as concentration and temperature and (2) to understand the reaction mechanism, that is, the number of steps involved and the nature of intermediates formed. In the light of these facts, the kinetics of fluoride sorption onto DE was tested along the rate of chemical reaction and the likely mechanism controlling the sorption rate (Chang, 1977). A number of mechanisms control sorption rate. These include (1) diffusion from the bulk solution to a film layer surrounding the adsorbent particle, (2) diffusion from the film to particle surface, "film diffusion", (3) migration inside the adsorbent particle by "surface diffusion" or diffusion within liquid-filled pores, "pore diffusion" and (4) uptake of adsorbate by chemisorption, physisorption, ion exchange or complexation (Weber and DiGiano, 1996; Gulipalli et al., 2011). The models for determining sorption mechanisms are of two types. These are reaction-based and diffusion-based models (Sundaram et al., 2008). Diffusions in sorption experiments are classified generally as external or internal. External diffusion is the migration of the adsorbate from the bulk solution through a film layer surrounding the adsorbent particle to the particle surface while intra-particle diffusion is the migration of the adsorbate by surface diffusion through the pores of the adsorbent particles (Weber and DiGiano, 1996; Gulipalli et al., 2011).

11.6.2.1 Pseudo first and second order models

The sorption data obtained from the equilibration of mixtures of 0.4 g of adsorbent and 50 ml of 8 mg/l fluoride solutions with initial pH 2 for 5, 10, 20, 30, 40 and 50 min at 298 K and shaking speed of 200 rpm were used. The order for the sorption process was tested by fitting the sorption data into the Lagergren pseudo-first and second order model (Lagergren, 1898). The pseudo-first-order plots didn't give a linear plot indicating the sorption of fluoride ions on diatomaceous earth is not a first-order process. It was therefore expedient to apply the pseudo-second-order model. The plot of values against time t gave a straight line ($R^2 = 0.992$) as shown in Figure 11.12. The closeness of the calculated q_e (0.2302) to the experimental q_e (0.2562) is an indication that fluoride sorption onto DE is a second-order process. As a result, fluoride is mainly chemisorbed onto DE as opposed to physisorption which is characterized by weak van der Waals forces. The results of the calculated pseudo-first-order and pseudo-second-order parameters are presented in Table 11.7.

Table 11.7. Pseudo-first-order and pseudo-second-order parameters

Time (min)	C_t	q_t	$q_e - q_t$	$\log (q_e - q_t)$	t/q_t
5	6.10	0.2375	0.0187	-1.728	21.0526
10	6.10	0.2375	0.0187	-1.728	42.1053
20	6.25	0.2187	0.0375	-1.426	91.4495
30	5.95	0.2562	0	-	117.096
40	6.10	0.2375	0.0187	-1.728	168.421
50	6.20	0.2250	0.0312	-1.506	222.222

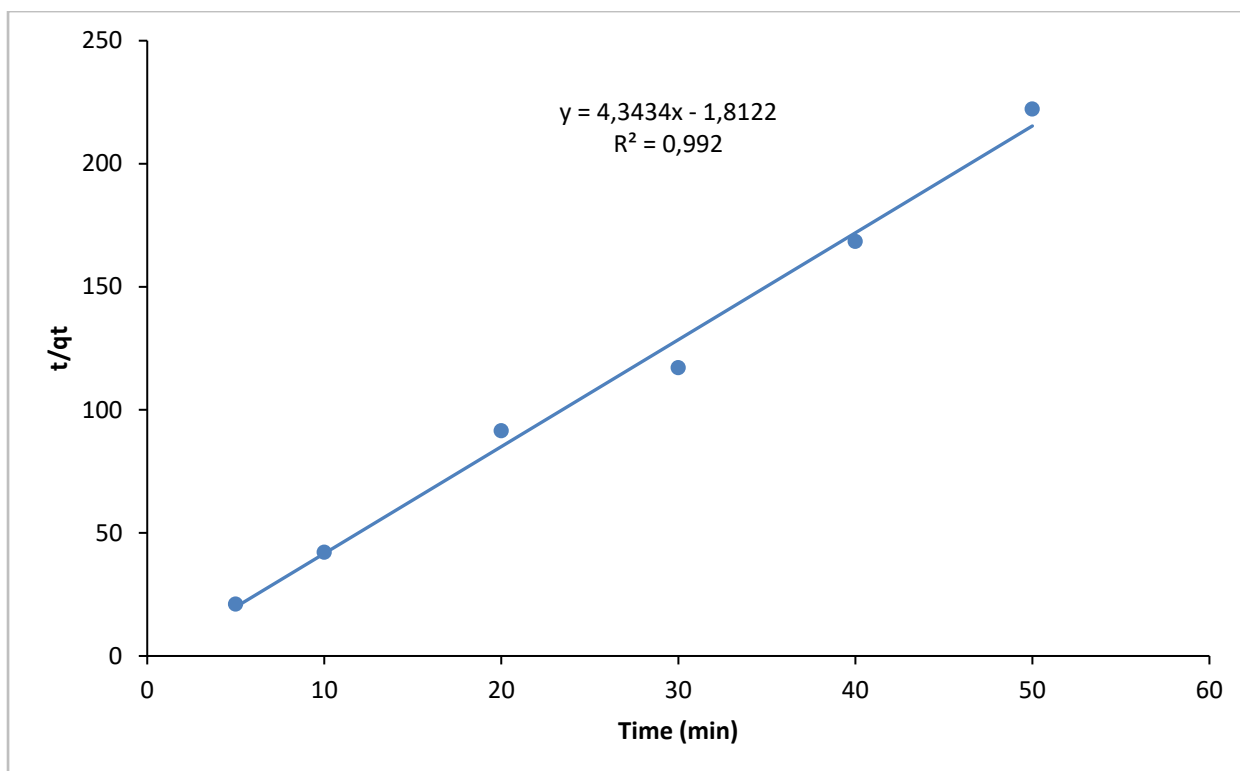


Figure 11.12. Pseudo-second-order plots for equilibration at different contact times (initial fluoride concentration: 8 mg/ℓ, volume of solution: 50 mℓ, adsorbent dosage: 0.4 g, initial pH: 2, temperature: 298 K and shaking speed: 200 rpm).

11.6.2.2 *Intra-particle diffusion model*

The possibility of intra-particle diffusion being the mechanism controlling the rate of adsorption of fluoride on diatomaceous earth was evaluated using the Weber-Morris model (Weber and Morris, 1963). If the plot of against is linear, then, the sorption process would be controlled only by intra-particle diffusion. However, the plots gave a sinusoidal curve (Figure 11.13), showing that the sorption rate was not likely controlled by intra-particle diffusion.

11.6.2.3 *External diffusion model*

The likelihood of external diffusion being the rate-controlling step was also tested using the model by Lee et al. (1999). If a straight line is obtained from the plot of against the adsorption time t , then, external diffusion controls the sorption process. The plot of against t for the first 30 min of sorption gave a straight line (Figure 11.14a) as described by Khraisheh et al. (2002). The linear plot obtained for the entire equilibration times (Figure 11.14b) is evidence that external diffusion was the rate-controlling mechanism for the sorption process.

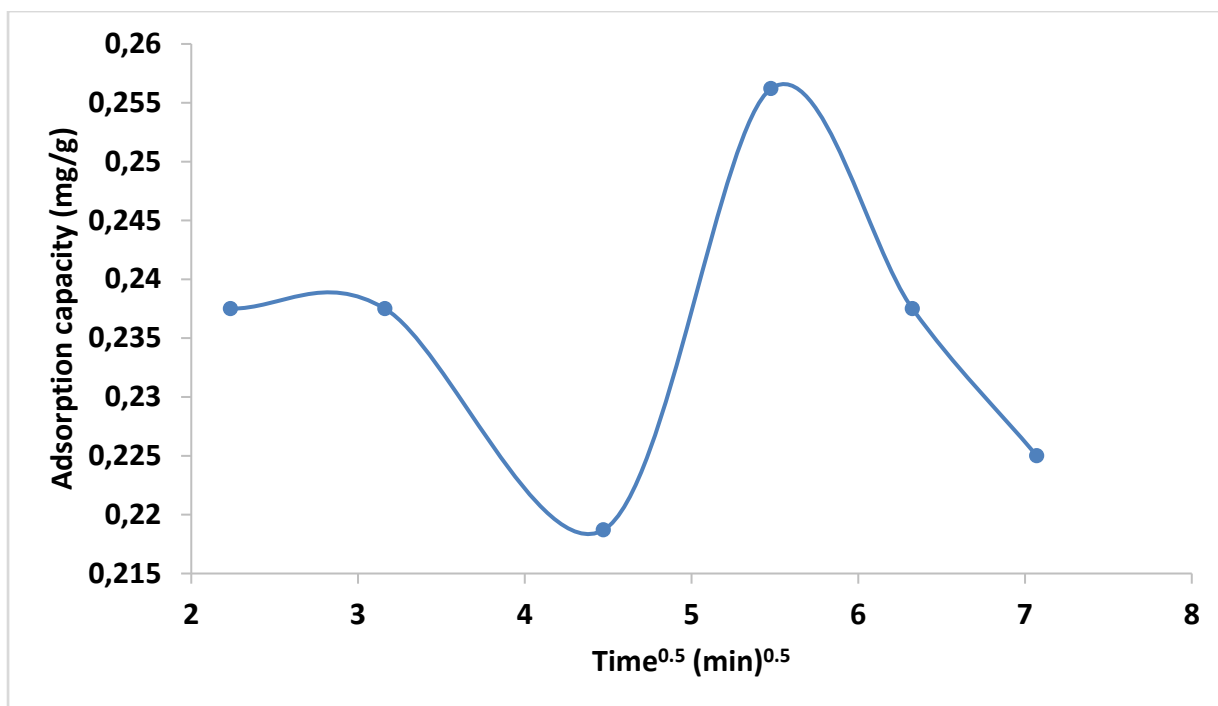


Figure 11.13. Verification of intra-particle diffusion using Weber-Morris model (initial fluoride concentration: 8 mg/l, volume of solution: 50 ml, adsorbent dosage: 0.4 g, initial pH: 2, temperature: 298 K and shaking speed: 200 rpm).

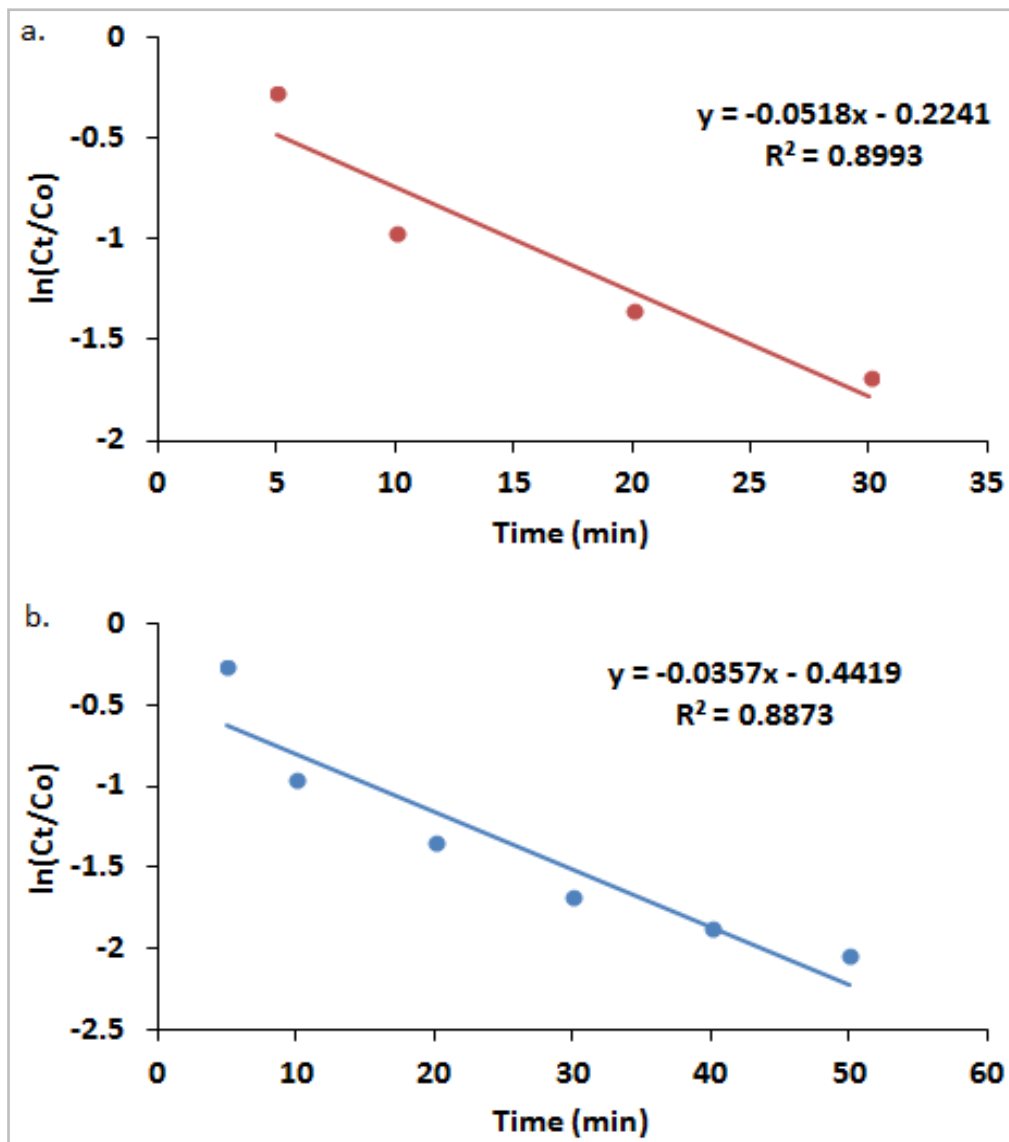


Figure 11.14. External diffusion plots a. for contact time up to 30 min and b. for all contact time (initial fluoride concentration: 8 mg/l, volume of solution: 50 ml, adsorbent dosage: 0.4 g, initial pH: 2, temperature: 298 K and shaking speed: 200 rpm).

11.7 EVALUATION OF METALS, NON-METALS AND ANIONS RELEASE FROM DIATOMACEOUS EARTH

The safety of the DE for use in defluoridation of drinking water was evaluated by determining the extent of metals and anionic chemical species released from the adsorbent into treated water at different equilibrium pH and contact times. The analysis of metals leached into treated water was necessary because of their toxic effect if concentrations exceed the limit recommended by SANS 241-1 (2015). The supernatants from the batch experiments of contact time (Figure 11.6) and initial pH (figure 6.8) were analysed for major and trace elements using inductively coupled plasma-mass spectrometer (ICP-MS). The results of the metal and non-metal species analysed are presented in Tables 11.8-11.11. It was observed that all the metal and non-metal species released from the adsorbent into treated water were at trace levels and so the use of the DE for defluoridation might not portend danger as far as metal and non-metal release is concerned. The concentration of each species released into water was virtually independent of contact time. The amount of each metal species released in water was a function of pH. The high concentrations of sodium observed were due to the NaOH used for necessary pH adjustment. The concentration of silicon in water was appreciably high at high equilibrium pH probably because of the increase in dissolution of silicon at high pH. The lowest silica dissolution was at the equilibrium pH of 2.05. Anions evaluated included Cl⁻, Br⁻, SO₄²⁻, PO₄³⁻, NO₂⁻ and NO₃⁻. Except for Cl⁻ whose average concentration was 391.3 mg/l in the supernatants because HCl was used to achieve an initial pH of 2.0, none of the anions was detectable by the instrument at a detection limit of 1 mg/l.

11.8 DEFLUORIDATION OF FIELD GROUNDWATER

The effectiveness of raw DE in fluoride removal from water was tested on a field groundwater (Siloam water) containing 6 mg/l F⁻ and 3 mg/l PO₄³⁻. The anions NO₃⁻, and SO₄²⁻ were not detected. A mixture of the field water and 0.4 g/50 ml of DE with initial pH 2 was equilibrated for 30 min at the shaking speed of 200 rpm. The concentrations of anions on dilution and after equilibration are reported in Table 11.12. The per cent fluoride removal was 14.6%. The reduction of PO₄³⁻ concentration from 2.4 to 1.4 mg/l, representing 41.7% phosphate removal is an indication that phosphate is a high competitor with fluoride in sorption onto DE.

Table 11.8. Concentrations of anions in raw and treated field groundwater

Anion	Concentration in raw field groundwater (mg/l)	Concentration in treated field groundwater (mg/l)
F ⁻	4.8	4.1
NO ₃ ⁻	ND	ND
PO ₄ ³⁻	2.4	1.4
SO ₄ ²⁻	ND	10

ND = Not detected.

Table 11.9. Concentration of chemical species in treated water at different initial pH values (mg/ℓ)

pH₀	pH_e	Al	Ca	Fe	K	Mg	Na	P	S	Si	Sr	B
2	2.05	9.25	16.76	0.11	21.09	1.12	45.69	0.06	0.26	9.92	0.12	<0.05
4	4.27	9.26	1.68	8.02	8.16	0.43	32.14	0.11	0.51	60.81	0.01	<0.05
6	6.30	5.29	0.66	7.44	4.44	0.32	25.80	0.10	0.42	48.84	0.00	<0.05
7	7.11	4.63	0.50	6.73	3.66	0.28	23.30	0.11	0.37	43.56	0.00	<0.05
9	7.62	5.20	0.60	6.91	3.34	0.30	24.35	0.09	0.22	43.22	0.01	<0.05
10	8.91	5.67	0.61	6.34	4.43	0.33	31.22	0.08	0.15	43.60	0.01	<0.05
11	10.59	15.98	1.49	18.37	8.34	1.00	74.26	0.12	0.17	104.50	0.02	<0.05
12	11.96	23.41	1.95	26.22	12.56	1.48	345.30	0.17	0.24	147.60	0.02	0.06

Table 11.10. Concentration of chemical species in treated water at different initial pH values (µg/ℓ)

pH₀	pH_e	Ti	V	Cr	Mn	Co	Ni	Cu	Zn	As	Se	Mo	Cd	Sn	Sb	Ba	Hg	Pb
2	2.05	2.15	3.26	0.39	237.57	0.60	5.27	4.49	21.51	0.53	0.67	<0.05	0.34	<0.04	0.03	50.03	<0.01	0.77
4	4.27	409.43	5.47	2.74	80.14	0.44	3.05	3.42	28.35	1.52	4.49	1.67	0.11	1.18	0.11	5.89	0.02	3.59
6	6.30	320.84	5.64	2.24	46.90	0.33	2.17	4.39	22.68	1.54	7.34	1.66	0.03	0.90	0.13	4.03	0.01	3.04
7	7.11	291.14	5.50	2.15	41.09	0.30	1.81	3.36	20.14	1.52	6.24	1.40	0.07	0.63	0.08	3.85	<0.01	2.80
9	7.62	290.08	5.49	2.17	43.02	0.39	1.86	3.55	21.90	1.63	4.47	1.39	0.15	0.68	0.23	3.26	0.02	2.70
10	8.91	329.39	5.59	2.20	42.65	0.37	2.06	3.94	23.22	1.93	7.46	1.25	0.07	0.87	0.13	4.69	0.02	3.15
11	10.59	882.62	16.56	5.10	116.89	0.97	5.01	8.28	66.93	3.11	14.80	3.20	0.08	3.65	0.13	11.89	0.02	7.86
12	11.96	1076.1	19.01	6.14	138.69	1.26	5.87	13.44	83.74	4.25	20.45	7.32	0.19	8.29	0.47	16.43	0.06	10.29

Table 11.11. Concentration of elements in treated water at different contact times (mg/ℓ)

Time (min)	Al	Ca	Fe	K	Mg	Na	P	S	Si	Sr	B
5	8.09	15.05	0.07	20.12	0.76	127.20	0.06	0.19	11.58	0.10	0.3591
10	8.04	15.39	0.08	20.45	0.83	118.10	0.04	0.17	11.39	0.11	0.3649
20	8.46	15.79	0.07	20.28	0.84	47.51	0.07	0.18	7.44	0.11	<0.05
30	9.25	16.76	0.11	21.09	1.12	45.69	0.06	0.26	9.92	0.12	<0.05
40	8.50	15.61	0.07	20.58	0.83	89.95	0.04	0.17	11.11	0.11	0.1831
50	8.60	15.61	0.07	20.30	0.87	45.18	0.03	0.16	10.03	0.11	<0.05

Table 11.12. Concentration of elements in treated water at different contact times (µg/ℓ)

Time (min)	Ti	V	Cr	Mn	Co	Ni	Cu	Zn	As	Se	Mo	Cd	Sn	Sb	Ba	Hg	Pb
5	1.30	2.96	0.47	175.84	0.47	4.62	11.75	19.42	0.58	0.08	<0.05	0.31	<0.04	0.07	19.55	<0.01	0.57
10	1.77	2.96	0.47	198.65	0.51	4.80	8.68	20.88	0.50	0.13	<0.05	0.38	<0.04	0.02	20.96	<0.01	0.55
20	0.84	2.54	0.34	203.26	0.47	4.61	4.14	18.30	0.48	0.17	<0.05	0.33	<0.04	0.03	18.13	<0.01	0.37
30	2.15	3.26	0.39	237.57	0.60	5.27	4.49	21.51	0.53	0.67	<0.05	0.34	<0.04	0.03	50.03	<0.01	0.77
40	1.25	2.47	0.41	199.54	0.48	4.51	5.95	21.42	0.43	0.14	<0.05	0.35	<0.04	0.02	19.69	<0.01	0.43
50	1.38	2.28	0.35	210.18	0.49	4.64	3.62	19.32	0.40	0.19	<0.05	0.36	<0.04	0.01	18.29	<0.01	0.36

11.9 SUMMARY

Physicochemical and mineralogical properties of raw diatomaceous earth (DE) have been ascertained and moreover its groundwater defluoridation potential evaluated. X-ray fluorescence analysis reveals that major component in diatomaceous earth is silica (83.1%), while Al_2O_3 and Fe_2O_3 are minor components while X-ray diffraction reveals that it is largely amorphous. Optimum defluoridation conditions were established through batch reactions. These were: contact time: 30 min, adsorbent dosage: 8 g/l, pH 2, temperature: 298 K and shaking speed: 200 rpm. For a solution with initial 8 mg/l F^- concentration, % fluoride removal at optimum conditions ranged from 23.4-25.6%. The sorption data could adequately be described by Freundlich isotherm model. Evaluation of the sorption kinetics showed that fluoride sorption process followed Lagergren pseudo second-order kinetics suggesting chemisorption mechanism of fluoride removal. Raw DE was observed to have low capacity for fluoride adsorption moreover, PO_4^{3-} in field water was observed to reduce its fluoride uptake capacity. ICP-MS analysis of treated water revealed that metal and non-metal species were released at trace levels. There was no detectable release of anions into water. Diatomaceous earth would be safe for application in defluoridation of groundwater since there is no danger of recontamination of product water. However, its low fluoride adsorption capacity and the fact that its optimum adsorption is at pH 2 will be a limitation in its application for household defluoridation devices. Surface modification to increase its fluoride adsorption capacity is recommended.

12 EVALUATION OF GROUNDWATER DEFLUORIDATION USING TRIMETAL MG/CE/MN OXIDE-MODIFIED DIATOMACEOUS EARTH

12.1 INTRODUCTION

In developing countries such as South Africa, most rural communities rely on groundwater as a source of drinking water (Ncube and Schutte, 2005). This is mainly due to inadequate supply of clean water or none at all. Surface waters in the rural areas are susceptible to pollution by human and animal faecal matter (Obi et al., 2002). Groundwater is usually free from pathogens that are characteristics of surface water if it is protected from contamination. While the consumption of groundwater reduced cases of water-borne diseases new problems emerged (Daw, 2004). One of the challenges of groundwater is high salinity and high fluoride in selected geological zones. Health impact associated with high fluoride in drinking water is fluorosis and is attributed to consumption of water with concentration > 1.5 mg/l. In the previous Chapter defluoridation potential of raw diatomaceous earth (DE) was evaluated. Obtained results indicated that raw diatomaceous earth (DE) has a low capacity for fluoride adsorption. In an attempt to increase its surface area and adsorption sites, this section investigates the use of metal oxides. Results presented in this section include;

- a. Optimization of synthesis conditions for Mg/Ce/Mn oxides impregnated diatomaceous earth.
- b. Fluoride adsorption potential/capacity of the Mg/Ce/Mn impregnated DE, optimization of adsorption conditions, adsorption isotherms and kinetics.
- c. Regeneration and reusability potential and chemical stability of Mn/Ce/Mn impregnated DE.

12.2 MATERIALS

All reagents and TISAB-III were obtained from Rochelle Chemicals & Lab Equipment CC, South Africa Ltd and they were of analytical grade. The DE for the study was obtained from natural deposits at Kariandusi in Gilgil District, Nakuru County, Kenya and a second supply sourced in South Africa. A stock solution containing 1000 mg/l fluoride was prepared by dissolving 2.21 g analytical grade sodium fluoride in 1 l of ultra-pure water (18.2 MΩ/cm). Fluoride solutions for batch experiments were prepared from fresh stock fluoride solution by appropriate dilution. A stock solution containing 1000 mg/l fluoride was prepared by dissolving 2.21 g NaF in 1 l of MilliQ water (18.2 MΩ/cm) and fluoride solutions for batch experiments were prepared from fresh stock fluoride solution by appropriate dilution. Field water was collected from a community borehole in Siloam, Vhembe district in South Africa.

12.3 METHODS

12.3.1 Preparation of solutions for DE modification

For the optimised modification of diatomaceous earth with Mg/Ce/Mn oxide, 50 ml of 0.25 M MgSO₄, 50 ml of 0.25 M CeCl₃·7H₂O and 100 ml of 0.25M MnCl₂·4H₂O solutions were prepared by dissolving 1.5046 g, 4.6573 g and 4.9478 g of the respective salts in MilliQ water in appropriate volumetric flasks and

then raising the volume to the etched mark by adding more MilliQ water. The flasks were stoppered and shaken to attain homogeneity.

12.3.2 Synthesis and optimization of synthesis conditions for pure Mg/Ce/Mn oxide and Mg/Ce/Mn oxide-modified diatomaceous earth

Synthesis of the pure oxides were initially prepared and their potential for fluoride adsorption and pH stabilization individually assessed. These were designated as follows: Ce oxide modified DE (Ce-DE) and Mn oxide modified DE (Mn-DE). This was done as part of the initial steps to establish which oxide played which part interms of fluoride adsorption and pH stability. After individual oxides were evaluated, next Ce/Mn bimetal oxide modified DE (Ce-Mn-DE) was prepared and tested for fluoride removal. In the third part of the synthesis process, the Ce/Mn bimetal oxide modified DE was then modified with Mg(OH)₂ in an attempt to stabilize the equilibrium pH at circum-neutral levels. The Mg(OH)₂ modified Ce/Mn bimetal oxide modified DE was prepared from a mixture of solutions of the salts of the three metal species at different proportions to obtain the optimum product (Table 12.1). The synthesised adsorbent was then characterised using several techniques (detailed in Appendix A). These included Cation Exchange Capacity (CEC), Point of Zero Charge (PZC), X-ray diffraction (XRD), X-ray fluorescence (XRF), Scanning Electron Microscopy (SEM), Scanning Electron Microscopy coupled with Energy Dispersive Spectroscopy (SEM-EDS), Transmission Electron Microscopy (TEM), Brunauer-Emmett-Teller (BET) and Fourier Transform Infrared (FTIR).

Table 12.1. Mixtures of salt solutions at different proportions

Volume of solution (mL)			Total volume (mL)
Mg ²⁺	Ce ³⁺	Mn ²⁺	
2.5	2.5	15.0	20
2.5	5.0	12.5	20
5.0	2.5	12.5	20
5.0	5.0	10.0	20
10	2.5	7.5	20
10	5.0	5.0	20

12.3.3 Batch and field groundwater adsorption experiments

Methods followed for batch and field fluoride adsorption studies are detailed in Appendix B. Equation 1 (Appendix C) was used to calculate the percentage of removal and adsorption capacity.

12.4 PHYSICOCHEMICAL AND MINERALOGICAL ANALYSIS OF THE TRIMETAL OXIDE MODIFIED DIATOMACEOUS EARTH

12.4.1 X-ray diffraction analysis (XRD)

Figure 12.1 shows the XRD spectra of Mg/Ce/Mn oxide-modified DE which indicates that the synthesized sorbent is an amorphous material.

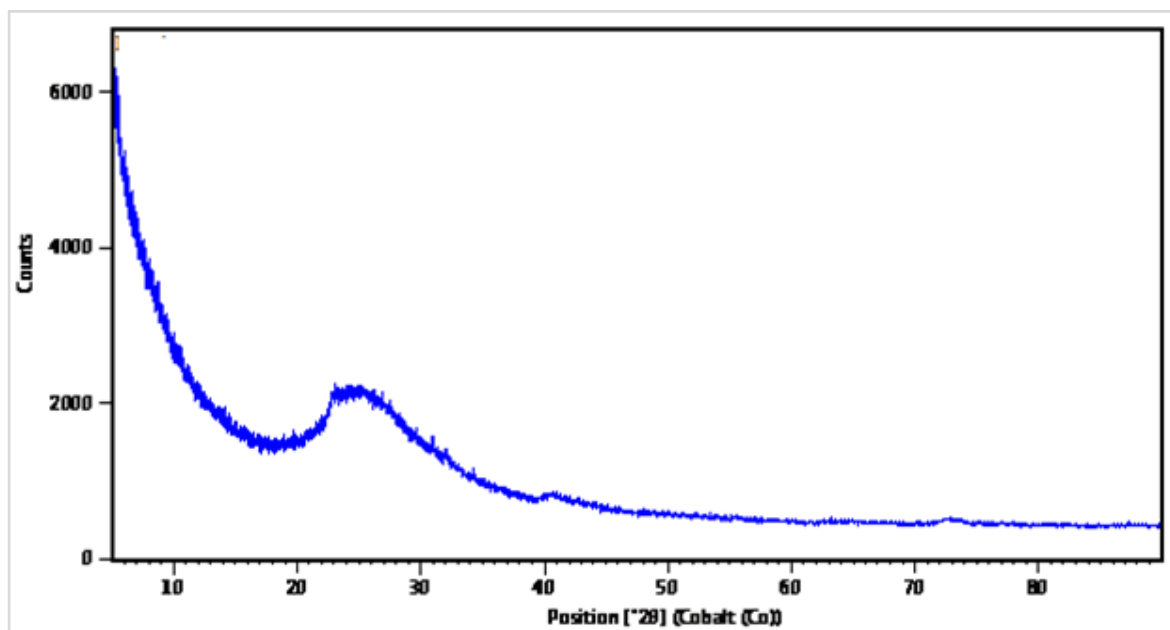


Figure 12.1. X-ray diffractogram of Mg/Ce/Mn oxide-modified diatomaceous earth.

12.4.2 Scanning electron microscopic analysis

Change in surface morphology on coating the DE with the trimetal oxide was examined by scanning the surface of the modified sorbent with scanning electron microscopy (SEM) (Hitachi X-650 scanning electron micro analyser equipped with CDU lead detector at 25 kV). The micrographs of the raw DE, trimetal oxide modified DE are presented in Figure 12.2. Coating of the raw DE with the trimetal oxide seems to mask the pores (Figure 12.2 e and f) as compared to raw (Figure 12.2 a and b). Scanning electron microscopy-energy dispersion X-ray (SEM-EDX) analysis of the surface shows increase in the average composition of Ce, Mg and Mn compared to raw DE (Figure 12.3). This confirms the loading of the oxides on the DE surface.

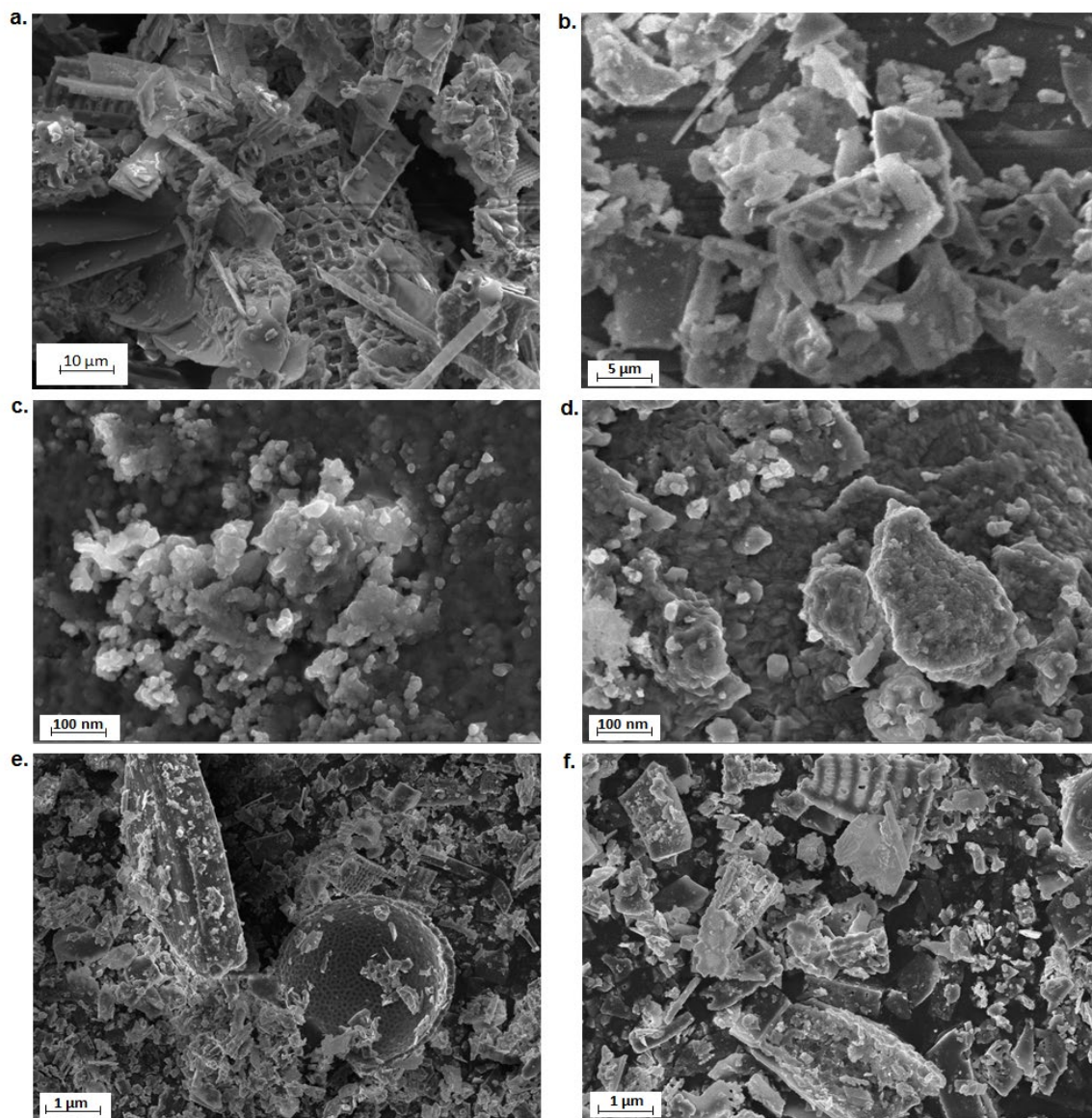


Figure 12.2. SEM images of raw diatomaceous earth (a and b), Mg/Ce/Mn oxide (c and d) and Mg/Ce/Mn oxide-modified diatomaceous earth (e and f).

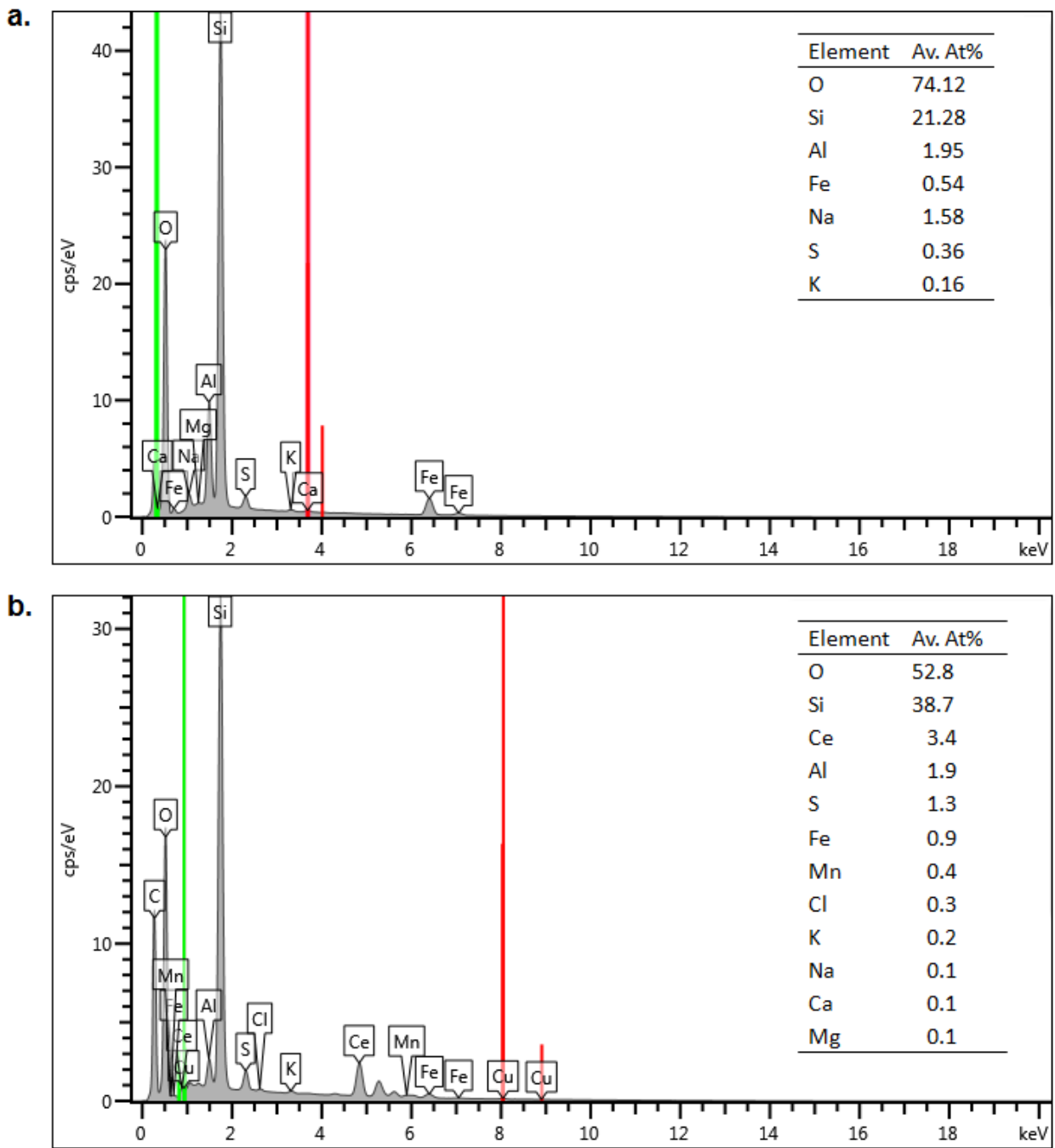


Figure 12.3. SEM-EDX spectra of a. raw diatomaceous earth and b. Mg/Ce/Mn oxide-modified diatomaceous earth.

12.4.3 High resolution transmission electron microscopic (HR-TEM) analysis

The structural integrity of the Mg/Ce/Mn oxide-modified DE was evaluated by High Resolution Transmission electron microscopy (HR-TEM) (JEM-2100 Transmission Electron Microscope). The micrographs are presented in Figure 12.4. Figure 12.4 a and b show aggregated particles of the Mg/Ce/Mn oxide, while Figures 12.3 c-f show the Mg/Ce/Mn oxide modified DE. The deposition of the trimetal metal oxide on the pores of the DE as indicated by the dark patches in the TEM images (Figure 12.4 b-f) indicates non-uniform deposition. The micrographs show the deposition was intense at some points and sparse at some. However, the noticeable dark patches are evidence that surface modification of DE occurred.

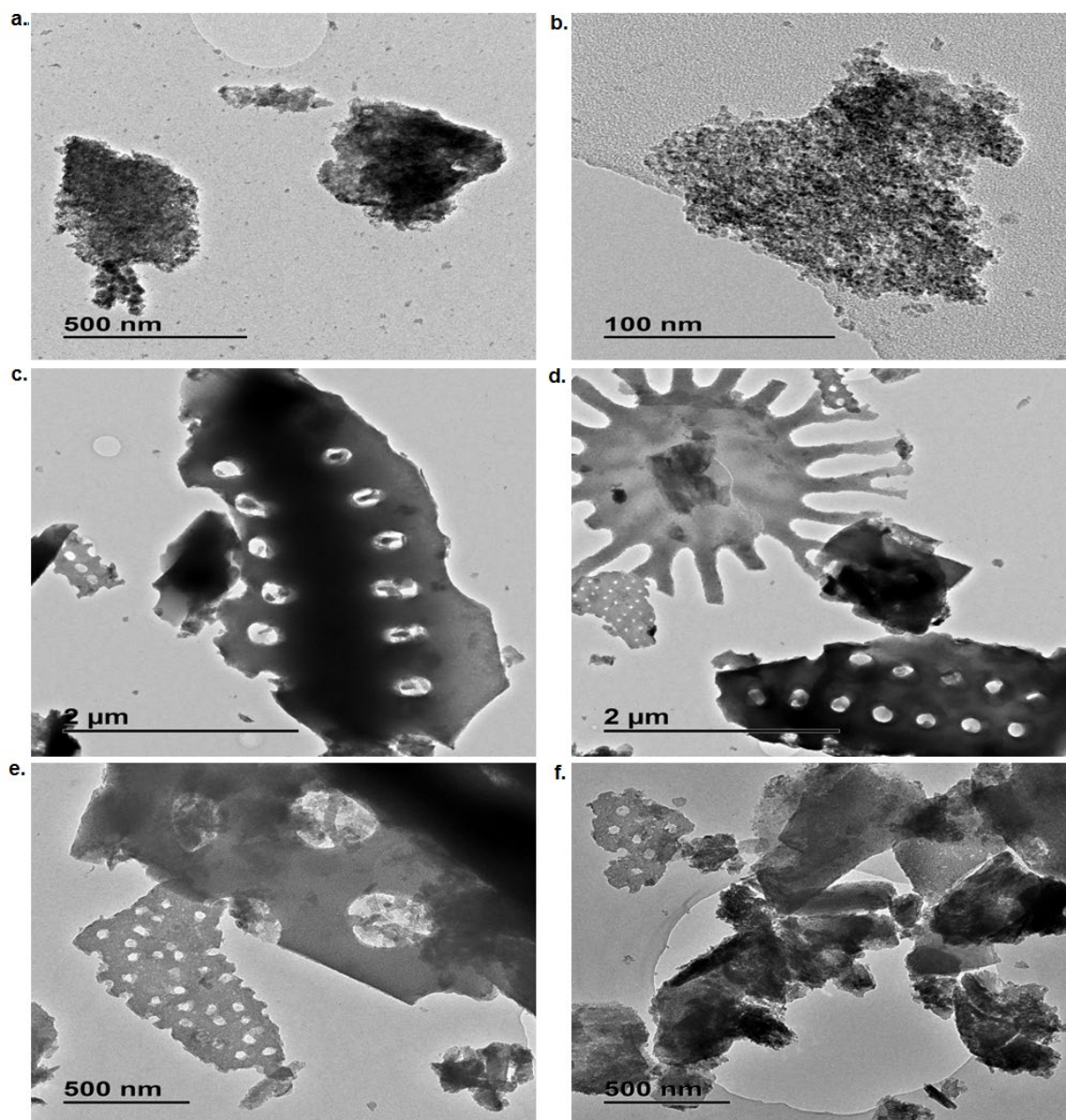


Figure 12.4. HR-TEM images of Mg/Ce/Mn oxide (a and b), Mg/Ce/Mn oxide-modified diatomaceous earth (c to f) and b to f.

12.4.4 Surface area analysis by Brunauer-Emmett-Teller method

The surface area and pore size of Mg/Ce/Mn oxide-modified DE were evaluated using the Brunauer-Emmett-Teller (BET) method (TriStar II *Surface Area and porosity*). Table 12.2 compares the values of the parameters evaluated for both raw and modified DE. There was a slight increase in the surface area of DE on modification. The increase in area was attributed to the deposits of the oxides on the surface and pores of DE. A plot of the pore volumes of the raw and modified sorbents (Figure 12.5) shows that the bulk of the pores lie within the mesopores range of 2-50 nm. Hence, the modified sorbent would be very permeable to water.

Table 12.2. Surface area, pore area and pore volume of the raw and Mg/Ce/Mn oxide-modified diatomaceous earth

Form of diatomaceous earth (DE)	Single point surf. area (m ² /g)	BET surf. area (m ² /g)	BJH adsorption cum. surf. area of pores (m ² /g)	BJH desorption cum. surf. area of pores (m ² /g)	Single point adsorption total pore vol. cm ³ /g)	BJH adsorption cum. vol. of pores (cm ³ /g)	BJH desorption cum. vol. of pores (cm ³ /g)
Raw DE	31.17	31.89	21.41	22.70	0.083	0.089	0.090
Mg/Ce/Mn oxide-modified DE	34.81	35.91	26.95	27.43	0.078	0.086	0.086

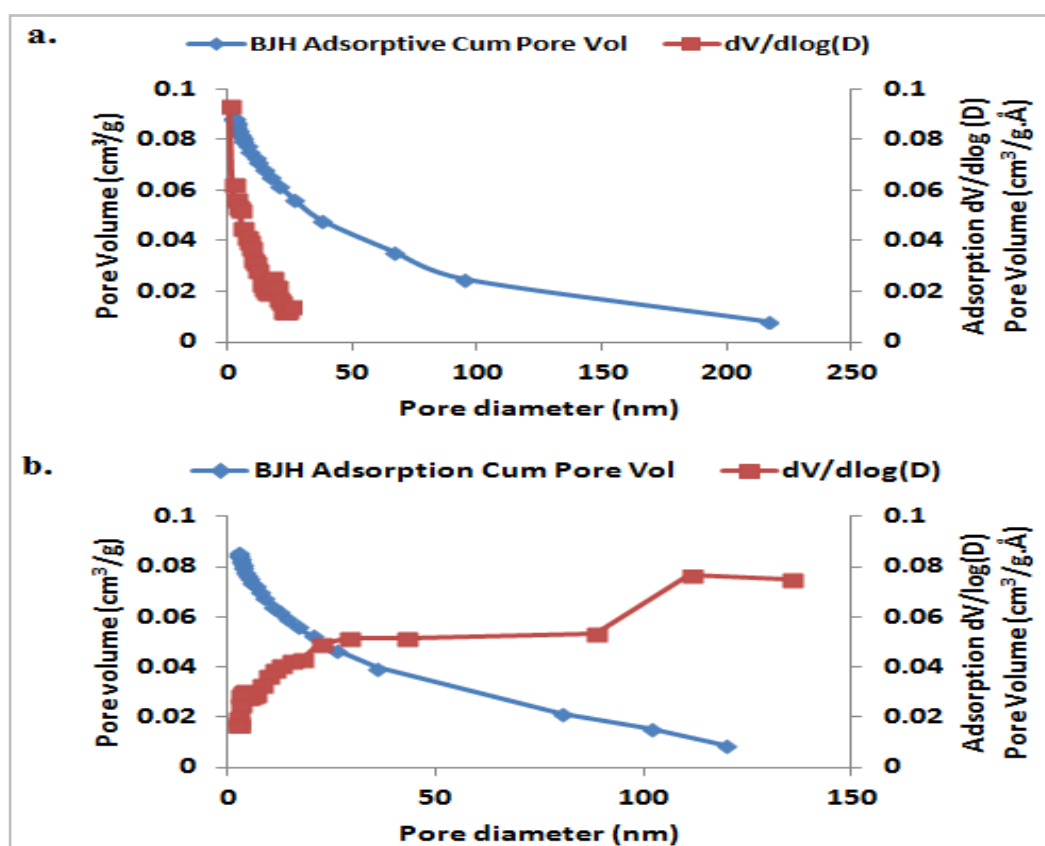


Figure 12.5. Plot of BJH adsorption pore volumes and BJH dV/dlog(D) pore volumes against pore diameter (D) for a. raw and b. Mg/Ce/Mn oxide-modified diatomaceous earth.

12.4.5 Fourier Transform Infra-Red (FTIR) Spectroscopy

The FTIR spectroscopic analysis of Mg/Ce/Mn oxide, Mg/Ce/Mn oxide-modified DE and fluoride-loaded modified DE were run to identify the functional groups in the materials as well as evaluate likely changes in the functional groups of the modified sorbent on contact with fluoride solution. The spectra of the trimetal oxide-modified and the fluoride-loaded DE are characteristically different from that of the pure Mg/Ce/Mn oxide. For the two, the fingerprints of the silica bands are distinct. It could therefore be readily observed from the spectrum of Mg/Ce/Mn oxide that the material has no silica component. Figure 12.6 shows that there was an increase in the transmittance of the band at the wavenumber 454 cm^{-1} for the modified DE. The band at 454 cm^{-1} represents the Si-O-H stretching vibration. With some of the OH groups replaced by fluoride ions, there was a decrease in the number of Si-O-H groups. Therefore, there was a decrease in the absorbance by the Si-O-H groups remaining. The bands around 3300 cm^{-1} for the three samples are for -OH from the adsorbed water molecules.

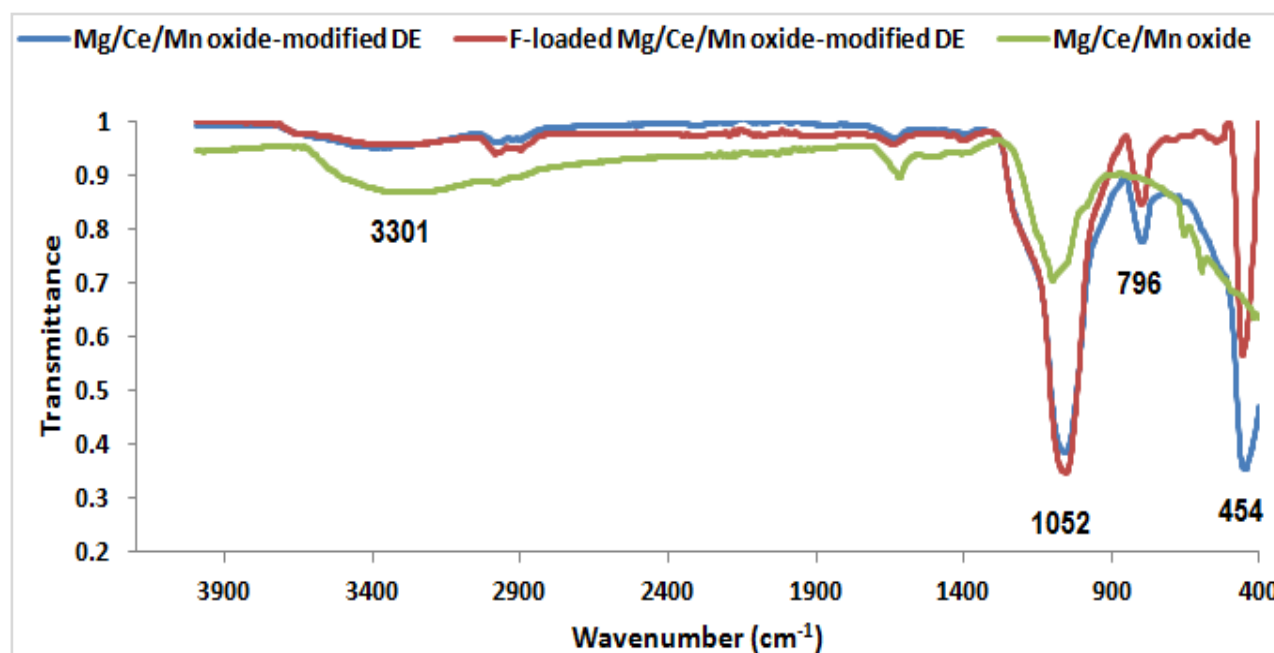


Figure 12.6. FTIR spectra of Mg/Ce/Mn oxide, Mg/Ce/Mn oxide-modified and F⁻ loaded Al/Fe oxide-modified diatomaceous earth.

12.4.6 pH at Point-of-zero-charge (pH_{pzc})

Figure 12.7 shows a plot of the change in pH ($p\Delta H = pH_e - pH_0$) against the initial pH. The pH_{pzc} is the abscissa at $p\Delta H$ equals zero. The pH_{pzc} at the evaluated KCl concentrations was 5.45.

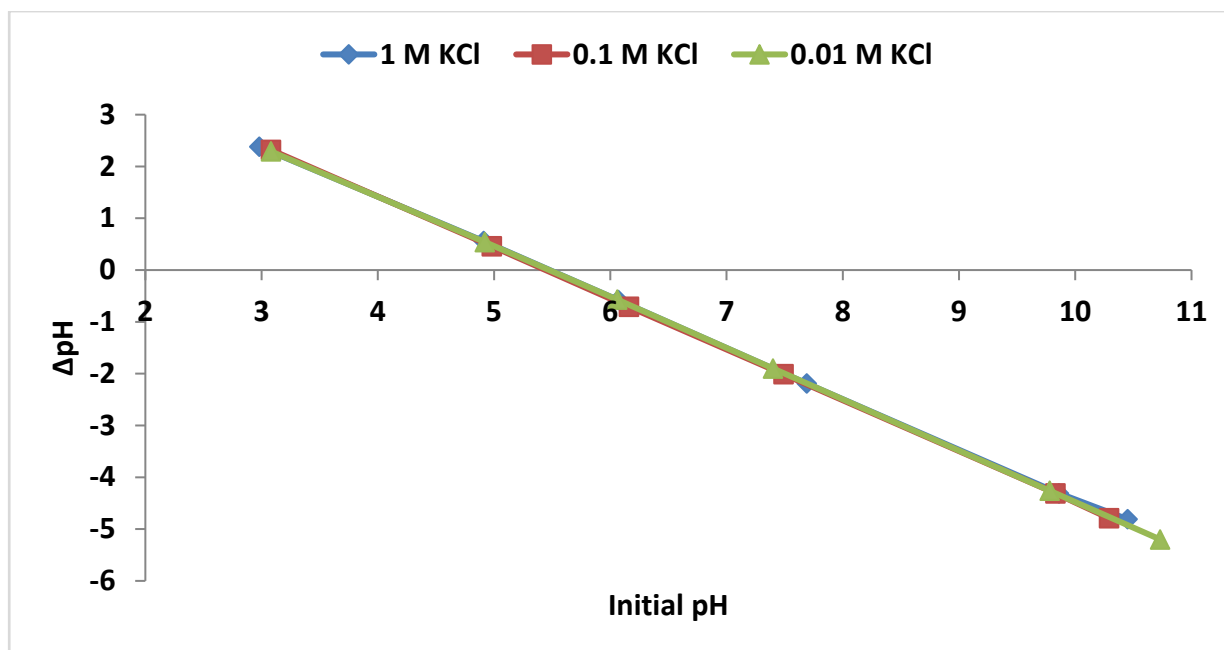


Figure 12.7. pH at point-of-zero charge of Mg/Ce/Mn oxide-modified DE evaluated in 1 M, 0.1 M and 0.01 M KCl (volume of solution: 25 ml, adsorbent dosage: 0.2 g, contact time: 24 h and shaking speed: 200 rpm).

12.4.7 Thermogravimetric analysis (TGA)

The thermograms of Mg/Ce/Mn oxide-modified DE and Mg/Ce/Mn oxide were compared by plotting the values of their per cent weight against the corresponding temperatures (Figure 12.8). It is observed that the trimetal oxide and the modified sorbent experienced loss in weight with increasing temperature. However, for the two samples, the second phase of weight loss did not occur at the same temperature. The second phase of weight loss began at $\approx 680^{\circ}\text{C}$ for Mg/Ce/Mn oxide while it was about 580°C for the Mg/Ce/Mn oxide modified DE. Beyond these respective temperatures there was possibly a near total loss of the constituent metal oxides. The almost constant weight noticeable for Mg/Ce/Mn oxide-modified DE from 680°C and above was due to the DE or silica content. There was no silica in the other sample. Hence, the sample showed the tendency of further weight loss. Therefore, the trimetal oxide-modified DE might not be suitable for use if calcined above 580°C .

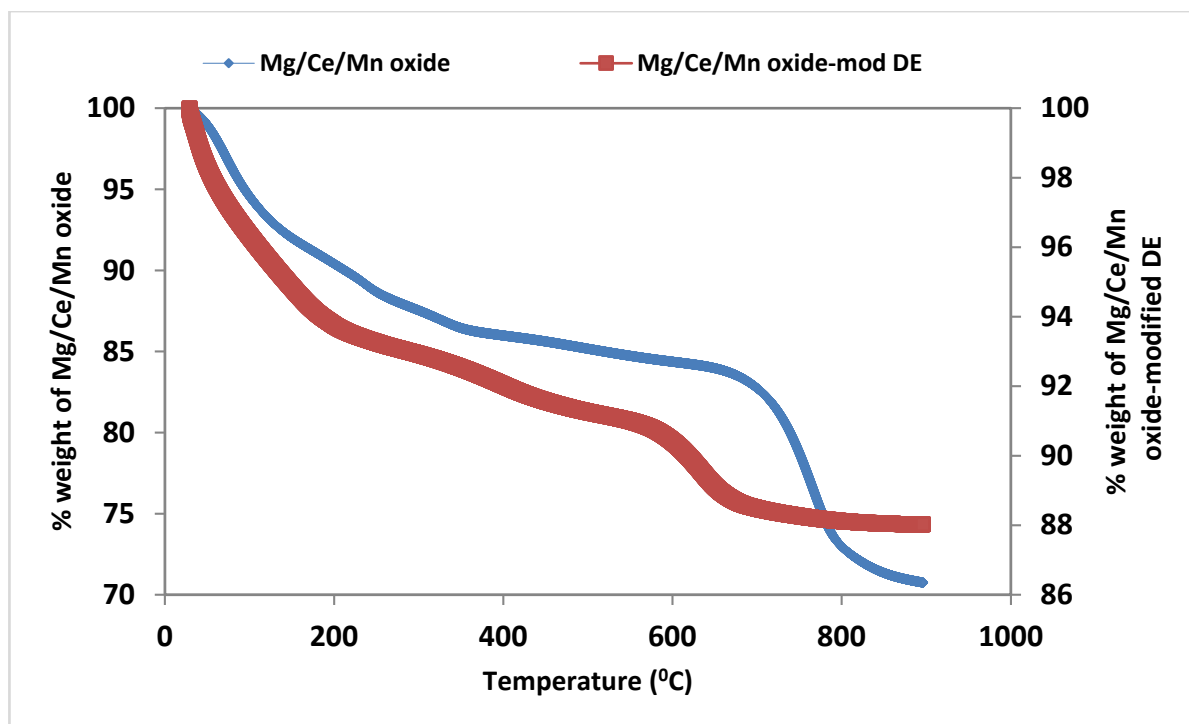


Figure 12.8. The thermograms of Mg/Ce/Mn oxide and Mg/Ce/Mn oxide-modified diatomaceous earth.

12.5 BATCH ADSORPTION EXPERIMENTS

12.5.1 Effect of contact time

The effect of contact time on fluoride removal was evaluated using three adsorbent dosages (0.1 g, 0.2 g and 0.3 g). The results of the per cent fluoride removal and the adsorption capacities with contact time are presented in Figure 12.9 a and b, respectively. There is no significant difference in the per cent fluoride removal at the contact times for the three evaluated dosages. At 20 min the system appears to attain equilibrium.

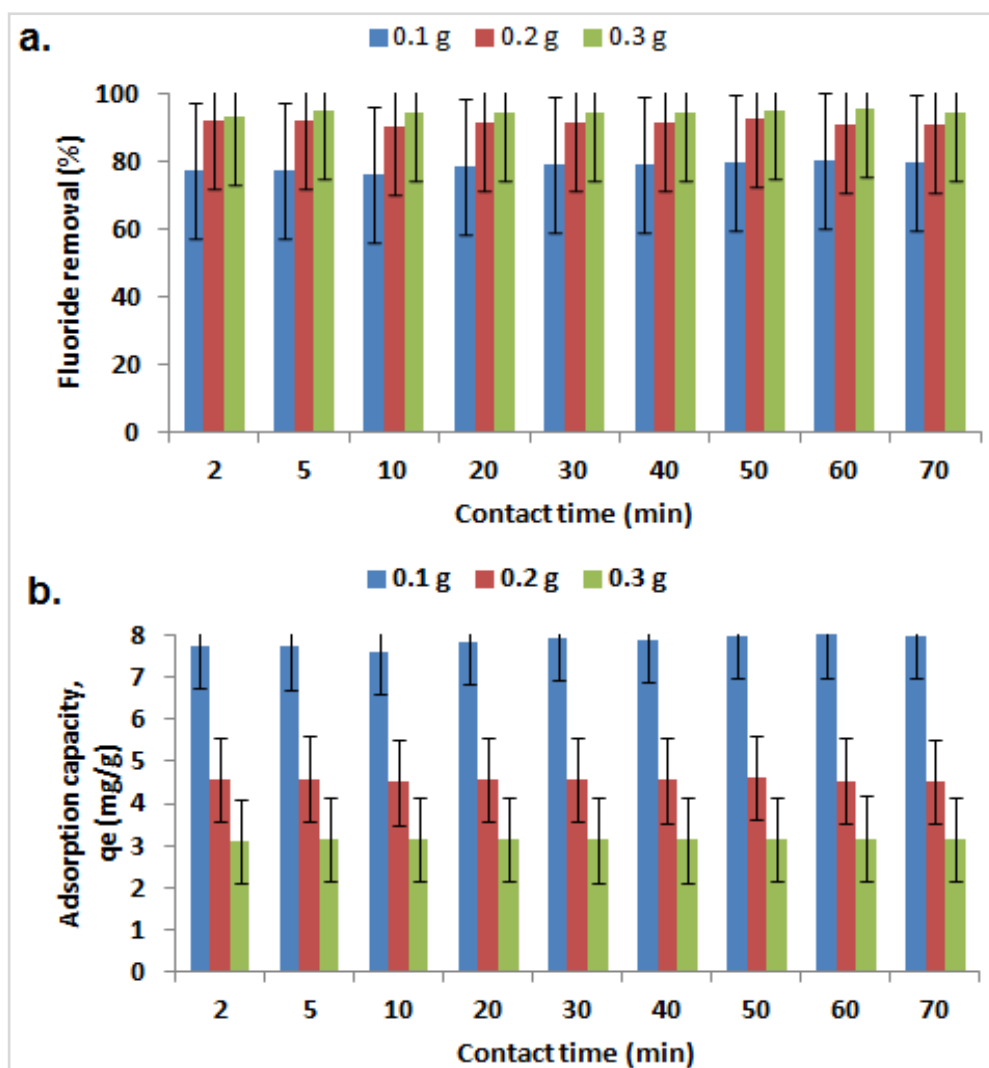


Figure 12.9. Variation of a. Per cent fluoride removal and b. adsorption capacity with contact time at various adsorbent dosages (initial fluoride concentration: 10 mg/l, volume of solution: 100 ml, shaking speed: 200 rpm and temperature: 297 K).

12.5.2 Effect of adsorbent dosage

Table 12.3 and Figure 12.10 shows the results of the equilibrium concentrations, the per cent fluoride removal and the adsorption capacities at various sorbent dosages. There was a quantitative rise in the per cent fluoride removal with increase in sorbent dosage from 0.1 g to 0.3 g (80.0% to 95.4%). There was only a marginal increase in the percent fluoride removal above a dosage of 0.3 g; the removal being 95.9% and 98.0% for dosages of 0.4 g and 1 g respectively, accounting for incremental difference of approximately 2%. As the sorbent dosage was being increased from 0.1 g to 0.3 g, the number of active sites for fluoride sorption was increasing. Above 0.3 g, there was overlap of active sorption sites that offered mass transfer resistance hence no significant change in adsorption. The adsorption capacity reduced expectedly as the sorbent dosage increased again due to resistance in mass transfer due to overlap of adsorption sites.

Table 12.3. Percent (%) fluoride removal and adsorption capacity at various adsorbent dosages

Adsorbent dosage (g)	C_e (mg/l)	% F- removal	q_e (mg/g)	pH_0	pH_e
0.1	2.00	80.0	8.00	6.58	6.38
0.2	0.92	90.8	4.54	6.27	6.21
0.3	0.46	95.4	3.18	6.23	6.31
0.4	0.42	95.9	2.40	6.29	6.13
0.6	0.34	96.7	1.61	6.20	6.18
0.8	0.25	97.6	1.22	6.19	6.18
1.0	0.20	98.0	0.98	6.22	6.17

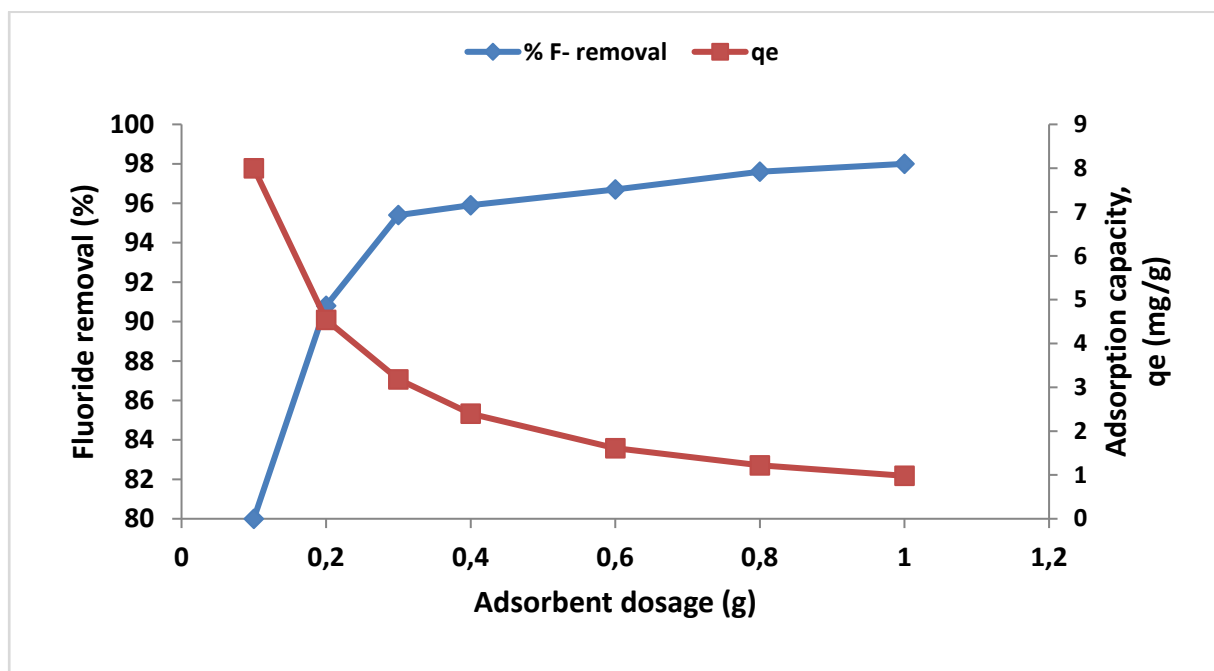


Figure 12.10. Per cent fluoride removal and adsorption capacity as a function of adsorbent dosage (initial fluoride concentration: 10 mg/l, contact time: 60 min, shaking speed: 200 rpm and temperature: 297 K).

12.5.3 Effect of adsorbate concentration

The effect of adsorbate concentration on fluoride adsorption by the trimetal oxide-modified DE was evaluated at temperatures of 297 K, 310 K and 326 K. Figure 12.11 shows the trends in the variation of per cent fluoride removal and adsorption capacity with the equilibrium concentration. The per cent fluoride removal increased slightly with increase in the initial fluoride concentration from 10 to 30 mg/l. However, the increase in fluoride removal was only marginal leading to a cluster of points up to the initial fluoride concentration of 50 mg/l (data not shown).

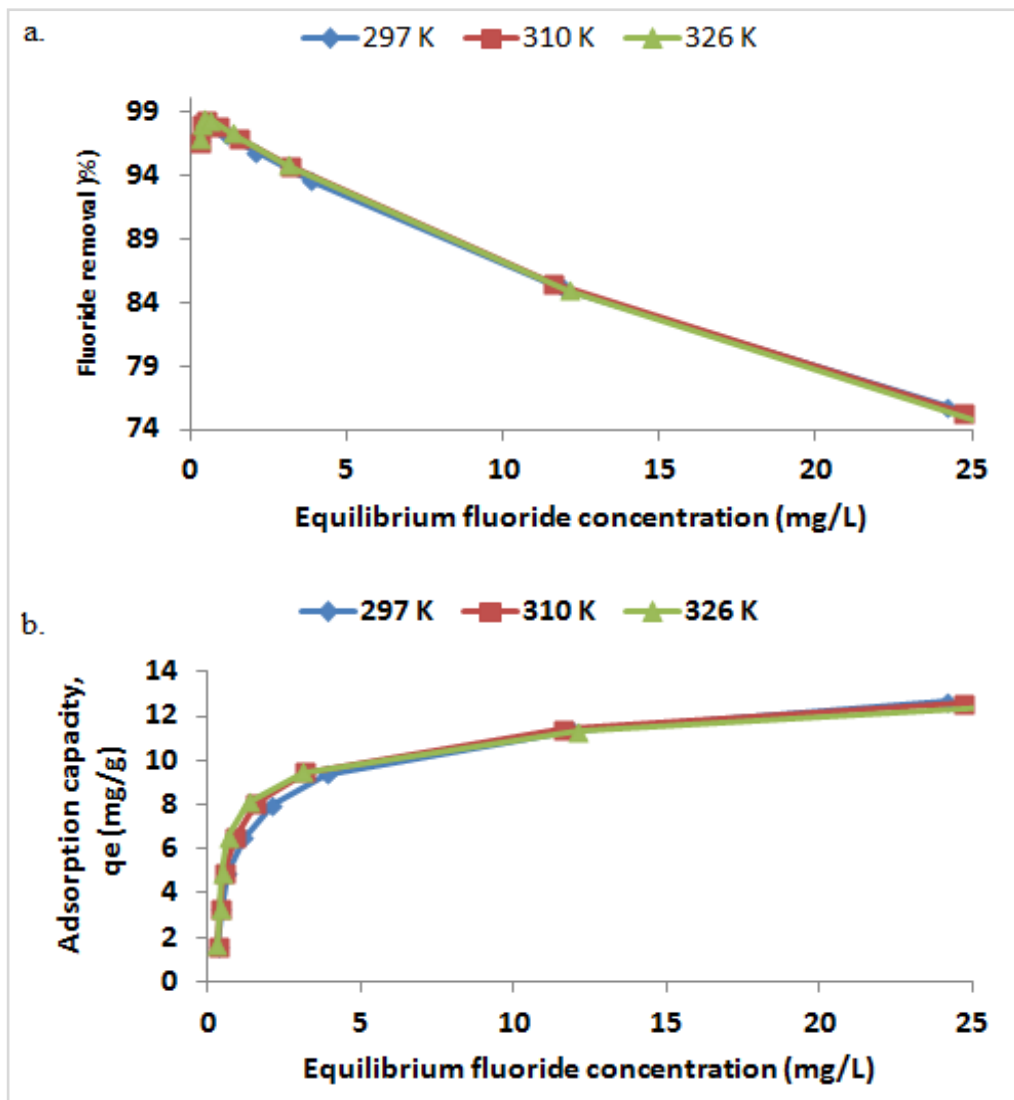


Figure 12.11. Variation of a. per cent fluoride removal and b. adsorption capacity with equilibrium fluoride concentration at different temperatures (contact time: 60 min, volume of solution: 100 mL, and shaking speed: 200 rpm).

Within the range of 10-50 mg/l fluoride, the per cent fluoride removal was directly related to the initial concentration of fluoride. Fluoride concentration was a driving force for fluoride removal. The percent fluoride removal decreased as the initial fluoride concentration increased above 50 mg/l. This was because the active sorption sites on the adsorbent surface were getting close to being saturated with adsorbed fluoride. The fluoride removal pattern was the same at the three evaluated temperatures. The adsorption capacity of the adsorbent increased significantly as the equilibrium fluoride concentration increased and tending toward a constant value at the higher fluoride concentrations. The adsorbent was nearing saturation at higher fluoride concentrations and hence the reduction in the steepness of the curve. The optimum adsorption capacities were obtained for solutions with the initial concentration of 100 mg/l at the three evaluated temperatures.

12.5.4 Effect of pH

The effect of pH on fluoride removal was evaluated by varying the initial pH of the fluoride solution in the range of 2-12 by addition of 0.1 M HCl or 0.1 M NaOH. Experiments were carried out at a temperature of 297 K. Table 12.4 and Figure 12.12 show the per cent fluoride removal as a function of both initial and equilibrium pH of solutions. The highest fluoride removal (96.6%) was obtained for the fluoride solution with initial pH 3.91 (equilibrium pH = 6.07). The value was however not appreciably different from those of other solutions whose equilibrium pH values were within a close range. Fluoride removal was low (61.6%) for the fluoride solution with initial pH 2.05 (equilibrium pH = 2.56). The lowest fluoride removal of 4% was obtained at high equilibrium pH of 11.06. For the defluoridation of groundwater, the most appropriate initial pH range of water with the use of the adsorbent is approximately 4-9. Below or above this pH range there would be low fluoride removal. The p_Hpzc of Mg/Ce/Mn oxide-modified DE is evaluated to be 5.45. It therefore follows that the surface of sorbent was negatively charged in solutions at which the equilibrium pH was greater than p_Hpzc. Fluoride removal would be ion-exchange in which the hydroxyl ions at the surface were being exchanged for the fluoride ions. In the sorbent composite, the dominant metal oxide/hydroxide responsible for fluoride removal is Ce oxide/hydroxide as reported in Table 12.4.

Table 12.4. Percent fluoride removal at different solution pH values

pH ₀	pH _e	C _e (mg/ℓ)	% F ⁻ removal
2.05	2.56	3.46	61.6
3.91	6.07	0.30	96.6
6.49	6.18	0.40	95.6
9.02	6.24	0.41	95.4
11.00	6.98	0.79	91.3
12.02	11.06	8.64	4.00

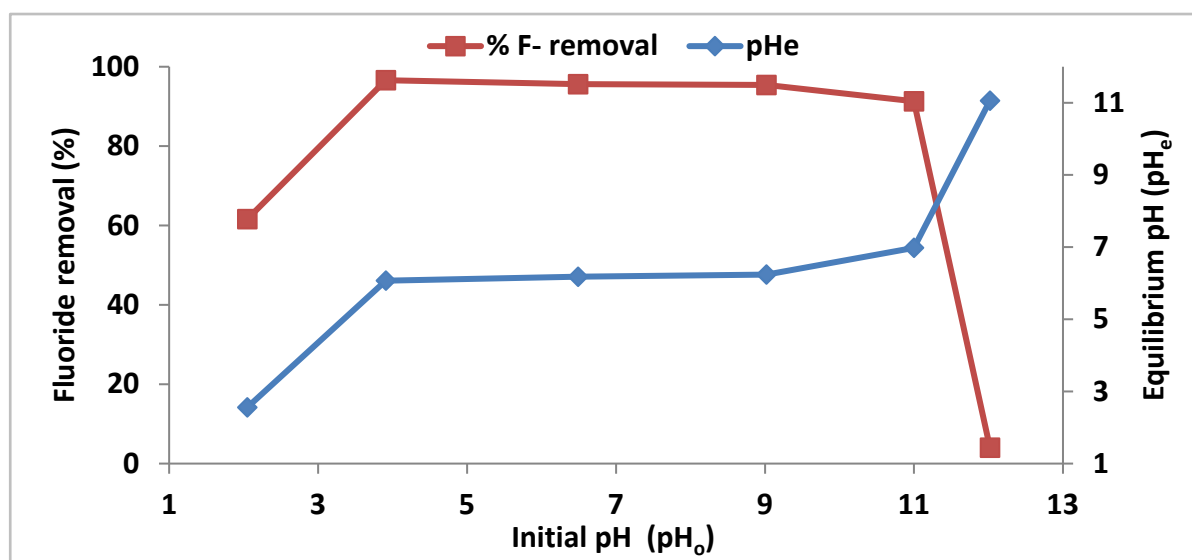


Figure 12.12. Fluoride removal as a function of initial solution pH (initial fluoride concentration: 9 mg/ℓ, volume of solution: 100 mL, contact time: 60 min, shaking speed: 200 rpm and temperature: 297 K).

12.5.5 Effect of temperature

The effect of temperature on fluoride sorption was evaluated at 297 K, 310 K and 326 K. The per cent fluoride removal was equal at all evaluated temperatures. The same trend was observed for the adsorption capacity at different fluoride concentrations and temperatures (Figure 12.13). Change in temperature therefore had no effect on the fluoride sorption.

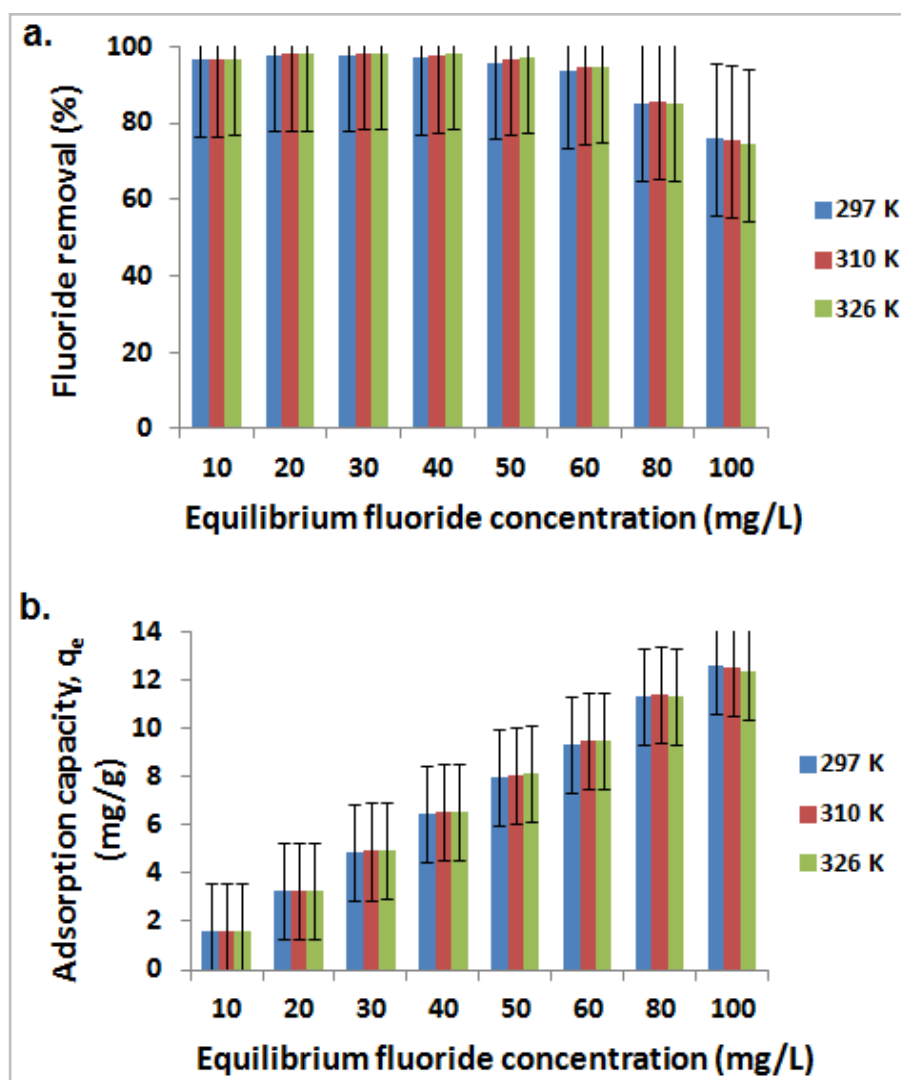


Figure 12.13. Variation of a. per cent fluoride removal and b. adsorption capacity with temperatures (contact time: 60 min, volume of solution: 100 mL, and shaking speed: 200 rpm).

12.5.6 Effect of co-existing anions

The effect of each of the anions Cl^- , NO_3^- , CO_3^{2-} , SO_4^{2-} and PO_4^{3-} on fluoride sorption was evaluated at separate defluoridation experiments. At the end of equilibration, the supernatants obtained after centrifuging mixtures were analysed for fluoride. The blank of the determination was the competing anion-free solution. Hence, the per cent fluoride removal in the blank was the optimum value. The percent fluoride removal varied with the type of anion (Figure 12.14 and Table 12.5). The presence of Cl^- , NO_3^- and SO_4^{2-} in solution was observed to enhance fluoride removal as the amount of fluoride removed increased slightly. CO_3^{2-} appeared to be competing with fluoride in solution as it lowered the amount of fluoride removal slightly from 96.7% to 95.3%. The presence of PO_4^{3-} in solution had no effect on fluoride removal. The equilibrium pH ranged between 6.17 and 6.28.

Table 12.5. Percent fluoride removal in the presence of co-existing anions (Initial 10 mg/ℓ F⁻)

Co-existing anion	Equilibrium F ⁻ Concentration (mg/ℓ)	% F ⁻ removal	pH _o	pH _e
Blank	0.332	96.7	6.20	6.18
Cl ⁻	0.237	97.6	6.34	6.22
CO ₃ ²⁻	0.473	95.3	6.34	6.28
NO ₃ ⁻	0.274	97.3	6.28	6.18
SO ₄ ²⁻	0.247	97.5	6.41	6.17
PO ₄ ³⁻	0.340	96.6	6.15	6.22

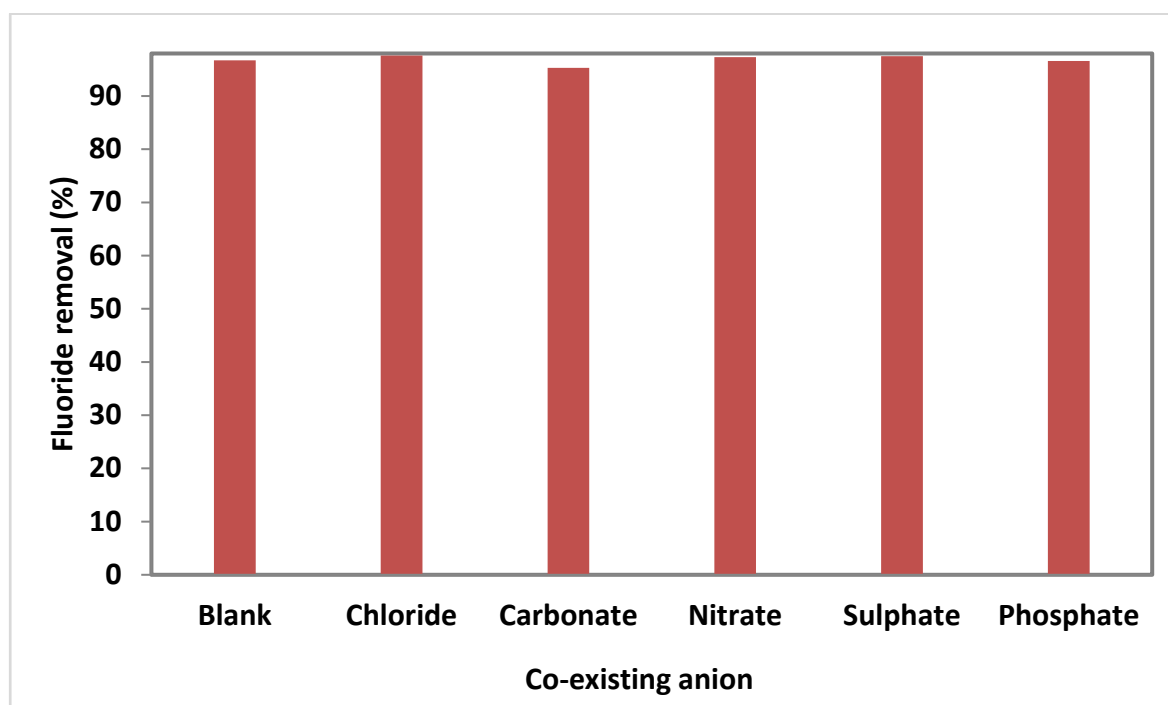


Figure 12.14. Per cent fluoride removal in the presence of co-existing anions (initial F⁻ concentration: 10 mg/ℓ, initial anion concentration: 5 mg/ℓ, volume of solution: 100 mL, contact time: 60 min, shaking speed: 200 rpm and temperature: 297 K).

12.6 ASSESSMENT OF METAL LEACHING FROM SORBENT AT VARIOUS EQUILIBRIUM PH VALUES

The chemical stability of the adsorbent is a crucial factor during the adsorption process. This is important to avoid secondary contaminant of the treated water. Supernatants from the batch adsorption experiments on effect of pH were subjected to ICP-MS analysis to quantify the chemical species released into solution at pH of media employed. The results of leachability of the chemical species used in modification of the DE are presented in Figure 12.15. The most leached metal at all the pH values was cerium. The loss was as high as 202.27 mg/l at the lowest pH. There was no difference in the amounts of manganese leached at pH range 6.07-6.24. Lowest loss of 0.12 mg/l for Mn was observed highest equilibrium pH 11.06. Magnesium was probably completely in the form of $Mg(OH)_2$ at this pH. Generally, metal leaching increased as the solution pH decreased. The order of loss of metals was $Ce > Mn > Mg$. Residual Mg was below SANS limits while Mn was above the limits. SANS doesn't give any guidelines limits for Ce in drinking water.

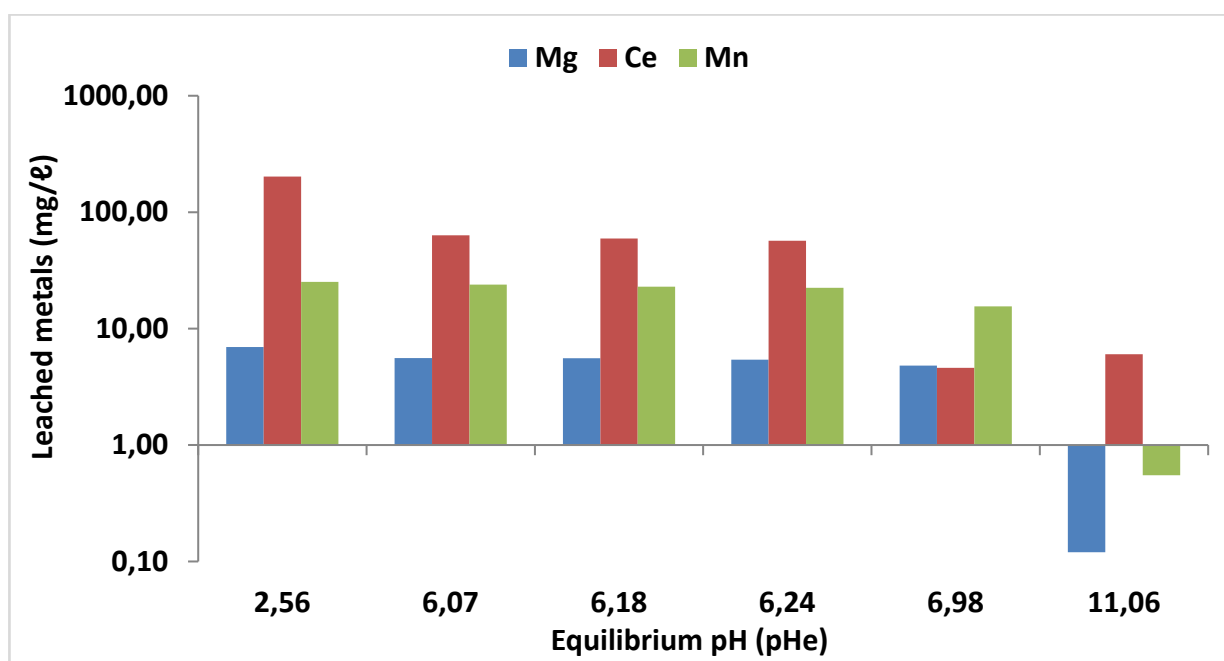


Figure 12.15. Concentration of leached metals as a function of equilibrium pH (initial fluoride concentration: 9 mg/l, volume of solution: 100 ml, contact time: 60 min, temperature: 297 K and shaking speed: 200 rpm).

12.7 DEFLUORIDATION OF FIELD WATER

The concentration of fluoride in field water was reduced from 5.53 to 0.40 mg/l after 100 ml of the water was contacted with 0.6 g of adsorbent for 60 min. Thus, the per cent fluoride removal was 83.2%. The initial and equilibrium pH values were 6.92 and 6.80 respectively. The concentrations of the various parameters evaluated in raw and treated water are reported in Table 12.6.

Table 12.6. Concentrations of competing anions in raw and treated field water

Anion in water	C_o (mg/ℓ)	C_e (mg/ℓ)	% anion removal	SANS 241-1 (2015) (mg/ℓ)
F ⁻	5.53	0.40	92.8	<1
Cl ⁻	31.60	65.14	-106.1	<200
Br ⁻	2.08	ND	≈100	-
NO ₃ ⁻	1.13	ND	≈100	<50
SO ₄ ²⁻	11.90	80.88	-580	<400
PO ₄ ³⁻	ND	ND	-	-

ND: Not detected

It is observed that the adsorbent removed all the competing anions except chloride and sulphate below the detection limits. The increase in the concentration of chloride in the treated water was as a result of the leaching of the chloride from the adsorbent. The source could be the HCl used in the treatment of the raw DE and sulphate salts used for modification of the DE. The full chemical analysis of the field water before and after defluoridation is presented in Figures 12.16 and 12.17. All chemical species evaluated in the raw and treated field water were below SANS 241-1 (2015) and WHO guidelines for Drinking-water Quality (WHO, 2011) except for Mn.

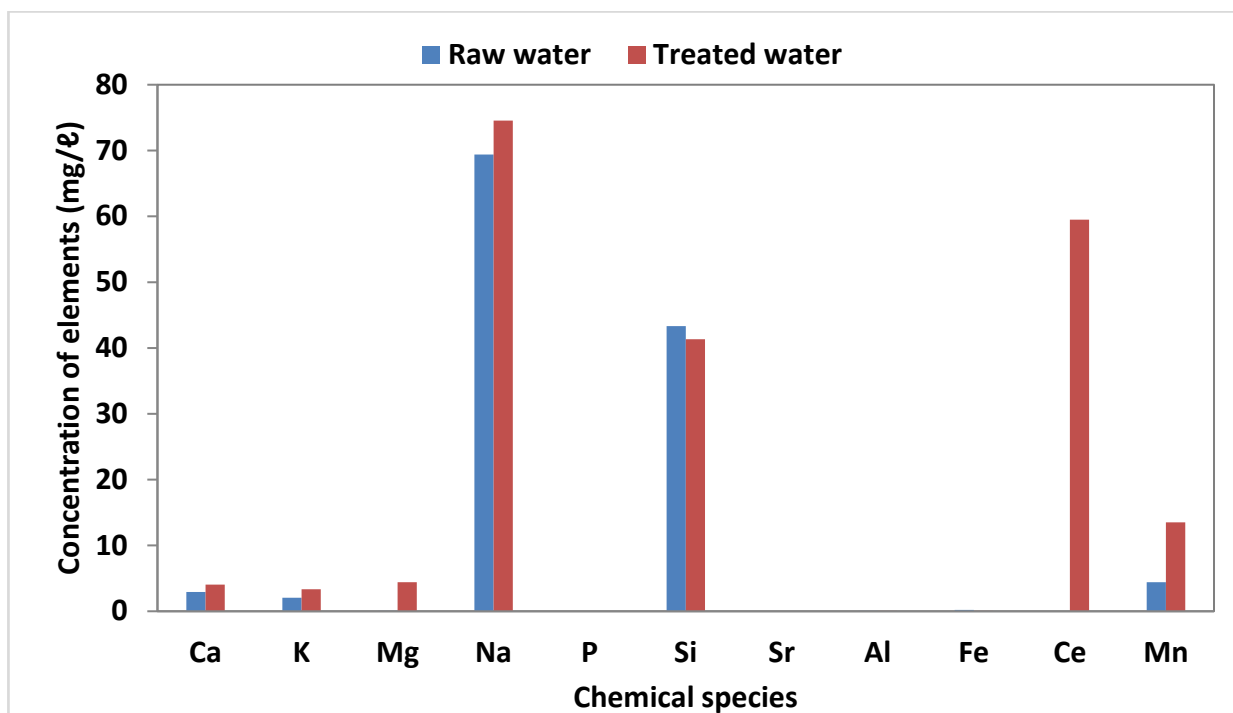


Figure 12.16. Concentrations of elements in treated field water in mg/ℓ

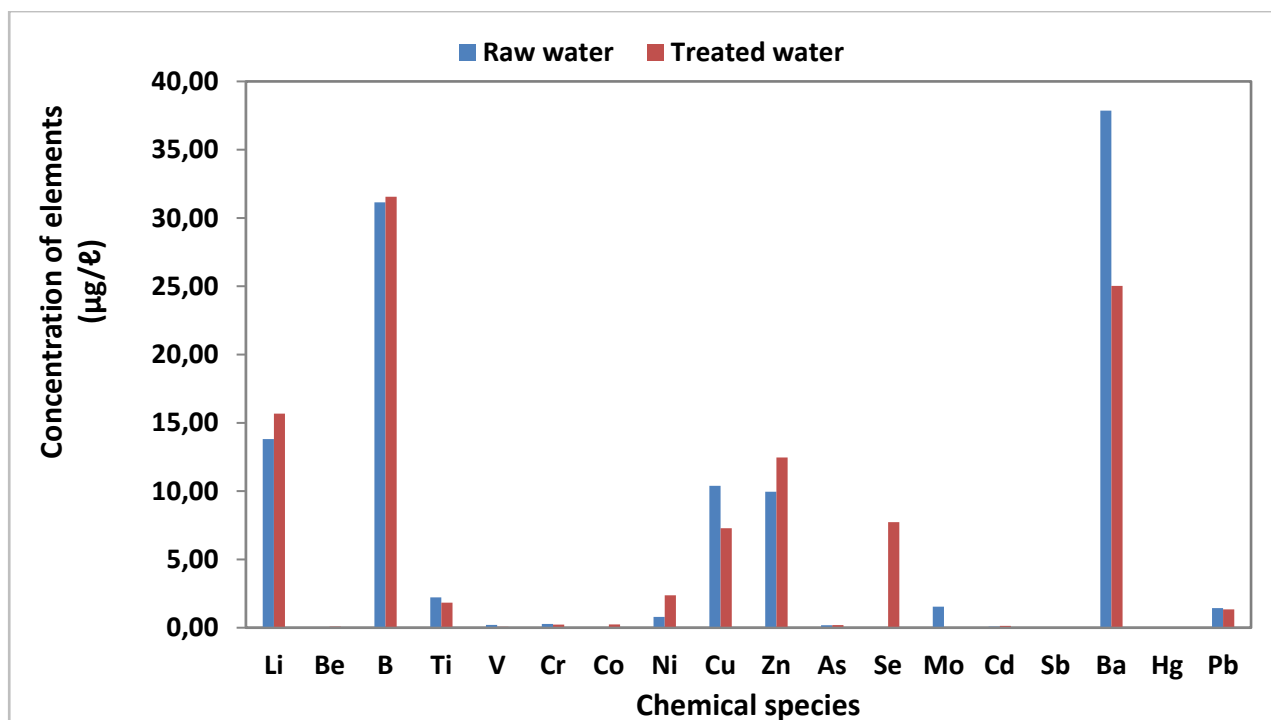


Figure 12.17. Concentrations of elements in treated field water in µg/ℓ (volume of water: 100 mℓ, adsorbent dosage: 0.6 g, contact time: 50 min, shaking speed: 200 rpm).

12.8 REGENERATION AND REUSABILITY OF SPENT SORBENT

The results of regeneration and reusability of the spent adsorbent are presented in terms of percent fluoride removal (Figure 12.18). Regeneration of spent sorbent using 0.01 M NaOH appeared inappropriate because of the appreciable loss of silica at high pH. This implies that there was high loss of the support material for the Mg/Ce/Mn oxide. With the use 0.01 M NaOH solution, the difference between the values of per cent fluoride removal at the first and second defluoridation cycles was too high; a reduction from 97.6 to 15.0% confirming significant loss in adsorption capacity. The low trend of fluoride removal with regenerated sorbent continued until the fourth cycle. NaOH was therefore observed to be a poor regenerant for the adsorbent. The performance of the spent sorbent regenerated with 0.1 M K₂SO₄ solution in defluoridation was fairly better than that observed with the use of 0.01 M NaOH. The values of per cent fluoride removal at the second, third and fourth cycles were 60.8%, 40.6% and 35.0% respectively. At the second cycle defluoridation of 10 mg/ℓ fluoride solution using a sorbent dosage of 0.8 g/100 mℓ, the initial concentration of fluoride was reduced to 3.92 mg/ℓ. This value is much higher than the SANS 241-1 (2015) limit of 1.5 mg/ℓ fluoride in drinking water. Regeneration and reusability of spent Mg/Ce/Mn oxide-modified DE would be a limitation in application of this adsorbent in home based defluoridation devices.

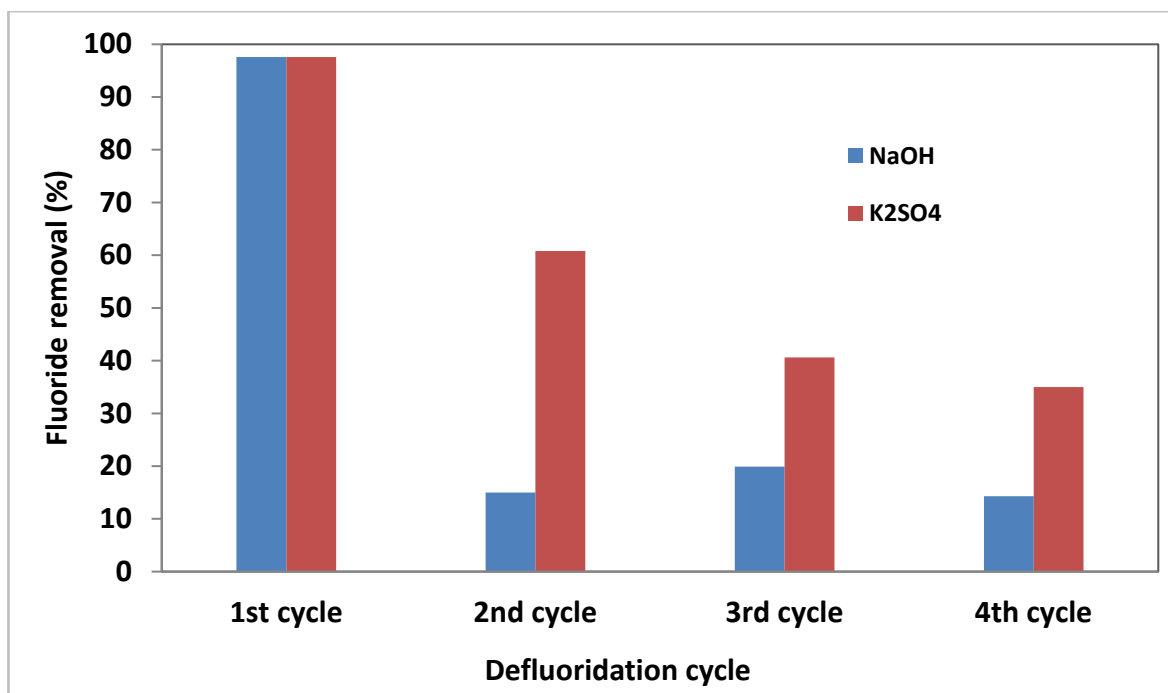


Figure 12.18. Percent (%) fluoride removal as a function of defluoridation cycle using 0.01 M NaOH and 0.1 M K₂SO₄ as regenerants (initial fluoride concentration: 10 mg/ℓ, volume of solution: 100 mℓ, adsorbent dosage: 0.8 g contact time: 60 min, temperature: 297 K and shaking speed: 200 rpm).

12.9 ADSORPTION MODELLING

12.9.1 Isotherms

The sorption data at evaluated temperatures were fitted to both Langmuir and Freundlich models to evaluate which of the two models better describe the sorption process. The plot of values against gives a straight line for the sorption data. Langmuir plots at 297 K, 310 K and 326 K gave straight lines with high correlation coefficients as shown in Figure 12.19. This is an indication that the data can adequately be described by the Langmuir model. Possible multisite adsorption of fluoride onto a rough sorbent surface was evaluated using the Freundlich adsorption isotherm. Where $1/n$ values are much less than 1, the adsorbents are heterogeneous (Papageorgiou et al., 2006). The plot of against C_e for the sorption data at 297 K, 310 K and 326 K gave straight lines with lower correlation coefficients compared to those of the corresponding Langmuir isotherm (Figure 12.20). Langmuir isotherm therefore gave a better fit for the sorption data. So, the sorption process is better described as a monolayer adsorption onto a smooth surface. The values of the parameters of the two isotherms are reported in Table 12.7.

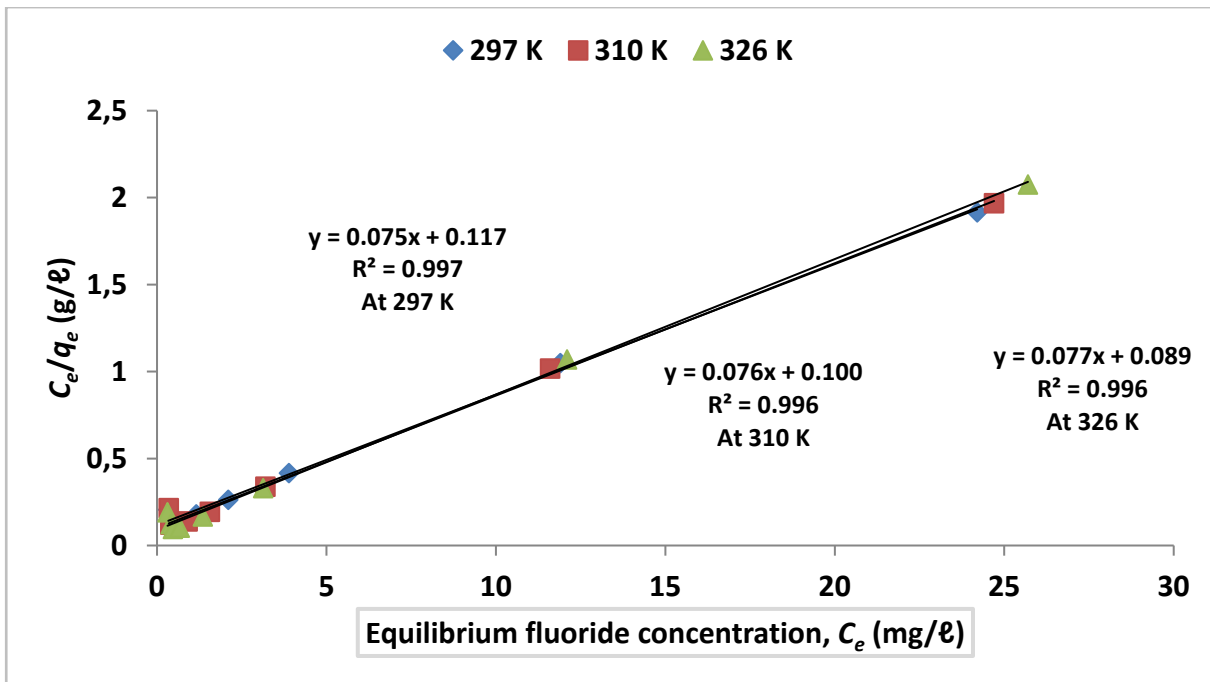


Figure 12.19. Langmuir isotherm plots at 297 K, 310 K and 326 K (contact time: 60 min, adsorbent dosage: 0.6 g, volume of solution: 100 mL, shaking speed: 200 rpm).

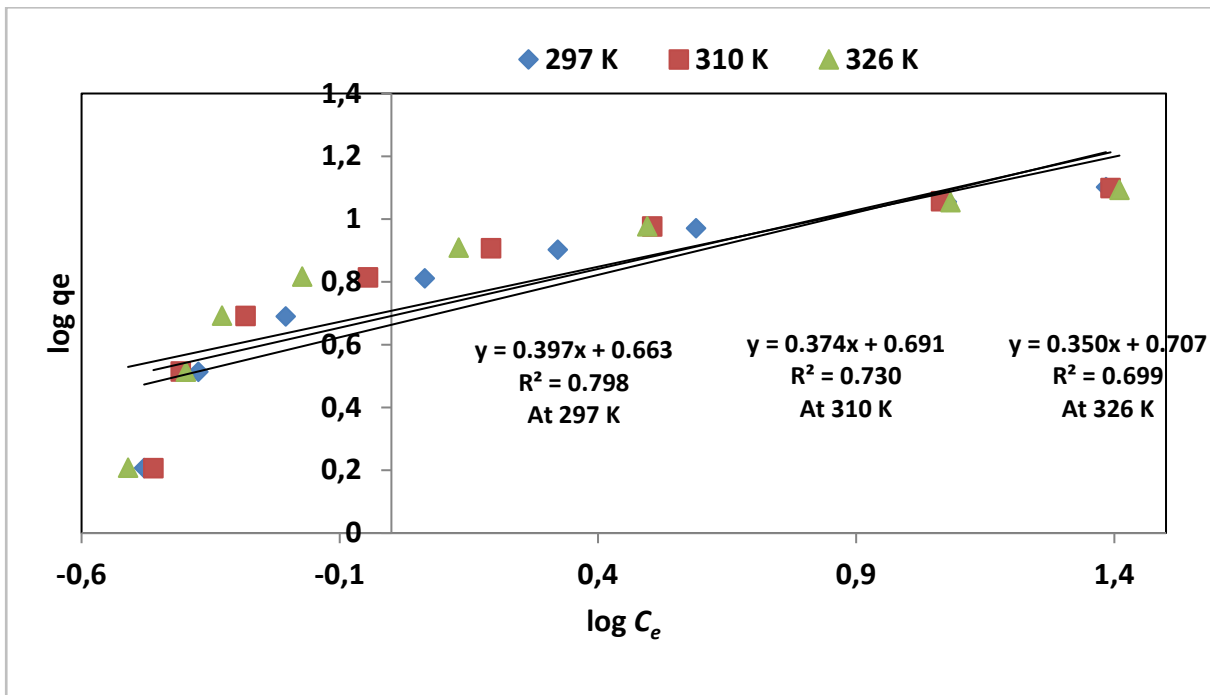


Figure 12.20. Freundlich isotherm plots at 297 K, 310 K and 326 K (contact time: 60 min, adsorbent dosage: 0.6 g, volume of solution: 100 mL, shaking speed: 200 rpm).

Table 12.7. Calculated Langmuir and Freundlich isotherm parameters

Temp (K)	Langmuir isotherm constants				Freundlich isotherm constants		
	$q_m(\text{mg/g})$	$K_L(\ell/\text{mg})$	$K_L(\text{m}^3/\text{kg})$	R^2	$1/n$	$K_F(\text{mg/g})$	R^2
297	13.33	0.641	641.0	0.997	0.397	4.603	0.798
310	13.16	0.760	760.0	0.996	0.374	4.909	0.730
326	12.99	0.865	865.2	0.996	0.350	5.093	0.699

The favourability of adsorption at the various concentrations used for the Langmuir isotherm plots was evaluated using the dimensionless separation factor, R_L , which is an essential feature of Langmuir model described by (Weber and Chakravorti, 1974). R_L describes the shape of the isotherm to be unfavourable if $R_L > 1$, linear if $R_L = 1$ and favourable if $0 < R_L < 1$ (Weber and Chakravorti, 1974). The condition $0 < R_L < 1$ was fulfilled for all the initial concentrations considered at the evaluated temperatures as shown in Figure 12.21. Hence, adsorption was favourable at those fluoride concentrations.

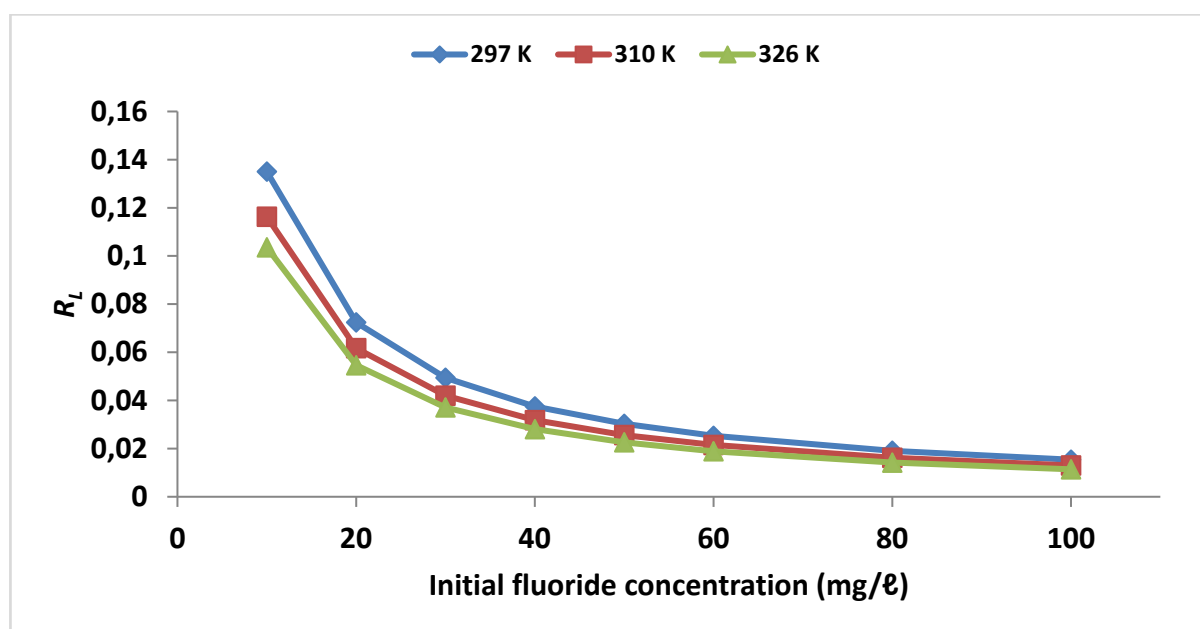


Figure 12.21. Values of dimensionless separation factor, R_L at different initial fluoride concentrations.

12.9.2 Adsorption thermodynamics

Temperature, like other factors such as concentration influences the spontaneity of a chemical process among other driving forces. However, the spontaneity of a chemical reaction is wholly determined by a thermodynamic quantity defined as the Gibbs free energy change, ΔG° (Jenkins, 2008). For a spontaneous sorption process, ΔG° must have a negative value. The Gibbs free energy change calculated for the sorption data at the evaluated temperatures have negative values (Table 12.8). Plotting $\ln K_L$ against $1/T$ gave a straight line (Figure 12.22) from which ΔH° was calculated to be 8 281.58 J/mol.

Table 12.8. Adsorption thermodynamic parameters

T (K)	$1/T$ (1/K)	$\ln K_L$	K_L (m ³ /kg)	ΔG° (J/mol)
297	0.003367	6.4630	641.0	15,958.89
310	0.003226	6.6333	760.0	17,096.32
326	0.003067	6.7630	865.2	18,330.09

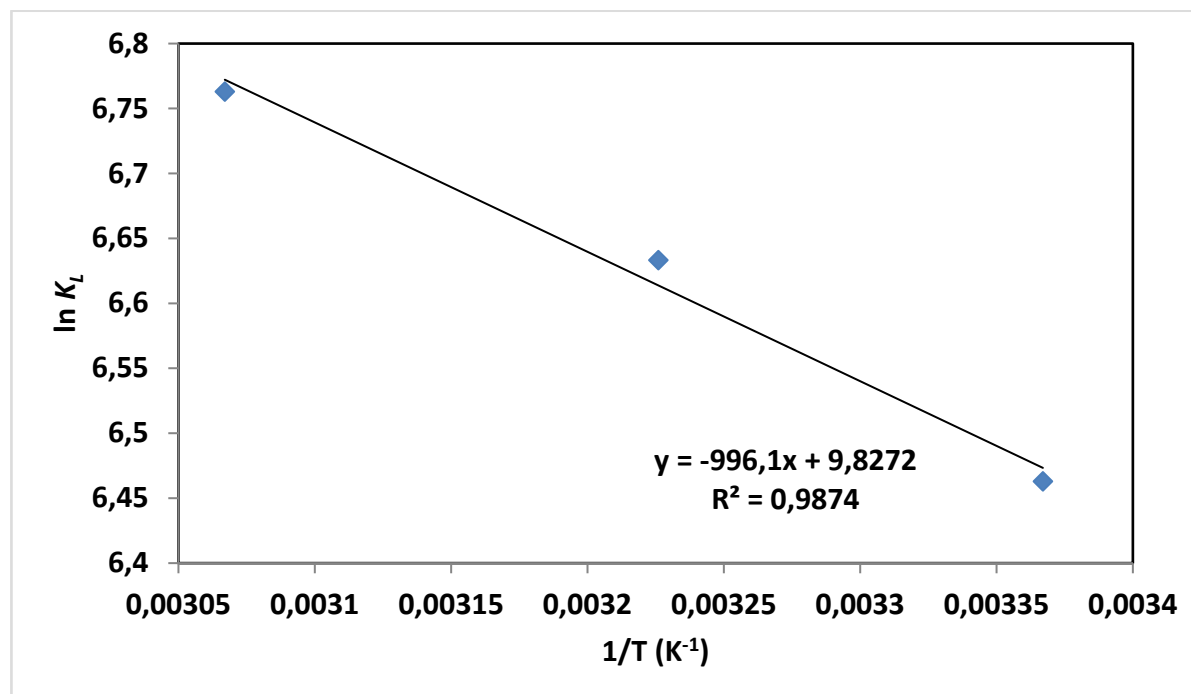


Figure 12.22. $\ln K_L$ as a function of reciprocal of adsorption temperatures.

12.9.3 Adsorption kinetics

12.9.3.1 Pseudo-first- and second-order models

The reaction-based models, the Lagergren pseudo-first-order model (Lagergren, 1898) and the pseudo-second-order model were used to evaluate the kinetic order of the fluoride sorption. The plots as shown in Figure 12.23 revealed that the Lagergren pseudo-first-order model could not adequately describe the kinetics of the adsorption process. However, the pseudo-second-order kinetic model plot of values against time t for adsorbent dosages of 0.1, 0.2 and 0.3 g gave linear plots with very high correlation coefficients (Figure 12.24). The better fit of the data to the model is an indication that the pseudo-second-order model was the appropriate kinetic model to describe the data. Fluoride adsorption was therefore by chemisorption, that is, fluoride uptake was a chemical process. The values of the experimental q_e , the calculated q_e and pseudo-second-order constants for 0.1 g, 0.2 g and 0.3 g dosages are summarized in Table 12.9.

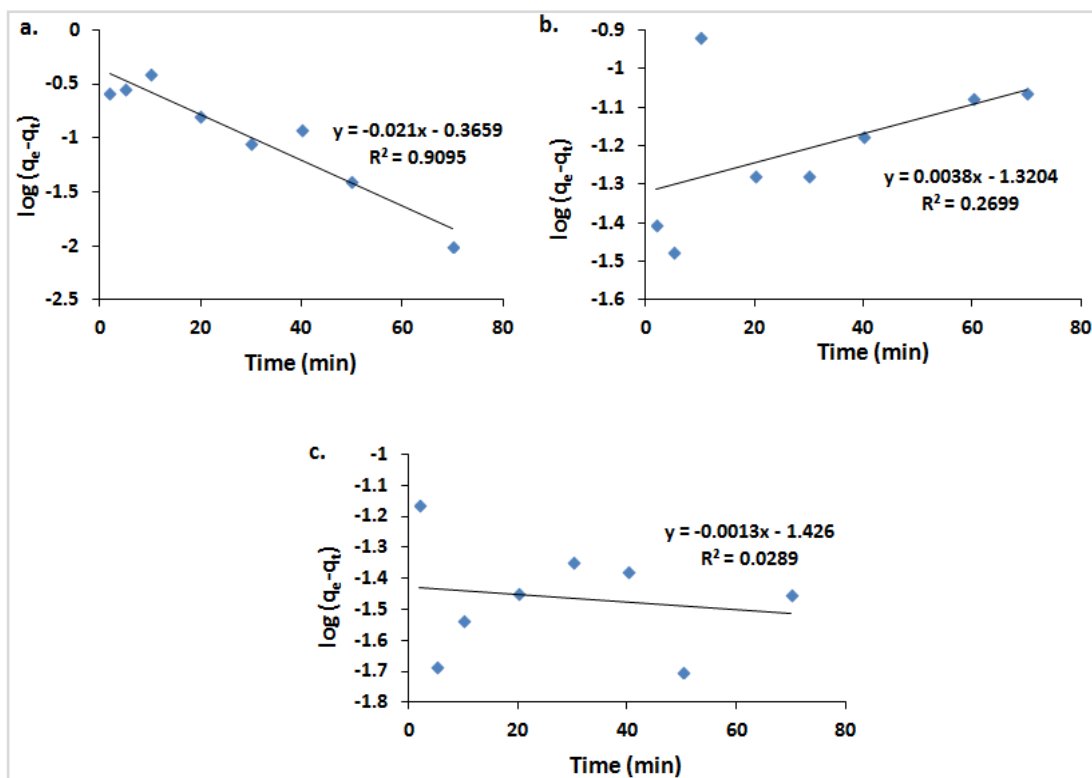


Figure 12.23. Pseudo-first-order plots for a. 0.1 g, b. 0.2 g and c. 0.3 g sorbent (initial fluoride concentration: 10 mg/l, volume of solution: 100 ml, shaking speed: 200 rpm and temperature: 297 K).

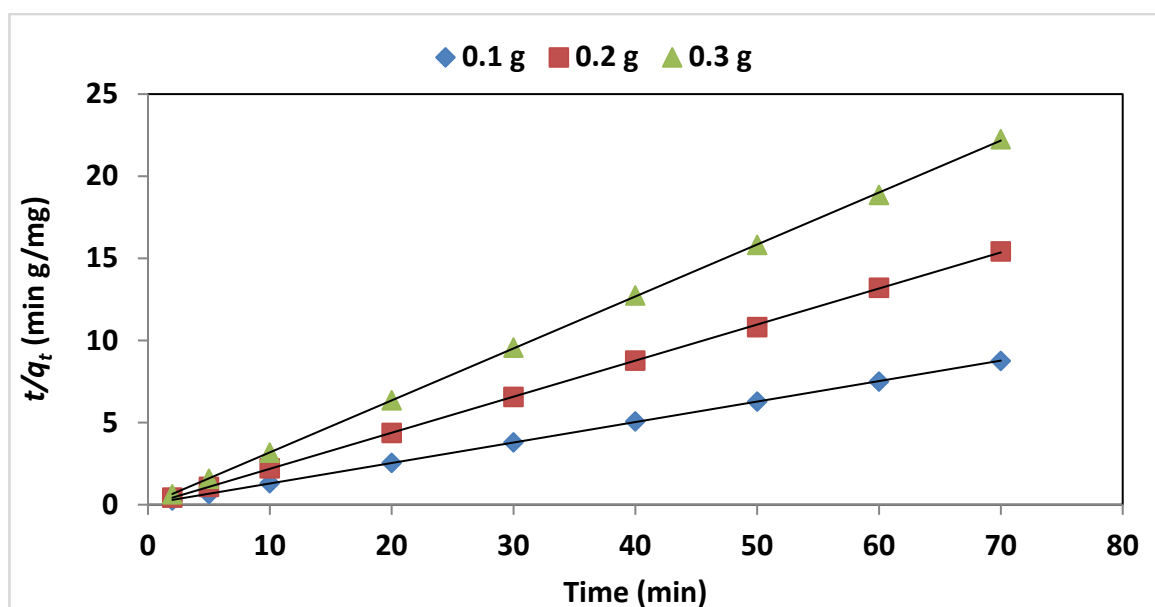


Figure 12.24. Pseudo-second-order plots for 0.1, 0.2 and 0.3 g sorbent (initial fluoride concentration: 10 mg/l, volume of solution: 100 ml, shaking speed: 200 rpm and temperature: 297 K).

Table 12.9. Pseudo-second-order parameters at different adsorbent dosages

Adsorbent dosage (g)	Equation	Experimental q_e (mg/g)	Calculated q_e (mg/g)	k_2 (L mg ⁻¹ min ⁻¹)
0.1	$y = 0.124x + 0.043$	8.0000	8.0645	0.3576
0.2	$y = 0.219x - 0.013$	4.6245	4.5662	-3.6893
0.3	$y = 0.316x + 0.019$	3.1810	3.1646	5.2556

12.9.3.2 Diffusion models

The mechanisms controlling sorption rate include 1) diffusion from the bulk solution to a film layer surrounding the adsorbent particle, 2) diffusion from the film to particle surface, “film diffusion”, 3) migration inside the adsorbent particle by “surface diffusion” or diffusion within liquid-filled pores, “pore diffusion” and 4) uptake of adsorbate by chemisorption, physisorption, ion exchange or complexation (Weber and DiGiano, 1996; Gulipalli et al., 2011). Basically, migration of adsorbate is either from the bulk of the solution to the surface of particle (external diffusion) or through the pores of the particles (intra-particle diffusion). Diffusion models are principally based on these two types of diffusion.

Intra-particle diffusion

The model by Weber and Morris (1963) is a commonly used model to evaluate intra-particle diffusion. The model was used to appraise the possibility of intra-particle diffusion of fluoride solution being the sorption rate controlling step. The migration of adsorbate through the pores of adsorbate could be an adsorption rate limiting step if on the account of the size of the adsorbate there is a measure of difficulty in its migration through the adsorbent. Modelling the experimental kinetic data with the intra-particle diffusion model showed that diffusion of fluoride through the pores of the adsorbent was not the mechanism controlling process (Figure 12.25). This fact is further substantiated by comparing the ionic radius of fluoride or its diameter to the minimum pore diameter of the adsorbent determined by BET analysis. The ionic radius of fluoride is 1.33 Å (Ruben, 1985). Hence, the ionic diameter of fluoride is 2.66 Å. The minimum pore diameter of the adsorbent as determined by BET was 20.12 Å. It therefore follows that fluoride ions would migrate through the pores of the adsorbent without restraint. The much lower size of fluoride ion to the pore size does suffice to conclude that intra-particle diffusion could not be the sorption rate controlling step.

External diffusion

The external diffusion model by Lee et al. (1999) is a commonly used model for evaluating external diffusion as a likely sorption rate limiting process in adsorption. The plots were bilinear for the kinetic data obtained at the three evaluated sorbent dosages (Figure 12.26). The first linear portion was from 2-20 min contact time, while the second linear portion was from 30 to 70 min contact time. The bilinear plots indicate a two-mode influence of external diffusion on the sorption rate. External diffusion is therefore the rate limiting step for the fluoride sorption.

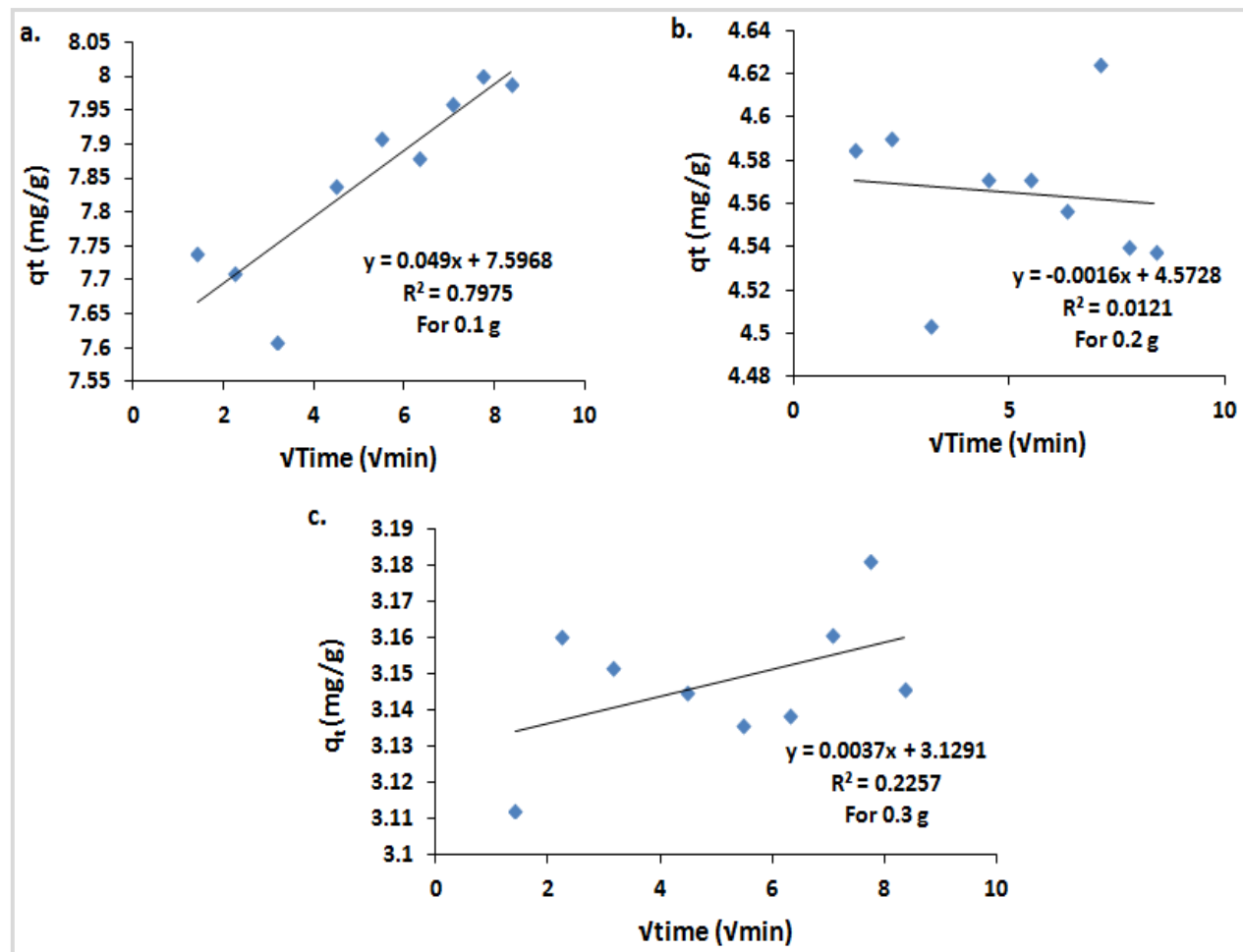


Figure 12.25. Weber-Morris intra-particle diffusion plot for a) 0.1 g, b) 0.2 g and c) 0.3 g sorbent (initial fluoride concentration: 10 mg/ℓ, volume of solution: 100 mℓ, shaking speed: 200 rpm and temperature: 297 K).

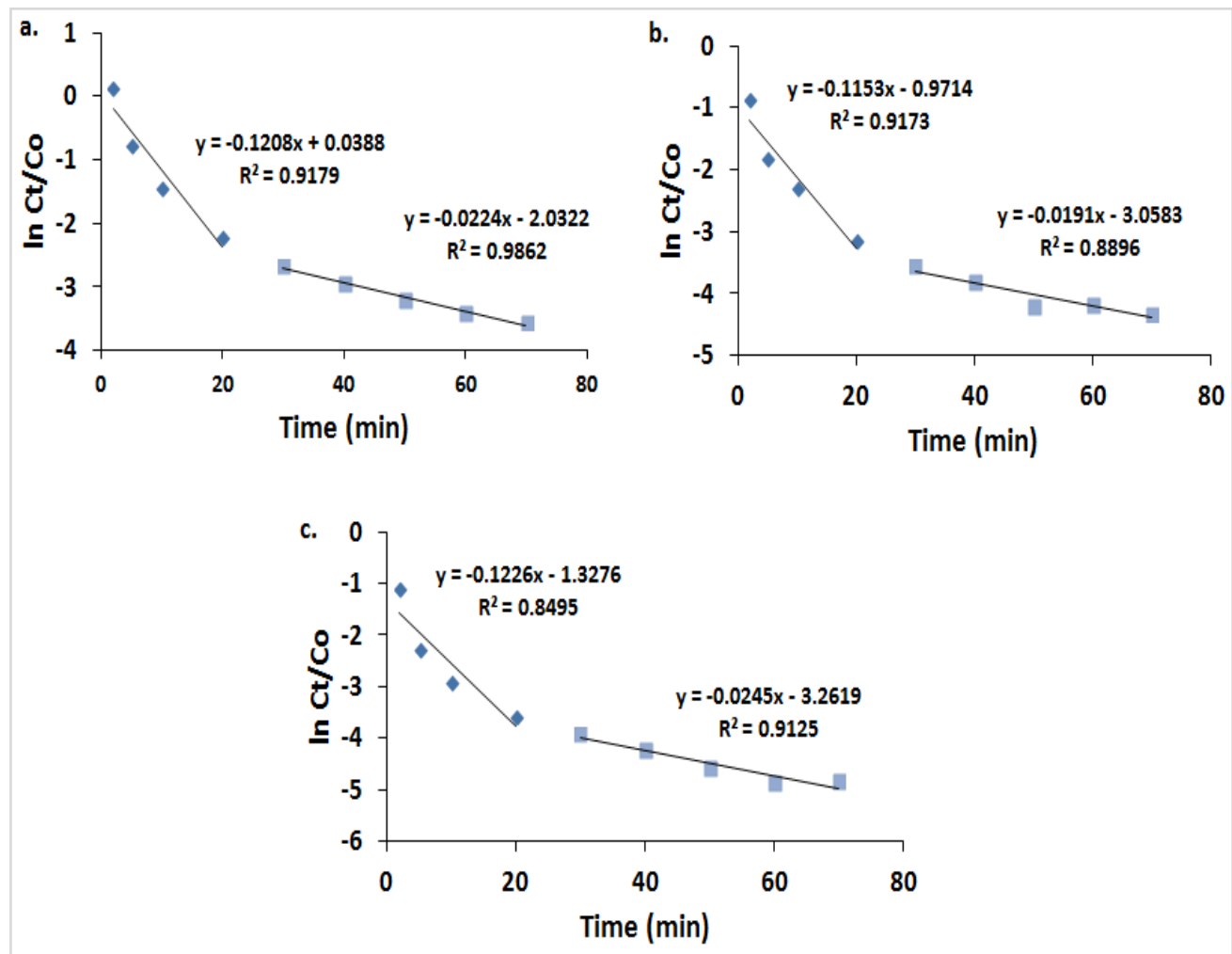


Figure 12.26. External diffusion plots for 0.1 g, 0.2 g and 0.3 g sorbent dosages (initial fluoride concentration: 10 mg/ℓ, volume of solution: 100 mℓ, shaking speed: 200 rpm and temperature: 297 K).

12.10 SUMMARY

Diatomaceous earth (DE) was successfully modified by co-precipitating a composite of Mg/Ce/Mn oxide/hydroxides on its surface and pores. The modified product was characterized and applied in batch defluoridation of groundwater water. The sorbent displayed high fluoride removal potentials (> 93% fluoride removal) for solutions with initial fluoride concentration of 10 mg/l - 60 mg/l at sorbent dosage of 0.6 g/100 ml (contact time: 60 min, 200 rpm and temperature: 297 K). The optimum fluoride uptake capacity was 12.63 mg/g for an initial solution of 100 mg/l fluoride. Fluoride removal was >91% with an initial concentration of 9 mg/l fluoride over a pH range of ~ 4 to 11 at a sorbent dosage of 0.6 g/100 ml. The equilibrium pH was greater than the sorbent's pHPzc of 5.45. Fluoride removal was attributed to the exchange of the hydroxyl groups at the sorbent surface with fluoride ions. Sorption data fitted better to Langmuir isotherm than Freundlich isotherm. Kinetically the sorption data was adequately described by the Lagergren pseudo-second-order kinetic model indicating chemisorption was the main fluoride removal mechanism. External diffusion was observed to be the sorption rate limiting step. TGA confirmed that the trimetal oxide coated diatomaceous earth would be thermally stable at < 580°C. The presence of competing anions such as Cl⁻, NO₃⁻, CO₃²⁻, SO₄²⁻ and PO₄³⁻ didn't affect the defluoridation efficiency of the adsorbent, moreover the equilibrium pH ranged between 6-6.28 with the product water requiring no pH adjustment. A shortcoming of the adsorbent would be the leaching of Ce, Mg and Mn which would affect the quality of the product water and this would be its limitation in its application in household defluoridation devices.

13 EVALUATION OF GROUNDWATER DEFLUORIDATION USING AL/FE OXIDE-IMPREGNATED DIATOMACEOUS EARTH

13.1 INTRODUCTION

In the previous Chapter, raw DE has been shown to possess a low fluoride removal potential and moreover optimum adsorption potential was only observed at pH of 2. The application of raw DE for fluoride removal in drinking water would be limited by the fact that it exhibits fluoride removal at very low pH since this would require pH adjustment of the product water. To overcome this challenge, this Chapter presents findings on attempts to modify the surface properties of the diatomaceous earth with a view to increasing its pH_{pzc} to circum-neutral pH and also increase its surface area and hence create more active sites for adsorption of fluoride. DE has pores which can be coated with metal hydroxides/oxides having high affinity for fluoride through precipitation of metal ions from their salts in solution. DE is nonorganic so cannot undergo degradation to foul water. Another advantage is the fact that it is stable at the operating temperature. It is reported that the pore structure of DE start to collapse at 900°C. Also, complete dehydration of the material occurs from 900 to 1200°C (Ibrahim and Selim, 2012) meaning DE is thermally stable and can retain its structure even after calcination at high temperatures. Thus, this Chapter presents findings on the following:

- a. Optimization of synthesis conditions for Al/Fe impregnated diatomaceous earth.
- b. Evaluation of the fluoride adsorption potential/capacity of the Al/Fe impregnated DE. optimization of adsorption conditions, adsorption isotherms and kinetics.
- c. Application for field groundwater treatment
- d. Regeneration, reusability potential and chemical stability of Al/Fe impregnated DE

13.2 MATERIALS

All reagents and TISAB-III were obtained from Rochelle Chemicals & Lab Equipment CC, South Africa Ltd and they were of analytical grade. The DE for the study was obtained from natural deposits at Kariandusi in Gilgil District, Nakuru County, Kenya and a second supply sourced in South Africa. A stock solution containing

1000 mg/l fluoride was prepared by dissolving 2.21 g analytical grade sodium fluoride in 1 l of ultra-pure water (18.2 MΩ/cm). Fluoride solutions for batch experiments were prepared from fresh stock fluoride solution by appropriate dilution. A stock solution containing 1000 mg/l fluoride was prepared by dissolving 2.21 g NaF in 1 l of MilliQ water (18.2 MΩ/cm) and fluoride solutions for batch experiments were prepared from fresh stock fluoride solution by appropriate dilution. Field water was collected from a community borehole in Siloam, Vhembe district in South Africa.

13.3 METHODS

13.3.1 Optimising the modification of DE with Al₂O₃ and Fe₂O₃

Diatomaceous earth (DE) was prepared as described in Section 11.3.1. DE was modified separately with Al₂O₃ and Fe₂O₃. The effects of agitation speed and contact time on the loading of the oxide coats on diatomaceous earth were evaluated in an attempt to establish the optimum conditions for the modification process. This was achieved by analysis of the residue Al, Fe in the supernatants. For Al analysis, 0.2 g of each of the with Al₂O₃-modified DE samples and raw DE sample (for blank) was weighed into 250 ml plastic bottles containing 50 ml of 3 M HNO₃. The bottles were tightly corked and the mixtures were heated at 60°C for 2 h to dissolve Al₂O₃. After heating, the mixtures were cooled to room temperature and then filtered through membrane filters. The filtrates were analysed for Al using ICP-MS. Analysis of Fe in the supernatants resulting from the precipitation of Fe (OH)₃ on DE at different shaking speeds and contact times using ICP-MS was used to evaluate the optimum conditions for modification of DE with Fe₂O₃.

13.3.2 Al/Fe oxide modification of diatomaceous earth at optimum conditions

One hundred millilitres of solution containing a mixture of 0.25 M of Al³⁺ and 0.25 M Fe³⁺ were prepared by dissolving 8.3304 g of Al₂(SO₄)₃.18H₂O and 4.9985 g of Fe₂(SO₄)₃.xH₂O respectively. The two metal ions were therefore contained in the solution at equal proportions as the optimum mixture ratio for the modification of DE as earlier determined. The 100 ml of the solution of Al³⁺ and Fe³⁺ were transferred into a litre plastic bottle. A mass of 15 g of raw DE was dispersed in the solution and shaken on a reciprocating shaker at 200 rpm for 20 min to ensure proper soaking. Al₂(OH)₃ and Fe₂(OH)₃ were co-precipitated on DE by adjusting the pH to 8.2 with rapid stirring. The mixture was then shaken on a reciprocating shaker for an optimum shaking speed of 100 rpm for 50 min (optimum contact time) to ensure complete precipitation on the DE. The mixture was centrifuged to remove excess NaOH while the solid was washed with MilliQ water until the wash could not turn phenolphthalein red. Finally, the mixture was centrifuged to discard the supernatants. The solid was scooped out of the centrifuge tubes and dried in the oven at 110 °C for 8 hours, cooled in a desiccator and stored in corked plastic bottles to avoid moisture.

13.3.3 Characterisation of the adsorbents

The adsorbents were characterised using several techniques (detailed in Appendix A). These included Cation Exchange Capacity (CEC), Point of Zero Charge (PZC), X-ray diffraction (XRD), X-ray fluorescence (XRF), Scanning Electron Microscopy (SEM), Scanning Electron Microscopy coupled with Energy Dispersive Spectroscopy (SEM-EDS), Transmission Electron Microscopy (TEM), Brunauer-Emmett-Teller (BET) and Fourier Transform Infrared (FTIR).

13.3.4 Batch and field groundwater adsorption experiments

The defluoridation potentials of Al₂O₃, Fe₂O₃ and Al/Fe oxide-modified DE adsorbents were evaluated by conducting batch experiments (detailed in Appendix B). Methods followed for field groundwater defluoridation studies are also detailed in Appendix B. Appendix C details models used for describing the adsorption process.

13.4 SYNTHESIS OF AL₂O₃- AND FE₂O₃-MODIFIED DIATOMACEOUS EARTH

13.4.1 Effect of shaking speed on synthesis of Al₂O₃- and Fe₂O₃-modified DE

The results of ICP-MS analysis of the two-metal species in the supernatants after blank correction are reported in Table 13.1. Results showed that the highest amount of Al(OH)₃ precipitated on DE at the agitation speed of 100 rpm. Dissolution of Al from Al₂O₃-modified DE was highest for the modification done at 100 rpm. The lowest concentration of Fe in supernatant corresponding to modification shaking speed of 200 rpm is an indication that the highest precipitation of Fe(OH)₃ on DE occurred at 200 rpm. Lowest amount of Fe in supernatant was observed at shaking speed of 200 rpm (Table 12.1). Therefore, the optimum synthesis of Al₂O₃-and Fe₂O₃-modified DE occurred at the shaking speeds of 100 and 200 rpm respectively.

Table 13.1. Effect of shaking speed on modification of diatomaceous earth with Al₂O₃ and Fe₂O₃

Shaking speed in rpm	Concentration of dissolved Al ³⁺ (mg/ℓ)	Concentration of Al ³⁺ From DE (mg/g)	Concentration of Fe species in supernatant (mg/ℓ)
100	197.61	49.40	0.90
150	153.49	38.37	1.20
200	124.30	31.07	0.84
250	107.90	26.97	2.16

13.4.2 Effect of contact time

The effect of contact time was evaluated following the procedure explained in section 3.4, chapter 5 of appendix D. However, the Al₂(SO₄)₃-DE-NaOH and FeCl₂-DE-NaOH mixtures in the 250 ml bottles were equilibrated at 200 rpm for 10, 20, 30, 40, 50 and 60 min contact times. The supernatants from Al (OH)₃-DE-NaOH mixtures were discarded as the dry solids were to be treated for metal analysis by ICP-MS. The supernatants from Fe (OH)₂-DE-NaOH were also prepared for ICP-MS analyses as previously described. The results of the Al and Fe analysis are reported in Table 13.2. Results indicate that the optimum contact times were 50 and 60 min respectively for DE modification with Fe₂O₃ and Al₂O₃.

Table 13.2. Effect of contact time on modification of diatomaceous earth with Al₂O₃ and Fe₂O₃

Contact time (min)	Concentration of dissolved Al ³⁺ (mg/ℓ)	Concentration of Al ³⁺ from DE (mg/g)	Concentration of residual Fe species in supernatant (mg/ℓ)
0	0	0	0
10	121.40	30.35	1.28
20	115.20	28.80	1.24
30	124.30	31.07	1.15
40	114.70	28.67	1.16
50	119.70	29.92	1.02
60	137.90	34.47	1.20

13.5 PHYSICOCHEMICAL AND MINERALOGICAL CHARACTERIZATION

13.5.1 Surface area and pore volume of Al/Fe oxide-modified DE

The surface area, pore area and volume of Al/Fe oxide modified DE were analysed using the Brunauer-Emmett-Teller (BET) method using Micromeritics TriStar II *Surface Area and porosity*. The results of analysis are reported in Table 13.3. The values of the single point surface area, BET surface area and the BDH adsorption cumulative area of the Al/Fe oxide-modified DE are more than double those of the raw diatomaceous earth. This is evidence that coating of raw diatomite with Al/Fe oxide was successful. Increase in surface area of adsorbent implies an increase in active adsorption sites. There was a corresponding increase in pore volume of the adsorbent. The increase in pore surface area and volume is an indication that the percolation of water through the particles of adsorbent during defluoridation would be more readily achieved.

Table 13.3. Comparison of the surface area, and pore area and volume of the raw and Al/Fe oxide-modified diatomaceous earth

Form of diatomaceous earth (DE)	Single point surf. area (m ² /g)	BET surf. area (m ² /g)	BJH adsorption cum. surf. area of pores (m ² /g)	BJH desorption cum. surf. area of pores (m ² /g)	Single point adsorption total pore vol. (cm ³ /g)	BJH adsorption cum. vol. of pores (cm ³ /g)	BJH desorption cum. vol. of pores (cm ³ /g)
Raw DE	31.17	31.89	21.41	22.70	0.083	0.089	0.090
Al-Fe oxide-modified DE	67.79	70.73	61.31	64.78	0.113	0.122	0.124

The plot of pore volume against pore diameter for both raw and Al/Fe oxide-modified DE is shown in Figure 13.1. About 88% of the pores had their diameter within the range of 2-50 nm (mesopores range). The raw and Al/Fe oxide-modified DE can be described as mesoporous materials. This finding further confirms that the adsorbent would be very permeable to water during defluoridation.

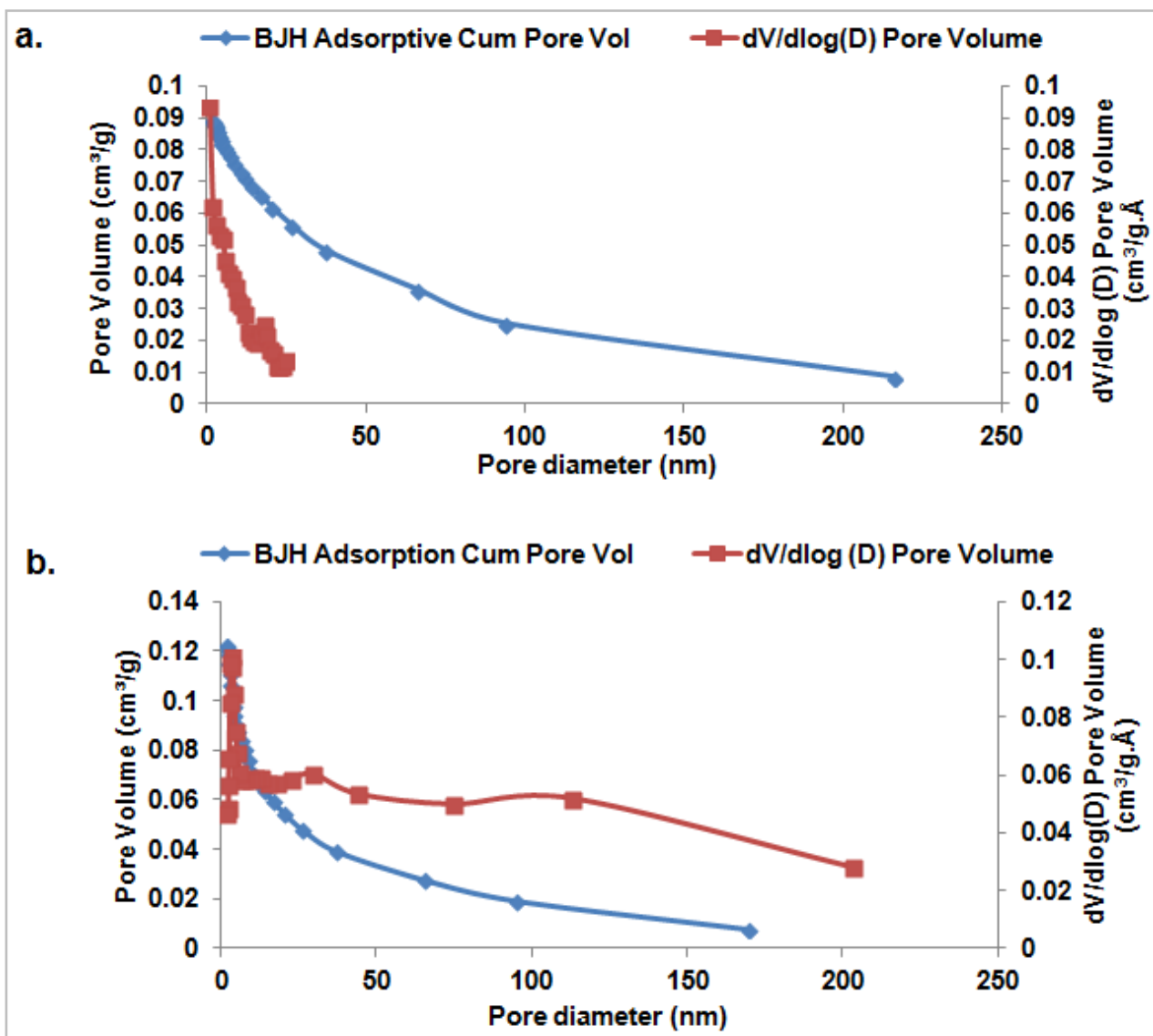


Figure 13.1. Plot of BJH adsorption pore volume and BJH $dV/d\log(D)$ pore volume against pore diameter (D) for a. raw and b. Al/Fe oxide-modified diatomaceous earth.

13.5.2 Morphological analysis of raw and Al/Fe oxide-modified diatomaceous earth by scanning electron microscope

The surface morphology of the modified DE was probed by scanning with Hitachi X-650 scanning electron micro analyser equipped with CDU lead detector at 25 kV. The SEM micrographs (b) and (c) of pure binary Al/Fe oxide are presented in Figure 13.2 show that the particles of the oxides are of nano size as opposed to micrographs (a) of raw diatomaceous earth. Micrographs (d), (e) and (f) represents the Al/Fe oxide-modified DE. The particles of Al/Fe oxide deposited in the pores of DE are particularly visible in micrographs (e) and (f). The micrographs show the differences in the pore's sizes and appearance of DE before and after modification. The pores of the modified DE appeared almost completely filled by Al_2O_3 and Fe_2O_3 deposits as opposed to the clear, net-like pores in the raw DE (a). The near closure of the pores of the modified DE is evidence that the surface of the raw DE was modified.

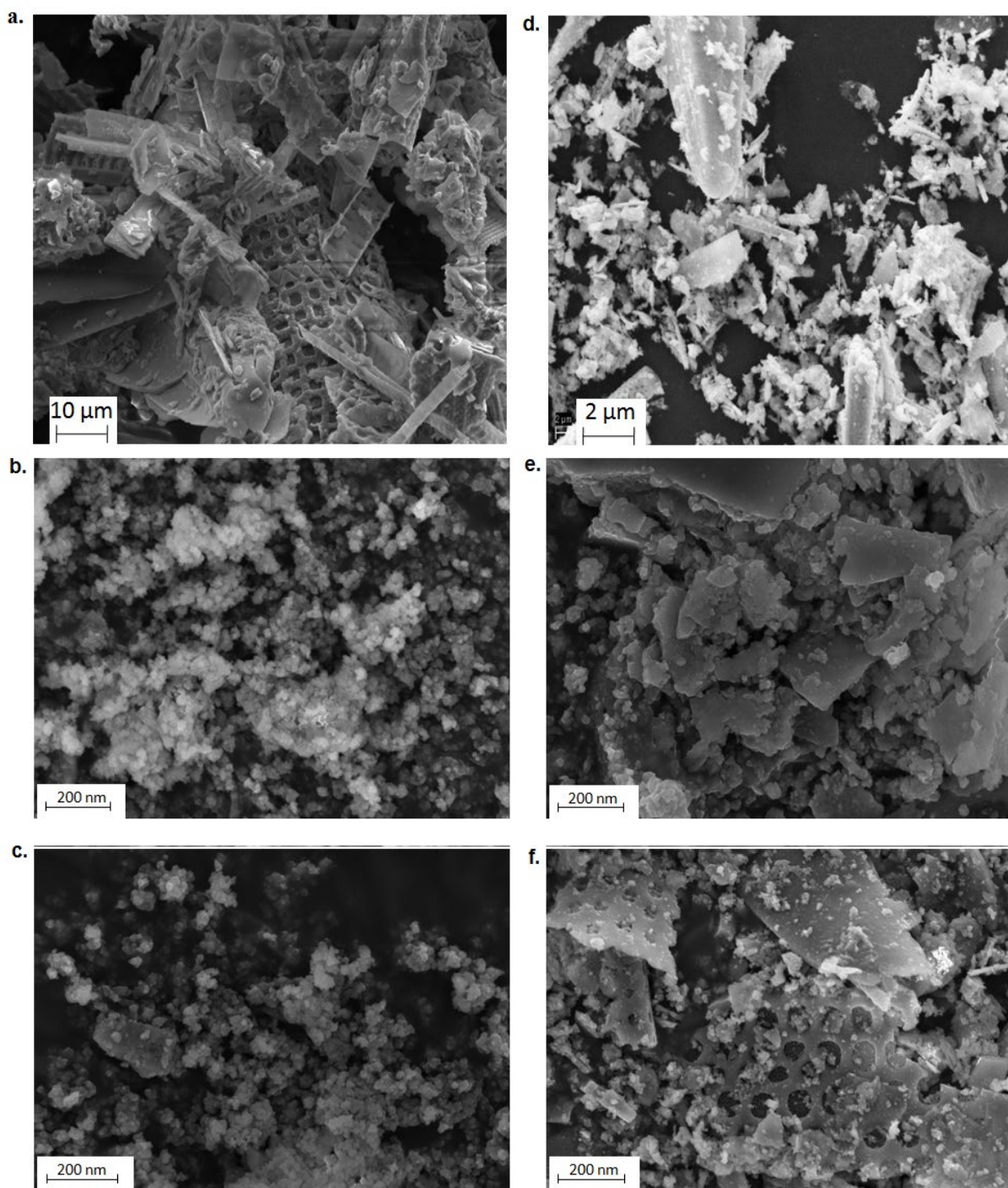


Figure 13.2. SEM images of a. raw diatomaceous earth, b. and c. Al/Fe oxide and d. to f. Al/Fe oxide-modified diatomaceous earth.

13.5.3 Scanning Electron Microscope-Energy dispersive X-ray spectroscopy (EDX)

The results of the scanning electron microscopy energy dispersive spectroscopy (EDX) of the raw and Al/Fe oxide-modified DE are presented in Figure 13.3. The results show an increase in the average per cent atoms of Al and Fe in Al/Fe oxide-modified DE over those of the raw DE.

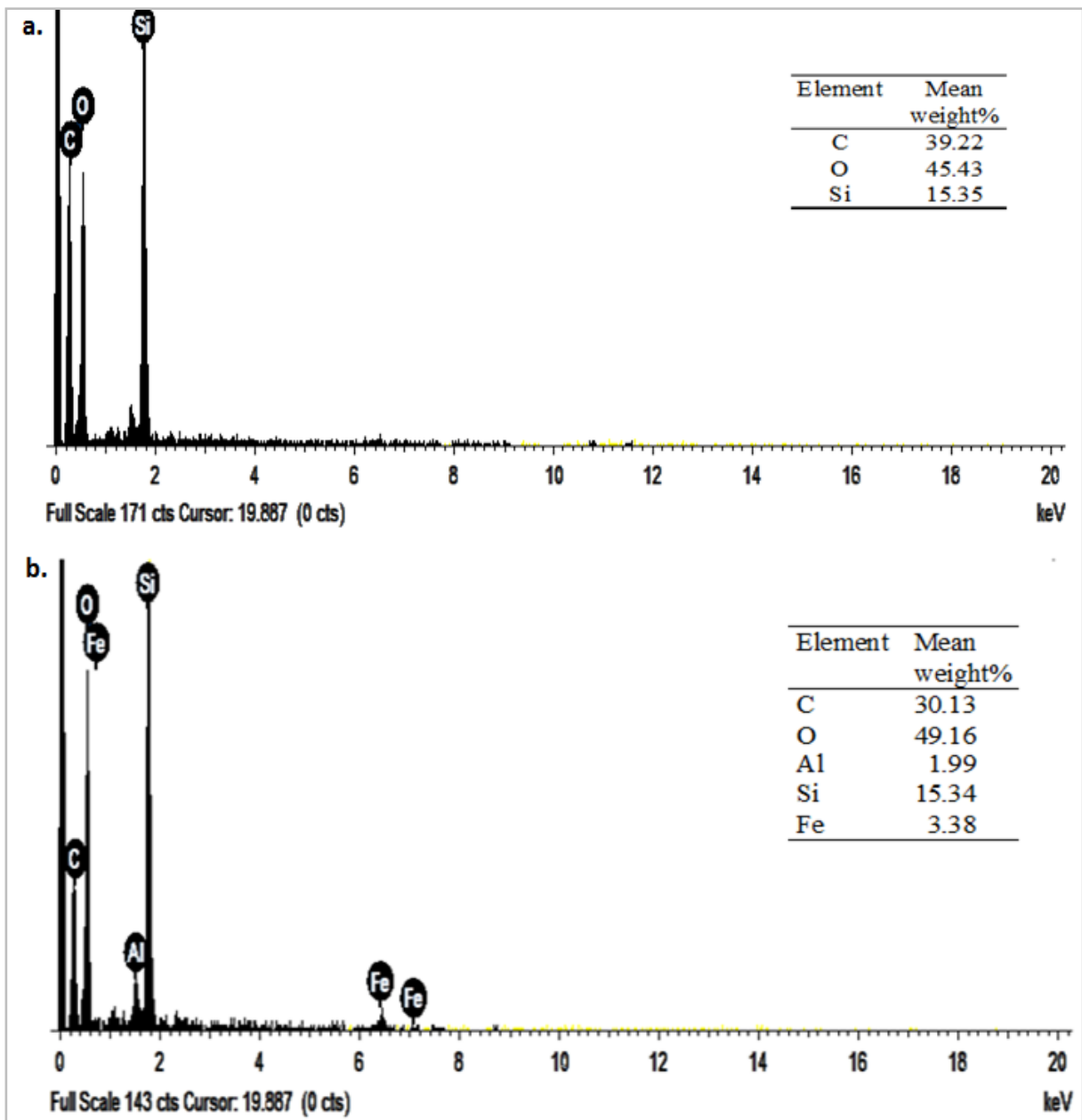


Figure 13.3. Energy dispersive spectrograph of (a). raw diatomaceous earth and (b). Al/Fe oxide-modified diatomaceous earth.

13.5.4 Morphological analysis of raw and Al/Fe oxide-modified diatomaceous earth by transmission electron microscope

Further morphological evaluation of the Al/Fe modified DE was done by transmission electron microscopy (TEM) using JEM-2100 Electron Microscope. The micrographs of the pure binary Al/Fe oxide and Al/Fe oxide-modified DE are presented in Figure 13.4. The TEM micrograph (a) is for the pure binary Al/Fe oxide. The deposition of the binary metal oxide on the pores of the DE is observed as dark patches in the TEM micrographs (b) to (f) of Al/Fe oxide-modified DE. The deposition was not uniform. The deposition was intense at some points and sparse at others. However, the noticeable dark patches are evidence that surface deposition of the oxides on DE surface occurred.

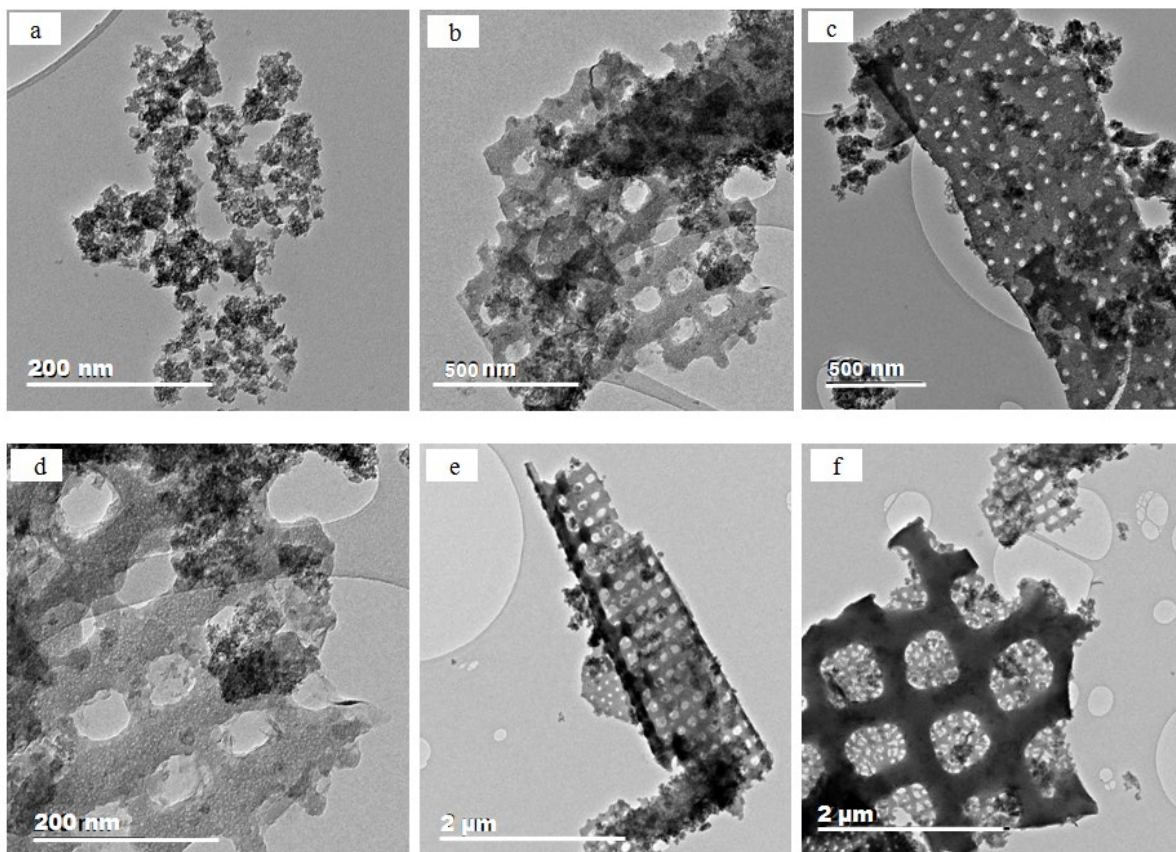


Figure 13.4. TEM images of (a) Al/Fe oxide and (b) to (f) Al/Fe oxide-modified diatomaceous earth.

13.5.5 Fourier Transform Infra-Red (FTIR) Spectroscopy

The FTIR spectroscopic analysis of pure binary Al/Fe oxide, Al/Fe oxide-modified DE and fluoride-loaded modified DE was done to identify the groups of atoms at the surface of the adsorbents and to evaluate the possible changes in the functional groups of the modified sorbent on contact with fluoride solution (Fig 13.5). There is increase in the transmittance of the Si-O-H stretching vibration at 453 cm^{-1} for the fluoride-treated DE. This could be attributed to the formation of Si-F bonds on fluoride adsorption which reduced the number of Si-O-H bonds on the adsorbent surface.

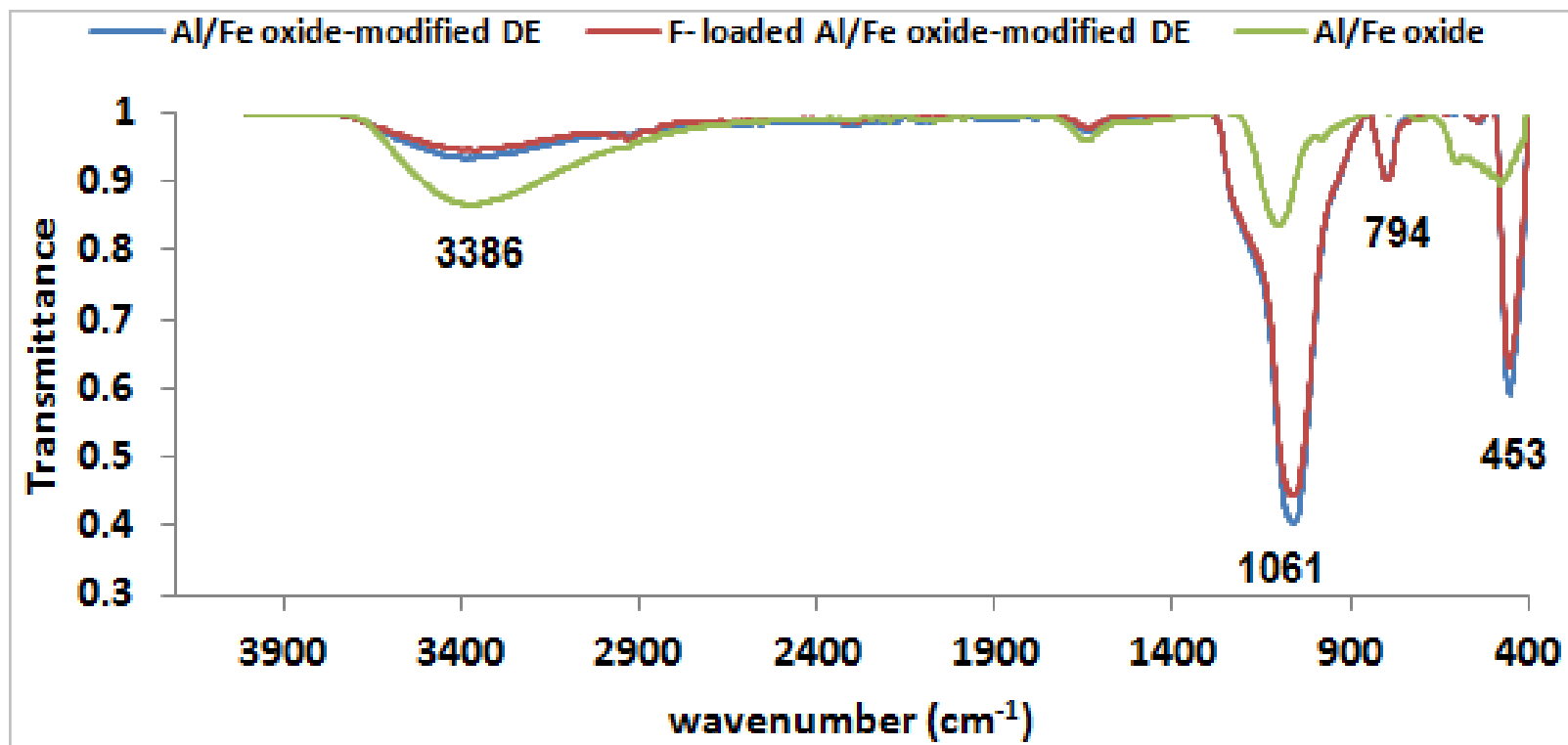


Figure 13.5. FTIR spectra of Al/Fe oxide, Al/Fe oxide-modified and F-loaded Al/Fe oxide modified diatomaceous earth.

The same trend is noticed for the transmittance at 1061 cm⁻¹ for Si-O-Si stretching vibration for possible replacement of -O-Si group with F⁻ with accompanying reduction in absorbance by Si-O-Si. Thus, there is evidence of interaction of F⁻ with surface functional groups in Al/Fe modified DE during adsorption process.

13.5.6 X-ray fluorescence (XRF) analysis

Chemical composition of raw and Al/Fe oxide-modified DE is presented in Table 13.4. Significant difference was observed in the percentages of Al₂O₃, Fe₂O₃ and SiO₂ for the two adsorbents. While there was increase in the per cent compositions of Al₂O₃ and Fe₂O₃ in the modified DE, the value of SiO₂ decreased. The increase in the values of the two metal oxides is indicative of the precipitation and deposition of the binary metal oxide on DE.

Table 13.4. Chemical composition of raw and Al/Fe oxide modified DE

Metal oxide	Raw diatomaceous earth	Al/Fe oxide modified diatomaceous earth
Al ₂ O ₃	4.01	9.85
CaO	0.24	0.19
Cr ₂ O ₃	0	0.01
Fe ₂ O ₃	2.96	12.46
K ₂ O	0.75	0.38
MgO	0.11	0.15
MnO	0.04	0.06
Na ₂ O	0.61	1.92
P ₂ O ₅	0.04	0.02
SiO ₂	84.17	66.09
TiO ₂	0.17	0.14
L.O.I	7.52	8.82
Total	100.6	100.9

13.5.7 X-ray diffraction (XRD) analysis

The XRD spectrum of DE of Al/Fe oxide-modified DE is presented in Figure 13.6. From Figure 13.6, it can be observed that the material is completely amorphous. An amorphous material has a wider surface area than a crystalline material. The larger the surface area of an adsorbent the larger the number of active sites on the adsorbent surface.

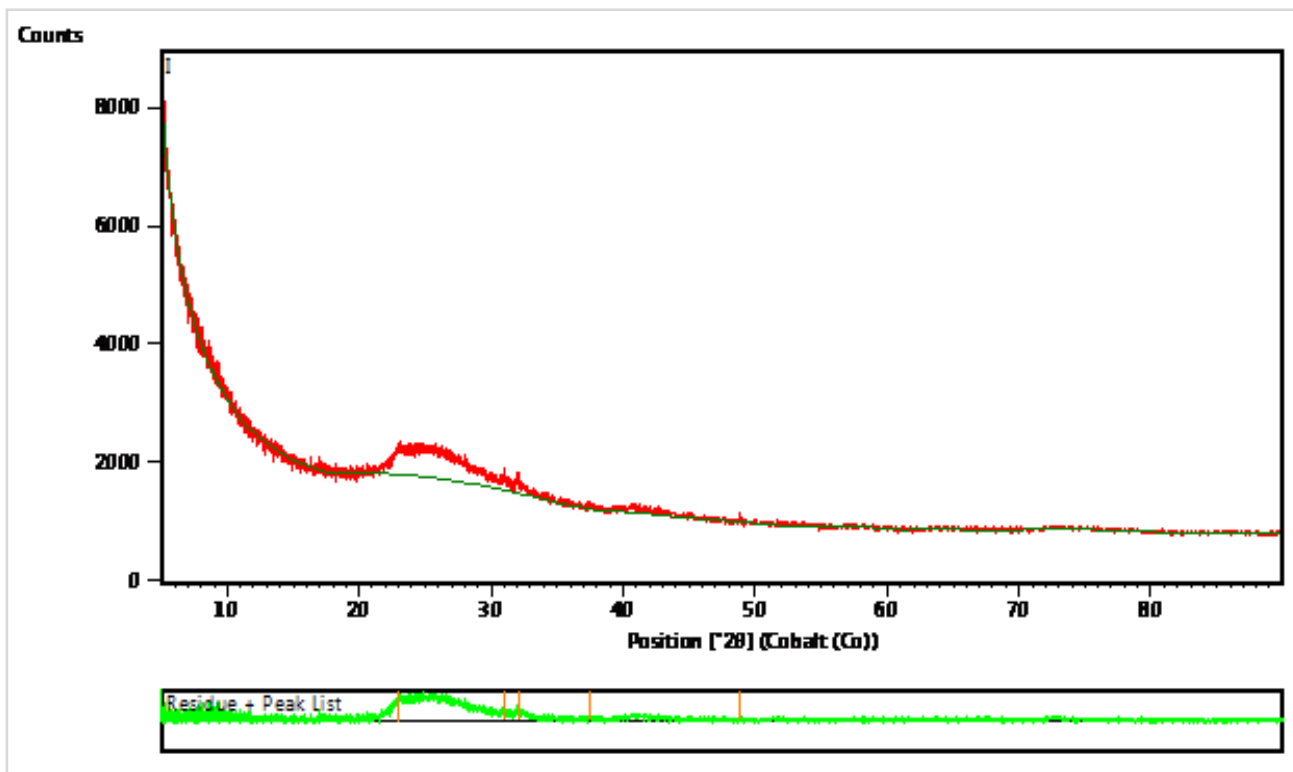


Figure 13.6. X-ray spectrum of Al/Fe oxide-modified diatomaceous earth.

13.5.8 pH at point-of-zero charge pH_{pzc}

The pH at point-of-zero charge of the prepared Al/Fe oxide-modified DE was evaluated using 0.01, 0.1 and 1 M KCl ionic strengths. pH was adjusted to a desired value with 0.1 M HCl and 0.1 M NaOH. The adjusted pH constituted the initial pH (pH_0) while final pH after equilibration. pH (pH_e) was determined. The change in pH ($\Delta pH = pH_e - pH_0$) was plotted against the initial pH of KCl solution to obtain the pH_{pzc} on the x-axis. The profiles of the plots for the adsorbent in the solutions at various ionic strengths are presented in Figure 13.7. In the plots, the pH_{pzc} is the abscissa for ΔpH equals zero. This is the point where the curve crosses the horizontal axis. The values of pH_{pzc} for 1, 0.1 and 0.01 M KCl were 5.75, 6.00 and 6.25 respectively. Therefore, the pH_{pzc} of Al/Feoxide-modified DE was 6.0 ± 0.2 . At $pH \geq 6.0 \pm 0.2$, fluoride removal from solution will be by exchange of fluoride ions with the hydroxyl ions on the surface of the sorbent. At $pH < 6.0 \pm 0.2$, fluoride removal will be by electrostatic attraction of fluoride ions to the electropositive sorbent's surface.

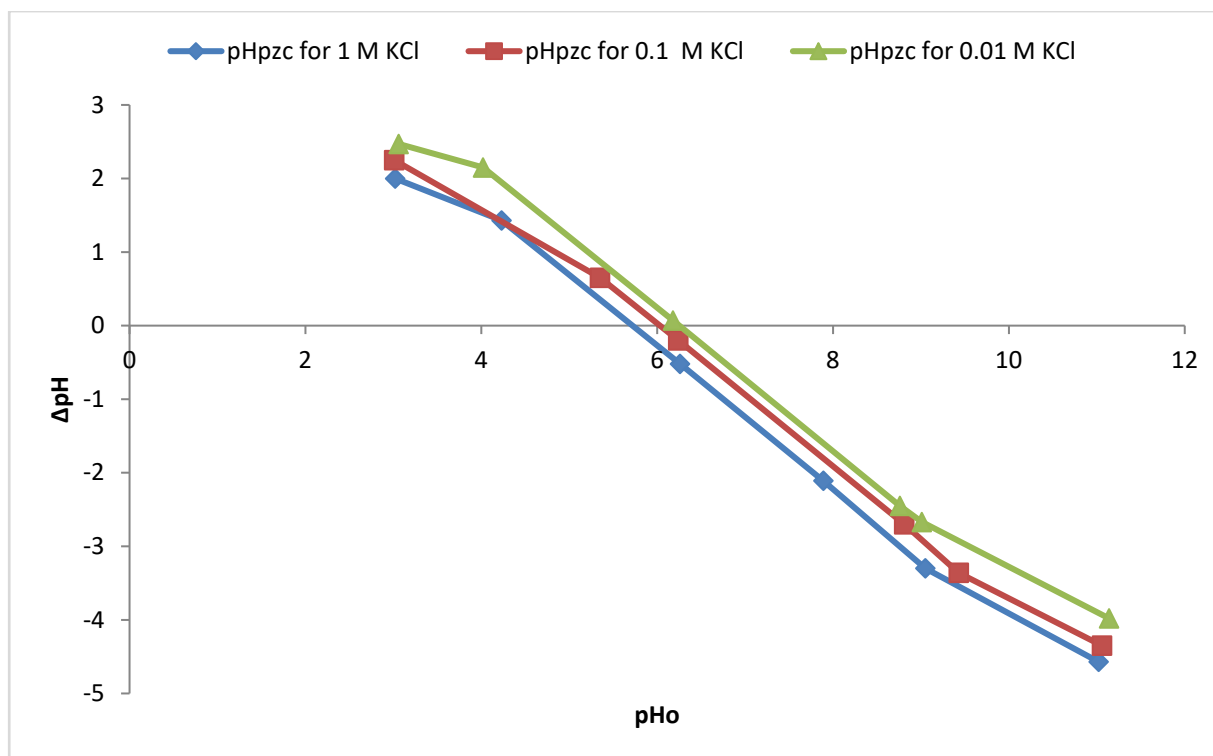


Figure 13.7. Variation of initial solution pH with ΔpH of solutions at 0.01, 0.1 and 1 M KCl for Al/Fe modified DE (vol 50 mL, adsorbent dosage: 0.5 g, contact time: 24 h and shaking speed: 200 rpm).

13.5.9 Thermogravimetric analysis (TGA)

The stability of Al/Fe oxide-modified DE and pure binary Al/Fe oxide was evaluated by carrying out thermogravimetric analysis of the adsorbent using TGA Q500 V20.13 Build 39. The heating in the furnace was done to a maximum temperature of 900°C. The per cent weight of sample at each temperature was plotted against the corresponding temperature in order to compare the trends in the variation of the masses of samples as the furnace temperature increased. The thermograms of Al/Fe oxide-modified DE and Al/Fe oxide were compared by plotting the per cent weight against the corresponding temperature (Figure 13.8). It is observed that the thermograms had a similar trend. There was a progressive weight loss with increasing temperature except for a narrow region around 600°C which showed a steady state or constant mass. Weight loss was more pronounced at temperature above 600°C. The limit of temperature stability of the samples was 600°C. This observation explains why there was a remarkable decline in the per cent fluoride removal for adsorbents calcined temperatures above 600°C (Figure 13.8).

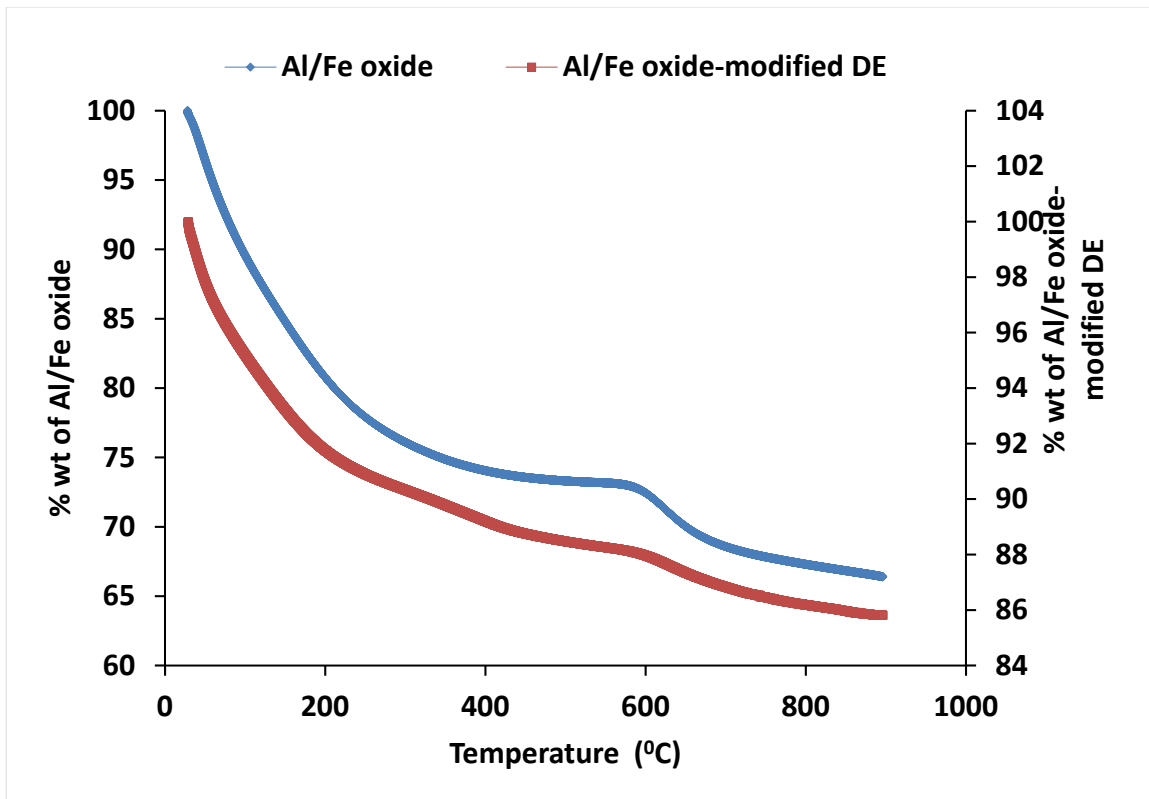


Figure 13.8. The thermograms of Al/Fe oxide and Al/Fe oxide-modified diatomaceous earth.

13.6 OPTIMIZATION OF ADSORPTION CONDITIONS FOR FLUORIDE REMOVAL USING AL/FE OXIDE-MODIFIED DE

13.6.1 Effect of contact time on fluoride removal

Figure 13.9 presents the variation of % fluoride removal and adsorption capacity of Al/Fe modified DE with contact time. It is observed that the kinetics of fluoride adsorption was rapid and was accomplished within 5 minutes of contact. The system seemed to achieve equilibrium within a short time. Further increase in contact time didn't result in appreciable increase in fluoride removal. A similar trend in fluoride removal was reported by Yao et al. (2009) with the use of neodymium-modified chitosan for defluoridation of water. The mean difference between the percent fluoride removal at 5 min and 50 min contact times at the evaluated dosages was approximately 1%.

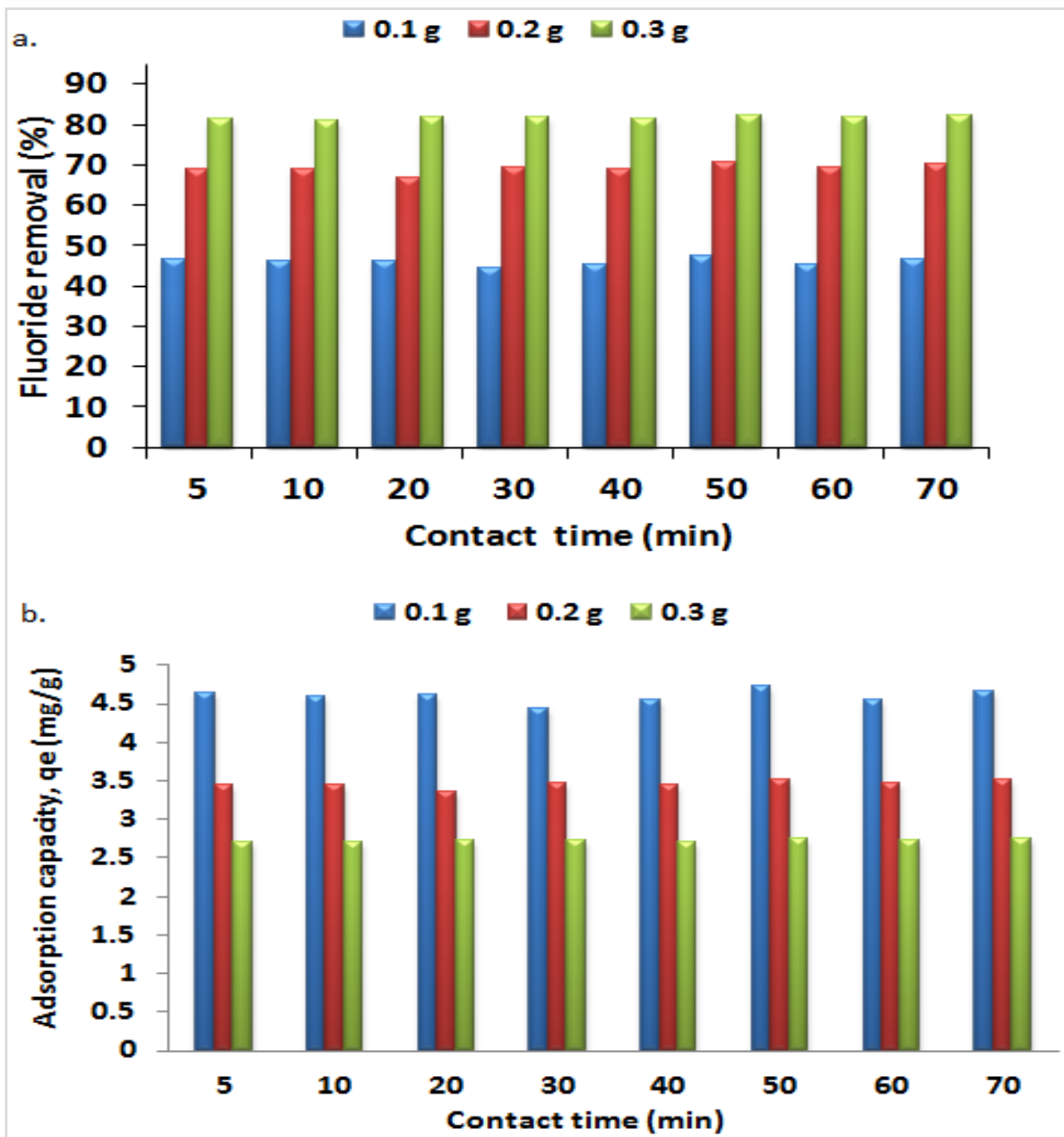


Figure 13.9. Variation of a. per cent fluoride removal and b. adsorption capacity with contact time at adsorbent doses of 0.1, 0.2 and 0.3 g (initial fluoride concentration: 10 mg/l, volume of solution: 100 ml, and temperature: 297 K and shaking speed: 200 rpm).

13.6.2 Effect of Al/Fe oxide-modified DE dosage on fluoride removal

Figure 13.10 shows the variation of per cent fluoride removal and adsorption capacity with adsorbent dosage. The per cent fluoride removal increased significantly from 0.1 g to 0.6 g, this is attributed to the increase in adsorption sites with increasing dosage. The observed increase in fluoride adsorption with increasing sorbent dosage has been reported by several authors (Shimelis et al., 2006; Meenakshi et al., 2008; Yao et al., 2009). At dosages greater than 0.6 g, there was no significant increase in fluoride removal. On the contrary the adsorption capacity was observed to decrease with increasing adsorbent dosage, this is attributed to resistance to intra-particle diffusion as the adsorbent surface becomes increasingly covered with adsorbate species. A compromise between appropriate adsorbent dosage that will give appreciable operating adsorption capacity is always adopted. A compromise dosage of 0.6 g was adopted. The aim was to achieve a high fluoride removal at an adsorbent dosage as low as possible.

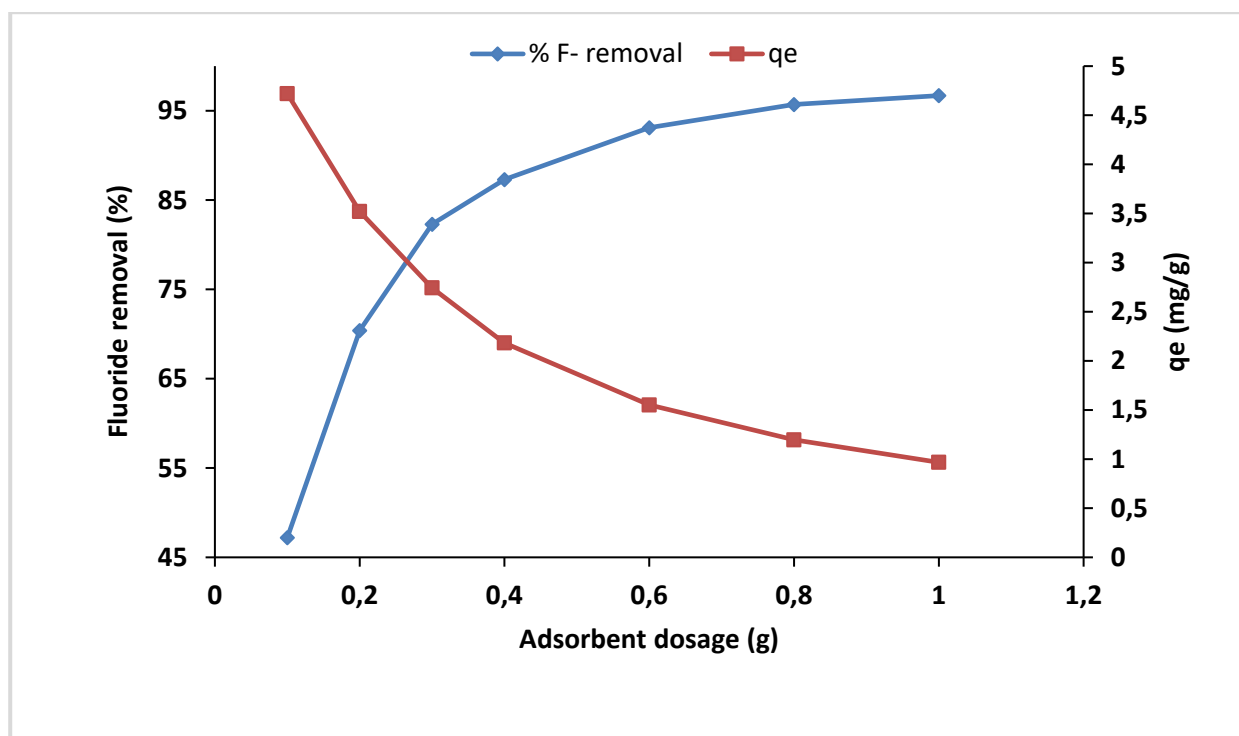


Figure 13.10. Variation of per cent fluoride removal and adsorption capacity with adsorbent dosage (initial fluoride concentration: 10 mg/l, volume of solution: 100 ml, shaking speed: 200 rpm and temperature: 297 K).

13.6.3 Effect of adsorbate concentration on fluoride removal by Al/Fe DE

Figure 13.11 presents the variation of the per cent fluoride removal and adsorption capacity of Al/Fe DE with the equilibrium fluoride concentrations. The trends are similar at the three evaluated temperatures. The per cent fluoride removal decreased with increasing initial fluoride concentration. Similar results were reported by Wambu et al. (2011) and Sakhare et al. (2012). However, the adsorption capacity of the adsorbent was observed to increase with increasing adsorbate concentration with maximum adsorption capacity being recorded at 100 mg/l adsorbate concentration (data not shown in the figure).

The adsorbent capacity recorded at 100 mg/l F⁻ concentration were 7.63, 6.97 and 7.25 mg/g at 297, 317 and 329 K respectively. The increase in the equilibrium pH with increasing initial fluoride concentration

could be attributed to the fact that fluoride being highly electronegative formed hydrogen bonds with water molecules. Hence, there was a progressive increase in the concentration of hydroxyl ions as the initial concentration of fluoride increased.

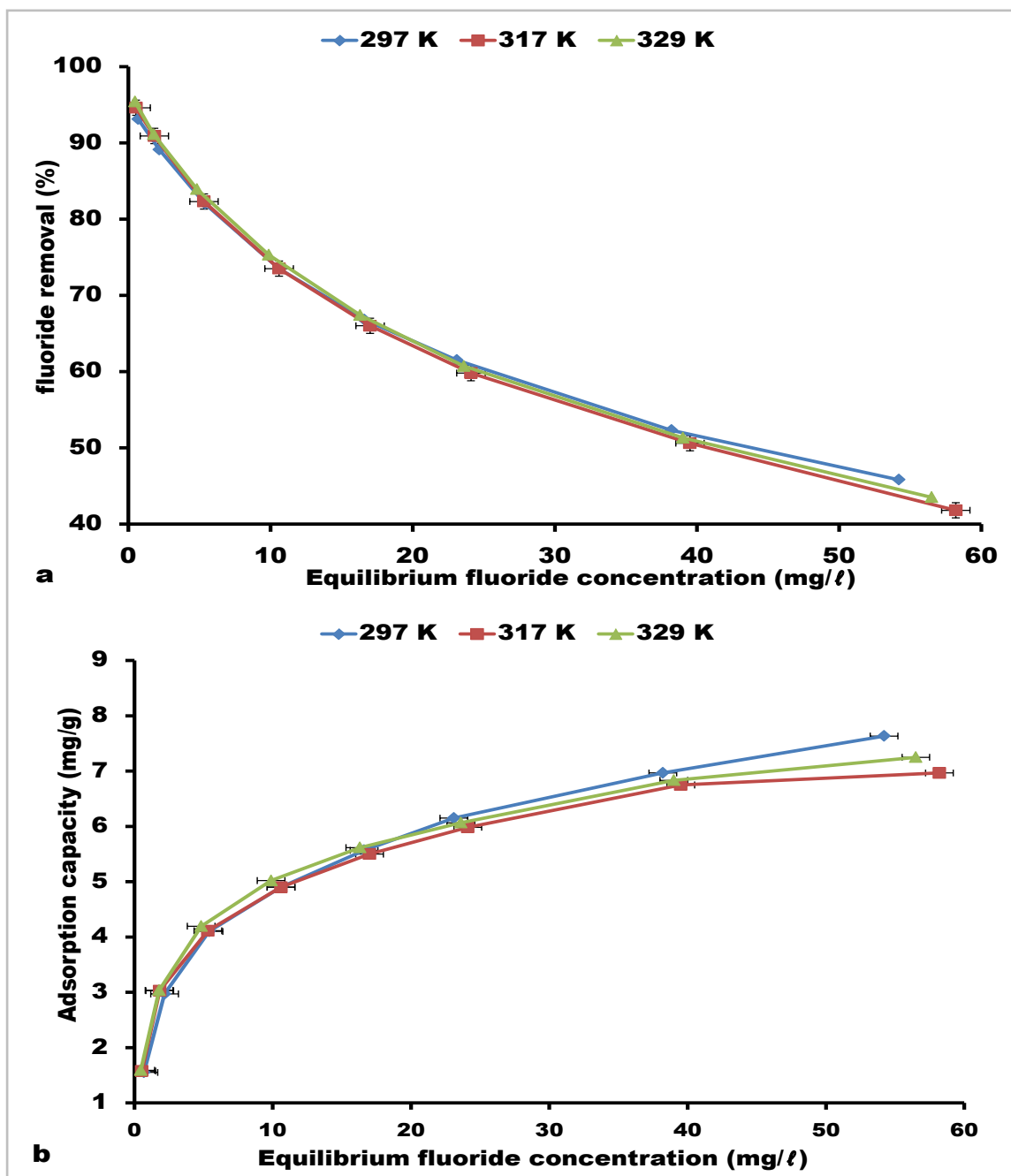


Figure 13.11. a). Variation of per cent fluoride removal and, b). adsorption capacity with adsorbate concentration at 297, 317, and 329 K (contact time: 50 min, volume of solution: 100 mL and shaking speed: 200 rpm).

13.6.4 Effect of pH on fluoride adsorption

It is widely reported that pH has an effect on adsorption of fluoride onto adsorbents and it is an important parameter in the adsorption process (Tripathy et al., 2006; Nasr et al., 2011). The effect of pH on fluoride

sorption onto Al/Fe oxide-modified DE was evaluated. The results of variation of percentage fluoride removal and other parameters with initial pH are presented in Table 13.5 and Figure 13.12. The highest fluoride removal occurred at equilibrium pH of 6.70 and initial pH 7.02. The least fluoride removal was observed at the highest pH. Significant fluoride removal occurred within the pH range 4.3 to 8.8. The pHPzc of Al/Fe oxide-modified DE was calculated to be 6.0 ± 0.2 . Below the pHPzc the adsorbent surface is positively charged and therefore attracts negatively charged fluoride, resulting to fluoride removal from solution.

Table 13.5. Effect of equilibrium pH on fluoride sorption

pH ₀	pH _e	C ₀ (mg/ℓ)	C _e (mg/ℓ)	% F ⁻ removal	q _e (mg/g)
2.00	2.51	11.25	8.16	27.5	0.5150
4.25	4.58	11.25	6.21	44.8	0.8400
7.02	6.70	11.25	0.86	92.3	1.7308
8.79	8.12	11.25	3.40	69.8	1.3083
10.94	10.49	11.25	11.2	0.44	0.0083
12.00	11.12	11.25	11.2	0.44	0.0083

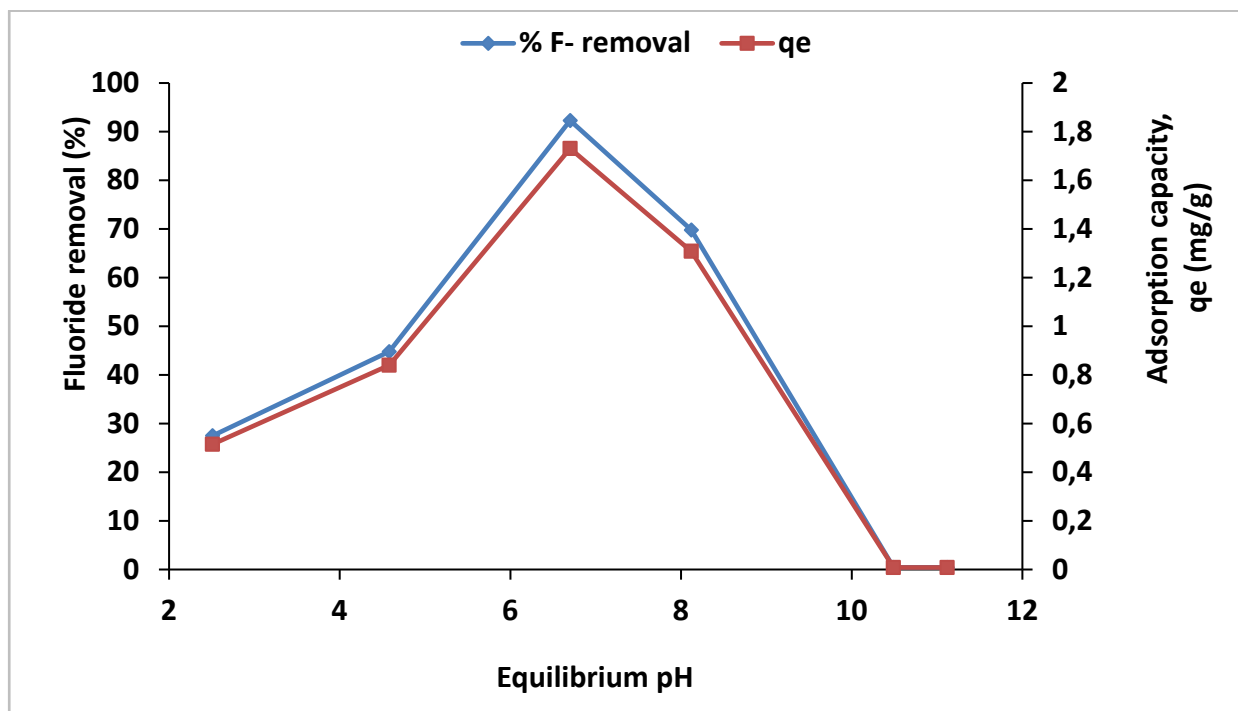


Figure 13.12. Variation of per cent fluoride removal and adsorption capacity with equilibrium pH (initial fluoride concentration: 11.25 mg/ℓ, volume of solution: 100 mL, temperature: 297 K, shaking speed: 200 rpm).

Contrary to reports that highest fluoride removal occurs at lower pH with most adsorbents, the low fluoride removal observed at low and high pH with this adsorbent could be attributed to loss of aluminium and iron oxides at low and high pH. It is reported that at pH < 5, Al₂O₃ dissolves leading to loss of adsorbent. At pH > 7, silicate and hydroxyl ions compete more strongly with fluoride ions for exchange sites (Bishop and Sansoucy, 1978; Shrivastava and Vani, 2009). Dissolution of silica matrix which acted as support for the Al/Fe oxide was evident from the light brown colloidal phase observed in the media at these pH values. As

an amphoteric oxide, Al_2O_3 would react with OH^- to form soluble species leading to further loss of the adsorbent.

Figure 13.13 shows the extent of loss of metal species at different values of media pH supporting the assertion of dissolution of Al_2O_3 and silica support matrix. The loss of Al^{3+} was least at pH 6.70, its value being close to that of Fe^{3+} . The same trend was observed for the two-metal species at pH 8.12 where the next higher fluoride removal occurred. The significant loss of Al^{3+} occurred at very high acidity and at very high alkalinity (Fig 13.13). Hence, fluoride removal was correspondingly low at that pH. That the concentrations of Al^{3+} and Fe^{3+} were low within the pH range 4.58 to 8.8 is evident of the chemical integrity and stability of the adsorbent at these pH conditions.

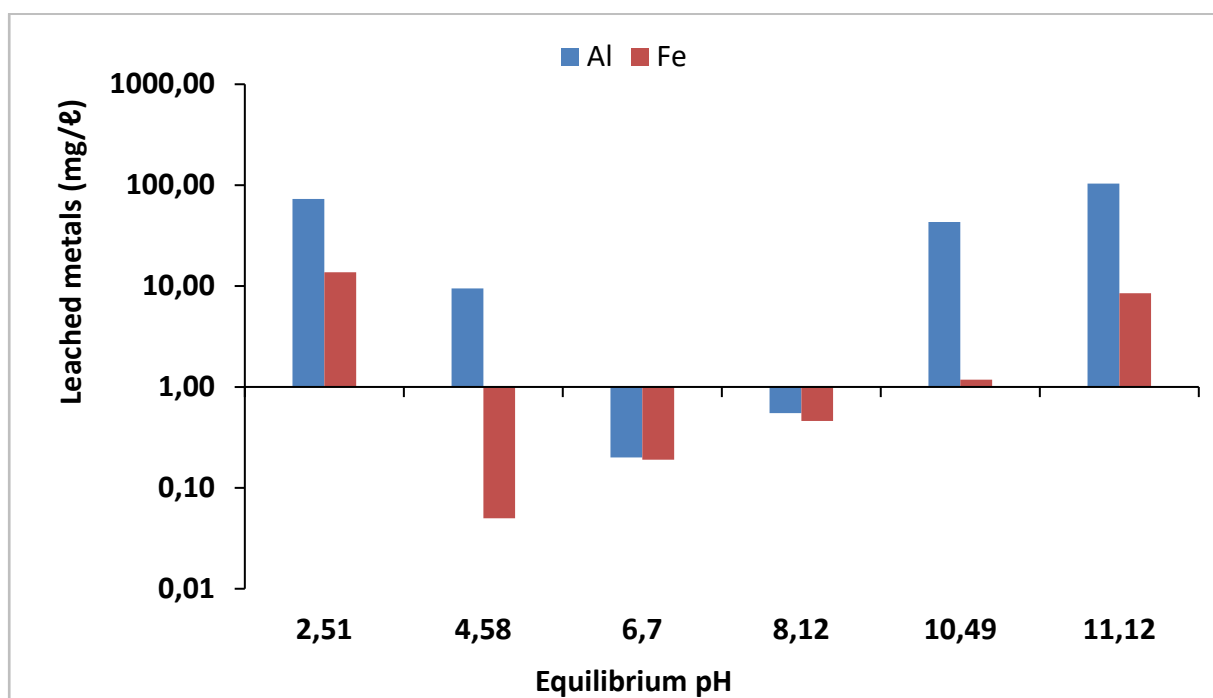


Figure 13.13. Leached metals as a function pH (initial fluoride concentration: 11.25 mg/l, volume of solution: 100 mL, temperature: 297 K, shaking speed: 200 rpm).

13.6.5 Effect of temperature

The effect of temperature on per cent fluoride removal and adsorption capacity was evaluated at 297 K, 317 K and 329 K and the results are presented in Figure 13.14. There was no significant change in per cent fluoride removal at the evaluated temperatures. This was also observed for the adsorption capacity. This implies that change in temperature had no effect on the sorption process. Therefore, the sorption process could be carried out at ambient temperatures. The feasibility of fluoride sorption even at the ambient temperature is confirmed by the negative value of the Gibbs free energy ($\Delta G^\circ = -12\,905.04$ J/mol) at 297 K. Hence, Al/Fe oxide-modified DE is appropriate for removal of excess fluoride from drinking water at room temperature.

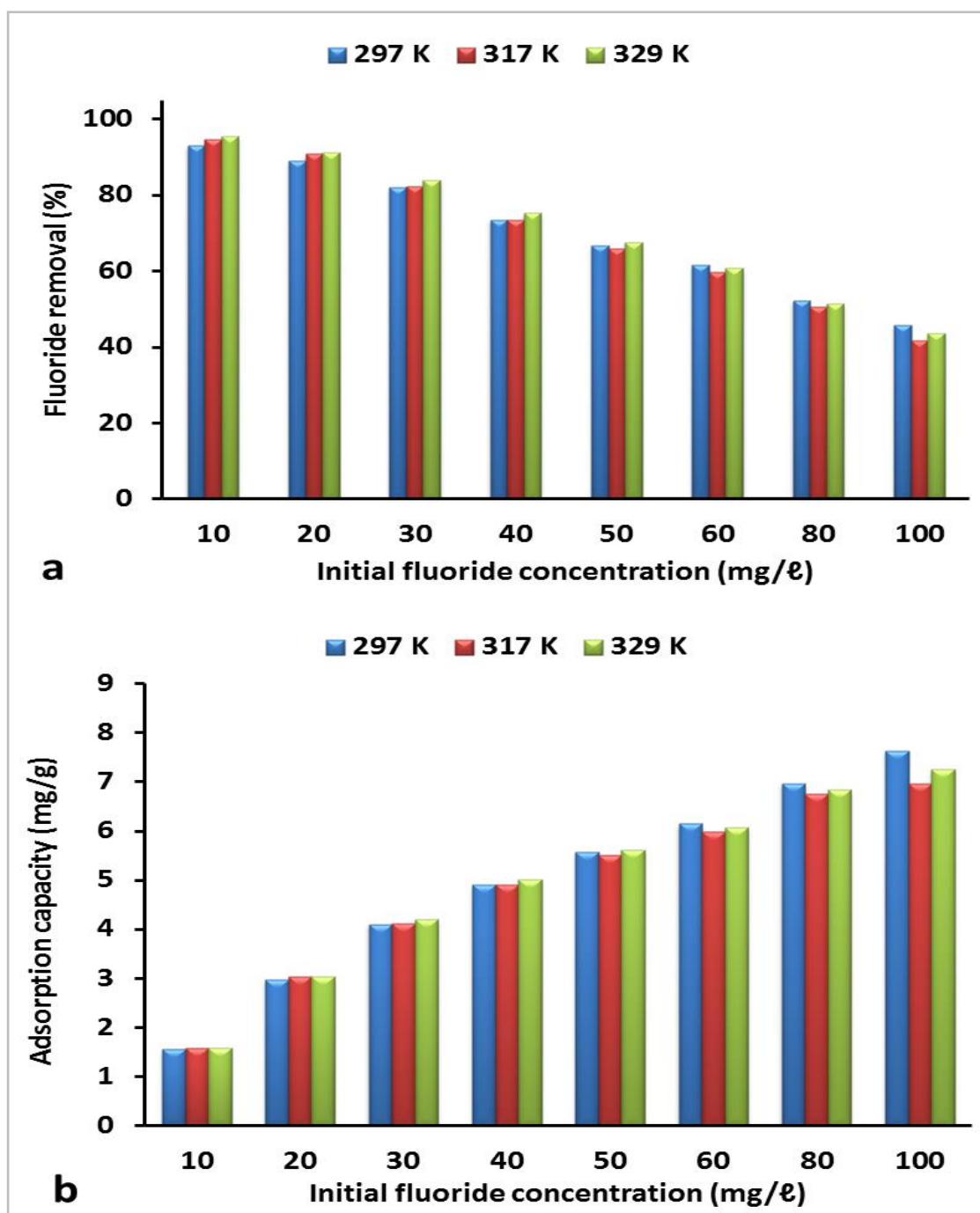


Figure 13.14. a) Per cent fluoride removal and, b) adsorption capacity as a function of temperature (contact time: 50 min, temperature: 297, 317, and 329 K, volume of solution: 100 ml and shaking speed: 200 rpm).

13.6.6 Evaluation of defluoridation efficiency of different Al/Fe oxide-modified diatomaceous earth samples

The results of the fluoride analysis of the supernatants obtained from contacting 0.4 g of different Al/Fe oxide-modified DE samples are presented in Table 13.6. The optimum defluoridation was obtained for AF-D3 which resulted from equal mixtures of equimolar Al^{3+} and Fe^{2+} solutions. Modification with combined

oxides was done at the mixture ratio 1:1. It therefore follows that modification involving addition of equal volumes of Al^{3+} and Fe^{2+} salts would give Al/Fe oxide-modified DE with highest defluoridation efficiency.

Table 13.6. Per cent fluoride removal by co-precipitated metal oxide-modified DE from different metal ratios

Sample of modified DE	$\text{Al}_2\text{O}_3/\text{Fe}_2\text{O}_3$ -	pH_e	C_e (mg/l)	% fluoride removal
AF-D1		7.26	6.74	15.8
AF-D2		7.31	5.52	31.0
AF-D3		7.26	4.69	41.4
AF-D4		7.31	4.94	38.3
AF-D5		7.25	5.61	29.9

A-Al, F-Fe

Adsorbents prepared in Table 13.6 used Fe^{2+} solution as the feedstock which required leaving the solution in the open for some time for complete oxidation of Fe^{2+} to Fe^{3+} . The process of leaving $\text{Fe}(\text{OH})_2$ -DE-NaOH solids in air for hours to accomplish oxidation of Fe^{2+} to Fe^{3+} led to much loss of diatomaceous earth since silica is highly soluble at alkaline pH. To avoid loss of material, Fe^{3+} salt was used in subsequent modifications requiring Fe^{3+} in the composite. With the use of Fe^{3+} salt, no further oxidation of metal was required. Therefore, $\text{Fe}_2(\text{SO}_4)_3 \cdot x\text{H}_2\text{O}$ was used in place of $\text{FeCl}_2 \cdot 4\text{H}_2\text{O}$. The results of the per cent fluoride removal following equilibration of mixtures of fluoride solution and adsorbent are reported in Table 13.7.

Table 13.7. Percent fluoride removal using different metal oxide-modified DE samples

Modified DE	pH_0	pH_e	C_e (mg/l)	% F ⁻ removal
ADE	6.90	6.56	0.345	96.55
FDE	6.55	6.50	6.280	37.20
AFDE	6.51	6.43	0.302	96.98

ADE – Al diatomaceous earth, FDE – Fe diatomaceous earth, AFDE – Al, Fe diatomaceous earth

Results show that Al_2O_3 - Fe_2O_3 -modified DE (AFDE) had the highest defluoridation potential (96.98% fluoride removal) of the three modified DE samples and closely followed by Al-DE (96.66% fluoride removal). Fe_2O_3 -modified DE had the least defluoridation potential. There was no pH adjustment of mixtures since pH adjustment would not be practicable in the application of adsorbents in domestic defluoridation units. Diatomaceous earth was impregnated with Al/Fe oxides through co-precipitation with $\text{Fe}^{3+}/\text{Al}^{3+}$ solutions, NaOH was used to adjust the pH for the optimum precipitation of the oxides. An optimum pH of 8.2 was used. Contact time for optimum precipitation was established. The Al/Fe impregnated DE was dried at 110°C for hours and was then ready for use.

13.7 EVALUATION OF THE DE MODIFICATION WITH Al_2O_3 - AND Fe_2O_3 THROUGH ANALYSIS OF SUPERNATANTS

13.7.1 Relationship between leached metals and adsorbent dosage

It was necessary to evaluate the potential of Al/Fe oxide-modified DE to leach Al and Fe species in treated water during the adsorption process since it has an impact on the quality of the product water. Supernatants at various equilibrium pH were analysed for residual Al and Fe. Samples of supernatants obtained from the contact of various sorbent dosages with 10 mg/l fluoride solution at different equilibrium pH values were analysed for Al and Fe in an attempt to determine the chemical stability of the adsorbent. The results are

presented in Figure 13.15. The concentrations of Al and Fe species were in trace levels. The average equilibrium pH of solution was 6.59 ± 0.09 .

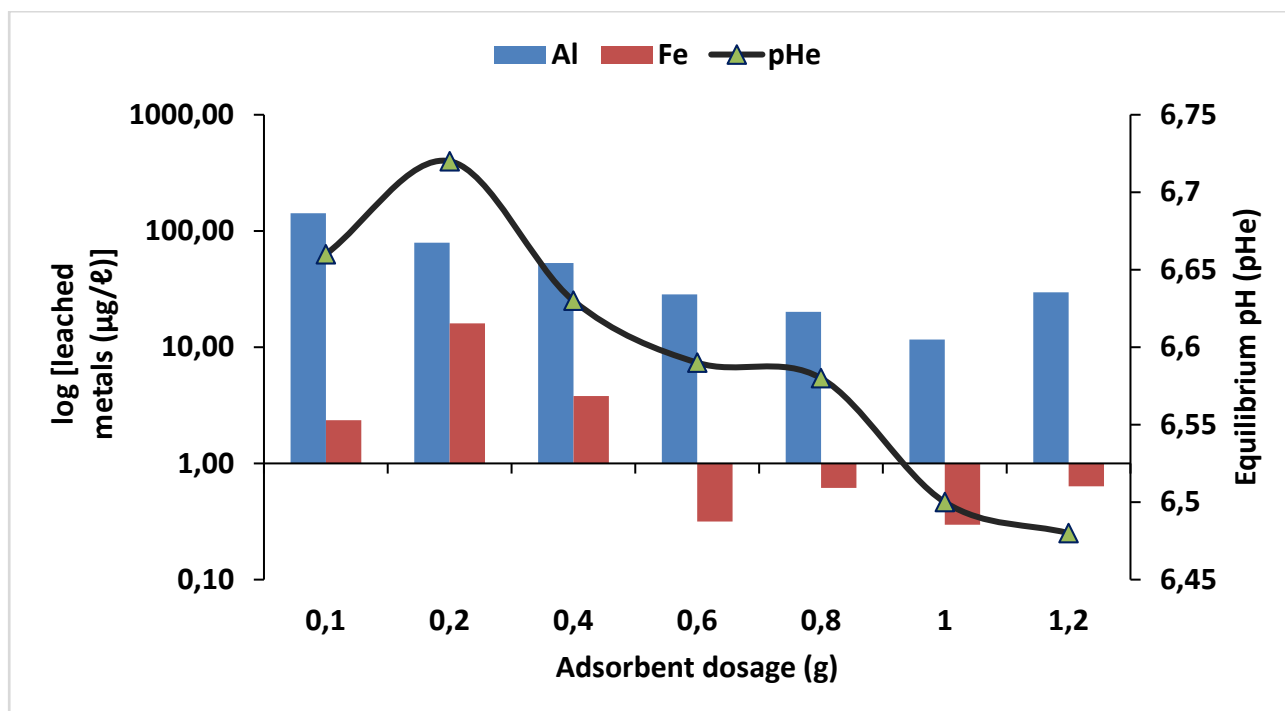


Figure 13.15. Concentration of leached metals as a function of adsorbent dosage (initial fluoride concentration: 10 mg/ℓ, volume of solution: 100 mL, contact time: 50 min, temperature: 297 K and shaking speed: 200 rpm).

13.7.2 Effect of co-existing anions on F⁻ sorption

In groundwater, other anions exist with fluoride and would probably compete with fluoride for adsorption sites. Some of the common anions in groundwater include NO₃⁻, CO₃²⁻, SO₄²⁻ and PO₄³⁻ ions (Chen et al., 2011). The effect of each anion on fluoride adsorption was evaluated separately. The simulated fluoride-rich groundwater was prepared by spiking with a competing anion, the defluoridation was then tested in the presence of the competing anion. The effect of SO₄²⁻, NO₃⁻, CO₃²⁻ and PO₄³⁻ as co-existing anions on fluoride sorption was evaluated. The per cent fluoride removal in competing anion-free supernatant was taken to be the optimum value and designated blank (Table 13.8). Results indicated that the per cent fluoride removal varied with the type of anion. The order in which the anions competed with fluoride was SO₄²⁻ < NO₃⁻ < CO₃²⁻ ≈ PO₄³⁻. There was no significant difference between CO₃²⁻ and PO₄³⁻ in competition with fluoride. Negatively charged ions are naturally attracted to positively charged cations. The extent of attraction is dependent on the magnitude of charge and size of ion. Usually anions with higher charge density are more strongly attracted to cations than the univalent anions. This explains why PO₄³⁻ competed highly with F⁻ for adsorption than other anions. The equilibrium pH ranged between 6.80 and 6.98.

Table 13.8. Effect of co-existing anions on fluoride adsorption (Initial adsorbate conc: 10 mg/l F⁻)

Anion	Conc. of added anion (mg/l)	C _e (mg/l)	% F ⁻ removal	pH ₀	pH _e
Blank	0	0.69	93.1	6.85	6.77
CO ₃ ²⁻	5	1.59	84.1	6.99	6.98
PO ₄ ³⁻	5	1.61	83.9	6.92	6.87
NO ₃ ⁻	5	1.42	85.8	6.86	6.82
SO ₄ ²⁻	5	1.37	86.3	6.82	6.80

Further studies were carried out to determine the extent to which the concentration of phosphate could affect fluoride removal. The concentration of phosphate was varied from 2 to 5 mg/l. From the results, a concentration as low as 2 mg/l phosphate in water containing 10 mg/l fluoride could lower the per cent fluoride removal by about 8%. Increasing the phosphate concentration to 5 mg/l only caused a slight further decrease in fluoride removal (Table 13.9).

Table 13.9. Effect of phosphate ion concentration on fluoride removal (Initial adsorbate conc: 10 mg/l F⁻)

PO ₄ ³⁻ (mg/l)	% F ⁻ removal	pH ₀	pH _e	C _e (mg/l)
-	93.1	6.65	6.59	0.69
2	85.2	6.74	6.78	1.48
3	84.9	6.82	6.78	1.51
4	84.8	6.89	6.85	1.52
5	83.9	6.92	6.87	1.61

13.7.3 Metal speciation calculations

The supernatants obtained when 0.6 g of Al/Fe oxide-modified DE was equilibrated with 100 ml of 11.25 mg/l fluoride solution at different pH values were analysed for Al and Fe using ICP-MS. PHREEQC geochemical model was used to calculate the activity of the various species of Al and Fe in the solutions. The necessary data required for the calculations included the pH, the metal concentrations as determined by ICP-MS, equilibrium fluoride concentrations and the equilibration temperature. The logarithms of the metal species concentrations were plotted against the pH to evaluate how the concentration of each species varied with pH and the species that would actually be responsible for fluoride removal at specific pH.

PHREEQC geochemical model was used to calculate the speciation of Al and Fe ions in supernatant solutions for equilibration of 0.6 g of Al/Fe oxide-modified DE and 100 ml of 11.25 mg/l fluoride solutions at various pH. The plots of the logarithms of activities of the various species of the metal species and fluoride ions against pH are presented in Figures 13.16 and 13.17. The equilibrium pH values of 6.70 and 8.12 are greater than the pH_{pzc} of Al/Fe oxide-modified DE calculated to be 6.0 ± 0.2. Above the pH_{pzc}, the adsorbent surface is negatively charged. Fluoride removal above the pH_{pzc} is attributed to ion-exchange as OH⁻ ions would predominate over H⁺ or more appropriately H₃O⁺ ions. Figure 6.62 shows that at the equilibrium pH values of 6.70 and 8.12, the sorbent surface would only be negatively charged because of Al(OH)₄⁻ and Fe(OH)₄⁻.

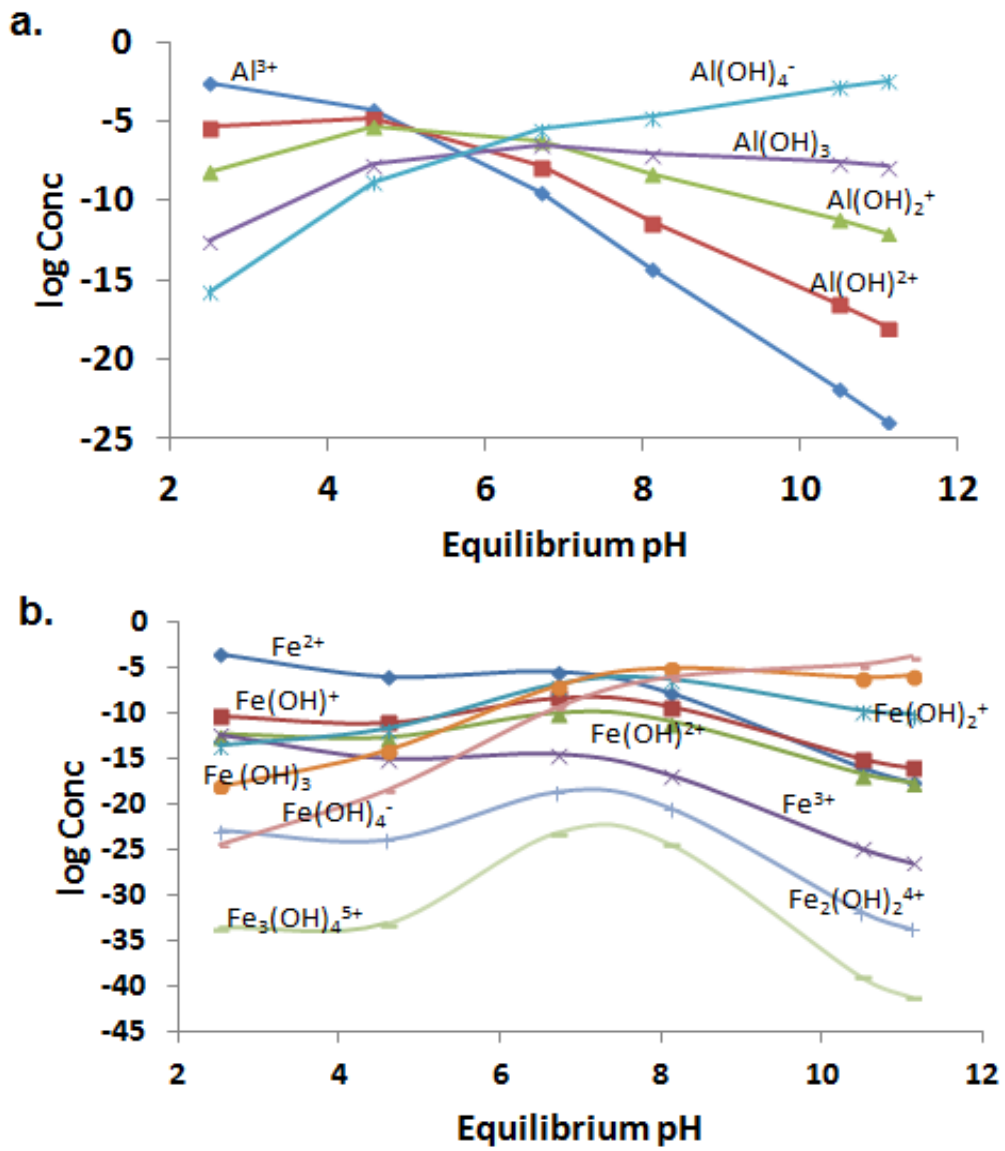


Figure 13.16. Variation of concentrations of species of a. Al and b. Fe at different pH values.

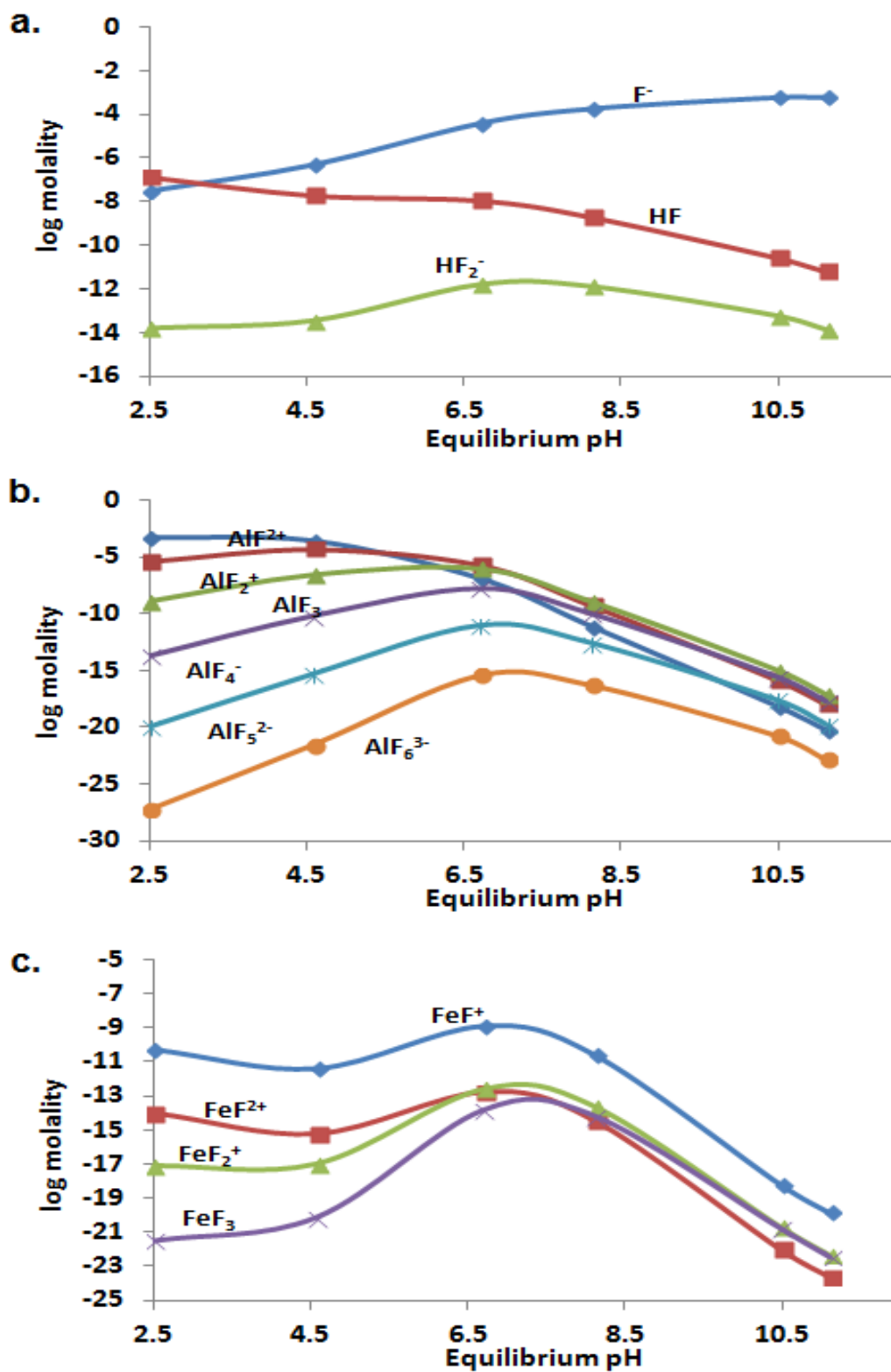


Figure 13.17. Variation of concentrations of a. fluoride species, b. Al-F complexes and c. Fe-F complexes at different pH values.

13.7.4 Effect of calcination

Al/Fe oxide modified diatomaceous earth was calcined at various temperatures to evaluate the effect of calcination on fluoride removal. The calcined adsorbents were then tested for fluoride removal using batch methods described in earlier sections. Similar samples were prepared and calcined at various temperatures and their chemical stability with respect to dissolution of the Al/Fe oxides evaluated in presence of HNO₃. The dissolved metal species were analysed by ICP-MS. Results of effect of calcination of Al/Fe oxide modified DE on fluoride removal are presented in Table 13.10 and Figure 13.18. Results indicate that the optimum calcination temperature was 200°C (473 K) which exhibited the highest fluoride removal. Fluoride removal for sorbent heated at 200°C was only slightly higher than sorbent dried at 110°C. Calcination is therefore not necessary considering the high cost of energy of calcination.

Table 13.10. Per cent fluoride removal and adsorption capacity at various calcination temperatures (Initial conc: 10 mg/ℓ)

Calcination temperature(°C)	pH ₀	pH _e	C _e (mg/ℓ)	% F ⁻ removal	q _e (mg/g)
110	6.878	6.951	0.695	93.1	1.551
200	6.710	6.930	0.524	94.8	1.580
400	6.765	6.820	0.766	92.3	1.539
600	6.859	6.916	1.460	85.4	1.423
900	7.795	8.186	9.610	3.9	0.065

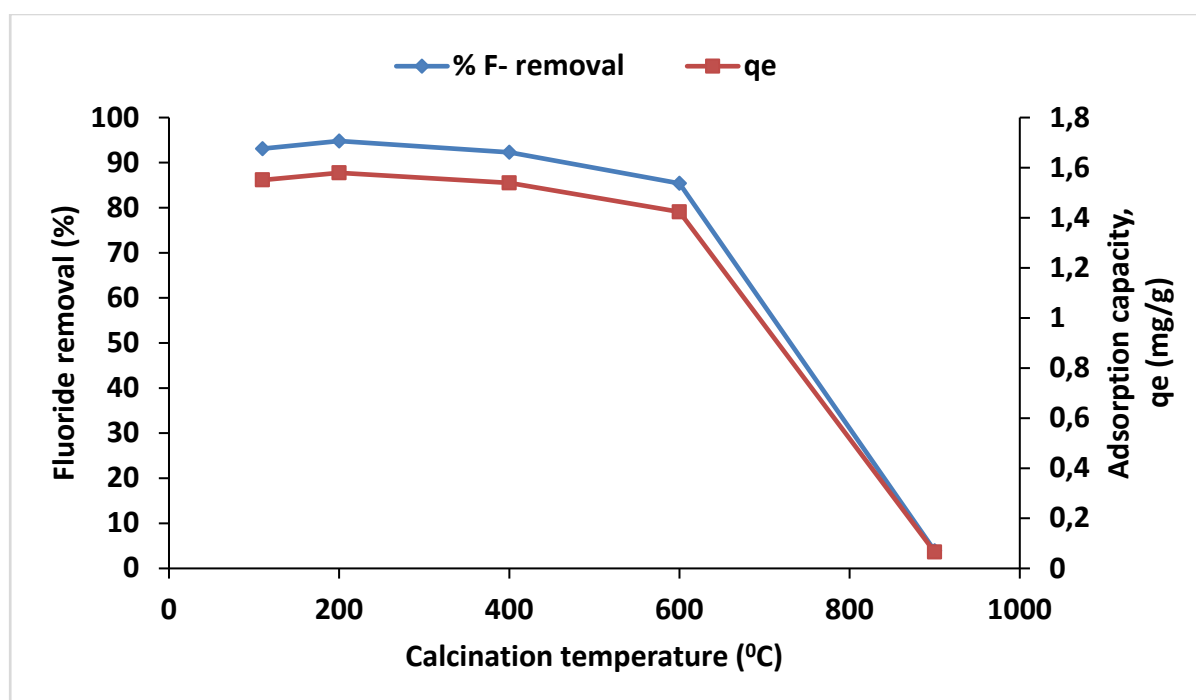


Figure 13.18. Variation of per cent fluoride removal and adsorption capacity with calcination temperature (initial fluoride concentration: 10 mg/ℓ, volume of solution: 100 mL, contact time: 50 min and shaking speed: 200 rpm).

The progressive reduction in the per cent fluoride removal as the calcination temperature increased must be due to loss of metals from the adsorbent by evaporation. At 900°C (1173 K), the structure of DE which served as a support for the Al/Fe oxide was completely destroyed (Ibrahim and Selim, 2012). This

development is corroborated by the inability of separation of the adsorbent-fluoride mixture by centrifugation. The particles which looked like very tiny strands of cotton could not settle. These must have arisen from the weakened DE structure which was readily broken apart during equilibration. For the stability evaluation of the adsorbent at different calcination temperatures, the results of the metal analysis after blank correction are reported in Table 13.11. The low metal concentrations in the adsorbent at calcination temperature above 600°C (Table 13.11 and Figure 13.19) explains why a very low fluoride removal was recorded for the sample calcined at 900°C. The adsorbent is quite unstable at temperatures above 600°C. There was a substantive loss of metals through evaporation.

Table 13.11. Concentration of major elements in calcined adsorbent at different temperatures

Temperature (°C)	Al (mg/ℓ)	Fe (mg/ℓ)	Si (mg/ℓ)
105	311.7	443.6	26.55
200	314.5	451.2	26.40
400	328.6	464.4	29.48
600	350.3	475.0	32.91
700	176.2	150.3	28.77
800	129.2	88.43	27.22

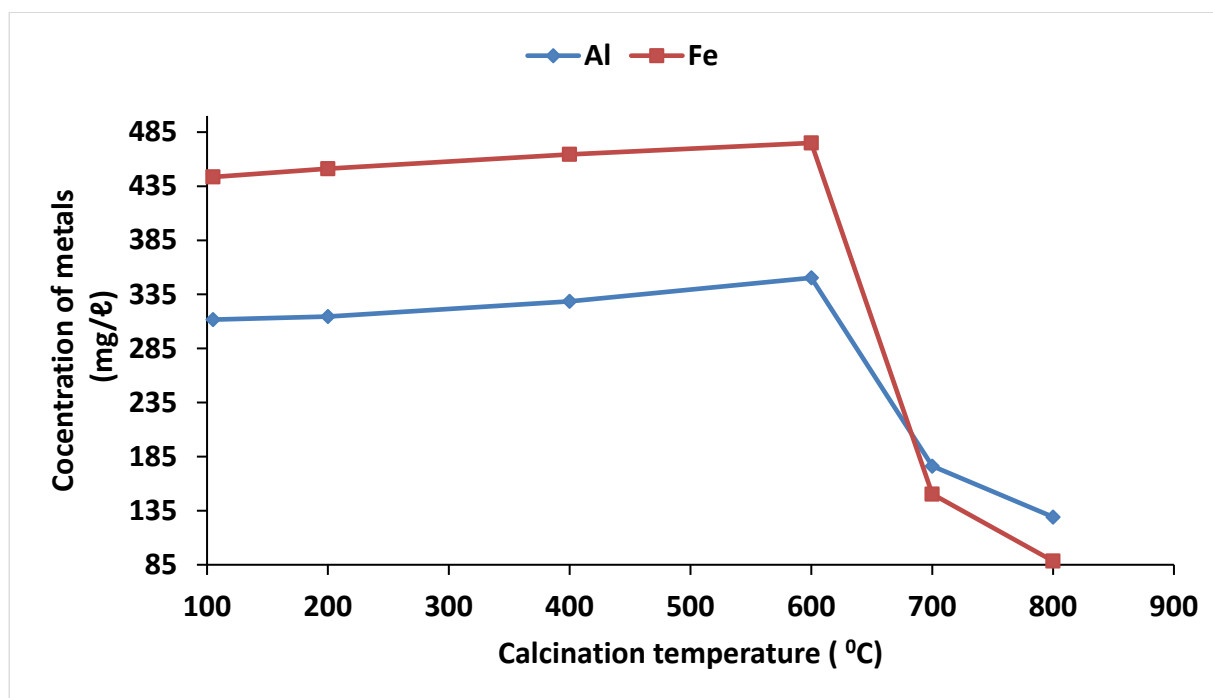


Figure 13.19. Residual metal species concentration in Al/Fe oxide-modified DE at different calcination temperatures (Adsorbent dosage: 0.5 g/50 mL of acid solution).

13.8 ADSORPTION MODELING

13.8.1 Isotherm models

Using the linearised Langmuir equation by Kinniburgh (1986) the obtained values were plotted against the sorption data (Fig 13.20) for temperatures 297 K, 317 K and 329 K. The adsorption data at all temperatures was adequately described by the Langmuir model with strong correlation factor observed ($R^2=0.99-0.995$). This is an indication the process was a monolayer adsorption.

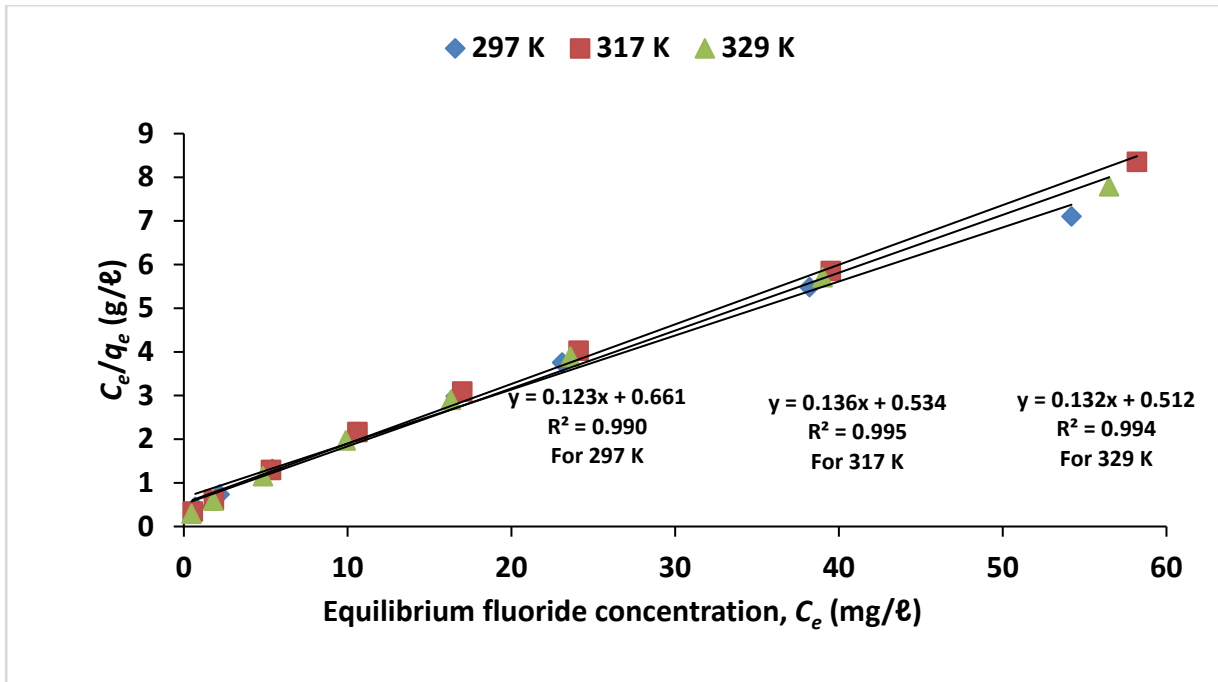


Figure 13.20. Langmuir isotherm plots at 297, 317 and 329 K (contact time: 50 min, volume of solution: 100 mL, adsorbent dosage: 0.6 g and shaking speed: 200 rpm).

The possibility of a multi-site adsorption was evaluated by fitting sorption data into the Freundlich isotherm, where $1/n$ values are much less than 1, the adsorbents are heterogeneous (Papageorgiou et al., 2006). The values of K_F and $1/n$ can be computed from the plots of against C_e . The plot of against C_e for the sorption data at 297 K, 317 K and 329 K returned high correlation coefficients (Figure 13.21). The adsorption data fitted better to Langmuir than Freundlich isotherm. Nevertheless, the heterogeneity of the adsorbent is established by the low values of the parameter $1/n$ (Table 13.12). It can be inferred that fluoride sorption occurred at both the smooth surfaces and the multi-sites of the adsorbent since the correlation coefficients were very high.

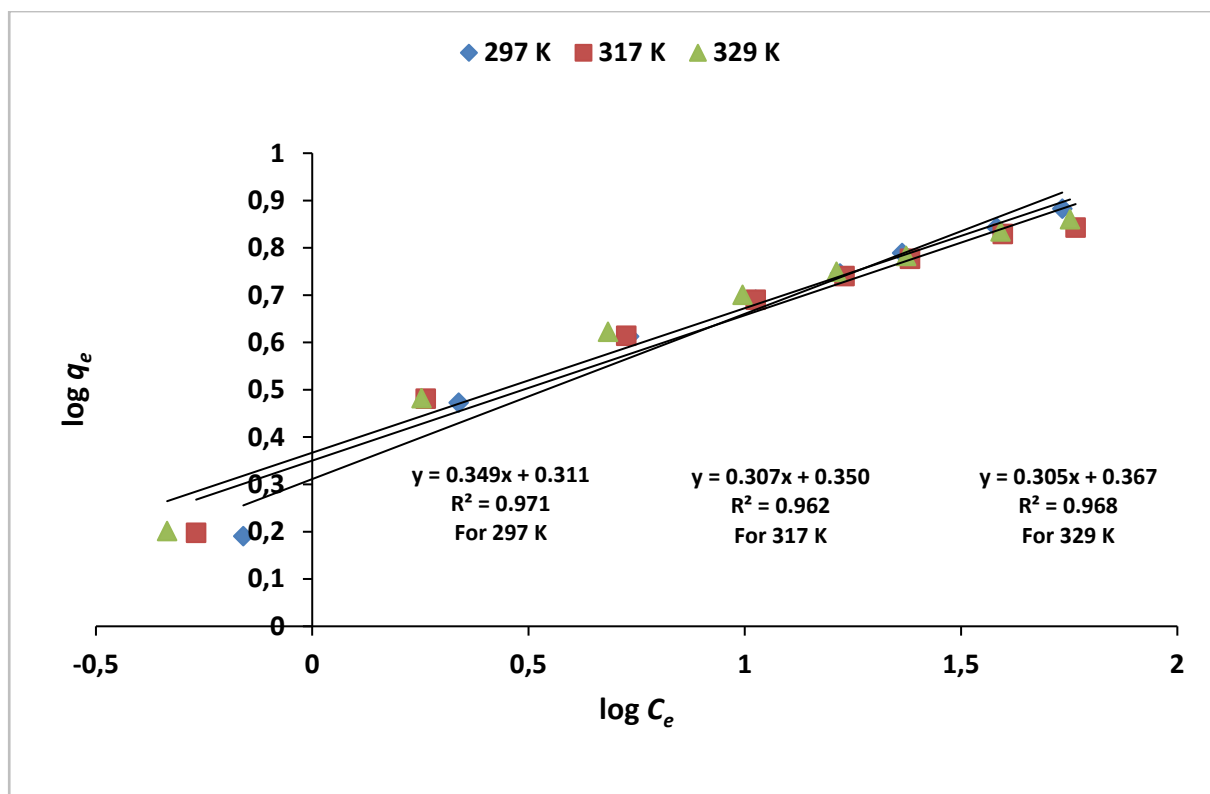


Figure 13.21. Freundlich isotherm plots at 297 K, 317 K and 329 K (contact time: 50 min, volume of solution: 100 mL, adsorbent dosage: 0.6 g, shaking speed: 200 rpm).

Table 13.12. Calculated Langmuir and Freundlich isotherm parameters

Temperature (°K)	Langmuir isotherm constants			Freundlich isotherm constants		
	$q_m(\text{mg/g})$	$K_L(\text{l/mg})$	R^2	$1/n$	K_F	R^2
297	8.1301	0.1861	0.990	0.349	2.0464	0.971
317	7.3529	0.2547	0.995	0.307	2.2387	0.962
329	7.5758	0.2578	0.994	0.305	2.3281	0.968

Dimensionless separation factor, R_L which is an essential feature of Langmuir model was used to evaluate favourability of fluoride adsorption at the various initial fluoride concentrations (Figure 13.22). R_L describes the shape of the isotherm to be unfavourable if $R_L > 1$, linear if $R_L = 1$ and favourable if $0 < R_L < 1$ (Weber and Chakravorti, 1974). The condition $0 < R_L < 1$ was fulfilled for all the initial concentrations considered at the evaluated temperatures (Figure 13.22). Hence, adsorption was favourable at those fluoride concentrations.

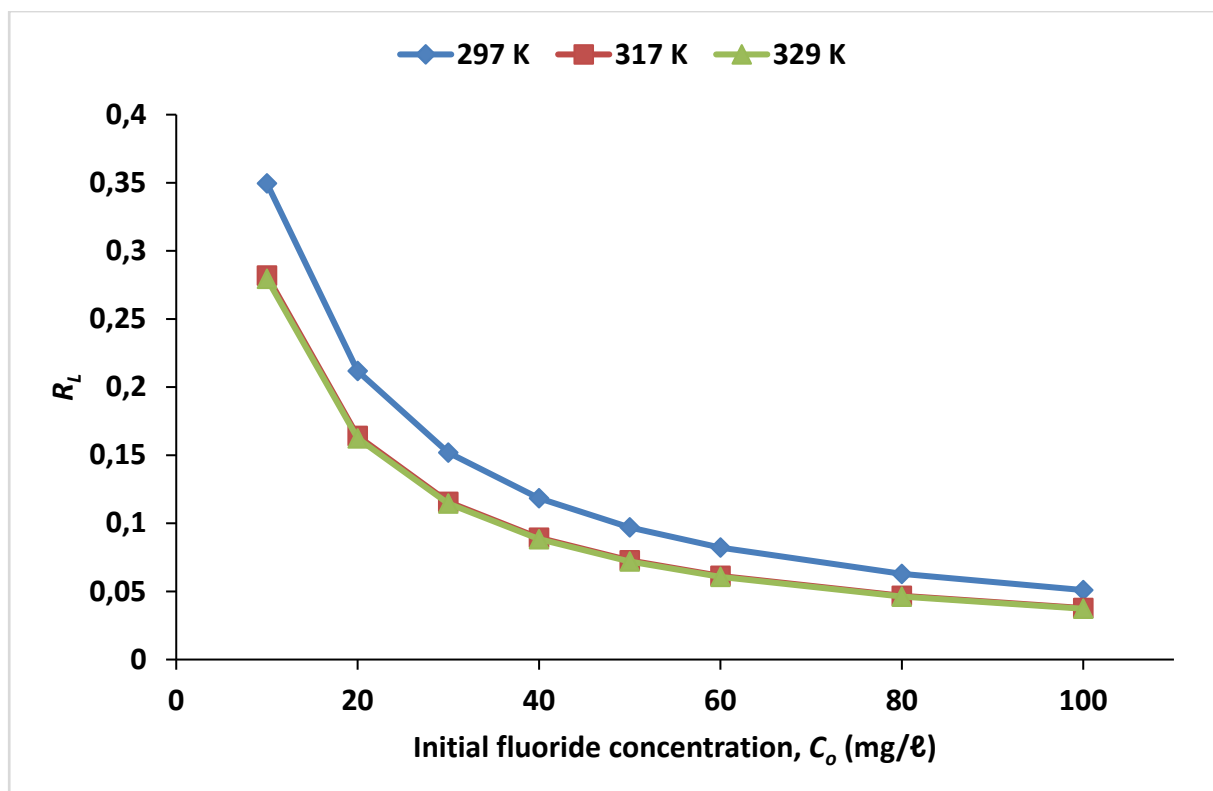


Figure 13.22. Values of dimensionless separation factor, R_L at different initial fluoride concentrations.

13.8.2 Adsorption thermodynamics

Temperature influences the spontaneity of a chemical process among other driving forces. However, the spontaneity of a chemical reaction is wholly determined by a thermodynamic quantity defined as the Gibbs free energy change, ΔG (Jenkins, 2008). The relationship between standard Gibbs free energy (and other thermodynamic functions) is presented in Appendix C. The standard Gibbs free energy change calculated for the sorption data at the evaluated temperatures have negative values (Table 13.13). This confirms the spontaneity of the sorption process at those temperatures. The standard enthalpy change (ΔH°) for fluoride sorption experiment at 297 K, 317 K and 329 K was evaluated graphically from the slope of the linear plot of $\ln K_L$ against $1/T$ (Figure 12.23).

Table 13.13. Adsorption thermodynamic parameters

$T(K)$	$1/T(1/K) \times 10^3$	$\ln K_L$	$K_L(m^3/kg)$	$\Delta G^\circ J/mol$
297	3.367	5.226	186.1	-12 905
317	3.155	5.540	254.7	-14 601
329	3.040	5.552	257.8	-15 186

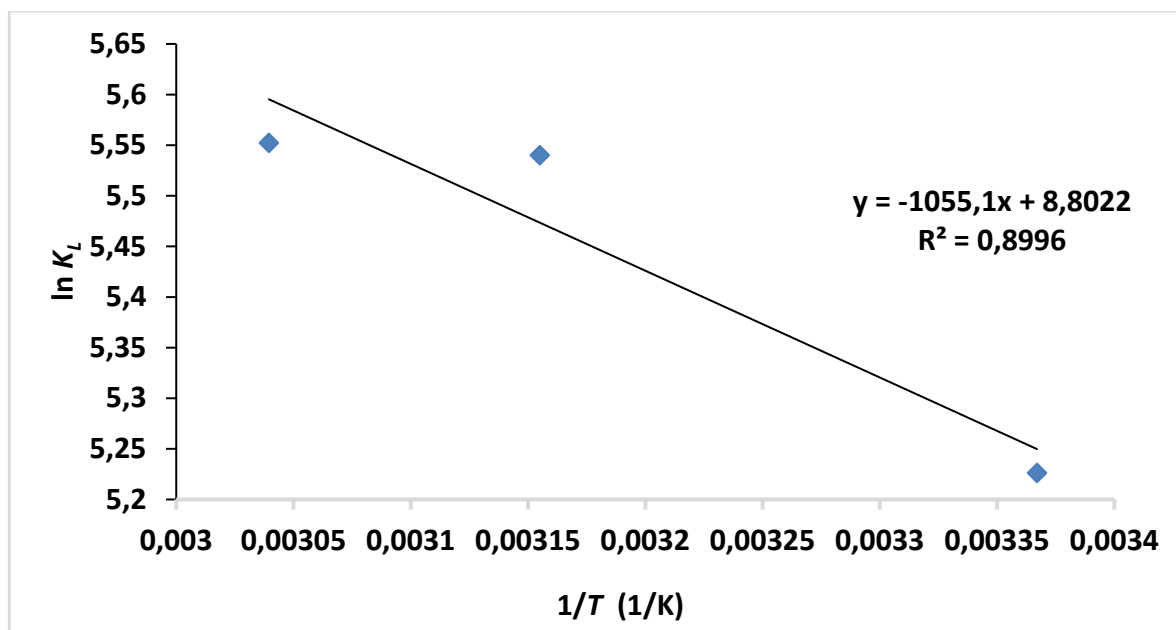


Figure 13.23. $\ln K_L$ as a function of reciprocal of adsorption temperatures.

The standard enthalpy change for the sorption of fluoride on Al/Fe oxide-modified DE was obtained from the slope of the linear plot of $\ln K_L$ against $1/T$ (Fig 12.23). The slope of the linear plot is -1055. Therefore,

$$-\frac{\Delta H^0}{R} = -1055$$

Hence, $\Delta H^0 = 8771.27$ J/mol.

The positive value of the standard enthalpy change is an indication that the fluoride sorption onto Al/Fe oxide-modified DE is endothermic.

13.8.3 Adsorption kinetics

The kinetics of the adsorption process were evaluated using the Lagergren pseudo-first and pseudo-second order kinetic models. The scatter plots indicate that the pseudo first-order model was not applicable to the sorption process (Figure 13.24). However, high correlation values were obtained confirming the kinetic data was well described by the pseudo-second order model suggesting chemisorption process (Figure 12.25). The calculated q_e and the experimental q_e were compared. The closeness of the two values as shown in Table 12.14 is an indication that the pseudo-second-order model adequately described the adsorption kinetics.

Table 13.14. Pseudo-second-order parameters at different adsorbent dosages

Adsorbent dosage (g)	Experimental q_e (mg/g)	Calculated q_e (mg/g)	k_2 ($\ell \text{ mg}^{-1} \text{ min}^{-1}$)
0.1	4.651	4.720	0.670
0.2	3.521	3.520	0.625
0.3	2.740	2.743	2.258

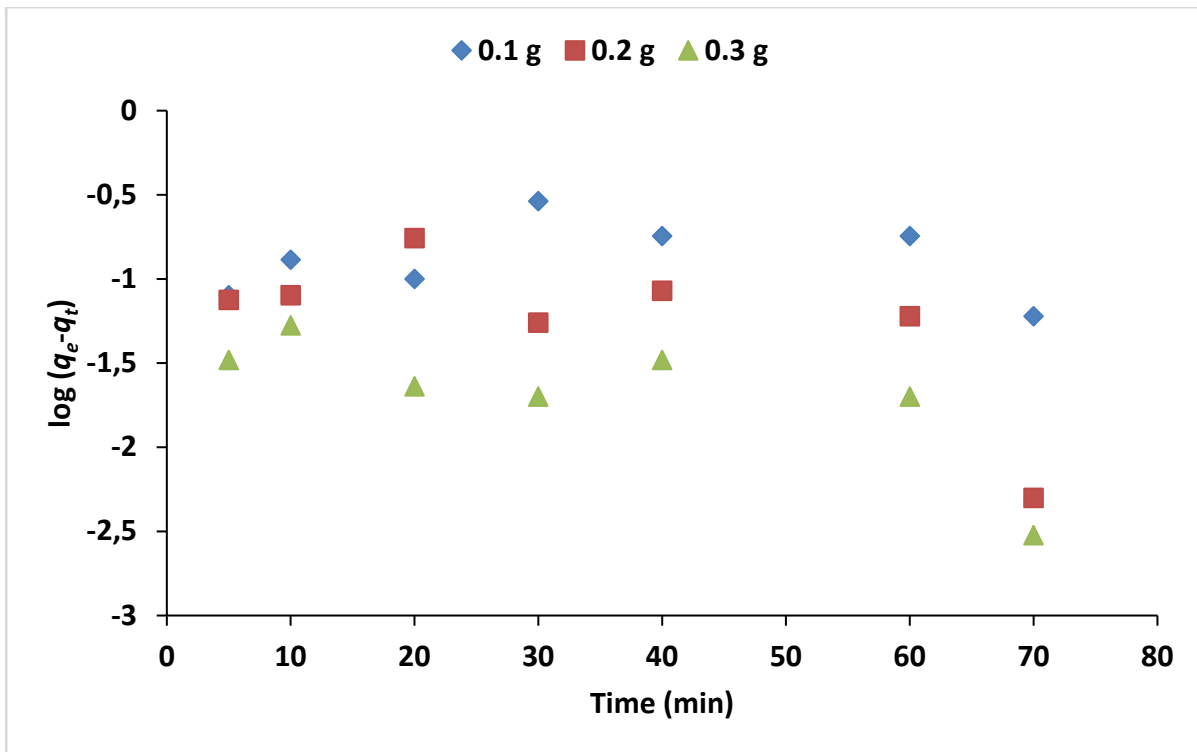


Figure 13.24. Pseudo-first-order profiles at different adsorbent dosages of a. 0.1 g, b. 0.2 g and c. 0.3 g of Al/Fe oxide-modified DE (initial fluoride concentration: 10 mg/ℓ, volume of solution: 100 mℓ, temperature: 297 K and shaking speed: 200 rpm).

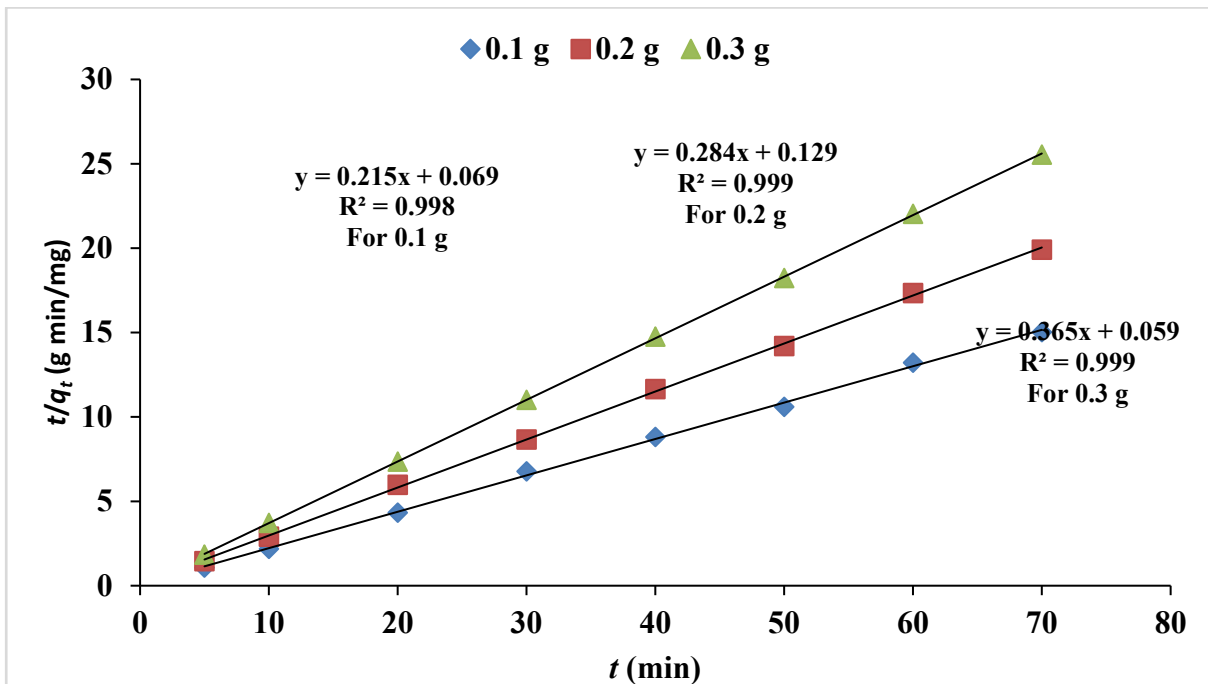


Figure 13.25. Pseudo-second-order profile at different adsorbent dosages (initial fluoride concentration: 10 mg/ℓ, volume of solution: 100 mℓ, temperature: 297 K and shaking speed: 200 rpm).

13.8.4 Adsorption mechanisms

13.8.4.1 Intra-particle diffusion

The probable mechanism controlling the sorption rate was evaluated using the intra-particle diffusion model by Weber and Morris (1963). The intra-particle diffusion plots for the three dosages evaluated are presented in Figure 13.26, showing poor correlations. The minimum pore diameter of the adsorbent as determined by BET was 20.112 Å. The ionic radius of fluoride is 1.33 Å (Ruben, 1985). There was therefore no resistance to diffusion of fluoride ions through the adsorbent. This explains why intra-particle diffusion could not have been the sorption rate limiting step.

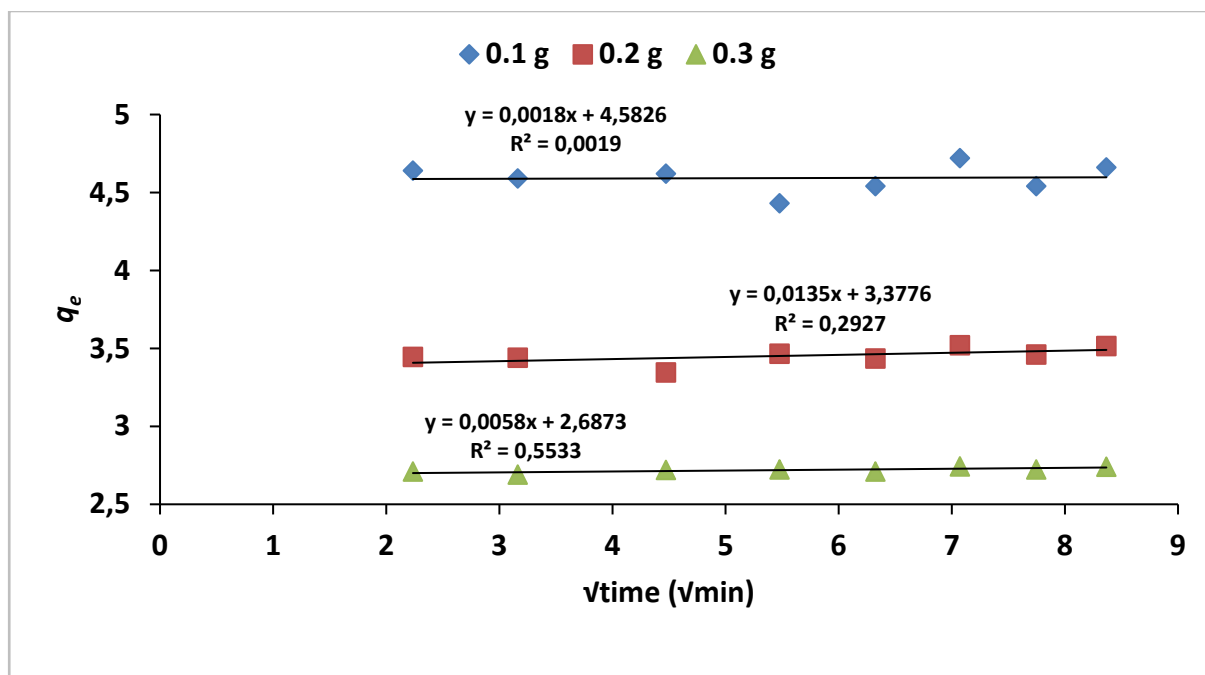


Figure 13.26. Intra-particle diffusion profile at different adsorbent dosages of 0.1 g, 0.2 g and 0.3 g (initial fluoride concentration: 10 mg/l, volume of solution: 100 ml, temperature: 297 K and shaking speed: 200 rpm).

13.8.4.2 External diffusion

The external diffusion model by Lee et al. (1999) was used to evaluate the possibility of external diffusion being the rate controlling step. Similarly, low correlation coefficients were observed indicating external diffusion was not the rate controlling process (Figure 13.27). The probable mechanism controlling the rate of fluoride sorption onto the adsorbent is the ion-exchange at the adsorbent surface.

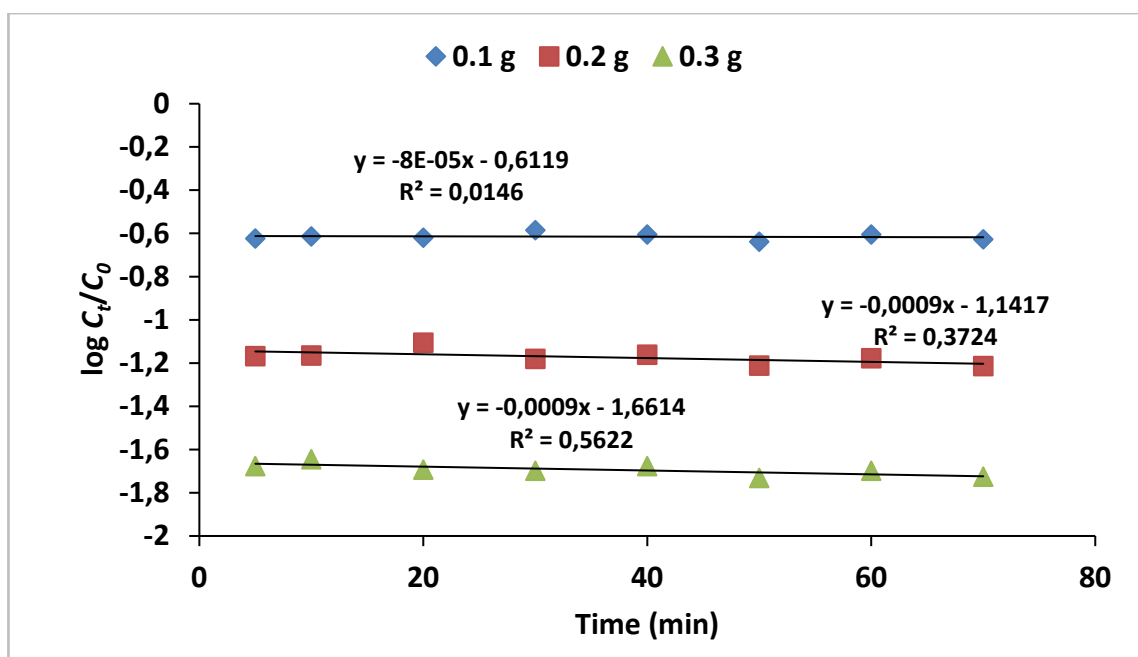


Figure 13.27. External diffusion profiles at adsorbent dosages of 0.1 g, 0.2 g and 0.3 g (initial fluoride concentration: 10 mg/ℓ, volume of solution: 100 mℓ, temperature: 297 K and shaking speed: 200 rpm).

13.9 DEFLUORIDATION OF FIELD WATER

The performance of Al/Fe oxide-modified DE in field groundwater defluoridation was evaluated by batch technique. The concentration of fluoride in field water was reduced from 5.53 to 0.93 mg/ℓ after 100 mℓ of the water was contacted with 0.6 g of adsorbent for 50 min. Thus, the per cent fluoride removal was 83.2%. The initial and equilibrium pH values were 6.92 and 6.80 respectively. The concentrations of the various parameters evaluated in raw and treated field water are reported in Table 13.15. Results indicate that the adsorbent removed all the competing anions except chloride to below the detection limits. The increase in the concentration of chloride in the treated was as a result of the leaching of the chloride from the adsorbent. The source could be the HCl used in the pre-treatment of the raw DE. The full chemical analysis of the field water before and after defluoridation was done using ICP-MS. From the results presented in Tables 13.16 and 13.17, all the chemical species evaluated in the raw and treated field water were below SANS 241-1 (2015) limits. Hence, the treated water would be chemically safe for drinking.

Table 13.15. Concentrations of competing anions in raw and treated field water

Co-existing anion	Concentration in raw water (mg/ℓ)	Concentration in treated water (mg/ℓ)	SANS 241-1 (2015) (mg/ℓ)
Cl ⁻	31.6	40.9	<200
Br ⁻	2.08	ND	-
NO ₃ ⁻	1.13	ND	<50
SO ₄ ⁻	11.9	ND	<400
PO ₄ ³⁻	ND	ND	-

ND: Not detected

Table 13.16. Concentrations of chemical species in raw and treated field water in mg/ℓ

Sample	concentration mg/ℓ								
	Ca	K	Mg	Na	P	Si	Sr	Al	Fe
Raw field water	2.93	2.06	0.072	69.38	<0.01	43.32	0.024	0.067	0.210
Treated field water	1.70	1.70	0.084	99.53	<0.01	18.11	0.012	0.139	0.129
SANS 241-1 (2015) (mg/ℓ)	<150	<50	<70	<200	-	-	-	<0.3	<0.2

Table 13.17. Concentrations of elements in raw and treated field water in µg/ℓ

Sample	concentration µg/ℓ																	
	Li	Be	B	Cd	Ti	V	Cr	Mn	Sb	Co	Ni	Cu	Zn	As	Se	Mo	Ba	Hg
Raw field water	13.81	<0.039	31.14	0.07	2.22	0.20	0.28	4.40	0.01	0.04	0.79	10.39	9.96	0.18	<0.456	1.54	37.86	0.01
Treated field water	2.62	<0.039	27.60	0.06	1.14	0.07	0.26	15.90	0.01	0.04	1.03	3.17	3.19	0.16	<0.456	0.40	4.43	0.01
SANS 241-1 (2015)	-	-	-	3	-	<200	-	<100	-	<500	<150	<1000	<5000	<10	<20	-	-	<1

SANS-South African National Standards: Drinking Water

13.10 REGENERATION AND REUSABILITY OF SPENT SORBENT

Desorption study was carried out to evaluate the reusability of the adsorbent. The solutions used to regenerate the spent sorbent included 0.01 M NaOH, 0.01 M Na₂CO₃ and 0.1 M K₂SO₄ solutions. The regeneration was done for several cycles with reduction in adsorption potential being evaluated. The values of the per cent fluoride removal by the regenerated sorbents across the various defluoridation cycles are presented in Table 13.18. Regeneration of spent Al/Fe oxide-modified DE using 0.1 M K₂SO₄ solution proved to be the most reliable of the evaluated regenerants. By the third defluoridation cycle, a dosage of 0.8 g/100 ml was efficient enough to reduce the concentration of 10 mg/l fluoride by 67.2%. With the use of 0.01 M NaOH and 0.01 M Na₂CO₃ for fluoride desorption from the fluoride-loaded (spent) sorbent, the per cent fluoride removal at the first and higher defluoridation cycles were far less than that observed for the blank. The lowest regeneration potential was observed with the use of Na₂CO₃. Both reagents gave a high desorption pH which led to appreciable loss of silica, the framework of DE – the support for the coated binary metal oxide. The dissolution of silica implied loss of Al/Fe oxide. This was evident from the intense brown colour of the supernatants which showed the loss of Fe³⁺ from the adsorbent.

Table 13.18. Comparison of the sorbent regeneration potentials for selected reagents

Defluoridation cycle	% F⁻ removal with NaOH as regenerant	% F⁻ removal with K₂SO₄ as regenerant	% F⁻ removal with Na₂CO₃ as regenerant
Blank	95.7	95.7	95.7
1st cycle	26.4	92.0	19.2
2nd cycle	27.8	81.8	8.6
3rd cycle	26.2	67.2	-
4th cycle	28.8	-	-

Figure 13.28 shows the trend in the concentration of dissolved silica in a batch experiment with raw DE at different pH values. Significant loss of silica occurred at pH above 9. Both NaOH and Na₂CO₃ solutions are therefore considered inappropriate for the regeneration of spent Al/Fe oxide-modified DE.

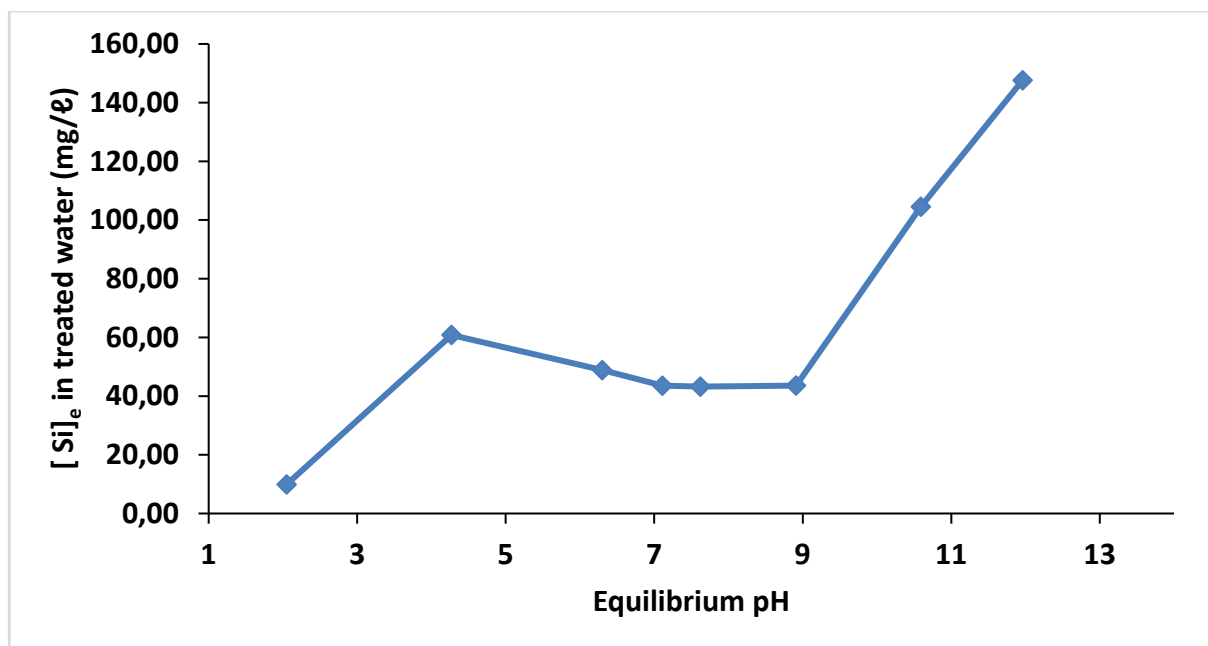


Figure 13.28. Loss of silica from diatomaceous earth as a function of solution pH (initial fluoride concentration: 10 mg/l, dosage of raw DE: 0.4 g/50 ml, shaking speed: 200 rpm, temperature: 297 K).

13.11 SUMMARY

Diatomaceous earth (DE) was successively modified by co-precipitation of Al/Fe oxides and its fluoride adsorption potential evaluated. Results indicate that Al/Fe oxide-modified DE has a high fluoride removal potential. At optimum contact time of 50 min, adsorbent dose of 0.6 g/100 ml and mixing rate of 200 rpm, the adsorbent with pH_{pzc} 6.0 ± 0.2 reduced the concentration of fluoride in fluoride-spiked water from 10 to 0.69 mg/l. The optimum adsorption capacity of the adsorbent was 7.633 mg/g for a solution containing initially 100 mg/l fluoride. The equilibrium pH of the suspensions ranged between 6.77 and 8.26 for various initial fluoride solutions. At optimum conditions the adsorbent reduced fluoride in field water from 5.53 mg/l to 0.93 mg/l. The sorption data could adequately be described by both Langmuir and Freundlich isotherms but fitted better to Langmuir. Kinetic data fitted adequately to Lagergren pseudo-second order model implying mainly chemisorption process. The adsorption mechanisms involved ion-exchange of the hydroxyl ions on the sorbent with fluoride in solution. The ion-exchange was probably the sorption rate controlling step since neither the external diffusion nor intra-particle diffusion was confirmed to be the rate controlling step. The adsorption process occurred at circum-neutral pH and at room temperature making the adsorbent suitable for application in field pH conditions. This pH of adsorption makes the adsorbent particularly suitable for application in household treatment devices since no pH adjustment of product water will be required.

14 EVALUATION OF GROUNDWATER DEFLUORIDATION BY AL/FE OXIDE-MODIFIED DIATOMACEOUS EARTH IN A FIXED-BED COLUMN

14.1 INTRODUCTION

The fluoride removal capacity of a sorbent is usually first evaluated through batch method while optimizing the adsorption parameters such as contact time, sorbent dosage, adsorbate concentration, solution pH and temperature as reported in literature (Karthikeyan et al., 2005; Jagtap et al., 2011; Izuagie et al., 2015; Tang and Zhang, 2016). The batch method of defluoridation involves weighing a known mass of sorbent into a set of bottles containing solutions of fluoride of the same or different concentrations, and shaking the corked bottles of mixtures on a reciprocating shaker for a specified time. Sorbents proven through batch method to have sufficiently high defluoridation performance may qualify for defluoridation performance appraisal in a continuous flow mode in fixed-bed column adsorption filter as in the case of many reports (Ghorai and Pant, 2004; Ma et al., 2011; Davila-Rodriguez et al., 2012; Ghosh et al., 2015). A sorbent with low fluoride removal tendency, even at optimized conditions in batch experiments would most likely have poor fluoride uptake capacity in a fixed-bed column. Al/Fe oxide-modified diatomaceous earth demonstrated a high fluoride removal potential in batch method as reported in Chapter 13 of this report, where a dosage of 0.6 g/100 ml reduced the fluoride in artificial water containing 10 mg/l fluoride by 93.1%. Moreover, no leaching of chemical species was observed making the adsorbent safe to use for household groundwater defluoridation. It is therefore pertinent to evaluate the fluoride removal performance of the sorbent in a fixed-bed column which mimics its true application in point-of-use devices.

14.2 MATERIALS

All reagents and TISAB-III were obtained from Rochelle Chemicals & Lab Equipment CC, South Africa Ltd and they were of analytical grade. The DE for the study was obtained from natural deposits at Kariandusi in Gilgil District, Nakuru County, Kenya and a second supply sourced in South Africa. A stock solution containing 1000 mg/l fluoride was prepared by dissolving 2.21 g analytical grade sodium fluoride in 1 l of ultra-pure water (18.2 MΩ/cm). Fluoride solutions for batch experiments were prepared from fresh stock fluoride solution by appropriate dilution. A stock solution containing 1000 mg/l fluoride was prepared by dissolving 2.21 g NaF in 1 l of MilliQ water (18.2 MΩ/cm) and fluoride solutions for batch experiments were prepared from fresh stock fluoride solution by appropriate dilution. Field water was collected from a community borehole in Siloam, Vhembe district in South Africa.

14.3 METHODS

14.3.1 Adsorbent and adsorbate preparation

The methods and procedures for the synthesis and optimisation of metal oxide impregnation of diatomaceous earth (DE) in the fixed bed column experiments are presented in detail in Chapter 13.

14.3.2 Reactor set up

The apparatus for the fixed-bed continuous flow experiments comprised a fixed-bed column adsorption filter, a glass beaker containing the influent fluoride solution, a peristaltic pump, a fixed-bed column, Teflon tubing to convey influent and effluent fluoride solutions and a measuring cylinder to collect the treated water. The column was made from a polypropylene syringe tube having an internal diameter of 2 cm and a length of 10 cm (cross sectional area of 12.56 cm²). In each experiment, the column was packed with a definite mass of Al/Fe oxide-modified DE in-between two strips of 11 µm pore size Whatman filter paper cut to shape. Each paper was sandwiched between two wire gauzes to provide support. The lower gauze sat on a narrow tight-fitting plastic ring with another ring placed over the upper gauze such that the two rings served as seals to prevent the escape of sorbent from both ends of the packing as well as hold the filter papers and gauzes firmly in fixed positions. Glass wool was placed at both ends of the packing followed by inert beads to ensure consistent packing as well as condition the flow stream of influent solution (Kelly, 1992). The setup is as illustrated in Figure 14.1.

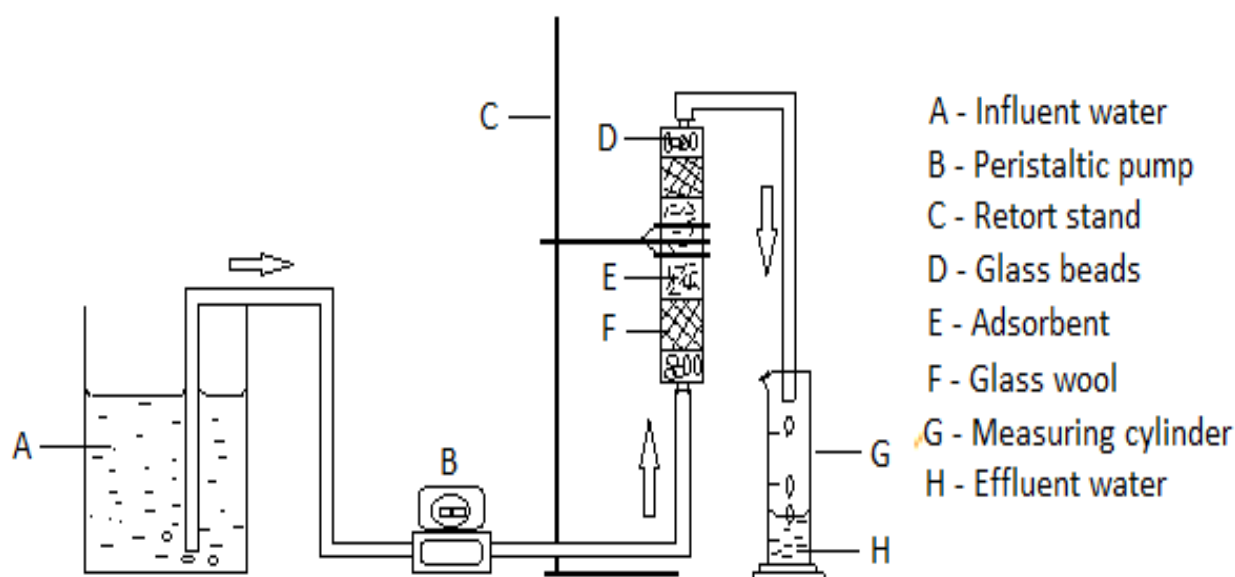


Figure 14.1. Schematic diagram of a fixed-bed column continuous flow set up.

14.3.3 Evaluation of adsorption parameters

The artificial fluoride water to be defluoridated (influent fluoride solution) was stored in a litre plastic bottle. The water was poured from the bottle into a 100-ml Erlenmeyer beaker from time to time throughout the duration of experiment. The water was drawn out of the beaker continuously through a Teflon tubing of 3.8 mm diameter using a Gilson peristaltic pump and fed into the Al/Fe oxide-modified DE-packed column by upward flow. All experiments were carried out at room temperature and influent pH was 6.5 ± 0.5 . The effluent (treated water) was collected with measuring cylinders at 10 min intervals for fluoride analysis using Total Ionic Strength Adjustment Buffer III (TISAB III)-added standard fluoride solutions-calibrated fluoride ion-selective electrode (ORION VERSASTAR Advanced Electrochemistry meter fluoride ion-selective electrode). Parameters evaluated include; flow rate, sorbent mass/bed depth, initial fluoride concentration and adsorption capacity.

14.3.4 Fixed bed column defluoridation studies

Field water containing 9.14 mg/l fluoride was passed through 1 g of sorbent packed column as in other experiments at a flow rate of 0.62 ml/min. The resulting effluent was collected at intervals of 10 min. The concentration of fluoride and other coexisting anions Cl^- , SO_4^{2-} , PO_4^{3-} and NO_3^- in each processed water collection was analysed.

14.3.4.1 Chemical analysis of processed water

The samples of effluent collected from the column for the period of experiment were analysed using Inductively Coupled Plasma-Mass Spectrometer (ICP-MS) or Inductively Coupled Plasma-Atomic Emission Spectrometer (ICP-AES) as applicable to the elements to be analysed. The objective of analysis was to evaluate the extent of release of chemical species from the sorbent into the processed water over a period of defluoridation time. Ten millilitres of each collection were acidified with 2 ml of 3 M HNO_3 before analysis. Sample blank was also analysed for correction purposes.

14.3.4.2 Microbial tests

The presence of total coliforms in water samples indicates the possible presence of opportunistic bacteria such as *Klebsiella* and *Enterobacter* that can multiply in water environments and pathogens such as *Salmonella* spp, *Shigella* spp, *V. cholerae*, *C. jejuni*, *C. coli*, *Y. enterocolitica* and pathogenic *E. coli* especially when detected in conjunction with other faecal coliforms. These organisms can cause diseases such as gastroenteritis, salmonellosis, dysentery, cholera and typhoid fever (DWAF, 1996). Fluoride-rich groundwater samples were spiked with 10 ml of wastewater effluent from a local wastewater treatment plant. Water samples, before and after passing through the prepared column (1 g adsorbent, 1 rpm flow rate) were analysed in triplicate for the presence of *E. coli* and other coliforms using the membrane filtration technique. The raw water was diluted up to 10^{-2} , and then a 100 ml of water sample was filtered through a sterile 47-mm diameter membrane filter inserted in a filtration unit. The membrane filters were placed right side up on the Petri Dish containing an absorbent pad soaked in the culture medium. Plates for enumeration of total coliform bacteria were inverted and incubated at 37°C for 24 hours. *E. coli* bacteria and other coliform bacteria were enumerated on m-Endo Total Coliform Broth used for the recovery of *E. coli* and coliform organisms and used according to supplier's instructions (Merck, Darmstadt, Germany). Blue colonies were counted as positive colonies for total *E. coli* bacteria and Red for other coliforms, a combination of the two counts gave the total coliform count.

14.4 EVALUATION OF ADSORPTION PARAMETERS

14.4.1 Effect of flow rate

The effect of flow rate on fluoride sorption was evaluated using a column packed with 1 g (1 cm bed height) of sorbent and influent fluoride concentration of 8.3 mg/l. The flow rate was varied from 0.62-1.32 mg/l. In each experiment, the effluent collected at 10 min intervals was analysed for residual fluoride. Column breakthrough analysis data was analysed. Breakthrough curves were used to illustrate the efficiency of the adsorbent in defluoridation of groundwater in a fixed bed. The effect of influent flow rates on the adsorption of fluoride was evaluated at flow rates of 0.62, 1.18, and 1.32 ml/min respectively at adsorbent mass of 1 g and $C_e = 10$ mg/l. Figure 14.2 shows the breakthrough curves at different influent flow rates. The breakthrough time decreased from 110 min at 0.62 ml/min to 20 min at 1.32 ml/min. Volumes of water treated at breakthrough point at 0.62, 1.18 and 1.32 ml/min flow rate were found to be 75.5, 30 and 18 ml respectively. This could be attributed to the fact that higher flow rates lead to decrease contact time between the adsorbate and adsorbent and therefore fluoride ions do not have enough time to penetrate and diffuse into the pores of adsorbent.

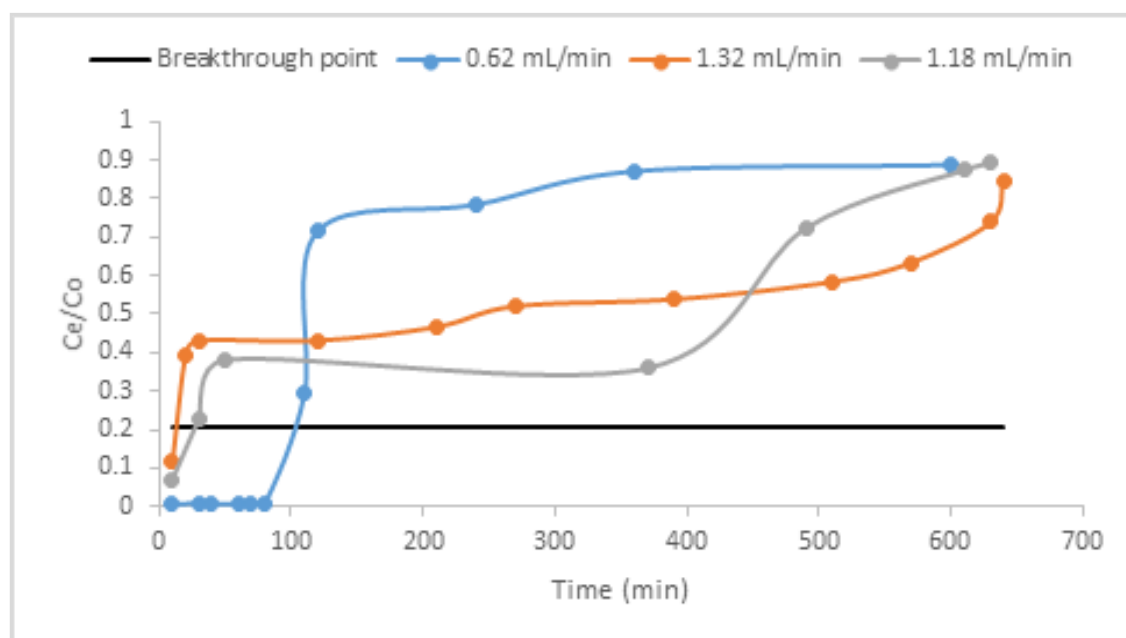


Figure 14.2. Breakthrough curves at different influent flow rates (influent concentration: 10 mg/l, sorbent dosage: 1 g, particle size <250 μ m, N=3).

14.4.2 Effect of sorbent mass/bed depth

The effect of bed depth/adsorbent mass was evaluated by packing the column respectively with 0.5, 0.85 and 1 g of sorbent corresponding to bed height of 0.5, 0.85 and 1 cm. The concentration of fluoride in the influent was kept at 8.7 mg/l. The flow rate was maintained at 0.62 ml/min. The effluent was collected with a measuring cylinder at 10 min intervals. Each collection was then analysed for residual fluoride. Figure 14.3 shows the breakthrough curves at different bed heights/sorbent mass. The bed heights of 0.5, 0.85 and 1 cm corresponds to sorbent mass of 0.1, 0.76 and 1 g respectively. It is observed that the breakthrough time increased from 20 min at 0.5 cm to 100 min at 1 cm. For 0.5 cm and 0.75 cm the breakthrough occurred at the same time. The increase in breakthrough time and volume may be attributed

to the increase in number of active sites that are available for F⁻ adsorption with increased bed height and sorbent mass. Furthermore, at lower bed height the solution has limited time to contact with the bed compared to higher bed height. This phenomenon is explained by the EBCT value which was found to be increasing with increasing bed height (Table 14.1). The volume of water treated at 0.5, 0.85 and 1 cm were found to be 7, 8 and 12.4 ml respectively. The number of BV treated for 0.5, 0.85 cm and 1 cm were 0.0012, 0.01 and 0.0075 respectively. On the other hand, the adsorbent exhaustion rate was found to decrease with increasing bed height (Table 14.1). The results show that the column performs better at 1 g bed mass.

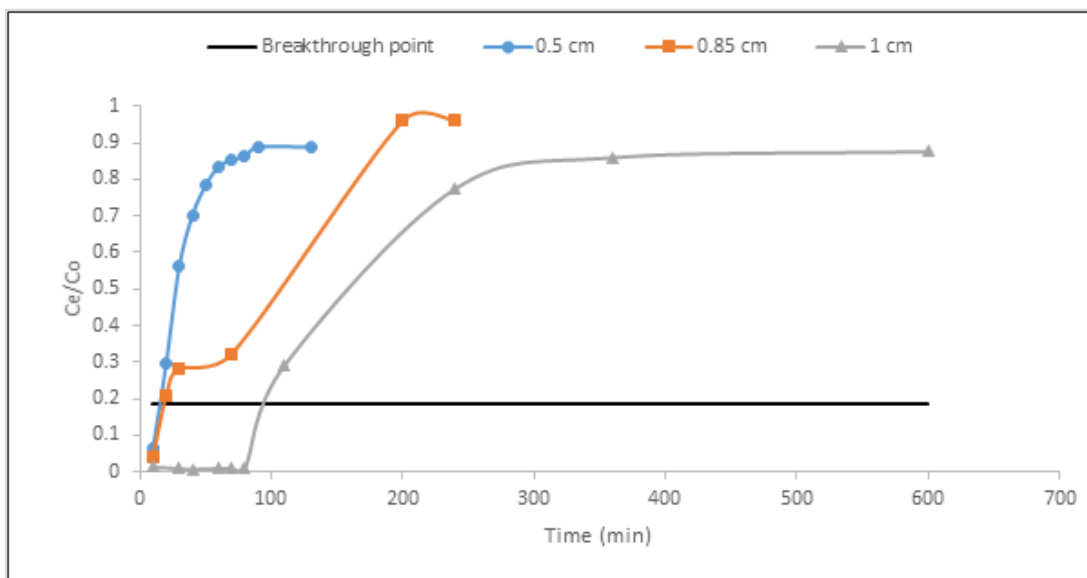


Figure 14.3. Breakthrough curves at different sorbent masses/bed height (influent concentration: 8.17 mg/l, inflow rate 0.62 ml/min, particle size <250 μm, N=3).

Table 14.1. Breakthrough curve parameters for F⁻ adsorption onto Al/Fe oxide modified DE at different operating conditions

F (ml/min)	H (cm)	C _i (mg/l)	V _B (ml)	q _B (mg/g)	V _E (ml)	q _E (mg/g)	EBCT (min)	AER (g/l)	BV
0.62	0.5	8.17	8	0.11	78	0.014	0.8	62.5	0.0012
0.62	0.85	8.17	12.4	0.15	148	0.055	1.37	60.48	0.001
0.62	1	8.17	75	0.35	432	0.34	1.61	13.33	0.079
0.62	1	8.3	75	0.33	432	0.021	1.61	13.33	0.079
1.18	1	8.3	24	0.09	756	0	0.84	38.46	0.002
1.32	1	8.3	13.2	0.21	755	0.018	0.75	76.92	0.00025
0.62	1	5	200	0.44	672	0.12	1.61	5	0.015
0.62	1	10	75	0.25	120	0.23	1.61	13.3	0.005
0.62	1	20	44.5	0.18	110	0.2	1.61	22	0.003

*f= flow rate (ml/min), H=bed height (cm), C_i=initial concentration (mg/l), V_B=Volume at breakthrough (ml), q_B= capacity at breakthrough point (mg/g), V_E=volume at exhaustion point (ml), q_E=capacity at exhaustion point (mg/g), EBCT= empty bed contact time (min), AER=Adsorbent exhaustion rate (g/l), BV= Number of Bed volumes.

14.4.3 Effect of initial fluoride concentration

Having evaluated the optimum bed height, the effect of the initial fluoride concentration on the breakthrough was evaluated using solutions with initial fluoride concentrations of 3.5, 10 and 18 mg/l. The fluoride

solutions were fed into the fixed-bed column containing 1 g of sorbent at a flow rate of 0.62 mL/min. Treated water was collected at 10 min intervals and analysed for fluoride as described in previous subsections. Values of C_e/C_0 were plotted against time to obtain the breakthrough curves. Figure 14.4 shows the breakthrough curves as a function of initial influent fluoride concentration. From the results it is observed that the breakthrough points for 3.5, 10 and 18 mg/L were achieved after 240, 90 and 50 min respectively. The volume of water treated at breakthrough points for 3.5, 9 and 17 mg/L F^- initial concentrations were 200, 75.5 and 45.5 mL respectively. This could be attributed to the fact that as the concentration increases, the driving force for mass transfer also increases leading to faster saturation of the adsorbent's active sites. Higher flow rates lead to less penetration of adsorbate species into the interior surface of particles in fixed beds leading to early breakthrough. Appearance of early breakthrough point and low breakthrough volume for high influent concentration indicates rapid exhaustion of the fluoride removal capacity of the bed. Similar observations have been reported by Ghosh et al. (2014) and Setshedi et al. (2014). The AER values for 3.5, 10 and 18 mg/L initial concentrations were found to be 5, 13.33 and 22.22 g/L. The number of BV treated decreased with increasing initial concentration (Table 14.1). The results showed that the fixed-bed column performed better at low concentration.

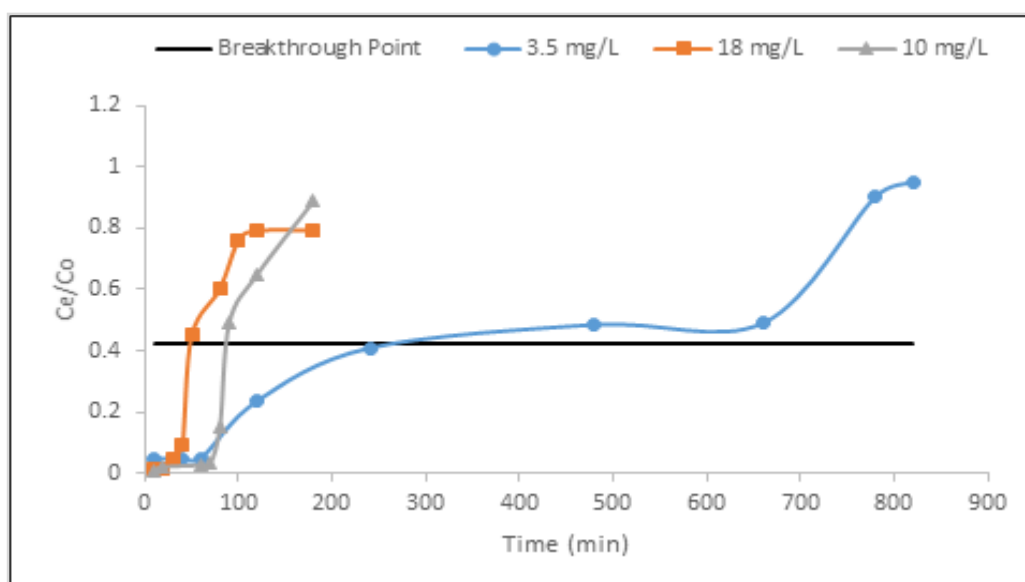


Figure 14.4. Breakthrough curves at different initial fluoride concentrations as function of time (sorbent dosage: 1 g and influent flow rate of 0.62 mL/min, particle size <250 μ m, N=3).

14.4.4 Evaluation of adsorption capacity by batch method

Mixtures of 100 mL each of 3, 5 and 7 mg/L fluoride solutions and 1 g of sorbent in coked 250 mL plastic bottles were equilibrated at room temperature in a reciprocating thermostated water bath shaker (Daihan LabTech Model LSB-015S) at a shaking speed of 200 rpm for 50 min – the optimum contact time (Izuagie et al., 2016). The purpose was to compare the adsorption capacities under batch method with those of fixed-bed continuous flow method while maintaining the same initial fluoride concentrations and sorbent dosage. After equilibration, mixtures were centrifuged and the resulting supernatants were analysed for fluoride. The results of the per cent fluoride removal and adsorption capacity in batch defluoridation mode for a 100 mL of 3, 5 and 7 mg/L fluoride solutions are presented in Table 14.2. The determined adsorption capacities were compared with values obtained for the fixed-bed continuous flow regime. More fluoride was adsorbed per unit mass of the adsorbent in the batch than in the continuous flow fixed bed mode. This could be attributed to the aggressive agitation in the batch mode that reduced mass transfer resistance to

the adsorbent surface leading to increased contact between adsorbate species and adsorbent adsorption active sites. The value of C_t was obtained from the breakthrough plots where the volume of processed water was 100 mL.

Table 14.2. Percent F⁻ removal and adsorption capacity in batch and continuous flow fixed bed

C_o (mg/L)	% F ⁻ removal	C_e (mg/L)	q_e (mg/g)	* q_t (mg/g)	% difference in adsorption capacity
3	96.3	0.111	0.2889	0.2256	6.33
5	96.6	0.168	0.4832	0.4370	4.62
7	96.1	0.274	0.6726	0.5789	9.37

* q_t was the bed capacity at the point where the volume of processed water was 100 mL for the fixed bed continuous flow process.

14.5 DEFLUORIDATION OF FIELD WATER

Figure 14.5 shows the breakthrough curve for fluoride removal onto Al/Fe oxide modified for fluoride-rich groundwater. The efficiency of fixed-bed column packed with Al/Fe oxide modified DE in treatment of fluoride-rich groundwater was tested by treating field water collected from community borehole in Lephalale (23°38'30.9"S 27°45'07.8"E). The physicochemical parameters of the field water before and after treatment are presented in Table 14.3. The results show that the breakthrough point was achieved after 120 min of contact time and the volume of treated water collected was found to be 74.4 mL. Field water was treated using 1 g of adsorbent at a flow rate of 0.62 mL/min. The analysis showed that Al/Fe oxide modified DE also adsorbed other co-existing anions such as Cl⁻, SO₄²⁻, PO₄³⁻ and NO₃⁻ and hence the quality of treated water was improved.

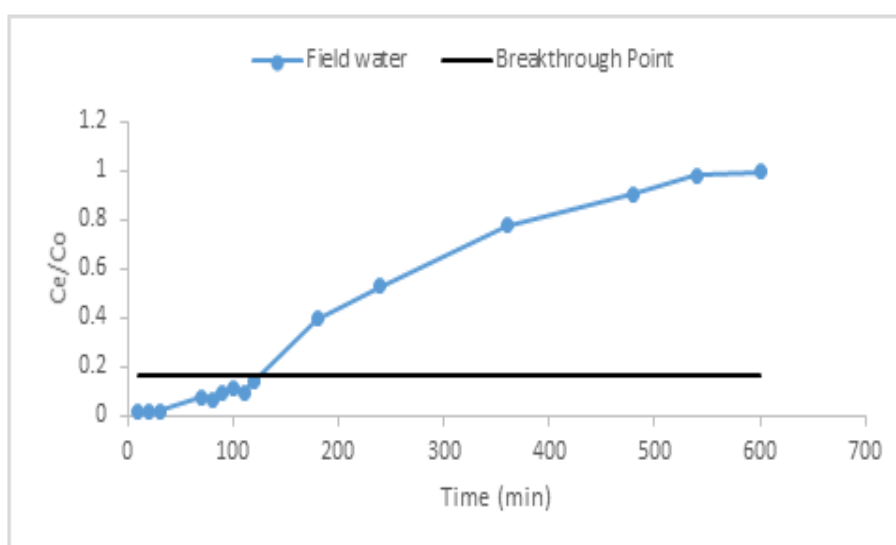


Figure 14.5. Field water defluoridation in a fixed bed-column packed with 1 g Al/Fe oxide modified DE and flow rate of 0.62 mL/min, particle size <250 μm, N=3.

Table 14.3. Physicochemical parameters of feed water and effluent water at breakthrough point

	pH	F ⁻	Cl ⁻	NO ₃ ⁻	SO ₄ ²⁻	PO ₄ ³⁻
Feed water (mg/ℓ)	8.91	9.14	78.9	32.89	22.52	0.94
Breakthrough point (mg/ℓ)	7.42	1.5	44.97	17.31	3.6	ND
SANS-241 (mg/ℓ)	5-9.7	1.5	300	50	500	-

Figure 14.6 a and b shows the petri dishes after incubation before and after fixed bed treatment of the wastewater spiked fluoride-rich groundwater. The results of the experiments showed that the fabricated column and material was effective in removing both *E. coli* and other coliform bacteria in conjunction with fluoride. Both *E. coli* and total coliform were reduced from $\geq 30\,000$ cfu/100 ml to 0 cfu/100 ml after passing through the fixed bed column. DE consists of the amorphous silica-based cell wall of diatoms, and the various species of diatoms have different morphologies and sizes of natural pores (Michen et al., 2011). These properties give the material a high surface area and porosity, making it suitable for use in filtration. Using latex particles with a mean diameter of 140, 260 and 450 nm which mimic the size of small-sized bacteria to investigate the performance of the DE-based depth filter, Michen et al. (2011), demonstrated that the removal of most bacteria is not due to the size exclusion principle as stated in literature. Michen et al. (2011) demonstrated that the adsorption of latex particles onto a noticeable number of adsorption sites in the depth of the filter. Based on that it is clear that the adsorption mechanism is likely to play a significant role in bacteria removal in DE filters working on the depth filtration principle. De Cortalezzi et al. (2014), reported that iron oxide coated alumina filters showed improved removal capacity compared to the stand-alone material when tested in batch mode, as inner pore sites that otherwise would be considered inaccessible due to long diffusion times become operational.

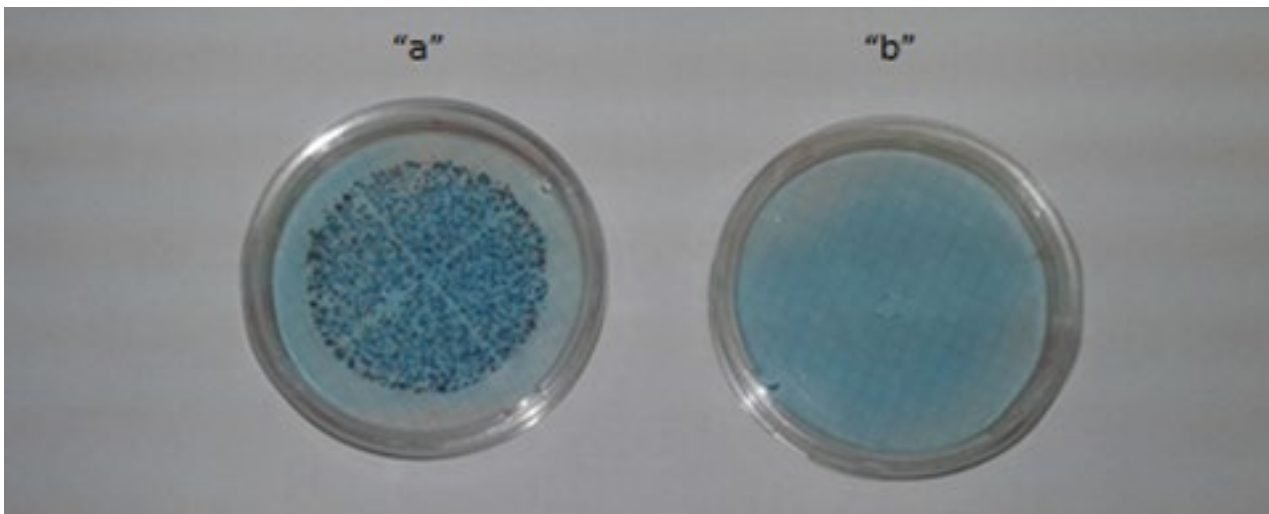


Figure 14.6. Petri Dishes after incubation showing 'a' before & 'b' after treatment

Since the present study applied Al/Fe oxide-modified diatomaceous earth in a fixed-bed column, it can be assumed that adsorption was the main mechanism involved in the removal of faecal coliform bacteria, due to the high surface area and porosity of DE improved by Al/Fe oxide-modification. This is also supported by LeChevallier and Au (2004) who state that the effective removal of microbes by granular filtration cannot rely on physical straining alone, at least at the initial stage of a filter run. According to LeChevallier and Au (2004), the removal of particles by granular filtration is considered to involve two steps: transport of particles from suspension to filter medium, followed by attachment of particles to the medium. The transport step depends on the physical and hydrodynamic properties of the system. Transport mechanisms include diffusion, interception and sedimentation. Factors such as size and density of microbes, size and depth of filter medium, and filtration rate affect transport efficiency and attachment is determined by the surface and solution chemistry of the system. Coating of granular media with other positively charged metal oxides and hydroxides of iron, aluminium, calcium or magnesium makes it more effective for removing and retaining the negatively charged bacteria by electrostatic adsorption (Chaudhuri & Sattar, 1986). In positively charged filter media bacteria reductions of 90->99% was recorded in the present study and have also been reported by LeChevallier and Au (2004).

A separate sample from a community borehole in Siloam was also run through the fixed bed to test the leaching potential of the adsorbent under dynamic flow conditions. Sample collected from the treatment of the field water was subjected to full chemical analysis by ICP-MS/AES to evaluate possible leaching of chemical species and secondary contamination of the product water. Results of analysis are presented in Table 14.4. All the evaluated chemical species in the effluents and raw field water were at trace levels. This indicates the adsorbent is chemically stable and poses no secondary contamination risk to the processed water. The high concentration of Na (168.84 mg/l) in the first effluent sample was reduced by 49% by the second sampling time and could be attributed to residue Na from the NaOH used to activate the diatomaceous earth.

14.6 SUMMARY

Al/Fe oxide-modified diatomaceous earth was evaluated for its defluoridation potential of fluoride-rich groundwater in a fixed bed column. Several operation parameters were evaluated and optimized, these included, influent flow rate, influent fluoride concentration and adsorbent mass/bed height. Increasing flow rate led to a decrease in breakthrough volume, while increase in bed height/adsorbent mass increased the breakthrough volume confirming observation made by other researchers. The adsorbent capacity of the fixed bed at 100 ml breakthrough volume compared well with adsorbent capacity for batch experiments for the same volume treated. The breakthrough volume also increased with decreasing influent fluoride concentrations. The adsorbent effectively removed fluoride from groundwater and exhibited high adsorption capacity. Moreover it was able to adsorb other co-existing anions further improving the quality of the water. The adsorbent slightly lowered the pH of the treated water but remained within the SANS 241 guidelines. The adsorbent was observed to be chemically stable under the employed treatment conditions with minimal leaching of chemical species observed. This is an advantage since there will be no risk of secondary contamination of the processed water. Microbial tests confirmed that the adsorbent can simultaneously remove fluoride and pathogens further making the water safe for drinking.

Table 14.4. Elemental analysis of processed Siloam water by ICP-MS/ICP-AES (conc in µg/ℓ except for Ca, K, Na, P and Si)

Sampling Time (min)	Al (µg/ℓ)	V (µg/ℓ)	Cr (µg/ℓ)	Mn (µg/ℓ)	Fe (µg/ℓ)	Co (µg/ℓ)	Ni (µg/ℓ)	Cu (µg/ℓ)	Zn (µg/ℓ)	Cd (µg/ℓ)	Ca (mg/ℓ)	K (mg/ℓ)	Na (mg/ℓ)	P (mg/ℓ)	Si (mg/ℓ)
10	322.4	0.50	0.52	5.76	348.8	0.62	2.88	12.7	12.0	0.99	6.09	2.68	168.8	0.02	37.1
20	171.8	0.11	0.29	4.58	88.8	0.17	1.16	6.50	6.79	0.29	2.45	2.71	86.0	1.20	41.7
30	208.4	0.28	0.27	6.55	91.4	0.14	1.10	6.62	6.14	0.23	2.35	2.84	81.7	1.20	43.7
40	265.0	0.52	0.41	7.82	107.6	0.18	2.08	8.90	10.20	0.41	2.76	3.15	82.9	0.01	45.9
60	244.1	1.00	0.28	4.94	132.4	0.13	1.06	6.49	5.77	0.27	2.11	2.90	78.3	1.20	46.0
80	238.1	1.36	0.25	4.04	163.7	0.11	0.98	6.52	5.82	0.24	2.00	2.83	76.4	1.20	46.4
100	669.6	1.78	0.29	5.36	804.7	0.12	1.06	6.57	7.59	0.22	2.00	2.89	76.1	0.01	47.4
130	187.1	1.96	0.23	3.06	139.7	0.09	0.99	6.58	6.20	0.18	1.96	2.84	75.0	1.20	46.9
Raw water	97.4	2.69	0.29	3.55	58.7	0.06	0.93	6.53	7.31	0.14	2.50	2.82	70.9	1.20	48.7

15 CONCLUSIONS & RECOMMENDATIONS

Groundwater is the source of drinking water in most rural communities of sub-Saharan Africa and Asian countries due partly to inadequate water supply. However, some of the groundwater contains high F⁻ concentration that is detrimental to health. Consumption of groundwater with F⁻ concentration > 1.5 mg/l can lead to development of dental fluorosis and dental carries. This groundwater requires partial defluoridation to the required limits. There are several technologies that have been developed for defluoridation of groundwater. They are of several categories: ion exchange and precipitation processes, membrane process such as reverse osmosis, donnan dialysis, electro dialysis and nanofiltration. All these are high-cost technologies that require electrical power and technical expertise and are therefore not appropriate for defluoridation of groundwater in rural areas. Appropriate technologies for domestic and rural community groundwater defluoridation have been developed, these include precipitation-coagulation or adsorption-based technologies aluminium sulphate-based coagulation-flocculation sedimentation. However, the techniques are limited in fluoride removal and suffer high residual sulphate. Of all the defluoridation techniques, adsorption methods have been identified as the most appropriate for application in rural communities. The challenge is to come up with high capacity, cheap adsorbents based on locally available materials. This study was an attempt to fabricate high capacity, cheap adsorbents based on locally available aluminosilicate-rich, smectite-rich clay soils, bentonite clay and diatomaceous earth. The clay soils, bentonite and diatomaceous earth have been modified using high charge metal cations or their oxides, mixed to form composites and their fluoride adsorption capacity evaluated at various optimized conditions in batch scale.

In the first part of this study, bentonite clay was modified with Fe³⁺/Fe-oxides and blended with clay soils to make ceramic pellets. Modification of the bentonite clay with Fe-oxides increased the surface area compared to the raw bentonite. The Fe-oxides modified bentonite showed high F⁻ adsorption, >70% F⁻ removal was observed over the pH range 2-12 which is significant for field defluoridation of groundwater since no pH adjustment will be required. Moreover, the residual concentration of chemical species in the treated water at initial pH of 6-9, were below the WHO drinking water guidelines. Solution pH played a major role in fluoride removal by Fe-oxides modified bentonite clay with maximum adsorption being observed at pH 2. The adsorption kinetics could be described by pseudo second order model suggestion chemisorption process. Ceramic pellets prepared through calcination were observed to have low fluoride adsorption capacity.

In the second part bentonite clay was successfully modified by intercalation of Mn²⁺ in the interlayers through ion exchange. At 3 mg/l F⁻ concentration and 1 g/100 l volume and 30 min contact time, a maximum F⁻ removal of 84.0% was achieved at the optimized pH 2. Regeneration study revealed that Mn²⁺ bentonite can be successfully regenerated with 0.1 M NaOH. Stability assessment showed that there is minimal release of chemical species from the adsorbent at various pH levels. Fluoride adsorption onto Mn²⁺ bentonite occurred via ligand exchange at lower pH and ion exchange at higher pH. Mn²⁺ bentonite clay showed low F⁻ adsorption capacity compared to other adsorbent reported in the literature. The optimal adsorption capacity was at low pH which would limit application in rural areas due to requirement for pH adjustment.

Bentonite clay was also activated and converted into Na-bentonite which was then coated with MnO₂ via in-situ oxidation process. The MnO₂ coated bentonite was then blended with locally available black clay soil and fabricated into ceramic pellets. Coating Na-bentonite with MnO₂ led to the formation of new mineral phases such as cryptomelane (KMn₈O₁₆), jacobsite (Mn₆Fe₄)O₄ and pyrolusite (MnO₂). Coating increased the percentage composition of Mn in the Na-bentonite and this diluted the percentage of other oxides such as SiO₂, Al₂O₃, MgO and Fe₂O₃. Optimum conditions for fluoride removal were found to be, 30 min contact time at 250 rpm, 1.5 g/100 ml adsorbent dosage, 5 mg/l adsorbate concentration, and pH of 8 for the MnO₂-coated bentonite clay. Maximum F⁻ removal of ≈94.66% was achieved under optimum conditions for the MnO₂ coated bentonite clay. The adsorption data fitted well to Langmuir adsorption isotherm while the kinetics data fitted well to pseudo second order model. Intra-particle diffusion model of Weber-Morris indicated that the removal

of fluoride by MnO₂ coated Na-bentonite is a highly complex process, involving boundary layer diffusion and intra-particle diffusion as well as equilibrium adsorption. Sorption of fluoride occurred via ligands exchange mechanism at pH below 3 and at pH above 3 via ion exchange mechanism. In an attempt to increase stability and hand lability of the adsorbent, ceramic pellets were fabricated at various calcination temperatures through optimization of various operational parameters, optimum ratio for mixing MnO₂ coated Na-bentonite/smectite-rich clay soils for fabrication of the composite pellets was established to be 1:3 and calcination temperature was 550°C. XRF analysis showed that SiO₂, Al₂O₃, MnO and Fe₂O₃ are the major oxides of the clay composite. Mineralogical characterisation of the clay composite showed the presence of quartz, albite, cryptomelane and microcline as the main minerals of the calcined pellets. Pellets prepared under the established optimum conditions removed ≈63.3% F⁻ from an initial F⁻ concentration of 10 mg/ℓ.

In the third part raw diatomaceous earth (DE) was evaluated for its capacity to adsorb fluoride from groundwater. Maximum per cent fluoride removal and adsorption capacity for DE were 25.62% and 0.653 mg/g, respectively, for 8 mg/ℓ fluoride solution at optimum adsorption conditions. Sorption data was well described by Freundlich isotherm, thus showing multi-site adsorption onto the heterogeneous DE surface. The sorption kinetic was observed to be a pseudo-second-order kinetic process. Hence, fluoride uptake was mainly by chemisorption. The mechanism controlling the sorption rate was found to be external diffusion of fluoride from the bulk solution to the thin film on the surface of the adsorbent particles. Release of metal and non-metal species from DE was observed to be at trace level while there was no detectable release of anions from the adsorbent. Phosphate was observed to have a negative effect on fluoride adsorption at low pH. Diatomaceous earth is a poor fluoride adsorbent even at optimum pH of 2. It was therefore recommended that with the advantage of its porous structure and excellent flow of water, the surface could be modified by coating with high charge metal oxides with high affinity for fluoride thus creating a potentially high capacity adsorbent for fluoride removal in groundwater.

Diatomaceous Earth (DE) was successively modified by co-precipitation of Al/Fe oxides and its fluoride adsorption potential evaluated. Results of batch experiments indicate that Al/Fe oxide-modified DE has a high fluoride removal potential. Co-existing ions were observed to have an effect on the adsorption of F⁻. At 5 mg/ℓ co-existing anion concentration, reduction in % F⁻ removal was at most 9.2% for PO₄³⁻. The effect of co-existing anions was observed to be of the following order: SO₄²⁻ < NO₃⁻ < CO₃²⁻ ≈ PO₄³⁻. The synthesized adsorbent was effective in defluoridation of field groundwater at optimized conditions registering 83.2% fluoride removal with an equilibrium pH ≈ 6.86. Minimal leaching of Al, Fe and Si from the adsorbent was observed at this pH range. Adsorption data was adequately described by Langmuir and Freundlich isotherms confirming both monolayer and multi-site adsorption of F⁻ onto the adsorbent surface. Sorption process was better modelled using the pseudo-second-order model confirming uptake of F⁻ by chemisorption. Adsorption rate limiting step was most probably ion exchange or attraction of F⁻ to the sorbent surface. The adsorbent could adequately be regenerated using K₂SO₄ solution. The results indicate that Al/Fe oxide modified DE is a potential adsorbent for defluoridation of groundwater and can be easily regenerated for reuse making it suitable for point of use defluoridation devices in rural communities.

The Al/Fe oxide modified DE was identified as highly stable chemically and also had high adsorption capacity at circum-neutral pH range which is crucial for fluoride-rich groundwater treatment. Its defluoridation potential was also evaluated in a fixed bed continuous flow. Operational parameters such as flow rate, adsorbent mass/bed height and influent fluoride concentration were observed to determine the effectiveness of the fixed bed. When testing the fixed bed column in defluoridation of field groundwater, it was found that 1 g of Al/Fe oxide modified DE packed column can treat a maximum of volume 75 mℓ at the breakthrough point and the breakthrough point was achieved after 120 min. Furthermore, the concentrations of other co-existing ions such as Cl⁻, NO₃⁻, SO₄²⁻ and PO₄³⁻ were decreased after treatment. The adsorbent was observed to be chemically stable under the employed treatment conditions with minimal leaching of chemical species observed. This is an advantage since there will be no risk of secondary contamination of the processed water. Moreover, microbial tests using wastewater spiked fluoride-rich groundwater showed that the adsorbent can

simultaneously remove fluoride and pathogens of faecal origin commonly found in surface water further enhancing the quality and safety of drinking water.

In the third part diatomaceous earth (DE) was successively modified by co-precipitation of Mg/Ce/Mn oxides and its fluoride adsorption potential evaluated. Presence of MgO in the composite was crucial in raising the pH of treated water. The major active component in the sorbent was the Ce oxide. However, without the presence of MgO in the composite, the pH of treated water was very low. High fluoride removal, > 91%, was observed for fluoride solutions with initial concentration of 9 mg/l over a wide initial pH range (~ 4 to 11) using a sorbent dosage of 0.6 g/100 ml. This indicates the adsorbent can be applied for treatment of field fluoride-rich water with no need for pH adjustment. The sorption data fitted better to Langmuir isotherm while kinetic data fitted better to pseudo-second-order model. The equilibrium pH of treated water was above the pH_{pzc} indicating fluoride removal was by exchange of hydroxyl ions on the sorbent surface. The sorption rate limiting step was observed to be external diffusion with the bilinear plots indicating a two-mode influence of external diffusion on the sorption rate. K₂SO₄ solution was established to be a suitable regenerant for Mg/Ce/Mn trimetal oxide modified diatomaceous earth. However, it was observed that the regenerated spent sorbent could only be suitable for defluoridation of groundwater containing much less than 10 mg/l fluoride. A shortcoming of the adsorbent would be the leaching of Ce in the adsorption media which would affect the quality of the product water

The developed adsorbents had varying adsorption capacity, from moderate to high as compared to adsorbents reported in literature and also low-high chemical stability in the treatment media. The raw clays and diatomaceous earth had adsorption capacity ranging from 0.08-0.34 mg/g. Modification of the clays with various metal cations and their oxides increased their adsorption capacity (0.65-1.59 mg/g). The modified DE had adsorption capacity ranging from 0.6-1.73 mg/g. These adsorbents exhibited potential for application in household defluoridation devices based on their chemical stability and suitable adsorption capacity. Moreover, the Al/Fe modified DE showed capability of removing common pathogens of faecal origin found in surface water further enhancing the quality and safety of drinking water. However, more techno-economic evaluation and optimization of the Al/Fe, Mg/Ce/Mn-oxide modified DE/clay soils composites/mixtures is highly recommended for fabrication of ceramic candles and discs for application in household water treatment devices.

REFERENCES

1. ABAIRE, B., ZEWGE, F. and ENDALEW, M. (2009). Water, sanitation and hygiene: sustainable development and multisectoral approaches. Operational experiences on small scale community defluoridation systems. 34th WEDC International Conference, Addis Ababa, Ethiopia
2. ABDULRAHMANI, A. (1996). Fluoride content in drinking water supplies of Riyadh, Saudi
3. ABEBE, L.S., SMITH, J.A., NARKIEWICZ, S., OYANEDEL-CRAVER, V., CONAWAY, M., SINGO, A., SAMIE, A., MOJAPELO, P., BRANT, J. and DILLINGHAM, R. (2014). Ceramic water filters impregnated with silver nanoparticles as a point-of-use water-treatment intervention for HIV-positive individuals in Limpopo Province, South Africa: A pilot study of technological performance and human health benefits. *Journal of Water and Health*. 12: 288-300.
4. ABRAHAMS, L.C. (1946). The masticatory apparatus of Calvinia and Namaqualand in the North Western Cape of the Union of South Africa. *Journal of the Dental Association of South Africa*. 1: 4-9.
5. ADIHIKARY, S.K., TIPNIS, U.K., HARKARE, W.P. and GOVINDA, K.P. (1989). Defluoridation Africa
6. AGONAFIR, A. and AMBELU, A. (2007). Treatment duration and adsorption capacity of crushed bricks in the removal of fluoride from drinking water. *Ethiopia J Health Sci*. 17: 2.
7. AHMEDIN, H. (2007). Selection of clay adsorbents and determination of the optimum condition for defluoridation of groundwater in rift valley region. MSc Thesis. Department of Chemical Engineering. Addis Ababa University, Ethiopia.
8. ALSHAMERI, A., YAN, C., AL-ANI, Y., DAWOOD, A.S., IBRAHIM, A., ZHOU, C. and WANG, H. (2014). An investigation into the adsorption removal of ammonium by salt activated Chinese (Hulaodu) natural zeolite: Kinetics, isotherms, and thermodynamics. *Journal of the Taiwan Institute of Chemical Engineers*. 45: 554-564.
9. AMINA, C., LHADI, L.K., YOUNSI, A. and MURDY, J. (2004). Environmental impact of an urban landfill on a coastal aquifer. *J. Afr. Earth Sci*. 39: 509-516.
10. AMOR, Z., TAKY, M., MALKI, S., NICOLAS, S. and ELMIDAOU, A. (2001). Fluoride removal from brackish water by electrodialysis. *Desalination*. 133: 215-223.
11. ANWAR, F. (2003). Assessment and analysis of industrial liquid waste and sludge disposal and surface water resources and dental fluorosis in Kenya. *Fluoride*. 18: 4-11.
12. APPELA, C., LENA, Q., MA, R. and KENNELLEY, D.R.E. (2003). Point of zero charge determination in soils and minerals via traditional methods and detection of electroacoustic mobility. *Geoderma*. 113: 77-93.
13. APPELO, C.A.J. and POSTMA, D. (1994). *Geochemistry, groundwater and pollution*, Rotterdam: Balkema.
14. ARAMI, M., LIMAE, N.Y. and MAHMOODI, N.M. (2008). Evaluation of the adsorption kinetics and equilibrium for the potential removal of acid dyes using a biosorbent. *Chem Eng J*. 139: 2-10.
15. ARGAW, A. and FARIS, K. Development of appropriate defluoridation technologies for Ethiopian communities. A thesis submitted to the School of Environmental Health, Public Health Faculty, Jimma University, Ethiopia. Unpublished MSc Thesis.
16. ARGAW, A., KEBEDE, F. (2005). Development of appropriate defluoridation technologies for Ethiopian communities. *J Civil. Eng, JKUAT*. 8: 79-88.
17. ARNESEN, A.K.M., ABRAHAMSEN, G., SANDVIK, G. and KROGSTAD, T. (1995). Aluminium-smelters and fluoride pollution of soil solution in Norway. *Sci. Total Environ*. 163: 39-53.
18. AUDINOS, R. (1997). Ion-exchange membrane processes for clean industrial chemistry. *Chem. Eng. Technol*. 20: 247-258.
19. AYOUB, S. and GUPTA, A.K. (2006). Fluoride in drinking water: A review on the status and stress effects. *Environ. Sci. Technol*. 36: 433-487.
20. AYOUB, S., GUPTA, A., VENUGOPAL, K. and BHAT, T. (2008). A Conceptual Overview on Sustainable Technologies for the Defluoridation of Drinking Water Critical Reviews in Environmental Science and Technology. 38: 401-470.

-
21. BABLIA, K. (1996). Studies of water defluoridation using activated carbons and activated carbons loaded separately with Magnesia, Alumina and Calcium. MSc Thesis. University of Dar es Salaam, Tanzania.
 22. BABU, C.A., SUJISH, D., MURUGAPPA, M.S., MOHANAKRISHNAN, G., KALYANASUNDARAM, P. and RAJ, B. (2011). A comprehensive treatment method for defluoridation of drinking water. *Indian J. of Chemical Technology*. 18: 314-318.
 23. BAILEY, K., CHILTON, J., DAHI, E., LENNON, M., JACKSON, P. and FAWELL, J. (eds) (2006). *Fluoride in Drinking Water*. IWA Publishing (on behalf of the World Health Organization), London.
 24. BARDECKI, C.J. (1974). Fluoride probability in Tanzania waters. *Maji Review*. 1: 55-61.
 25. BATISTELLA, L., VENQUIARUTO, L.D., DI LUCCIO, M., OLIVEIRA, J.V., PERGHER, S.B.C., MAZUTTI, M.A., DE OLIVEIRA, D., MOSSI, A.J., TREICHEL, H. and DALLAGO, R. (2011). Evaluation of acid activation under the adsorption capacity of double layered hydroxides of Mg-Al-CO₃ type for fluoride removal from aqueous medium. *Ind. Eng. Chem. Res.* 50: 6871-6876.
 26. BENEFIELD, L.D., JUDKINS, J.F. and BARRON, L. (1982). *Process chemistry for water and wastewater treatment*, prentice hall, Englewood cliffs, New Jersey.
 27. BENNAJAH, M., GOURICH, B., ESSADKI, A.H., VIAL, C.H. and DELMAS, H. (2009). Defluoridation of Morocco drinking water by Electrocoagulation/electro-flotation in an electrochemical external-loop airlift reactor. *Chemical Engineering Journal*. 148: 122-131.
 28. BHATNAGAR, A., KUMAR, E. and SILLANPÄÄB, M. (2011). Fluoride removal from water by adsorption- A review, *Chem. Eng. J.* 10: 5-28.
 29. BISHOP, P.L. and SANCOUCY, G. (1978). Fluoride removal from drinking water by fluidized activated alumina adsorption. *J. AWWA*. 70: 554-559.
 30. BJORVATN, K. and BARDBSEN. A. (1995). Use of activated clay for defluoridation of water. In: *Proceedings of the First International Workshop on Fluorosis and Defluoridation of Water*, Dahi, E., and Bregnhøj, H., Eds., International Society for Fluoride Research, Auckland, pp. 40-45.
 31. BJORVATN, K., BARDBSEN, A. and TEKLEHAIMAN, O.T. (1997). Defluoridation of drinking water by use of clay/soil. *Proceedings of the 2nd International Workshop on Fluorosis Prevention and Defluoridation of Water*. Nazareth, Ethiopia, November 19-25.
 32. BOHN, H.L., MCNEAL, B.I. and O'CONNOR, G. (1975). *Soil chemistry*. A Wiley-interscience publication. New York: John Wiley and Sons.
 33. BOTHA, F.S. and VAN ROOYEN, J.L. (2001) Affordable water resources development in the Limpopo Province, South Africa. *J. Afr. Earth Sci.* 33: 687-692.
 34. BOWER, C.A. and HATCHER, J.T. (1967). Adsorption of fluoride by soils and minerals. *Soil Sci.* 103: 151-154.
 35. BOYLE, D.R. and CHAGNON, M. (1995). An incidence of skeletal fluorosis associated with groundwaters of the carboniferous basin Gaspé region, Quebec, Canada. *Environmental Geochemistry and Health*. 17: 5-12.
 36. BREGNHØJ, H., DAHI, E. and JENSEN, M. (1997). Modelling defluoridation of water in bone char columns. In: *Proceedings of the First International Workshop on Fluorosis and Defluoridation of Water 18-22 October 1995, Tanzania*, The International Society for Fluoride Research, Auckland.
 37. BULUSU, K.R. and NAWLAKHE, W.G. (1990). Defluoridation of Water with Activated Alumina Continuous System. *Indian Journal of Environmental Health*. 32: 197.
 38. CAI, H., CHEN, G., PENG, C., ZHANG, Z., DONG, Y., SHANG, G., ZHU, X., GAO, H. and WAN, X. (2015). Removal of fluoride from drinking water using tea waste loaded with Al/Fe oxides: A novel, safe and efficient bio sorbent. *Applied Surface Science*. 328: 34-44
 39. CENGELÖGLU, Y., KIR, E., ERSOZ, M. (2002). Removal of fluoride from aqueous solution by using red mud. *Sep. Purif. Technol.* 28: 81-86.
 40. CHANG, R. (1977). *Physical chemistry with applications to biological systems*. New York: Macmillan Publishing Co, Inc.
 41. CHATURVEDI. A., PATHAK, K.C. and SINGH, V.N. (1988). Fluoride removal from water by adsorption on China clay. *Appl. Clay Sci.* 3: 337-346.

-
42. CHAUDHURI, M. and SATTAR, S.A. (1988). Removal of human rotavirus from water by coal-based sorbents. Proceedings – first biennial water quality symposium: Microbiological aspects, Banff, Alberta, Canada.
 43. CHAUHAN, V.S., DWIVEDI, P.K. and IYENGER, L. (2007). Investigations on activated alumina based domestic defluoridation units. *Journal of Hazardous Materials*. B139: 103-107.
 44. CHEN, N., ZHANG, Z., FENG, C., LI, M., CHEN, R. and SUGIURA, N. (2011a). Investigations on the batch and fixed-bed column performance of fluoride adsorption by Kanuma mud. *Desalination*. 268: 76-82.
 45. CHEN, N., ZHANG, Z., FENG, C., LI, M., ZHU, D. and SUGIURA, N. (2011). Studies on fluoride adsorption of iron-impregnated granular ceramics from aqueous solution. *Journal of material and physics*. 125: 293-298.
 46. CHEN, N., ZHANG, Z., FENG, C., LI, M., ZHU, D., CHEN, R. and SUGIURA, N. (2010). An excellent fluoride sorption behaviour of ceramic adsorbent. *Journal of Hazardous Materials*. 183: 460-465.
 47. CHEN, N., ZHANG, Z., FENG, C., ZHU, D., YANG, Y. and SUGIURA, N. (2011). Preparation and characterization of porous granular ceramic containing dispersed aluminium and iron oxides as adsorbents for fluoride removal from aqueous solution. *Journal of Hazardous Materials*. 186: 863-868.
 48. CHEN, N., ZHANG, Z., FENG, C., LI, M., ZHU, D. and SUGIURA, N. (2011). Studies on fluoride adsorption of iron-impregnated granular ceramics from aqueous solution. *Journal of material and physics*. 125: 293-298
 49. CHIBI, C. and HAARHOFF, J. (2000). A Promising Approach to Fluoride Removal in Rural Drinking Water Supplies. Presented at WISA 2000 Biennial Conference, Sun City, South Africa, 28 May-1 June 2000
 50. CHIDAMBARAM, C., RAMANTHAN, A.L. and VASUDEVAN, S. (2003). Fluoride studies in water using natural materials. *Technical Note. Water SA*. 29: 339-344.
 51. CHOUBISA, S.L. and SOMPURA, K. (1996). Dental fluorosis in tribal villages of Dungepur district (Rajasthan). *Pollution Research*. 15: 45-47.
 52. CLIFFORD, M.J. and KENNEDY, R. (1978). Activated alumina: Rediscovered adsorbent for fluoride, humic acids and silica. *Industrial Water Engineering*. 15: 6-12.
 53. COETZEE, P.P., COETZEE, L., PUKA, R. and MUBENGA, S. (2006). Characterisation of selected South African clays for defluoridation of natural waters. A report to Water Research Commission. Pretoria, South Africa.
 54. COETZEE, P.P., COETZEE, L.L., PUKA, R. and MUBENG, S. (2003). Characterization of selected South African clays for defluoridation of natural water. *Water SA*. 29: 331-338.
 55. CRINI, G. (2006). Non-conventional low-cost adsorbents for dye removal: A review. *Bioresour Technol*. 197: 1061-1085.
 56. DABROWSKI, A. (2001). Adsorption-from theory to practice. *Adv. Colloid Interface Sci*. 93:135-224.
 57. DACOSTA, F.A., MUZERENGI, C., MHLONGO, S.E. and MUKWEVHO, G.F. (2013). Characterization of clays for making ceramic pots and water filters at Mukondeni village, Limpopo province, South Africa. *ARNP Journal of Engineering and Applied Sciences*. 11: 927-932.
 58. DAHI, E. (1996). Contact precipitation for defluoridation of water. Paper presented at 22nd WEDC Conference, New Delhi, 9-13 September, WEDC.
 59. DAHI, E. (1997). Development of the contact precipitation method for appropriate defluoridation of water. *Proceeding of 2nd International Workshop on Fluorosis and Defluoridation of Water*, Eds. E Dahi E & J M Nielsen; *Int. Soc. Fluoride Res. Dunedin, New Zealand*.
 60. DAHI, E. (2000). The State of Art of Small Community Defluoridation of Drinking Water. *3rd International Workshop on Fluorosis Prevention and Defluoridation of Water*, Chiang Mai, Thailand, pp. 137-167
 61. DAI JC and HUANG JT 1991). Surface modification of clays and clay rubber composite. *App. Clay Sci*. 15: 51-65.
 62. DAIFULLAH, A.A.M., YAKOUT, S.M. and ELREEFY, S.A. (2007). Adsorption of fluoride in aqueous solutions using KMnO₄-modified activated carbon derived from steam pyrolysis of rice straw. *Journal of Hazardous Materials*. 147: 633-643.

-
63. DAVILA-RODRIGUENZ, J.L., ESCOBAR-BARRIOS, V.A. and RANGEL-MENDEZ, J.R. (2012). Removal of fluoride from drinking water by a chitin-based biocomposite in fixed-bed columns. *J. Fluorine Chem.* 140: 99-103.
 64. DAW, R.K. (2004). Experiences with Domestic Defluoridation in India. People-centred Approaches to Water and Environmental Sanitation. 30th WEDC International Conference, Vientiane, Lao.
 65. DAY, F.H. (1963). *The chemical elements in nature*. Harrap p. 306. London, England.
 66. Defluoridation of Water; *Int. Soc. Fluoride Res.* 109-114.
 67. DENGGA, M.E. (2013). Evaluation of the fluoride adsorption capacity of locally available clay in Vhembe district. A Honors mini-thesis. School of Environmental Sciences. University of Venda.
 68. DEPARTMENT OF WATER AFFAIRS AND FORESTRY (DWAF) (1996). *South African Water Quality Guidelines for Domestic Use*, 1st ed., Department of Water Affairs and Forestry, Pretoria. Available from: www.dwaf.gov.za.
 69. DIEYE, A. (1995). *Defluoridation des eaux par dialyse ionique croise*, Thesis, University of
 70. DUBININ, M.M. (1960). The potential theory of adsorption of gases and vapours for adsorbents with energetically non-uniform surface. *Chem. Rev.* 60: 235-266.
 71. DURGAPRASAD, P. and SIVARAM, P. (2007). Case studies of user managed safe drinking water and health projects in India. *Asian-Pacific Journal of Rural Development.* 17: 95-112.
 72. DUROV, S.A. (1948). Natural waters and graphical representation of their composition. *Dokl. Akad. Nauk. USSR.* 59:87-90.
 73. EDMUNDS, W.M. and SMEDLEY, P.L. (1996). Groundwater geochemistry and health: An overview. In Appleton, Fuge and McCall (Eds). *Environmental Geochemistry and Health*. Geological Society Special Publication. 113: 91-105.
 74. ELAZHAR, F., TAHAIKT, M., ZOUAHRI, A., TAKY, M., HAFSI, M. and ELMIDAOU, A. (2013). Defluoridation by electrodialysis: Performances and cost comparison. *World Applied Sciences Journal.* 22: 844-850.
 75. EREN, E., AFSIN, B. and ONAL, Y. (2009). Removal of lead ions by acid activated and manganese oxide-coated bentonite. *Journal of Hazardous Materials.* 161: 677-685.
 76. ESWAR, P. and DEVARAJ, C.G. (2011). Water defluoridation: Field studies. *Indian Journal of Dental Advancements.* 3: 526-533.
 77. FAWELL, J., BAILEY, K., CHILTON, J., DAHI, E., FEWTRELL, L. and MAGARA, Y. (2006). *Fluoride in drinking water*. Published on behalf of World Health Organization by IWA Publishing, London.
 78. FEENSTRA, L., VASAK, L. and GRIFFIOEN, J. (2007). *Fluoride in groundwater: Overview and evaluation of removal methods*. International groundwater resources assessment centre. Report nr. SP 2007-1.
 79. FIDALGO D. CORTALEZZI, M.M.F., GALLARDO, M.V. & YRAZU, F., GENTILE, G.J., OPEZZO, O., PIZARRO, R., POMA, H.R. & RAJAL, V.B (2014). Virus removal by iron oxide ceramic membranes. *Journal of Environmental Chemical Engineering*, 2: 1831-1840.
 80. FIGUEIREDO, S.A., LOUREIRO, J.M. and BOAVENTURA, R.A. (2005). Natural waste materials containing chitin as adsorbents for textile dyestuffs: batch and continuous studies. *Water Res.* 39: 4142-4152.
 81. FREUNDLICH, H.M.F. (1906). Over the adsorption in solution. *Journal of Physical Chemistry.* 57: 370-485.
 82. GACIRI, S.J. and DAVIES, T.C. (1993). The occurrence and geochemistry of fluoride in some natural waters of Kenya. *Journal of Hydrology.* 143: 395-412.
 83. GANDHI, N., SIRISHA, D., ASTHANA, S. and MANJUSHA, A. (2012). Adsorption studies of fluoride on multani matti and red soil. *Res. J. Chem. Sci.* 2: 32-37.
 84. GAVRILOAIEI, D.I. and GAVRILOAIEI, T. (2008). Determination of surface charge for metal oxides. *Anal. St. Univ. "Al. I. Cuza", Geologie, Tomul LIV.* pp.11-18.
 85. GHANDI, R. (1993). *Prevention and Control of Fluorosis in India*. Water Board, Ministry of
 86. Resources, Government of India. Rajiv Gandhi National Drinking Water Mission.
 87. GHORABA, S.A. and KHAN, A.D. (2013). Hydrochemistry and groundwater quality assessment in Baluchistan Province, Pakistan. *IJRRAS* 17: 185-199.

-
88. GHORAI, S. and PANT, K.K. (2004). Investigations on the column performance of fluoride adsorption by activated alumina in a fixed-bed. *Chem. Eng. J.* 98: 165-173.
 89. GHORAI, S. and PANT, K.K. (2005). Equilibrium, kinetics and breakthrough studies for adsorption of fluoride on activated alumina, *Sep. Purif. Technol.* 42: 265-271.
 90. GHOSH, A., CHAKRABARTI, S., BISWAS, K. and GHOSH, U.C. (2015). Column performances on fluoride removal by agglomerated Ce (IV)-Zr (IV) mixed oxide nanoparticles packed fixed-beds. *J. Environ. Chem. Eng.* 3: 653-661.
 91. GHOSH, A., CHAKRABARTI, S. and GHOSH, U.C. (2014). Fixed-bed column performance of Mn-incorporated iron(III) oxide nanoparticle agglomerates on As (III) removal from the spiked groundwater in lab bench scale. *Chemical Engineering Journal.* 248: 18-26.
 92. GHOSH, A., PAL, M., BISWAS, K., GHOSH, U.C. and MANNA, B. (2015). Manganese oxide incorporated ferric oxide Nano composites (MIFN): A novel adsorbent for effective removal of Cr(VI) from contaminated water. *Journal of Water Process Engineering.* 7: 176-186
 93. GITARI, W.M., NGULUBE, T., MASINDI, V. and GUMBO, J.R. (2013). Defluoridation of groundwater using Fe³⁺ – modified bentonite clay: optimization of adsorption conditions. *Desalin. Water Treat.* 53, pp. 1578-1590.
 94. GOLDBERG, S. (2005). *Equations and Models Describing Adsorption Processes in Soils*. Soil Science Society of America, 677 S. Segoe Road, Madison, WI 53711, USA. *Chemical Processes in Soils.* SSSA Book Series, no. 8.
 95. GOSWAMI, A. and PURKAIT, M.K. (2013). Defluoridation of Water by Schwertmannite. *World Academy of Science, Engineering and Technology.* 73.
 96. GULIPALLI, C.H.S., PRASAD, B. and WASEWAR, K.L. (2011). Batch study, equilibrium and kinetics of adsorption of selenium using rice husk ash (RHA). *Journal of Engineering Science and Technology.* 6: 586-605.
 97. GUMBO, F.J. and MKONGO, G. (1995). Water defluoridation for rural fluoride-affected communities in Tanzania. 1st International Workshop on Fluorosis Prevention and Defluoridation of Water; *Int. Soc. Fluoride Res.* 109-114.
 98. HACKETT, C., HACKETT, T., HARSH, D. and SCHRIDER, S. (2013). Assessing the establishment of a ceramic water filter factory in Limpopo Province, South Africa. *Public:* 9-12.
 99. HAMMER, M.J. (1986). Need for fluoridation of desalinated water supplies. *Aqua* 4: 179-182.
 100. HARON, M.J. and YUNUS, W.M.Z.W. (2001). Removal of fluoride ion from aqueous solution by a cerium-poly(hydroxamic acid) resin complex. *J. Environ. Sci. Health Part A – Toxic/Hazard. Subst. Environ. Eng.* 36: 727-734.
 101. HASSEN, A. (2007). Selection of clay adsorbents and determination of the optimum condition for defluoridation of ground water in rift valley region. MSc thesis. School of Graduate Studies. Addis Ababa University. Chemical Engineering (Process Engineering Stream).
 102. HAUGE, S., O`STERBERG, R., BJORVATN, K., SELVIG, K.A. (1994). Defluoridation of drinking water with pottery: effect of firing temperature. *Scandinavian journal of dental research.* 102: 329-333.
 103. HEM JD (1985) Study and interpretation of the chemical characteristics of natural water, U.S. Geological Survey, United States Government Printing Office.
 104. HEM, J.D. (1989). Study and interpretation of the chemical characteristics of natural water. *Water Supply Paper 2254*, 3rd edition, US Geological Survey, Washington, D. C.
 105. HICHOOR, M., PERSIN, F., SANDEAUX, J. and GAVACH, C. (2000). Fluoride removal from waters by Donnan dialysis. *Se. Purif. Technol.* 18: 1-11.
 106. HIEMSTRA, T. and VAN RIEMSDIJK, W.H. (2000). Fluoride adsorption on Geoethite in relation to different types of surface sites. *J. Colloid Interface Sci.* 225: 94-104.
 107. HIREMATH, S.S. (2006). *Textbook of Preventive and Community Dentistry.* Bangalore: Elsevier India.
 108. HO, Y.S., WASE, D.A.J. and FORSTER, C.F. (1995). Batch Nickel removal from aqueous solution by Sphagnum moss peat. *Water Research.* 29: 1327-1332.
 109. HOLT, P.K., BARTON, G.W. and MITCHELL, C.A. (2005). The future for Electrocoagulation as a localised water treatment technology. *Chemosphere.* 59: 355-367.

-
110. HU, C.Y., LO, S.L. and KUAN, W.H. (2003). Effects of co-existing anions on fluoride removal in electrocoagulation (EC) process using aluminium electrodes. *Water Research*. 37: 4513-4523.
 111. HUANG, C.H. and XU, T.W. (2006). Cleaner production by using electrodialysis in organic or aqueous-organic systems. In: C.V. Loeffe, (Editor). *Trends in Conservation and Recycling of Resources (83-97)*. New York: Nova Science Publishers.
 112. HUANG, C.H., XU, T.W., ZHANG, Y.P., XUE, Y.H. and CHEN, G.W. (2007). Application of electrodialysis to the production of organic acids: state-of-the-art and recent developments (review). *J. Membr. Sci.* 288: 1-12.
 113. IBRAHIM, S.S. and SELIM, A.Q. (2012). Heat treatment of natural diatomite. *Physicochemical Problems of Mineral Processing*. 48: 413-424.
 114. IBRAHIM, Y.E., AFFAN, A.A. and BJORVATN, K. (1995). Prevalence of fental fluorosis in Sudanese children from two villages with 0.25 and 2.56 ppm fluoride in the drinking water. *Int. J. Paediatr. Dent.* 5: 223-229.
 115. IYENGER, L. (2005). Defluoridation of Water using Activated Alumina Technology: Studies carried out at IIT Kanpur. Prepared for UNICEF, New Delhi.
 116. IZUAGIE, A.A. (2016). Defluoridation of groundwater using raw, heat-treated and metal oxide-modified diatomaceous earth. PhD Thesis. University of Venda
 117. IZUAGIE, A.A., GITARI, W.M. and GUMBO, J.R. (2015). Defluoridation of groundwater using diatomaceous earth: optimization of adsorption conditions, kinetics and leached metals risk assessment. *Desalin. Water Treat.* DOI: 10.1080/19443994.2015.1083894.
 118. IZUAGIE, A.A., GITARI, W.M. and JABULANI, R.G. (2016). Synthesis and performance evaluation of Al/Fe oxide coated diatomaceous earth in groundwater defluoridation: Towards fluorosis mitigation, *Journal of Environmental Science and Health, Part A*. DOI: 10.1080/10934529.2016.1181445
 119. JACOBSEN, P. and DAHL, E. (1997). Bone char-based bucket defluoridation in Tanzania households. *Proceedings of the 2nd International Workshop on Fluorosis Prevention and Defluoridation of Water*. Nazareth, Ethiopia, November 19-25.
 120. JAGTAP, S., YENKIE, M.K.N., LABHSETWAR, N. and RAYALU, S. (2011). Defluoridation of drinking water using chitosan based mesoporous alumina. *Micropor. Mesopor. Mat.* 142: 454-463.
 121. JAIN, S. and JAYARAM, R.V. (2009). Removal of fluoride from contaminated drinking water using unmodified and aluminium hydroxide impregnated blue lime stone waste. *Sep. Sci. Technol.* 44:1436-1451.
 122. JANARDHANA, C., RAO, G.N., SATHISH, R.S. and LAKSHMAN, V.S. (2006). Study on defluoridation of drinking water by impregnation of metal ions in activated charcoal. *Indian Journal of Chemical Technology*. 13: 414-416.
 123. JENKINS, H.D.B. (2008). *Chemical thermodynamics at a glance*. Oxford: Blackwell Publishing Ltd., Oxford.
 124. JIA, Y., ZHU, B.S., ZHANG, K.S., JIN, Z., LUO, T., YU, X.Y., KONG, L.T. and LIU, J.H. (2015). Porous 2-line ferrihydrite/byerite composite (LFBC): Fluoride removal performance and mechanism. *Chemical Engineering Journal*. 268: 325-336.
 125. JIANG, J. and ZENG, J. (2003). Comparison of modified montmorillonite adsorbents. Part II: The effects of the type of raw clays and modification conditions on the adsorption performance. *Chemosphere*. 53: 53-62.
 126. JIMMY, L., HUMPHREY, G.E. and KELLER, I.I. (1997). *Separation process technology*, McGraw-Hill, New York.
 127. JOSHI, S.V., MEHTA, S.H., RAO, A.P. and RAO, A.V. (1992). Estimation of sodium fluoride using HPLC in reverse osmosis experiments, *Water Treat.* 10: 307-312.
 128. KALAVATHY, M.H., KARTHIKEYAN, T., RAJGOPAL, S. and MIRANDA, L.R. (2005). Kinetic and isotherm studies of Cu (II) adsorption onto H₃PO₄ activated rubber wood sawdust. *J. Colloid Interface Sci.* 292: 354-362.
 129. KALIBATONGA, P.D. (2004). Adsorption of heavy metals from solution by South African industrial clay. A Thesis submitted at Tshwane University of Technology.

-
130. KAMBLE, S., DIXIT, P., RAYALU, S.S. and LABHSETWAR, N.K. (2009). Defluoridation of drinking water using chemically modified bentonite clay. *Desalination and water treatment journal*. 249: 687-693.
 131. KAPOOR, A. and VIRARAGHAVAN, T. (1998). Use of immobilized bentonite in removal of heavy metals from wastewater. *J. Environ. Eng. ASCE*. 124:1020-1024.
 132. KARTHIKEYAN, G., ANDAL, M.N. and SUNDAR, S.G. (1999). Defluoridation Property of Burnt Clay, *Journal of Indian Water Works Association*. 31: 291-300.
 133. KARTHIKEYAN, G., PIUS, A. and ALAGUMUTHU, G. (2005). Fluoride adsorption studies of montmorillonite clay. *Indian J. Chem. Technol*. 12: 263-272.
 134. KASS, A., YECHIELI, Y., VENGOSH, A. and STARINSKY, A. (2005). The impact of freshwater and wastewater irrigation on the chemistry of shallow groundwater: a case study from the Israeli Coastal aquifer. *J. Hydrol*. 300: 314-331.
 135. KAU, P.M.H., SMITH, D.W. and BINNING, P. (1997). Fluoride detention by kaolin clay. *J. Contamin. Hydrol*. 28: 267-288.
 136. KAU, P.M.H., SMITH, D.W. and BINNING, P. (1998). Experimental sorption of fluoride by kaolinite and bentonite. *Geoderma*. 84: 89-108.
 137. KELLY, T.W. (1992). Determination of Adsorption Capacities using Packed-Bed Breakthrough Tests. Unpublished MSc Thesis, B. S. Illinois State University, Urbana-Champaign.
 138. KHRAISHEH, M.A.M., AL-DEGS, Y.S. and MCMINN, W.A.M. (2014). Remediation of wastewater containing heavy metals using raw and modified diatomite. *Chemical Engineering Journal*. 99: 177-184.
 139. KHRAISHEH, M.A.M., AL-DEGS, Y.S., ALLEN, S.J. and AHMAD, M.N. (2002). Elucidation of controlling steps of reactive dye adsorption on activated carbon. *Industrial and Engineering Chemistry Research*. 41: 1651-1651.
 140. KILLEDAR, D.J. and BHARGAVA, D.S. (1998). An overview of Defluoridation methods (part-1) *Jour of Institution of public Health Engineers*. 1: 6-13.
 141. KILLEDAR, D.J. and BHARGAVA, D.S. (1990). Feasibility of fluoride adsorption on bone charcoal. *J. Inst. Eng*. 70: 47-49.
 142. KINNIBURGH, D.G. (1986). General purpose adsorption isotherms. *Environmental Science and Technology*. 20: 895-904.
 143. KLOOS, H. and TEKLEHAIMANOT, R. (1999). Distribution of fluoride and fluorosis in Ethiopia and prospects for control. *Trop Med Intern Health*. 4: 355-364.
 144. LAGERGREN, S. (1898). Zur theorie der sogenannten adsorption gelöster stoffe (About the theory of so-called adsorption of soluble substances). *Kungliga Svenska Vetenskapsakademiens. Handlingar*. 24: 1-39.
 145. LANGMUIR, D. (1997). *Aqueous environmental geochemistry*. Prentice-Hall, Inc. Upper Saddle River: New Jersey.
 146. LECHEVALLIER, M.W. and AU, K.K. (2004). *Water treatment and pathogen control: Process efficiency in achieving safe drinking-water*. WHO drinking-water quality Series, IWA Publishing, London.
 147. LEE, C.K., LOW, K.S. and CHEW, S.L. (1999). Removal of anion dyes by water hyacinth roots. *Advances in Environmental Research*. 3: 343-351.
 148. LI, Y., DU, Q., WANG, J., LIU, T., SUN, J., WANG, Y., WANG, Z., XIA, Y. and XIA, L. (2013). Defluoridation from aqueous solution by manganese oxide coated graphene oxide. *Journal of Fluorine Chemistry*. 148: 67-73
 149. LIAO, P., ISMAEL, Z.M., ZHANG, W., YUAN, S., TONG, M. and WANG, K. (2012). Adsorption of dyes from aqueous solutions by microwave modified bamboo charcoal. *Chem Eng J*. 195: 339-346.
 150. LIU, J., LI, W.Y., LIU, Y.G., ZENG, Q.H. and HONG, S. (2014). Titanium (IV) hydrate based on chitosan template for defluoridation from aqueous solution. *Appl. Surf. Sci.* 293: 46-54.
 151. LOGANATHAN, P., VIGNESWARAN, S., KANDASAMY, J. and NAIDU, R. (2013). Review: Defluoridation of drinking water using adsorption processes. *Journal of Hazardous Materials*. 248: 1-19.
 152. LV, G., WU, L., LIAO, L., ZHANG, Y., ZHAOHUI, Y. (2012). Preparation and characterization of red mud sintered porous materials for water defluoridation. *Journal of Applied Clay Science*. 74:95-101.

-
153. MA, Y., SHI, F., ZHENG, X., MA, J. and GAO, C. (2011). Removal of fluoride from aqueous solution using granular acid-treated bentonite (GHB): batch and column studies. *J. Hazard. Mater.* 185: 1073-1080.
 154. MAY., WANG, S.G., FAN, M., GONG, W.X. and GAO, B.Y. (2009). Characteristics and defluoridation performance of granular activated carbons coated with manganese oxides. *Journal of Hazardous Materials.* 168: 1140-1146.
 155. MADEJOVA, J. and KOMADEL, P. (2001). Baseline studies of the clay minerals society source clays: infrared methods. *Clays and Clay Minerals.* 49: 410-432.
 156. MAITI, A., BASU, J.K. and DE, S. (2011). Chemical treated laterite as promising fluoride adsorbent for aqueous system and kinetic modelling. *Desalination.* 265: 28-36.
 157. MAKHADO, A.R., BOLOGOA, T. and KNIGHT, R. (2006) Fluoride removal from rural spring water using wood ash. A correspondence, CSIR. South Africa.
 158. MALIYEKKAL, S.M., SHARMA, A.K., PHILIP, L. (2006). Manganese-oxide-coated alumina: a promising sorbent for defluoridation of water. *Water Res.* 40: 3497-3506.
 159. MALIYEKKAL, S.M., SHUKLA, S., PHILIP, L. and NAMBI, I.M. (2008). Enhanced fluoride removal from drinking water by magnesia-amended activated alumina granules, *Chem. Eng. J.* 140: 183-192.
 160. MAMERI, N., YEDDOU, A.R., LOUNICI, H., GRIB, H., BELHOCINE, D. and BARIOU, B. (1998). Defluoridation of septentrional Sahara water of North Africa by electrocoagulation process using bipolar aluminium electrodes. *Water Res.* 32: 1604-1610.
 161. MANDAL, S. and MAYADEVI, S. (2009). Defluoridation of water using as-synthesized Zn/Al/Cl anionic clay adsorbent: equilibrium and regeneration studies. *J. Hazard. Mater.* 167: 873-878.
 162. MARAIS, S. (1998). "Fluorides and Human Health", Fluorides and Nitrates in Rural Water Supplies. WRC Workshop, 9-10 March 1998, Mmabatho
 163. MARIAPPAN, P. and VASUDEVAN, T. (2011). Domestic defluoridation techniques and sector approach for fluorosis mitigation. Pages 1-11 (Accessed on 2014 Mar. 4th). Available from: URL: www.twadboard.gov.in
 164. MARIAPPAN, R., VAIRAMUTHU, R. and GANAPATHY, A. (2015). Use of chemically activated cotton nut shell carbon for the removal of fluoride contaminated drinking water: Kinetics evaluation. *Chinese Journal of Chemical Engineering.* 23: 1-12
 165. MASAMBA, W.R.L., SAJIDU, S.M.I., THOLE, B. and MWATSETEZA, J.F. (2005). Water defluoridation using Malawi's locally sourced gypsum. *Phys. Chem. Earth, A/B/C.* 30: 846-849.
 166. MAUGHAN-BROWN, H. (1935). Our Land. Is our population satisfactory? The results of inspection of school ages. *South African Medical Journal.* 9: 822.
 167. MCCAFFREY, L.P. and WILLIS, J.P. (1993). Distribution of fluoride-rich groundwater in the eastern parts of Bophuthatswana, relationship to bedrock and soils and constraints on drinking water supplies: a preliminary report. *Africa Needs Ground Water. An International Ground Water Convention*, 1, pp. 1-8.
 168. MCCAFFREY, L.P., WILLIS, J.P. (2001). Distribution of Fluoride-Rich Groundwater in the Eastern and Mogwase Regions of the Northern and North-West Province. WRC Report No. 526/1/01 1.1-9.85 Pretoria. South Africa
 169. MCCAFFREY, L.P. (1998). PhD Thesis, University of Cape Town, 1998: In Chibi, C; Haarhoff, J (2000). A Promising Approach to Fluoride Removal in Rural Drinking Water Supplies. Presented at WISA 2000 Biennial Conference, Sun City, South Africa, 28 May-1 June 2000
 170. MEENAKSHI, S.K. and MAHESHWARI, R.C. (2006). Fluoride in drinking water and its removal. *Journal of Hazardous Matter.* 137: 456-463
 171. MICHEN, B., DIATTA, A., FRITSCH, J., ANEZIRIS, C. and GRAULE, T. (2011). Removal of colloidal particles in ceramic depth filters based on diatomaceous earth. *Separation and purification technology,* 81: 77-87.
 172. MJENGERA, H. and MKONGO, G. (2003). Appropriate defluoridation technology for use in fluorotic areas in Tanzania. *Physics and Chemistry of the Earth.* 28: 1097-1104.
 173. MOGES, G., ZEWGE, F. and SOCHER, M. (1996). Preliminary investigations on the defluoridation of water using fired clay chips, *J. African Earth Sciences.* 22: 479-482.

-
174. MOHAMEDBAKR, H. (2010). Diatomite: Its characterization, modifications and applications. *Asian Journal of Materials Science*. 2: 121-136.
 175. MOHAPATRA, M.A.S., MISHRA, B.K., DION, E.G. and SINGH, P. (2009). Review of fluoride removal from drinking water. *Journal of Environmental Management*. 91: 67-77
 176. MOLLAH, M.Y.A., SCHENNACH, R., PARGA, J.R. and COCKE, D.L. (2001). Electrocoagulation montmorillonite clay. *Indian Journal of Chemical Technology*. 12: 263-272.
 177. MORAIS, F.I., PAGE, A.L. and LUND, L.J. (1976). The effect of pH, salt concentration, and nature of electrolytes on the charge characteristics of Brazilian tropical soils. *Soil Sci. Soc. Am. J.* 40: 521-527.
 178. MUDZIELWA, N.A. (2016). Synthesis, characterization and performance evaluation of groundwater defluoridation capacity of smectite-rich clay soils and Mn-modified bentonite clay composites. MSc Thesis. University of Venda.
 179. MULLER, W.J. (1998). Finding the optimum: Fluoridation of potable water in South Africa. *Water SA*. 24: No 1.
 180. MUNZHELELE (1998). Fluorspar. Personal communication. Department of Minerals and Energy. South Africa. In Ncube EJ (2002) The distribution of fluoride in South African Groundwater and the impact thereof on dental health. MSc Dissertation. Water Utilization. University of Pretoria, South Africa.
 181. MURPHY, H.M., MCBEAN, E.A. and FARAHBAKHS, K. (2009). Appropriate technology – a comprehensive approach for water and sanitation in the developing world. *Technol. Soc.* 31: 158-167.
 182. MURRAY, J.J. (Ed.) (1986). *Appropriate Use of Fluorides for Human Health*, World Health Organization, Geneva.
 183. MURUGAN, M. and SUBRAMANIAN, E. (2006). Studies on defluoridation of water by Tamarind seed, an unconventional biosorbent. *Journal of Water and Health*. 4: 453-461.
 184. MWANIKI, D.L. (1992). Fluoride sorption characteristics of different grades of bone charcoal, based on batch tests. *J. Dent. Res.* 71:1310-1315
 185. NAGENDRA RAO, C.R. (2003). Fluoride and Environment – A Review. In Martin JB, Madha Suresh V and Vasantha Kumaran T eds. *Proceedings of the Third International Conference on Environment and Health*. Chennai, India 15-17 December 2003. Department of Geography, University of Madras and Faculty of Environmental Studies, York University. pp. 386-399: Chennai.
 186. NAIR, K.R. and GITONGA, J.N. (1985). Correlation between occurrence of fluoride in ground and surface water resources and dental fluorosis in Kenya. *Fluoride*. 18: 4-11.
 187. NAMASIVAYAM, C. and YAMUNA, R.T. (1995). Adsorption of direct red 12B, biogas residual slurry: equilibrium and rate processes. *Environ Poll.* 89: 1-7.
 188. NANYARO, J.T., ASWATHANARAYANE, U., MUNGURE, J.S. and LAHERMO, P.W. (1984). A geochemical model for the abnormal fluoride concentrations in waters in parts of Northern Tanzania. *Journal of African Earth Sciences*. 2: 129-140.
 189. NÄSLUND, J. and SNELL, L. (2005). GIS mapping of fluoride contaminated groundwater in Nakuru and Baringo District, Kenya: A minor field study. MSc Thesis, Lulea University of Technology, Sweden.
 190. NASR, A.B., CHARCOSSET, C., AMAR, R.B. and WALHA, K. (2013). Defluoridation of water by nanofiltration. *Journal of Fluorine Chemistry*. 150: 92-97.
 191. NASR, A.B., WALHA, K., CHARCOSSET, C. and AMAR, R.B. (2011). Removal of fluoride ions using cuttlefish bones. *Journal of Fluorine Chemistry*. 132: 57-62.
 192. NAYAK, P. (2002). Review aluminium: impacts and disease. *Envtl. Res. Sec.* A89: 101-115.
 193. NCUBE, E.J. (2002). The distribution of fluoride in South African Groundwater and the impact thereof on dental health. MSc Dissertation. Water Utilization. University of Pretoria, South Africa.
 194. NCUBE, E.J. and SCHUTTE, C.F. (2005). The occurrence of fluoride in South African groundwater: A water quality and health problem. *Water SA*. 31: 35-40.
 195. NGULUBE, T. (2016). Synthesis, characterization and performance evaluation of iron(III) oxide coated bentonite clay – silica-rich reddish black Mukondeni clay soils composites for the defluoridation of groundwater. MSc Thesis. University of Venda.
 196. NHMRC and ARMCANZ (2005). *Australian drinking water guidelines*, National Health and Medical Research Council and the Agriculture and Resource Management Council of Austria and New Zealand, 2004.

-
197. NUR, T., LOGANATHAN, P., NGUYEN, T.C., VIGNESWARAN, S., SINGH, G. and KANDASAMY, J. (2014). Batch and column adsorption and desorption of fluoride using hydrous ferric oxide: Solution chemistry and modelling. *Chemical Engineering Journal*. 247: 93-102.
 198. NYAORA, M.W.K., TOLE, M.P., DAVIES, T.C. (2001). The contribution of drinking water towards dental fluorosis: A case study of Njoro Division, Nakuru District, Kenya. *Environmental Geochemistry and Health*. 24: 123-130.
 199. OBI, C.L., POTGIETER, N., BESSONG, P.O. and MATSAUNG, G. (2002). Assessment of the microbial quality of river water sources in rural Venda communities in South Africa. *Water SA*. 28: 287-292.
 200. OCKERSE, T. (1941). Endemic fluorosis in the Kenhardt and Gordonia districts, South Africa. *Journal of the American Dental Association*. 28: 936-941.
 201. OCKERSE, T. (1947). Endemic fluorosis in South Africa. A PhD Thesis submitted to University of Witwatersrand. South Africa.
 202. OCKERSE, T. and Meyer, H.P. (1941). Endemic fluorosis in the Pilansberg area and the occurrence of fluorine in the Saltpan, Pretoria district. *South African Dental Journal*. 15: 62.
 203. ODIYO, J.O. and MAKUNGO, R. (2012). Fluoride concentrations in groundwater and impact on human health in Siloam Village, Limpopo Province, South Africa. *Water SA*. 38: 731-736.
 204. ODONNEL, T.A. (1973). *The chemistry of fluoride*. Elmsford, NY: Pergamon Press.
 205. OLADOJA, N.A. and HELMREICH, B. (2014). Batch defluoridation appraisal of aluminium oxide infused diatomaceous earth. *Chemical Engineering Journal*. 258: 51-61
 206. OMUETI, J. and JONES, R.L. (1977). Fluoride adsorption by Illinois soils. *J. Soil Sci*. 28: 546-572.
 207. ONYANGO, M.S., KOJIMA, Y., AOYI, O., BERNADO, E.C. and MATSUDA, H. (2004). Adsorption equilibrium modelling and solution chemistry dependence of fluoride removal from water by trivalent-cation-exchanged zeolite F-9. *J. Colloid Interface Sci*. 279: 341-350.
 208. OREMUSOVÁ, J. (2007). *Manual for laboratory practice in physical chemistry for students of pharmacy*, Department of Physical Chemistry, Faculty of Pharmacy, Comenius University, Bratislava, in Slovak
 209. OREN, O., YECHIELI, Y., BOHLKE, J.K. and DODY, A. (2004). Contamination of groundwater
 210. OZCAN, A., OZCAN, A.S. and GOK, O. (2007). Adsorption kinetics and isotherms of anionic dye of reactive blue19 from aqueous solutions onto DTMA-sepiolite, in: A.A. Lewinsky (Ed.), *Hazardous Materials and Wastewater-Treatment, Removal and Analysis*, Nova Science Publishers, New York.
 211. OZEAN, A.S., ERDEN, B. and OZEAN, A. (2005). Adsorption of acid blue 193 from aqueous solutions onto BTMA activated bentonite. *Colloid and surfaces. A. Physicochem. Eng. Aspects*. 266: 73-81.
 212. PADMASIRI, J.P. (1998). Low cost defluoridation of drinking water by means of brick chips. *Proceedings of the 2nd International Workshop on Fluorosis and Defluoridation of Water*. Nazareth, 19-22 November 1997. The International Society for Fluoride Research, Auckland.
 213. PANDAY, K.K., PRASAD, G. and SINGH, V.N. (1985). Copper (II) removal from aqueous solutions by fly ash. *Water Res*. 19: 869-873.
 214. PAPAGEORGIOU, K.S., KATSAROS, K.F., KOUVELOU, P.E., NOLAN, W.J., LEDEIT, H. and KANELLOPOULOS, K.N. (2006). Heavy metal sorption by calcium alginate beads from *Laminaria digitate*. *Journal of Hazardous Materials*. 137: 1765-1772. Paris XII.
 215. PARK, G.A. (1965). The isoelectric points of solid oxides, solid hydroxides and aqueous hydroxy complex systems. *Chem. Rev*. 65: 177-198.
 216. PAUDYAL, H., PANGENI, B., INOUE, K., KAWAKITA, H., OHTO, K. and ALAM, S. (2013). Adsorptive removal of fluoride from aqueous medium using a fixed bed column packed with Zr (IV) loaded dried orange juice residue. *Bioresource Tech*. 146: 713-720.
 217. PAUDYAL, H., PANGENI, B., INOUE, K., KAWAKITA, H., OHTO, K., HARADA, H. and ALAM, S. (2011). Adsorptive removal of fluoride from aqueous solution using orange waste loaded with multi-valent metal ions. *J. Hazard. Mater*. 192: 676-682.
 218. PERROTT, K.W., SMITH, B.F.L. and INKSON, R.H.E. (1976). The reaction of fluoride with soils and soil minerals. *J. Soil Sci*. 27: 348.
 219. PHE (2001). *Protection of the Human Environment. Fluoride in drinking water*, a World Health Organization paper, www.unicef.org/programme/wes/info.

-
220. PIDDENAVAR, R. and KRISHNAPPA, P. (2013). Review on defluoridation techniques of water. *The International Journal of Engineering and Science*.2: 86-94
221. PIPER, A.M. (1944). A graphic procedure in the geochemical interpretation of water analysis. *American Geophysical Union Transactions*. 25: 914-923.
222. PONTIUS, F.W. (1991). Fluoride regulation and water fluoridation. *J. Am. Water Works*
223. *Process. Separation and Purification Technology* 56: 184-191.
224. PUGAZHENTHI, G. and KUMAR, A. (2005). Chromium (VI) separation from aqueous solution using anion exchange membrane. *AIChE J.* 51: 2001-2010.
225. PUREMADI (2013). Annual Newsletter. Issue 1. www.puremadi.org
226. QADEER, R., HANIF, J., KHAN, M. and SALEM, M. (1995). Uptake of uranium ions by molecular sieve, *Radiochim. Acta.* 68: 197-201.
227. QIAN, J., SUSHEELA, A.K., MUDGAL, A. and KEAST, G. (1999). Fluoride in water: An Overview. UNICEF Publication on Water, Environment sanitation and Hygiene, pp. 11-13.
228. RAI, M., PATHAN, M., KHAN, A., FAROOQUI, M. and ZAHEER, A. (2004). A study of the removal of dyes by goda sand. *J. Indian Chem. Soc.* 81: 484-487.
229. RAJKOVIC, M.B. and NOVAKOVIC, I.D. (2007). Determination of fluoride content in drinking water and tea infusions using fluoride ion selective electrode. *Journal of Agricultural Sciences.* 52: 155-168.
230. RAJU, N.J., DEY, S. and DAS, K. (2009). Fluoride contamination in groundwaters of Sonbhadra District, Uttar Pradesh, India. *Curr. Sci.* 96: 975-985.
231. RAKSHIT, P.K. (2004). Studies on the estimation of fluoride and defluoridation of drinking water. A project report submitted to the department of Chemical Engineering, Indian Institute of Science. India.
232. RAO, N.R. and PRASAD, P.R. (1997). Phosphate pollution in the groundwater of lower Vamsadhara river basin, India, *Environmental geology.* 31: 117-122.
233. RAO, S.M., REDDY, B.V.V., LAKSHMIKANTH, S. and AMBIKA, N.S. (2009). Re-use of fluoride contaminated bone char sludge in concrete. *Journal of Hazardous Materials.* 166:751-756.
234. RAWHARI, S. (1986). Incidence of microbial, fluoride and nitrate pollution in groundwater. Seminar on technology transfer in water supply and sanitation in developing areas. Bophuthatswana, Mmabatho. 1-17.
235. RIVETT, M., DREWES, J., BARRETT, M., CHILTON, S., APPLEYARD, S., DIETER, H.H., WAUCHOPE, D. and FASTNER, J. (2006). Chapter b4. Chemicals: health relevance transport and attenuation. In: Schmoll O, Howard G, Chilton J and Chorus J (eds) *Protecting Groundwater for Health: Managing the Quality of Drinking Water Sources.* WHO Drinking Water Quality Series, IWA publishing, London.
236. ROBERT, E.T. (1988). *Mass Transfer Operations*, 3rd Ed
237. ROSS, D.S. and KETTERINGS, Q. (2011). Recommended Methods for Determining Soil Cation Exchange Capacity Chapter 9. Cooperative Bulletin No. 493 Recommended Soil Testing Procedures for the North-eastern United States: 75-86.
238. RUBEN, S. (1985). *Handbook of the elements.* La Salle Illinois: Open Court Publishing Company
239. RURAL WATER SUPPLY HEALTH STANDARD COMMITTEE (1974). Temporary standards of quality of domestic water in Tanzania. *Maji Review.* 1: 69-71. (Ministry of Water
240. SADIJU, S., KAYIRA, C., MASAMBA, W. and MWATSETEZA, J. (2012). Defluoridation of groundwater using bauxite: rural domestic defluoridation technology. *Environment and Natural Resources Research.* 2: 1-9.
241. SADIJU, S.M.I., MASAMBA, W.R.L., THOLE, B. and MWATSETEZA, J.F. (2008). Groundwater fluoride levels in villages of Southern Malawi and removal studies using bauxite. *Int. J. Phys. Sci.* 3: 1-11.
242. SAKHARE, R.S. and JAMKHADE, P.G. (2012). Absorption ratio method for estimation drotaverine hydrochloride and mefenamic acid in their combined tablet dosage form. *International Research Journal of Pharmacy.* 3: 212-214.
243. SARACCO, G. (2003). Ionic membrane technologies for the recovery of valuable chemicals from waste waters. *Ann. Chim.* 93: 817-826.
244. SARI, A. and TUZE, M. (2013). Adsorption of silver from aqueous solution onto raw vermiculite and manganese oxide-modified vermiculite. *Microporous and Mesoporous Materials,* 170: 155-163

-
245. SARKAR, M.B., APARNA, P.P., PARTHA, R.S., ASIT. R.S. (2007). Design and operation of fixed bed laterite column for the removal of fluoride from water. *Chem. Eng. J.* 131: 329-335
 246. SCHOEMAN, J.J. (2009). Performance of a water defluoridation plant in a rural area in South Africa. *Water SA.* 35: No. 1.
 247. SCHOEMAN, J.J. and BOTHA, G.R. (1985). An evaluation of the activated alumina process for fluoride removal from drinking-water and some factors influencing its performance. *Water SA.* 11: No. 1.
 248. SCHWERTMANN, U. and FECHTER, C. (1982). The point of zero charge of natural and synthetic ferrihydrites and its relation to adsorbed silicate. *Clay Minerals.* 17: 471-476.
 249. SEMMENS, B. and MEGGY, A.B. (1996). The reaction of kaolin with fluorides. *J. Appl. Chem.* 16: 122.
 250. SETSHEDI, K.Z., BHAUMIK, M., ONYANGO, M.S. and MAITY, A. (2014). Breakthrough studies for Cr(VI) sorption from aqueous solution using exfoliated polypyrrole-organically modified montmorillonite clay nanocomposite. *Journal of Industrial and Engineering Chemistry.* 20: 2208-2216.
 251. SHANG, Y. and GUO, H. (2013). Fluoride adsorption on modified natural siderite: Optimization and performance. *Chemical Engineering Journal.* 223:183-191
 252. SHIMELIS, B., ZEWGE, F. and CHANDRAVANSHI, B.S. (2006). Removal of excess fluoride from water by aluminium hydroxide. *Bulletin of the Chemical Society of Ethiopia.* 20: 17-34.
 253. SHRIKANT, S.P. and NITIN, W.I. (2012). Studies on defluoridation – a critical review. *Journal of Engineering Research and Studies.* 3: 111-119.
 254. SHRIVASTAVA, B.K. and VANI, A. (2009). Comparative study of defluoridation technologies in India. *Asian Journal of Experimental Sciences.* 23: 269-274.
 255. SIMONS, R. (1993). Trace element removal from ash dam waters by nanofiltration and diffusion dialysis. *Desalination.* 89: 325-341.
 256. SMET, J. (1992). Fluoride in drinking water. In: Frencken, JE (ed.) *Endemic fluorosis in developing countries. Report of a symposium held in Delft, the Netherlands, April 27th 1990.* pp98.
 257. SMITH, H.R. and SMITH, L.C. (1937). Bone Contact Removes Fluorine. *Water Works Engineering,* 90: 600-608.
 258. SORG, T.J. (1978). Treatment technology to meet the interim primary drinking water regulations for inorganics. *J. Am. Water Work Assoc.* 70: 105-112.
 259. SOUTH AFRICAN NATIONAL STANDARD (2015). *Drinking Water. Part 1: Microbiological, physical, aesthetic and chemical determinants.* SANS 241-1: 2015
 260. SPARK, D.L. (1997). *Environmental soil chemistry.* 2nd ed. Amsterdam: Academic Press.
 261. SRIMURALI, M. and KARTHIKEYAN, J. (2008). Activated alumina: defluoridation of water and household application – a study. Twelfth International Water Technology Conference, IWTC12. Alexandria, Egypt
 262. SRIMURALI, M., PRAGATHI, A. and KARTHIKEYAN, J. (1998). A study on removal of fluorides from drinking water by adsorption onto low-cost materials. *Environ Pollut.* 99: 285-289.
 263. STAZ, J. (1938). Dental caries in South Africa. *South African Journal of Medical Science.* 3: 2-25.
 264. STIFF, H.A. JR. (1951). The interpretation of chemical water analysis by means of patterns: *Journal of Petroleum Technology.* 3: 15-17.
 265. STRATHMANN, H. (2004). *Ion-exchange membrane separation processes (Membrane Science and Technology Series 9).* Amsterdam: Elsevier.
 266. SUN, Y.B., FANG, Q.H., DONG, J.P., CHENG, X.W. and XU, J.Q. (2011). Removal of fluoride from drinking water by natural stilbite zeolite modified with Fe (III). *Desalination.* 277: 121-127.
 267. SUNDARAM, C.S., VISWANATHAN, N. and MEENAKSHI, S. (2008). Defluoridation chemistry of synthetic hydroxyapatite at nano scale: equilibrium and kinetic studies. *Journal of Hazardous Materials.* 155: 206-215.
 268. SUSHEELA, A.K. (2001), *Treatise on Fluorosis, Fluorosis Research and Rural Development Foundation, India.*
 269. SWISS CENTRE FOR DEVELOPMENT CO-OPERATION IN TECHNOLOGY AND MANAGEMENT (SKAT) (2003). Household water treatment 1 (Technical brief No. 58) *Waterlines.* January 2003; 21: 3.

-
270. TALABI, A.O. and TIJANI, M.N. (2013). Hydrochemical and stable isotopic characterization of shallow groundwater system in the crystalline basement terrain of Ekiti area, southwestern Nigeria. *Appl. Water Sci.* 3:229-245.
271. TAMER, M.N., KOROGLU, B.K., ARSLAN, C., AKDOGAN, M., KOROGLU, M., ÇAM, H. and YILDIZ, M. (2007). Osteosclerosis due to endemic fluorosis. *Sci. Total Environ.* 373: 43-48.
272. TAMURA, H.A., MITA, K., TANAKA, A. and ITO, M. (2001). Mechanism of hydroxylation of metal oxide surfaces. *J. Colloid Interface Sci.* 243: 202-207.
273. TANG, D. and ZHANG, G. (2016). Efficient removal of fluoride by hierarchical Ce-Fe bimetal oxides adsorbent: thermodynamics, kinetics and mechanism. *Chem. Eng. J.* 283: 721-729.
274. TCHOMGUI-KAMGA, E., ALONZO, V., NANSEU-NJIKI, C.P., AUDEBRAND, N., NGAMENI, E. and DARCHEN, A. (2010). Preparation and characterization of charcoals that contain dispersed aluminium oxide as adsorbents for removal of fluoride from drinking water. *Carbon.* 48: 333-343.
275. TENG, S., WANG, S., GONG, W., LIU, X. and GAO, B. (2009). Removal of fluoride by hydrous manganese oxide-coated alumina: Performance and mechanism. *Journal of Hazardous Materials.* 168: 1004-1011.
276. TERI, E.M. (1982). Endemic fluorosis: some clinical and epidemiological aspects of fluorosis with specific reference to Maji ya Chai area, Arusha Region. A report on Domestic water health Standards with Emphasis on Fluoride. Arusha, Tanzania. Ministry of Water and Energy. 83-93.
277. THAKRE, D., RAYALU, S., KAWADE, R., MESHARAM, S., SUBRT, J. and LABHSETWAR, N. (2010). Magnesium incorporated Bentonite clay for defluoridation of drinking water. *Journal of Hazardous Materials.* 180: 122-130.
278. THILAGAVATHY, P. and SANTHI, T. (2014). Kinetics, Isotherms and Equilibrium Study of Co (II) Adsorption from Single and Binary Aqueous Solutions by *Acacia nilotica* Leaf Carbon Chinese. *Journal of Chemical Engineering.* 22: 1193-1198.
279. THOLE, B. (2011). Defluoridation kinetics of 200°C calcined bauxite, gypsum, and magnesite and breakthrough characteristics of their composite filter. *Journal of Fluorine Chemistry.* 132: 529-535.
280. THOLE, B., MTALO, F.W. and MASAMBA, W.R.L. (2011). Water Defluoridation with 150-300°C Calcined Bauxite-Gypsum-Magnesite Composite (B-G-Mc) filters. *Water Resources Management VI, Wit Transactions on Ecology and Environment.* 145: 383-393.
281. THOLE, B., MTALO, F.W. and MASAMBA, W.R.L. (2012). Effect of particle size on loading capacity and water quality in water defluoridation with 200°C calcined bauxite, gypsum, magnesite and their composite filter. *African Journal of Pure and Applied Chemistry.* 6: 26-34.
282. TOHIDI, N. and RAMEZ, V. (1997). Preparation of Iron and Steel Burden, Tehran University. 577.
283. TOMAR, V., PRASAD, S., KUMAR, D. (2014). Adsorptive removal of fluoride from aqueous media using citrus limonum (lemon) leaf. *Microchem. J.* 112: 97-103.
284. TOMAR, V., PRASAD, S. and KUMAR, D. (2013). Adsorptive removal of fluoride from water samples using Zr-Mn composite material. *Microchem. J.* 111: 116-124.
285. TOOR, M., JIN, B., DAI, S. and VIMONOSES, V. (2014). Activating natural bentonite as a cost effective adsorbent for removal of Congo red in waste water. *J. industrial and engineering chemistry.* 21: 653-661
286. TOR, A. (2006). Removal of fluoride from an aqueous solution by using montmorillonite. *Desalination.* 201: 267-276.
287. TRAN, C.D., DURİ, S., DELNERI, A. and FRANKO, M. (2013). Chitosan – cellulose composite materials: preparation, characterisation and application for removal of microcystin. *J Hazard Material.* 10: 252-366.
288. TRIPATHY, S.S., BERSILLON, J-L. and GOPAL, K. (2006). Removal of fluoride from drinking water by adsorption onto alum-impregnated activated alumina. *Sep. Purif. Technol.* 50: 310-317.
289. TYERYAR, M., HACKETT, C., HARSH, D. and HACKETT, T. (2012). Establishing a ceramic water filter factory in Limpopo Province, South Africa. *Public.* 104-110.
290. UNDERWOOD, E.J. (1977). Trace elements In Human and Animal nutrition (4th edition) Academic press, New York, San Francisco, London.

-
291. UNUABONAH, E.I., ADEBOUAL, K.O. and DAWODU, A.A. (2008). Equilibrium kinetic and sorbent design studies on the adsorption of Aniline blue dye by sodium tetra borate – modified Kaolinite clay adsorbent. *J. Hazard Mater.* 157: 397-409.
 292. UNUABONAH, E.I., ADEBOWALE, K.O. and OLU-OWOLABI, B.I. (2007). Kinetic and thermodynamic studies of the adsorption of lead (II) ions onto phosphate-modified kaolinite clay. *J. Hazard. Mater.* 144: 386-395.
 293. US PUBLIC HEALTH DRINKING WATER STANDARDS (1962). US Public Health Service, Washington, DC.
 294. VENKOBACHAR, C., IYENGAR, L. and MUDGAL, A. (1997). Household defluoridation of drinking water using activated alumina technology. Proceedings of the 2nd international workshop on fluorosis and defluoridation of water, Addis Ababa, Ethiopia, November 19-22, 1997. Dunedin, New Zealand, International Society for Fluoride Research.
 295. VERMEULAN, T.H., VERMEULAN, K.R., and HALL, L.C. (1966). *Fundamental. Ind. Eng. Chem.* 5: 212-223.
 296. VHAHANGWELE, M., MUGERA, G.W., THOLISO, N. (2014). Defluoridation of drinking water using Al³⁺-modified bentonite clay: optimization of fluoride adsorption conditions. *Toxicol. Environ. Chem.* 96: 1-16.
 297. VIJAYARAHGAVAN, K., JEGAN, J.R., PALANIVELU, K. and VELAN, M. (2005). Nickel Recovery from Aqueous Solution using Crab Shell Particles. *Adsorption Science Technology.* 23: 303-311.
 298. VOUDRIAS, E., FYTIANOS, F. and BOZANI, E. (2002). Sorption Description isotherms of Dyes from aqueous solutions and Waste Waters with Different Sorbent materials. *Global Nest .The Int. J.* 4: 75-83.
 299. WAMBU, E.W., ONINDO, C.O., AMBUSSO, W.J. and MUTHAKA, G.K. (2011). Fluoride adsorption onto acid-treated diatomaceous mineral from Kenya. *Materials Sciences and Applications.* 2: 1654-1660.
 300. WANG, J., KANG, D., YU, X., GE, M. and CHEN, Y. (2015). Synthesis and characterization of Mg-Fe-La trimetal composite as an adsorbent for fluoride removal. *Chemical Engineering Journal.* 264: 506-513.
 301. WANG, J., XU, W., CHEN, L., JIA, Y., WANG, L., HUANG, X. and LIU, J. (2013). Excellent fluoride removal performance by CeO₂-ZrO₂ nanocages in water environment. *Chemical Engineering Journal.* 231: 198-205.
 302. WANG, Y., WANG, X., WANG, X., LIU, M., YANG, L., WU, Z., XIA, S. and ZHAO, J. (2012). Adsorption of Pb(II) in aqueous solutions by bamboo charcoal modified with KMnO₄ via microwave irradiation. *Colloids and Surfaces A: Physicochem. Eng. Aspects.* 414: 1-8.
 303. WANG, Y. and REARDON, E.J. (2001). Activation and regeneration of a soil sorbent for defluoridation of drinking water. *Appl. Geochem.* 16: 531-539.
 304. WARSHAW, C.M., ROSENBERG, P.E. and ROY, R. (1960). Changes effected in layer silicates by heating below 550°C. *Clay minerals bulletin.* 23: 113-125.
 305. WATER RESEARCH COMMISSION (2008). Knowledge for Growth on Development: Knowledge Review 2007/08. Water Research Commission, Pretoria.
 306. WEBER, T.W. and CHAKRAVORTI, R.K. (1974). Pore and solid diffusion models for fixed bed adsorbents. *AIChE Journal.* 20: 228-238.
 307. WEBER, W.J. and DIGIANO, F.A. (1996). Process dynamics in environmental systems. Environmental Science and Technology Series, New York: Wiley & Sons.
 308. WEBER, W.J. and MORRIS, J.C. (1963). Kinetics of adsorption on carbon from solution. *Journal of Sanitary Engineering Division/American Society of Civil Engineers.* 89: 31-60.
 309. WORLD HEALTH ORGANISATION (2004). Fluoride in drinking-water. WHO guidelines for drinking-water quality, Geneva.
 310. WORLD HEALTH ORGANISATION (2005). Bentonite, kaolinite, and selected clay minerals. Environmental health criteria. 231: ISBN 92 4 157231 0.
 311. WORLD HEALTH ORGANIZATION (1984). Guidelines for Drinking Water Quality. Vol. 2 (Health Criteria and other Supporting Information), part III, Chapter 8, WHO, Geneva.

-
312. WORLD HEALTH ORGANIZATION (2006). Chemical fact sheets: fluoride. In guidelines for drinking water quality (electric resource): incorporation first addendum. Recommendations. 1, 3rd ed., Geneva, 375-377.
 313. WORLD HEALTH ORGANIZATION (2011). Chemical fact sheets. Guidelines for Drinking-Water Quality, 4thed. Gutenberg, Malta
 314. WORLD HEALTH ORGANIZATION (WHO) (2000). Quality of Domestic Water Supplies. IWA Publishing, London, UK.
 315. WORLD HEALTH ORGANIZATION, Environmental Health Criteria (1984). Fluorine and Fluorides.
 316. WU, X., ZHANG, Y., DOU, X. and YANG, M. (2007). Fluoride removal performance of a novel Fe-Al-Ce trimetal oxide adsorbent. *Chemosphere*. 69: 1758-1764.
 317. XIANG, W., ZHANG, G., ZHANG, Y., TANG, D. and WANG, J. (2014). Synthesis and characterization of cotton-like Ca-Al-La composite as an adsorbent for fluoride removal. *Chemical Engineering Journal*. 250: 423-430.
 318. XU, M., WANG, H., DI LEI, D., QU, D., ZHAI, Y. and WANG, Y. (2013). Removal of Pb (II) from aqueous solution by hydrous manganese dioxide: Adsorption behavior and mechanism. *Journal of Environmental Sciences*. 25: 479-486
 319. XU, T.W. (2005). Ion exchange membranes: state of their development and perspective. *J. Membr. Sci*. 263: 1-29.
 320. YAO, R., MENG, F., ZHANG, L., MA, D. and WANG, M. (2009). Defluoridation of water using neodymium-modified chitosan. *Journal of Hazardous Materials*. 165: 454-460.
 321. YAO, Z.Y., QI, J.H. and WANG, L.H. (2010). Equilibrium, kinetic and thermodynamic studies on the biosorption of Cu (II) onto chestnut shell. *J. Hazard. Mater*. 174: 137-143.
 322. YI, Z., YING, X., HAO, C., BINGJIE, L., XIANG, G., DONGFENG, W. and PENG, L. (2014). La(III)-loaded bentonite/chitosan beads for defluoridation from aqueous solution. *Journal of rare earths*.32: 458-466.
 323. YUAN, P., WU, D.Q., HE, H.P. and LIN, Z.Y. (1997). The hydroxyl species and acid sites on diatomite surface: a combined IR and Raman study. *Applied Surface Science*, 227: 30-39.
 324. ZENI, M., RIVEROS, R., MELO, K., PRIMERI, R. and LORENZINI, S. (2005), Study on fluoride reduction in artesian wells-water from electrodialysis process. *Desalination*. 185: 214-244.
 325. ZEVENBERGEN, C., REEUWICK, L.P., FRAPPORTI, G., LOUWS, R.J. and SCHUILING, R.D. (1996). A simple method for defluoridation of drinking water at village level by adsorption on Ando soil in Kenya. *The Science of the Total Environment*. 188: 225-232.
 326. ZHANG, Y., CHENG, Y., BAO, F. and WANG, Y. (2006). Synthesis and magnetic properties of Fe₃O₄ nanoparticles. *Material Research bulletin*. 41: 525-529.
 327. ZHANG, Y., ZHAO, Y., ZHU, Y., WU, H., WANG, H. and LU, W. (2012). Adsorption of mixed cationic-nonionic surfactant and its effect on bentonite structure. *Journal of Environmental Sciences*. 24: 1525-1532
 328. ZHANG, Z., TAN, Y. and ZHONG, M. (2011). Defluoridation of wastewater by calcium chloride modified natural zeolite. *Desalination*. 276: 246-252
 329. ZHU, J., ZHAO, H. and NI, J. (2007). Fluoride distribution in electrocoagulation defluoridation Process. *Separation and Purification Technology* 56: 184-191.

APPENDIX A: ADSORBENT CHARACTERISATION METHODS

A1 Determination of Cation Exchange Capacity (CEC)

CEC was determined using the ammonium acetate method at pH 5.4 and pH 7.4 according to Chapman (1962)'s method. 0.5 g of the clay adsorbents was extracted using 25 ml aliquots of 1 M ammonium acetate. The samples were shaken for 15 min using a reciprocating shaker. After shaking, the samples were centrifuged at 30 000 rpm for 15 min. After centrifuging, the supernatant was decanted in a 250 ml bottle. The cumulative extract was brought to 100 ml and then filtered through 0.45 µm pore cellulose nitrate membranes. The filtrate was acidified by adding three drops of nitric acid and stored in the refrigerator until analysis by the Atomic Absorption Spectrometry (AAS). The samples were analysed for the availability of K⁺, Na⁺, Mg²⁺ and Ca²⁺

A2 Calculation of CEC per 1 g

Atomic weight Na = 23

Equivalent weight = Atomic weight/number of valences

Na⁺ = 23/1

By getting equivalent weight, the elements are now in equal terms

CEC is reported in meq/100 g, therefore the equivalent weights are multiplied by 10 to be converted to meq/100 g

Na⁺ = 23 * 10

CEC = Concentration of ions in mg/l/meq/100 g

A3 Determination of Point of Zero Charge (PZC)

To determine the point of zero charge (pHPZC) of the clay adsorbents, 40 ml of 0.1 M KCl was measured into 100 ml bottles. The initial pH of the solution was adjusted to pHs 2, 4, 6, 8, 10 and 12 by adding 0.1 M HCl and 0.1 M NaOH solutions. The total volume of the solution in each bottle was topped to 50 ml by adding KCl. Afterwards, 0.5 g of the clay was added to the solutions and the mixtures were then equilibrated for 24 h using a Daihan Labtech thermostatic waterbath shaker. After shaking, the final pH values of the solutions were measured. The difference between the initial and the final pH was plotted against the initial pH. The point of intersection of the resulting curve with the co-ordinate that gives the distance along the horizontal axis at which ΔpH = 0, was taken as the point of zero charge. The same procedure was repeated using 0.01 M and 0.001 M KCl.

A4 Determination of mineralogy by X-ray diffraction (XRD)

The clay samples were milled in a tungsten carbide vessel and prepared according to the standardised PANalytical backloading system, which provides nearly random distribution of the particles. The samples were analysed using a PANalytical X'Pert Pro powder diffractometer in θ-θ configuration with an X'Celerator detector and variable divergence and receiving slits with Fe filtered Co-Kα radiation (λ=1.789Å). The phases were identified using X'Pert Highscore plus software. The relative phase amounts (weight %) were estimated using the Rietveld method (Autoquan Program).

A5 Determination of elemental composition by X-ray fluorescence (XRF)

The powdered clay samples were milled in a tungsten-carbide milling pot to achieve particle sizes < 75 micron. The samples were dried at 100°C and roasted at 1000°C to determine Loss On Ignition (LOI). 1 g sample was mixed with 6 g Lithiumtetraborate flux and fused at 1050°C to make a stable fused glass bead. The Thermo Fisher ARL Perform'X Sequential XRF with OXSAS software was used for analysis.

A6 Determination of morphology by Scanning Electron Microscopy (SEM)

The morphology of the clay adsorbents was examined using a Hitachi X-650 Scanning Electron Micro-analyser equipped with a CDU-lead detector at 25 kV. Powdered samples were mounted on aluminum pegs and coated with a thin film of gold to make them conductive.

A7 Determination of surface area by Brunauer-Emmett-Teller (BET)

The surface area and pore size distribution of the clay adsorbents was determined using the BET method of analysis using a Micromeritics TriStar II 3020 Version 2.00. Nitrogen adsorption isotherms were obtained at liquid nitrogen temperature. Before the determination of the adsorption isotherm, 5.2187 g of the sample was degassed at 180°C for 48 h. The degassing process was meant to remove adsorbed gases and moisture. The clay was then placed in a N₂ stream and the mass change of the solid due to gas adsorbed was measured relative to the change in partial pressure of N₂.

A8 Determination of functional groups by Fourier Transform Infrared (FTIR)

To determine the functional groups in the clay adsorbents, 0.5 g sample of the clay was analysed by Fourier-transform infrared spectroscopy (FTIR) flow-through continuous reactor. The infrared spectra in transmission mode were recorded in the 4000-400 cm⁻¹ frequency region using a Bruker Alpha spectrometer. The measurements of the adsorption bands integrated intensity were made using OPUS software supplied by the Bruker instrument.

A9 Transmission Electron Microscopy (TEM)

Electron transparent thin slices of dust particles were prepared for TEM analysis of clay minerals then sliced with a microtome to obtain ultrathin (70 nm) cross sections of the embedded specimen. These sections were mounted on 400-mesh copper grids and analysed with a JEM-2100 Electron Microscope operating at 200 kV.

APPENDIX B: BATCH AND FIELD ADSORPTION EXPERIMENTS

B1 Adsorption of fluoride as a function of contact time

To evaluate the effect of contact time on the fluoride removal capacity of adsorbents, 100 ml of 10 mg/l F- solution was pipetted into 21, 250 ml bottles and 1 g, 2 g and 3 g of silica-rich reddish black Mukondeni clay soils were added to each separate bottle. The mixture was agitated for 1, 5, 10, 15, 30, 60, and 180 min at 250 rpm using the Stuart reciprocating shaker. The experiments were carried out in triplicate at room temperature (25°C) and the mean values reported. After equilibration, the mixtures were centrifuged for 10 min at 3000 rpm. The samples were analysed for F-, pH, Temp and EC using a Thermo Scientific Orion Versa Star Advanced Electrochemistry meter.

B2 Adsorption of fluoride as a function of adsorbent dosage

To evaluate the effect of adsorbent dosage on the fluoride removal capacity, 33 samples of 100 ml of 5, 10 and 15 mg/l F- solution were pipetted into 33, 250 ml bottles and 0.1 g, 0.3 g, 0.5 g, 0.7 g, 0.9 g, 1 g, 1.2 g, 1.5 g, 1.7 g, 1.9 g and 2 g of adsorbent were added to each bottle. The mixtures were then agitated for 60 min at 250 rpm using the Stuart reciprocating shaker. The experiments were carried out in triplicate at room temperature (25°C) and the mean values reported. After equilibration, the mixtures were centrifuged for 10 min at 3000 rpm. The samples were analysed for F-, pH, Temp and EC using a Thermo Scientific Orion Versa Star Advanced Electrochemistry meter.

B3 Adsorption of fluoride as a function of adsorbate concentration

To evaluate the effect of initial fluoride concentration on the fluoride removal capacity, 21 samples of 100 ml with 2, 5, 7, 9, 11, 13 and 15 mg/l F- solution was pipetted into 21, 250 ml bottles and 1 g and 2 g of adsorbent were added to each bottle separately. The mixtures were then agitated for 60 min at 250 rpm using the Stuart reciprocating shaker. The experiments were carried out in triplicate at room temperature (25°C) and the mean values reported. After equilibration, the mixtures were centrifuged for 10 min at 3000 rpm. The samples were analysed for F-, pH, Temp and EC using a Thermo Scientific Orion Versa Star Advanced Electrochemistry meter.

B4 Adsorption of fluoride as a function of temperature

To evaluate the effect of temperature on the fluoride removal capacity experiments were conducted at different temperatures of 298 K, 308 K and 318 K. The shaking process was done using a Daihan Labtech thermostatic water bath shaker.

B5 Adsorption of fluoride as a function of competing ions

To evaluate the effect of competing ions on the fluoride removal capacity, sulphate, carbonate, nitrate and phosphate ions were used. To each 250 ml bottle, 10 mg/l of fluoride and 10 mg/l of each competing ion was added. To one 250 ml bottle, no competing ion was added, this was used as a control. 1.5 g of adsorbent dosage was added to each bottle. The mixtures were then agitated for 60 min at 250 rpm using the Stuart reciprocating shaker. The experiments were carried out in triplicate at room temperature (25°C) and the mean values reported. After equilibration, the mixtures were centrifuged for 10 min at 3000 rpm. The samples were analysed for F-, pH, Temp and EC using a Thermo Scientific Orion Versa Star Advanced Electrochemistry meter.

B6 Adsorption of fluoride as a function of pH

To evaluate the effect of pH on the fluoride removal capacity, 100 ml with 9 mg/l of F- solution was pipetted into 6, 250 ml bottles. The pH of the solution was adjusted to 2, 4, 6, 8, 10 and 12 using 0.1 M of HCl and 0.1 M NaOH. 1.5 g of adsorbent dosage was added to each bottle. The mixtures were then agitated for 60 min at

250 rpm using the Stuart reciprocating shaker. The experiments were carried out in triplicate at room temperature (25°C) and the mean values reported. After equilibration, the mixtures were centrifuged for 10 min at 3000 rpm. The samples were analysed for F⁻, pH, Temp and EC using a Thermo Scientific Orion Versa Star Advanced Electrochemistry meter.

B8 Chemical stability testing

The chemical stability of the adsorbents was investigated by measuring the concentration of dissolved metals in the solution before and after fluoride adsorption experiments. The adsorbents (1.5 and 3 g) were added to 100 mL fluoride solution (10 mg/L) samples over a pH range of 2-12. The supernatant was separated through filtration using a 0.45 µm pore cellulose nitrate membranes after shaking for 60 min at 250 rpm using the Stuart reciprocating shaker. The concentration of dissolved metals was measured by inductively coupled plasma mass spectrometry (ICP-MS, DIONEX ICS-2100 from Thermo).

B9 Regeneration studies

The regeneration potential of the adsorbents was evaluated by using 0.01 M NaOH. A defluoridation experiment was done using 2 g of the adsorbent in a 100 mL, 10 mg/L F⁻ solution. The amount of fluoride adsorbed was noted and the adsorbent was dried in the oven for 12 h at 105°C. Afterwards the adsorbent was soaked into 100 mL, 0.01 M NaOH solution and the mixture was centrifuged at 50 000 rpm for 15 min. The amount of fluoride desorbed into the solution was recorded. The adsorbent was again washed by 100 mL MilliQ water to wash off any fluoride on the adsorbent and the amount of fluoride in the wash was recorded again. The desorbed adsorbent was again dried in the oven for 12 h at 105°C. The dried adsorbent was again used for another defluoridation experiment as described above. The same procedure using the same adsorbent was repeated until the adsorbent's fluoride removal capacity was at its lowest.

B10 Determination of pH, EC, TDS and F⁻

Fluoride concentrations were measured by a fluoride ion selective electrode (Thermo Scientific Orion Star A215 pH/Conductivity Benchtop Meter, USA) coupled to an 8157BNUMD Orion ROSS Ultra Triode pH/ATC electrode). A similar ion meter coupled with a pH, EC and TDS electrodes was used for measuring pH, EC and TDS of the treated samples. Before fluoride determination, a total ionic strength adjusting buffer (TISAB III) was added to the solutions in a ratio of 10:1 in order to maintain ionic strength and pH, and eliminate the interference effect of F⁻ ion complexing with metal cations.

B11 Determination of iron, aluminium, magnesium, cerium and manganese levels in treated water

It was necessary to evaluate the potential of the adsorbents to leach Al, Fe, Mg, Ce and Mn species into treated water especially when high doses of the adsorbents are used for fluoride removal from groundwater. The metals would be hazardous if their concentrations in treated water are not within the limits of the WHO guidelines for drinking water. Hence, 0.1, 0.2, 0.4, 0.6, 0.8, 1 and 1.2 g of adsorbent were weighed into 250 mL plastic bottles containing 100 mL of 10 mg/L fluoride solution and equilibrated for 50 min at 200 rpm. The mixtures were centrifuged and the supernatants analysed for the listed metals using inductively coupled plasma-mass spectrometer (ICP-MS).

B12 Full suite analysis of elements in field water using ICP-MS and ICP-AES

Full chemical analysis of the field water before and after defluoridation was done using Inductively Coupled Plasma-Mass Spectrometer (ICP-MS) and Inductively Coupled Plasma-Atomic Emission Spectrometer (ICP-AES). Trace elements were analysed on an Agilent 7700 quadrupole ICP-MS. The elements V, Cr, Mn, Fe, Co, Ni, Cu, Zn, As and Se were analysed under He-collision mode to remove polyatomic interferences. Major elements (Na, K, Ca, Mg, P and Si) were analysed on a Thermo ICap 6200 ICP-AES. The instrument was calibrated using NIST (National Institute of Standards and Technology, Gaithersburg MD, USA) traceable standards to quantify selected elements.

APPENDIX C: ADSORPTION MODELS

C1 Calculation of % F- removal and adsorption capacity

The % fluoride removal by the adsorbents was calculated by the following equation:

$$\% \text{ Removal} = \left(\frac{C_o - C_e}{C_o} \right) \times 100 \quad \text{Equation 1}$$

Where: C_o = initial F- concentration (mg/l)

C_e = Equilibrium F- concentration (mg/l)

The adsorption capacity of the adsorbents for fluoride adsorbed per unit mass of adsorbent (q) was calculated using the following formula:

$$q = (C_i - C_e) \quad \text{Equation 2}$$

Where: C_i = Initial F- concentration (mg/l)

C_e = F- concentration at equilibrium (mg/l)

V = Volume of F- solution (L)

m = Weight of adsorbent (g)

C2 Isotherm models

The concentration of an adsorbate (F⁻) in a bulk solution is in dynamic balance with that of the adsorbent interface. The analysis of equilibrium data helps to develop mathematical models that could be used for the quantitative description of the results. The equation parameters and the underlying assumptions of these equilibrium models are capable of predicting ion adsorption and generating vital information on the mechanism of sorption. The Langmuir, Freundlich and Dubinin-Radushkevich isotherms were tested in this study.

The Langmuir isotherm (Equation 3) assumes that adsorption cannot proceed beyond the monolayer and the ability of a molecule to be adsorbed at a given site is independent of the occupation of neighbouring sites (Zawani et al., 2009). The Langmuir isotherm is expressed as follows;

$$\frac{C_e}{Q_e} = \frac{1}{Q_m b} + \frac{C_e}{Q_m} \quad \text{Equation 3}$$

Where C_e is the equilibrium concentration (mg/l), Q_e is the amount adsorbed at equilibrium (mg/g), b represents the Langmuir isotherm constant and Q_m is the maximum adsorption capacity for a complete monolayer coverage.

Calculated R_L (separation factors) value indicates the adsorption nature to be either unfavourable if $R_L > 1$, linear if $R_L = 1$, favourable if $0 < R_L < 1$ and irreversible if $R_L = 0$.

Freundlich isotherm (Equation 4) describes the adsorption characteristics for heterogeneous surfaces (Krishnaiah and Vijaya, 2009).

$$\log Q_e = \frac{1}{n} \log C_e + \log K_F \quad \text{Equation 4}$$

K_f and $1/n$ are the Freundlich constants, describing the adsorption capacity and intensity respectively. The constants n and K_f were determined from the slope and the intercept respectively. The constant K_f is an approximate indicator of adsorption capacity, while $1/n$ is a function of the strength of adsorption in the adsorption process (Voudrias et al., 2002). If n lies between 1-10, this indicates a favourable sorption process (Goldberg, 2005).

The Dubinin-Radushkevich isotherm model is applied in order to investigate the mean free energy of adsorption. The linearized Dubinin-Radushkevich isotherm is expressed in equation (5)

$$\ln Q_e = \ln Q_D - 2B_D RT \ln \left(1 + \frac{1}{C_e} \right) \quad \text{Equation 5}$$

The apparent energy of adsorption from the isotherm was calculated from equation 6, as follows;

$$E = \frac{1}{(2B_D)^{1/2}} \quad \text{Equation 6}$$

Where Q_D is the Dubinin-Radushkevich isotherm constant, related to adsorption capacity of the adsorbent, B_D , represents free energy of sorption, T is the temperature in Kelvin and R , ideal gas constant. $\ln Q_e$ is plotted against $\ln (1+1/C_e)$ and the constants B_D and Q_D are extrapolated from the slope and intercept.

C3 Thermodynamics

In order to evaluate the feasibility of the adsorption process, thermodynamic parameters are evaluated. The standard free energy change ΔG is calculated using the following equations:

$$\Delta G = -RT \quad \text{Equation 7}$$

where ΔG is the free energy of sorption (kJ/mol), T is the temperature in Kelvin (K), R is the universal gas constant (8.314 J/mol/K) and K_a is the sorption equilibrium constant.

The sorption equilibrium constant K_a can be expressed in terms of enthalpy change (ΔH) and entropy change (ΔS) as a function of temperature (equation 8)

$$\ln K_a = \frac{\Delta H}{RT} + \frac{\Delta S}{RT} \quad \text{Equation 8}$$

where ΔH is the heat of sorption (kJ/mol) and ΔS is the standard entropy change (kJ/mol/K).

The values of ΔH and ΔS can be obtained from the slope and intercept of the Van Hoff's plot of $\ln (K_a)$ vs $1/T$. The positive value of enthalpy change suggests that the adsorption process is endothermic in nature.

C4 Adsorption kinetic models

Adsorption is a time-dependent process and it is very important to know the rate of the adsorption process for design purposes, the rate limiting steps and the mechanism of the adsorption process.

Pseudo first-order kinetics

The pseudo first-order kinetics equation is generally expressed as:

$$\frac{dq_t}{dt} = K_1 (q_e - q_t) \quad \text{Equation 9}$$

where q_e and q_t are the amounts of adsorbate adsorbed onto the surface of the adsorbent at equilibrium and at time, t respectively (mg/g) and K_1 is the rate constant of the first order adsorption process (l/min). Integrating equation (9) and applying the boundary conditions $t = 0$ to $t = t$ and $q_t = 0$ to $q_t = q_t$, gives the linear form of the equation (equation 10)

$$\log(q_e - q_t) = \log q_e - \frac{K_1 t}{2.303} \quad \text{Equation 10}$$

A plot of $\log(q_e - q_t)$ against t gives a straight line with K_1 and q_e as the slope and intercept respectively (Zawani et al., 2009).

Pseudo second-order kinetics

The pseudo second-order kinetics model which assumes that measured concentrations are equal to sorbent surface concentrations is generally expressed as (equation 11)

$$\frac{dq_t}{dt} = K_2 (q_e - q_t)^2 \quad \text{Equation 11}$$

where K_2 is the rate constant of the pseudo second-order adsorption process (g/m/h). After integrating equation (5.9) and applying the boundary conditions $t = 0$ to $t = t$ and $q_t = 0$ to $q_t = q_t$, a linear form of the equation is obtained as (equation 12)

$$\frac{t}{q_t} = \frac{1}{K_2 q_e^2} + \frac{t}{q_e} \quad \text{Equation 12}$$

A plot of t/q_t against t gives a straight line with K_2 and q_e as the intercept and slope respectively (Zawani et al., 2009).

Intra-particle and external diffusion models

There are three steps involved in adsorption of fluoride ions: (i) the fluoride ions diffuse from liquid phase to liquid-solid interface; (ii) the fluoride ions move from liquid-solid interface to solid surfaces; and (iii) the fluoride ions diffuse into the particle pores (Liao, 2012). To reveal the diffusion mechanisms of the adsorption of fluoride on the clay adsorbents, the kinetic results were analysed by using the Weber and Morris intraparticle diffusion model and the external diffusion model. To reveal the relative contribution of surface and intraparticle diffusion to the kinetic process, the kinetic adsorption data can be further fitted to diffusion models. The intraparticle diffusion is the rate controlling factor; uptake of the adsorbate varies with the square root of the time as described by the Weber Morris model. For the rate constant of intraparticle diffusion the equation can be written as:

$$qt = k_{id} t^{\frac{1}{2}} + C \quad \text{Equation 13}$$

Where K_{id} is intraparticle diffusion rate constant (mg/g/min) and qt is the amount of fluoride adsorbed at any time t (mg/g) and C is the intercept. Intraparticle diffusion is assumed to be the sole rate-controlling step if the regression of Qt versus $t^{1/2}$ is linear and the plot passes through the origin (Arami, 2008).

The likelihood of external diffusion being the rate controlling step was also tested using the model by Lee et al. (1999). The diffusion model is given as:

$$\ln \frac{C_t}{C_o} = -k_f \frac{A}{V} t$$

Equation 14

Where C_o is the initial fluoride concentration, C_t is the concentration at time t , A/V is the external adsorption area to the total solution volume, t is the adsorption time, and k_f is the external diffusion coefficient. If a straight line is obtained from the plot of $\ln C_t/C_o$ against t , then, external diffusion controls the sorption process.